ZOOPLANKTON AND NEKTON: GATEKEEPERS OF THE BIOLOGICAL PUMP

EDITED BY: Rainer Kiko, Morten Hvitfeldt Iversen, Amy Elizabeth Maas, Helena Hauss and Daniele Bianchi

PUBLISHED IN: Frontiers in Marine Science

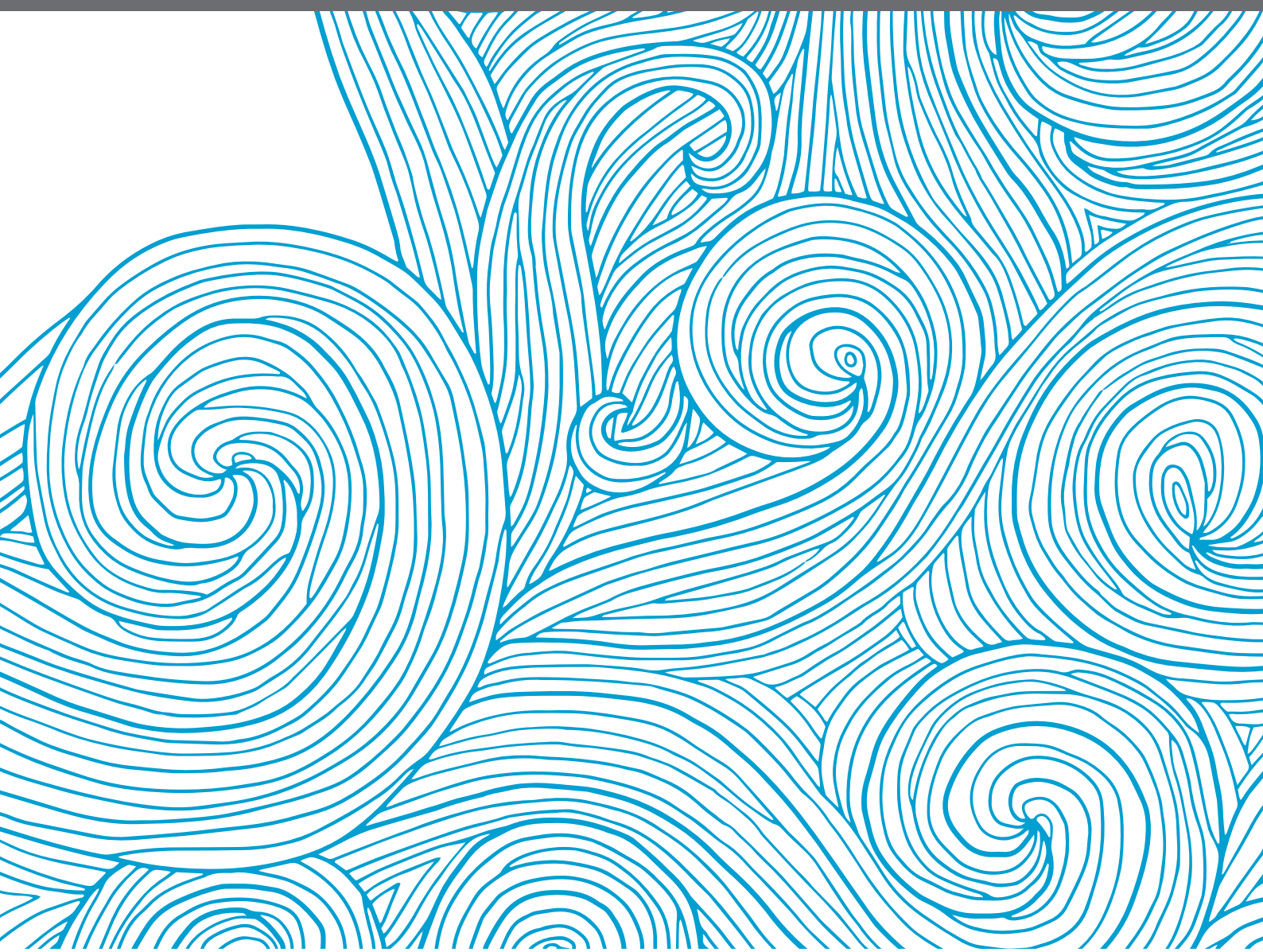

frontiers Research Topics

frontiers

ISSN 1664-8714
ISBN 978-2-88963-982-3
DOI 10.3389/978-2-88963-982-3

About Frontiers

Frontiers is more than just an open-access publisher of scholarly articles: it is a pioneering approach to the world of academia, radically improving the way scholarly research is managed. The grand vision of Frontiers is a world where all people have an equal opportunity to seek, share and generate knowledge. Frontiers provides immediate and permanent online open access to all its publications, but this alone is not enough to realize our grand goals.

Frontiers Journal Series

The Frontiers Journal Series is a multi-tier and interdisciplinary set of open-access, online journals, promising a paradigm shift from the current review, selection and dissemination processes in academic publishing. All Frontiers journals are driven by researchers for researchers; therefore, they constitute a service to the scholarly community. At the same time, the Frontiers Journal Series operates on a revolutionary invention, the tiered publishing system, initially addressing specific communities of scholars, and gradually climbing up to broader public understanding, thus serving the interests of the lay society, too.

Dedication to Quality

Each Frontiers article is a landmark of the highest quality, thanks to genuinely collaborative interactions between authors and review editors, who include some of the world's best academicians. Research must be certified by peers before entering a stream of knowledge that may eventually reach the public - and shape society; therefore, Frontiers only applies the most rigorous and unbiased reviews.
Frontiers revolutionizes research publishing by freely delivering the most outstanding research, evaluated with no bias from both the academic and social point of view. By applying the most advanced information technologies, Frontiers is catapulting scholarly publishing into a new generation.

What are Frontiers Research Topics?

Frontiers Research Topics are very popular trademarks of the Frontiers Journals Series: they are collections of at least ten articles, all centered on a particular subject. With their unique mix of varied contributions from Original Research to Review Articles, Frontiers Research Topics unify the most influential researchers, the latest key findings and historical advances in a hot research area! Find out more on how to host your own Frontiers Research Topic or contribute to one as an author by contacting the Frontiers Editorial Office: researchtopics@frontiersin.org

ZOOPLANKTON AND NEKTON: GATEKEEPERS OF THE BIOLOGICAL PUMP

Topic Editors:
Rainer Kiko, GEOMAR Helmholtz Center for Ocean Research Kiel, Germany
Morten Hvitfeldt Iversen, Alfred Wegener Institute Helmholtz Centre for Polar and Marine Research (AWI), Germany
Amy Elizabeth Maas, Bermuda Institute of Ocean Sciences, Bermuda
Helena Hauss, GEOMAR Helmholtz Center for Ocean Research Kiel, Germany
Daniele Bianchi, University of California, Los Angeles, United States

Citation: Kiko, R., Iversen, M. H., Maas, A. E., Hauss, H., Bianchi, D., eds. (2020). Zooplankton and Nekton: Gatekeepers of the Biological Pump. Lausanne: Frontiers Media SA. doi: 10.3389/978-2-88963-982-3

Table of Contents

04 ***Editorial: Zooplankton and Nekton: Gatekeepers of the Biological Pump***
Rainer Kiko, Daniele Bianchi, Christian Grenz, Helena Hauss, Morten Iversen, Sanjeev Kumar, Amy Maas and Carol Robinson

06 ***Mesozooplankton Community Composition Controls Fecal Pellet Flux and Remineralization Depth in the Southern Ocean***
Cecilia M. Liszka, Clara Manno, Gabriele Stowasser, Carol Robinson and Geraint A. Tarling

20 ***The Roles of Suspension-Feeding and Flux-Feeding Zooplankton as Gatekeepers of Particle Flux Into the Mesopelagic Ocean in the Northeast Pacific***
Michael R. Stukel, Mark D. Ohman, Thomas B. Kelly and Tristan Biard

36 ***Zooplankton and Micronekton Active Flux Across the Tropical and Subtropical Atlantic Ocean***
Santiago Hernández-León, María Pilar Olivar, María Luz Fernández de Puelles, Antonio Bode, Arturo Castellón, Cristina López-Pérez, Víctor M. Tuset and José Ignacio González-Gordillo

56 ***The Importance of Mesozooplankton Diel Vertical Migration for Sustaining a Mesopelagic Food Web***
Thomas B. Kelly, Peter C. Davison, Ralf Goericke, Michael R. Landry, Mark D. Ohman and Michael R. Stukel

74 ***Copepod Grazing Influences Diatom Aggregation and Particle Dynamics***
Jordan Toullec, Dorothée Vincent, Laura Frohn, Philippe Miner, Manon Le Goff, Jérémy Devesa and Brivaëla Moriceau

96 ***On the Estimation of Zooplankton-Mediated Active Fluxes in Oxygen Minimum Zone Regions***
Rainer Kiko and Helena Hauss

112 ***Mesozooplankton and Micronekton Active Carbon Transport in Contrasting Eddies***
Lian E. Kwong, Natasha Henschke, Evgeny A. Pakhomov, Jason D. Everett and Iain M. Suthers

129 ***Corrigendum: Mesozooplankton and Micronekton Active Carbon Transport in Contrasting Eddies***
Lian E. Kwong, Natasha Henschke, Evgeny A. Pakhomov, Jason D. Everett and Iain M. Suthers

132 ***Running the Gauntlet: Assessing the Threats to Vertical Migrators***
Bruce H. Robison, Rob E. Sherlock, Kim R. Reisenbichler and Paul R. McGill

142 ***Zooplankton-Mediated Fluxes in the Eastern Tropical North Atlantic***
Rainer Kiko, Peter Brandt, Svenja Christiansen, Jannik Faustmann, Iris Kriest, Elizandro Rodrigues, Florian Schütte and Helena Hauss

frontiers in Marine Science

EDITORIAL
published: 15 July 2020
doi: 10.3389/fmars.2020.00545

Editorial: Zooplankton and Nekton: Gatekeepers of the Biological Pump

Rainer Kiko[1]*, *Daniele Bianchi*[2], *Christian Grenz*[3], *Helena Hauss*[4], *Morten Iversen*[5,6], *Sanjeev Kumar*[7], *Amy Maas*[8] and *Carol Robinson*[9]

[1] Sorbonne Université, Laboratoire d'Océanologie de Villefranche-sur-Mer, Villefranche-sur-Mer, France, [2] Atmospheric & Oceanic Sciences, University of California, Los Angeles, Los Angeles, CA, United States, [3] Aix Marseille Université, Université Toulon, CNRS/INSU, IRD, Mediterranean Institute of Oceanography MIO UM 110, Marseille, France, [4] GEOMAR Helmholtz Centre for Ocean Research Kiel, Kiel, Germany, [5] Polar Biological Oceanography, Alfred Wegener Institut, Bremerhaven, Germany, [6] MARUM and University of Bremen, Bremen, Germany, [7] Physical Research Laboratory, Ahmedabad, India, [8] Bermuda Institute of Ocean Sciences, St. Georges, Bermuda, [9] School of Environmental Sciences, University of East Anglia, Norwich, United Kingdom

Keywords: zooplankton, nekton, biological pump, editorial, global ocean, zooplankton-particle interactions, export flux

Editorial on the Research Topic

Zooplankton and Nekton: Gatekeepers of the Biological Pump

Zooplankton and nekton organisms create and destroy particles in manifold ways. They feed on the diverse components of the plankton community and on detrital matter. They disaggregate these components, but also repackage them into fecal pellets. Zooplankton and nekton thereby contributes to the attenuation, but also to the export of vertically settling particles. Many zooplankton and nekton organisms also ascend to the surface layer of the ocean at dusk to feed during the dark hours, and return to midwater at the break of dawn. This diurnal vertical migration (DVM) shuttles organic matter from the surface ocean to deeper layers, where it is metabolized and excreted. This active flux (as opposed to the passive flux of sinking particles) can contribute substantially to the biological pump, the downward export of carbon and nutrients into the oceans interior. Due to their multiple roles in oceanic particle dynamics, zooplankton and nekton organisms can actually be considered the gatekeepers of the biological pump.

Several articles in this Research Topic deal with the contribution of zooplankton and nekton-mediated active flux to the total export of organic matter. Using biomass and enzyme transport system (ETS) assessments of respiratory flux for both mesozooplankton and micronekton communities, Hernández-León et al. estimated the total active transport of carbon (respiration, excretion, mortality, and egestion) along a transect in the Atlantic from the Canary Islands to Brazil. They found that active flux by these communities ranged from 25 to 80% of the total particulate organic carbon export at 150 m depth and that the importance of active flux increased with increasing surface productivity. Kwong et al. compared biomass, diel vertical migration, and active flux of mesozooplankton and micronekton across a range of mesoscale eddy structures along the east-coast of Australia during winter and spring. They found that although all eddy regimes had similar integrated biomass of mesozooplakton and micronekton, the organisms in the individual eddies had different migratory behavior, which resulted in contrasting importance of active flux. Kiko et al. assessed the impact of mesozooplankton DVM on elemental cycling at three stations in the Eastern Tropical North Atlantic. They found that approximately 31 to 41% of the total nitrogen loss from the upper 200 m of the water column was attributable to DVM mediated fluxes. They also suggest that gut flux—the flux created by migrators when they evacuate their gut at DVM-depth—and migrator mortality at DVM-depth contribute to an Intermediate Particle Maximum. In their study conducted in the Peruvian upwelling system (which features a severe midwater oxygen minimum zone), Kiko and Hauss concluded that the metabolic suppression

OPEN ACCESS

Edited by:
Hongbin Liu,
Hong Kong University of Science and Technology, Hong Kong

Reviewed by:
Hiroaki Saito,
The University of Tokyo, Japan

****Correspondence:***
Rainer Kiko
rainer.kiko@obs-vlfr.fr

Specialty section:
This article was submitted to Marine Biogeochemistry, a section of the journal Frontiers in Marine Science

Received: *20 May 2020*
Accepted: *15 June 2020*
Published: *15 July 2020*

Citation:
Kiko R, Bianchi D, Grenz C, Hauss H, Iversen M, Kumar S, Maas A and Robinson C (2020) Editorial: Zooplankton and Nekton: Gatekeepers of the Biological Pump. Front. Mar. Sci. 7:545. doi: 10.3389/fmars.2020.00545

of zooplankton metabolic activity at low oxygen needs to be considered when calculating active fluxes. This metabolic suppression results in a substantial reduction of both respiration and ammonium excretion within the OMZ core. Kelly et al. employed a linear inverse ecosystem model to explore carbon fluxes between the epipelagic and the mesopelagic zones in the California Current Ecosystem. The model was constrained by measurements from quasi-Lagrangian experiments spanning a wide range of conditions from upwelling to oligotrophic regions. They consistently found that active transport by mesozooplankton was important in supporting the mesopelagic carbon demand, and also highlighted the central importance of mesozooplankton in marine food webs.

During an austral summer cruise in the Southern Ocean, Liszka et al. studied the peculiarities of fecal pellet transport in the upper mesopelagic layer. They confirmed that zooplankton contributed to the carbon supply to deeper waters, but also ascertained their role in the breakdown and reworking of the fecal pellets as they sink. Stukel et al. used MOCNESS and UVP5 data combined with allometric equations to characterize the impact of different suspension and flux feeders on particle flux attenuation (assessed using drifting sediment traps and thorium isotope measurements) in the California upwelling ecosystem. They found that suspension feeders have a large impact on small, slow sinking particles, whereas the two investigated flux feeders (the pteropod *Limacina helicina* and phaeodarian Aulophaeridae) attenuated the flux of large, presumably fast settling particles, by about 10 to 20 % within the upper 100 m of the water column. Toullec et al. found that micro-turbulence created by the swimming activity of small copepods encouraged aggregate formation of suspended diatoms, while the stronger turbulence created by large, cruise feeding copepods prevented aggregation and caused large aggregates to fragment. This work may cast new light on the observations of phytoplankton aggregates being an important vector for carbon export at low latitudes, whereas zooplankton fecal pellets seem to be an important contributor to carbon flux at high latitudes.

Finally, Robison et al. used MBARI's extensive *in situ* ROV observations of organismal behaviors and abundances to calculate the threat potential to the migratory community from encounters with mid-water predators. Although these estimates do not yet provide a quantitative prediction of the mortality experienced by migrators, they help us to better comprehend this very poorly-sampled, but likely substantial, component of active flux.

A general theme in all contributions in this Research Topic is the need for size- and/or weight-specific parameterizations to estimate biomass, gut flux, mortality, predation potential, excretion, respiration or flux-interception potential. Efforts should be strengthened to collect, synthesize and compare these parameters, but further efforts are also needed to harmonize and share zooplankton and nekton distribution data across studies. Such efforts will enable modeling studies and model assessments, which could yield a more comprehensive understanding of the role of zooplankton and nekton as essential components of the biological pump.

AUTHOR CONTRIBUTIONS

All authors listed have made a substantial, direct and intellectual contribution to the work, and approved it for publication.

FUNDING

RK was supported by a Make Our Planet Great Again grant of the French National Research Agency within the Programme d'Investissements d'Avenir: reference ANR-19-MPGA-0012. MI was supported by the HGF Young Investigator Group SeaPump Seasonal and Regional Food Web Interactions with the Biological Pump: VH-NG-1000. HH received support from iAtlantic (EU H2020 grant agreement no. 818123) and from project CUSCO of the German Federal Ministry of Education and Research (BMBF). CR was supported by funds from The Leverhulme Trust (Grant RPG-2017-089) and the Natural Environment Research Council (NERC) of the United Kingdom (Grant NE/R000956/1). DB acknowledges support by the U.S. National Science Foundation under Grant 1635632. Funding for AM was provided by the NASA EXPORTS project (grant 80NSSC17K0654).

ACKNOWLEDGMENTS

We would like to thank the Frontiers team for their support and the following reviewers for their contribution to this Research Topic: Bingzhang Chen, John P. Dunne, Santiago Hernández-León, Kusum Komal Karati, Qian Li, Daria Martynova, Natalia Osma, Suzanne J. Painting, Jyothibabu Retnamma, HS, Rudi Schuech, Michael R. Stukel, Jun Sun, Geraint A. Tarling, and Xiaodong Wang.

Conflict of Interest: The authors declare that the research was conducted in the absence of any commercial or financial relationships that could be construed as a potential conflict of interest.

frontiers in Marine Science

ORIGINAL RESEARCH
published: 10 May 2019
doi: 10.3389/fmars.2019.00230

Mesozooplankton Community Composition Controls Fecal Pellet Flux and Remineralization Depth in the Southern Ocean

Cecilia M. Liszka[1,2], Clara Manno[1], Gabriele Stowasser[1], Carol Robinson[2] and Geraint A. Tarling[1]**

[1] British Antarctic Survey, Cambridge, United Kingdom, [2] School of Environmental Sciences, University of East Anglia, Norwich, United Kingdom

OPEN ACCESS

Edited by:
Christian Grenz,
UMR 7294 Institut Méditerranéen d'Océanographie (MIO), France

Reviewed by:
Daria Martynova,
Zoological Institute (RAS), Russia
Kusum Komal Karati,
Centre for Marine Living Resources and Ecology (CMLRE), India

***Correspondence:**
Cecilia M. Liszka
c.m.liszka.02@cantab.net
Geraint A. Tarling
gant@bas.ac.uk

Specialty section:
This article was submitted to Marine Ecosystem Ecology, a section of the journal Frontiers in Marine Science

Received: 11 December 2018
Accepted: 12 April 2019
Published: 10 May 2019

Citation:
Liszka CM, Manno C, Stowasser G, Robinson C and Tarling GA (2019) Mesozooplankton Community Composition Controls Fecal Pellet Flux and Remineralization Depth in the Southern Ocean. Front. Mar. Sci. 6:230. doi: 10.3389/fmars.2019.00230

Zooplankton fecal pellets (FPs) are important conduits of carbon from the surface to the deep ocean, as shown by their presence in deep-sea sediment traps. Zooplankton themselves are thought to play an important role in the breakdown and reworking of FPs as they sink, whilst processes such as diel vertical migration (DVM) may enhance the supply of carbon to the mesopelagic. However, comparatively little is known about the processes or variability of FP sinking/transport within the upper mesopelagic and how this relates to deeper ocean export. Profiles of FP type and size, and the contribution made by FPs to mesopelagic carbon flux to a depth of 400 m, were considered. Three contrasting locations in the Scotia Sea were compared, which together reflect the variability in physical regime and productivity encountered across the Southern Ocean. Comparing observed FPs with predictions from the mesozooplankton community, we show that, even at shallow depths, the smallest fraction of FP is under-represented, suggesting rapid remineralization, incorporation into larger aggregates or reworking into larger FPs, and that the flux is dominated by FPs from larger zooplankton. In contrast to models where POC attenuation rates are set to increase with temperature, we find that FP carbon flux attenuates rapidly in low productivity, colder regions dominated by krill, while remineralization is deeper in warmer areas where productivity is high and copepods dominate. This emphasizes the strong modulation of the zooplankton community on the supply and transfer of FP carbon between the epi- and mesopelagic. Evidence was found to suggest that DVM enhances FP flux across the upper mesopelagic, producing a pulse of fresh, dense material that may support secondary production and heterotrophic respiration in the mesopelagic. This illustrates that variability in flux at short (daily) as well as longer (seasonal) timescales may have important implications for the supply of FP carbon to deeper waters.

Keywords: copepods, euphausiids, Scotia Sea, biological carbon pump, sea-ice, export

INTRODUCTION

The Southern Ocean (SO) is an important region for the global uptake and sequestration of CO_2: whilst accounting for only 10% of global ocean area, it is responsible for >20% CO_2 uptake (Takahashi et al., 2002). The biological carbon pump (BCP) delivers photosynthetically derived organic material from the euphotic zone to the deeper ocean (Legendre et al., 2015), largely via the sinking of phytoplankton cells and detrital aggregates including molts, feeding webs, and carcasses. It therefore exerts an important control on the uptake of atmospheric CO_2 by the oceans. Whilst much of the SO is iron-limited and termed high nutrient-low chlorophyll (HNLC) (Martin, 1990; de Baar et al., 1995), there are also regions of exceptionally high productivity that may be of increased importance in driving the SO BCP. This includes areas of terrestrial iron input around archipelagos, where phytoplankton blooms can last up to 4 months (Whitehouse et al., 2008), and the seasonal ice edge where substantial seasonal diatom blooms are stimulated (Korb et al., 2005).

The BCP is enhanced by the passively sinking fecal pellets (FPs) of zooplankton and micronekton feeding in the epi- and upper mesopelagic, repackaging and converting small, slow-sinking phytoplankton cells into larger, faster-sinking agglomerates (Urrère and Knauer, 1981; Turner, 2015). Factors affecting FP export efficiency include temperature (Bendtsen et al., 2015; Marsay et al., 2015), season (Urban et al., 1993; Frangoulis et al., 2001), food type or availability, and FP composition or ballast (Francois et al., 2002; Ploug et al., 2008; Atkinson et al., 2012; Dagg et al., 2014), microbial colonization (Turner, 1979; Sampei et al., 2009; Belcher et al., 2016), and mechanical degradation (e.g., Sampei et al., 2009). Zooplankton are also important mediators of FP flux, transforming FPs via processes of ingestion (coprophagy), fragmentation (coprorhexy), and loosening (coprochaly) (Lampitt et al., 1990; Noji et al., 1991; Iversen and Poulsen, 2007), contributing to the export of carbon to the deep ocean and supporting the metabolism of mesopelagic biota (Buesseler et al., 2007; Steinberg et al., 2008; Robinson et al., 2010). FP export may be further augmented by the diel vertical migration (DVM) of zooplankton in response to feeding and survival cues (Angel, 1986; Emerson and Roff, 1987; Longhurst and Harrison, 1989). Deep FP production may therefore bypass the region of greatest zooplankton abundance and most rapid remineralization, expediting the transfer of organic carbon, nitrogen and phosphorous to meso- and bathypelagic depths (Urrère and Knauer, 1981).

Estimates of the contribution of FP carbon to export flux are subject to substantial temporal and spatial variability, ranging from <1% to ∼100% (González, 1992; González et al., 2000; Turner, 2002, 2015; Steinberg and Landry, 2017) and discrepancies between estimates of export to the 'twilight' zone (Buesseler et al., 2007; Burd et al., 2010) can be especially great at high latitudes (Maiti et al., 2013). Recent studies in the SO challenge assumptions of relationships between primary productivity (PP) or temperature to export efficiency (Maiti et al., 2013; Cavan et al., 2015; Marsay et al., 2015) and highlight the role of zooplankton–microbial interactions (Steinberg et al., 2008; Giering et al., 2014) or zooplankton trophic dynamics (Le Quéré et al., 2016) in resolving such discrepancies. Material collected in SO sediment traps demonstrates the importance of zooplankton mediated FP flux in this region, with well-preserved FPs being found at greater depths than expected from passive sinking alone (Wilson et al., 2013; Manno et al., 2015). Studies of FP morphology have also provided insight into the origin and repackaging of FPs throughout the water column (Turner, 2002; Wilson et al., 2008; Belcher et al., 2017a). Despite this, our knowledge of FP production and export processes in the SO remains hampered by a paucity of measurements at intermediate depths, particularly in the crucial region between the epi- and upper mesopelagic.

Evidence suggests that, where euphausiids are abundant and consume a diatom-rich diet, they can exert a strong control on export flux (Dagg et al., 2014). *Euphausia superba* is a central component of the SO ecosystem, linking PP and higher predators (Murphy et al., 2007) and their FPs have been found in deep sediment traps (Manno et al., 2015). However, Manno et al. (2015) also showed that variability in mesozooplankton community structure may be responsible for differences in deep FP export in the Scotia Sea. To better understand the role of zooplankton in the export of FPs to depth, we conducted a study at three contrasting locations within the Scotia Sea. This includes a naturally iron fertilized region with elevated PP and zooplankton abundances; a region of lower PP more characteristic of the wider SO; and an ice influenced region where seasonal diatom blooms occur and euphausiids can be particularly abundant (Lancraft et al., 1989; Atkinson et al., 2008).

We investigated FP morphology, vertical distribution and flux at six depths between the epi- and upper mesopelagic, to provide higher resolution insight into the supply and attenuation of zooplankton FPs on both sides of the mixed layer, beneath which exported material may be more likely to sink to depth. Our aim was to (i) establish the role of the zooplankton community in mediating FP flux to depth by comparing observed FP profiles with predictions based on the mesozooplankton community; and (ii) quantify the flux of FP carbon across the upper mesopelagic, from 5 to 400 m in different regimes within the SO. This will lead to an improved understanding of the factors affecting flux through the mesopelagic in three important and contrasting regimes typical of the SO.

MATERIALS AND METHODS

Study Area and Sampling

This study was conducted at three time-series stations in the Scotia Sea: P3, P2, and ICE, which were sampled at six depths over the top 400 m (**Figure 1**). The stations encompass different oceanic regimes which is reflected in zooplankton community compositions. P3 is situated downstream of South Georgia where it benefits from natural iron fertilization and is characterized by high levels of biological productivity and a diverse zooplankton community. P2 is situated upstream of South Georgia and receives low natural iron inputs. Its zooplankton community is similar in composition to P3 but often lower in abundance.

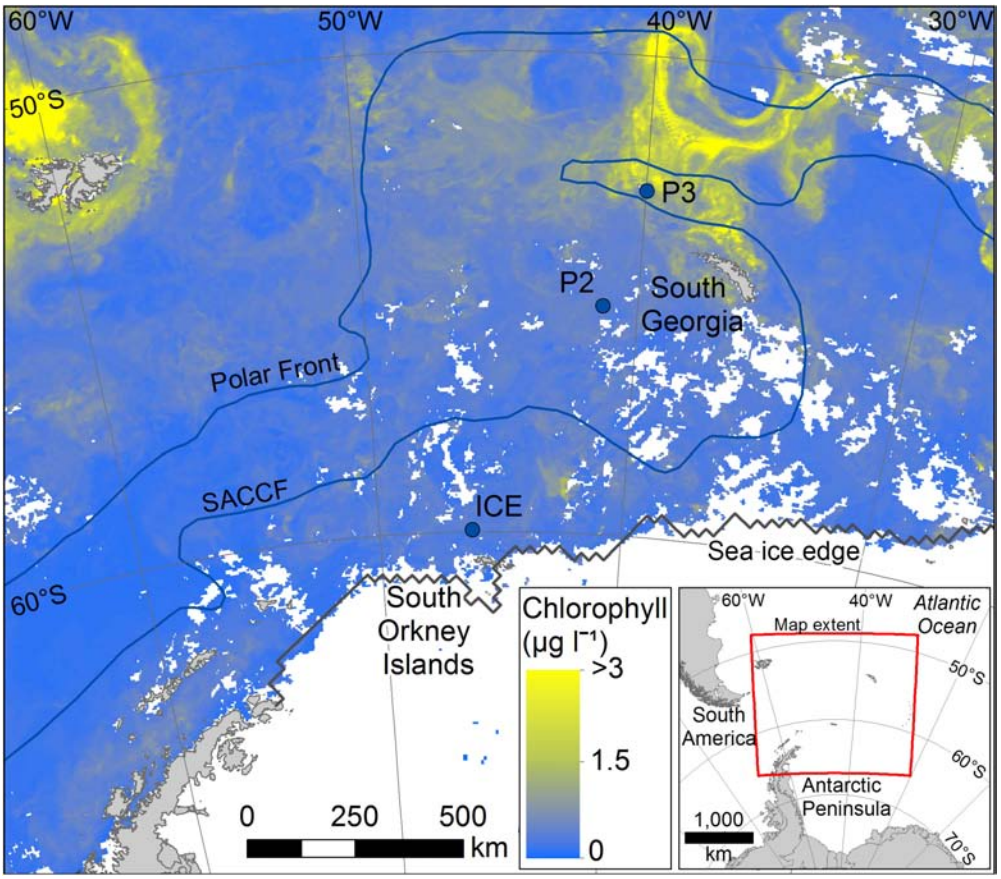

FIGURE 1 | Mean chlorophyll data for the period covering sampling (stations marked with filled blue circles). Data for the period 25/11/14 to 26/12/14 were taken from NASA MODIS website: https://oceandata.sci.gsfc.nasa.gov/MODIS-Aqua/Mapped/Rolling_32_Day/4km/chlor_a/2014/.

ICE is situated close to the ice edge where seasonal ice advance and retreat is an important feature and where euphausiids often dominate the zooplankton.

All samples were collected on board the Southern Ocean research cruise JR304 (Watkins et al., 2015) on the RRS James Clark Ross. The expedition took place in the austral spring/summer season, from 15 November 2014 to 17 December 2014.

Environmental and Hydrographic Data

An SBE 9Plus CTD was set up with instrumentation including a dual SBE 3Plus temperature sensor, SBE4C conductivity sensor and a fluorometer. Fluorescence was converted from volts into chlorophyll a (µg l^{-1}) using the manufacturer's calibration. Chlorophyll a concentrations were used as a proxy for phytoplankton biomass at each station.

Aqua MODIS 4 km, 32-day mean chlorophyll data were also obtained from NASA's Ocean Color Data website[1] for the study area to provide additional environmental context and indicate mean phytoplankton biomass around the stations before, after, and during the period of sampling.

[1]https://oceandata.sci.gsfc.nasa.gov/MODIS-Aqua/Mapped/Rolling_32_Day/4km/chlor_a/2014/

Sample Collection

Mesozooplankton samples were collected in order to predict the abundance and size spectra of FPs produced from within the upper 200 m for comparison with direct observations of FPs from bottle samples. Motion-compensated Bongo nets with a 200 µm mesh net (57 cm mouth diameter, 2.8 m long) were deployed at all time-series stations throughout the cruise (see **Table 1**). Nets were deployed vertically to 200 m depth during morning and evening, as close as possible to 12 h apart, in order to sample populations throughout the diurnal cycle. Samples were passed through a stacked sieve onto a 200 µm mesh and immediately frozen and stored at −80°C. Once back at the laboratory they were defrosted and immediately fixed in 100% ethanol in preparation for analysis.

An SBE32 carousel water sampler holding 24 12 L Niskin bottles and attached to a SBE 11Plus deck unit was deployed for collection of water for FP and phytoplankton analysis at three stations, ICE, P2, and P3 (see **Table 1**). Six bottles were fired at each station, one at each of the following depths: 5 m, 20 m, 40 m, 100 m, 200 m, and 400 m. These depths were selected to give good coverage throughout the mixed layer and the undersampled portion of the upper mesopelagic between the base of the mixed layer and deep sediment traps.

TABLE 1 | Details of sampling undertaken in the Scotia Sea, Southern Ocean during cruise JR304.

Station	Sample type	Date	Time (GMT)	Latitude	Longitude
ICE	Bongo (N)	25/11/2014	21:18	59.9623 S	46.1597 W
ICE	Bongo (D)	26/11/2014	07:20	59.9624 S	46.1601 W
ICE	CTD	26/11/2014	17:29	59.9629 S	46.1602 W
P2	Bongo (N)	28/11/2014	19:44	55.2484 S	41.2639 W
P2	Bongo (D)	29/11/2014	09:05	55.2478 S	41.2648 W
P2	CTD	29/11/2014	03:41	55.2476 S	41.2661 W
P3	Bongo (D)	13/12/2014	06:26	52.8121 S	39.9723 W
P3	Bongo (N)	13/12/2014	21:17	52.8118 S	39.9726 W
P3	CTD	13/12/2014	22:56	52.8118 S	39.9726 W

In sample type, Bongo refers to Bongo net deployments made over 0–200 m with 200 μm mesh and analyzed for mesozooplankton abundance and size spectra; D and N represent whether the sample was the day or night sample, respectively; CTD refers to 12 L water bottle samples obtained through CTD deployments and analyzed for fecal pellets.

Once on deck, water was gently siphoned out of the Niskin bottles via a piece of silicone tubing, which had been pre-rinsed three times with 0.22 μm filtered seawater (FSW), into pre-rinsed 20 L carboys. To ensure collection of all possible fecal material from the funneled base of the Niskin bottles, the base of each bottle was opened, rinsed with FSW, and the water collected in separate sterile 250 mL Nalgene bottles.

The contents of the carboys and Nalgene bottles were then gently filtered through a 53 μm mesh and bottles rinsed through with FSW. The contents of the mesh were backwashed into a 250 mL sterile Nalgene bottle using a 5% borax-buffered formalin-seawater solution.

Formalin-preserved samples were stored in the shipboard chemical cupboard in the dark until arrival back at the laboratory, where they were stored in the dark at ambient temperature and analyzed within 21 months.

Sample Analysis

Mesozooplankton

Mesozooplankton samples were split using a Folsom Plankton Splitter, according to the density of the sample, and final splits were analyzed using two methods. The first half of the final fraction split was transferred to a beaker and topped up to 500 mL. Three 25 mL aliquots were extracted and analyzed for abundance and size spectra using ZooScan (CNRS and Hydroptic) and Ecotaxa (Picheral et al., 2017), a semi-automated software package for digital zooplankton analysis. The second half of the final split was preserved in 35 mL 95% ethanol and analyzed by the Plankton Sorting and Identification Center Morski Instytut Rybacki, Poland. Samples were classified to the lowest possible taxonomic resolution for additional semi-quantitative and contextual information about the taxonomic composition of samples.

Fecal Pellets

The contents of Nalgene bottles (generally between 100 mL and 200 mL) were filtered onto a 53 μm mesh, gently rinsed and backwashed into petri dishes. Petri dishes were examined under a light microscope (Olympus SZX16 with SDF PLAPO 0.5XPF and 1.6XPF objectives) for whole or fragmented FPs and other organic matter (e.g., diatoms, protozoa, and detritus). FPs were photographed using a Canon EOS 70D camera. Observations related to type and abundance of sample content, lens and magnification of photographs were recorded.

FPs were categorized into morphological type: cylindrical, spherical, ovoid or ellipsoidal. Images were visually examined and length (L) and width (W) measured with the imaging software, ImageJ (Rasband, 1997/2016). Where the item was an irregular shape, e.g., wider at the top than the bottom, measurements of each part were made and an average taken. FP volume was calculated using the geometric formulae for sphere, cylinder and ellipsoid/ovoid (González et al., 2000; Manno et al., 2015). Since spherical items included some that were a slightly irregular shape, the radius was taken as half of the average of both the L and W measurements. FP carbon content was calculated using mean conversion factors specific to the Scotia Sea for spring-early autumn calculated by Manno et al. (2015): 0.052 mg C mm^{-3} for ovoid/ellipsoidal; 0.035 mg C mm^{-3} for spherical; and 0.030 mg C mm^{-3} for cylindrical FPs.

A number of FPs, including many spherical items that were too small to identify clearly with the magnification of the light microscope alone, were examined further with Scanning Electron Microscopy (SEM). Samples were filtered onto 53 μm mesh, rinsed to remove formalin and backwashed into a petri dish. They were then pipetted gently onto PELCO double coated carbon conductive tabs, excess water was pipetted off and the stub was allowed to air dry. Samples were analyzed with a Hitachi TM3000 SEM and associated software.

Estimates of FP numbers are likely to represent a minimum per sample due to unavoidable losses incurred during transfer stages, despite care taken to minimize this.

Phytoplankton Analysis

Samples were visually assessed for the number of phytoplankton species and their comparative abundances. The most common species were identified and their abundances across stations and depth were assessed semi-quantitatively.

Data Analysis and Statistics

Mesozooplankton

Following Ecotaxa image processing and verification, data were analyzed in RStudio (V.1.0.136) (R Core Team, 2016), converting object length in pixels [estimated with ZooScan as the object's major axis (Gorsky et al., 2010)] to prosome length (PL, mm) and using this value to classify zooplankton into 0.1 mm size spectra bins, ranging from 0–0.1 mm to 5.9–6.0 mm.

Counts per sample were calculated by multiplying abundance (as quantified from ZooScan samples) up to the 500 mL subsample from which the aliquots originated and then by the relevant split. Counts per sample were converted to individuals m^{-3} by dividing by the volume filtered (calculated from the net mouth area multiplied by the depth of haul). These values were multiplied by 200 (the depth of haul in m) to determine individuals m^{-2}.

An Anderson–Darling *k* sample test was performed on pairs of day/night samples to examine whether the distributions of prosome size spectra differed statistically. Day/night abundances from each station were averaged in order to account for any changes in the taxonomic composition of the mixed layer resulting from any normal or reverse patterns of DVM in the mesozooplankton community.

The predicted FP size (volume, *FPV*) from these animals was calculated as a function of prosome length (*PL*) following Eq. (1):

$$\log_{10} FPV = \theta \log_{10}(PL) + n \quad (1)$$

where θ of 2.58 and *n* of 5.4 have been taken from known relationships derived and adapted from Mauchline (1998) and Stamieszkin et al. (2015).

Predicted FP size was compared with actual FP size by comparing the frequency distributions of each using an Anderson–Darling *k* sample test.

Following taxonomic analysis, the percent contributions of individual taxa to the whole sample was calculated.

Fecal Pellets

Fecal pellet abundance m^{-3} was calculated by dividing abundance per sample by the volume of the Niskin sampling bottle (12 L) and multiplying by 1,000. The same calculation was used to calculate the volume and carbon of FPs m^{-3}.

To investigate a difference in FP volume over depth, ANOVA tests were carried out for each station (Shapiro–Wilks and Kruskal–Wallis). Volumes of FPs from 5 m, 20 m, 40 m, and 100 m were also combined into a 0–100 m depth bin and 200 m and 400 m were combined into a 200–400 m depth bin to investigate whether FP volume changed significantly from the upper to lower mesopelagic and the same ANOVA tests were applied.

Fecal pellet flux was calculated following the methodology set out in Dagg et al. (2014) according to Eq. (2):

$$FP\,flux(g\,C\,m^{-2}\,d^{-1}) = \frac{\sum (w_s \times C)}{V} \quad (2)$$

where w_s is the FP sinking velocity, *C* is FP carbon content (g C), and *V* is the sample volume (m^3).

Fecal pellet sinking velocity (w_s, m d^{-1}) was calculated using an empirically derived relationship adapted from Komar et al. (1981), Eq. (3), which has been shown to represent the settling velocities of mixed copepod and euphausiid FPs of different dimensions from a number of datasets.

$$w_s = \left(1.21 \times 10^3\right) \times L^2 \left(\frac{L}{W}\right)^{-1.664} \quad (3)$$

where *L* is FP length (cm) and *W* is FP diameter (cm).

Statistics were carried out in SigmaPlot V.13.0.0.83 (Systat Software Inc.) and RStudio (V.1.0.136) (R Core Team, 2016).

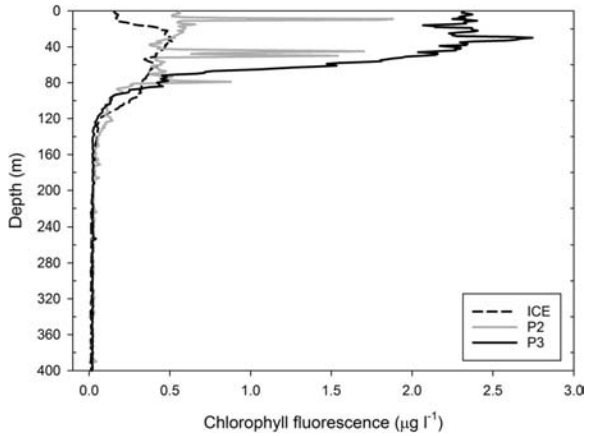

FIGURE 2 | Profiles of chlorophyll a concentrations (μg l^{-1}) based on fluorescence measurements at ICE, P2, and P3. Measurements were taken with CTD casts from which water samples were obtained.

RESULTS

Environmental and Hydrographical Context

Chlorophyll a fluorescence profiles obtained from CTD instrumentation (**Figure 2**) are used as a proxy for the phytoplankton biomass. All three stations exhibited subsurface chlorophyll a maxima and high levels of chlorophyll a were found as deep as 100 m. The highest value was observed at P3 with a chlorophyll a maximum of 2.7 μg l^{-1} at ∼30 m, although it was consistently >2 μg l^{-1} between 0 and 50 m, remaining at >0.5 μg l^{-1} as deep as 80 m and only reaching a minimum below 120 m. The lowest value was observed at ICE where peak chlorophyll a at ∼35 m was 0.5 μg l^{-1}, followed by a secondary peak of ∼0.4 μg l^{-1} at ∼70 m, with values remaining between 0.1 and 0.4 μg l^{-1} as deep as 120 m. At P2, chlorophyll a in the top 100 m was relatively constant at ∼0.5 μg l^{-1} from 0 to 65 m with sharp peaks >1.5 μg l^{-1} at ∼10 and 45 m and 0.9 μg l^{-1} at ∼80 m, possibly indicating some surface-level disruption to the water column from wind or storm turbulence.

Mesozooplankton Abundance and Distribution

Table 2 shows the percent contribution of the most abundant taxa in the mesozooplankton community. Copepods comprised the majority of the mesozooplankton at all stations (80% at P2 to 93% at ICE). At P2 and P3, the mesozooplankton community was dominated by cyclopoids, especially *Oithona* spp., which comprised 40% of the total, and copepod nauplii (11% and 16%, respectively), whilst at ICE, *Oithona* spp. (61%) and *Microcalanus* adults (14%) dominated.

Due to the ability of larger euphausiids to avoid the Bongo net, adult euphausiids were almost absent at all stations but younger stages (calytopes, furcilia, and juveniles) comprised 4% at ICE, 1% at P2 and <1% at P3. Another important group at P2

TABLE 2 | Detailed taxonomic composition of mesozooplankton samples from 0 to 200 m at ICE, P2, and P3 grouped to species/stage (copepods), genus (euphausiids), and major group for all other taxa.

	ICE		P2		P3	
Copepods	m^{-3}	%	m^{-3}	%	m^{-3}	%
C. propinquus ≥ CV	5	0.2%	22	1.1%	0	0.0%
Metridia adult	49	2.0%	3	0.1%	3	0.1%
C. acutus 1–4	7	0.3%	42	2.0%	27	0.6%
Metridia 4–5	45	1.8%	3	0.2%	61	1.3%
Ctenocalanus adult	15	0.6%	56	2.7%	11	0.2%
Clausocalanus 1–5	39	1.6%	85	4.1%	109	2.3%
Metridia 1–3	34	1.4%	25	1.2%	347	7.3%
Ctenocalanus 1–5	12	0.5%	112	5.4%	14	0.3%
Microcalanus adult	330	13.6%	4	0.2%	19	0.4%
Oncaea spp.	26	1.1%	30	1.5%	75	1.6%
Oithona spp.	1483	61.1%	836	40.3%	1920	40.2%
Microcalanus 1–5	61	2.5%	1	0.1%	3	0.1%
Copepod nauplius	8	0.3%	234	11.3%	742	15.5%
Other calanoids 1–5	5	0.2%	97	4.7%	465	9.7%
Other unidentified calanoids	53	2.2%	69	3.3%	5	0.1%
Euphausiids						
Euphausiid calyptopis	102	4.2%	23	1.1%	9	0.2%
Other						
Appendicularian	5	0.2%	52	2.5%	52	1.1%
Chaetognatha	38	1.6%	4	0.2%	5	0.1%
Foraminifera	3	0.1%	283	13.6%	650	13.6%

Only taxa contributing ≥1% to the total are included. 'm^{-3}' is the concentration of individuals per unit volume, '%' is the % contribution of each respective taxa to total sample abundance.

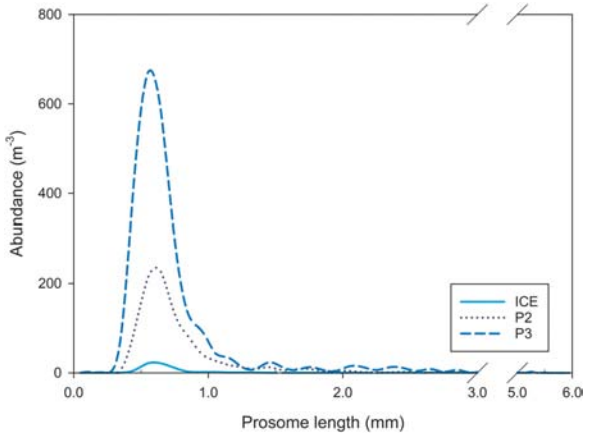

FIGURE 3 | Mesozooplankton abundance and size spectra based on prosome length (PL) at ICE, P2, and P3.

and P3 was the Foraminifera, comprising 14% at both stations, but <1% at ICE.

An Anderson–Darling *k* sample test found no significant difference between the day and night nets ($p > 0.05$). The two nets were therefore combined into an average for each station. Abundance at P2 (>910 m^{-3}) was over 12 times greater than at the ICE station (<75 m^{-3}) and P3 abundances (>2,500 inds m^{-3}) were almost three times greater than at P2 (individual station plots are in **Supplemetary Figure S1**).

Mesozooplankton size range (PL, mm; **Figure 3**) did not vary substantially between stations (median PL 0.35–5.15 mm at ICE, 0.35–5.05 at P2, and 0.35–5.25 mm at P3) with the range between modes being just 0.04 mm (modal peak abundance, x0(P3) = 0.60 mm, x0(ICE) = 0.62 mm, and x0(P2) = 0.64 mm).

Fecal Pellet Morphology and Size

Examples of the different morphological types identified as seen under the light microscope and SEM microscope are shown in **Figures 4** and **5**, respectively.

The contribution of FPs of different morphological type to total FP number and volume varied across depth and between stations (**Figure 6**). At ICE, cylindrical FPs dominated the flux in both abundance and volume over all depths, contributing most to the flux at 20 m (89% of total volume) and remaining the dominant contributor until 400 m. Ellipsoidal and ovoid FPs were also important, together contributing over 50% at 5 m and ≥40% at 40 m and 400 m but demonstrating no clear pattern. Spherical FPs were most prominent at 40 m in both abundance and volume although they only contributed 10% of flux, attenuating rapidly below 40 m.

At P2, ovoid and spherical FPs strongly dominated in abundance and volume at all depths (≥73% in the top 200 m, 65% at 400 m), with only small contributions from cylindrical or ellipsoidal FPs. Despite this, the contribution of cylindrical FPs to FP volume generally increased with depth, from 3% at 5 m to 27% at 400 m, although there was no apparent pattern to ellipsoidal FPs.

At P3, the contribution of cylindrical FPs dominated in both number and volume over the top 200 m, although the overall mix was much more heterogeneous. Both ovoid and ellipsoidal FPs were fairly significant contributors, on average contributing 27% to total volume over all depths. Spherical FPs tended to increase in importance with depth however and, by 400 m, had become the greatest contributor to total volume (47%).

Fecal pellet abundance (m^{-3}) (**Figure 6**, left panel) throughout the upper water column (0–100 m) differed between stations, although at all stations there was some attenuation between 100 and 200 m followed by an increase at 400 m. FP volume (mm^3; **Figure 6**, right panel) increased at ICE to a 40 m maximum, decreasing slightly at 100 m and substantially thereafter; a bimodal peak in volume was exhibited at 20 m and 100 m at P2; whilst at P3, FP volume increased substantially to a 100 m peak before attenuating.

The mean size of FPs (measured in volume, mm^3) at each depth across stations is shown in **Figure 7**. At ICE, FP size was greatest at 100 m (0.0063 mm^3) although a similar size peak occurred at 20 m (0.0062 mm^3). This was comprised mainly of FPs of a cylindrical morphology. At P2, mean size was greatest at 20 m (0.0074 mm^3), comprised largely of ovoid and spherical FPs, with a secondary peak at 100 m before decreasing to a 400 m minimum. At P3, FP size peaked at 40 m (0.0043 mm^3) before decreasing slightly to 200 m and more substantially at 400 m.

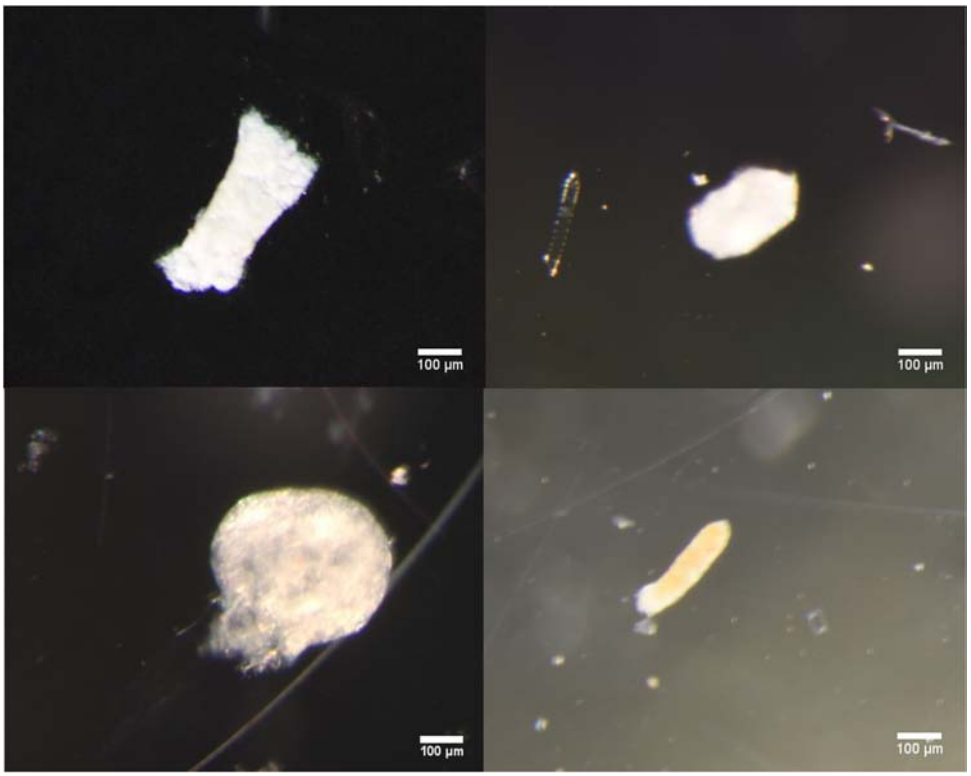

FIGURE 4 | Clockwise from top left: Light microscope images of broken cylindrical, intact ovoid, partially broken ellipsoidal, and spherical fecal pellets typical of those found in samples.

The size spectra (volume, mm^3) of FPs encountered at each station ranged from <0.0001–0.045 (ICE), <0.0001–0.043 (P2), and <0.0001–0.018 (P3). No significant difference (Shapiro–Wilk's and Mann–Whitney *U*-statistic) was found in FP volume between those found in the 0–100 m depth range and those from 200 to 400 m. Predicted FP size spectra ranged from <0.0001–0.016 (ICE), <0.0001–0.015 (P2), and <0.0001–0.017 (P3). At all three stations, the majority (>80%) of predicted FPs occurred in the 0.0002–0.01 mm^3 size range.

Distributions of predicted FP size spectra, based on the mesozooplankton community in the top 200 m, and actual FP size spectra of FPs encountered in the top 200 m at each station, are shown in **Figure 8**. Anderson–Darling *k* sample tests revealed significant differences ($p < 0.0001$) between the size spectra of FPs predicted from zooplankton community size structure and those actually observed (based on volume), both between 0 and 200 m and 0 and 400 m depth (total FP sampled depth). In particular, many more FPs were predicted to occur in the smaller size fraction but most FPs were observed at the larger end of the size spectrum.

Fecal Pellet Sinking Rates and Carbon Flux

The mean sinking velocities of FPs at each depth, as calculated from the relationship derived by Komar et al. (1981), are presented in **Figure 9**. Sinking rates were generally highest at P2 and lowest at P3. At ICE there was an increase in mean sinking speed to a maximum of 270 m d^{-1} at 100 m, followed by a decrease to 82 m d^{-1} at 400 m. At P2, there was a strong decrease in sinking velocity with depth from 437 m d^{-1} maximum at 20 m to 192 m d^{-1} at 400 m. At P3, there was a slight increase in sinking rate to 218 m d^{-1} maximum at 40 m followed by a steady decrease to 115 m d^{-1} at 400 m.

This was reflected in the flux of carbon over depth (mg C m^{-2} d^{-1}) as calculated from FP sinking rates, shown in **Figure 10**. Overall, P2 exhibited the greatest attenuation and P3 the least, although by 400 m, the station with lowest flux was ICE (9 mg C m^{-2} d^{-1}) while P2 exhibited the greatest 400 m flux despite strong attenuation (67 mg C m^{-2} d^{-1}). Stations differed in the depth of peak flux: at ICE, flux peaked at 40 m before attenuating strongly; at P2 the peak occurred at 20 m followed by rapid attenuation; whilst at P3 flux gradually increased to 100 m and then decreased to 400 m.

Phytoplankton Composition

A semi-quantitative analysis revealed some differences in phytoplankton between stations, although, at all stations, the phytoplankton was dominated by diatoms. Phytoplankton was sparsest at ICE, with only *Corethron* spp. observed in relatively low abundances. P2 exhibited a more diverse phytoplankton community, with moderate abundances of *Fragilariopsis* spp. and low abundances of *Thalassiothrix* spp. and *Thalassiosira* spp.

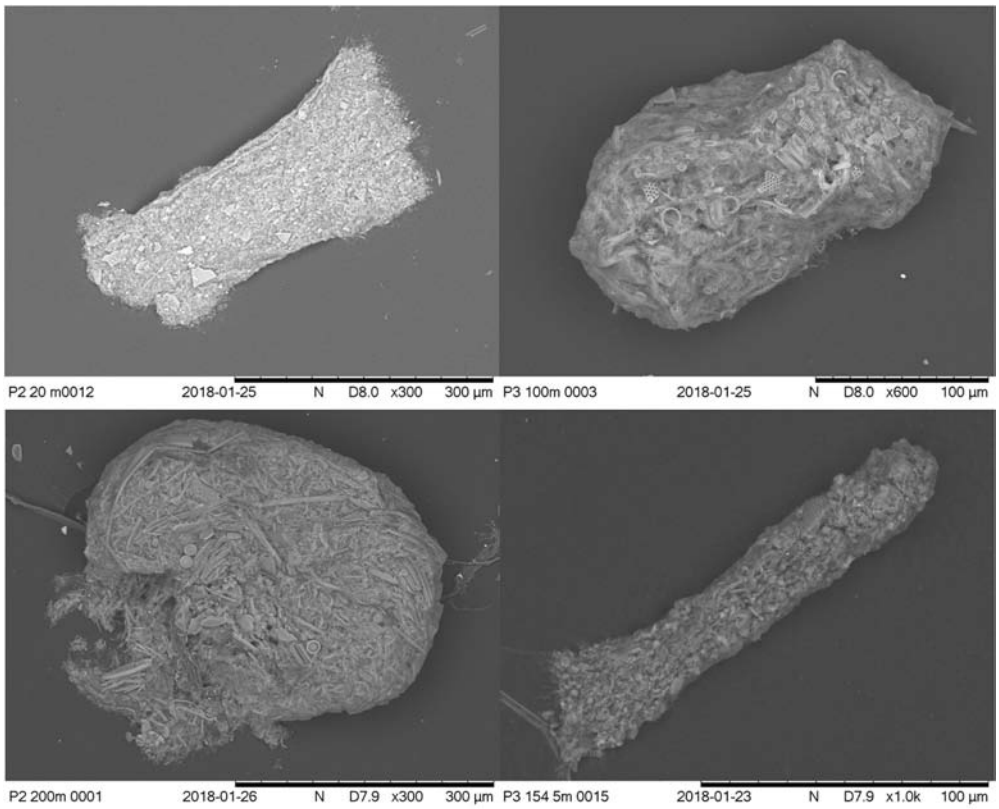

FIGURE 5 | Clockwise from top left: SEM images of broken cylindrical, intact ovoid, partially broken ellipsoidal, and spherical fecal pellets typical of those found in samples. Images show evidence of organic material, peritrophic membrane (on ovoid and spherical FPs) and diatom fragments.

The greatest diversity of phytoplankton species occurred at P3, where *Eucampia* spp. was most frequently observed, along with moderate abundances of *Fragilariopsis* spp. and *Pseudo-nitzschia* and low abundances of *Corethron* spp. and *Thalassiosira* spp.

Diatoms, organic detritus and zooplankton were sparsest at ICE across all depths. At P2, diatoms were observed as deep as 100 m but in greatest abundance at 20 and 40 m. In addition, occasional zooplankton and other specimens were observed within the samples, including copepods and their nauplii, euphausiid larvae, pteropods, polychaete worms, Foraminifera and egg masses. The highest concentration of material was encountered at P3 where diatoms, organic detritus and zooplankton were abundant to 40 m. Copepods of varying sizes were the most abundant type of zooplankton observed, although pteropods were also found. Below 40 m, material became sparser but zooplankton, diatoms and organic detritus were still evident at 100, 200, and 400 m.

DISCUSSION

Across the upper mesopelagic, we found that FPs of the smallest mesozooplankton were rapidly lost whilst larger FPs contributed disproportionately to FP flux and export out of the mixed layer. In ice-influenced regions, where the zooplankton community is generally euphausiid-dominated, we found mesozooplankton contributed comparatively little to FP flux compared to lower latitude regions, although high fluxes to the deep sea were likely to have been driven by episodic, swarm events. Higher export out of the mixed layer, followed by deep but strong attenuation, occurred north of the SACCF where the mesozooplankton was most abundant and dominated by copepods. In contrast, shallower attenuation and lower export flux occurred at ICE, suggesting that remineralization depth cannot be predicted by temperature alone but requires an understanding of the zooplankton community structure.

Is the Mesozooplankton Community a Good Predictor of FP Export?

At all stations, the size spectra of FPs found in the top 200 m deviated strongly from that predicted based on the size structure of the mesozooplankton community sampled over the same depth, especially at the smallest end of the size spectrum. Based on our predictions, we expected >85% of FPs produced to be $\leq$0.0002 mm^3 at all stations, yet found 78% (ICE) to 97% (P2) of FPs to be >0.0002 mm^3, up to nine times greater than expected. FPs with volumes of ∼0.0001 mm^3 often corresponded to those with one dimension <60 µm suggesting that one reason for not observing the very smallest FPs was the choice of mesh size. However, considering how few of the very smallest FPs were observed, a reduction in mesh size may not alter this result to any

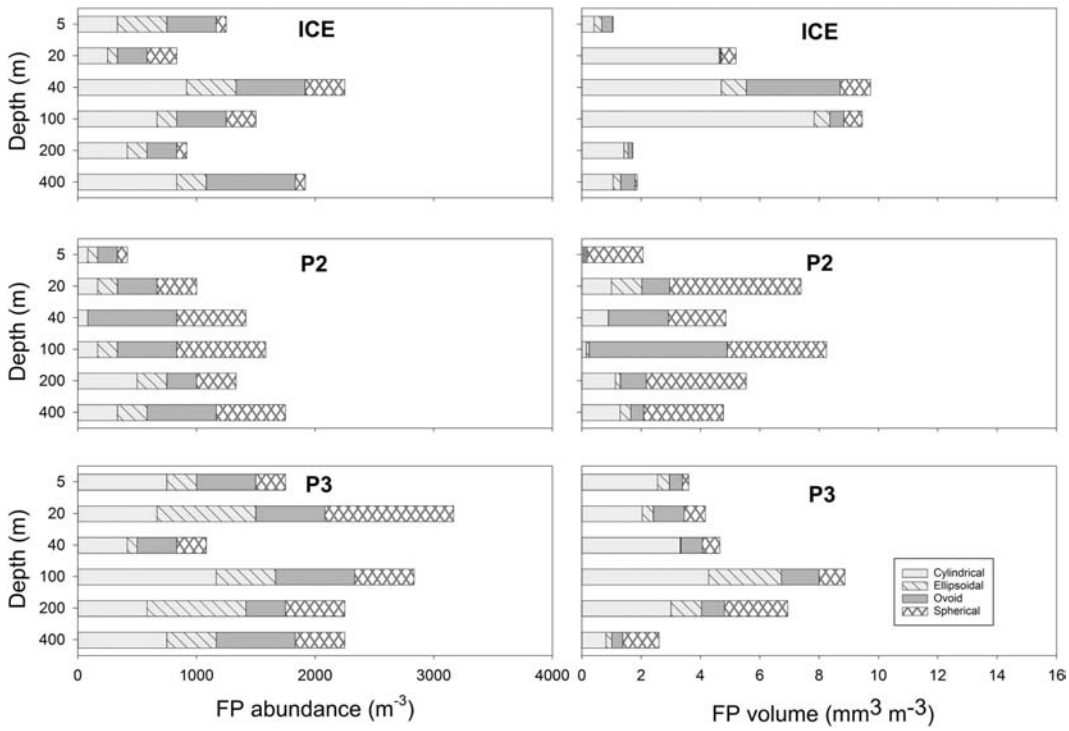

FIGURE 6 | (Left) Total abundance of FPs at each station, stacked by contribution of different morphological type. **(Right)** Total volume of FPs at each station, stacked by contribution by different morphological type.

meaningful degree. Nevertheless, removing FPs $\leq$0.0001 mm^3 from consideration still left between 6% (ICE) and 14% (P2) of the smallest predicted FPs unaccounted for. This implies that FPs originating from the smallest members of the zooplankton community including copepods of the abundant genus *Oithona* (Gonzalez and Smetacek, 1994; Dahms et al., 2015) are rapidly remineralized and that export is therefore dominated by FPs of the relatively less abundant but larger copepods such as *Calanus* and *Metridia* spp.

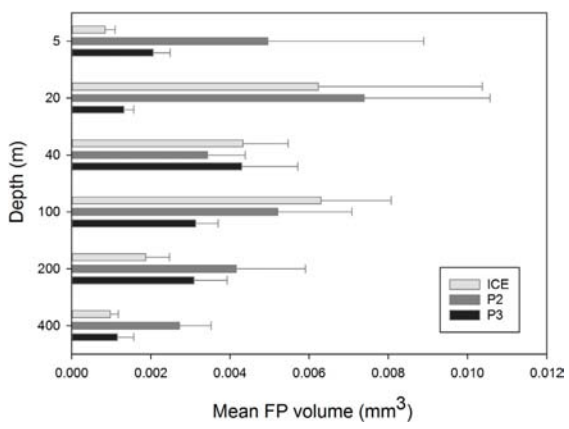

FIGURE 7 | Plot of the mean size (volume, mm^3) of FPs across depth at ICE, P2, and P3.

There was no significant difference in the size distribution in observed FPs between the upper four depths and bottom two depths at each station; however, the mean FP volume over depth showed a tendency first to increase (to 100 m at ICE, 20 m at P2 and 40 m at P3) before decreasing to 400 m. This suggests that the rate of production of smaller FPs in the surface waters exceeded their loss, whether to zooplankton-mediated coprophagy, coprorhexy, and coprochaly at depths of greater chlorophyll a concentration; or to the microbial or physical breakdown of particles as they sink. Conversely, as FPs sink through the mixed layer and light penetration and chlorophyll decrease, we suggest that the ingestion and breakdown of smaller FPs by other biota may increase as FPs contribute more to food intake. In addition, since small FPs produced in the mixed layer (between 40 and 80 m in this study) are less likely than larger ones to sink to deeper waters, this may contribute to an enhanced encounter rate of smaller particles in mixed layer waters and a shallower depth of their remineralization.

Similar patterns have been observed elsewhere: Lane et al. (1994) found that the larger FPs of the copepod species *Calanus finmarchicus* were important mediators of downward flux in the North Atlantic Bight, whilst the FPs of smaller copepods such as *Centropages typicus* were, on the whole, recycled. More recently, Belcher et al. (2017a) used Marine Snow Catcher and sediment trap data to conclude that the smallest FPs were not efficiently transferred from meso- to bathypelagic depths in the Scotia Sea and that they would represent only a small contribution to the flux of carbon. The present data represents the portion

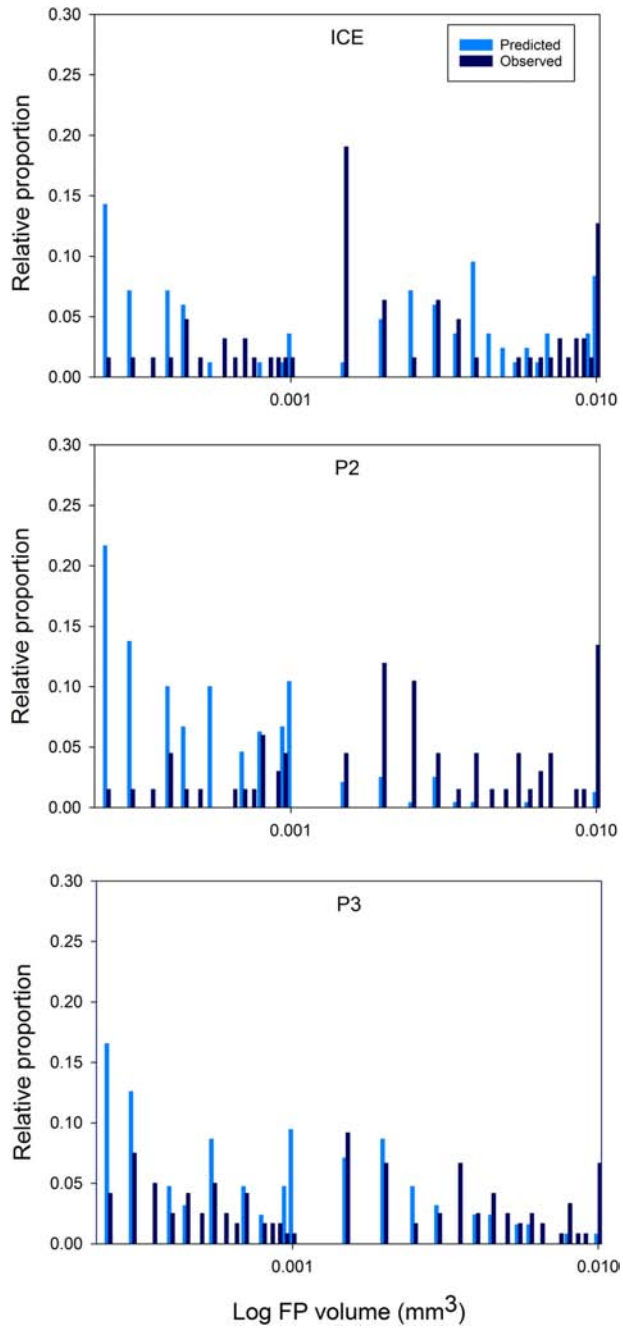

FIGURE 8 | Area plots of predicted versus observed FP size distributions over 0–200 m. FPs ≥ 0.0002 mm^3 are plotted as the log FP volume (mm^3) against the proportion of the total for each FP size class (as a percentage).

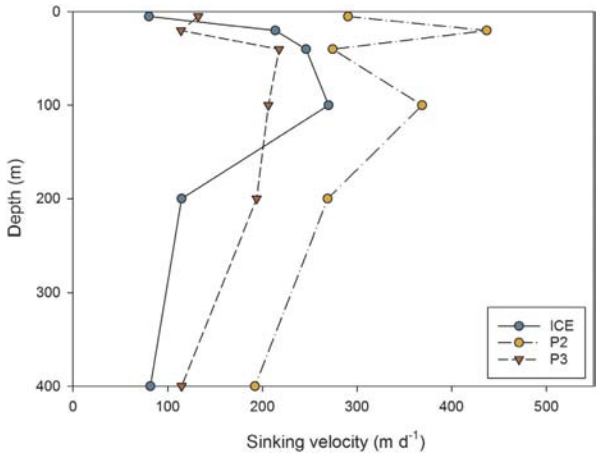

FIGURE 9 | Average FP sinking velocity (m d^{-1}) at different depths through the upper water column at ICE, P2, and P3 stations.

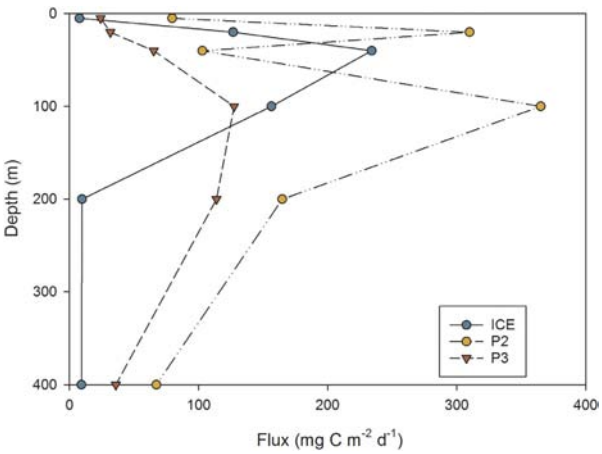

FIGURE 10 | FP flux (mg C m^{-2} d^{-1}) at different depths through the upper water column at ICE, P2, and P3 stations.

of the water column above their Marine Snow Catcher data (from 110 m below the mixed layer) and an intermediate depth of 400 m and suggests that, as well as not being transferred from meso- to bathypelagic depths, the smallest particles are in fact remineralized soon after production, regardless of depth or oceanographic regime. Although the importance of the microbial community colonizing zooplankton FPs, whether in breaking down the organic content of feces or as a direct food source, has long been appreciated (Johannes and Satomi, 1966; Poulsen and Iversen, 2008; Svensen et al., 2012), Svensen et al. (2012) also found that degradation of FPs by the microbial community and biota <200 μm is unlikely to retard the sinking rates of larger copepod FPs sufficiently to retain them at the surface.

At the larger end of the size spectrum (>0.0002 mm^3), some differences between the three stations emerge. At ICE, there is a peak in observed FPs in the 0.0015–0.002 mm^3 size range which is not predicted from the mesozooplankton community, and more deviation from the expected distribution than is seen at P2 or P3. The majority of the missing peak is comprised of cylindrical FPs typical of euphausiids. Due to the ability of euphausiids to avoid Bongo nets, they are not effectively captured by this method. However, taxonomic analysis found two to eight times as many euphausiid calyptopes at ICE than at P2 or P3, and for mesozooplankton abundance in the top 200 m to be up to one

order of magnitude lower at ICE. Euphausiids are known to be an important component of the macrozooplankton community in much of the Scotia Sea (e.g., Ward et al., 2012) and to have large, fast sinking FPs (Fowler and Small, 1972). A study identifying bioregions of the Scotia Sea found communities in the colder waters to the south of the SACCF and close to the ice edge to be typified by a greater proportion of small zooplankton such as copepods of *Oithona* and *Oncaea* spp. and cyclopoid nauplii, and the large *Euphausia superba* (Ward et al., 2012). This is consistent with the present results which show the FP community at ICE to be largely comprised of cylindrical FPs and few small FPs, and for *Oithona* spp. to be most abundant here compared to either P2 or P3. For this region therefore, the mesozooplankton community alone is an insufficient predictor of FP export in the upper mesopelagic and euphausiids are more influential in FP carbon export over intermediate depths.

Additionally, at P3 and P2, the number of predicted FPs in the 0.001–0.0015 mm^3 range were scarce in the observations. This corresponds to mesozooplankton with a prosome length of 1.8–2.1 mm, equivalent to, for example, copepodite stages of *Calanoides acutus*, *Scolecithricella* spp., and *Euchaeta* spp., and older stages of *Metridia* spp. Taxonomic analysis revealed the presence of most of these species at both stations. One explanation could be that our model is predicting what should occur in the absence of any biological or physical changes, yet FPs immediately become subject to processes which act to change their size and shape, including the coprophagous consumption of FPs (Gonzalez and Smetacek, 1994) and fragmentation of FPs by zooplankton in surface waters (Iversen and Poulsen, 2007). The implication is that physical, mechanical, and biological processes play an important role in reducing FP size, decoupling expected and observed FP size distributions, such that the overlying mesozooplankton community is not a direct predictor of FP size in the upper mesopelagic.

Race to the Bottom: Large, Dense FPs Are Biggest Contributors to Flux

Mean sinking rates calculated in this study ranged from 80 to 437 m d^{-1} across stations (range 5–1,919 m d^{-1}). This means that the majority of particles will have sunk past 400 m within 1–3 days. Horizontal advection could potentially move these particles between 12 and 40 km over that time (assuming an average velocity magnitude for the Scotia Sea of 15 cm s^{-1}, Tarling and Thorpe, 2014). This may introduce variability into our observations that can only be fully quantified through wider scale ($\sim$50 km^2) surveys. Here, we assume that our values represent mean levels at each station, pending further small- to mesoscale studies into spatial heterogeneity.

Comparing between stations, P3 had the slowest mean sinking rates, although they were also similar to ICE. FPs at P2 displayed the fastest sinking rates, also contributing to the greatest calculated carbon fluxes. FP sinking rates can be highly variable, ranging from 36 to 376 m d^{-1} (mixed zooplankton FPs, Smayda, 1969), 20 to 101 m d^{-1} (mixed copepods, Small et al., 1979), and 15 to 862 m d^{-1} (euphausiids, Fowler and Small, 1972; Belcher et al., 2017b). Sinking velocity is related to FP density which is affected by food type (Bienfang, 1980) or concentration (Small et al., 1979; Dagg and Walser, 1986) and ballast (Ploug et al., 2008). Since diets naturally high in mineral ballast and diatom frustules tend to produce denser, faster-sinking FPs (Small et al., 1979; Bienfang, 1980; Ploug et al., 2008), FPs originating from the characteristic diatom community of the Scotia Sea, and based on a herbivorous diet, should therefore be faster-sinking than those of similar dimensions and originating from a flagellate or omnivorous diet (Frangoulis et al., 2001). In addition, the fastest sinking FPs were found at P2 where the FP assemblage was dominated by ovoid and spherical FPs, as also observed in the Weddell Sea by Cadée et al. (1992). Many of the FPs found at P2 were densely packed with the silica frustules of diatoms, the mineral ballasting of which is likely to contribute to higher FP sinking rates.

Attenuation of FP Carbon Flux Is Strongly Modulated by Zooplankton

North of the SACCF at P2 and P3, FP carbon flux increased from the surface to a mid-depth maxima of 100 m situated below the thermocline. However, to the south at ICE, FP flux peaked within the mixed layer at a depth of 40 m. Here, a deep chlorophyll a maximum between 40 and 80 m suggests that most FPs resulted from production above or within this depth. At P2 and P3, chlorophyll a in the top 60–80 m was up to $>$2.0 $\mu g\ l^{-1}$ higher than at ICE. This corresponded to zooplankton abundances over the top 200 m that were at least an order of magnitude higher, with substantially greater export beneath the mixed layer. This suggests that mesozooplankton play a greater role in the deeper export of FPs in the more productive waters of the northern Scotia Sea, with elevated production of FPs from autotrophic feeding to at least 80 m, and their sinking from above, likely fuelling a deeper dwelling zooplankton community. Despite this, fluxes at all stations demonstrated a high degree of attenuation from the flux maxima, decreasing by an order of magnitude by 400 m, suggesting efficient processes of remineralization in the intermediate depths of the upper mesopelagic.

At ICE, cylindrical FPs typical of euphausiids dominated the flux at 100 m, after which there was strong attenuation. This agrees with a previous study by Cavan et al. (2015) who observed 82% of FPs in the seasonal ice zone to be of euphausiid origin, and for a large decrease in flux to occur with depth. In a separate study, Dagg et al. (2014) found their FP samples to be comprised almost entirely of cylindrical types and for euphausiids to comprise almost half of the abundance in net samples. Euphausiids were episodically abundant, had a diet rich in diatoms, and were the dominant contributor to FP flux, although the flux decreased when food quality was lower. Whilst direct adult euphausiid abundances for this study were not available, our findings confirm that where the community is euphausiid dominated, they contribute proportionately more to the export of organic material from the surface. Nevertheless, the strong attenuation of flux between 100 and 400 m also shows that, despite these pellets being an important component of export out of the mixed layer, only a small fraction eventually reaches the deeper mesopelagic.

Whilst the attenuation depth was equally deep at P2 as at P3, overall fluxes were greater at P2 and there was an additional peak at 20 m. This also corresponds to the presence of a number of predominantly ovoid and spherical FPs across the upper 200 m in the size range 0.002–0.003 mm^3, as well as increased numbers in sizes up to 0.007 mm^3, consistent with copepods such as *C. acutus* stages CIV and CV or *C. propinquus* stages CIV and CV. SEM analysis showed these to be densely packed, often comprised of diatom fragments and with fully or partially intact membranes. Examination of sampling times revealed that the P2 CTD sample had been collected 4 h after sunset, whilst ICE was sampled in the middle of the day and P3 1 h prior to sunset. Despite attempts to capture the diel cycle by sampling during night and day, sampling constraints meant that the mesozooplankton samples at P2 were collected approximately 4 h prior to sunset and 2 h after sunrise. This raises the possibility that FPs captured at P2 were the result of recent production from vertically migrating zooplankton that were missed by the net sampling. Zooplankton composition at P2 is similar to P3 yet abundances in this study were almost three times lower. However, in the oceanic Scotia Sea, the proportion of zooplankton in the top 100 m can increase from 45 to 60% between midday and midnight, with an additional secondary biomass peak between 150 and 300 m found at midnight (Ward et al., 1995). Larger copepods such as *C. acutus* and *C. propinquus* undertake deeper DVMs than smaller species or younger stages (Atkinson et al., 1992; Ward et al., 1995). This supports the hypothesis that zooplankton not captured by the Bongo nets were responsible for an additional pulse of FP production during the night between 20 and 100 m which may have been too recent to be subjected to the same degree of breakdown, degradation or sinking loss as daytime samples. Assuming that the animals were actively feeding, this would explain the production of fresh, high volume FPs, many of which still had intact or partially intact peritrophic membranes. It also illustrates that estimates of FP flux may be affected by diel variability in zooplankton distribution and that more work is required to understand the importance of short-term (diel) variability of FP flux.

An additional feature of the FP flux profile at P2 is a reduction in flux at 40 m, followed by a subsequent increase at 100 m. The chlorophyll a profile from the same CTD shows spikes in chlorophyll a biomass throughout a deep mixed layer, suggesting a possible earlier disturbance of the water column. The reduction in flux at 40 m corresponds to low chlorophyll a, whilst the peaks in flux at 20 m and 100 m are directly below peaks in chlorophyll a, suggesting active feeding within or above chlorophyll a layers which resulted in the densely packed, labile FPs observed just below. The presence of a diversity of zooplankton specimens in bottle samples supports the presence of a mid-depth community at 100 m, which may be feeding on FPs raining down from above and further contributing to the secondary peak in flux observed at 100 m.

CONCLUSION

ICE is separated from P2 and P3 by the SACCF, representing a difference in surface water temperatures of up to 5°C and supporting different zooplankton communities. At global scales, POC remineralization is found to increase with temperature (Marsay et al., 2015) but, at the regional scale of our study, we found zooplankton community interactions were the dominant influence on remineralization rates (Belcher et al., 2016). Shallowest remineralization occurred at the coldest station, ICE, where zooplankton abundances were lower and dominated by euphausiids, while remineralization was deeper in the warmer waters to the north, where zooplankton abundances were high and dominated by copepods. We propose that, at sites of higher zooplankton abundance, the fragmentation and consumption of FPs is able to sustain further zooplankton production and microbial respiration in the twilight zone, contributing to a deep pool of dissolved organic carbon (DOC) and deeper remineralization by the microbial community. The absence of the smallest FPs from even shallow depths illustrates how FP supply to the mesopelagic is determined by the presence of larger zooplankton, demonstrating the strong modulation by the zooplankton community on the supply and transfer of FPs between the epi- and upper mesopelagic in the SO.

AUTHOR CONTRIBUTIONS

CL carried out the fieldwork and sample collection with support from GT and other scientists on board JR304. CL carried out the sample and statistical analysis with support from CM and GT. CL wrote the manuscript with input from GT, CM, CR, and GS.

FUNDING

This work was funded by a NERC studentship granted through the EnvEast Doctoral Training Partnership (Grant No. NE/L002582/1) at the University of East Anglia. Fieldwork was supported by the British Antarctic Survey Ecosystems Programme and the Western Core Box and SCOOBIES Projects on board the *RRS James Clark Ross*.

ACKNOWLEDGMENTS

We would like to acknowledge the master, crew, and scientists aboard the *RRS James Clark Ross* during cruise JR304. We thank Laura Gerrish for providing **Figure 1** and the Plankton Sorting and Identification Center Morski Instytut Rybacki, Poland for their assistance with sample analysis.

SUPPLEMENTARY MATERIAL

The Supplementary Material for this article can be found online at: https://www.frontiersin.org/articles/10.3389/fmars.2019.00230/full#supplementary-material

FIGURE S1 | Average mesozooplankton abundance and size spectra based on prosome length at ICE (top), P2 (middle) and P3 (bottom).

REFERENCES

Angel, M. V. (1986). Vertical migrations in the oceanic realm: possible causes and probable effects. *Contrib. Mar. Sci.* 27, 47–70.

Atkinson, A., Schmidt, K., Fielding, S., Kawaguchi, S., and Geissler, P. A. (2012). Variable food absorption by *Antarctic krill*: relationships between diet, egestion rate and the composition and sinking rates of their fecal pellets. *Deep Sea Res. II Top. Stud. Oceanogr.* 59–60, 147–158. doi: 10.1016/j.dsr2.2011.06.008

Atkinson, A., Siegel, V., Pakhomov, E., Rothery, P., Loeb, V., Ross, R., et al. (2008). Oceanic circumpolar habitats of *Antarctic krill*. *Mar. Ecol. Prog. Ser.* 362, 1–23. doi: 10.3354/meps07498

Atkinson, A., Ward, P., Williams, R., and Poulet, S. A. (1992). Diel vertical migration and feeding of copepods at an oceanic site near South Georgia. *Mar. Biol.* 113, 583–593. doi: 10.1007/bf00349702

Belcher, A., Iversen, M., Manno, C., Henson, S. A., Tarling, G. A., and Sanders, R. (2016). The role of particle associated microbes in remineralization of fecal pellets in the upper mesopelagic of the Scotia Sea, Antarctica. *Limnol. Oceanogr.* 61, 1049–1064. doi: 10.1002/lno.10269

Belcher, A., Manno, C., Ward, P., Henson, S. A., Sanders, R., and Tarling, G. A. (2017a). Copepod faecal pellet transfer through the meso-and bathypelagic layers in the Southern Ocean in spring. *Biogeosciences* 14:1511–1525. doi: 10.5194/bg-14-1511-2017

Belcher, A., Tarling, G., Manno, C., Atkinson, A., Ward, P., Skaret, G., et al. (2017b). The potential role of *Antarctic krill* faecal pellets in efficient carbon export at the marginal ice zone of the South Orkney Islands in spring. *Polar Biol.* 40, 2001–2013. doi: 10.1007/s00300-017-2118-z

Bendtsen, J., Hilligsøe, K. M., Hansen, J. L. S., and Richardson, K. (2015). Analysis of remineralisation, lability, temperature sensitivity and structural composition of organic matter from the upper ocean. *Prog. Oceanogr.* 130, 125–145. doi: 10.1016/j.pocean.2014.10.009

Bienfang, P. (1980). Herbivore diet affects fecal pellet settling. *Can. J. Fish. Aquat. Sci.* 37, 1352–1357. doi: 10.1139/f80-173

Buesseler, K. O., Lamborg, C. H., Boyd, P. W., Lam, P. J., Trull, T. W., Bidigare, R. R., et al. (2007). Revisiting carbon flux through the ocean's twilight zone. *Science* 316, 567–570.

Burd, A. B., Hansell, D. A., Steinberg, D. K., Anderson, T. R., Arístegui, J., Baltar, F., et al. (2010). Assessing the apparent imbalance between geochemical and biochemical indicators of meso-and bathypelagic biological activity: what the@ $?! is wrong with present calculations of carbon budgets? *Deep Sea Res. II Top. Stud. Oceanogr.* 57, 1557–1571. doi: 10.1016/j.dsr2.2010.02.022

Cadée, G. C., González, H., and Schnack-Schiel, S. B. (1992). Krill diet affects faecal string settling. *Polar Biol.* 12, 75–80. doi: 10.1007/978-3-642-77595-6_8

Cavan, E. L., Le Moigne, F. A. C., Poulton, A. J., Tarling, G. A., Ward, P., Daniels, C. J., et al. (2015). Attenuation of particulate organic carbon flux in the Scotia Sea, Southern Ocean, is controlled by zooplankton fecal pellets. *Geophys. Res. Lett.* 42, 1–10.

Dagg, M. J., Jackson, G. A., and Checkley, D. M. (2014). The distribution and vertical flux of fecal pellets from large zooplankton in Monterey Bay and coastal California. *Deep Sea Res. I Oceanogr. Res. Pap.* 94, 72–86. doi: 10.1016/j.dsr.2014.09.001

Dagg, M. J., and Walser, W. E. (1986). The effect of food concentration on fecal pellet size in marine copepods. *Limnol. Oceanogr.* 31, 1066–1071. doi: 10.4319/lo.1986.31.5.1066

Dahms, H.-U., Tseng, L.-C., and Hwang, J.-S. (2015). Biogeographic distribution of the cyclopoid copepod genus Oithona – from mesoscales to global scales. *J. Exp. Mar. Biol. Ecol.* 467, 26–32. doi: 10.1016/j.jembe.2015.02.009

de Baar, H. J. W., De Jong, J. T. M., Bakker, D. C. E., Löscher, B. M., Veth, C., Bathmann, U., et al. (1995). Importance of iron for plankton blooms and carbon dioxide drawdown in the Southern Ocean. *Nature* 373, 412–415. doi: 10.1038/373412a0

Emerson, C. W., and Roff, J. C. (1987). Implications of fecal pellet size and zooplankton behaviour to estimates of pelagic-benthic carbon flux. *Mar. Ecol. Prog. Ser.* 35, 251–257. doi: 10.3354/meps035251

Fowler, S. W., and Small, L. F. (1972). Sinking rates of euphausiid fecal pellets. *Limnol. Oceanogr.* 17, 293–296. doi: 10.4319/lo.1972.17.2.0293

Francois, R., Honjo, S., Krishfield, R., and Manganini, S. (2002). Factors controlling the flux of organic carbon to the bathypelagic zone of the ocean. *Glob. Biogeochem. Cycles* 16, 34-1–34-20.

Frangoulis, C., Belkhiria, S., Goffart, A., and Hecq, J.-H. (2001). Dynamics of copepod faecal pellets in relation to a *Phaeocystis* dominated phytoplankton bloom: characteristics, production and flux. *J. Plankton Res.* 23, 75–88. doi: 10.1093/plankt/23.1.75

Giering, S. L., Sanders, R., Lampitt, R. S., Anderson, T. R., Tamburini, C., Boutrif, M., et al. (2014). Reconciliation of the carbon budget in the ocean's twilight zone. *Nature* 507, 480–483. doi: 10.1038/nature13123

González, H. E. (1992). The distribution and abundance of krill faecal material and oval pellets in the scotia and weddell seas (Antarctica) and their role in particle flux. *Polar Biol.* 12, 81–91. doi: 10.1007/978-3-642-77595-6_9

González, H. E., Ortiz, V. C., and Sobarzo, M. (2000). The role of faecal material in the particulate organic carbon flux in the northern humboldt current, Chile (23 S), before and during the 1997–1998 El Niño. *J. Plankton Res.* 22, 499–529. doi: 10.1093/plankt/22.3.499

Gonzalez, H. E., and Smetacek, V. (1994). The possible role of the cyclopoid copepod *Oithona* in retarding vertical flux of zooplankton faecal material. *Mar. Ecol. Prog. Ser.* 113, 233–246. doi: 10.3354/meps113233

Gorsky, G., Ohman, M. D., Picheral, M., Gasparini, S., Stemmann, L., Romagnan, J.-B., et al. (2010). Digital zooplankton image analysis using the ZooScan integrated system. *J. Plankton Res.* 32, 285–303. doi: 10.1093/plankt/fbp124

Iversen, M. H., and Poulsen, L. K. (2007). Coprorhexy, coprophagy, and coprochaly in the copepods *Calanus helgolandicus*, *Pseudocalanus elongatus*, and *Oithona similis*. *Mar. Ecol. Prog. Ser.* 350, 79–89. doi: 10.1021/acs.est.5b05905

Johannes, R. E., and Satomi, M. (1966). Composition and nutritive value of fecal pellets of a marine crustacean. *Limnol. Oceanogr.* 11, 191–197. doi: 10.4319/lo.1966.11.2.0191

Komar, P. D., Morse, A. P., Small, L. F., and Fowler, S. W. (1981). An analysis of sinking rates of natural copepod and euphausiid fecal pellets. *Limnol. Oceanogr.* 26, 172–180. doi: 10.4319/lo.1981.26.1.0172

Korb, R. E., Whitehouse, M. J., Thorpe, S. E., and Gordon, M. (2005). Primary production across the Scotia Sea in relation to the physico-chemical environment. *J. Mar. Syst.* 57, 231–249. doi: 10.1016/j.jmarsys.2005.04.009

Lampitt, R. S., Noji, T., and Von Bodungen, B. (1990). What happens to zooplankton faecal pellets? Implications for material flux. *Mar. Biol.* 104, 15–23. doi: 10.1007/bf01313152

Lancraft, T. M., Torres, J. J., and Hopkins, T. L. (1989). Micronekton and macrozooplankton in the open waters near antarctic ice edge zones (Ameriez 1983 and 1986). *Polar Biol.* 9, 225–233. doi: 10.1007/bf00263770

Lane, P., Smith, S., Urban, J., and Biscaye, P. (1994). Carbon flux and recycling associated with zooplanktonic fecal pellets on the shelf of the Middle Atlantic Bight. *Deep Sea Res. II Top. Stud. Oceanogr.* 41, 437–457. doi: 10.1016/0967-0645(94)90031-0

Le Quéré, C., Buitenhuis, E. T., Moriarty, R., Alvain, S., Aumont, O., Bopp, L., et al. (2016). Role of zooplankton dynamics for Southern Ocean phytoplankton biomass and global biogeochemical cycles. *Biogeosciences* 13, 4111–4133. doi: 10.5194/bg-13-4111-2016

Legendre, L., Rivkin, R. B., Weinbauer, M. G., Guidi, L., and Uitz, J. (2015). The microbial carbon pump concept: potential biogeochemical significance in the globally changing ocean. *Prog. Oceanogr.* 134, 432–450. doi: 10.1016/j.pocean.2015.01.008

Longhurst, A. R., and Harrison, W. (1989). The biological pump: profiles of plankton production and consumption in the upper ocean. *Prog. Oceanogr.* 22, 47–123. doi: 10.1016/0079-6611(89)90010-4

Maiti, K., Charette, M. A., Buesseler, K. O., and Kahru, M. (2013). An inverse relationship between production and export efficiency in the Southern Ocean. *Geophys. Res. Lett.* 40, 1557–1561. doi: 10.1002/grl.50219

Manno, C., Stowasser, G., Enderlein, P., Fielding, S., and Tarling, G. A. (2015). The contribution of zooplankton faecal pellets to deep-carbon transport in the Scotia Sea (Southern Ocean). *Biogeosciences* 12, 1955–1965. doi: 10.5194/bg-12-1955-2015

Marsay, C. M., Sanders, R. J., Henson, S. A., Pabortsava, K., Achterberg, E. P., and Lampitt, R. S. (2015). Attenuation of sinking particulate organic carbon flux through the mesopelagic ocean. *Proc. Natl. Acad. Sci. U.S.A.* 112, 1089–1094. doi: 10.1073/pnas.1415311112

Martin, J. H. (1990). Glacial-interglacial CO2 change: the iron hypothesis. *Paleoceanography* 5, 1–13. doi: 10.1029/pa005i001p00001

Mauchline, J. (1998). "Physiology," in *The Biology of Calanoid Copepods*, eds J. H. S. Blaxter, A. J. Southward, and P. A. Tyler (London: Academic Press).

Murphy, E. J., Watkins, J. L., Trathan, P. N., Reid, K., Meredith, M. P., Thorpe, S. E., et al. (2007). Spatial and temporal operation of the Scotia Sea ecosystem: a review of large-scale links in a krill centred food web. *Philos. Trans. R. Soc. B Biol. Sci.* 362, 113–148. doi: 10.1098/rstb.2006.1957

Noji, T. T., Estep, K. W., Macintyre, F., and Norrbin, F. (1991). Image analysis of faecal material grazed upon by three species of copepods: evidence for coprorhexy, coprophagy and coprochaly. *J. Mar. Biol. Assoc.* 71, 465–480.

Picheral, M., Colin, S., and Irisson, J. O. (2017). *EcoTaxa, a tool for the Taxonomic Classification of Images*.Available at: http://ecotaxa.obs-vlfr.fr (accessed date August 09, 2017).

Ploug, H., Iversen, M., and Fischer, G. (2008). Ballast, sinking velocity and apparent diffusivity in marine snow and zooplankton fecal pellets: implications for substrate turnover by attached bacteria. *Limnol. Oceanogr.* 53, 1878–1886. doi: 10.4319/lo.2008.53.5.1878

Poulsen, L. K., and Iversen, M. H. (2008). Degradation of copepod fecal pellets: key role of protozooplankton. *Mar. Ecol. Prog. Ser.* 367, 1–13. doi: 10.3354/meps07611

R Core Team (2016). *R: A Language and Environment for Statistical Computing*. Vienna: R Foundation for Statistical Computing. Available at: https://www.r-project.org/

Rasband, W. S. (1997/2016). *ImageJ*. Bethesda, MD: U. S. National Institutes of Health.

Robinson, C., Steinberg, D. K., Anderson, T. R., Arístegui, J., Carlson, C. A., Frost, J. R., et al. (2010). Mesopelagic zone ecology and biogeochemistry–a synthesis. *Deep Sea Res. II Top. Stud. Oceanogr.* 57, 1504–1518. doi: 10.1016/j.dsr2.2010.02.018

Sampei, M., Forest, A., Sasaki, H., Hattori, H., Makabe, R., Fukuchi, M., et al. (2009). Attenuation of the vertical flux of copepod fecal pellets under Arctic sea ice: evidence for an active detrital food web in winter. *Polar Biol.* 32, 225–232. doi: 10.1007/s00300-008-0523-z

Small, L., Fowler, S., and Ünlü, M. (1979). Sinking rates of natural copepod fecal pellets. *Mar. Biol.* 51, 233–241. doi: 10.1021/acs.est.5b05905

Smayda, T. J. (1969). Some measurements of the sinking rate of fecal pellets. *Limnol. Oceanogr.* 14, 621–625. doi: 10.1038/srep00716

Stamieszkin, K., Pershing, A. J., Record, N. R., Pilskaln, C. H., Dam, H. G., and Feinberg, L. R. (2015). Size as the master trait in modeled copepod fecal pellet carbon flux. *Limnol. Oceanogr.* 60, 2090–2107. doi: 10.1002/lno.10156

Steinberg, D. K., and Landry, M. R. (2017). Zooplankton and the ocean carbon cycle. *Annu. Rev. Mar. Sci.* 9, 413–444. doi: 10.1146/annurev-marine-010814-015924

Steinberg, D. K., Van Mooy, B. A., Buesseler, K. O., Boyd, P. W., Kobari, T., and Karl, D. M. (2008). Bacterial vs zooplankton control of sinking particle flux in the ocean's twilight zone. *Limnol. Oceanogr.* 53, 1327–1338. doi: 10.1002/bies.201400100

Svensen, C., Wexels Riser, C., Reigstad, M., and Seuthe, L. (2012). Degradation of copepod faecal pellets in the upper layer: role of microbial community and *Calanus finmarchicus*. *Mar. Ecol. Prog. Ser.* 462, 39–49. doi: 10.3354/meps09808

Takahashi, T., Sutherland, S. C., Sweeney, C., Poisson, A., Metzl, N., Tilbrook, B., et al. (2002). Global sea–air Co_2 flux based on climatological surface ocean pco2, and seasonal biological and temperature effects. *Deep Sea Res. II Top. Stud. Oceanogr.* 49, 1601–1622. doi: 10.1016/s0967-0645(02)00003-6

Tarling, G. A., and Thorpe, S. E. (2014). Instantaneous movement of krill swarms in the antarctic circumpolar current. *Limnol. Oceanogr.* 59, 872–886. doi: 10.4319/lo.2014.59.3.0872

Turner, J. T. (1979). Microbial attachment to copepod fecal pellets and its possible ecological significance. *Trans. Am. Microsc. Soc.* 98, 131–135.

Turner, J. T. (2002). Zooplankton fecal pellets, marine snow and sinking phytoplankton blooms. *Aquat. Microb. Ecol.* 27, 57–102. doi: 10.3354/ame027057

Turner, J. T. (2015). Zooplankton fecal pellets, marine snow, phytodetritus and the ocean's biological pump. *Prog. Oceanogr.* 130, 205–248. doi: 10.1016/j.pocean.2014.08.005

Urban, J., Mckenzie, C., and Deibel, D. (1993). Nanoplankton found in fecal pellets of macrozooplankton in coastal Newfoundland waters. *Bot. Mar.* 36, 267–282.

Urrère, M. A., and Knauer, G. A. (1981). Zooplankton fecal pellet fluxes and vertical transport of particulate organic material in the pelagic environment. *J. Plankton Res.* 3, 369–387. doi: 10.1093/plankt/3.3.369

Ward, P., Atkinson, A., Murray, A., Wood, A., Williams, R., and Poulet, S. (1995). The summer zooplankton community at South Georgia: biomass, vertical migration and grazing. *Polar Biol.* 15, 195–208.

Ward, P., Atkinson, A., Venables, H. J., Tarling, G. A., Whitehouse, M. J., Fielding, S., et al. (2012). Food web structure and bioregions in the Scotia Sea: a seasonal synthesis. *Deep Sea Res. II Top. Stud. Oceanogr.* 59–60, 253–266. doi: 10.1016/j.dsr2.2011.08.005

Watkins, J., Belcher, A., Duret, M., Enderlein, P., Fielding, S., Floter, S., et al. (2015). *JR304 Western Core Box & Moorings Cruise Report*. Cambridge: British Antarctic Survey.

Whitehouse, M. J., Korb, R. E., Atkinson, A., Thorpe, S. E., and Gordon, M. (2008). Formation, transport and decay of an intense phytoplankton bloom within the high-nutrient low-chlorophyll belt of the Southern Ocean. *J. Mar. Syst.* 70, 150–167. doi: 10.1016/j.jmarsys.2007.05.003

Wilson, S., Ruhl, H., and Smith, K. Jr. (2013). Zooplankton fecal pellet flux in the abyssal Northeast Pacific: a 15 year time-series study. *Limnol. Oceanogr.* 58, 881–892. doi: 10.4319/lo.2013.58.3.0881

Wilson, S. E., Steinberg, D. K., and Buesseler, K. O. (2008). Changes in fecal pellet characteristics with depth as indicators of zooplankton repackaging of particles in the mesopelagic zone of the subtropical and subarctic North Pacific Ocean. *Deep Sea Res. II Top. Stud. Oceanogr.* 55, 1636–1647. doi: 10.1016/j.dsr2.2008.04.019

Conflict of Interest Statement: The authors declare that the research was conducted in the absence of any commercial or financial relationships that could be construed as a potential conflict of interest.

frontiers in Marine Science

ORIGINAL RESEARCH
published: 12 July 2019
doi: 10.3389/fmars.2019.00397

The Roles of Suspension-Feeding and Flux-Feeding Zooplankton as Gatekeepers of Particle Flux Into the Mesopelagic Ocean in the Northeast Pacific

Michael R. Stukel[1,2], Mark D. Ohman[3], Thomas B. Kelly[1] and Tristan Biard[4]*

[1] Department of Earth, Ocean, and Atmospheric Science, Florida State University, Tallahassee, FL, United States, [2] Center for Ocean-Atmospheric Prediction Studies, Florida State University, Tallahassee, FL, United States, [3] Scripps Institution of Oceanography, University of California, San Diego, San Diego, CA, United States, [4] Laboratoire d'Océanologie et de Géosciences, Wimereux, France

OPEN ACCESS

Edited by:
Rainer Kiko, GEOMAR Helmholtz Centre for Ocean Research Kiel, Germany

Reviewed by:
John Patrick Dunne, Geophysical Fluid Dynamics Laboratory (GFDL), United States
Hiroaki Saito, The University of Tokyo, Japan
Santiago Hernández-León, University of Las Palmas de Gran Canaria, Spain

***Correspondence:**
Michael R. Stukel
mstukel@fsu.edu

Specialty section:
This article was submitted to Marine Biogeochemistry, a section of the journal Frontiers in Marine Science

Received: *26 March 2019*
Accepted: *26 June 2019*
Published: *12 July 2019*

Citation:
Stukel MR, Ohman MD, Kelly TB and Biard T (2019) The Roles of Suspension-Feeding and Flux-Feeding Zooplankton as Gatekeepers of Particle Flux Into the Mesopelagic Ocean in the Northeast Pacific. Front. Mar. Sci. 6:397. doi: 10.3389/fmars.2019.00397

Zooplankton are important consumers of sinking particles in the ocean's twilight zone. However, the impact of different taxa depends on their feeding mode. In contrast to typical suspension-feeding zooplankton, flux-feeding taxa preferentially consume rapidly sinking particles that would otherwise penetrate into the deep ocean. To quantify the potential impact of two flux-feeding zooplankton taxa [Aulosphaeridae (Rhizaria), and *Limacina helicina* (euthecosome pteropod)] and the total suspension-feeding zooplankton community, we measured depth-stratified abundances of these organisms during six cruises in the California Current Ecosystem. Using allometric–scaling relationships, we computed the percentage of carbon flux intercepted by flux feeders and suspension feeders. These estimates were compared to direct measurements of carbon flux attenuation (CFA) made using drifting sediment traps and ^{238}U–^{234}Th disequilibrium. We found that CFA in the shallow twilight zone typically ranged from 500 to 1000 μmol organic C flux remineralized per 10-m vertical depth bin. This equated to approximately 6–10% of carbon flux remineralized/10 m. The two flux-feeding taxa considered in this study could account for a substantial proportion of this flux near the base of the euphotic zone. The mean flux attenuation attributable to Aulosphaeridae was 0.69%/10 m (median = 0.21%/10 m, interquartile range = 0.04–0.81%) at their depth of maximum abundance (∼100 m), which would equate to ∼10% of total flux attenuation in this depth range. The maximum flux attenuation attributable to Aulosphaeridae reached 4.2%/10 m when these protists were most abundant. *L. helicina*, meanwhile, could intercept 0.45–1.6% of carbon flux/10 m, which was slightly greater (on average) than the Aulosphaeridae. In contrast, suspension-feeding zooplankton in the mesopelagic (including copepods, euphausiids, appendicularians, and ostracods) had combined clearance rates of 2–81 L m^{-3} day^{-1} (mean of 19.6 L m^{-3} day^{-1}). This implies a substantial impact on slowly sinking particles, but

a negligible impact on the presumably rapidly sinking fecal pellets that comprised the majority of the material collected in sediment traps. Our results highlight the need for a greater research focus on the many taxa that potentially act as flux feeders in the oceanic twilight zone.

Keywords: biological pump, carbon export, remineralization length scale, mesozooplankton ecology, pteropods, marine biogeochemistry, sinking particles, marine snow

INTRODUCTION

Zooplankton play diverse roles in the cycling of many elements in the ocean including iron, zinc, sulfur, and mercury (Fowler, 1977; Asher et al., 2016; Baines et al., 2016; Schmidt et al., 2016; Gorokhova et al., 2018). However, their greatest importance to global biogeochemistry is likely derived from their roles in the biological carbon pump (BCP; Buitenhuis et al., 2006; Turner, 2015; Steinberg and Landry, 2017). The BCP refers to the processes that transport organic carbon fixed by phytoplankton in the euphotic zone into the mesopelagic realm (Silver and Gowing, 1991; Ducklow et al., 2001; Siegel et al., 2016). The BCP leads to net transport of CO_2 from the surface ocean into the deep ocean where it can be sequestered for periods of decades to millennia (DeVries et al., 2012). Estimates of the present magnitude of the BCP range from 5 to 12 Pg C year^{-1} (Henson et al., 2011; Laws et al., 2011; Siegel et al., 2014; DeVries and Weber, 2017), however, the responses of mesozooplankton and the BCP to future climate change remain unknown.

Research on the role of mesozooplankton in the BCP has focused primarily on the epipelagic zone where the relationship between zooplankton and the BCP can change based on the community composition of phytoplankton and zooplankton. Zooplankton can play an important role in combining smaller particles into large, rapidly sinking fecal pellets (Bruland and Silver, 1981; Komar et al., 1981; Turner, 2002; Wilson et al., 2008) and promote aggregation and sinking through discarded mucous feeding webs (Alldredge, 1976; Hansen et al., 1996; Robison et al., 2005). Zooplankton can also decrease the magnitude of the biological pump when their grazing activities exert top-down control on phytoplankton production (Glibert, 1998; Goericke, 2002) or fragment larger particles into smaller ones (Dilling and Alldredge, 2000), and also play an important role in nutrient regeneration in the euphotic zone (Frangoulis et al., 2005; Alcaraz et al., 2010; Saba et al., 2011). Active transport by diel vertically migrating zooplankton is also an important (potentially dominant) component of the biological pump in many marine ecosystems (Steinberg et al., 2000; Hannides et al., 2009; Bianchi et al., 2013; Stukel et al., 2018b; Archibald et al., 2019; Hernández-Leon et al., unpublished; Kelly et al., unpublished; Kiko et al., unpublished).

Although fewer studies have quantified zooplankton impacts in the mesopelagic, zooplankton play a substantial role in consuming, disaggregating, and transforming sinking particles (Steinberg and Landry, 2017). These organisms may play a substantial role in modulating marine snow flux in the mesopelagic (Lampitt et al., 1993) and have been hypothesized to play roles as "gatekeepers" that modulate carbon transfer from the euphotic zone to the mesopelagic (Jackson and Checkley, 2011). However, zooplankton are phylogenetically and functionally diverse with a wide array of feeding strategies (Kiørboe, 2011). It is thus important to consider the relative importance of zooplankton with different feeding modes. For instance, suspension-feeding salps and crustaceans may consume particles in relative proportion to their abundance in the water column, although they may show selectivity based on particle size or other characteristics (Fuchs and Franks, 2010). In contrast, a flux-feeding pteropod will intercept particles in proportion to the speed with which they sink through the water column (Jackson et al., 1993), while cruise-feeding zooplankton may search for and colonize large aggregates (Kiørboe and Thygesen, 2001). Yet other taxa may break aggregates apart due to their swimming and feeding behaviors or partially consume fecal pellets leading to breakage and decreased settling velocities (Goldthwait et al., 2004; Iversen and Poulsen, 2007). Understanding these interactions is important to understanding observed decadal scale changes in carbon flux attenuation (CFA) in the mesopelagic (Lomas et al., 2010).

In this study we investigate the relative importance of representatives of two groups of flux-feeding zooplankton (phaeodarians and euthecosome pteropods) with respect to sinking particle flux attenuation. Phaeodarians are a group of siliceous protists from the supergroup Rhizaria that typically thrive in the deep ocean (Nakamura and Suzuki, 2015). We focus in this manuscript on one group of large Phaeodaria (Aulosphaeridae) that have a typical diameter of ∼2-mm and are common in the shallow twilight zone in the CCE (Ohman et al., 2012; Biard et al., 2016, 2018). These mesopelagic phaeodarians are likely flux feeders that have relatively slow (for protists) growth rates and rely on the rain of sinking particles from above for their food (Gowing, 1986, 1989; Gowing and Bentham, 1994; Stukel et al., 2018a). Euthecosome pteropods are pelagic molluscs that produce large mucous feeding webs to trap food, including swimming zooplankton and sinking particles (Gilmer and Harbison, 1986; Lalli and Gilmer, 1989). We focus on the species *Limacina helicina*, which is common in cold waters worldwide from the Antarctic to the Arctic including the California Current (Hunt et al., 2010; Bednaršek et al., 2012). *L. helicina* produces a mucous feeding web with a typical diameter of 40–55 mm (Gilmer and Harbison, 1986). We draw our data from a decade's worth of field campaigns with differing objectives and hence changing methodology. We thus do not intend this to be a definitive assessment of the role of flux feeders in the mesopelagic ecosystem. Rather we intend it as an initial quantitative investigation of the differing roles of suspension feeders and two specific taxa of flux feeders.

We find that each of these flux feeders has the potential to mediate a substantial portion of the CFA in the shallow twilight zone, although their impact is greatly reduced in the deeper mesopelagic. In contrast, suspension-feeding zooplankton are abundant through the mesopelagic, but likely only play a substantial role in the attenuation of the flux of slowly sinking particles. There is, however, substantial uncertainty around our core conclusions, and we hope that this uncertainty will spur future targeted investigations.

MATERIALS AND METHODS

Field Sampling

In situ measurements were made on six process cruises of the CCE LTER Program (P0704, April 2007; P0810, October 2008; P1106, June 2011; P1208, August 2012; P1408, August 2014; and P1604 April 2016, **Figure 1**). On these cruises, we used a quasi-Lagrangian sampling scheme to track water parcels for a period of 2–5 days while quantifying biotic and abiotic standing stocks and rates (Landry et al., 2009, 2012). After preliminary site surveys with a free-fall Moving Vessel Profiler (Ohman et al., 2012), quasi-Lagrangian experiments (hereafter referred to as "cycles") were initiated with the deployment of a surface-tethered drifting sediment trap with a 3 × 1-m drogue centered at 15-m depth to track the mixed layer (Stukel et al., 2013). A second, identically drogued, experimental array was deployed and recovered daily while being used as a platform for *in situ* incubations (Landry et al., 2009). During each cycle, paired day–night Multiple Opening and Closing Net and Environmental Sensing System (MOCNESS) net tows were used to determine vertical patterns of mesozooplankton abundance (Powell and Ohman, 2015). On approximately 10 CTD-Niskin rosette casts per cycle, we used an Underwater Vision Profiler (UVP5) to determine vertical profiles of rhizarians (Ohman et al., 2012; Biard et al., 2018). We also measured the vertical flux (and flux attenuation) of sinking particles using the aforementioned drifting sediment traps and measurements of water column ^{238}U–^{234}Th deficiency (Stukel et al., 2015). We divided our Lagrangian experiments into oligotrophic cycles (<0.5 μg Chl a L^{-1}) or high biomass cycles (>0.5 μg Chl a L^{-1}). For details on cruise conditions, see **Supplementary Materials**.

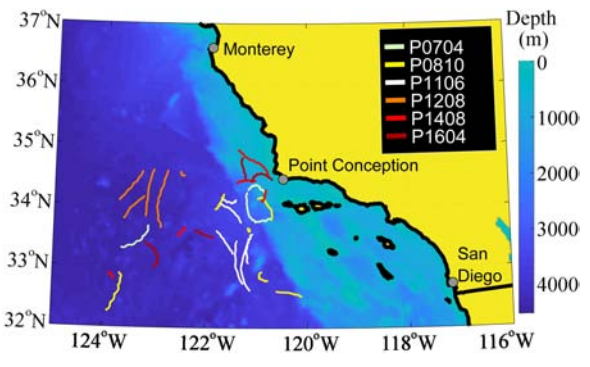

FIGURE 1 | Study region showing Lagrangian tracks of each experimental cycle (color coded by cruise). Blue shading show bathymetry.

Zooplankton Collection and Enumeration

Mesozooplankton depth-stratified abundances were determined from day–night MOCNESS tows (1 m^2 net, 202-μm mesh) on the P0704 and P0810 cruises (typically two pairs of tows per cycle). Each net collected organisms over a ∼50-m depth interval with consecutive nets tripped from a depth of 450 m to the surface. Samples were preserved in 1.8% formaldehyde and analyzed using a ZooScan digital scanner with ZooProcess software (Gorsky et al., 2010). Zooplankton were sorted into broad taxonomic groups (e.g., copepods, euphausiids, doliolids, etc.) using machine learning algorithms, the taxonomic assignments of 100% of the vignettes validated manually, then automatically sized (as Feret diameter). Organismal length was then used with allometric equations (see below) to quantify organism biomass and clearance rate. For additional details on ZooScan processing, see Stukel et al. (2013), Powell and Ohman (2015), and Ohman and Romagnan (2016). On two cycles from the P1208 cruise, these samples were also sorted to enumerate the abundance of pteropods, specifically *L. helicina* (Bednaršek and Ohman, 2015).

Because they are not well preserved in net tows, large rhizarians (>600-μm) were quantified using an UVP5 (Picheral et al., 2010; Biard et al., 2016). The UVP5 is an *in situ* imaging camera that was mounted downward facing on the bottom of the ship's CTD-Niskin rosette and deployed an average of 10 times per Lagrangian cycle. It reliably images organisms that are >600-μm in diameter, although avoidance issues should be expected for strongly swimming taxa. The UVP5 images a volume of ∼1 L per image at ∼6 Hz. Data were analyzed as described in Biard et al. (2016, 2018). Briefly, images were automatically analyzed to separate out vignettes representing organisms or marine snow aggregates. ZooProcess software was utilized to generate morphometric information (e.g., diameter) and classify the organisms into broad taxonomic groups. Classifications were then 100% manually validated. Phaeodarian taxonomic groups included Aulosphaeridae, which was the dominant rhizarian present and is the only group of organisms enumerated by UVP5 that is utilized in this study.

Sediment Trap Deployments

VERTEX-style particle interceptor tube (PIT) sediment traps were deployed at the beginning and recovered at the end of each cycle (Knauer et al., 1979; Stukel et al., 2013). PITs consisted of a polycarbonate tube with 7-cm inner diameter and 8:1 aspect ratio with a baffle on top comprised of 13 smaller, beveled tubes. On the P0704 cruise, PITs were deployed at a depth of 100 m. On P0810, P1106, and P1208, PITs were deployed at a depth of 100 m and near the base of the euphotic zone (as estimated based on fluorescence profiles from MVP transects) if the base of the euphotic zone was shallower than 75 m. On the P1408 and P1604 cruises, PITs were deployed at the base of the euphotic zone, 100 m, and 150 m.

PITs were deployed with a dense formaldehyde-filtered seawater brine. Deployments lasted from 2.25 to 4.25 days. After

recovery, the interface separating brine water from overlying ambient seawater was identified and the overlying seawater was immediately removed. Samples were then gravity filtered through a 200-μm mesh filter, the filter examined under a stereomicroscope, and swimming zooplankton removed. Three to five replicates per depth were filtered through pre-combusted GF/F filters and used for particulate organic carbon analyses (¼ to ½ of a tube). An additional three samples were filtered through pre-combusted quartz (QMA) filters and used for C:^{234}Th ratio measurements (Stukel et al., 2019). On the P0704, P0810, and P1604 cruises, two replicates (one half tube each) per depth were saved in formaldehyde and analyzed under a stereomicroscope to quantify fecal pellet abundance (Stukel et al., 2013; Morrow et al., 2018). For detailed methods and information on additional analyses made from these traps, see Gutierrez-Rodriguez et al. (2018), Morrow et al. (2018), and Stukel et al. (2019).

^{234}Th Analyses

Water column ^{234}Th activity was measured (typically two profiles per cycle and 10–12 depths per profile, spanning the upper 200 m of the water column) using standard small volume techniques (Benitez-Nelson et al., 2001; Pike et al., 2005). Briefly, 4-L samples were spiked with tracer ^{230}Th and thorium was co-precipitated with manganese oxide. Samples were beta counted on a RISO low-level background beta counter and re-counted >6 half-lives later. Samples were dissolved and spiked with ^{229}Th. The $^{229:230}$Th ratio was determined by inductively coupled plasma mass spectrometry to determine the yield of the initial thorium filtration. For additional details, see Stukel et al. (2019). ^{238}U–^{234}Th deficiency was quantified after determining ^{238}U activity from relationships with salinity published in Owens et al. (2011). ^{238}U–^{234}Th deficiency was combined with sediment trap organic carbon flux measurements to estimate twilight zone CFA as outlined below.

Carbon Flux Attenuation

Within the CCE, which has high mesoscale variability and pronounced horizontal currents, we consider our drifting sediment traps to provide a more accurate estimate of carbon flux than ^{234}Th (see **Supplementary Materials**). Our supposition that the sediment traps have no substantial over- or under-collection bias is supported by a total of 56 paired sediment trap and ^{238}U–^{234}Th deficiency measurements showing good agreement (see "Results" section). Consequently, we use sediment trap values of carbon flux at deployment depths (typically near the base of the euphotic zone and at 100 m) and utilize ^{238}U–^{234}Th measurements to generate smooth profiles of CFA above, between, and below sediment trap deployment depths. Specifically, carbon flux at a depth horizon (D) can be quantified from ^{238}U–^{234}Th deficiency using a steady-state without advection equation:

$$\text{Flux}\,(D) = \text{CTh}(D) \times \int_0^D \lambda_{234} \times \text{Def}(z)dz \qquad (1)$$

where CTh(D) is the C:^{234}Th ratio of sinking particles at the depth horizon of interest, λ_{234} is the ^{234}Th decay constant, and Def(z) is the ^{238}U–^{234}Th deficiency at depth z, which is equal to the activity of ^{238}U minus the activity of ^{234}Th. CFA can thus be calculated from the first derivative of Eq. 1:

$$\text{CFA} = \frac{\partial\left(\text{CTh}(D)\right)}{\partial z} \times \int_0^D \left(\lambda_{234} \times \text{Def}(z)\right) dz + \lambda_{234} \times \text{Def}(D) \times \text{CTh}(D) \qquad (2)$$

Stukel et al. (2019) found a strong relationship between the C:^{234}Th ratio of sinking particles and the ratio of vertically integrated POC to vertically integrated total water column ^{234}Th (^{V}C:^{234}Th$_{tot}$). Using this equation allows us to determine CTh(D) as a smoothly varying function of D. For additional details see **Supplementary Appendix S1**.

Particle Sinking Speed

We estimate sinking speeds from microscopic analyses of fecal pellets collected in the sediment traps (Stukel et al., 2013; Morrow et al., 2018) and a relationship between fecal pellet size and sinking rate. A strong relationship between size and sinking speed is a consistent finding of studies that have quantified fecal pellet sinking rates (Small et al., 1979; Giesecke et al., 2010; Turner, 2015). Using fecal pellet sinking rate as a function of equivalent spherical diameter (ESD) data reviewed in Stukel et al. (2014), a power-law relationship suggests that sinking speed can be predicted from ESD:

$$\text{SinkingSpeed} = 436 \times \text{ESD}^{0.85} \qquad (3)$$

where sinking speed is in units of m day^{-1} and ESD is in units of mm. This relationship is derived from multiple studies spanning a range of taxonomic groups including appendicularians (Ploug et al., 2008), copepods and euphausiids (Smayda, 1971; Turner, 1977; Small et al., 1979; Yoon et al., 2001; Ploug et al., 2008), chaetognaths (Giesecke et al., 2010), and thaliaceans and pteropods (Bruland and Silver, 1981; Madin, 1982; Yoon et al., 2001). We thus expect it to be broadly representative of sinking rates of fecal pellets produced by the mixed zooplankton assemblages encountered in the southern CCE.

Flux-Feeding Calculations

The impact of flux-feeding zooplankters (such as a thecosome pteropod or phaeodarian) on particle flux can be quantified based on the effective cross-sectional area over which particles are collected (Jackson et al., 1993):

$$\frac{\partial F}{\partial z} = -\sigma_x N_x F \qquad (4)$$

where F is the flux of sinking particles and N_x is the numerical concentration of suspension feeders (N_{Aulo} is the abundance of Aulosphaeridae and N_{ptero} is the abundance of pteropods; all a function of depth). σ_x is the cross-sectional area over which the organisms are intercepting particles: $\sigma_x = \pi/4 \times \text{ESD}_{eff}^2$. Following Stukel et al. (2018a), ESD_{eff} is the effective diameter over which the organisms collect sinking particles and is dependent on both the diameter of the collection apparatus and

the average cross-sectional area of sinking particles. For the CCE, the effective diameter of sinking fecal pellets was calculated as D_{par} = 403 μm. We then calculate:

$$\sigma_{Aulo} = \frac{\pi}{4}\left(1.25 \times ESD_{Aulo} + D_{par}\right)^2 \quad (5)$$

$$\sigma_{ptero} = \frac{\pi}{4}\left(ESD_{Web} + D_{par}\right)^2 \quad (6)$$

where ESD_{Aulo} is the equivalent spherical diameter of Aulosphaeridae cells (measured separately by UVP5 for each cell) and ESD_{web} is the equivalent spherical diameter of a pteropod feeding web [assumed to be 45 mm based on summary in Gilmer and Harbison (1986)]. The factor of 1.25 in Eq. 6 represents the ratio of cell diameter (reported by UVP5) to diameter including radial spines.

Suspension-Feeding Calculations

The impact of suspension-feeding zooplankton (within which we include both true filter-feeders, e.g., appendicularians, and other organisms such as some herbivorous copepods that may use feeding currents that can be modeled as suspension-feeding) on particle flux attenuation can be calculated as:

$$\frac{\partial F}{\partial z} = -\frac{CR_0}{S} N_x F \quad (7)$$

where N_x is the number concentration of suspension feeders with a clearance rate of CR_0, and S is the sinking speed of the particles. The impact of suspension-feeding zooplankton thus depends on the range of sinking speeds of sinking particles. We calculated clearance rates using the allometric scaling relationship determined in Kiørboe (2011):

$$CR_0 = 10^{a+b\times\log_{10}(BC)} \times Q_{10}^{(T-15)/10} \quad (8)$$

where CR_0 is the clearance rate (mL day^{-1}), BC is the individual carbon content (g), a = 7.31 (±0.27), b = 1.01 (±0.05), and the Q_{10} used to account for temperature effects was assumed (following Hansen et al., 1997) to be 2.8.

We utilized zooplankton data from nighttime MOCNESS tows sorted into broad taxonomic and size groups using ZooScan. The choice to use only nighttime biomass likely leads to a conservative estimate of flux attenuation, because it excludes the activity of diel vertical migrants. This decision was made because these vertical migrants likely feed primarily in the surface layers and are not actively feeding at depth. The carbon biomass of individual organisms was determined using length:carbon relationships for different taxa as outlined in Table 1 of Stukel et al. (2013). We calculated clearance rates for four groups of potentially suspension-feeding mesozooplankton: copepods, euphausiids, appendicularians, and ostracods, while recognizing that some taxa include omnivores or predators. Nauplii and doliolids were also sorted in the samples, but their biomasses were low and hence are not considered further. Other taxa, including chaetognaths, were abundant, but are not suspension feeders.

RESULTS

Carbon Flux and Carbon Flux Attenuation

We used two independent estimates of particle flux (sediment traps and ^{238}U–^{234}Th) to test whether or not our estimates of particle flux (and particle flux attenuation) suffered from methodological biases (**Figure 2**). Comparisons between ^{234}Th flux collected in sediment traps and ^{234}Th flux estimated from ^{238}U:^{234}Th disequilibrium [computed using a one-dimensional, steady-state model without upwelling, Savoye et al. (2006)] showed strong agreement, with occasional outliers. The median ratio of sediment trap-derived flux to deficiency-derived flux was 0.998 suggesting near perfect agreement on a typical deployment. However, the overall mean of the sediment trap dataset was 6% higher than that of the Th deficiency dataset, suggesting that when there was a substantial disagreement, the sediment trap results were likely to be higher. This is not surprising in a dynamic system, where bloom decay can lead to spikes in particle export on faster time-scales than the approximately monthly temporal integration time-scale of ^{238}U–^{234}Th deficiency approaches. The overall agreement between sediment trap and thorium-based approaches suggests that our sediment traps had neither an over- nor an under-collection bias. Furthermore, our results suggest that although ^{234}Th-derived flux may not perfectly match with contemporaneous processes occurring in the surface layer, there is no reason to suspect that flux attenuation calculations based on ^{234}Th measurements will have a systematic bias.

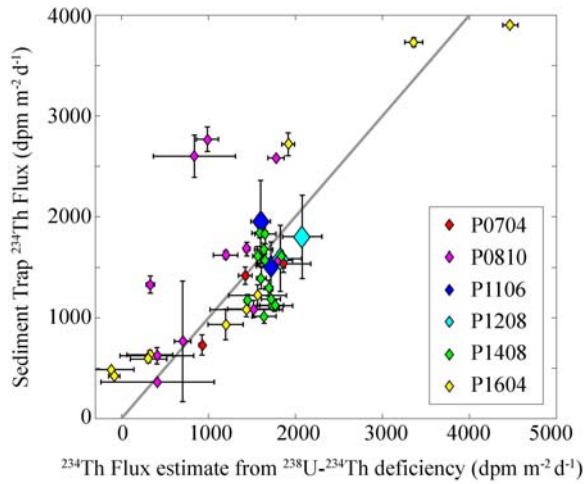

FIGURE 2 | Comparison of sediment trap and ^{238}U–^{234}Th deficiency measurements. *Y*-axis is ^{234}Th flux directly measured in sediment traps. *X*-axis is ^{234}Th flux estimated during the same cycle from ^{238}U–^{234}Th deficiency using a one-dimensional steady-state model without upwelling or diffusion. Note that for the P1106 and P1208 cruises, we plot only two data points each (representing cruise average results at the base of the euphotic zone or at 100 m). These cruise averages were used instead of a separate point for each cycle, because at the smaller spatial scales sampled on these "front" cruises ^{234}Th spatial patterns are likely driven as strongly by advection as by contemporaneous sinking flux.

Across the 30 Lagrangian cycles, POC flux (measured by sediment trap) at 100 m depth ranged from 2.6 to 24.9 mmol C m^{-2} day^{-1}. Export was higher in coastal areas than in the oligotrophic, offshore domain and there was a strong correlation between POC flux and both primary productivity and surface chl. When independent sediment trap export measurements were made at the base of the euphotic zone and at 100 m depth, the correlation (Spearman's ρ) between flux at these two depths was 0.72 (p = 0.002). This across-depth correlation was substantially weaker when only data from frontal regions (P1106 and P1208 Cruises) were analyzed (ρ = 0.49, p = 0.36) than when non-front data were considered (ρ = 0.92, $p = 4.5 \times 10^{-4}$). For all paired samples, the median ratio of sediment trap flux at 100 m to sediment trap flux near the base of the euphotic zone (shallow trap depths varied from 47 to 70 m) was 0.72, suggesting that approximately 28% of sinking POC could be expected to be remineralized before a depth of 100 m on these cycles.

To determine continuous profiles of carbon flux and CFA, we merged sediment trap data with ^{234}Th data. We restricted this flux attenuation analysis to the depth range from the base of the euphotic zone to a depth of 150 m, because at deeper depths we cannot constrain the C:^{234}Th ratio with certainty. The depth range of our flux attenuation calculations thus corresponds with the upper twilight zone, where zooplankton roles in flux attenuation have been hypothesized to be particularly important (Jackson and Checkley, 2011). CFA in the upper twilight zone was highly variable (**Figure 3A**). When comparing across all cycles, flux attenuation decreased with depth from a mean (across all cycles) flux attenuation of 913 μmol C m^{-2} day^{-1} decrease in flux over a 10 m depth range between 80 and 90 m (interquartile range was 57–874 μmol C m^{-2} day^{-1}/10 m) to a mean of 495 μmol C m^{-2} day^{-1}/10 m (interquartile = 328–692 μmol C m^{-2} day^{-1}/10 m) between 140 and 150 m depth. Additional patterns can be seen when considering the oligotrophic and high biomass cycles separately. For the oligotrophic cycles, the base of the euphotic zone (1% light level) was typically in the range of 60–80 m. We thus considered flux attenuation starting at the deeper limit of this range. Flux attenuation increased with depth from a mean of 231 μmol C m^{-2} day^{-1}/10 m (interquartile = −82 to 418.5) in the 80–90 m depth range to a mean of 503 μmol C m^{-2} day^{-1}/10 m (interquartile = 233–799) in the 100–110 m depth range. Beneath this depth flux attenuation declined gradually (**Figure 3B**). For the high biomass cycles a similar pattern was seen. Flux attenuation over the 50–60 m depth range in the high biomass cycles averaged 595 μmol C m^{-2} day^{-1}/10 m (interquartile = −338 to 1221) and increased to 1503 μmol C m^{-2} day^{-1}/10 m (interquartile = 514–1.981) in the 80–90 m depth range.

In contrast to absolute flux attenuation, the percentage of flux remineralized over a 10-m depth range did not decrease beneath 100 m (**Figures 3D–F**). Instead, relative flux attenuation increased somewhat from near the base of the euphotic zone to 150 m. This pattern was relatively consistent when restricting analyses to the oligotrophic cycles (**Figure 3E**), but was less distinct in the high biomass cycles (**Figure 3F**). Nevertheless, across depth and regions, relative CFA was typically in the range of 6–10% of carbon flux remineralized over a 10-m depth range. The median relative flux attenuation in the shallow twilight zone varied from 6.0 to 9.0% of flux/10 m (mean ranged

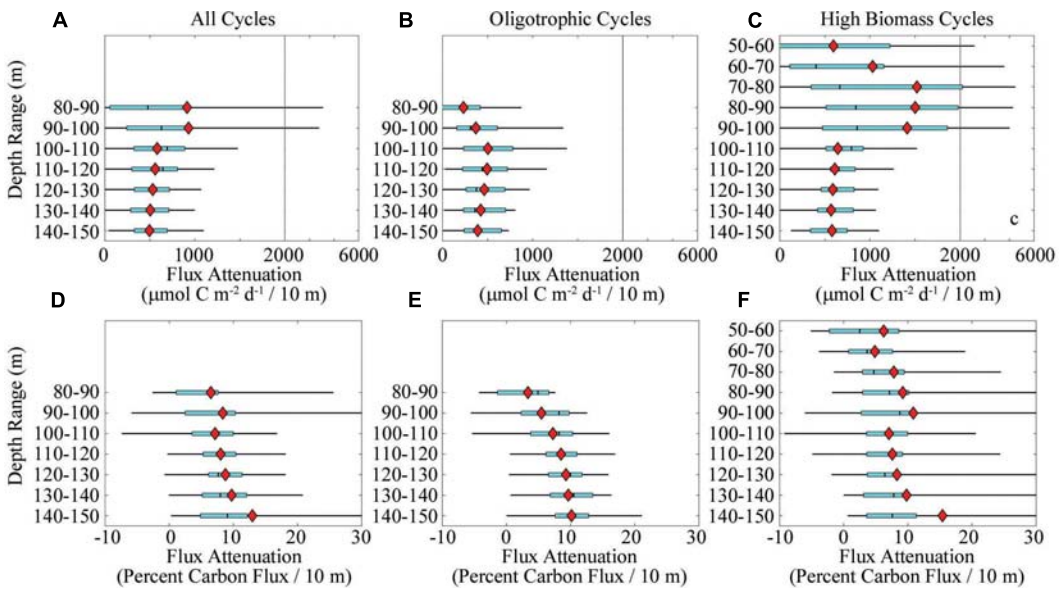

FIGURE 3 | Carbon flux attenuation determined by merging sediment trap and ^{238}U–^{234}Th deficiency data. Panels **(A–C)** show absolute flux attenuation over 10 m depth bins (note break in flux scale at 2000 μmol C m^{-2} day^{-1}/10 m). Panels **(D–F)** show relative flux attenuation over 10 m depth bins. In all panels, light blue boxes show quartiles (median is black line) and thin black lines show 95% confidence intervals (computed using MATLAB function quantile). Red diamonds are arithmetic mean value. Panels **(A)** and **(D)** show data for all cycles. Panels **(B)** and **(E)** show data for cycles with surface chl <0.5 μg Chl a L^{-1}. Panels **(E)** and **(F)** show data for cycles with surface chl >0.5 μg Chl a L^{-1}.

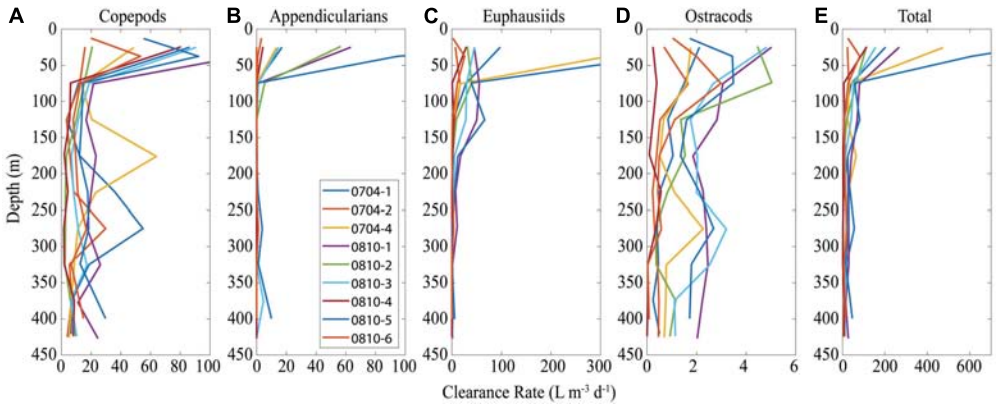

FIGURE 4 | Clearance rates for copepods **(A)**, appendicularians **(B)**, euphausiids **(C)**, ostracods **(D)**, and the sum of all four groups **(E)**. Each plot shows results within 50-m bins as collected by MOCNESS tows and computed using Eq. 8.

from 6.5 to 13%/10 m). This sets a reasonable expectation for the amount of flux attenuation that must be mediated by the combined mesopelagic microbial, mesozooplankton, and nekton communities.

Suspension-Feeding Zooplankton and Particle Flux Attenuation

Suspension-feeding crustaceans are the most abundant (by carbon biomass) ecological category of zooplankton in the CCE (Lavaniegos and Ohman, 2007). To quantify the potential role of these suspension feeders, we utilized data from nighttime MOCNESS tows in the CCE. Suspension-feeder biomass in the mesopelagic was typically dominated by copepods and euphausiids (**Supplementary Figure S2**). Between 100 and 450 m depth, copepod biomass was typically in the range of 1–3 mg C m^{-3}. Euphausiid biomass was almost always <1 mg C m^{-3} at depths deeper than 200 m (and typically <0.4 mg C m^{-3}) but was greater in the shallow mesopelagic. Ostracods had substantially lower biomass, never exceeding 0.6 mg C m^{-3} in the mesopelagic. Appendicularians, while occasionally abundant in the euphotic zone, were also relatively minor contributors to total suspension-feeder biomass in the mesopelagic.

Community clearance rates ranged from 2 to 81 L m^{-3} day^{-1} in the mesopelagic, which corresponds to mesozooplankton clearing between 0.2 and 8.1% of the water each day (**Figure 4**). Clearance rates were dominated by copepods and euphausiids, with copepods dominating beneath 150 m and both having substantial contributions at shallower depths.

The impact of suspension feeders on particle flux attenuation depends on the average sinking rates of particles. We chose P0704-1 as a cycle with typical community clearance rates and calculated flux attenuation for particles with a full range of sinking speeds (**Figure 5**). For particles with a sinking speed of 1 m day^{-1}, nearly all flux would be consumed by suspension feeders within 50 m of the depth of particle creation. By contrast, for particles sinking at a speed of 10 m day^{-1}, only ∼70% of flux would be expected to be consumed before particles reach a depth of 450 m. For particles sinking at a rate of >50 m day^{-1}, the impact of suspension feeders becomes negligible. Comparing data from all cycles, we see a similar pattern. If particles sink at 1 m day^{-1}, anywhere from ∼5 to 50% of sinking particles would be consumed over a 10 m depth range (**Figure 6A**). For particles sinking with a speed of 10 m day^{-1}, particle flux attenuation was typically <4%/10 m and for particles sinking at a speed of 100 m day^{-1}, particle flux attenuation was always <1%/10 m and typically <0.4%/10 m.

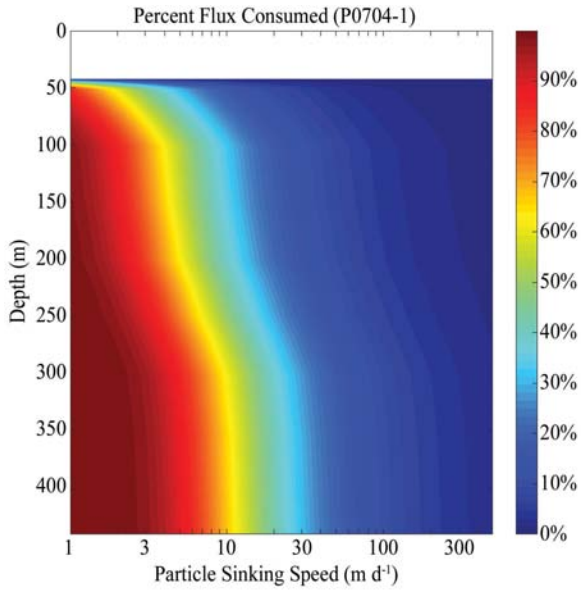

FIGURE 5 | Cumulative percent carbon flux consumed by suspension feeders by a certain depth for particles with different sinking speeds (*x*-axis). Data is for P0704 Cycle 1.

To investigate typical particle sinking speeds, we measured the abundance and size of recognizable fecal pellets collected in sediment traps. These pellets were almost always the dominant visually identifiable component of the sinking material, although

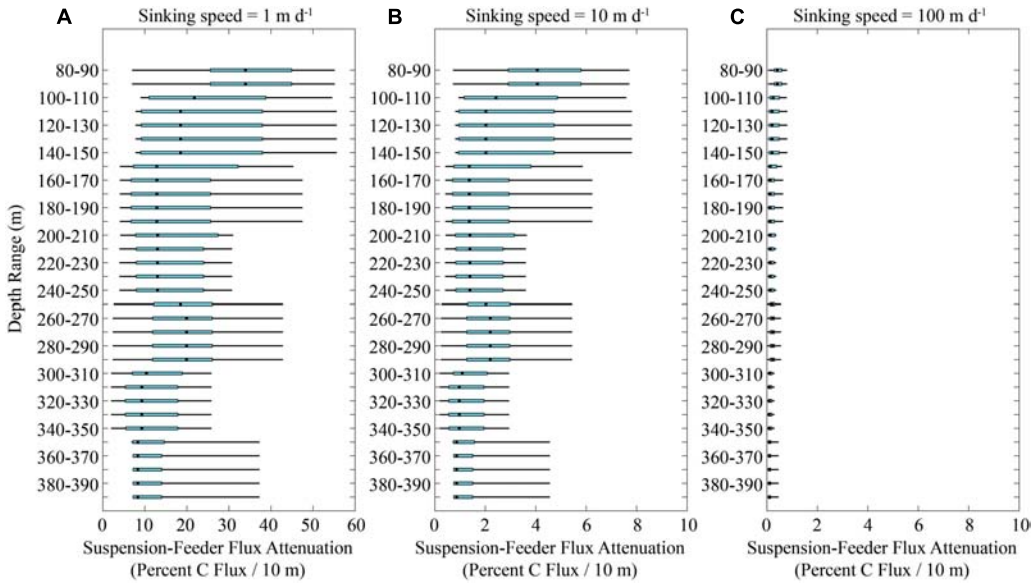

FIGURE 6 | Computed carbon flux attenuation mediated by suspension-feeding copepods, euphausiids, appendicularians, and ostracods if particles are sinking at 1 m day^{-1} **(A)**, 10 m day^{-1} **(B)**, or 100 m day^{-1} **(C)**. Light blue boxes show quartiles (median is black line) and thin black lines show 95% confidence intervals (computed using MATLAB function quantile).

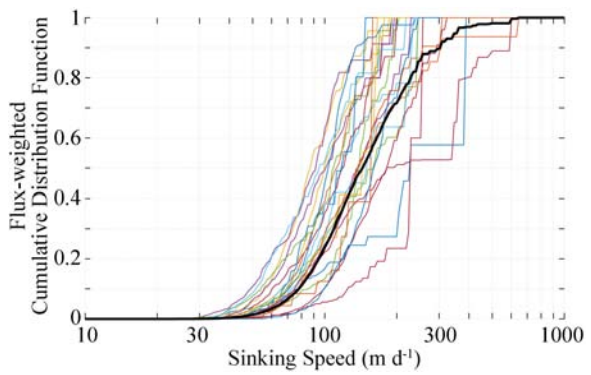

FIGURE 7 | Flux weighted cumulative distribution function for fecal pellets with different sinking speeds. Fecal pellet sinking speeds were calculated from morphometric measurements of fecal pellets collected in sediment traps and Eq. 3. Colored lines are results from individual samples. Black line is the flux-weighted mean of all samples.

in the oligotrophic regions the identifiable pellets typically comprised less than half of total carbon flux. We applied allometric–scaling relationships between sinking speed and fecal pellet size to estimate fecal pellet settling velocities. Across all samples, half of the fecal pellet carbon flux was mediated by pellets sinking at a speed slower than 141 m day^{-1} (**Figure 7**). Only 10% of the flux was due to pellets sinking slower than 78 m day^{-1} and only 1% was derived from pellets sinking slower than 46 m day^{-1}. Even for the cycle most dominated by small fecal pellets, half of the pellet flux was due to pellets sinking faster than 85 m day^{-1}. When considering these results in light of the calculated impact of suspension-feeding zooplankton on flux attenuation of particles with average sinking speeds in the range of 100 m day^{-1}, it becomes clear that suspension-feeding mesozooplankton are not likely to be playing a dominant role in CFA in the mesopelagic. This does not mean, however, that they play no role in flux attenuation. Rather, the abundance and activity of suspension feeders in the epipelagic may be the reason that so few slowly sinking particles were collected in sediment traps beneath the euphotic zone.

Flux-Feeding Zooplankton and Particle Flux Attenuation

To investigate the potential role of flux- feeding zooplankton in CFA, we quantified the abundances of two prominent taxa of flux feeders in the CCE: Aulosphaeridae (a phaeodarian) and *L. helicina* (a thecosome pteropod). These are certainly not the only flux-feeding zooplankton in the CCE, hence our calculations of the total contribution of flux feeders should be considered quite conservative.

Aulosphaeridae abundance consistently peaked in the shallow twilight zone between 50 and 150 m depth (**Figures 8A–E**). Abundances were substantially higher on the P0810 and P1106 cruises (peak cycle average abundances reaching >500 cells m^{-3}) than on the warm period cruises (P1408 and P1604, peak abundances <50 cells m^{-3}). Unlike most other plankton community and biogeochemical measurements, there was not a strong correlation between Aulosphaeridae abundance and primary productivity (cf. Biard and Ohman, 2019). Using Eqs 4 and 5, we quantified the potential impact of Aulosphaeridae on CFA (**Figures 8F–H**). Despite high variability, Aulosphaeridae often had an important role in flux attenuation. Near the depth

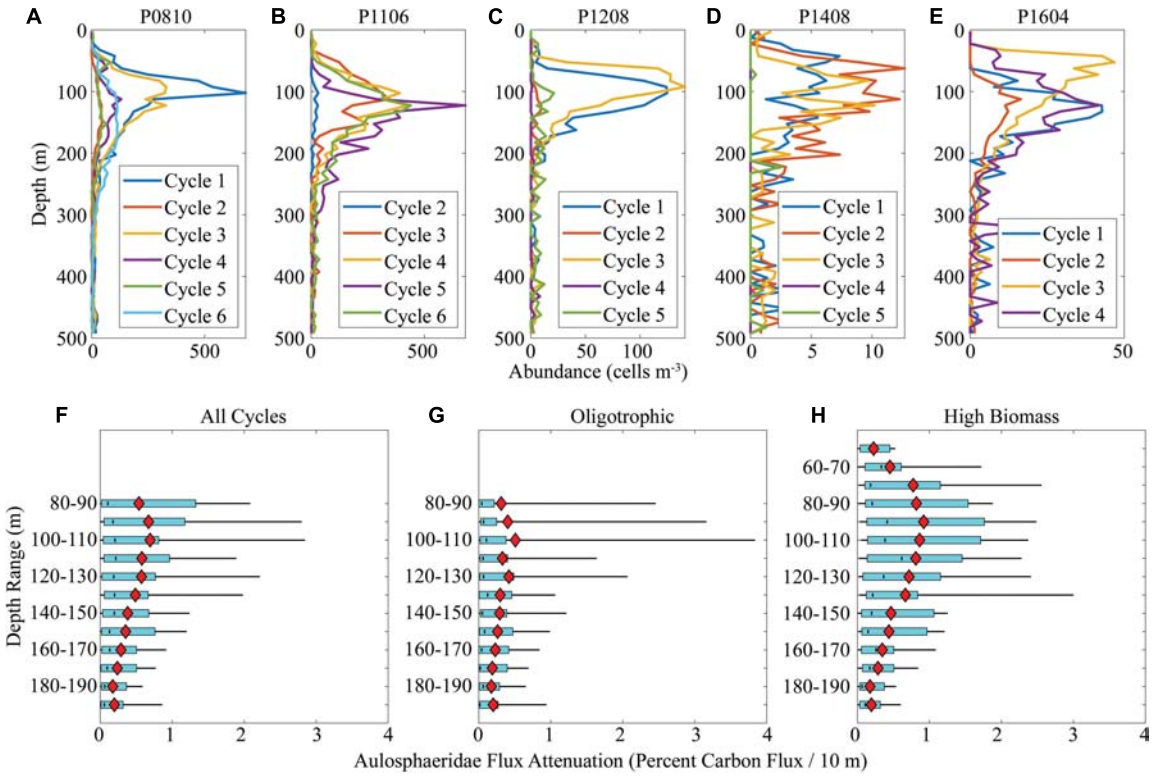

FIGURE 8 | Abundance **(A–E)** and flux attenuation **(F–H)** of Aulosphaeridae. Note the different *x*-axis scales used in panels **(A–E)** that were necessary because of high inter-cruise variability in Aulosphaeridae abundance. Panels **(F–H)** show computed flux attenuation mediated by Aulosphaeridae. Light blue boxes show quartiles (median is black line) and thin black lines show 95% confidence intervals (computed using MATLAB function quantile). Red diamonds are arithmetic mean value.

of peak Aulosphaeridae abundance (∼100 m), the mean (across all cycles) flux attenuation attributable to Aulosphaeridae was 0.69%/10 m (median = 0.21%/10 m, interquartile range = 0.04–0.81%). The maximum Aulosphaeridae flux attenuation (Cycle P0810-1, 100–110 m depth range) was 4.2%/10 m. For comparison, the total flux attenuation mediated by all abiotic and biotic factors (as assessed using sediment traps and ^{234}Th) was typically in the range of 6–10%/10 m. Thus, the Aulosphaeridae (a single family of phaeodarians) can play a substantial role in CFA, although at most times its contribution is <5% of total flux attenuation.

Limacina helicina was only quantified in MOCNESS samples from two cycles (P1208-3, which had a 31-m deep euphotic zone, and P1208-4, which had a 70-m euphotic zone). *L. helicina* abundances typically declined from peak abundances of ∼0.5–2 individuals m^{-3} in the upper 100 m of the water column to <0.2 individuals m^{-3} beneath 100 m depth (**Figure 9A**). We computed (using Eqs 4 and 6) the potential role of *L. helicina* in intercepting sinking particles and found that they could potentially intercept between 4 and 10% of sinking particles between the base of the euphotic zone and a depth of 400 m (**Figure 9B**). However, their impact was concentrated just below the base of the euphotic zone, where on Cycle P1208-3 they consumed an average of 1.2–1.6% of carbon flux/10 m and on P1208-4 they consumed an average of 0.45–0.81%/10 m (**Figures 9C,D**). As for the Aulosphaeridae, the evidence suggests that this species can intercept a substantial portion of the sinking particles, but their impact is concentrated on the region immediately beneath the euphotic zone.

DISCUSSION

Zooplankton as Gatekeepers to the Mesopelagic

Zooplankton play diverse roles in the epi- and mesopelagic (Steinberg and Landry, 2017). Our results show that suspension-feeding mesozooplankton (especially copepods and euphausiids) are abundant in the twilight zone and can have substantial clearance rates on the magnitude of 50 L m^{-3} day^{-1} (**Figure 4** and **Supplementary Figure S2**). However, these clearance rates are not sufficient to give them a meaningful impact on CFA of the particles sinking at ∼100 m day^{-1}, which dominate flux in the region (**Figures 5**, **6**). Instead, their activity leads to near complete consumption of slowly sinking particles near the base of the euphotic zone. This is likely a general result, because studies focused on *in situ* measurement of particle sinking speeds often find typical velocities on the order of 100 m day^{-1} beneath the euphotic zone (Alldredge and Gotschalk, 1988; Trull et al., 2008; Armstrong et al., 2009; McDonnell and Buesseler, 2010;

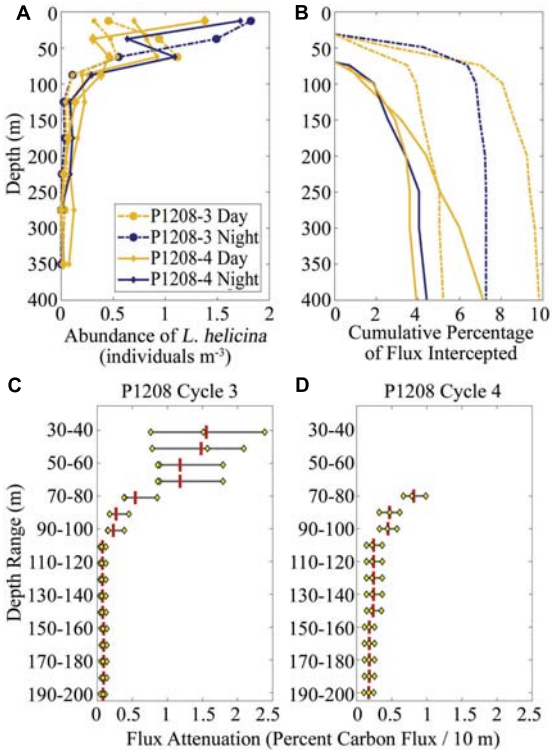

FIGURE 9 | Importance of pteropods to flux attenuation. The abundance of *Limacina helicina* in MOCNESS tows conducted during two cycles on the P1208 cruise from Bednaršek and Ohman (2015) **(A)**. The cumulative percentage of flux intercepted by *L. helicina* based on abundances measured during each MOCNESS tow and assuming a 45-mm diameter for the mucous feeding web **(B)**. Cumulative percentage flux is calculated starting at the base of the euphotic zone (1% light level), which was at 30 m on P1208-3 and 70 m on P1208-4. Panels **(C)** and **(D)** show computed flux attenuation mediated by Aulosphaeridae. Black line shows the range of values measured on the three tows for each Cycle (which are depicted as yellow diamonds). Vertical red line is arithmetic mean.

Jackson et al., 2015). It may also partially explain the rapid decrease in marine snow abundance beneath the euphotic zone (Lampitt et al., 1993; Jackson and Checkley, 2011), particularly if these aggregates are assumed to have heterogeneous compositions that lead to a wide range of sinking speeds.

We also note that our calculations were based on nighttime net tows, thus largely excluding any potential impacts of diel vertically migrating suspension feeders. This decision was based on the assumption that diel vertical migrants feed primarily in the surface layers, not at depth. If we calculate clearance rates based on daytime net tows, we find increased mesopelagic clearance rates, particularly at depths between 150 and 250 m. However, this increased clearance rate (daytime values were typically 50% higher than nighttime values) still resulted in a low impact of suspension-feeders on rapidly sinking (100 m day^{-1}) particles (median across all cycles was <0.4%/10 at all depths), except for Cycle P0810-3. During this cycle, abundant vertically migrating euphausiids were present and, if they were feeding at depth, the total suspension-feeding community could have been responsible for attenuation of 4% of C flux/10 m during daytime hours (in the depth range 200–250 m). Notably, *Euphausia pacifica* (one of the dominant euphausiids in the CCE) has been shown to play an important role in disaggregation of marine snow in the euphotic zone (Dilling and Alldredge, 2000). However, it is unlikely that they swim as rapidly at their daytime resting depths as they do while actively feeding in the surface ocean. It is thus not currently possible to extrapolate their potential impacts on rapidly sinking particles.

Despite their comparatively weak capacity for intercepting rapidly sinking particles, suspension-feeding zooplankton in the mesopelagic have substantial carbon demands in the CCE (Kelly et al., unpublished) and many other ecosystems (Hernández-Leon and Ikeda et al., 2005; Steinberg et al., 2008b; Burd et al., 2010; Robinson et al., 2010; Schukat et al., 2013; Proud et al., 2017). Potential food sources include slowly sinking particles produced in the euphotic zone, free-living mesopelagic protists, particle-attached protists and microbes that may have been released from sinking particles, and carnivory on vertically migrating or mesopelagic resident zooplankton. Slowly sinking particles may also be generated from rapidly sinking particles through the swimming or feeding actions of mesozooplankton (Dilling and Alldredge, 2000; Goldthwait et al., 2004; Iversen and Poulsen, 2007). Indeed, such particle transformations, whether mediated by zooplankton, microbes, or abiotic processes, are likely to continually generate additional slowly sinking particles throughout the water column. However, these slowly sinking particles should not be expected to contribute substantially to particle flux in regions with abundant suspension-feeding zooplankton, because the suspension feeders will efficiently consume slowly sinking particles (e.g., **Figure 6A**).

In contrast, flux-feeding zooplankton can be substantial loss terms for rapidly sinking particles. The mean percentage flux attenuation for Aulosphaeridae in the shallow mesopelagic was 0.69%/10-m depth horizon corresponding to the depth of maximum Aulosphaeridae abundance (**Figure 8**). For comparison, in the same depth range total flux averaged 7.1%/10 m (**Figure 3**). This implies that a single family of giant Rhizaria (∼2-mm) may be responsible for nearly 10% of the flux attenuation in the layer immediately beneath the euphotic zone. Similarly, the pteropod *L. helicina* is abundant beneath the euphotic zone and may be responsible for ∼10–20% of total flux attenuation in the depth ranges where it is most common. These are certainly not the only flux feeders in the CCE. Many other pteropod and rhizarian taxa occur in the CCE (Kling and Boltovskoy, 1995; Bednaršek and Ohman, 2015; Biard and Ohman, 2019). Flux feeding has also been suggested for the copepods *Neocalanus cristatus* and *Spinocalanus antarcticus* (Dagg, 1993; Kosobokova et al., 2002) and the polychaetes *Poeobius* and *Poecilochaetus* (Hamner et al., 1975; Uttal and Buck, 1996; Christiansen et al., 2018). Flux feeding may also be a part-time feeding mode used by a diverse class of organisms during low food periods. For instance, in the absence of phytoplankton prey, the copepod *Acartia tonsa* will behave as a non-motile feeder that will occasionally feed on fecal pellets that pass within its detection radius (Poulsen and Kiorboe, 2005). It is unknown if such behavior is widespread amongst the abundant diel vertically

migrating zooplankton that spend half of their life in the low-prey mesopelagic environment. Another similar strategy has been termed "active flux feeding" or "plume finding" by Stemmann et al. (2004b) and involves cruise-feeding copepods that detect the solute plume behind a sinking aggregate (Kiørboe and Thygesen, 2001), leading to capture rates that are dependent on sinking speed. We could not quantify the impact of this feeding strategy, because the taxa that utilize it have not been identified. However, if it is widespread amongst mesopelagic copepods [as assumed by Stemmann et al. (2004a)] it would lead to substantially greater attenuation of particle flux in the twilight zone.

Also of import, these flux feeders not only intercept and consume sinking particles, but also produce sinking fecal pellets. *L. helicina* fecal pellets have been shown to contribute 19% of the POC flux in a coastal bay near Antarctica (Manno et al., 2009), while "mini-pellets" produced by phaeodarians were abundant contributors to sinking flux in the Eastern Tropical Pacific and Northeast Atlantic (Gowing and Silver, 1985; Lampitt et al., 2009). Furthermore, due to their dense aragonite shells and siliceous tests, respectively, dead pteropods and phaeodarians likely contribute substantially to sinking flux and are often found in sediment trap material (Takahashi and Honjo, 1981; Bathmann et al., 1991; Fabry and Deuser, 1992; Michaels et al., 1995; Biard et al., 2018). Future research will need to focus on the roles of these organisms in transforming not just the quantity but also the quality of sinking particles in the mesopelagic.

Microbes and Zooplankton in the Mesopelagic

The abundance (and impact on flux attenuation) of suspension-feeding and flux-feeding zooplankton generally decreases with depth in the mesopelagic. In particular, the flux-feeding zooplankton that we believe play a disproportionately strong role in twilight zone flux attenuation both decreased sharply in abundance beneath a depth of ∼100 m. However, the percentage (but not absolute magnitude) of CFA increased slightly with depth between 80 and 150 m depth (**Figure 3**). While the substantial variability in flux attenuation profiles prevents us from making definitive conclusions about these patterns, this mismatch between flux attenuation patterns determined from bulk flux estimates (sediment traps and ^{234}Th) and the abundance of flux feeders points to the importance of other sources of carbon remineralization. Stemmann et al. (2004a) suggested based on modeling results for the Mediterranean Sea that flux feeders may be particularly important in the shallow twilight zone, while microbial degradation becomes increasingly important at the lower particle concentrations experienced in deeper waters. Such a result seems plausible for multiple reasons. First, free-living zooplankton will have substantially greater difficulty obtaining sufficient energy for basal metabolic needs and respiration in the deeper ocean, while particle-attached microbes should have ample food at all depths. Second, the abundance of particle-attached microbes on a sinking particle may be expected to increase with age (and depth) of the particle, because it may be continually colonized by new microbes while it sinks, and these microbes are likely to multiply on the sinking particle.

Results from other studies in the CCE can highlight the potential impact of microbes. Simon et al. (1990) estimated that marine snow turnover times with respect to bacterial remineralization ranged from 20 to 100 d. This is similar to the turnover times expected to be mediated by suspension-feeding zooplankton, and suggests that bacteria have only a minor impact on the flux of rapidly sinking particles. However, Samo et al. (2012) measured bacterial carbon production rates (including particle-attached and free-living bacteria) at a depth of 100 m that ranged from ∼10 to 100 μmol C m^{-3} day^{-1}. For comparison, we quantified that the total flux attenuation at this depth was 75 μmol C m^{-3} day^{-1} (median = 66 μmol C m^{-3} day^{-1}; 95% confidence interval of up to 313 μmol C m^{-3} day^{-1}). It is also unclear whether decomposition rates for marine snow aggregates are comparable to those of the fecal pellets that dominate sediment trap material in the CCE. Gowing and Silver (1983) suggested that fecal pellets collected near our study region had substantial contributions of interior bacteria that likely originated as enteric or ingested, but digestion-resistant bacteria. These communities would likely be substantially different, and with different biogeochemical impacts, than those found on aggregates.

Heterotrophic protists can also play dominant roles in the microbial communities consuming fecal pellets (Poulsen and Iversen, 2008). Gutierrez-Rodriguez et al. (2018) used 18S sequencing to investigate protistan sequences in sediment traps on our P1408 cruise. They found a consistent and substantial increase in the relative contribution of dinophytes in un-preserved trap samples relative to formaldehyde-preserved trap samples. Dinophytes typically increased from <10% of total protistan reads to >50%, despite deployment times that were only 3.25 days. Stramenopiles (mainly heterotrophic nanoflagellate taxa) also increased in the unpreserved samples. This suggests potentially rapid growth rates for these protists on sinking particles, with a commensurate role in feeding on either detritus contained in the sinking particles or other microbial taxa transported within the particles.

Multiple studies from other regions have investigated the differing roles of zooplankton and microbes in the mesopelagic (Simon et al., 2002; Robinson et al., 2010; Steinberg and Landry, 2017). Steinberg et al. (2008b) found that bacterial carbon demand exceeded zooplankton demand in the North Pacific subtropical gyre by a factor of 3, although the two were approximately equal in the subarctic gyre. The combined respiration of these two groups was found to be larger than that entering the mesopelagic through sinking particles, a result that has been consistently found in other regions including the subtropical and north Atlantic (Boyd et al., 1999; Reinthaler et al., 2006; Baltar et al., 2009). There are also likely to be extensive synergistic and antagonistic interactions between zooplankton and microbes in the mesopelagic. Zooplankton egestion and excretion at depth provide available organic matter for bacteria (Hannides et al., 2009; Saba et al., 2011; Kiko et al., 2016). Release of organic matter mediated by extracellular enzymes produced by bacteria may contribute to the formation of plumes behind sinking particles that aid zooplankton's abilities to

find such particles (Kiørboe and Thygesen, 2001; Arnosti, 2011). The microbial communities themselves may also serve as nutrient- and carbon-rich food sources for zooplankton (Wilson et al., 2010). It is even possible that fragmentation of particles by mesozooplankton serves to enhance microbial activity and trophic transfer to mesozooplankton (Mayor et al., 2014). Unraveling these potential interactions will require collaborative efforts between microbial and zooplankton ecologists and biogeochemists.

Epipelagic-Mesopelagic Coupling in the CCE

Our result that suspension-feeding zooplankton are abundant in the mesopelagic, but play only minor roles in consuming sinking particles, raises important questions about how they satisfy their metabolic demands. Based on results from our P0704 and P0810 cruises, Kelly et al. (unpublished) estimated that total mesozooplankton (mostly suspension-feeders) respiration in the mesopelagic ranged from 3.2 to 18 mg C m^{-2} day^{-1} across these cruises. These values substantially exceed the total carbon that we calculate suspension-feeders would be able to consume from rapidly sinking particles settling through the mesopelagic. However, the Kelly et al. (unpublished) results also suggest a resolution to this apparent imbalance. Diel vertically migrating taxa were abundant in the region and their active transport provides substantial energy subsidies to mesopelagic food webs. Mesopelagic resident organisms derive energy directly (through predation) and indirectly (through their release of dissolved organic carbon that supports microbial communities) from vertical migrants. Indeed, results showed that nearly half of the organic matter consumed by mesopelagic resident mesozooplankton was derived (directly or indirectly) from foodweb pathways that originated with active transport by vertical migrants rather than pathways originating from sinking particle flux (Kelly et al., unpublished).

This highlights an important reality of mesopelagic ecosystems. Although we most often think of these ecosystems as being supported by sinking particles (and to a lesser extent diel vertical migration), mesopelagic communities feature complex ecological relationships between particle-attached and free-living bacteria, protistan bacterivores, and zooplankton (Robinson et al., 2010). These zooplankton communities are diverse and have many feeding modes including suspension-feeding (likely on protists and suspended organic matter), flux-feeding, predation, and parasitism (Steinberg et al., 2008a; Wilson et al., 2010; Bode et al., 2015). The quality (in addition to quantity) of sinking particles also changes with depth as these particles are modified by microbial and zooplankton communities, new particles are created through defecation, mortality, molting, and discarded feeding webs, and particle size spectra are reshaped by aggregation and disaggregation (Wakeham et al., 1997; Burd and Jackson, 2009; Turner, 2015). Future studies are necessary to fully investigate the impacts of these different feeding traits on the BCP (Barton et al., 2013) and the impacts that future warming, ocean acidification, changes in optical attenuation, and potential shoaling of the oxycline may have on mesopelagic zooplankton communities (Richardson, 2008; Wishner et al., 2013; Cripps et al., 2014; Hauss et al., 2016; Ohman and Romagnan, 2016).

CONCLUSION

Our results offer compelling evidence that two flux-feeding zooplankton taxa (the phaeodarian Aulophaeridae and the pterpopod *L. helicina*) can exert substantial impact on sinking particles in the shallow twilight zone. Both taxa have the capacity to consume greater than 1% of sinking particles per 10-m vertical depth range at the depths at which they are most abundant, which equates to ∼10–20% of total CFA across those same depth ranges (typically the first 50–100 m beneath the euphotic zone). These are unlikely to be the only flux feeders in the mesopelagic. Indeed many other rhizarians and pteropods are found in the CCE and many other taxa are suspected of full or part-time flux-feeding behavior. Flux-feeders are likely particularly important in consuming rapidly sinking particles that would otherwise penetrate into the deep ocean. The abundance of suspension-feeding zooplankton in the ocean suggests that slowly sinking particles will have a relatively minor contribution to sinking carbon flux in the mesopelagic because they will be rapidly consumed. While our results suggest that feeding mode leads to very different biogeochemical importance for these functional groups of zooplankton, substantial work is needed to directly quantify the impact of these organisms *in situ* and to investigate the spatial and temporal distributions of each feeding trait amongst the diverse zooplankton communities found in the ocean (Barton et al., 2013). The qualitatively different impact of each feeding mode on remineralization length scales in the ocean further suggests that flux feeders should be included in modeling efforts undertaken to investigate marine carbon sequestration.

DATA AVAILABILITY

The datasets generated for this study are available on request to the corresponding author.

AUTHOR CONTRIBUTIONS

MS and TK were responsible for the sediment trap and thorium measurements. MO was responsible for the MOCNESS zooplankton data. MO and TB were responsible for the UVP deployments. TB was responsible for the UVP rhizarian analyses. MS wrote the manuscript. All authors edited the final version of the manuscript.

FUNDING

This work was funded by the NSF Bio OCE grants to the CCE LTER Program: OCE-0417616, OCE-1026607, OCE-1637632, and OCE-1614359. A portion of this work was performed at the

National High Magnetic Field Laboratory, which is supported by the National Science Foundation Cooperative Agreement No. DMR-1644779 and the State of Florida.

ACKNOWLEDGMENTS

We thank the captains and crews of the R. V. Melville, R. V. Thompson, and R. V. Sikuliaq as well as our many collaborators in the CCE LTER Program, without them this study would not have been possible. We also thank N. Bednaršek for the pteropod enumerations. Data used in this manuscript can be found on the CCE LTER DataZoo website: https://oceaninformatics.ucsd.edu/datazoo/catalogs/ccelter/datasets.

SUPPLEMENTARY MATERIAL

The Supplementary Material for this article can be found online at: https://www.frontiersin.org/articles/10.3389/fmars.2019.00397/full#supplementary-material

REFERENCES

Alcaraz, M., Almeda, R., Calbet, A., Saiz, E., Duarte, C. M., Lasternas, S., et al. (2010). The role of arctic zooplankton in biogeochemical cycles: respiration and excretion of ammonia and phosphate during summer. *Polar Biol.* 33, 1719–1731. doi: 10.1007/s00300-010-0789-9

Alldredge, A. L. (1976). Discarded appendicularian houses as sources of food, surface habitats, and particulate organic matter in planktonic environments. *Limnol. Oceanogr.* 21, 14–23.

Alldredge, A. L., and Gotschalk, C. (1988). In situ settling behavior of marine snow. *Limnol. Oceanogr.* 33, 339–351. doi: 10.1016/j.scitotenv.2016.09.115

Archibald, K. M., Siegel, D. A., and Doney, S. C. (2019). Modeling the impact of zooplankton diel vertical migration on the carbon export flux of the biological pump. *Global Biogeochem. Cycles* 33, 181–199. doi: 10.1029/2018gb005983

Armstrong, R. A., Peterson, M. L., Lee, C., and Wakeham, S. G. (2009). Settling velocity spectra and the ballast ratio hypothesis. *Deep Sea Res. II* 56, 1470–1478. doi: 10.1016/j.dsr2.2008.11.032

Arnosti, C. (2011). "Microbial extracellular enzymes and the marine carbon cycle," in *Annual Review of Marine Science*, Vol. 3, eds C. A. Carlson and S. J. Giovannoni (Palo Alto: Annual Reviews), 401–425. doi: 10.1146/annurev-marine-120709-142731

Asher, E., Dacey, J., Stukel, M., Long, M., and Tortell, P. (2016). Processes driving seasonal variability in DMS, DMSP, and DMSO concentrations and turnover in coastal Antarctic waters. *Limnol. Oceanogr.* 62, 104–124. doi: 10.1002/lno.10379

Baines, S. B., Chen, X., Twining, B. S., Fisher, N. S., and Landry, M. R. (2016). Factors affecting Fe and Zn contents of mesozooplankton from the Costa Rica Dome. *J. Plankton Res.* 38, 331–347. doi: 10.1093/plankt/fbv098

Baltar, F., Arístegui, J., Gasol, J. M., Sintes, E., and Herndl, G. J. (2009). Evidence of prokaryotic metabolism on suspended particulate organic matter in the dark waters of the subtropical North Atlantic. *Limnol. Oceanogr.* 54, 182–193. doi: 10.4319/lo.2009.54.1.0182

Barton, A. D., Pershing, A. J., Litchman, E., Record, N. R., Edwards, K. F., Finkel, Z. V., et al. (2013). The biogeography of marine plankton traits. *Ecol. Lett.* 16, 522–534. doi: 10.1111/ele.12063

Bathmann, U. V., Noji, T. T., and Von Bodungen, B. (1991). Sedimentation of pteropods in the Norwegian Sea in autumn. *Deep Sea Res. Part A Oceanogr. Res. Pap.* 38, 1341–1360. doi: 10.1016/0198-0149(91)90031-a

Bednaršek, N., Možina, J., Vogt, M., O'brien, C., and Tarling, G. (2012). The global distribution of pteropods and their contribution to carbonate and carbon biomass in the modern ocean. *Earth Syst. Sci. Data* 4, 167–186. doi: 10.5194/essd-4-167-2012

Bednaršek, N., and Ohman, M. D. (2015). Changes in pteropod distributions and shell dissolution across a frontal system in the California current system. *Mar. Ecol. Progr. Ser.* 523, 93–103. doi: 10.3354/meps11199

Benitez-Nelson, C. R., Buesseler, K. O., Van Der Loeff, M. R., Andrews, J., Ball, L., Crossin, G., et al. (2001). Testing a new small-volume technique for determining Th-234 in seawater. *J. Radioanal. Nuclear Chem.* 248, 795–799.

Bianchi, D., Galbraith, E. D., Carozza, D. A., Mislan, K. A. S., and Stock, C. A. (2013). Intensification of open-ocean oxygen depletion by vertically migrating animals. *Nat. Geosci.* 6, 545–548. doi: 10.1038/ngeo1837

Biard, T., Krause, J. W., Stukel, M. R., and Ohman, M. D. (2018). The significance of giant phaeodarians (Rhizaria) to biogenic silica export in the california current ecosystem. *Global Biogeochem. Cycles* 32, 987–1004. doi: 10.1029/2018gb005877

Biard, T., and Ohman, M. D. (2019). Vertical niche definition of test-bearing protists (Rhizaria) into the twilight zone revealed by in situ imaging. *bioRxiv*

Biard, T., Stemmann, L., Picheral, M., Mayot, N., Vandromme, P., Hauss, H., et al. (2016). In situ imaging reveals the biomass of giant protists in the global ocean. *Nature* 532, 504–507. doi: 10.1038/nature17652

Bode, M., Hagen, W., Schukat, A., Teuber, L., Fonseca-Batista, D., Dehairs, F., et al. (2015). Feeding strategies of tropical and subtropical calanoid copepods throughout the eastern Atlantic Ocean - Latitudinal and bathymetric aspects. *Progr. Oceanogr.* 138, 268–282. doi: 10.1016/j.pocean.2015.10.002

Boyd, P. W., Sherry, N. D., Berges, J. A., Bishop, J. K. B., Calvert, S. E., Charette, M. A., et al. (1999). Transformations of biogenic particulates from the pelagic to the deep ocean realm. *Deep Sea Res. Part II Top. Stud. Oceanogr.* 46, 2761–2792. doi: 10.1016/s0967-0645(99)00083-1

Bruland, K. W., and Silver, M. W. (1981). Sinking rates of fecal pellets from gelatinous zooplankton (salps, pteropods, doliolids). *Mar. Biol.* 63, 295–300. doi: 10.1007/bf00395999

Buitenhuis, E., Le Quere, C., Aumont, O., Beaugrand, G., Bunker, A., Hirst, A., et al. (2006). Biogeochemical fluxes through mesozooplankton. *Global Biogeochem. Cycles* 20:18.

Burd, A. B., Hansell, D. A., Steinberg, D. K., Anderson, T. R., Aristegui, J., Baltar, F., et al. (2010). Assessing the apparent imbalance between geochemical and biochemical indicators of meso- and bathypelagic biological activity: what the @$#! is wrong with present calculations of carbon budgets? *Deep Sea Res. II* 57, 1557–1571. doi: 10.1016/j.dsr2.2010.02.022

Burd, A. B., and Jackson, G. A. (2009). Particle Aggregation. *Annu. Rev. Mar. Sci.* 1, 65–90.

Christiansen, S., Hoving, H.-J., Schütte, F., Hauss, H., Karstensen, J., Körtzinger, A., et al. (2018). Particulate matter flux interception in oceanic mesoscale eddies by the polychaete Poeobius sp. *Limnol. Oceanogr.* 63, 2093–2109. doi: 10.1002/lno.10926

Cripps, G., Lindeque, P., and Flynn, K. J. (2014). Have we been underestimating the effects of ocean acidification in zooplankton? *Glob. Chang. Biol.* 20, 3377–3385. doi: 10.1111/gcb.12582

Dagg, M. (1993). Sinking particles as a possible source of nutrition for the large calanoid copepod Neocalanus cristatus in the subarctic Pacific Ocean. *Deep Sea Res. Part I* 40, 1431–1445. doi: 10.1016/0967-0637(93)90121-i

DeVries, T., Primeau, F., and Deutsch, C. (2012). The sequestration efficiency of the biological pump. *Geophys. Res. Lett.* 39:L13601. doi: 10.1029/2012GL051963

DeVries, T., and Weber, T. (2017). The export and fate of organic matter in the ocean: new constraints from combining satellite and oceanographic tracer observations. *Global Biogeochem. Cycles* 31, 535–555. doi: 10.1002/2016gb005551

Dilling, L., and Alldredge, A. L. (2000). Fragmentation of marine snow by swimming macrozooplankton: a new process impacting carbon cycling in the sea. *Deep Sea Res. I* 47, 1227–1245. doi: 10.1016/s0967-0637(99)00105-3

Ducklow, H. W., Steinberg, D. K., and Buesseler, K. O. (2001). Upper ocean carbon export and the biological pump. *Oceanography* 14, 50–58. doi: 10.5670/oceanog.2001.06

Fabry, V., and Deuser, W. (1992). Seasonal changes in the isotopic compositions and sinking fluxes of euthecosomatous pteropod shells in the Sargasso Sea. *Paleoceanography* 7, 195–213. doi: 10.1029/91pa03138

Fowler, S. W. (1977). Trace elements in zooplankton particulate products. *Nature* 269:51. doi: 10.1038/269051a0

Frangoulis, C., Christou, E. D., and Hecq, J. H. (2005). "Comparison of marine copepod outfluxes: nature, rate, fate and role in the carbon and nitrogen cycles," in *Advances in Marine Biology*, Vol. 47, ed. D. Smith (London: Academic Press Ltd.), 253–309. doi: 10.1016/s0065-2881(04)47004-7

Fuchs, H. L., and Franks, P. J. S. (2010). Plankton community properties determined by nutrients and size-selective feeding. *Mar. Ecol. Progr. Ser.* 413, 1–15. doi: 10.3354/meps08716

Giesecke, R., Gonzalez, H. E., and Bathmann, U. (2010). The role of the chaetognath Sagitta gazellae in the vertical carbon flux of the Southern Ocean. *Polar Biol.* 33, 293–304. doi: 10.1007/s00300-009-0704-4

Gilmer, R., and Harbison, G. (1986). Morphology and field behavior of pteropod molluscs: feeding methods in the families Cavoliniidae, Limacinidae and Peraclididae (Gastropoda: Thecosomata). *Mar. Biol.* 91, 47–57. doi: 10.1007/bf00397570

Glibert, P. M. (1998). Interactions of top-down and bottom-up control in planktonic nitrogen cycling. *Hydrobiologia* 363, 1–12. doi: 10.1073/pnas.0809671106

Goericke, R. (2002). Top-down control of phytoplankton biomass and community structure in the monsoonal Arabian Sea. *Limnol. Oceanogr.* 47, 1307–1323. doi: 10.4319/lo.2002.47.5.1307

Goldthwait, S., Yen, J., Brown, J., and Alldredge, A. (2004). Quantification of marine snow fragmentation by swimming euphausiids. *Limnol. Oceanogr.* 49, 940–952. doi: 10.4319/lo.2004.49.4.0940

Gorokhova, E., Soerensen, A. L., and Motwani, N. H. (2018). Mercury-methylating bacteria are associated with zooplankton: a proof-of-principle survey in the Baltic Sea. *bioRxiv*

Gorsky, G., Ohman, M. D., Picheral, M., Gasparini, S., Stemmann, L., Romagnan, J. B., et al. (2010). Digital zooplankton image analysis using the ZooScan integrated system. *J. Plankton Res.* 32, 285–303. doi: 10.1093/plankt/fbp124

Gowing, M. (1989). Abundance and feeding ecology of Antarctic phaeodarian radiolarians. *Mar. Biol.* 103, 107–118. doi: 10.1007/bf00391069

Gowing, M. M. (1986). Trophic biology of phaeodarian radiolarians and flux of living radiolarians in the upper 2000 m of the North Pacific central gyre. *Deep Sea Res.* 33, 655–674. doi: 10.1016/0198-0149(86)90059-2

Gowing, M. M., and Bentham, W. N. (1994). Feeding ecology of phaeodarian radiolarians at the VERTEX North Pacific time series site. *J. Plankton Res.* 16, 707–719. doi: 10.1093/plankt/16.6.707

Gowing, M. M., and Silver, M. W. (1983). Origins and microenvironments of bacteria mediating fecal pellet decomposition in the sea. *Mar. Biol.* 73, 7–16. doi: 10.1007/bf00396280

Gowing, M. M., and Silver, M. W. (1985). Minipellets - a new and abundant size class of marine fecal pellets. *J. Mar. Res.* 43, 395–418. doi: 10.1357/002224085788438676

Gutierrez-Rodriguez, A., Stukel, M. R., Lopes Dos Santos, A., Biard, T., Scharek, R., Vaulot, D., et al. (2018). High contribution of Rhizaria (Radiolaria) to vertical export in the California Current Ecosystem revealed by DNA metabarcoding. *ISME J.* 13, 964–976. doi: 10.1038/s41396-018-0322-7

Hamner, W., Madin, L., Alldredge, A., Gilmer, R., and Hamner, P. (1975). Underwater observations of gelatinous zooplankton: Sampling problems, feeding biology, and behavior1. *Limnol. Oceanogr.* 20, 907–917. doi: 10.4319/lo.1975.20.6.0907

Hannides, C. C. S., Landry, M. R., Benitez-Nelson, C. R., Styles, R. M., Montoya, J. P., and Karl, D. M. (2009). Export stoichiometry and migrant-mediated flux of phosphorus in the North Pacific Subtropical Gyre. *Deep Sea Res. I* 56, 73–88. doi: 10.1016/j.dsr.2008.08.003

Hansen, J. L. S., Kiorboe, T., and Alldredge, A. L. (1996). Marine snow derived from abandoned larvacean houses: sinking rates, particle content and mechanisms of aggregate formation. *Mar. Ecol. Progr. Ser.* 141, 205–215. doi: 10.3354/meps141205

Hansen, P. J., Bjornsen, P. K., and Hansen, B. W. (1997). Zooplankton grazing and growth: scaling within the 2-2,000-mu m body size range. *Limnol. Oceanogr.* 42, 687–704. doi: 10.4319/lo.1997.42.4.0687

Hauss, H., Christiansen, S., Schütte, F., Kiko, R., Edvam Lima, M., Rodrigues, E., et al. (2016). Dead zone or oasis in the open ocean? Zooplankton distribution and migration in low-oxygen modewater eddies. *Biogeosciences* 13, 1977–1989. doi: 10.5194/bg-13-1977-2016

Henson, S. A., Sanders, R., Madsen, E., Morris, P. J., Le Moigne, F., and Quartly, G. D. (2011). A reduced estimate of the strength of the ocean's biological carbon pump. *Geophys. Res. Lett.* 38:L04606.

Hernandez-Leon, S., and Ikeda, T. (2005). A global assessment of mesozooplankton respiration in the ocean. *J. Plankton Res.* 27, 153–158. doi: 10.3389/fmicb.2017.01358 doi: 10.1093/plankt/fbh166

Hunt, B., Strugnell, J., Bednarsek, N., Linse, K., Nelson, R. J., Pakhomov, E., et al. (2010). Poles apart: the "bipolar" pteropod species *Limacina helicina* is genetically distinct between the Arctic and Antarctic oceans. *PLoS One* 5:e9835. doi: 10.1371/journal.pone.0009835

Iversen, M. H., and Poulsen, L. K. (2007). Coprorhexy, coprophagy, and coprochaly in the copepods *Calanus helgolandicus*, *Pseudocalanus elongatus*, and *Oithona similis*. *Mar. Ecol. Progr. Ser.* 350, 79–89. doi: 10.1021/acs.est.5b05905

Jackson, G. A., Checkley, D. M. Jr., and Dagg, M. (2015). Settling of particles in the upper 100 m of the ocean detected with autonomous profiling floats off California. *Deep Sea Res. I* 99, 75–86. doi: 10.1016/j.dsr.2015.02.001

Jackson, G. A., and Checkley, D. M. (2011). Particle size distributions in the upper 100 m water column and their implications for animal feeding in the plankton. *Deep Sea Res. I* 58, 283–297. doi: 10.1016/j.dsr.2010.12.008

Jackson, G. A., Najjar, R. G., and Toggweiler, J. R. (1993). Flux feeding as a mechanism for zooplankton grazing and its implications for vertical particulate flux. *Limnol. Oceanogr.* 38, 1328–1331. doi: 10.4319/lo.1993.38.6.1328

Kiko, R., Hauss, H., Buchholz, F., and Melzner, F. (2016). Ammonium excretion and oxygen respiration of tropical copepods and euphausiids exposed to oxygen minimum zone conditions. *Biogeosciences* 13, 2241–2255. doi: 10.5194/bg-13-2241-2016

Kiørboe, T. (2011). How zooplankton feed: mechanisms, traits and trade-offs. *Biol. Rev.* 86, 311–339. doi: 10.1111/j.1469-185x.2010.00148.x

Kiørboe, T., and Thygesen, U. H. (2001). Fluid motion and solute distribution around sinking aggregates. II. Implications for remote detection by colonizing zooplankters. *Mar. Ecol. Progr. Ser.* 211, 15–25. doi: 10.3354/meps211015

Kling, S. A., and Boltovskoy, D. (1995). Radiolarian vertical distribution patterns across the southern California current. *Deep Sea Res. I* 42, 191–231. doi: 10.1016/0967-0637(94)00038-t

Knauer, G. A., Martin, J. H., and Bruland, K. W. (1979). Fluxes of particulate carbon, nitrogen, and phosphorus in the upper water column of the Northeast Pacific. *Deep Sea Res.* 26, 97–108. doi: 10.1016/0198-0149(79)90089-x

Komar, P. D., Morse, A. P., Small, L. F., and Fowler, S. W. (1981). An analysis of sinking rates of natural copepod and euphausiid fecal pellets. *Limnol. Oceanogr.* 26, 172–180. doi: 10.4319/lo.1981.26.1.0172

Kosobokova, K., Hirche, H.-J., and Scherzinger, T. (2002). Feeding ecology of Spinocalanus antarcticus, a mesopelagic copepod with a looped gut. *Mar. Biol.* 141, 503–511. doi: 10.1007/s00227-002-0848-z

Lalli, C. M., and Gilmer, R. W. (1989). *Pelagic Snails: The Biology of Holoplanktonic Gastropod Mollusks*. Palo Alto, CA: Stanford University Press.

Lampitt, R., Salter, I., and Johns, D. (2009). Radiolaria: major exporters of organic carbon to the deep ocean. *Global Biogeochem. Cycles* 23:GB1010.

Lampitt, R., Wishner, K., Turley, C., and Angel, M. (1993). Marine snow studies in the Northeast Atlantic Ocean: distribution, composition and role as a food source for migrating plankton. *Mar. Biol.* 116, 689–702. doi: 10.1007/bf00355486

Landry, M. R., Ohman, M. D., Goericke, R., Stukel, M. R., Barbeau, K. A., Bundy, R., et al. (2012). Pelagic community responses to a deep-water front in the California current ecosystem: overview of the A-front study. *J. Plankton Res.* 34, 739–748. doi: 10.1093/plankt/fbs025

Landry, M. R., Ohman, M. D., Goericke, R., Stukel, M. R., and Tsyrklevich, K. (2009). Lagrangian studies of phytoplankton growth and grazing relationships in a coastal upwelling ecosystem off Southern California. *Prog. Oceanogr.* 83, 208–216. doi: 10.1016/j.pocean.2009.07.026

Lavaniegos, B. E., and Ohman, M. D. (2007). Coherence of long-term variations of zooplankton in two sectors of the California current system. *Prog. Oceanogr.* 75, 42–69. doi: 10.1016/j.pocean.2007.07.002

Laws, E. A., D'sa, E., and Naik, P. (2011). Simple equations to estimate ratios of new or export production to total production from satellite-derived estimates of sea surface temperature and primary production. *Limnol. Oceanogr. Methods* 9, 593–601. doi: 10.4319/lom.2011.9.593

Lomas, M., Steinberg, D. K., Dickey, T., Carlson, C., Nelson, N., Condon, R. H., et al. (2010). Increased ocean carbon export in the sargasso sea linked to climate variability is countered by its enhanced mesopelagic attenuation. *Biogeosciences* 7, 57–70. doi: 10.5194/bg-7-57-2010

Madin, L. P. (1982). Production, composition, and sedimentation of salp fecal pellets in oceanic waters. *Mar. Biol.* 67, 39–45. doi: 10.1007/bf00397092

Manno, C., Tirelli, V., Accornero, A., and Fonda Umani, S. (2009). Importance of the contribution of *Limacina helicina* faecal pellets to the carbon pump in Terra Nova Bay (Antarctica). *J. Plankton Res.* 32, 145–152. doi: 10.1093/plankt/fbp108

Mayor, D. J., Sanders, R., Giering, S. L., and Anderson, T. R. (2014). Microbial gardening in the ocean's twilight zone: detritivorous metazoans benefit from fragmenting, rather than ingesting, sinking detritus: fragmentation of refractory detritus by zooplankton beneath the euphotic zone stimulates the harvestable production of labile and nutritious microbial biomass. *Bioessays* 36, 1132–1137. doi: 10.1002/bies.201400100

McDonnell, A. M. P., and Buesseler, K. O. (2010). Variability in the average sinking velocity of marine particles. *Limnol. Oceanogr.* 55, 2085–2096. doi: 10.4319/lo.2010.55.5.2085

Michaels, A. F., Caron, D. A., Swanberg, N. R., Howse, F. A., and Michaels, C. M. (1995). Planktonic sarcodines (Acantharia, Radiolaria, Foraminifera) in surface waters near Bermuda: abundance, biomass and vertical flux. *J. Plankton Res.* 17, 131–163. doi: 10.1093/plankt/17.1.131

Morrow, R. M., Ohman, M. D., Goericke, R., Kelly, T. B., Stephens, B. M., and Stukel, M. R. (2018). Primary productivity, mesozooplankton grazing, and the biological pump in the california current ecosystem: variability and response to El niño. *Deep Sea Res. I* 140, 52–62. doi: 10.1016/j.dsr.2018.07.012

Nakamura, Y., and Suzuki, N. (2015). "Phaeodaria: diverse marine cercozoans of world-wide distribution," in *Marine Protists*, eds S. Ohtsuka, T. Suzaki, T. Horiguchi, N. Suzuki, and F. Not (Berlin: Springer), 223–249. doi: 10.1007/978-4-431-55130-0_9

Ohman, M. D., Powell, J. R., Picheral, M., and Jensen, D. W. (2012). Mesozooplankton and particulate matter responses to a deep-water frontal system in the southern California current system. *J. Plankton Res.* 34, 815–827. doi: 10.1093/plankt/fbs028

Ohman, M. D., and Romagnan, J. B. (2016). Nonlinear effects of body size and optical attenuation on diel vertical migration by zooplankton. *Limnol. Oceanogr.* 61, 765–770. doi: 10.1002/lno.10251

Owens, S. A., Buesseler, K. O., and Sims, K. W. W. (2011). Re-evaluating the 238U-salinity relationship in seawater: implications for the 238U-234Th disequilibrium method. *Mar. Chem.* 127, 31–39. doi: 10.1016/j.marchem.2011.07.005

Picheral, M., Guidi, L., Stemmann, L., Karl, D. M., Iddaoud, G., and Gorsky, G. (2010). The underwater vision profiler 5: an advanced instrument for high spatial resolution studies of particle size spectra and zooplankton. *Limnol. Oceanogr. Methods* 8, 462–473. doi: 10.4319/lom.2010.8.462

Pike, S. M., Buesseler, K. O., Andrews, J., and Savoye, N. (2005). Quantification of 234Th recovery in small volume sea water samples by inductively coupled plasma-mass spectrometry. *J. Radioanal. Nucl. Chem.* 263, 355–360. doi: 10.1007/s10967-005-0594-z

Ploug, H., Iversen, M. H., and Fischer, G. (2008). Ballast, sinking velocity, and apparent diffusivity within marine snow and zooplankton fecal pellets: implications for substrate turnover by attached bacteria. *Limnol. Oceanogr.* 53, 1878–1886. doi: 10.4319/lo.2008.53.5.1878

Poulsen, L. K., and Iversen, M. H. (2008). Degradation of copepod fecal pellets: key role of protozooplankton. *Mar. Ecol. Prog. Ser.* 367, 1–13. doi: 10.3354/meps07611

Poulsen, L. K., and Kiorboe, T. (2005). Coprophagy and coprorhexy in the copepods *Acartia tonsa* and *Temora longicornis*: clearance rates and feeding behaviour. *Mar. Ecol. Prog. Ser.* 299, 217–227. doi: 10.3354/meps299217

Powell, J. R., and Ohman, M. D. (2015). Changes in zooplankton habitat, behavior, and acoustic scattering characteristics across glider-resolved fronts in the Southern California current system. *Prog. Oceanogr.* 134, 77–92. doi: 10.1016/j.pocean.2014.12.011

Proud, R., Cox, M. J., and Brierley, A. S. (2017). Biogeography of the global ocean's mesopelagic zone. *Curr. Biol.* 27, 113–119. doi: 10.1016/j.cub.2016.11.003

Reinthaler, T., Van Aken, H., Veth, C., Arístegui, J., Robinson, C., Williams, P. J. L. B., et al. (2006). Prokaryotic respiration and production in the meso-and bathypelagic realm of the eastern and western North Atlantic basin. *Limnol. Oceanogr.* 51, 1262–1273. doi: 10.4319/lo.2006.51.3.1262

Richardson, A. J. (2008). In hot water: zooplankton and climate change. *Ices J. Mar. Sci.* 65, 279–295. doi: 10.1093/icesjms/fsn028

Robinson, C., Steinberg, D. K., Anderson, T. R., Arístegui, J., Carlson, C. A., Frost, J. R., et al. (2010). Mesopelagic zone ecology and biogeochemistry – a synthesis. *Deep Sea Res. II* 57, 1504–1518. doi: 10.1016/j.dsr2.2010.02.018

Robison, B. H., Reisenbichler, K. R., and Sherlock, R. E. (2005). Giant larvacean houses: rapid carbon transport to the deep sea floor. *Science* 308, 1609–1611. doi: 10.1126/science.1109104

Saba, G. K., Steinberg, D. K., and Bronk, D. A. (2011). The relative importance of sloppy feeding, excretion, and fecal pellet leaching in the release of dissolved carbon and nitrogen by Acartia tonsa copepods. *J. Exp. Mar. Biol. Ecol.* 404, 47–56. doi: 10.1016/j.jembe.2011.04.013

Samo, T. J., Pedler, B. E., Ball, G. I., Pasulka, A. L., Taylor, A. G., Aluwihare, L. I., et al. (2012). Microbial distribution and activity across a water mass frontal zone in the California current ecosystem. *J. Plankton Res.* 34, 802–814. doi: 10.1093/plankt/fbs048

Savoye, N., Benitez-Nelson, C., Burd, A. B., Cochran, J. K., Charette, M., Buesseler, K. O., et al. (2006). 234Th sorption and export models in the water column: a review. *Mar. Chem.* 100, 234–249. doi: 10.1016/j.marchem.2005.10.014

Schmidt, K., Schlosser, C., Atkinson, A., Fielding, S., Venables, H. J., Waluda, C. M., et al. (2016). Zooplankton gut passage mobilizes lithogenic iron for ocean productivity. *Curr. Biol.* 26, 2667–2673. doi: 10.1016/j.cub.2016.07.058

Schukat, A., Bode, M., Auel, H., Carballo, R., Martin, B., Koppelmann, R., et al. (2013). Pelagic decapods in the northern benguela upwelling system: distribution, ecophysiology and contribution to active carbon flux. *Deep Sea Res. Part I Oceanogr. Res. Pap.* 75, 146–156. doi: 10.1016/j.dsr.2013.02.003

Siegel, D. A., Buesseler, K. O., Behrenfeld, M. J., Benitez-Nelson, C. R., Boss, E., Brzezinski, M. A., et al. (2016). Prediction of the export and fate of global ocean net primary production: the EXPORTS science plan. *Front. Mar. Sci.* 3:22. doi: 10.3389/fmars.2016.00022

Siegel, D. A., Buesseler, K. O., Doney, S. C., Sailley, S. F., Behrenfeld, M. J., and Boyd, P. W. (2014). Global assessment of ocean carbon export by combining satellite obervations and food-web models. *Global Biogeochem. Cycles* 28, 181–196. doi: 10.1002/2013gb004743

Silver, M. W., and Gowing, M. M. (1991). The "particle" flux: origins and biological components. *Prog. Oceanogr.* 26, 75–113. doi: 10.1016/0079-6611(91)90007-9

Simon, M., Alldredge, A. L., and Azam, F. (1990). Bacterial carbon dynamics on marine snow. *Mar. Ecol. Prog. Ser.* 65, 205–211. doi: 10.3354/meps065205

Simon, M., Grossart, H. P., Schweitzer, B., and Ploug, H. (2002). Microbial ecology of organic aggregates in aquatic ecosystems. *Aquat. Microb. Ecol.* 28, 175–211. doi: 10.3354/ame028175

Small, L. F., Fowler, S. W., and Unlu, M. Y. (1979). Sinking rates of natural copepod fecal pellets. *Mar. Biol.* 51, 233–241. doi: 10.1021/acs.est.5b05905

Smayda, T. J. (1971). Normal and accelerated sinking of phytoplankton in sea. *Mar. Geol.* 11, 105–122. doi: 10.1016/0025-3227(71)90070-3

Steinberg, D. K., Carlson, C. A., Bates, N. R., Goldthwait, S. A., Madin, L. P., and Michaels, A. F. (2000). Zooplankton vertical migration and the active transport of dissolved organic and inorganic carbon in the Sargasso Sea. *Deep Sea Res. I* 47, 137–158. doi: 10.1016/s0967-0637(99)00052-7

Steinberg, D. K., Cope, J. S., Wilson, S. E., and Kobari, T. (2008a). A comparison of mesopelagic mesozooplankton community structure in the subtropical and subarctic North Pacific Ocean. *Deep Sea Res. II* 55, 1615–1635. doi: 10.1016/j.dsr2.2008.04.025

Steinberg, D. K., Van Mooy, B. A. S., Buesseler, K. O., Boyd, P. W., Kobari, T., and Karl, D. M. (2008b). Bacterial vs. zooplankton control of sinking particle flux in the ocean's twilight zone. *Limnol. Oceanogr.* 53, 1327–1338. doi: 10.1002/bies.201400100

Steinberg, D. K., and Landry, M. R. (2017). Zooplankton and the ocean carbon cycle. *Annu. Rev. Mar. Sci.* 9, 413–444. doi: 10.1146/annurev-marine-010814-015924

Stemmann, L., Jackson, G. A., and Gorsky, G. (2004a). A vertical model of particle size distributions and fluxes in the midwater column that includes biological and physical processes-part II: application to a three year survey in the NW mediterranean sea. *Deep Sea Res. I* 51, 885–908. doi: 10.1016/j.dsr.2004.03.002

Stemmann, L., Jackson, G. A., and Ianson, D. (2004b). A vertical model of particle size distributions and fluxes in the midwater column that includes biological and physical processes-part I: model formulation. *Deep Sea Res. I* 51, 865–884. doi: 10.1016/j.dsr.2004.03.001

Stukel, M. R., Kahru, M., Benitez-Nelson, C. R., Decima, M., Goericke, R., Landry, M. R., et al. (2015). Using lagrangian-based process studies to test satellite algorithms of vertical carbon flux in the eastern North Pacific Ocean. *J. Geophys. Res. Oceans* 120, 7208–7222. doi: 10.1002/2015jc011264

Stukel, M. R., Biard, T., Krause, J., and Ohman, M. D. (2018a). Large phaeodaria in the twilight zone: their role in the carbon cycle. *Limnol. Oceanogr.* 63, 2579–2594. doi: 10.1002/lno.10961

Stukel, M. R., Décima, M., Landry, M. R., and Selph, K. E. (2018b). Nitrogen and isotope flows through the costa rica dome upwelling ecosystem: the crucial mesozooplankton role in export flux. *Global Biogeochem. Cycles* 32, 1815–1832. doi: 10.1029/2018gb005968

Stukel, M. R., Kelly, T. B., Aluwihare, L. I., Barbeau, K. A., Goericke, R., Krause, J. W., et al. (2019). The carbon:234thorium ratios of sinking particles in the California current ecosystem 1: relationships with plankton ecosystem dynamics. *Mar. Chem.* 212, 1–15. doi: 10.1016/j.marchem.2019.01.003

Stukel, M. R., Mislan, K. A. S., Décima, M., and Hmelo, L. (2014). "Detritus in the pelagic ocean," in *Eco-DAS IX Symposium Proceedings*, ed. P. F. Kemp (Waco, TX: Association for the Sciences of Limnology and Oceanography), 49–76.

Stukel, M. R., Ohman, M. D., Benitez-Nelson, C. R., and Landry, M. R. (2013). Contributions of mesozooplankton to vertical carbon export in a coastal upwelling system. *Mar. Ecol. Prog. Ser.* 491, 47–65. doi: 10.3354/meps10453

Takahashi, K., and Honjo, S. (1981). vertical flux of radiolaria: a taxon-quantitative sediment trap study from the Western Tropical Atlantic. *Micropaleontology* 27, 140–190.

Trull, T. W., Bray, S. G., Buesseler, K. O., Lamborg, C. H., Manganini, S., Moy, C., et al. (2008). In situ measurement of mesopelagic particle sinking rates and the control of carbon transfer to the ocean interior during the vertical flux in the global ocean (VERTIGO) voyages in the North Pacific. *Deep Sea Res. II* 55, 1684–1695. doi: 10.1016/j.dsr2.2008.04.021

Turner, J. T. (1977). Sinking rates of fecal pellets from marine copepod *Pontella meadii*. *Mar. Biol.* 40, 249–259. doi: 10.1007/bf00390880

Turner, J. T. (2002). Zooplankton fecal pellets, marine snow and sinking phytoplankton blooms. *Aquat. Microb. Ecol.* 27, 57–102. doi: 10.3354/ame027057

Turner, J. T. (2015). Zooplankton fecal pellets, marine snow, phytodetritus and the ocean's biological pump. *Prog. Oceanogr.* 130, 205–248. doi: 10.1016/j.pocean.2014.08.005

Uttal, L., and Buck, K. (1996). Dietary study of the midwater polychaete poeobius meseres in monterey bay, California. *Mar. Biol.* 125, 333–343. doi: 10.1007/bf00346314

Wakeham, S. G., Lee, C., Hedges, J. I., Hernes, P. J., and Peterson, M. J. (1997). Molecular indicators of diagenetic status in marine organic matter. *Geochim. Cosmochim. Acta* 61, 5363–5369. doi: 10.1016/s0016-7037(97)00312-8

Wilson, S. E., Steinberg, D. K., and Buesseler, K. O. (2008). Changes in fecal pellet characteristics with depth as indicators of zooplankton repackaging of particles in the mesopelagic zone of the subtropical and subarctic North Pacific Ocean. *Deep Sea Res. II* 55, 1636–1647. doi: 10.1016/j.dsr2.2008.04.019

Wilson, S. E., Steinberg, D. K., Chu, F. L. E., and Bishop, J. K. B. (2010). Feeding ecology of mesopelagic zooplankton of the subtropical and subarctic North Pacific Ocean determined with fatty acid biomarkers. *Deep Sea Res. I* 57, 1278–1294. doi: 10.1016/j.dsr.2010.07.005

Wishner, K. F., Outram, D. M., Seibel, B. A., Daly, K. L., and Williams, R. L. (2013). Zooplankton in the eastern tropical north pacific: boundary effects of oxygen minimum zone expansion. *Deep Sea Res. Part I Oceanogr. Res. Pap.* 79, 122–140. doi: 10.1016/j.dsr.2013.05.012

Yoon, W. D., Kim, S. K., and Han, K. N. (2001). Morphology and sinking velocities of fecal pellets of copepod, molluscan, euphausiid, and salp taxa in the northeastern tropical Atlantic. *Mar. Biol.* 139, 923–928. doi: 10.1007/s002270100630

Conflict of Interest Statement: The authors declare that the research was conducted in the absence of any commercial or financial relationships that could be construed as a potential conflict of interest.

frontiers in Marine Science

ORIGINAL RESEARCH
published: 02 September 2019
doi: 10.3389/fmars.2019.00535

Zooplankton and Micronekton Active Flux Across the Tropical and Subtropical Atlantic Ocean

Santiago Hernández-León[1], María Pilar Olivar[2], María Luz Fernández de Puelles[3], Antonio Bode[4], Arturo Castellón[5], Cristina López-Pérez[2], Víctor M. Tuset[2] and José Ignacio González-Gordillo[6]*

[1] Instituto de Oceanografía y Cambio Global, IOCAG, Universidad de Las Palmas de Gran Canaria, Unidad Asociada ULPGC-CSIC, Canary Islands, Spain, [2] CSIC, Institut de Ciències del Mar, Barcelona, Spain, [3] Centro de Baleares, Instituto Español de Oceanografia, Palma, Spain, [4] Centro Oceanográfico de A Coruña, Instituto Español de Oceanografia, A Coruña, Spain, [5] CSIC, Unidad de Tecnología Marina, Barcelona, Spain, [6] Instituto Universitario de Investigación Marina, Universidad de Cádiz, Cádiz, Spain

Quantification of the actual amount of carbon export to the mesopelagic layer by both zooplankton and micronekton is at present a gap in the knowledge of the biological pump. These organisms perform diel vertical migrations exporting carbon through respiration, excretion, mortality, and egestion during their residence at depth. The role of zooplankton in active flux is nowadays partially assessed. However, micronekton active flux is scarcely known and only a few studies addressed this downward transport. Even less is known about the capacity of both communities to export carbon in the ocean. Here, we show the results of zooplankton and micronekton active flux across a productivity gradient in the tropical and subtropical Atlantic Ocean. Biomass vertical distribution from the surface up to 800 m depth by day and night was studied during April 2015 in a transect from 9°S to 25°N, covering from the quite oligotrophic zone off Brazil to the meso- and eutrophic areas of the equator, Guinea Dome, and the oceanic upwelling off Northwest Africa. Zooplankton and micronekton migrant biomass was estimated from day and night catches at different layers of the water column using MOCNESS-1 (1 m^2 mouth area) and Mesopelagos (35 m^2) nets, respectively. Respiratory flux was assessed by measuring the enzymatic activity of the electron transfer system (ETS) of organisms at depth. Results showed a close relationship between migrant biomass and respiratory flux in zooplankton and micronekton as expected. Using a rather conservative 50% of efficiency for the net used to capture micronekton, respiratory flux resulted in similar values for both communities. Gravitational (passive) flux measured using sediment traps increased from the oligotrophic toward the meso- and eutrophic zones. Total active flux (including respiration and estimated mortality, excretion, and gut flux) by zooplankton and micronekton accounted for about 25% of total flux (passive plus active) in oligotrophic zones. Total active flux also increased toward meso- and eutrophic zones, reaching about 80% of total flux and being at least twofold higher than passive flux. These results alert about an important underestimation of the ocean biological pump using only passive flux measurements.

Keywords: biological pump, passive flux, active flux, zooplankton, micronekton, Atlantic Ocean

OPEN ACCESS

Edited by:
Amy Elizabeth Maas, Bermuda Institute of Ocean Sciences, Bermuda

Reviewed by:
Qian P. Li, Chinese Academy of Sciences, China
Natalia Osma, University of Concepción, Chile

****Correspondence:***
Santiago Hernández-León
shernandezleon@ulpgc.es

Specialty section:
This article was submitted to Marine Biogeochemistry, a section of the journal Frontiers in Marine Science

Received: *28 March 2019*
Accepted: *15 August 2019*
Published: *02 September 2019*

Citation:
Hernández-León S, Olivar MP, Fernández de Puelles ML, Bode A, Castellón A, López-Pérez C, Tuset VM and González-Gordillo JI (2019) Zooplankton and Micronekton Active Flux Across the Tropical and Subtropical Atlantic Ocean. Front. Mar. Sci. 6:535. doi: 10.3389/fmars.2019.00535

INTRODUCTION

The biological carbon pump exports organic matter from the euphotic to the mesopelagic zone through diverse mechanisms. Sinking particles and the active transport by diel vertical migrants are two main processes, jointly with physical mixing of particulate and dissolved organic matter (Buesseler et al., 2007). Passive or gravitational flux due to particulate organic carbon (POC) sinking is, by far, the most studied mechanism (see Honjo et al., 2008; Guidi et al., 2015). However, active flux, the transport of organic matter performed by organisms due to feeding at night in the epipelagic layer and their egestion (Angel, 1989), metabolism (Longhurst et al., 1990), and mortality (Zhang and Dam, 1997) during their daylight permanence at depth remains partially unknown. More than two decades of research provided a relatively important data set about zooplankton active flux. However, modeling the biological pump is still a challenge due to (1) the limited knowledge of downward transport in different areas of the ocean, and (2) the almost nescience about the actual amount of carbon transported by micronektonic organisms. The latter mechanism is, at present, an important gap in our assessment of the biological pump.

Diel vertical migrants are organisms showing a high diversity and a wide size spectrum. They spread from relatively small crustaceans, mainly large copepods and euphausiids, to micronektonic forms such as fishes (mainly myctophids), large crustaceans (mainly decapods), and cephalopods. This wide spectrum entails serious difficulties for the study of the importance of these organisms in the carbon pump. The use of different types of nets of different meshes and sizes, and depth stratified sampling covering most of the mesopelagic zone are time-consuming ship operations in standard oceanographic cruises. Moreover, expertise in a rather complex taxonomy from zooplankton to micronekton is also needed. Thus, the study of these migrants becomes a rather arduous and expensive subject to obtain a complete picture of the biological pump.

Zooplankton is known to perform diel vertical migrations transporting a significant fraction of organic matter to deep waters (Longhurst et al., 1990). The amount of carbon transported based on respiration at depth (respiratory flux) is somehow related to primary productivity as the biomass of the vertical migrant community is larger in meso- and eutrophic areas of the ocean (Yebra et al., 2018; Hernández-León et al., 2019b). This active flux is quite variable and accounts for less than 4% (Le Borgne and Rodier, 1997) to more than 100% (Yebra et al., 2018) of the POC flux. Micronekton active flux is poorly known simply because its study requires large nets which are not a standard in oceanographic cruises. In fact, there are only a handful of works studying their role in transporting carbon downward, most of them on single groups of organisms such as fishes (Hopkins et al., 1996; Davison et al., 2013; Hudson et al., 2014) or decapods (Schukat et al., 2013; Pakhomov et al., 2018). Assessment of active flux by both zooplankton and micronekton are, to our knowledge, limited to two studies (Hidaka et al., 2001; Ariza et al., 2015). Only respiratory fluxes in those studies ranged from 14 to 55% of the POC flux. Although the latter range is based in only two studies, they suggest that total active flux (considering mortality, excretion, and gut flux) in relation to POC flux by both communities (zooplankton and micronekton) could be significant, and sometimes larger than particle sinking rates (see Yebra et al., 2018).

In this sense, besides the magnitude of the migrant biomass, community structure of pelagic communities also change with productivity. For instance, large organisms increase in areas characterized by abundant resources for feeding (Frost, 1974). Thus, migrant biomass and, therefore, active flux should also change in different productive regimes. Moreover, some populations of large zooplankton could perform seasonal migrations, accumulating lipids in the epipelagic zone and respiring them at depth, promoting the so-called lipid pump (Jónasdóttir et al., 2015). Thus, our knowledge of total active flux and their sources of variability are still quite limited.

In order to study the natural variability of active flux by zooplankton and micronekton in the ocean, we performed a transect of stations from the quite oligotrophic waters off Brazil to the meso- and eutrophic waters off the Northwest African upwelling. The goal of the study was to estimate active flux by both communities in a gradient of productivity at the basin scale from subtropical to equatorial and tropical Atlantic Ocean. We performed vertical profiles of zooplankton and micronekton during day and by night in order to study their vertical migrations, to assess migrant biomass, and to measure the enzymatic activity of the electron transfer system (ETS) as a proxy for respiration rates of these organisms in the water column. Respiratory flux was estimated in both zooplankton and micronekton as a basis to assess total active flux in tropical and subtropical ecosystems.

MATERIALS AND METHODS

Sampling took place during the "Migrants and Active Flux In the Atlantic ocean" (MAFIA) cruise on board the R. V. "Hespérides" along the tropical and subtropical Atlantic Ocean. We sailed from Salvador de Bahía (Brazil) to the Canary Islands (Spain) from March 31st to April 29th, 2015 (**Figure 1**). Vertical profiles of temperature, conductivity, oxygen, fluorescence, and pressure were obtained using a CTD (Seabird 911 plus) mounted on a rosette sampler equipped with 12 l Niskin bottles. Fluorescence obtained in vertical profiles (0–200 m) was converted to chlorophyll using samples at discrete depths for calibration. Chlorophyll *a* was measured filtering 500 ml of Niskin water samples through a 25 mm Whatman GF/F filter and freezing it at −20°C until their analysis in the laboratory. We extracted pigments by placing the filter in 90% acetone at −20°C in the dark during 24 h. They were measured on a Turner Design 10A Fluorometer, previously calibrated with pure Chl *a* (Yentsch and Menzel, 1963), and measured following the acidification method by Strickland and Parsons (1972). Temperature, salinity, oxygen, and chlorophyll sections were represented using Ocean Data View and the DIVA gridding procedure (Schlitzer, 2016).

Passive flux was measured at 150 m depth using a free-drifting multi-trap array having eight cylinders following the model described by Knauer et al. (1979) using the procedure

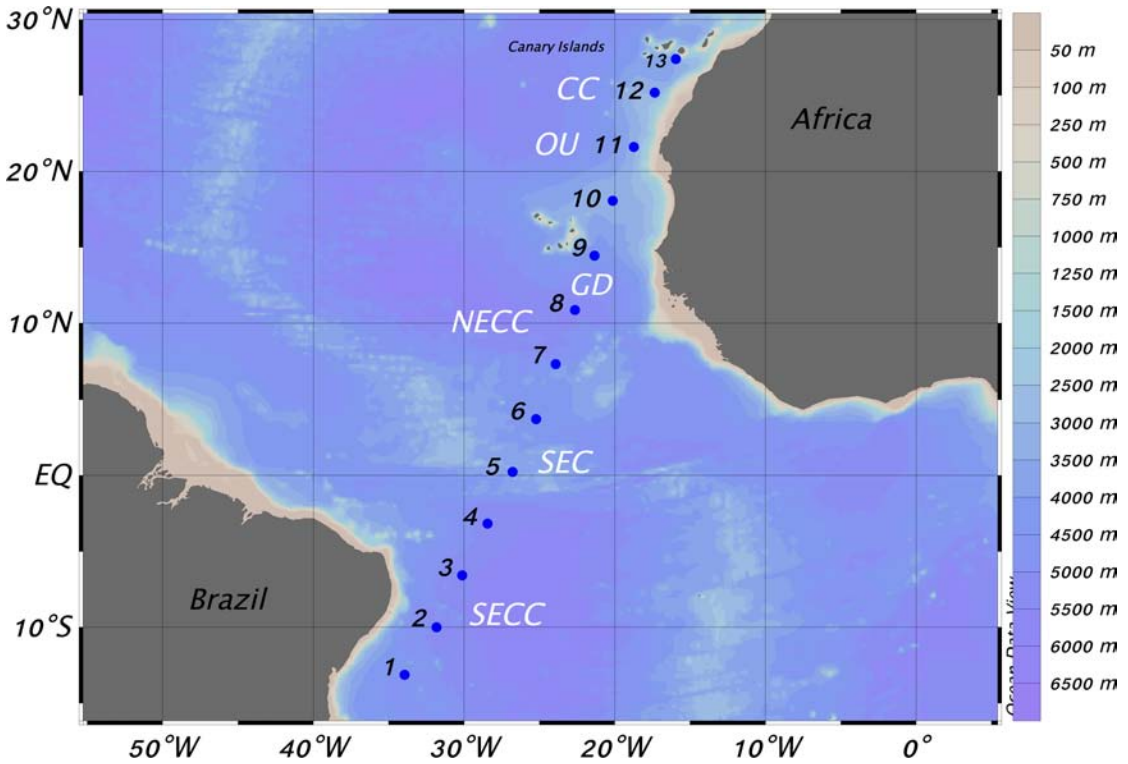

FIGURE 1 | Location of stations carried out in the tropical and subtropical Atlantic Ocean during the Mafia Cruise. CC, Canary Current; OU, Oceanic Upwelling; GD, Guinea Dome; NECC, North Equatorial Counter Current; SEC, South Equatorial Current; SECC, South Equatorial Counter Current (see text).

described in Hernández-León et al. (2019b). In short, the trap was deployed during approximately 24 h with cylinders containing filtered seawater and a high salinity (~45 g·l^{-1} NaCl analytical reagent grade) to increase density. No poisons were added to retard bacterial decomposition. After recovering, swimmers (different zooplanktonic organisms, mainly copepods) were removed and samples were filtered onto pre-combusted (450°C for 12 h) 25 mm Whatman GF/F filters. They were frozen at −20°C until analysis in a Carlo Erba CHNSO 1108 elemental analyzer (UNESCO, 1994).

Zooplankton samples were obtained using a MOCNESS-1 net with a 1 m^2 mouth opening area, fitted with 200 μm mesh size (Wiebe et al., 1976). Oblique hauls were made at about 1.5–2.5 knots during day and night from stations 2 to 12 (**Figure 1**), and from 800 m depth to the surface in eight strata: 800–600, 600–500, 500–400, 400–300, 300–200 m, the lower thermocline layer (200 m – ca. 100 m), the upper thermocline layer (ca. 100–50 m), and the upper mixed layer (ca. 50–0 m) (see Olivar et al., 2018b). Immediately after sampling, organisms were gently collected and samples for enzymatic measurements were picked up, frozen in liquid nitrogen (−196°C), and later preserved at −80°C. After this, the entire sample was preserved in 5% buffered formalin and seawater. On board, a subsample from each layer was stained using Rose Bengal and later photographed using a Nikon D800 digital camera (36 MP) using a macro lens (MicroNikkor 600 mm f/2.8G ED) over a white LED backlight. Images were taken at 1850 dpi resolution and later processed using ZooImage1 according to Grosjean and Denis (2007). Organisms were classified in six groups (copepods, chaetognaths, euphausid-like, gelatinous, other zooplankton, and particles-like). Body area was converted to biomass in terms of dry weight using the empirical relationships given by Hernández-León and Montero (2006), and improved by Lehette and Hernández-León (2009) for the different organisms. Dry weight was converted to carbon units assuming that carbon is 40% of dry weight (Dam and Peterson, 1993).

Micronekton samples were obtained using a Mesopelagos midwater trawl (Meillat, 2012) with an average mouth opening of 35 m^2 and a total length of 50 m. Mesh opening changed from 30 mm at the mouth to 4 mm at the end where a multi-sampler, able to collect samples in five different layers, was installed. Details of the system are given elsewhere (Olivar et al., 2017). Hauls were made at about 2–3 knots during day and night from 800 m to the surface in five consecutive layers (800–700, 700–400, 400–200, 200–100, and 100–0 m) except for station 1 which was restricted to the upper 150 m depth. The multi-sampler failed to obtain samples in areas or strata with abundant large gelatinous zooplankton or sargassum-weeds, so some stations were not considered for active flux. On board, organisms were sorted and classified to, at least, the family taxa, and wet weight (Ww) measured using a marine precision balance POLS S-182 P-15 (precision 2 g). Thereafter, samples were frozen for later species identification and dry weight measurements in the laboratory. Selected species of fishes and decapods were also

frozen in liquid nitrogen and stored at −80°C for later ETS activity analysis. Leptocephali, relatively abundant at night in the upper surface layer of station 6, were removed from the migratory organisms as their residence depth during day expanded from surface to ca. 300 m (Castonguay and McCleave, 1987; Olivar et al., 2018b). Wet weight of fishes were converted to dry weight (Dw) using the Dw/Ww ratio of 0.23 obtained for the cruise specimens (López-Pérez, unpublished), similar to the ratios given by Childress and Nygaard (1973). The ratio used for crustaceans was the one given by Pakhomov et al. (2018) of 0.179. Carbon biomass was obtained assuming that it was 40% of dry weight (Bailey et al., 1995; Lindsay, 2003; and mean value obtained from 79 individuals examined in an earlier study on stable isotope analyses by Olivar et al., 2018a).

Frozen samples were homogenized at the laboratory in a Teflon pestle at 0−4°C to avoid degradation of enzyme activity and proteins. ETS activity was measured following the method of Packard (1971) modified by Owens and King (1975), Kenner and Ahmed (1975), and Gómez et al. (1996). Samples were homogenized and centrifuged thereafter at 4000 rpm at 0°C for 10 min. An aliquot was subsampled from the homogenate and incubated at 16°C for zooplankton and 18°C for micronekton, and darkness using NADH, NADPH, succinate, and a tetrazolium salt (INT) as the artificial electron acceptor. After 20 min, the incubation was stopped with a quench solution. The ETS activity was estimated spectrophotometrically at 490 nm with a turbidity baseline of 750 nm. In order to correct ETS activity for *in situ* temperature, we used the Arrhenius equation and an activation energy of 15 kcal·mol^{-1} (Packard et al., 1975). Protein content was determined using the method of Lowry et al. (1951) modified by Rutter (1967), and using bovine serum albumin (BSA) as the standard. Zooplankton protein content was converted to dry weight using the ratio of 2.49 recently given by Hernández-León et al. (2019a) for zooplankton in subtropical waters. This ratio was also used to convert ETS activity and respiration rates data from previous estimates of respiratory flux in subtropical waters (Hernández-León et al., 2019b) and then compared to the results of the present study. ETS activity in micronekton was measured in the whole animal. Organisms were homogenized and a sub-sample taken for the ETS assay. We converted wet weight (Ww) to dry weight using the above mentioned ratio, and into protein (Prot) using the average Dw/Prot ratios given by Bailey et al. (1995) of 2.21 for fishes, and 2.48 for crustaceans.

Night minus day of integrated biomass profiles in the upper 200 m layer were used as an estimate of the zooplankton and micronekton migrant biomass. Cephalopods were excluded from our estimations as they did not showed a significant biomass, probably due to escapement. Migrant biomass values were converted to carbon units as shown above. For zooplankton we assumed no net avoidance. However, night minus day biomass for micronekton was estimated for two different capture efficiencies of the net (20 and 50%). No data about Mesopelagos trawl efficiency is, to our knowledge, available. This is an important shortcoming of our research as it is known that mesopelagic fish biomass in the ocean could be an order of magnitude higher than fishes captured using trawls due to their poor capture efficiency (Koslow et al., 1997; Kloser et al., 2009; Yasuma and Yamamura, 2010; Kaartvedt et al., 2012). Based on comparison between acoustics and net sampling, estimations of catchability for large mid-water trawls normally vary between 6 and 13% (Gjøsaeter, 1984; May and Blaber, 1989). Koslow et al. (1997) found a similar value of 14% using a Young Gadoic Pelagic Trawl (YGPT, opening mouth of 105 m^2). Nets such as MOHT trawl (5 m^2, Oozeki et al., 2004) showed capture efficiencies of 14% for gas-bearing organisms (e.g., mesopelagic fishes), and 38% for large non-gas-bearing (e.g., decapods) fauna (Davison, 2011). Similarly, a 33.3% catch efficiency was estimated for the 10 m^2 MOCNESS net by Pakhomov et al. (2018). Thus, we assumed the Mesopelagos trawl to catch between 20 and 50% of the biomass of fishes and crustaceans, and therefore, we estimated biomass using a quite conservative capture efficiency of 50%. In any case, values for an efficiency of 20% are also provided for comparison.

Respiratory flux in zooplankton was determined using the average ETS activity (in $\mu lO_2 \cdot mg\ protein^{-1} \cdot h^{-1}$) in the 200–800 m layer (considered as the residence depth of migrants), and multiplied by the migrant biomass obtained in the epipelagic layer. In micronekton, respiratory flux was determined for fishes and crustaceans using the average ETS activity (in $\mu lO_2 \cdot mg\ protein^{-1} \cdot h^{-1}$) for myctophids and decapods obtained during the survey, assuming an activation energy of 15 kcal·mol^{-1} (Packard et al., 1975) and correcting for the average temperature in the 200–800 m layer. A quite conservative respiration to ETS (R/ETS) ratio of 0.5 was used as in zooplankton this ratio normally varies between 0.5 and 1, mainly depending on the food availability to organisms (see Hernández-León and Gómez, 1996). A residence time at depth of 12 h was also assumed for both communities. To convert respiration into carbon units, a respiratory quotient (CO_2 respired/O_2 consumed) of 0.97 (Omori and Ikeda, 1984) was used.

Respiratory flux is only a component of active flux as mortality, excretion, and gut flux should also be considered. In these sense and in order to compare these conservative estimates of active flux with POC flux, we assessed total active flux by zooplankton and micronekton derived from respiratory flux. In zooplankton, mortality was estimated from growth assuming steady-state conditions in the mesopelagic zone (growth = mortality) using the equation of Ikeda and Motoda (1978) relating respiration and growth, and assuming gross growth (growth/ingestion) and assimilation efficiencies of 30 and 70%, respectively (see review in Omori and Ikeda, 1984). Excretion was assessed using the values of Steinberg et al. (2000) making up 24% of the respired plus excreted carbon. Gut flux was no added in the total zooplankton active flux assessment as gut passage time in zooplankton is short (<1 h, Dam and Peterson, 1988), and we assume that fecal pellets are released in the epipelagic zone, and thus, included in the sediment trap data. We are aware that this is not completely true as large copepods and euphausiids have longer gut passage times. However, because of the uncertainty in this transport and in order to be conservative in our estimations we did not add this flux.

Active flux by micronekton including mortality, excretion, and gut flux was also obtained from respiratory flux. Mortality was estimated from growth assuming steady-state conditions,

and using the growth/metabolism ratio of 0.66 given by Brett and Groves (1979). Excretion was estimated as in zooplankton (see above), gut flux assuming that carnivorous organisms egest an amount equivalent to the 40% of the respired carbon (Brett and Groves, 1979), and they transport feces to the mesopelagic because of their density and the long gut passage time of large animals. Thus, we used an egestion equivalent to 80% of the respired carbon as in Ariza et al. (2015) because of their residence at depth and their long gut passage time. Because of this, micronektonic migrants should egest after the downward migration. Thus, the egestion should be double in relation to respiration during 24 h. We are also aware that carbon egestion by marine fishes is also higher because they also release carbonate precipitates as a by-product of osmoregulation (see Wilson et al., 2009). In order to be also conservative in our estimations we did not consider this carbon egestion.

Primary production was obtained from remote sensing data following Behrenfeld and Falkowski (1997) through the Ocean Productivity web site[1] for the specific dates of the cruise and using the Vertical Generalized Production Model (VGPM). Values were averaged every 0.5° of longitude around the stations in order to account for the strong variability in the very productive upwelling zones, and because of the comparatively low turnover of zooplankton and micronekton.

RESULTS

Hydrography and Productivity

The section carried out covered the tropical and subtropical Atlantic Ocean from the very oligotrophic, high stratified waters off Brazil (**Figure 2A**) to the meso- and eutrophic waters off the Northwest African upwelling. Descriptions of the physical scenario were published elsewhere (Olivar et al., 2017; Armengol et al., 2019). In short, we moved from the South Equatorial Counter Current (SECC, stations 1–3) observing there a deep thermocline and high salinity (**Figure 2B**). Stations 4–6 were located in the South Equatorial Current (SEC) and the Intertropical Convergence Zone (ITCZ). The mid-ocean upwelling was close to station 6 and the North Equatorial Current (NEC) was near station 8. The Oxygen Minimum Zone (OMZ, **Figure 2C**) expanded from the south to stations 8 and 9, coinciding with the Guinea Dome, where the minimum dissolved oxygen values were observed. Northern stations were marked by the oceanic upwelling off Cape Blanc (Northwest Africa) except station 12 which was performed in the oceanic waters of the Canary Current.

As expected, we found a sharp chlorophyll gradient from the southern stations to the north, showing a deep chlorophyll maximum (DCM) related to the thermocline, and being shallower northward (**Figure 2D**). Chlorophyll *a* concentration at the DCM also increased northward and displayed higher values at those stations where the thermocline was shallower (**Figure 3A**). POC flux showed low values increasing northward in areas of high primary production (**Figure 3B**). Higher POC fluxes were observed in the Guinea Dome and in the oceanic upwelling off Cape Blanc. Primary production sharply increased north of the Guinea Dome and remained high through the oceanic upwelling off Cape Blanc, decreasing in the Canary Current (**Figure 3B**).

Zooplankton and Micronekton Biomass

Vertical profiles of zooplankton biomass were obtained from stations 2 to 12 during day and night (**Figure 4**). The gradient of productivity observed in fluorescence, chlorophyll *a*, and primary production was also observed in the zooplankton biomass, displaying quite low values in the SECC and SEC but increasing northward of the ITCZ (station 7). Zooplankton biomass was always higher at night in the epipelagic zone as the consequence of the diel vertical migration. Largest values of zooplankton migrant biomass were found in station 8 related to the Guinea Dome and in the oceanic upwelling off Northwest Africa (station 11, **Figure 5A**). The magnitude of this vertical migration was also related to the zooplankton biomass, showing higher migrant biomass in both stations 8 and 11 (**Table 1**). Variability of zooplankton migrant biomass was considerable, and changed over two orders of magnitude from the oligotrophic to the eutrophic waters.

Micronekton migrant biomass, as also expected, increased from the oligotrophic to the meso- and eutrophic stations in the Guinea Dome, and the upwelling off Northwest Africa (**Figure 5A**). Large migrant crustaceans increased north of the ITCZ coinciding with the lowest oxygen values in the water column, while fish migrant biomass showed less variability along the transect (**Figure 5B**). Micronekton biomass changed depending on the capture efficiency (CE) used to convert the catch to biomass (see Material and Methods). Differences between our quite conservative 50% CE, and the 20% CE were rather high (see **Figure 5A**), and illustrate the implications of the criteria used to estimate micronekton biomass. In any case, replicated hauls performed with the Mesopelagos trawl showed quite close values (see station 11 in **Figure 5A**).

Zooplankton and Micronekton Respiratory Flux

Zooplankton ETS activity profiles showed higher values in the epipelagic zone as expected from the higher temperature there (**Figure 6**). An increasing trend was also observed in the mesopelagic zone along the transect as temperature was higher at depth in the northern stations (**Table 1**). We also found statistically significant higher ETS activities during the day compared to night values in the mesopelagic zone (*t*-test for independent values, $p < 0.001$, **Figure 7A**). This higher activity was observed coinciding with the expected residence depth of migrants but also related to the oxygen minimum zone (see Hernández-León et al., 2019a).

Micronekton ETS activities were obtained in the epipelagic zone by night and at mesopelagic depths by day for fish (myctophids and bristlemouths) and crustaceans (decapods and euphausiids). Organisms captured by the Mesopelagos trawl sampling the entire water column were also corrected for the average temperature at 200–800 m layer (**Table 2** and **Figure 7B**).

[1] http://www.science.oregonstate.edu/ocean.productivity/index.php

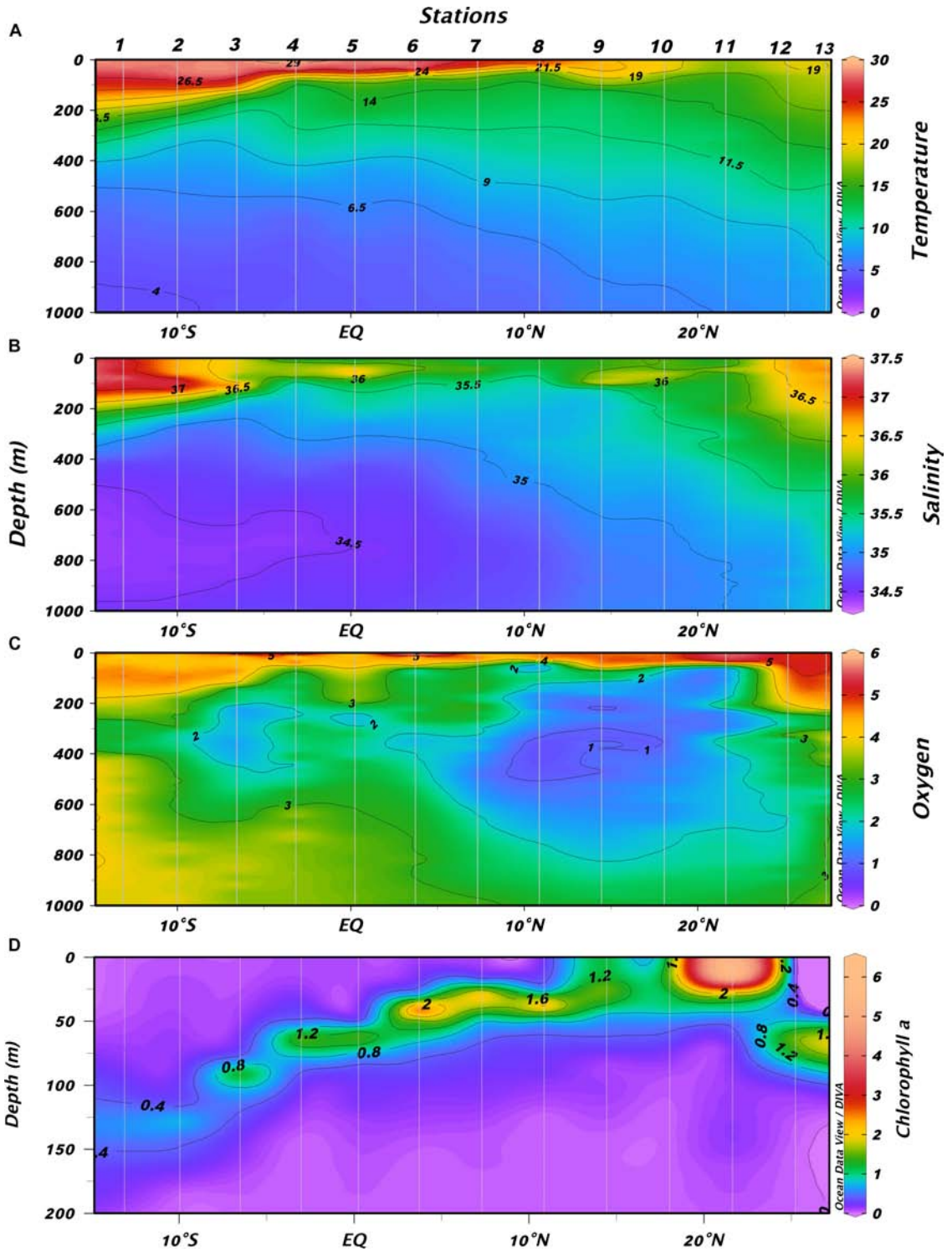

FIGURE 2 | Vertical distribution of **(A)** temperature (°C), **(B)** salinity, **(C)** oxygen (ml·l^{-1}), and **(D)** chlorophyll (mg·m^{-3}) along the transect performed in the tropical and subtropical Atlantic Ocean during the cruise.

ETS values along the transect were quite variable but, in general, increased north of the ITCZ (**Figure 7B**). We used all the ETS values from **Figure 7B** to derive respiration rates for the different groups at the average temperature for the 200–800 m layer at each station (**Table 1**). Myctophids showed values in the range 0.18–1.13 $\mu lO_2 \cdot mg\ Dw^{-1} \cdot h^{-1}$ (average 0.44 ± 0.31 SD),

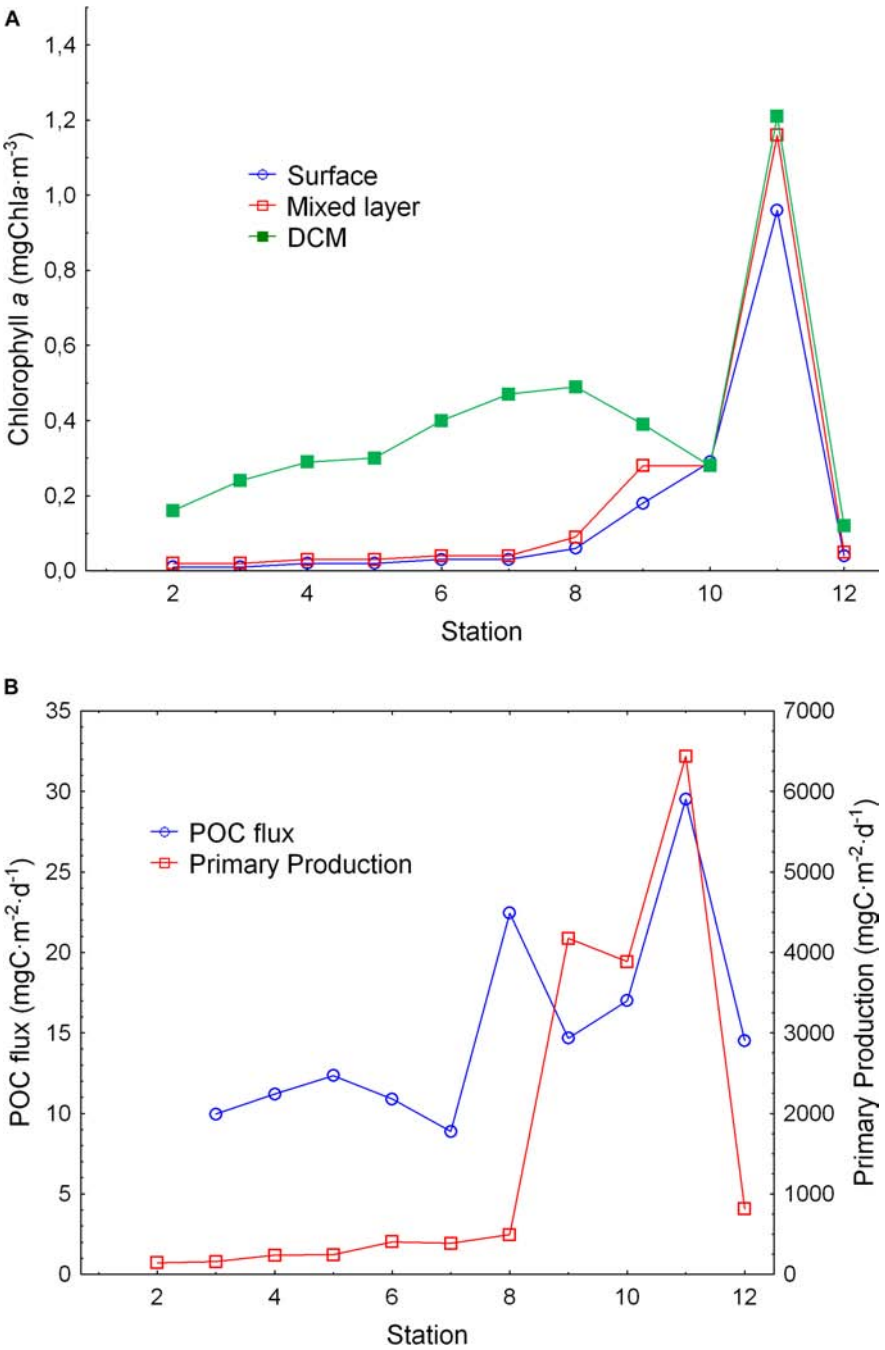

FIGURE 3 | (A) Chlorophyll at the surface (empty dots), mixed layer (empty squares), and at deep chlorophyll maximum (full squares). **(B)** POC flux (dots) and primary production (squares) obtained from remote sensing (VGPM model) along the transect performed during the cruise.

while respiration in bristlemouths was more variable and in the range 0.03–0.64 $\mu lO_2 \cdot mg\ Dw^{-1} \cdot h^{-1}$ (average 0.25 ± 0.24 SD). Respiration rates of decapods were in the range 0.03–2.29 $\mu lO_2 \cdot mg\ Dw^{-1} \cdot h^{-1}$ (average 0.66 ± 0.67 SD).

Respiratory flux by zooplankton was obtained from the migrant biomass and respiration rates by day averaged for the 200–800 m layer (**Table 1**). Values were higher in stations showing higher migrant biomass. Respiratory flux was highly correlated to migrant biomass as expected (as respiratory flux is a function of migrant biomass). This regression (**Figure 8A**) is given in order to compare to other results in the literature. In this sense, our values were highly comparable to previous studies also performed at the large-scale (**Figure 8A**, Hernández-León et al., 2019b). The new equation calculated using data from

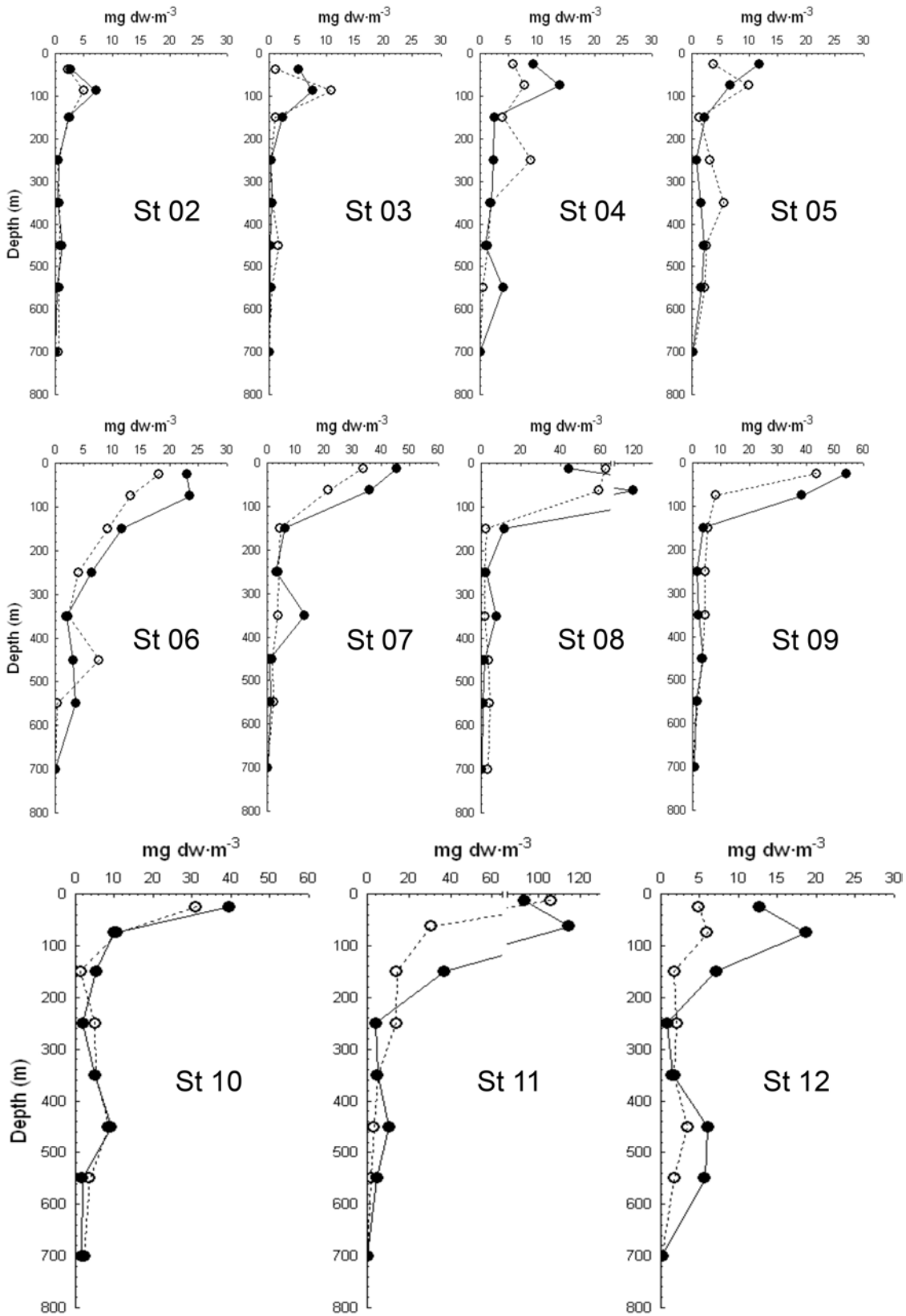

FIGURE 4 | Vertical distribution of zooplankton biomass during day (empty dots) and night (black dots) at the different stations along the Atlantic Ocean transect.

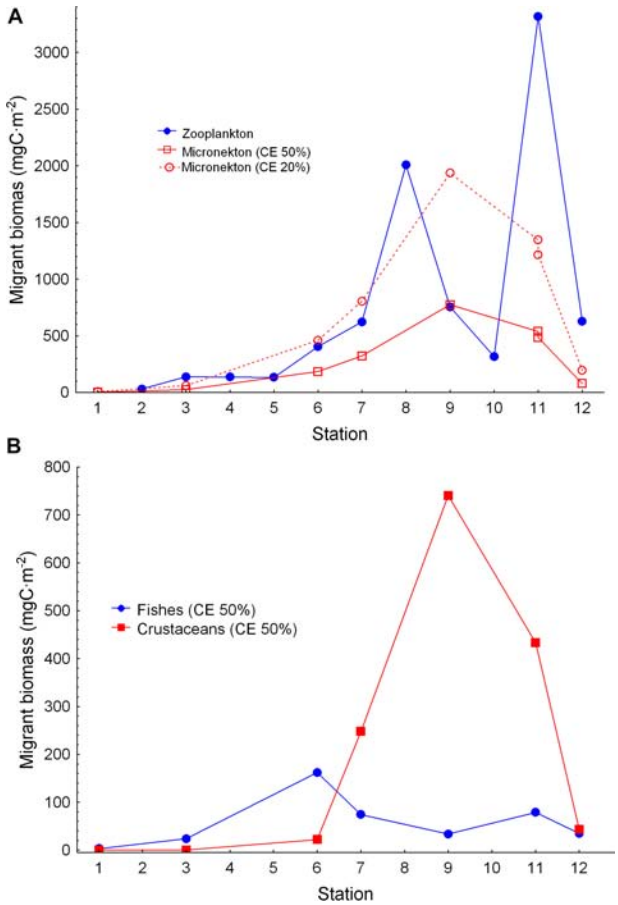

FIGURE 5 | (A) Zooplankton and micronekton migrant biomass (night minus day in the epipelagic zone) along the Atlantic transect. Micronekton migrant biomass was estimated at 20 and 50% of capture efficiency (see text) and it is depicted here for comparison. **(B)** Fish and crustacean migrant biomass along the transect.

both studies showed a highly significant correlation (r^2 = 0.866, $p < 0.001$, n = 20). The values from Hernández-León et al. (2019b) were recalculated using the same dry weight/protein ratio as used here and given by Hernández-León et al. (2019a) from a recent review of this ratio for subtropical waters. Respiratory flux by micronekton (myctophids and decapods) using the quite conservative capture efficiency of 50% was also highly correlated to migrant biomass, and relatively similar to the respiratory flux by zooplankton obtained in this study (**Figure 8B**).

Total Active Flux

We found a significant relationship between zooplankton and micronekton total active flux (Log_{10} Micronekton flux = −0.670 + 1.165·Log_{10} Zooplankton flux; r^2 = 0.756, $p < 0.05$, n = 6, see **Supplementary Figure S1**). So, in order to have a better picture of micronekton active flux and because of the limited set of data for this community (only seven stations), we used this relationship to estimate the total flux of micronekton for the other four stations (stations 4, 5, 8, and 10). Large values of zooplankton and micronekton flux were observed in the Guinea Dome (station 8) and in the upwelling zone off Northwest Africa (**Figure 9A**). Comparing POC flux and total active flux by both zooplankton and micronekton (**Figure 9B** and **Table 3**) we observed relatively constant values of POC flux along the transect with some larger values in the Guinea Dome and the oceanic upwelling off Cape Blanc, but also quite high values of total active flux coinciding with both upwelling areas. This is a striking result as active flux in both productive areas was observed between three and fivefold the POC flux (**Figure 9B**). These differences are clearly observed comparing the proportion of the different fluxes (zooplankton, micronekton, and POC flux) along the tropical and subtropical transect (**Figure 10**). As observed, POC flux is the most important component in very oligotrophic systems such as the SECC, but it sharply decreased as productivity increased northward. In the meso- and/or eutrophic zones of the Guinea Dome and the oceanic upwelling off Northwest Africa, POC flux was only 16–25% of total flux considered in this study (**Figure 10**).

Finally, despite the low number of both joint zooplankton and micronekton flux assessments, we found significant relationships between primary production obtained from remote sensing and total active flux (**Figure 11A**). Similarly, we observed primary production and POC flux also significantly correlated (**Figure 11B**). Total active flux was more variable than POC flux as noted from the different slopes, indicating a more important response of zooplankton and micronekton to an increase in productivity.

DISCUSSION

Zooplankton and micronekton vertical distribution, migrant biomass, and respiratory flux concurrently with passive flux were studied in a sharp gradient of productivity along a transect in the tropical and subtropical Atlantic Ocean. This is to our knowledge the first attempt to estimate these fluxes at the basin scale, and one of the very few assessments of both zooplankton and micronekton active flux in the ocean. We observed respiratory flux closely related to the migrant biomass as expected (**Figure 8**). This relationship in zooplankton was in accordance with a previous study, also at the large-scale in the Atlantic Ocean in a sharp gradient from the upwelling zone off Northwest Africa to central gyre waters (Hernández-León et al., 2019b). Respiratory flux in micronekton was also closely related to migrant biomass. However, the absolute value of this flux is still pending on the capture efficiency of the trawl used for sampling. This is an important shortcoming of our active flux assessment and clearly identifies a research subject for future studies. Besides trawl sampling, the role of new technologies such as optical systems and *in situ* acoustic systems should be developed to advance this knowledge.

Another feature of our sampling was the important role of decapods in the most productive area, and coinciding with the sharp oxygen minimum zones (OMZs) observed along our transect. This is similar to the results by Vereshchaka et al. (2016) who also found a high biomass of decapods in the tropical

TABLE 1 | Average temperature and zooplankton migrant biomass, ETS activity, respiration rates, and respiratory flux along the tropical and subtropical Atlantic Ocean.

Station	Average Temperature 200–800 m(°C)	SD	Migrant biomass ($mgC \cdot m^{-2}$)	Average sp. ETS at 200–800 m by day ($\mu lO_2 \cdot mg\ prot^{-1} \cdot h^{-1}$)	SD	Respiration at depth by day ($\mu lO_2 \cdot mg\ prot^{-1} \cdot h^{-1}$)	Respiration atdepth by day ($\mu lO_2 \cdot mg \cdot dw^{-1} \cdot h^{-1}$)	Respiration at depth by day (d^{-1})	Respiratory flux ($mgC \cdot m^{-2} \cdot d^{-1}$)	Respiratory flux ($mgC \cdot m^{-2} \cdot 12\,h^{-1}$)	POC flux ($mgC \cdot m^{-2} \cdot d^{-1}$)	Respiratory flux/POC (%)
2	7.47	2.61	29.5	4.73	2.57	2.37	0.95	0.03	0.9	0.4		
3	7.23	2.05	138.1	3.26	2.39	1.63	0.65	0.02	2.8	1.4	10.0	14.1
4	7.73	2.62	135.9	3.36	2.09	1.68	0.67	0.02	2.9	1.4	11.2	12.8
5	7.99	2.42	133.2	6.79	3.47	3.39	1.36	0.04	5.7	2.8	12.4	22.9
6	7.76	2.22	405.3	3.64	2.83	1.82	0.73	0.02	9.2	4.6	10.9	42.4
7	8.71	2.10	622.2	3.90	2.64	1.95	0.78	0.02	15.2	7.6	8.9	85.6
8	9.00	1.94	2007.5	6.63	6.07	3.32	1.33	0.04	83.3	41.6	22.5	185.5
9	9.56	1.59	755.3	4.70	2.00	2.35	0.94	0.03	22.2	11.1	14.7	75.6
10	9.71	1.81	317.5	2.71	1.23	1.36	0.54	0.02	5.4	2.7	17.0	15.8
11	10.48	1.84	3316.5	3.51	1.78	1.75	0.70	0.02	72.7	36.4	29.5	123.2
12	11.54	2.43	626.4	2.72	1.47	1.36	0.55	0.02	10.7	5.3	14.5	36.7
									Average	10.5	15.1	61.5
									SD	14.5	6.4	56.9

Respiratory flux was estimated for 12 h of organisms residence at depth during daylight hours. POC flux is also given and compared to the respiratory flux (in %). SD, standard deviation.

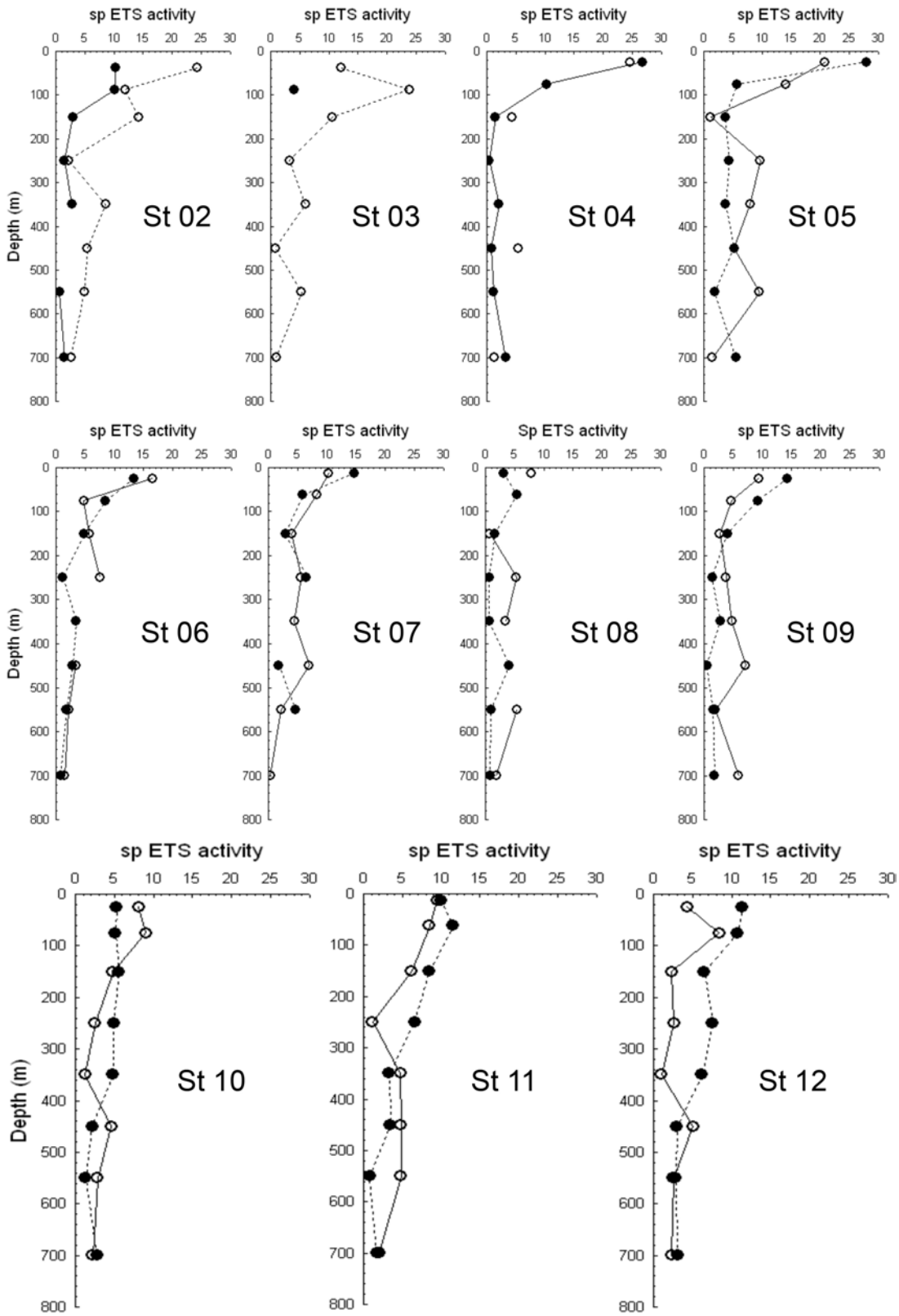

FIGURE 6 | Vertical profiles of zooplankton ETS activity (in $\mu lO_2 \cdot mg\ protein^{-1} \cdot h^{-1}$) along the transect. Empty dots are daylight activity values, while black dots are nighttime ETS activity.

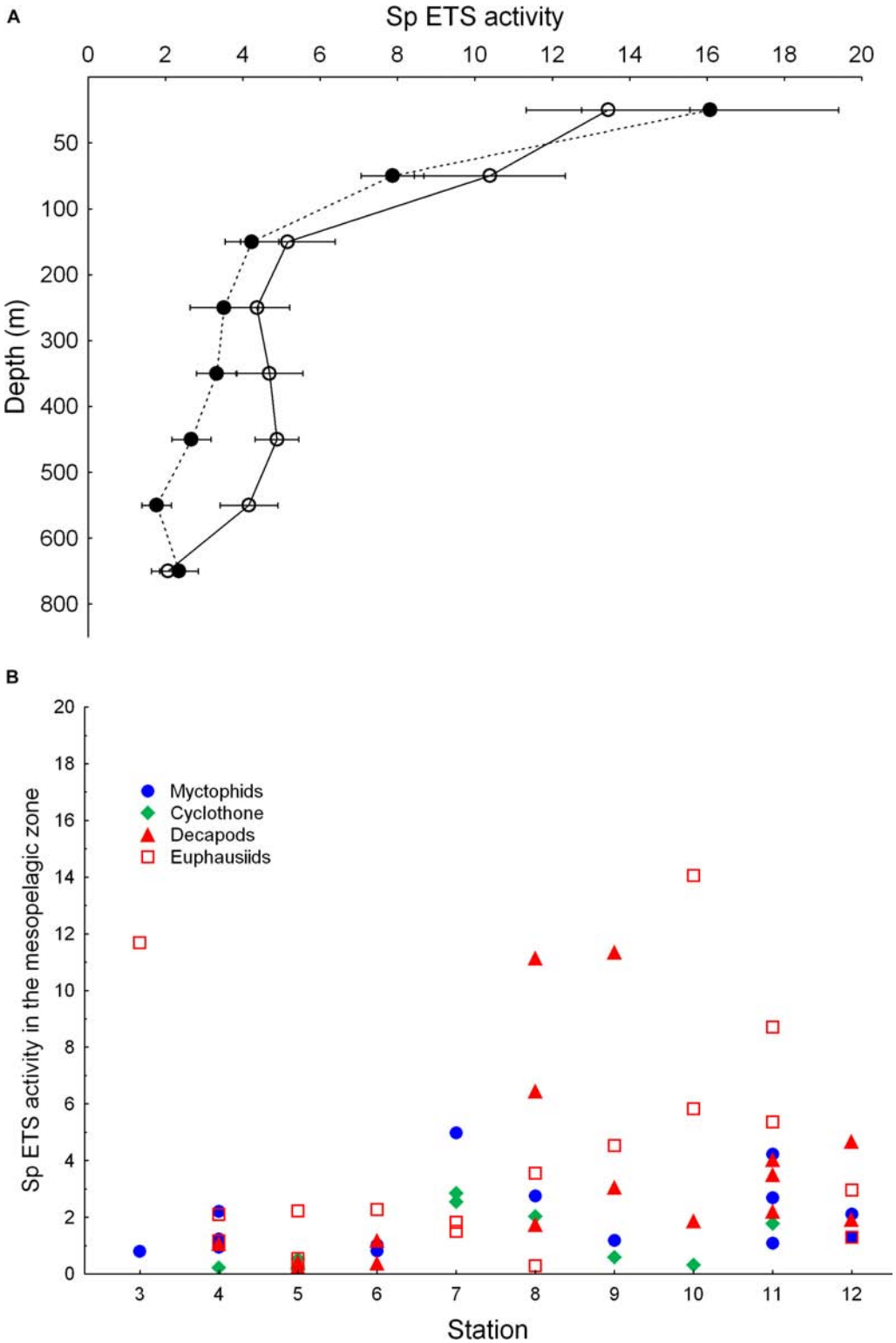

FIGURE 7 | (A) Vertical distribution of average zooplankton specific ETS activity (in $\mu lO_2 \cdot mg\ protein^{-1} \cdot h^{-1}$) during daytime (empty dots) and nighttime (black dots). Observe the higher ETS activity during daylight hours in the mesopelagic zone. **(B)** Specific ETS activity (in $\mu lO_2 \cdot mg\ protein^{-1} \cdot h^{-1}$) of fishes and crustaceans sampled in the mesopelagic zone along the transect. Organisms captured in the whole water column were analyzed for ETS and the activity calculated for the mesopelagic temperature given in **Table 1**.

TABLE 2 | Micronekton migrant biomass using 20 and 50% of capture efficiency for the Mesopelagos trawl and respiration rates, respiratory flux obtained using both capture efficiencies along the tropical and subtropical Atlantic Ocean.

Station	CE 50% Migrant biomass fishes ($mgC \cdot m^{-2}$)	CE 20% Migrant biomass fishes ($mgC \cdot m^{-2}$)	CE 50% Respiration ($mgC \cdot m^{-2} \cdot d^{-1}$)	CE 20% Respiration ($mgC \cdot m^{-2} \cdot d^{-1}$)	CE 50% Respiratory flux fishes ($mgC \cdot m^{-2} \cdot 12\,h^{-1}$)	CE 20% Respiratory flux fishes ($mgC \cdot m^{-2} \cdot 12\,h^{-1}$)
1	3.0	7.5	0.04	0.11	0.02	0.05
3	23.7	59.2	0.33	0.83	0.17	0.41
6	161.7	404.4	2.26	5.66	1.13	2.83
7	74.1	185.3	1.04	2.59	0.52	1.30
9	33.5	83.8	0.47	1.17	0.23	0.59
11	106.3	265.7	1.49	3.72	0.74	1.86
11	51.3	128.3	0.72	1.80	0.36	0.90
12	34.6	86.5	0.48	1.21	0.24	0.61
Mean	61.0	152.6			0.43	1.07
SD	51.7	129.1			0.36	0.90
	CE 50% Migrant biomass crustaceans ($mgC \cdot m^{-2}$)	**CE 20% Migrant biomass crustaceans ($mgC \cdot m^{-2}$)**	**CE 50% Respiration ($mgC \cdot m^{-2} \cdot d^{-1}$)**	**CE 20% Respiration ($mgC \cdot m^{-2} \cdot d^{-1}$)**	**CE 50% Respiratory flux crustaceans ($mgC \cdot m^{-2} \cdot 12\,h^{-1}$)**	**CE 20% Respiratory flux crustaceans ($mgC \cdot m^{-2} \cdot 12\,h^{-1}$)**
1	0.00	0.00	0.00	0.00	0.00	0.00
3	0.00	0.00	0.00	0.00	0.00	0.00
6	21.99	54.97	0.46	1.15	0.23	0.58
7	247.69	619.24	5.20	13.00	2.60	6.50
9	740.72	1851.81	15.56	38.89	7.78	19.44
11	431.80	1079.49	9.07	22.67	4.53	11.33
11	433.78	1084.46	9.11	22.77	4.55	11.39
12	43.14	107.84	0.91	2.26	0.45	1.13
Mean	239.9	599.7			2.52	6.30
SD	274.3	685.7			2.88	7.20
	CE 50% Migrant biomass fish + crustaceans ($mgC \cdot m^{-2}$)	**CE 20% Migrant biomass fish + crustaceans ($mgC \cdot m^{-2}$)**	**CE 50% Respiratory flux fish + crustaceans ($mgC \cdot m^{-2} \cdot 12\,h^{-1}$)**	**CE 20% Respiratory flux fish + crustaceans ($mgC \cdot m^{-2} \cdot 12\,h^{-1}$)**	**CE 50% Respiratory flux/POC (%)**	**CE 20% Respiratory flux/POC (%)**
1	3.0	7.5	0.02	0.05		
3	23.7	59.2	0.17	0.41	1.7	4.2
6	183.7	459.3	1.36	3.41	12.5	31.3
7	321.8	804.5	3.12	7.80	35.2	87.9
9	774.2	1935.6	8.01	20.03	54.6	136.4
11	538.1	1345.2	5.28	13.19	17.9	44.7
11	485.1	1212.8	4.91	12.28	16.6	41.6
12	77.7	194.3	0.70	1.74	4.8	12.0
Mean	300.9	752.3	2.95	7.37	20.5	51.2
SD	278.7	696.8	2.90	7.25	18.5	46.4

Respiratory flux was estimated for 12 h of organisms residence at depth during daylight hours. POC flux is also given and compared to the respiratory flux (in %). SD, standard deviation.

zone, in a similar transect in the Atlantic Ocean. Previous papers emphasized the importance of mesopelagic fishes in relation to decapods and large euphausiids in the micronekton flux (Ariza et al., 2015). This was the case in our transect for the oligotrophic and equatorial zones. However, decapods were abundant in the most productive zones (**Figure 5B**). Important values of the respiratory flux was also observed for these organisms by Schukat et al. (2013) in upwelling zones, thus, their role in active flux could be considerable. We also observed decapod abundance to match not only the most productive areas but also the OMZs. Many migrant decapods are known to be adapted to survive at quite low oxygen concentrations (Childress, 1975). These organisms are able to regulate their respiration to live aerobically in these OMZs. Thus, this observation could explain at least in part, the large biomass of decapods in the area related to the OMZs in this Atlantic transect.

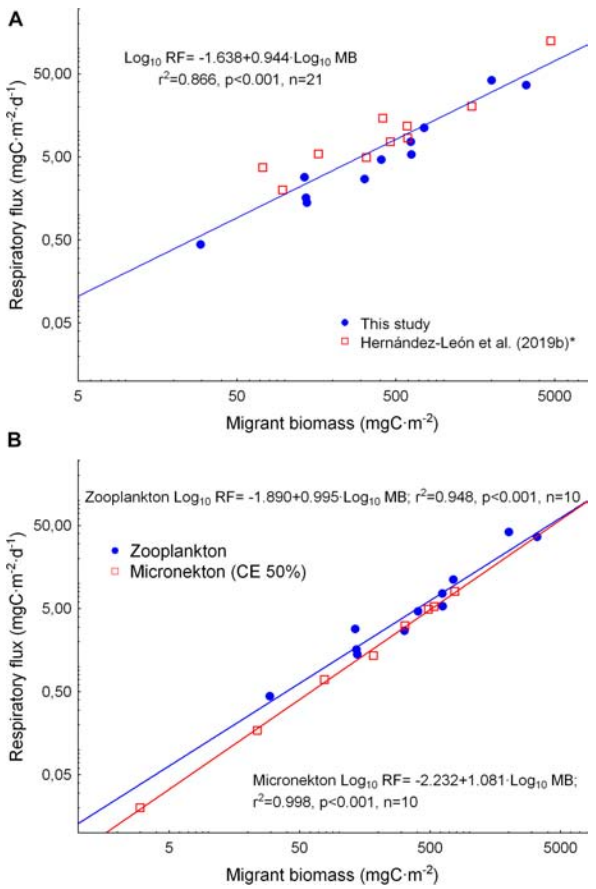

FIGURE 8 | (A) Relationship between zooplankton migrant biomass and respiratory flux for this study (filled dots) and results by Hernández-León et al. (2019b). The data from the latter authors were converted to the new Dw/Prot ratio of Hernández-León et al. (2019a). See text for details. **(B)** Comparison between migrant biomass and respiratory fluxes by zooplankton and micronekton in the present study using a 50% of capture efficiency for the Mesopelagos trawl.

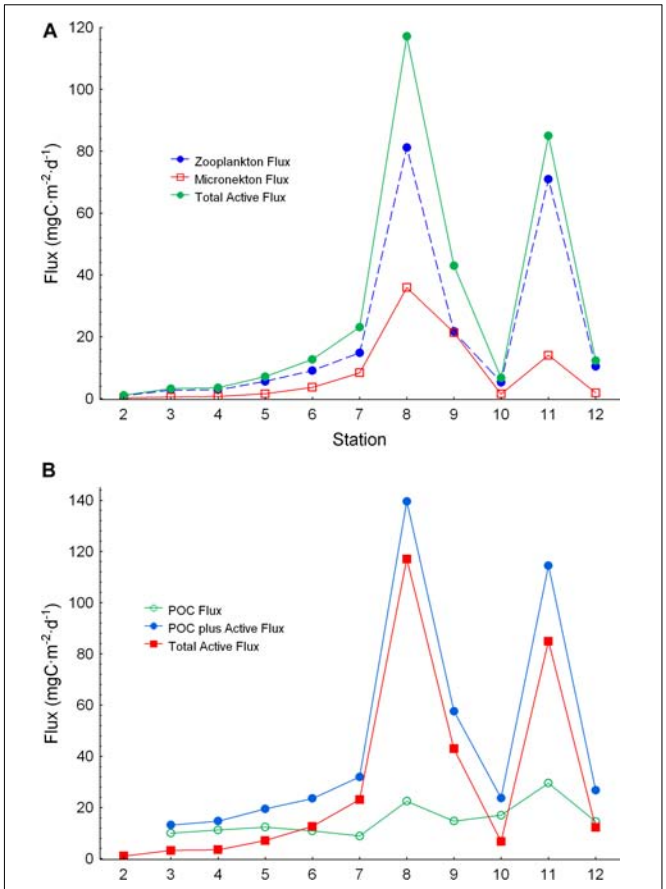

FIGURE 9 | (A) Active flux by zooplankton and micronekton using a 50% capture efficiency for the Mesopelagos trawl, and total active flux by both communities. **(B)** Comparison between total active flux and POC flux, and estimated total flux. Micronekton active flux for stations 4, 5, 8, and 10 were estimated from zooplankton active flux (see text).

In any case, our estimates of zooplankton and micronekton active flux were obtained using quite conservative values. Firstly, zooplankton biomass is always considered undersampled due to avoidance of nets by organisms, mainly large zooplankton which are the bulk of migrant biomass. The undersampling in micronekton was considered above (see section "Material and Methods") but here we used a 50% catch efficiency which is quite conservative. At least, there is no study showing values of the capture efficiency larger than the one used here. In order to keep our assessments conservative in both communities, ETS activity were converted to respiration rates (R) using a R/ETS ratio of 0.5. This ratio is also quite conservative as recently found for migrant copepods (Hernández-León et al., 2019a). These authors observed no differences in mesopelagic respiration between the R/ETS ratio of 1, and the values obtained using the equations of Ikeda (1985) and Ikeda (2014) derived from temperature, body weight, and depth. A R/ETS ratio between 0.5 and 1 during the residence time of migrant organisms at depth approaches better to respiration rates in nature as observed by Hernández-León et al. (2019a). However, we kept the lower value in order to maintain a conservative estimate of active flux. This criterion was also used to convert ETS activity to respiration rates in micronekton. Thus, our assessment of respiratory flux in both communities should be considered as a base line for this downward carbon transport in the ocean due to vertical migrants. In any case, ETS activities obtained were compared to previous studies (Ariza et al., 2015) and ranged closely, indicating that values were comparable in magnitude.

Higher active flux is expected in productive areas because organisms with a low turnover such as large zooplankton and micronekton could develop into high biomass because of the large and constant food supply. However, POC flux did not increase in a similar proportion in those productive areas. We found respiratory to POC flux ratios to increase toward the most productive area in the north, and quite high values in the Guinea Dome and the oceanic upwelling off Cape Blanc (>100%, **Table 1**). Similarly, Hernández-León et al. (2019b) found 2.5-fold higher POC flux in the most oligotrophic environment (a

TABLE 3 | Total active flux estimated as the sum of respiratory flux and estimated mortality, excretory, and gut flux performed by zooplankton and micronekton in comparison to primary production obtained by remote sensing (VGPM model) and POC flux obtained using sediment traps.

Station	Primary production ($mgC \cdot m^{-2} \cdot d^{-1}$)	SD	Zooplankton total active flux ($mgC \cdot m^{-2} \cdot 12\,h^{-1}$)	CE 50% Micronekton total active flux ($mgC \cdot m^{-2} \cdot 12\,h^{-1}$)	CE 20% Micronekton total active flux ($mgC \cdot m^{-2} \cdot 12\,h^{-1}$)	CE 50% Total active flux/POC (%)	CE 20% Total active flux/POC (%)
1				0.1	0.1	–	–
2	144	10	0.9	–	–	–	–
3	158	11	2.7	0.4	1.1	4.4	11.1
4	236	13	2.8	–	–	–	–
5	243	23	5.5	–	–	–	–
6	405	50	9.0	3.6	9.1	33.3	83.2
7	384	17	14.8	8.3	20.7	93.6	233.9
8	492	11	81.2	–	–	–	–
9	4175	578	21.6	21.3	53.3	145.2	362.9
10	3887	2383	5.2	–	–	–	–
11	6438	4409	70.9	14.0	35.1	47.5	118.9
11	–	–	–	13.1	32.7	44.3	110.7
12	814	90	10.4	1.8	4.6	12.7	31.8
Mean			20.5	7.8	19.6	54.4	136.1
SD			27.6	7.7	19.3	49.3	123.3

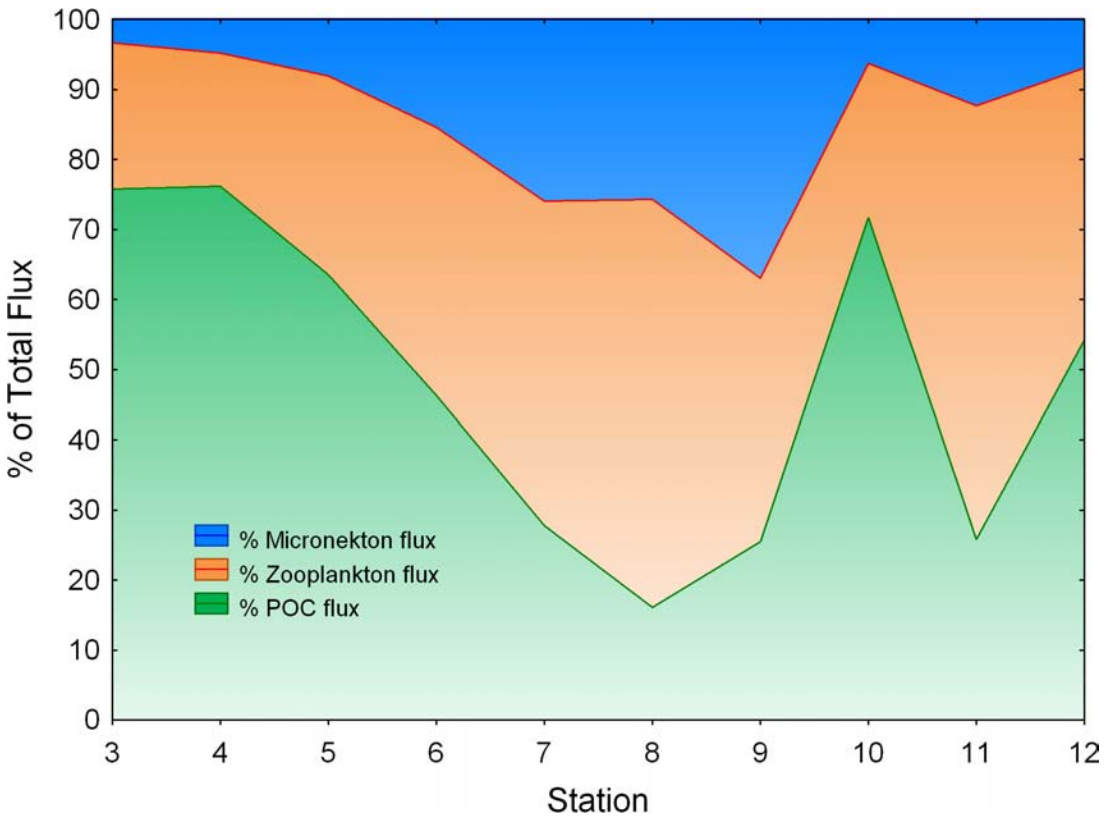

FIGURE 10 | Percentage of POC flux (lower), zooplankton active flux (middle), and micronekton flux using a 50% capture efficiency for the Mesopelagos trawl (upper). Observe the decreasing percentage of POC flux as productivity increases. Micronekton active flux for stations 4, 5, 8, and 10 were estimated from zooplankton active flux (see text).

longitudinal transect south of the Canary Islands) compared to the most productive zone sampled (a longitudinal transect departing from Cape Blanc along the Cape Vert Frontal Zone). Zooplankton respiratory flux was, on average, less than 10% of POC flux in the oligotrophic transect while it was higher than 40% in the most productive. They explained this relationship

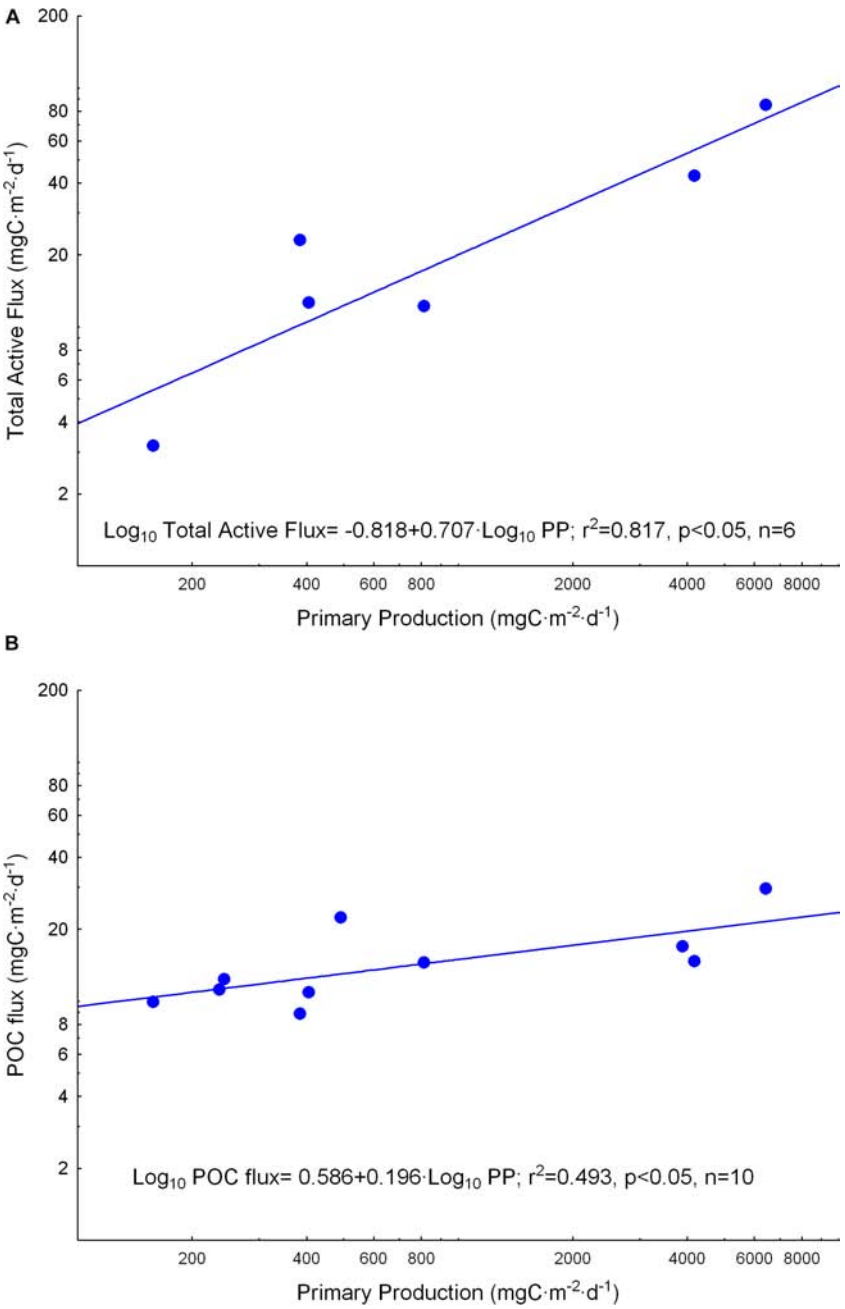

FIGURE 11 | Relationships between primary production obtained from remote sensing (VGPM model) and **(A)** total active flux by zooplankton and micronekton, and **(B)** particle organic carbon (POC) flux measured using drifting sediment traps at 150 m depth.

between POC and active fluxes as (1) the processing of particles by zooplankton, shaping the downward flux of particles, (2) the intense lateral transport of particles from the upwelling zone to the open ocean, or (3) both. The first explanation is supported by the zooplankton processing and fragmentation of particles through feeding in the epipelagic zone (Le Moigne et al., 2016; Cavan et al., 2017). However, in areas affected by upwelling, the offshore transport of particulate organic matter is known to be considerable (Lovecchio et al., 2017). This transport to the open ocean promotes lower sedimentation because of the lateral transport of particles, and longer residence times in the epipelagic zone, therefore, favoring the zooplankton and prokaryotes processing of particles in the upper layers. Our results in the oceanic upwelling off Cape Blanc could be affected by this offshore transport. In the Guinea Dome, lateral transport should also be important as we sampled in the area affected by the westward motion of the cyclonic structure, probably transporting the highly productive coastal upwelled waters. In this sense,

Armengol et al. (2019) showed a filament-like structure affecting station 8 in their surface map of primary production during the same oceanographic cruise (see their Figure 5). Whatever the effect of zooplankton or lateral advection, in areas of high primary production large organisms are favored (e.g., Frost, 1974), as constant energy fuels their longer lives, therefore, promoting a large biomass.

The large values of total active flux observed in areas of persistent productivity such as the mid-ocean upwelling, the Guinea Dome, or the oceanic upwelling off Cape Blanc suggests that the oceanic carbon pump is quite variable and active flux is not simply a constant value of POC flux as it is suggested in recent models (14–18%, Aumont et al., 2018; Archibald et al., 2019). In these studies as well as in the recent review by Steinberg and Landry (2017), active flux showed values lower than about 30 $mgC \cdot m^{-2} \cdot d^{-1}$ which is coincident with the values obtained during most of our Atlantic transect (**Figure 9B**). Thus, their models should reflect the general picture as about 70% of the ocean is oligotrophic. However, the magnitude of the biological carbon pump is quite variable as observed here in a sharp gradient of productivity along the tropical and subtropical Atlantic Ocean (**Figure 10**). Although most of the ocean is oligotrophic, mesoscale activity is widespread and it is known that there is an increase in productivity in these mesoscale structures maintained over long periods (McGillicuddy et al., 1998; Mahadevan, 2016). This increase in active flux by zooplankton related to mesoscale structures was observed long ago by Yebra et al. (2005) in an anticyclonic eddy shed by the Canary Islands. Recently, Yebra et al. (2018) also showed large active flux values by zooplankton in the Alboran gyre in the Mediterranean Sea. Thus, the development of zooplankton and micronekton related to mesoscale eddies, rings, or oceanic frontal zones could promote sharp increments in the downward carbon transport due to active flux. Moreover, sustained natural (e.g., dust) or artificial (e.g., iron) fertilized areas should also promote an increase of low turnover communities such as zooplankton and micronekton vertical migrants in the long run, promoting vertical flux beyond the immediate effect of an increase in productivity in shallow waters.

In this sense, the large values of active flux observed in the Guinea Dome deserves some attention. Recently, Stukel et al. (2018) found a dominant role of vertical migrants in the biological pump in the Costa Rica Dome, an analogous physical structure to the open-ocean upwelling of the Guinea Dome. Using a different approach, they observed active transport by the pelagic fauna as the dominant vertical transport mechanism, and only 11–17% of export was due to other mechanisms (physical mixing and phytoplankton sinking). This high active flux in the Costa Rica Dome is similar to our results in the Guinea Dome, as we also observed a low proportion of POC flux compared to the zooplankton and micronekton downward transport. Stukel et al. (2018) explained the energy transfer from the characteristic small phytoplankton (cyanobacteria) of these physical structures to zooplankton due to the role of protists as an important intermediate trophic level in these upwelling systems. Armengol et al. (2019) during our cruise observed the Guinea Dome dominated by small cells (picoeukaryotes and *Synechococcus*), not showing a high microzooplankton biomass compared to other productive stations, but displaying relatively high autotroph growth rates at the surface layer. In any case, oceanic domes are physical structures promoting an important role of the pelagic fauna in the biological pump. Whatever the mechanism, continuous fueling of primary production, the role of protists, or both, the study of active flux in these oceanic structures seems of interest in order to understand the functioning of pelagic systems.

Finally, despite the limited data set of both zooplankton and micronekton active flux in the present study, we found primary production obtained from remote sensing quite well correlated to total active flux by both communities (**Figure 11A**). POC flux was also significantly correlated to primary production in our study (**Figure 11B**), but showed a lower slope, therefore, varying less than total active flux. This lower slope should be related to lateral advection and the processing of particles by zooplankton as discussed above. Thus, the role of zooplankton and micronekton in driving the biological pump seems of paramount importance. Further research is required to verify the former equation as it could allow the estimation of total active flux from remote sensing.

In summary, we observed a striking response of the biological pump in areas of persistent high primary production through the growth of zooplankton and micronekton vertical migrant populations. Their metabolism could promote an increase in the carbon flux of, at least, twofold the POC flux, promoting quite high active flux values (**Figure 9**). As observed, there is a small response of POC flux to gradients in productivity compared to the effect of the migrant fauna. So, in areas of high productivity most of the vertical flux is suggested to be performed by zooplankton and micronekton (**Figure 10**). Our assessment of active flux was quite conservative as we used a high capture efficiency for the micronekton trawl (50%), and a quite conservative estimation of respiration rates (R/ETS ratio of 0.5, see Hernández-León et al., 2019a). Thus, our results considering both zooplankton and micronekton communities open new avenues to evaluate the export of carbon in the ocean and the functioning of the pelagic realm. These results confirm the importance of the mesopelagic-migrant pump in driving the biological pump (Boyd et al., 2019).

DATA AVAILABILITY

The datasets generated for this study are available on request to the corresponding author.

AUTHOR CONTRIBUTIONS

SH-L designed and promoted this study, acted as cruise leader, and measured ETS activity. MO, CL-P, VT, and JG-G sampled, measured biomass, and classified micronekton organisms. MFP sampled and classified the zooplankton organisms. AB measured the passive flux. AC designed the multi-sampler and deployed the Mesopelagos net. All authors contributed to the interpretation and writing of the manuscript as well as discussion of results and comments on the manuscript.

FUNDING

This work was supported by projects "Migrants and Active Flux in the Atlantic Ocean" (MAFIA, CTM2012-39587-C04), and "Biomass and Active Flux in the Bathypelagic Zone" (Bathypelagic, CTM2016-78853-R) from the Spanish Ministry of Economy and Competitiveness.

ACKNOWLEDGMENTS

We would like to thank the two reviewers for their efforts to amend the manuscript. We are also indebted to the crew and other scientists on board the research vessel "Hespérides," and the technicians of the "Unidad de Tecnología Marina" (UTM) for their support and help during the cruise. This article is a publication of the Unidad Océano y Clima, Universidad de Las Palmas de Gran Canaria, a R&D&i CSIC-associated unit.

SUPPLEMENTARY MATERIAL

The Supplementary Material for this article can be found online at: https://www.frontiersin.org/articles/10.3389/fmars.2019.00535/full#supplementary-material

FIGURE S1 | Relationship between total active flux of zooplankton and micronekton.

REFERENCES

Angel, M. V. (1989). "Does mesopelagic biology affect the vertical flux?," in *Productivity of the Ocean: Present and Past*, eds W. H. Berger, V. S. Smetacek, and G. Wefer (New York, NY: Wiley), 155–173.

Archibald, K. M., Siegel, D. A., and Doney, S. C. (2019). Modeling the impact of zooplankton diel vertical migration on the carbon export flux of the biological pump. *Glob. Biogeochem. Cycles* 33, 181–199. doi: 10.1029/2018GB005983

Ariza, A., Garijo, J. C., Landeira, J. M., Bordes, F., and Hernández-León, S. (2015). Migrant biomass and respiratory carbon flux by zooplankton and micronekton in the subtropical northeast Atlantic Ocean (Canary Islands). *Prog. Oceanogr.* 134, 330–342. doi: 10.1016/j.pocean.2015.03.003

Armengol, L., Calbet, A., Franchy, G., Rodríguez-Santos, A., and Hernández-León, S. (2019). Planktonic food web structure and trophic transfer efficiency along a productivity gradient in the tropical and subtropical Atlantic Ocean. *Sci. Rep.* 9:2044. doi: 10.1038/s41598-019-38507-9

Aumont, O., Maury, O., Lefort, S., and Bopp, L. (2018). Evaluating the potential impacts of the diurnal vertical migration by marine organisms on marine biogeochemistry. *Glob. Biogeochem. Cycles* 32, 1622–1643. doi: 10.1029/2018GB005886

Bailey, T. G., Youngbluth, M. J., and Owen, G. P. (1995). Chemical composition and metabolic rates of gelatinous zooplankton from midwater and benthic boundary layer environments off Cape Hatteras, North Carolina, USA. *Mar. Ecol. Prog. Ser.* 122, 121–134. doi: 10.3354/meps122121

Behrenfeld, M. J., and Falkowski, P. G. (1997). Photosynthetic rates derived from satellite-based chlorophyll concentration. *Limnol. Oceanogr.* 42, 1–20. doi: 10.4319/lo.1997.42.1.0001

Boyd, P. W., Claustre, H., Levy, M., Siegel, D. A., and Weber, T. (2019). Multi-faceted particle pumps drive carbon sequestration in the ocean. *Nature* 568, 327–336. doi: 10.1038/s41586-019-1098-2

Brett, J. R., and Groves, T. D. D. (1979). Physiological energetics. *Fish Physiol.* 8, 280–352.

Buesseler, K. O., Antia, A. N., Chen, M., Fowler, S. W., Gardner, W. D., Gustafsson, O., et al. (2007). An assessment of the use of sediment traps for estimating upper ocean particle fluxes. *J. Mar. Res.* 65, 345–416. doi: 10.1357/002224007781567621

Castonguay, M., and McCleave, J. D. (1987). Vertical distributions, diel and ontogenetic vertical migrations and net avoidance of leptocephali of Anguilla and other common species in the Sargasso Sea. *J. Plankton Res.* 9, 195–214. doi: 10.1093/plankt/9.1.195

Cavan, E. L., Henson, S. A., Belcher, A., and Sanders, R. (2017). Role of zooplankton in determining the efficiency of the biological carbon pump. *Biogeosciences* 14, 177–186. doi: 10.5194/bg-14-177-2017

Childress, J. J. (1975). The respiratory rates of midwater crustaceans as a function of depth of occurrence and relation to the oxygen minimum layer off southern California. *Comp. Biochem. Physiol. Part A Physiol.* 50, 787–799. doi: 10.1016/0300-9629(75)90146-2

Childress, J. J., and Nygaard, M. H. (1973). The chemical composition of midwater fishes as a function of depth of occurence off southern California. *Deep Sea Res.* 20, 1093–1109. doi: 10.1016/0011-7471(73)90023-5

Dam, H. G., and Peterson, W. T. (1988). The effect of temperature on the gut clearance rate constant of planktonic copepods. *J. Exp. Mar. Biol. Ecol.* 123, 1–14. doi: 10.1016/0022-0981(88)90105-0

Dam, H. G., and Peterson, W. T. (1993). Seasonal contrasts in the diel vertical distribution, feeding behavior, and grazing impact of the copepod Temora longicornis in Long Island Sound. *J. Mar. Res.* 51, 561–594. doi: 10.1357/0022240933223972

Davison, P. C. (2011). *The Export of Carbon Mediated by Mesopelagic Fishes in the Northeast Pacific Ocean*. PhD Thesis, University of California, San Diego, CA.

Davison, P. C., Checkley, D. M. Jr., Koslow, J. A., and Barlow, J. (2013). Carbon export mediated by mesopelagic fishes in the northeast Pacific Ocean. *Prog. Oceanogr.* 116, 14–30. doi: 10.1016/j.pocean.2013.05.013

Frost, B. W. (1974). "Feeding processes at lower trophic levels in pelagic communities," in *The Biology of Oceanic Pacific*, ed. C. B. Miller (Corvallis, OR: Oregon State University Press), 59–77.

Gjøsaeter, J. (1984). Mesopelagic fish, a large potential resource in the Arabian Sea. *Deep Sea Res.* 31, 1019–1035. doi: 10.1016/0198-0149(84)90054-2

Gómez, M., Torres, S., and Hernández-León, S. (1996). Modification of the electron transport system (ETS) method for routine measurements of respiratory rates of zooplankton. *South Afr. J. Mar. Sci.* 17, 15–20. doi: 10.2989/025776196784158446

Grosjean, P., and Denis, K. (2007). *Zoo/PhytoImage Version 1.2–0. User's Manual*. Available at: http://www.sciviews.org/zooimage (accessed September 9, 2011).

Guidi, L., Legendre, L., Reygondeau, G., Uitz, J., Stemmann, L., and Henson, S. A. (2015). A new look at ocean carbon remineralization for estimating deep-water sequestration. *Glob. Biogeochem. Cycles* 29, 1044–1059. doi: 10.1002/2014gb005063

Hernández-León, S., and Gómez, M. (1996). Factors affecting the respiration/ETS ratio in marine zooplankton. *J. Plankton Res.* 18, 239–255. doi: 10.1093/plankt/18.2.239

Hernández-León, S., and Montero, I. (2006). Zooplankton biomass estimated from digitalized images in Antarctic waters: a calibration exercise. *J. Geophys. Res. Oceans* 111:C05s03. doi: 10.1029/2005JC002887

Hernández-León, S., Calles, S., and Fernández de Puelles, M. L. (2019a). The estimation of metabolism in the mesopelagic zone: disentangling deep-sea respiration. *Prog. Oceanogr.* 178. doi: 10.1016/j.pocean.2019.102163

Hernández-León, S., Putzeys, S., Almeida, C., Bécognée, P., Marrero-Diaz, A., Arístegui, J., et al. (2019b). Carbon export through zooplankton active flux in the Canary current. *J. Mar. Syst.* 189, 12–21. doi: 10.1016/j.jmarsys.2018.09.002

Hidaka, K., Kawaguchi, K., Murakami, M., and Takahashi, M. (2001). Downward transport of organic carbon by diel migratory micronekton in the western equatorial Pacific: its quantitative and qualitative importance. *Deep Sea Res. I* 48, 1923–1939. doi: 10.1016/s0967-0637(01)00003-6

Honjo, S., Manganini, S. J., Krishfield, R. A., and Francois, R. (2008). Particulate organic carbon fluxes to the ocean interior and factors controlling the biological

pump: a synthesis of global sediment trap programs since 1983. *Prog. Oceanogr.* 76, 217–285. doi: 10.1016/j.pocean.2007.11.003

Hopkins, T. L., Sutton, T., and Lancraft, T. M. (1996). The trophic structure and predation impact of a low latitude midwater fish assemblage. *Prog. Oceanogr.* 38, 205–239. doi: 10.1016/s0079-6611(97)00003-7

Hudson, J. M., Steinberg, D. K., Sutton, T. T., Graves, J. E., and Latour, R. J. (2014). Myctophid feeding ecology and carbon transport along the northern Mid-Atlantic Ridge. *Deep Sea Res. I* 93, 104–116. doi: 10.1016/j.dsr.2014.07.002

Ikeda, T. (1985). Metabolic rates of epipelagic marine zooplankton as a function of body mass and temperature. *Mar. Biol.* 85, 1–11. doi: 10.1007/bf00396409

Ikeda, T. (2014). Respiration and ammonia excretion by marine metazooplankton taxa: synthesis toward a global-bathymetric model. *Mar. Biol.* 161, 2753–2766. doi: 10.1007/s00227-014-2540-5

Ikeda, T., and Motoda, S. (1978). Estimated zooplankton production and their ammonia excretion in the Kuroshio and adjacent seas. *Fish. Bull.* 76, 357–367.

Jónasdóttir, S. H., Visser, A. W., Richardson, K., and Heath, M. R. (2015). Seasonal copepod lipid pump promotes carbon sequestration in the deep North Atlantic. *Proc. Natl. Acad. Sci. U.S.A.* 112, 12122–12126. doi: 10.1073/pnas.1512110112

Kaartvedt, S., Staby, A., and Aksnes, D. L. (2012). Efficient trawl avoidance by mesopelagic fishes causes large underestimation of their biomass. *Mar. Ecol. Prog. Ser.* 456, 1–6. doi: 10.3354/meps09785

Kenner, R. A., and Ahmed, S. I. (1975). Measurements of electron transport activities in marine phytoplankton. *Mar. Biol.* 33, 119–127. doi: 10.1007/bf00390716

Kloser, R. J., Ryan, T. E., Young, J. W., and Lewis, M. E. (2009). Acoustic observations of micronekton fish on the scale of an ocean basin: potential and challenges. *ICES J. Mar. Sci.* 66, 998–1006. doi: 10.1093/icesjms/fsp077

Knauer, G. A., Martin, J. H., and Bruland, K. W. (1979). Fluxes of particulate carbon, nitrogen, and phosphorus in the upper water column of the northeast Pacific. *Deep Sea Res. I* 26, 97–108. doi: 10.1016/0198-0149(79)90089-x

Koslow, J. A., Kloser, R. J., and Williams, A. (1997). Pelagic biomass and community structure over the mid-continental slope off southeastern Australia based upon acoustic and midwater trawl sampling. *Mar. Ecol. Prog. Ser.* 146, 21–35. doi: 10.3354/meps146021

Le Borgne, R., and Rodier, M. (1997). Net zooplankton and the biological pump: a comparison between the oligotrophic and mesotrophic equatorial Pacific. *Deep Sea Res. II* 44, 2003–2023. doi: 10.1016/s0967-0645(97)00034-9

Le Moigne, F. A., Henson, S. A., Cavan, E., Georges, C., Pabortsava, K., Achterberg, E. P., et al. (2016). What causes the inverse relationship between primary production and export efficiency in the Southern Ocean? *Geophys. Res. Lett.* 43, 4457–4466. doi: 10.1002/2016gl068480

Lehette, P., and Hernández-León, S. (2009). Zooplankton biomass estimation from digitized images: a comparison between subtropical and Antarctic organisms. *Limnol. Oceanogr. Methods* 7, 304–308. doi: 10.4319/lom.2009.7.304

Lindsay, D. J. (2003). Carbon and nitrogen contents of mesopelagic organisms: results from Sagami Bay, Japan. *JAMSTEC J. Deep Sea Res.* 22, 1–13.

Longhurst, A. R., Bedo, A. W., Harrison, W. G., Head, E. J. H., and Sameoto, D. D. (1990). Vertical flux of respiratory carbon by oceanic diel migrant biota. *Deep Sea Res. I* 37, 685–694. doi: 10.1016/0198-0149(90)90098-g

Lovecchio, E., Gruber, N., Münnich, M., and Lachkar, Z. (2017). On the long-range offshore transport of organic carbon from the Canary Upwelling System to the open North Atlantic. *Biogeosciences* 14, 3337–3369. doi: 10.5194/bg-14-3337-2017

Lowry, O. H., Rosebrough, N. J., Farr, A. L., and Randall, R. J. (1951). Protein measurement with the Folin phenol reagent. *J. Biol. Chem.* 193, 265–275.

Mahadevan, A. (2016). The impact of submesoscale physics on primary productivity of plankton. *Annu. Rev. Mar. Sci.* 8, 161–184. doi: 10.1146/annurev-marine-010814-015912

May, J. L., and Blaber, S. J. M. (1989). Benthic and pelagic fish biomass of the upper continental slope off eastern Tasmania. *Mar. Biol.* 101, 11–25. doi: 10.1007/bf00393474

McGillicuddy, D. J. Jr., Robinson, A. R., Siegel, D. A., Jannasch, H. W., Johnson, R., Dickey, T. D., et al. (1998). Influence of mesoscale eddies on new production in the Sargasso Sea. *Nature* 394, 263–266. doi: 10.1038/28367

Meillat, M. (2012). Essais du chalut mésopélagos pour le programme MYCTO 3D-MAP de l'IRD, à bord du Marion Dufresne. IFREMER Rapport de mission Marion Dufresne. R.INT.RBE/STH/LTH 2012–2015.

Olivar, M. P., Bode, A., López-Pérez, C., Hulley, P. A., and Hernández-León, S. (2018a). Trophic position of lanternfishes (Pisces: Myctophidae) of the tropical and equatorial Atlantic estimated using stable isotopes. *ICES J. Mar. Sci.* 76, 649–661. doi: 10.1093/icesjms/fsx243

Olivar, M. P., Contreras, T., Hulley, P. A., Emelianov, M., López, C., Tuset, V., et al. (2018b). Variation in the diel vertical distributions of larvae and transforming stages of oceanic fishes across the tropical and equatorial Atlantic. *Prog. Oceanogr.* 160, 83–100. doi: 10.1016/j.pocean.2017.12.005

Olivar, M. P., Hulley, P. A., Castellón, A., Emelianov, M., López, C., Tuset, V. M., et al. (2017). Mesopelagic fishes across the tropical and equatorial Atlantic: biogeographical and vertical patterns. *Prog. Oceanogr.* 151, 116–137. doi: 10.1016/j.pocean.2016.12.001

Omori, M., and Ikeda, T. (1984). *Methods in Marine Zooplankton Ecology*. New York, NY: John Wiley and Sons, 332.

Oozeki, Y., Hu, F., Kubota, H., Sugisaki, H., and Kimura, R. (2004). Newly designed quantitative frame trawl for sampling larval and juvenile pelagic fish. *Fish. Sci.* 70, 223–232. doi: 10.1111/j.1444-2906.2003.00795.x

Owens, T. G., and King, F. D. (1975). The measurement of respiratory electron transport system activity in marine zooplankton. *Mar. Biol.* 30, 27–36. doi: 10.1007/bf00393750

Packard, T. T. (1971). The measurement of respiratory electron transport activity in marine phytoplankton. *J. Mar. Res.* 29, 235–244.

Packard, T. T., Devol, A. H., and King, F. D. (1975). The effect of temperature on the respiratory electron transport system in marine plankton. *Deep Sea Res. I* 22, 237–249. doi: 10.1016/0011-7471(75)90029-7

Pakhomov, E. A., Podeswa, Y., Hunt, B. P., and Kwong, L. E. (2018). Vertical distribution and active carbon transport by pelagic decapods in the North Pacific Subtropical Gyre. *ICES J. Mar. Sci.* 76, 702–717. doi: 10.1093/icesjms/fsy134

Rutter, W. J. (1967). "Methods in developmental biology," in *Methods in Developmental Biology*, eds H. F. Wilt and N. K. Wessels (London: Academic Press), 671–684.

Schlitzer, R. (2016). *Ocean Data View*. Available at: http://odv.awi.de

Schukat, A., Bode, M., Auel, H., Carballo, R., Martin, B., Koppelmann, R., et al. (2013). Pelagic decapods in the northern Benguela upwelling system: distribution, ecophysiology and contribution to active carbon flux. *Deep Sea Res. I* 75, 146–156. doi: 10.1016/j.dsr.2013.02.003

Steinberg, D. K., Carlson, C. A., Bates, N. R., Goldthwait, S. A., Madin, L. P., and Michaels, A. F. (2000). Zooplankton vertical migration and the active transport of dissolved organic and inorganic carbon in the Sargasso Sea. *Deep Sea Res. I* 47, 137–158. doi: 10.1016/s0967-0637(99)00052-7

Steinberg, D. K., and Landry, M. R. (2017). Zooplankton and the ocean carbon cycle. *Annu. Rev. Mar. Sci.* 9, 413–444. doi: 10.1146/annurev-marine-010814-015924

Strickland, J. D., and Parsons, T. R. (1972). A practical handbook of seawater analysis. *Fish. Res. Board Canada* 167, 1–281.

Stukel, M. R., Décima, M., Landry, M. R., and Selph, K. E. (2018). Nitrogen and isotope flows through the Costa Rica Dome upwelling ecosystem: the crucial mesozooplankton role in export flux. *Glob. Biogeochem. Cycles* 32, 1815–1832. doi: 10.1029/2018gb005968

UNESCO (1994). *Protocols for the Joint Global Ocean Flux Study (JGOFS) Core Measurements. Manuals and Guides*, Vol. 29. Paris: UNESCO, 170.

Vereshchaka, A. L., Abyzova, G., Lunina, A. A., Musaeva, E., and Sutton, T. T. (2016). A novel approach reveals high zooplankton standing stock deep in the sea. *Biogeosciences* 13, 6261–6271. doi: 10.5194/bg-13-6261-2016

Wiebe, P. H., Burt, K. H., Boyd, S. H., and Morton, A. W. (1976). A multiple opening/closing net and environmental sensing system for sampling zooplankton. *J. Mar. Res.* 34, 313–326.

Wilson, R. W., Millero, F. J., Taylor, J. R., Walsh, P. J., Christensen, V., Jennings, S., et al. (2009). Contribution of fish to the marine inorganic carbon cycle. *Science* 323, 359–362. doi: 10.1126/science.1157972

Yasuma, H., and Yamamura, O. (2010). "Second micronekton inter-calibration experiment, MIE-2. Comparison between acoustic estimates," in *Report of the Advisory Panel on Micronekton Sampling Intercalibration Experiment*, eds E. Pakhomov and O. Yamamura (Sidney, BC: PICES), 51–56.

Yebra, L., Almeida, C., and Hernández-León, S. (2005). Vertical distribution of zooplankton and active flux across an anticyclonic eddy in the Canary Island waters. *Deep Sea Res. I* 52, 69–83. doi: 10.1016/j.dsr.2004.08.010

Yebra, L., Herrera, I., Mercado, J. M., Cortés, D., Gómez-Jakobsen, F., Alonso, A., et al. (2018). Zooplankton production and carbon export flux in the western Alboran Sea gyre (SW Mediterranean). *Prog. Oceanogr.* 167, 64–77. doi: 10.1016/j.pocean.2018.07.009

Yentsch, C. S., and Menzel, D. W. (1963). A method for the determination of phytoplanktonic chlorophyll and phaeophytin by fluorescence. *Deep Sea Res. I* 10, 221–231. doi: 10.1016/0011-7471(63)90358-9

Zhang, X., and Dam, H. G. (1997). Downward export of carbon by diel migrant mesozooplankton in the central equatorial Pacific. *Deep Sea Res. II* 44, 2191–2220.

Conflict of Interest Statement: The authors declare that the research was conducted in the absence of any commercial or financial relationships that could be construed as a potential conflict of interest.

frontiers in Marine Science

ORIGINAL RESEARCH
published: 13 September 2019
doi: 10.3389/fmars.2019.00508

The Importance of Mesozooplankton Diel Vertical Migration for Sustaining a Mesopelagic Food Web

Thomas B. Kelly[1,2]*, *Peter C. Davison*[3], *Ralf Goericke*[3], *Michael R. Landry*[3], *Mark D. Ohman*[3] and *Michael R. Stukel*[1,2]

[1] Department of Earth, Ocean and Atmospheric Science, Florida State University, Tallahassee, FL, United States, [2] Center for Ocean-Atmospheric Prediction Studies, Florida State University, Tallahassee, FL, United States, [3] Integrative Oceanography Division, Scripps Institution of Oceanography, San Diego, CA, United States

We used extensive ecological and biogeochemical measurements obtained from quasi-Lagrangian experiments during two California Current Ecosystem Long-Term Ecosystem Research cruises to analyze carbon fluxes between the epipelagic and mesopelagic zones using a linear inverse ecosystem model (LIEM). Measurement constraints on the model include ^{14}C primary productivity, dilution-based microzooplankton grazing rates, gut pigment-based mesozooplankton grazing rates (on multiple zooplankton size classes), ^{234}Th:^{238}U disequilibrium and sediment trap measured carbon export, and metabolic requirements of micronekton, zooplankton, and bacteria. A likelihood approach (Markov Chain Monte Carlo) was used to estimate the resulting flow uncertainties from a sample of potential flux networks. Results highlight the importance of mesozooplankton active transport (i.e., diel vertical migration) in supplying the carbon demand of mesopelagic organisms and sequestering carbon dioxide from the atmosphere. In nine water parcels ranging from a coastal bloom to offshore oligotrophic conditions, mesozooplankton active transport accounted for 18–84% (median: 42%) of the total carbon transfer to the mesopelagic, with gravitational settling of POC (12–55%; median: 37%), and subduction (2–32%; median: 14%) providing the majority of the remainder. Vertically migrating zooplankton contributed to downward carbon flux through respiration and excretion at depth and via mortality losses to predatory zooplankton and mesopelagic fish (e.g., myctophids and gonostomatids). Sensitivity analyses showed that the results of the LIEM were robust to changes in nekton metabolic demand, rates of bacterial production, and mesozooplankton gross growth efficiency. This analysis suggests that prior estimates of zooplankton active transport based on conservative estimates of standard (rather than active) metabolism are likely too low.

Keywords: biological carbon pump, export production, DVM, LIEM, active transport, inverse model, carbon export, ecosystem model

OPEN ACCESS

Edited by:
Helena Hauss,
GEOMAR Helmholtz Center for Ocean Research Kiel, Germany

Reviewed by:
Bingzhang Chen,
University of Strathclyde, United Kingdom
John Patrick Dunne,
Geophysical Fluid Dynamics Laboratory (GFDL), United States

***Correspondence:**
Thomas B. Kelly
tbk14@fsu.edu

Specialty section:
This article was submitted to Marine Biogeochemistry, a section of the journal Frontiers in Marine Science

Received: *29 March 2019*
Accepted: *31 July 2019*
Published: *13 September 2019*

Citation:
Kelly TB, Davison PC, Goericke R, Landry MR, Ohman MD and Stukel MR (2019) The Importance of Mesozooplankton Diel Vertical Migration for Sustaining a Mesopelagic Food Web. Front. Mar. Sci. 6:508. doi: 10.3389/fmars.2019.00508

INTRODUCTION

Although mesopelagic food webs are believed to depend entirely on productivity generated in the euphotic zone, reconciling mesopelagic metabolic demand with estimates of export has been challenging (del Giorgio and Duarte, 2002; Steinberg et al., 2008; Burd et al., 2010; Henson et al., 2011; Hannides et al., 2015). Due to large uncertainties in rate measurements for

meso- and bathypelagic organisms as well as low sampling resolution, steady-state budgets must either report wide ranges or otherwise exclude some processes, such as mortality and defecation of diel vertical migrators at depth. Even among recent studies, global carbon export budgets have been highly variable (Boyd and Trull, 2007; Henson et al., 2011, 2015; Laws et al., 2011; Siegel et al., 2014). Compounding this issue, several analyses have reported carbon demands by mesopelagic bacteria alone that exceed calculated carbon export (Ducklow and Harris, 1993; Burd et al., 2010), sometimes by an order of magnitude (Steinberg et al., 2008). This apparent imbalance between carbon supply to the mesopelagic and estimated metabolic demand suggests either that export estimates fail to capture important dynamics or that metabolic calculations are highly biased (Burd et al., 2010).

Some work has demonstrated that diel vertical migrators are important for net transfer of organic carbon from the euphotic zone to the mesopelagic, a transfer not measured with traditional carbon export methods (Morales, 1999; Steinberg et al., 2000). Since export by mesozooplankton is not captured by sediment traps or radioisotope disequilibria methods, we must rely on net tows coupled to assumptions about *in situ* respiration rates, or on indirect modeling syntheses. For example, using remote sensing fields and a size-structured ecosystem model, Archibald et al. (2019) found that global zooplankton diel vertical migration (DVM) can increase export production by 14% annually. This is consistent with previous modeling exercises based on zooplankton behavior (Bianchi et al., 2013) and community size structure (Aumont et al., 2018). Zooplankton behavior models argue that for DVM to be evolutionarily advantageous (Cohen and Forward, 2009), the energy expenditure should be offset by a commensurate reduction in predation risk. Using this modeled-behavior approach, Hansen and Visser (2016) found that 16–30% mid-latitude export production in the North Atlantic was likely due to DVM mesozooplankton. Each of these models note sensitivities to zooplankton biomass and the fraction of the zooplankton population that undergoes DVM, which are ecosystem metrics that are difficult to generalize.

Linear inverse ecosystem models (LIEM) have been shown to be a versatile and robust framework for integrating a wide range of ecosystem data (Vézina et al., 1988; Gontikaki et al., 2011; van Oevelen et al., 2012; Sailley et al., 2013; Stukel et al., 2018b). A LIEM combines an ecosystem network with observations and generalized constraints to determine possible energy flows through the ecosystem. Unlike a forward model (e.g., an NPZ model; Franks, 2002), the relationships between organisms are not prescribed by functional responses of model state variables (e.g., assuming a Monod functional form controls phytoplankton nutrient uptake responses or an Ivlev grazing formulation). Instead, the model includes all possible combinations of fluxes that are compatible with the assumed model structure and input constraints. The most likely ecosystem structure is then retrieved based on a random walk through the solution space (van den Meersche et al., 2009). This inverted approach has the advantage of not requiring *a priori* assumptions of functional ecological responses but instead relies on an assumed basic ecosystem structure (i.e., which functional groups should be included and who eats whom) and many independent constraints on the food web.

The California Current Ecosystem (CCE) is an eastern boundary current upwelling biome with extensive temporal and spatial variability. As a result of high mesozooplankton biomass and strong DVM (Stukel et al., 2013; Powell and Ohman, 2015; Ohman and Romagnan, 2016), we expect a substantial contribution to export production by diel vertical migrators and a commensurately important role in satisfying the mesopelagic carbon demand. Stukel et al. (2013) suggested that active transport could be responsible for 1.8–29% of total export in the CCE. However, their study focused only on active transport fluxes due to zooplankton respiration and only included basal metabolism. To more thoroughly investigate the potential importance of active transport, we designed a two-layer LIEM, which includes non-living organic matter, primary producers, zooplankton, and planktivorous nekton organized into two layers: an epipelagic and a mesopelagic ecosystem. Using extensive data from two cruises of the CCE Long-Term Ecological Research (LTER) Program in the southern California Current region, our LIEM data synthesis suggests that active transport of carbon from the epipelagic down to depth is a significant mechanism supporting the mesopelagic carbon demand. Although previous studies have indicated that active transport may be responsible for 10–30% of total carbon flux (Yebra et al., 2005; Bianchi et al., 2013; Hansen and Visser, 2016; Aumont et al., 2018; Archibald et al., 2019), our LIEM suggests that 20–80% of carbon export in the CCE can be attributed to mesozooplankton DVM.

MATERIALS AND METHODS

Ecosystem Data

The data presented here (**Appendix A**) were collected during two cruises of the California Current Ecosystem Long Term Ecological Research (CCE LTER) program (P0704 in April 2007; P0810 in Oct. 2008). On these cruises, *in situ* drift arrays were used for quasi-Lagrangian tracking of water parcels for periods of 3–5 days (Landry et al., 2009, 2012), while the water column was repeatedly sampled for the following variables: CTD-derived physical data, phytoplankton diversity and biomass (flow cytometry, epifluorescence microscopy, and pigment analyses, Taylor et al., 2012), primary production ($H^{14}CO_3^-$ uptake, Morrow et al., 2018), mesozooplankton biomass and community analyses (paired day-night bongo and Multiple Opening and Closing Net with Environmental Sampling System, MOCNESS net tows, Ohman et al., 2012; Powell and Ohman, 2012), microzooplankton biomass (epifluorescence microscopy), microzooplankton grazing (dilution method, Landry et al., 2009), mesozooplankton grazing (gut pigment methods, Landry et al., 2009), meso- and epipelagic micronekton biomass and metabolic demands (see section Phytoplankton, Bacteria, and Protist Constraints; Oozeki net trawls, multi-frequency EK60 echosounder, and individual-based metabolic model, Davison et al., 2013, 2015), bacterial production (^{3}H-leucine uptake, Samo et al., 2012), and gravitational particle export (sediment traps and ^{234}Th:^{238}U disequilibrium, Stukel et al.,

2013). The use of a quasi-Lagrangian sampling framework also allowed us to assess net rates of change of phytoplankton biomass. Bulk rates and associated errors for the 3–5 day cycles were calculated by averaging vertically integrated rates or biomasses for each experimental cycle. The data and detailed methods can be found on the CCE LTER Datazoo website (http://oceaninformatics.ucsd.edu/datazoo/data/ccelter/datasets) and/or in published manuscripts cited above.

The quasi-Lagrangian experiments (hereafter "cycles" of repeated measurements in the same water parcel) spanned much of the physical, chemical, and ecological variability of the CCE domain (**Table 1**, **Figure 1**) which allowed us to classify cycles according to nutrient conditions, the primary driver of ecosystem variability within the CCE (Landry et al., 2012). Cycle classification was defined as: nutrient-limited cycles which were conducted in off-shore, low nutrient regions (P0704-2, P0810-2, P0810-6); transition region cycles which were characterized by low surface nutrient concentrations and intermediate NPP and biomass (P0810-1, P0810-3, P0810-4); and upwelling cycles in which surface nutrient concentrations and phytoplankton growth rates were highest (P0704-1, P0704-4, P0810-5; **Table 1**).

Phytoplankton, Bacteria, and Protist Constraints

Daily *in situ* primary productivity measurements using $H^{14}CO_3^-$ uptake (^{14}CPP) were conducted at 6–8 depths spanning the euphotic zone using 4 L incubations subsampled in triplicate (Morrow et al., 2018). A 250 mL dark bottle was used to correct for non-photosynthetic ^{14}C uptake. Contemporaneously, *in situ* dilution experiments, using the two-treatment approach of Landry et al. (2008), were conducted to measure protistan zooplankton grazing rates and chlorophyll-*a* growth rates (Landry et al., 2009). Chlorophyll to carbon ratios were determined by the ratio of vertically integrated chlorophyll-a growth rates and ^{14}CPP. Euphotic zone primary production and protistan zooplankton gazing rates were vertically integrated and averaged by cycle.

Rates of ^{3}H-leucine incorporation into bacteria were measured in triplicate at multiple depths during each cycle (Samo et al., 2012). Each profile was vertically integrated and then averaged by cycle in order to determine production rates of epipelagic bacteria. Additionally, upper and lower bounds for mesopelagic bacterial production were calculated by integrating bacterial production attenuation curves and scaling by the epipelagic bacterial production (Equation 1).

$$Mesopelagic\ BP = BP_{100} \int_{100}^{450} \left(\frac{z}{z_0}\right)^{-\alpha} dz \quad (1)$$

where BP_{100} is the measured BP rate at 100 m and α (BP attenuation factor) = 1.47 (Yokokawa et al., 2013) for the lower limit and $\alpha = 0$ (i.e., no attenuation) for the upper limit.

TABLE 1 | Overview of conditions for each cycle along with the attributed classifications: upwelling, transition region, and nutrient limited.

Cycle	Classification	Surface Chl (μg Chl a L^{-1})	^{14}C Primary productivity (mg C m^{-2} d^{-1})	Mesozooplankton biomass (mg C m^{-2})
P0704-1	Upwelling	1.35	1,233	2,695
P0704-2	Nutrient limited	0.22	587	391
P0704-4	Upwelling	0.99	2,314	1,715
P0810-1	Transition region	0.45	554	740
P0810-2	Nutrient limited	0.20	484	528
P0810-3	Transition region	0.72	892	923
P0810-4	Transition region	1.05	674	832
P0810-5	Upwelling	1.47	1,672	1,098
P0810-6	Nutrient limited	0.22	325	628

Mesozooplankton and Nekton Constraints

Data for the mesozooplankton constraints comes primarily from day-night paired oblique bongo net tows through the epipelagic (for grazing rates) or day-night paired 202 μm mesh MOCNESS tows taken at 9 depth horizons spanning the upper 450 m (for biomass and metabolism estimates). MOCNESS samples were analyzed by ZooScan digital scanner (Gorsky et al., 2010; Ohman et al., 2012), vignettes provisionally classified using machine learning methods, then 100% manually validated. Organisms were sorted (Stukel et al., 2013) into groups including euphausiids, nauplii, copepods, appendicularians, siphonophores, and "other crustaceans". For this study, we separated the mesozooplankton community into two size classes (i.e. <1 and >1 mm ESD) of grazers and one compartment for gelatinous predators (siphonophores). We also partitioned the large and small mesozooplankton into non-vertically migrating epipelagic residents, vertical-migrators, or mesopelagic resident communities. Biomass estimates of non-migrating epipelagic mesozooplankton were calculated from day time net tows in the upper 100 m, while the non-migrating, mesopelagic biomass was calculated based on nighttime mesopelagic (100–450 m) net tows (Stukel et al., 2013). We note that epipelagic estimates are likely conservative due to net avoidance. Biomass estimates for the DVM mesozooplankton were calculated by averaging the difference in the night and day epipelagic biomass estimates with the difference in the day and night mesopelagic biomass estimates. This approach was used in order to be the most consistent with both the epipelagic and mesopelagic biomass estimates for non-vertically migrating biomass. For a list of abbreviations used for all model compartments, see **Table 2**.

Minimum respiration estimates for each mesozooplankton group were calculated using published temperature-length-basal respiration relationships (Ikeda et al., 2001). Oxygen consumption was converted to carbon units using the scale factor 9.88×10^{-3} mg C d^{-1} (μL O_2 h^{-1})$^{-1}$. Mesozooplankton grazing on phytoplankton was calculated from gut pigment contents of oblique bongo net tow tows (202 μm mesh, D = 0.71 m) and estimated gut passage rates (Dam and Peterson, 1988). Carbon-based grazing rates were then calculated from chlorophyll (Chl) consumption, and C:Chl ratios computed as the ratio of NPP to chlorophyll-specific growth rates obtained from the dilution experiments. Mesozooplankton grazing rates were size fractionated as above. Mesozooplankton gut contents

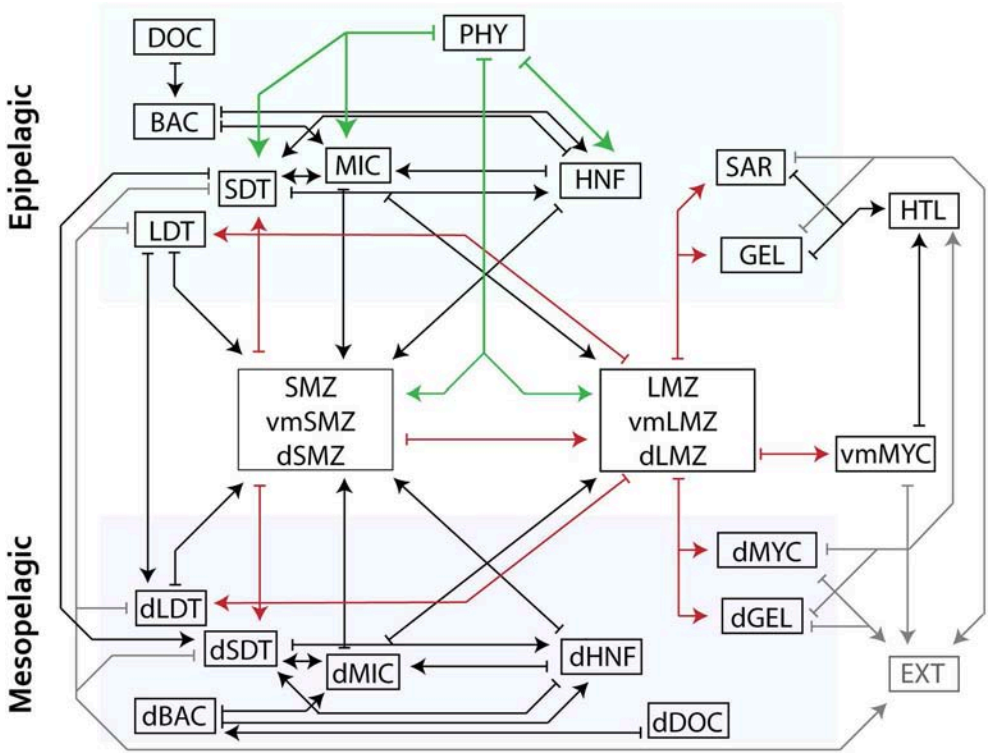

FIGURE 1 | Schematic of model structure organized into distinct layers (epipelagic, DVM, and mesopelagic) where arrows indicate a model flow. Mesozooplankton compartments are shown in aggregated boxes (i.e., small mesozooplankton consisting of SMZ, vmSMZ, and dSMZ are shown together). For clarity, green arrows indicate grazing while red highlight mesozooplankton flows. Closure terms ("EXT") are in gray. Production of DOC is not shown but would flow from each living compartment to DOC/dDOC. Losses to respiration are also not shown. See **Table 2** for abbreviations.

samples were improperly frozen for P0810-5, P0810-6, and most of P0810-4. In order to provide estimates for these grazing rates, average grazing rates from the cycle with the same classification were used (e.g., P0810-5 was an upwelling cycle so grazing rates were averaged from the other upwelling cycles). Conservative uncertainty estimates were set to be 2x the error calculated by propagation of error. This higher level of uncertainty is a reasonable compromise given the data limitations. For additional details on gut pigment processing, see Landry et al. (2009).

Nekton biomass was estimated based on catches made by a 5 m^2 Matsuda-Oozeki-Hu net trawl (Davison et al., 2013). For each station, epipelagic net tows were conducted at night after the ascent of the deep scattering layer. Preserved specimens from each net tow were identified to species and measured. Fish were classified as either non-vertical migrating or vertically migrating based on species. An individual based model was then used to determine metabolic rates and requirements for each nekton population: resident epipelagic, diel vertical migrant, and resident mesopelagic (Davison et al., 2013).

Export Production

VERTEX-style sediment traps consisting of 8–12 tubes per depth were deployed and recovered at the start and end of each cycle (Knauer et al., 1979; Stukel et al., 2013). Tubes were filled with a hypersaline, poisoned brine solution. Upon recovery >200-μm swimming mesozooplankton taxa were manually removed during inspection under a stereomicroscope. Samples for C and N or C:^{234}Th ratios were filtered through pre-combusted glass fiber and quartz filters, respectively, prior to analysis on a CHN elemental analyzer or a RISO beta multi-counter.

^{234}Th:^{238}U disequilibrium measurements were made at 12 depths spanning the upper 200 m at the start and end of each cycle using standard small-volume procedures (Benitez-Nelson et al., 2001; Pike et al., 2005). Thorium-234 export rates were then computed using a 1-box steady state model (Savoye et al., 2006). The C:^{234}Th ratio measured from sediment trap particles was used to convert to carbon export. For additional details, see Stukel et al. (2019).

Subduction of POC provides an alternative mechanism for the export of organic matter to the mesopelagic, that is not measured by either sediment traps or ^{234}Th profiles, which only record gravitational settling of particles. A three-dimensional particle advection model was used to determine a range of possible subduction rates (Stukel et al., 2018c). The maximum and minimum estimates of particle subduction were used as bounds on two size-fractionated subduction flows within the LIEM.

Linear Inverse Model

We developed a LIEM for the CCE to investigate mechanisms of epipelagic-mesopelagic coupling. The LIEM consists of 140 flows (i.e., ecosystem fluxes, **Supplemental Table 2**)

TABLE 2 | Names and abbreviations of all model compartments.

	Epipelagic abbreviation	Name	Mesopelagic abbreviation
Organisms	PHY	Phytoplankton	
	HNF	Heterotrophic Nanoflagellates	dHNF
	MIC	Microzooplankton	dMIC
	SMZ, vmSMZ	Small Mesozooplankton	dSMZ, vmSMZ
	LMZ, vmLMZ	Large Mesozooplankton	dLMZ, vmLMZ
	SAR	Sardines and other planktivorous fish	
		Non-DVM Myctophids	dMYC
	GEL	Gelatinous Predators	dGEL
	vmMYC	Vertically Migrating Myctophids	vmMYC
	BAC	Bacteria	dBAC
POC& DOC	SDT	Small Detritus	dSDT
	LDT	Large Detritus	dLDT
	DOC	Dissolved Organic Matter	dDOC
Closures	HTL	Higher Trophic Levels	HTL
	RES	Respiration	dRES
	EXT	Fecal Matter & External	EXT

An abbreviation in the left column indicates inclusion in the epipelagic, while an abbreviation in the right column indicates inclusion in the mesopelagic. Each abbreviation is a distinct compartment in the LIEM with the prefix "vm" signifying vertical migration and "d" signifying the mesopelagic.

and 24 compartments (i.e., standing stocks; **Table 2**) organized into two layers: the surface epipelagic and a deeper mesopelagic ecosystem (defined as 100–450 m depth to match with *in situ* measurements). The epipelagic and mesopelagic ecosystems consist of 73 flows and 64 flows, respectively, with four explicit flows (particle sinking and subduction) and three implicit flows (active transport) linking the two layers (**Figure 1**). Three vertically migrating compartments (small and large mesozooplankton and nekton) connect the epipelagic and mesopelagic through a transfer associated with DVM (i.e., respiration, excretion, and mortality). Constraints consist of 24 mass balance equations, 18 approximate equations (i.e., *in situ* rate measurements) and 133 inequalities, which are provided in the **Supplement Model Spreadsheet**.

The 18 approximate equations are ecosystem observations, which can be directly compared to flows within the model (**Appendix A**). These equations are net primary productivity (NPP), phytoplankton biomass net rate of change, protistan grazing, size-fractionated grazing rates (<1 and >1-mm) for epipelagic resident and DVM mesozooplankton, sediment trap and ^{234}Th-based export fluxes, bacterial production, and mesopelagic fish respiration, mortality and fecal pellet production rates. The model was provided an estimated value and associated uncertainty for each measurement.

Respiration, mesopelagic export, nekton fecal pellets, and losses to higher trophic levels were included as closure terms. Within the model, every organism loses carbon to respiration, DOC excretion, and defecation or mortality to detritus/fecal pellets. Grazing was allowed between organisms whose ecological roles and size ranges permit grazing (e.g., small mesozooplankton graze on nano- and microplankton; sardines consume only >1-mm mesozooplankton). Mass balance was required for each compartment. All compartments were assumed to be at steady state except for PHY, for which changes in biomass were measured (via Chl-*a* proxy) during each cycle and incorporated into the model. This flexibility was essential to capture the bloom phase of the ecosystem since dramatic shifts in Chl-*a* were observed during some cycles.

Inequality Constraints

The formulas used in the inequality constraints are provided in the **Supplement**. Upper and lower limit estimates of POC subduction from the epipelagic to the mesopelagic layer were taken from Stukel et al. (2018c), and minimum fecal pellet fluxes were assigned based on the assumption that recognizable fecal pellets in sediment trap material represented a lower limit on total fecal pellet flux. Minimum and maximum Gross Growth Efficiencies (GGE) were assigned according to previously accepted literature values: 10–40% GGE for protistan zooplankton (HNF & MIC) and gelatinous predators (Straile, 1997); 10–30% for mesozooplankton (Anderson et al., 2018); and 5–30% for bacteria (del Giorgio and Cole, 1998). The Absorption Efficiencies (AE) for all heterotrophs were limited to 50–90% (Conover, 1966).

Minimum respiration requirements were considered as both active respiration and basal respiration. Active respiration was set as a fraction of ingestion, and basal respiration was set as a function of biomass and temperature. Valid solutions fulfilled both criteria. Diel vertical migrator biomass, as determined from MOCNESS net tows, was used to calculate a minimum respiration based on temperature. DOC excretion was required to be >10% of ingestion (or 2% of NPP for phytoplankton) and less than respiration (or 35% of NPP). All inequality constraints are listed in **Supplemental Table 1**.

Model Solution

Because the LIEM is under-constrained, infinite possible solutions satisfy the equality, and inequality constraints. To choose mean solutions and determine uncertainties within the possible solution space, we use a Markov Chain Monte Carlo (MCMC) sampling method (Kones et al., 2009; van den Meersche et al., 2009; van Oevelen et al., 2010), which has been shown to reconstruct unmeasured flows more accurately than the L_2 minimum norm approach (Stukel et al., 2012, 2018a; Saint-béat et al., 2013). Implementation details are provided in the **Supplement Detailed Methods**.

As a metric for discussing model results with respect to the approximation equations (i.e., the observations), we use the model-observation misfit relative to the model uncertainty: $\Sigma = (X_{model} - X_{obs})/\sigma_{obs}$. Here X_{model} is the model prediction, X_{obs} is the observed value, and σ_{obs} is the standard deviation of the

observed value. The square of this quantity (Σ^2) is summed over all approximate equations yielding the solution cost function, and thus Σ is a proxy for disagreement between the LIEM and observations. Unless otherwise stated, LIEM solutions are given as ranges based on the mean solutions for each cycle as well as the median value for all cycles. Displaying data in this way allows us to highlight inter-cycle variability. For value and uncertainty in all rate constraints, see **Appendix A**.

Analyses and Model Comparisons

Indirect Analysis

An indirect analysis permits investigation of the contributions of carbon between any two compartments through indirect linkages. By taking the normalized matrix of flows between compartments (G) and the identity matrix (I), the matrix $(I\text{-}G)^{-1}$ provides all the indirect flows data (Kroes, 1977). In this way the contribution of the surface compartments to the deep ones can be ascertained even when no direct flows exist. For example, if the food chain were A B C, an indirect analysis would reveal that 100% of the flows to C go through A.

Independent DVM Estimates

A model to predict the export flux due to zooplankton DVM was recently published by Archibald et al. (2019), which adds a diel vertical migration module to the Siegel et al. (2014) ecosystem model. The Archibald et al. model parameterizes the export production based on NPP, size-fractionated grazing (i.e., protists and mesozooplankton), and the proportion of DVM mesozooplankton. The export production attributed to vertical migrators who defecate at depth is a function of total grazing, the gut clearance rate, and the proportion of zooplankton undergoing DVM (Equation 2).

$$Export_{twilight} = p_{DVM} \cdot (1 - f_{fec}) \cdot \left(m_{fec} \cdot G_m + n_{fec} \cdot G_n\right) \quad (2)$$

where p_{DVM} is the fraction of mesozooplankton that undergo DVM, and f_{fec} is the fraction of fecal pellets produced by diel vertical migrators in the euphotic zone. m_{fec} and n_{fec} are the proportions of grazing that are exported by mesozooplankton and protistan zooplankton, respectively. G_m and G_n are the grazing rates for mesozooplankton and protistan zooplankton, respectively.

The respiration conducted by vertically migrating zooplankton can be calculated based on the metabolic efficiency, fraction of mesozooplankton undergoing DVM, and their grazing rate (Equation 3).

$$Export_{resp} = p_{met} \cdot p_{dvm} \cdot f_{met} \cdot \left[\left(1 - m_{fec}\right) \cdot G_m + \frac{n_{fec}}{m_{fec}} \left(1 - m_{fec}\right) \cdot G_n\right] \quad (3)$$

where p_{met} is the temperature dependent metabolic rate with ΔT, the temperature difference between the mesopelagic and epipelagic and $p_{met} = 2^{(\Delta T/10)} / \left(2^{(\Delta T/10)} + 1\right)$. f_{met} is the metabolic efficiency of the zooplankton, assumed to be 0.50. We calculated active transport from Equations 3 and 4 following Archibald, but using the CCE-optimized parameter set that Stukel et al. (2015) determined for the Siegel et al. (2014) model. The fraction of mesozooplankton undergoing DVM (p_{dvm}) was calculated as described in Section Mesozooplankton and Nekton Constraints. Fecal pellet production for meso- and microzooplankton were set to $m_{fec} = 0.3$ and $n_{fec} = 0.06$ (Archibald et al., 2019), respectively.

Since the Archibald et al. model does not include mortality at depth as export and excludes any mesopelagic ingestion or excretion, the total export flux is the sum of Equations 2 and 3. To compare with the LIEM presented here, a modified LIEM active transport flux will be calculated using the total active transport for mesozooplankton and subtracting mesopelagic mortality.

RESULTS

In situ Ecosystem Observations

The locations for each study site were chosen to maximize the range of environmental conditions (**Figure 2**). Sea surface chlorophyll *a* (Chl *a*) varied from 0.2 to 1.5 mg Chl *a* m^{-3} with vertically-integrated primary productivity varying from 325 to 2,314 mg C m^{-2} d^{-1}. Productivity and biomass typically declined with distance from the Point Conception upwelling center. Most cycles were in water masses with steady or declining phytoplankton biomass (**Figure 2D**), with the exception of P0810-1. Sediment trap-derived carbon export at 100 m depth varied from 32 to 170 mg C m^{-2} d^{-1} (**Figure 2C**), with observed e-ratios (i.e., sediment trap export/^{14}CPP) ranging from 5 to 33%. Standing stock of zooplankton correlated positively with NPP and export (Spearman correlations of 0.36 and 0.40, respectively). Protistan zooplankton were responsible for grazing ∼50% of NPP (**Figure 2B**) while mesozooplankton grazed, on average, ∼30% of NPP with one exception (**Figure 2E**). The proportion of mesozooplankton biomass exhibiting DVM behavior ranged from 35 to 86% (median: 58%). Epipelagic bacterial production rates did not correlate with NPP but ranged from 22 to 400 mg C m^{-2} d^{-1} (**Figure 2F**), with the three lowest rates observed during the P0704 Cruise.

Model-Observation Mismatch

The LIEM solutions consistently show general agreement with all *in situ* observations except for modeled NPP, which is elevated by 18–56% (median: 22%) from ^{14}CPP estimates (**Figure 3A**), or 3.0–9.3 Σ (median: 3.6 Σ). This degree of misfit corresponds to 18–82% (median: 46%) of the total model-observation misfit. Model agreement with the sediment trap was high (−33–25%; **Figure 3E**) with a modeled e-ratio (i.e., sediment trap export/NPP) of 5–35% (median: 14%), which compares well to the observed e-ratio of 5–33% (median: 11%). Modeled protistan grazing rates and mesozooplankton grazing rates were reasonably close to observations (**Figure 3B**). Modeled microzooplankton (MIC) grazing was lower than observed for cycles P0704-2 (−2.8 Σ) but agreed reasonably well (−1.5– +0.1 Σ) for the other cycles (**Supplemental Figure 1**). For P0704-1, mesozooplankton grazing rates were lower than observations for SMZ (−1.8 Σ), total non-DVM grazing (−1.8 Σ) and for vmSMZ grazing (−1.6 Σ). During the course of this cycle, phytoplankton biomass declined (−322 mg C m^{-2} d^{-1}) and had high zooplankton

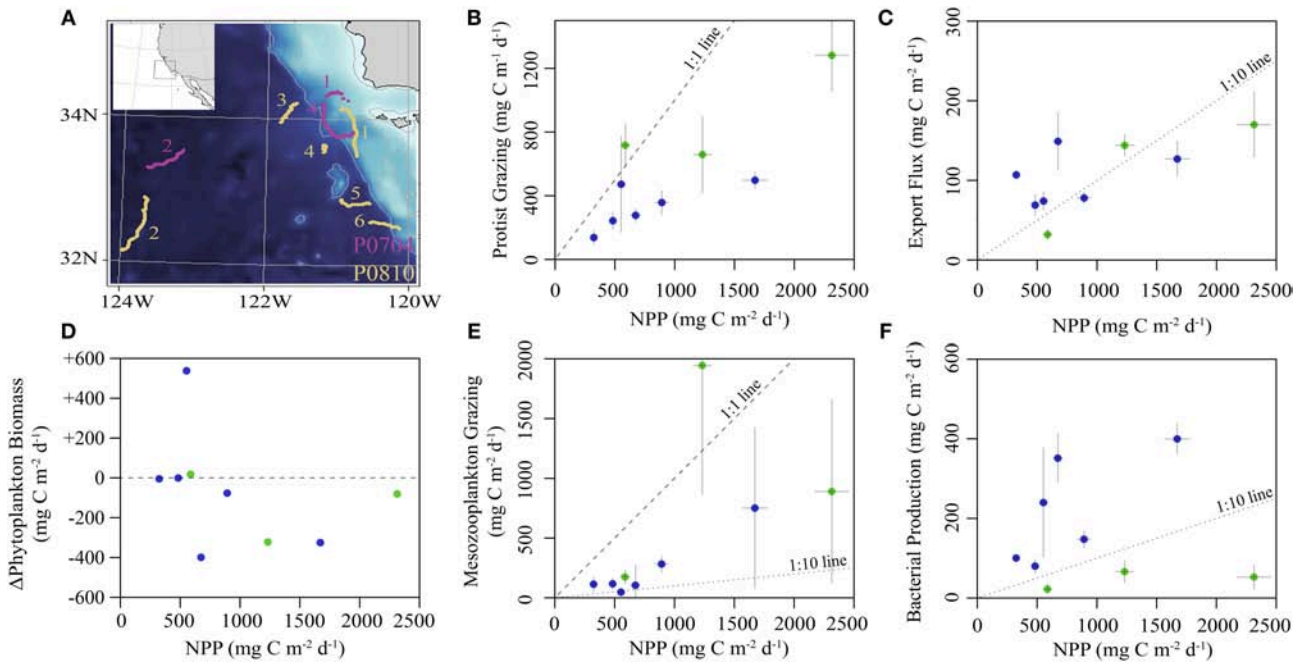

FIGURE 2 | (A) Bathymetric map of study region showing drift trajectories from each cycle (inset shows larger region). Numbers correspond to cycle for P0704 (purple) and P0810 (yellow). **(B–F)** Summary of *in situ* observations plotted against NPP: **(B)** protistan grazing, **(C)** export flux from sediment trap at 100 m, **(D)** observed rate of change of phytoplankton biomass, **(E)** mean mesozooplankton grazing, and **(F)** epipelagic bacterial production. Values are colored by cruise (P0704 = green, P0810 = blue). Dashed lines for reference slopes of 1:1, 1:10, or no change as indicated and error bars are ±1 SD.

grazing rates compared to the other cycles. This water parcel may have been in a declining bloom stage where observed grazing rates were unsustainable. Model-data agreement among the seven nekton-related observations (e.g., **Figure 3F**) was satisfactory ($|\Sigma| < 1$) except for P0810-1, which showed reduced vertically migrating nekton activity relative to estimates (vmMYC epipelagic respiration: $-1.5\ \Sigma$, vmMYC mesopelagic respiration: $-1.7\ \Sigma$, and vmMYC mesopelagic mortality: $-1.1\ \Sigma$). This cycle was along the edge of an anti-cyclonic eddy, where lateral gradients were likely high.

Epipelagic Ecosystem Model

According to the LIEM, phytoplankton respired 18–39% (median: 30%) of GPP, lost 14–26% (median: 18%) as DOC, lost 2–42% (median: 6%) to non-grazer mortality and the remaining 5–54% (median: 45%) was grazed by zooplankton. Modeled NPP ranged from 421 mg C m^{-2} d^{-1} to 2,750 mg C m^{-2} d^{-1} (median: 861 mg C m^{-2} d^{-1}). The LIEM suggested that protists and mesozooplankton had relatively similar grazing impacts on phytoplankton across all cycles, although the proportional role was greater for mesozooplankton in coastal regions and greater for protists under oligotrophic conditions. Between 14 and 47% (median: 33%) of NPP was grazed by protistan zooplankton (MIC + HNF) and 18–96% (median: 45%) by mesozooplankton (SMZ + vmSMZ + LMZ + vmLMZ). We note that protistan grazing rates normalized to NPP are slightly depressed relative to observations since model NPP was higher than observations while protistan grazing generally matched the observations (**Figure 3**; **Supplemental Figure 1**). 57–82% (median: 74%) of mesozooplankton grazing was by small mesozooplankton (SMZ + vmSMZ). Vertically migrating mesozooplankton were responsible for 52–89% (median: 63%) of total mesozooplankton grazing, 58–85% (median: 77%) of which was done by vmSMZ (i.e., vmSMZ grazing/total vm grazing).

Mortality relative to ingestion for mesozooplankton was similar for the different epipelagic mesozooplankton (i.e., SMZ, LMZ, vmSMZ, and vmLMZ): SMZ: 24–25%, vmSMZ: 23–25%, LMZ: 22–25%, and vmLMZ: 24–27%, as was fecal pellet production (between 30 and 40% of ingestion).

Overall, 19–44% (median: 29%) of NPP was transferred from the epipelagic to the mesopelagic with 3–8% (median: 5%) of NPP leaving the epipelagic through higher trophic levels (SAR + vmMYC). Gravitational settling and subduction of POC accounted for 12–55% (median: 37%) and 2–32% (medina:14%) of epipelagic export, respectively, while 18–84% (median: 41%) was through active transport of DVM mesozooplankton (vmSMZ + vmLMZ). Vertically migrating myctophids (vmMYC) transferred 2–6% (median: 4%) of total export. Section New Production, Export and DVM provides a more detailed description of export production.

The gross growth efficiencies (GGE) for each type of organism are shown in **Figure 4A**. Overall, BAC GGE was 7–29% (median: 25%) with an upper bound set to 30%. Notably, BAC GGE differed based on cruise, with P0704 cycles ranging between 8 and 13% and P0810 ranging between 23 and 29%. MIC

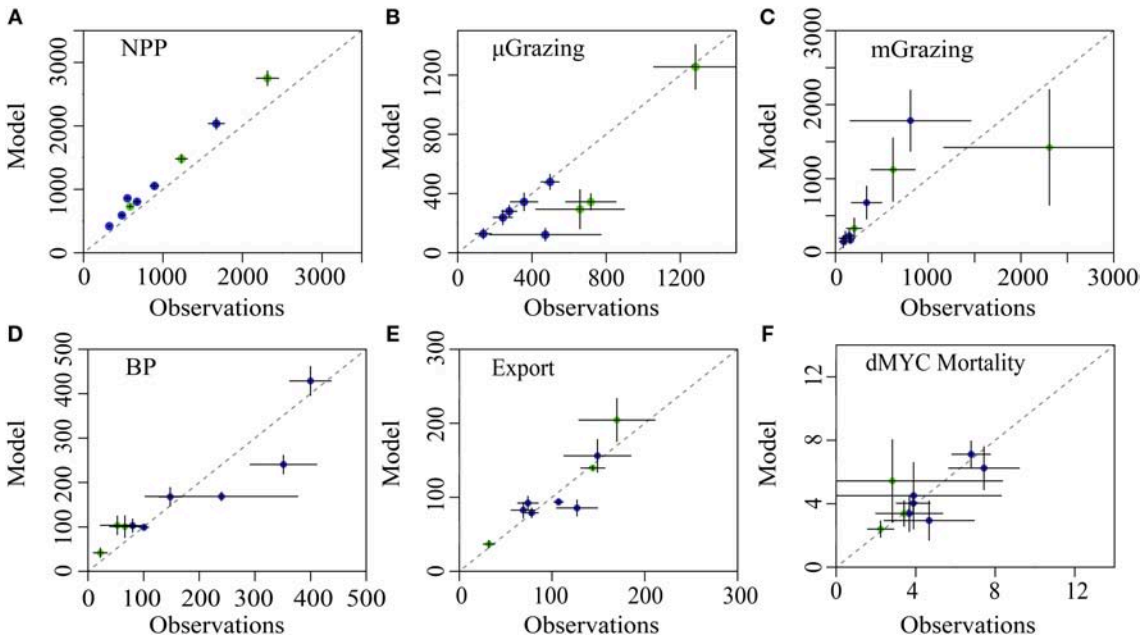

FIGURE 3 | Model-observation comparisons for selected measurements: **(A)** net primary productivity, **(B)** protistan zooplankton grazing, **(C)** mesozooplankton grazing, **(D)** epipelagic bacterial production, **(E)** sediment trap carbon export (@ 100 m), and **(F)** non-vertically migrating mesopelagic nekton mortality. Cruises are denoted by color (P0704 = green, P0810 = blue). Dashed line is 1:1 and error bars show 1 SD of uncertainty.

GGE was 35–38% (median: 37%), and HNF GGE ranged from 32 to 35% (median: 33%), which is slightly higher than typical estimates of protistan zooplankton GGE (Straile, 1997) although reported variability is high (Steinberg and Landry, 2017). GGEs for epipelagic mesozooplankton were consistently above 20%.

Trophic Level and Diets

Trophic levels for each organism (**Figure 4B**) were calculated by assuming that primary productivity, detritus and DOC were at trophic level 1. Trophic level indices were not affected by the overall cycle productivity (i.e., NPP), time of year, or by nutrient regime. The trophic level of small epipelagic mesozooplankton (SMZ) ranged from 2.2 to 2.5 (median: 2.2) and large mesozooplankton (LMZ) ranged from 2.2 to 2.9 (median: 2.6). The SAR trophic level was 3.3–3.8 (median: 3.5), and vmMYC was similar at 3.3–4.0 (median: 3.8). Modeling these higher trophic levels is important for structuring the ecosystem, and the nekton trophic levels found here are consistent with findings from ^{15}N amino acid studies (Choy et al., 2015).

The modeled mesozooplankton ingestion can be classified into four distinct dietary types: (1) Herbivory = phytoplankton diet, (2) Protistivory = protistan zooplankton diet, (3) Detritivory = detrital diet (i.e., SDT or LDT), and (4) Carnivory = mesozooplankton diet. Using this partitioning, the relative contributions of each dietary component were assessed for large, and small vertically migrating mesozooplankton compartments (**Figure 5**). The largest proportion of the diet for resident epipelagic mesozooplankton (i.e., SMZ & LMZ) was balanced between herbivory (19–57% median: 40%) and protistivory (26–59% median: 40%). Detritivory was 9–21% (median: 13%) of total diet. Inter-cycle variability in carnivory was low for resident epipelagic mesozooplankton and contributed 6–8% (median: 6%) of their diet.

Comparing the LIEM solutions between the nutrient limited and upwelling cycles, we found that large mesozooplankton (LMZ) grazing increased from 9–16% (median: 13%) in the nutrient limited cycles to 22–65% under upwelling conditions (median: 30%) of NPP. However, the overall diets of the mesozooplankton did not systematically change with nutrient condition.

New Production, Export and DVM

Total export ranged from 163 to 707 mg C m^{-2} d^{-1} (median: 282 mg C m^{-2} d^{-1}), with distinctly elevated values associated with upwelling cycles (**Figure 6A**). The fraction of export attributed to mesozooplankton DVM (vmSMZ + vmLMZ) covaried with nutrient regime: mesozooplankton active transport contributed 14–37% of total export under nutrient limited conditions and 44–84% under upwelling conditions (**Figure 6B**). There was no significant relationship ($p < 0.1$) between the total export efficiency (i.e., total export/NPP) and NPP (**Figure 6C**).

For vmSMZ, 77–80% (median: 80%) of their respiration took place in the epipelagic, along with 67–87% (median: 85%) of their DOC excretion. This is consistent with the suggestion that mesozooplankton respiration and excretion are elevated in the warmer epipelagic waters (Ikeda, 1985), where activity is highest.

The fate of active export flux is important for understanding the ecological impact of this carbon supply. Within the

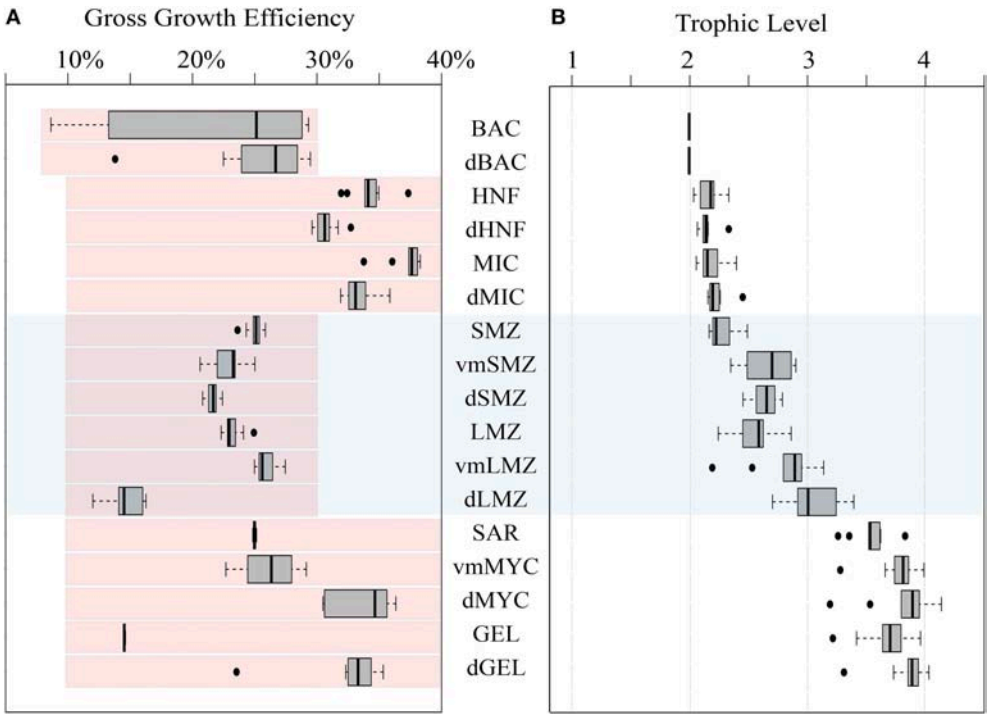

FIGURE 4 | (A) Box and whisker plot of GGE for organisms in the LIEM. Red shaded boxes indicate the permitted range of values constraining the LIEM. **(B)** Box and whisker plot of trophic levels for each zooplankton assuming detritus and primary productivity are trophic level 1, and bacteria are trophic level 2. Box and whisker plots show inter-quartile range and 95% C.I. as determined using the mean solutions for each cycle. For reference the mesozooplankton compartments are shaded across both figures. Abbreviations are explained in **Table 2**.

mesopelagic, mesozooplankton respired 11–104 mg C m^{-2} d^{-1} (median: 33 mg C m^{-2} d^{-1}) and excreted 7–116 mg C m^{-2} d^{-1} (median: 20 mg C m^{-2} d^{-1}; **Figure 7A**). Predation on vertically migrating mesozooplankton accounted for a loss of 23–352 mg C m^{-2} d^{-1} (median: 59 mg C m^{-2} d^{-1}) in the mesopelagic. Mesozooplankton fecal pellet production in the mesopelagic was 8–29 mg C m^{-2} d^{-1} (median: 13 mg C m^{-2} d^{-1}). Resident mesopelagic mesozooplankton were the dominant mortality term for the vertically migrating mesozooplankton (**Figure 7B**).

Mesopelagic Ecosystem

Deep bacteria (dBAC) made up 6–30% (median: 11%) of the mesopelagic protistan zooplankton diet with the remainder supplied by detritus/fecal pellets. Mesopelagic mesozooplankton (i.e., dSMZ & dLMZ) had a more variable diet than the epipelagic mesozooplankton (**Figure 5**), with detritivory ranging from 17 to 43% (median: 39%) of their diet, protistivory at 14–51% (median: 30%) and carnivory at 10–68% (median: 33%).

Systematic increases in trophic level between the epipelagic and mesopelagic resident zooplankton and nekton were observed (**Figure 4**). The trophic level of epipelagic microzooplankton (MIC) was 2.0–2.3 while dMIC was 2.3–2.5. Similar increases between the epipelagic and mesopelagic were observed for mesozooplankton, where SMZ had a trophic level of 2.2–2.5 (median: 2.2) dSMZ had a trophic level of 2.5–2.8 (median: 2.6). Likewise, dLMZ trophic levels were elevated by ∼0.4 relative to LMZ. The trophic level of dMYC (3.2–4.1) was more variable than the other micronekton (e.g., vmMYC: 3.5–4.0), illustrating a greater variability in diet.

Mesopelagic respiration is a useful diagnostic loss term for determining which organisms are responsible for the mesopelagic carbon demand (**Supplemental Figure 2**). Mesopelagic bacteria accounted for the largest proportion of mesopelagic respiration (31–41% median: 34%). High respiration of mesopelagic bacteria was found despite relatively high GGE for these organisms (median 26%, **Figure 4A**). Mesopelagic protistan zooplankton and resident mesozooplankton were responsible for 14–30% (median: 25%) and 14–24% (median: 15%), respectively. Resident gelatinous predators and myctophids are responsible for 4–8% of mesopelagic respiration combined. The proportion of export due to active transport covaried with resident mesopelagic respiration (**Figure 8A**), illustrating the coupling between active transport and mesopelagic activity in the LIEM. The effect of higher active transport relative to total export can be shown with an indirect analysis where the relative contribution of carbon from epipelagic detritus (i.e., a passive transport proxy) and vertically migrating mesozooplankton (i.e., an active transport proxy) in the diet of each organism can be measured. Indirect flux analyses show that a higher proportion of the carbon consumed by mesopelagic bacteria, protists, and mesozooplankton originated from passive rather than active

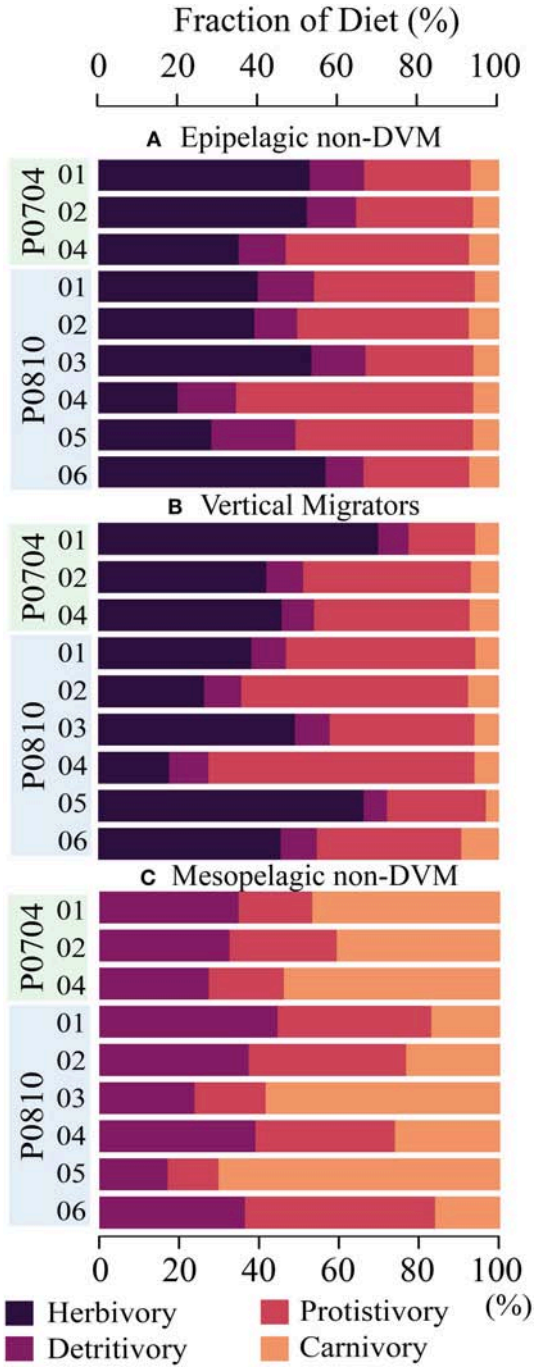

FIGURE 5 | Composition of diet for **(A)** epipelagic, non-DVM mesozooplankton, **(B)** vertically migrating mesozooplankton, and **(C)** mesopelagic, non-DVM mesozooplankton. Diet is partitioned into herbivory (darkest), protistivory, detritivory, and carnivory (lightest). Cycles are as indicated.

transport (**Figure 8B**). However, mesopelagic nekton (dMYC) were predominantly supported by carbon derived from active transport pathways.

DISCUSSION

Diel Vertical Migration and Active Transport in the CCE

In contrast to common assumption about the processes driving the biological pump, our results suggest that active transport may be as, if not more, important than sinking particle flux. We found that active transport (mesozooplankton and fish combined) was responsible for 39–606 mg C m^{-2} d^{-1} (median: 107 mg C m^{-2} d^{-1}), corresponding to 21–86% of total export to the mesopelagic, while sinking particles contributed 14–79%. This finding is not directly forced by an *a priori* assumption of the importance of active transport. Indeed, we placed no direct constraint on the amount of mesozooplankton mortality in the mesopelagic, and the minimum constraints on basal metabolism by zooplankton in the mesopelagic (Stukel et al., 2013) implied that active transport could have been as low as 2–40% of sinking flux (median: 18%). Nevertheless, the importance of active transport was a robust result of the inverse analyses. For P0810-6, the cycle with the lowest relative contribution of active transport to total export (21%), the total flux was 184 ± 23 mg C m^{-2} d^{-1} (95% CI) and active transport was 39 ± 21 mg C m^{-2} d^{-1} (95% CI). This cycle was oligotrophic and had the lowest ^{14}CPP measurements of any cycle on the two cruises. In contrast, cycle P0810-5 had the highest relative contribution of active transport (86 ± 4% of total export at the 95% CI). P0810-5 was on the coastal (i.e., high biomass) side of a strong frontal feature with high rates of primary productivity and large standing stocks of zooplankton.

Although these rates of active transport are higher than reported in many studies, they are fully consistent with mesozooplankton community dynamics in the CCE. The model suggests that total epipelagic mesozooplankton consumption on phytoplankton, protists, detritus, and other mesozooplankton ranged from 361 to 2,966 mg C m^{-2} d^{-1} (median: 1,006 mg C m^{-2} d^{-1}). Vertically stratified day-night net tows showed that 35–86% (median: 57%) of the mesozooplankton community was vertically migrating to depth each day and that most of these vertical migrants were copepods and euphausiids (Stukel et al., 2013). Our model results indicate that only 20–23% of respiration and 16–34% of excretion by vertical migrants occurred at depth. None of these assumptions are particularly aggressive. Furthermore, our results (**Figure 9**) are consistent with estimates of DVM in the zooplankton derived from the model of Archibald et al. (2019), if specific dynamics of the CCE are taken into account (e.g., zooplankton consume nearly all of NPP, Landry et al., 2009; microphytoplankton are negligible contributors to sinking flux, Stukel et al., 2013). Our estimates of the total export ratio 19–44% are also consistent with typical *f*-ratio estimates (new production to total export) in our study region, which varied from 0.23 to 0.40 (Krause et al., 2015). Our results thus do not arise from unusual parameterizations but instead may reflect the fact that estimates of active export using standard metabolism calculated from Ikeda (1985) and Ikeda et al. (2001) may be conservative underestimates.

Our results also reflect realistic coupling between the epipelagic and mesopelagic communities. Model results

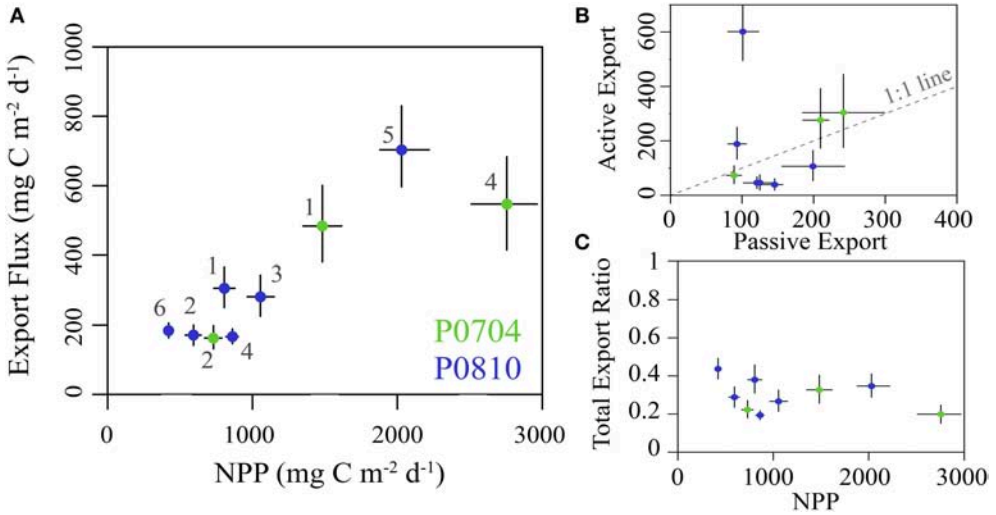

FIGURE 6 | (A) The sum of both passive and active carbon export flux from the epipelagic plotted against NPP. Cruises are color coded and error bars show the 95% CI for each value. **(B)** The total active flux due to DVM verses passive flux for each cycle (as in **A**). Dashed 1:1 line for reference. **(C)** The total export ratio (i.e., total epipelagic export/NPP) plotted against NPP and colored as in **(A)**. All values are in mg C m^{-2} d^{-1}.

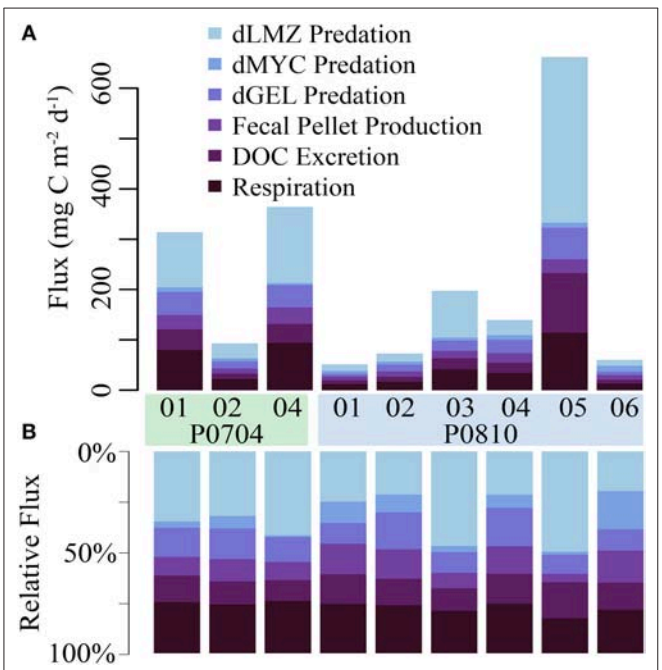

FIGURE 7 | The **(A)** net and **(B)** relative fate of vertically migrating mesozooplankton within the mesopelagic. Loss terms are color coded, and cruise and cycle are as shown. Abbreviations are explained in **Table 2**.

suggested that the carbon demand was equal to <1–4% (median: 1.1%) of NPP for mesopelagic fish, 1–7% (median: 3%) of NPP for predatory gelatinous zooplankton, 8–22% (median: 14%) of NPP for resident mesopelagic zooplankton, and 6–19% (median: 11%) of NPP for mesopelagic bacteria. These mesopelagic carbon demands must be met by carbon flux from the surface layer, the most likely sources of which are sinking particle flux (which we experimentally measured using two independent approaches) and active transport. While it is possible that both sediment traps and ^{238}U-^{234}Th disequilibrium underestimated sinking carbon flux, the inverse analysis offers compelling evidence that active transport is more likely to support mesopelagic fish and gelatinous predator communities. Although sinking particles can efficiently support bacterial production (as they are likely directly colonized by particle-attached bacteria), many fish and gelatinous zooplankton are predators that feed more on living organisms than on the sinking fecal pellets that typically dominate particle flux in the CCE. For these planktivorous organisms, sustaining their metabolism through a food chain supported by sinking particles would likely require one (if not more) trophic levels to separate them from the export source, depending on whether the sinking particles are consumed by filter- or flux-feeding zooplankton or by microbes (Stukel et al., 2019). Thus, sustaining the high carbon demand of mesopelagic myctophids with sinking particles requires substantially more total carbon flux than does sustaining it via active transport of the myctophids' prey.

Mesopelagic sources of mortality have implications for the fitness of vertical migrators. It is often assumed that DVM is ecologically advantageous when the costs associated with not feeding during the day and actively swimming to depth are offset by the benefits of reduced predation pressure and/or reduced metabolism at colder mesopelagic temperatures (Bianchi et al., 2013; Hansen and Visser, 2016; Morozov and Kuzenkov, 2016). Our model suggests that mortality normalized to ingestion is similar across all mesozooplankton compartments and across a wide range of ecosystem states (SMZ: 24–26%, LMZ: 22–25%, vmSMZ: 21–25%, vmLMZ: 25–27%, dSMZ: 21–23%, dLMZ: 19–23%). Even though vmSMZ experience similar predation to SMZ and dSMZ, approximately half of the predation on vertically

migrating zooplankton takes place in the mesopelagic, thereby transferring carbon to depth despite the fact that their excretion and respiration occur primarily in the epipelagic.

The comparable mortality experienced by vertically-migrating mesozooplankton in the mesozooplankton may seem counterintuitive in light of extensive research suggesting that the adaptive advantage of DVM may be to reduce predation (Ohman and Romagnan, 2016; Bandara et al., 2018). However, in the CCE, it is not particularly surprising when the large abundances of myctophids, gonostomatids, and other mesopelagic fish are considered. Davison et al. (2013) and Davison et al. (2015) demonstrated high biomass of these fish comprising both vertically-migrating and mesopelagic resident communities. Mesozooplankton may thus face as high, if not higher, predator abundance at mesopelagic depths than in the epipelagic, although colder temperatures and reduced irradiance may diminish predation rates at depth. DVM may remain advantageous as a lifestyle because if these organisms were present at the surface during the day then they might experience substantially greater predation than in the mesopelagic.

Sensitivity Analysis and Ecological Connections

The ecosystems generated in the 9 model runs were as varied as the cruise measurements: including observations from dynamic coastal blooms to quiescent oligotrophic communities. All 9 cycles had significantly elevated NPP compared to the observed ^{14}CPP (**Figure 3**; **Supplemental Figure 1**) with 95% CI from the MCMC random walk. Whether this result can be considered a model bias or is derived from possible systematic differences between ^{14}CPP and true net primary production (Peterson, 1980; Lefevre et al., 1997; Marra, 2009; Milligan et al., 2015) is not known. Compared to shorter ^{14}C labeling experiments (e.g. dawn-to-dusk, 8 h, pulse-chase), the 24 h incubations used here are generally thought to measure NPP rates directly (Milligan et al., 2015); however, long-term incubations are susceptible to biases introduced by heterotrophic processes and DOC excretion (Laws et al., 2000; Dickson et al., 2001). Since rapid consumption of net primary productivity by grazers, cell lysis, and excretion of DOC (all of which are explicitly included in the LIEM) will reduce the apparent ^{14}C-bicarbonate uptake rates, ^{14}CPP rates may be biased low, especially when turnover times are short. In fact, when comparing dilution-based growth rates with 24 h ^{14}CPP incubations in the equatorial Pacific, Landry et al. (2011) found that ^{14}CPP estimates needed to be adjusted upwards by 29% on average. An alternative explanation may stem from a bias in the MCMC approach used. Since the random walk is strictly required to yield solutions where flows are positive through the "mirror" algorithm, the region of permitted solutions is non-symmetric and may favor the broader solution-space of high NPP solutions (as noted in Stukel et al., 2012). A thorough investigation into the potential biases of the ^{14}CPP method of the MCMC solution algorithm are beyond the scope of this study, but the impact of a potential bias in modeled NPP are discussed below.

To test the model's sensitivity to the misfit with ^{14}CPP and to confirm that our results were not driven by a potential bias in the model, the LIEM was rerun assuming that ^{14}CPP uncertainty was 1/10th of the actual estimated uncertainty (i.e., 0.6% relative uncertainty). The model-observation misfit increased by nearly 2.5x with vmSMZ and SMZ grazing rates, myctophid metabolic estimates, and sediment trap export all reduced by $\sim$2 Σ relative to the standard model run. This result shows that the model needed to increase NPP in the standard model run in order to match the observed mesozooplankton grazing rate and myctophid metabolic requirements. However, the proportion of export resulting from active transport remained relatively unchanged. It varied from 106 to 641 mg C m^{-2} d^{-1} across the cycles (compared to 162 to 707 mg C m^{-2} d^{-1} in the standard model run). This suggests that our primary conclusions about export flux were not contingent on elevated model NPP.

Because bacterial activity in the mesopelagic was not measured, we set a high upper and low minimum bounds for bacterial production. For the minimum bound on mesopelagic BP, we chose an attenuation coefficient of $\alpha = 1.47$ (Yokokawa et al., 2013). This resulted in model-determined mesopelagic bacterial carbon demand that may have been lower than true *in situ* values. Other reported values for the attenuation of BP in the mesopelagic include slopes of $\alpha = 1.15$ (Tanaka and Rassoulzadegan, 2004) and 1.03 (Gasol et al., 2009), which would result in 25 and 36% higher estimates of mesopelagic BP, respectively. When the minimum mesopelagic bacterial production estimates were halved ($\alpha = 0.64$; Equation 1), the model responded by increasing NPP by +2% (inter-cycle median) and total export flux by 11%. Since passive particle flux is constrained by observations, passive flux increased by 0–12% (median: 4%) while active transport by mesozooplankton increased by 0–56% (median: 26%). Active transport by nekton was also elevated (0–14%, median: 10%). Model-observation misfit increased by an average of 17% with notable changes in NPP (+0.42 Σ), sediment trap flux (+0.34 Σ) and Thorium-234 flux (+0.22 Σ).

The standard model results were also robust to changes in other observations. When the nekton metabolic estimates were halved, export by vmMYC was reduced by 51% (inter-cycle median), a change of $<$ 5 mg C m^{-2} d$^{-1,}$ while other forms of export were unchanged. Increasing the upper limit of mesozooplankton GGE from 30 to 40% led to a $\sim$20% increase in mesozooplankton active transport and no change in nekton-derived active flux or passive flux.

Zooplankton basal respiration rates have been shown to be suppressed under low-oxygen conditions (Ekau et al., 2010; Seibel, 2011), such as those seen in the midwater oxygen minimum zones (OMZ) often encountered below the productive Eastern boundary current upwelling biomes (Chavez and Messié, 2009; Bettencourt et al., 2015). During our study periods, water-column dissolved oxygen concentrations fell below 44.7 μM (0.5 ml/l), indicating hypoxic conditions (Helly and Levin, 2004; Gilly et al., 2013), between 271 and 470 m water depth (**Supplemental Figure 3**). Notably, most of the zooplankton captured in our study were found at depths shallower than 300 m. While there are questions remaining with regard to how mesozooplankton respiration rates would be affected by the intermediate oxygen depletion observed in

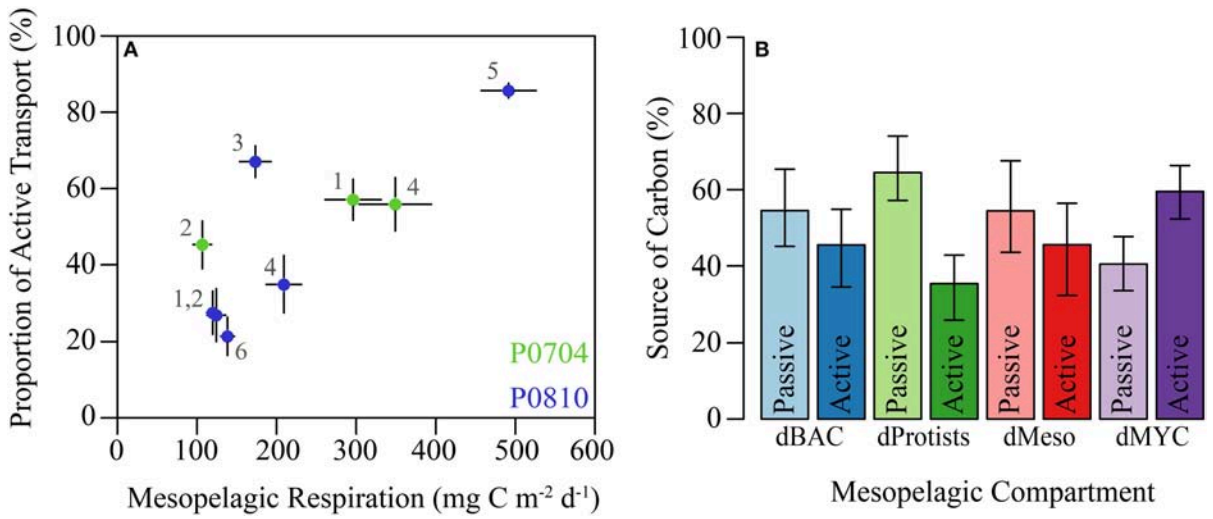

FIGURE 8 | (A) Proportion of active transport relative to total export verses total mesopelagic respiration by residents (i.e., dBAC, dHNF, dMIC, dSMZ, dLMZ, dMYC, dGEL). Cruises are colored and cycles are as shown. **(B)** Relative proportions of carbon demand supplied by passive or active flux for the indicated mesopelagic groups. Source was calculated using indirect flux analysis (Section Indirect analysis) to determine the indirect contribution epipelagic detritus (passive) and vertically migrating mesozooplankton (active). Error bars are ±1 SD.

our study (Teuber et al., 2013; Kiko et al., 2016), the model results are largely insensitive to a possible reduction in basal metabolism. In particular, the respiration rates of the mesopelagic organisms in the model were consistently higher than the basal metabolic constraint placed on them (typically >2x). Including ecological implications of the OMZ directly would be a valuable contribution to the field that necessitates a more depth-resolved model due to the importance of vertical gradients in oxygen and temperature.

Linear Inverse Models

LIEMs are powerful tools for assimilating diverse *in situ* measurements and constraints with a food web perspective. The use of a two-layer model (Jackson and Eldridge, 1992) is particularly powerful because it allows information from the mesopelagic to constrain epipelagic food web flows and vice versa. Compared to most previously published LIEMs, the model presented here includes many more *in situ* rate measurements, made possible by the suite of contemporaneous rate measurements made during quasi-Lagrangian experiments. When constrained by fewer rate measurements (Dubois et al., 2012; van Oevelen et al., 2012; Sailley et al., 2013), the LIEM solution relies more heavily on greater than/less than constraints derived from biomass measurements, leading to correspondingly higher uncertainty. This highlights a need for studies that simultaneously quantify the activity of many different plankton functional groups.

Since a LIEM is fundamentally a data-regression technique, our results are emergent from (A) our observations, (B) the assumptions used (e.g., GGE), and (C) the ecosystem structure of the model. Thus, we believe the resulting model solutions to be descriptive of the dominant *in situ* processes in the CCE LTER study region. However, it is important to note

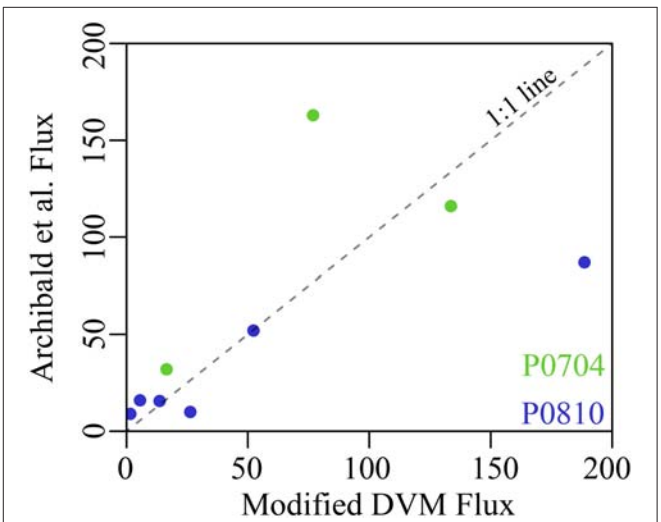

FIGURE 9 | Comparison between modeled mesozooplankton DVM flux without mesopelagic mortality and the predicted flux from Archibald et al. (2019) with CCE-specific parameterization following Stukel et al. (2015). Cruises are as colored (P0704 = green, P0810 = blue) and dashed line is a 1:1 reference line. Fluxes are shown in mg C m^{-2} d^{-1}.

that there were large uncertainties associated with some model flows, and that these could be quantified using the MCMC approach (**Supplemental Table 2**). We thus highly recommend the MCMC approach (Kones et al., 2009; van den Meersche et al., 2009), which has been shown to be robust in its ability to recover ecosystem rates relative to the L-2 minimum norm (Stukel et al., 2012; Saint-béat et al., 2013). Even more important is its ability to generate confidence intervals that realistically

represent the uncertainties in model outputs with respect to both measurements and under-determinacy of the model. For instance, for cycle P0810-6, we found that the 95% confidence interval for HNF ingestion of detritus was 5–127 mg C m^{-2} d^{-1}, providing no real knowledge of whether or not this connection was an important part of the ecosystem. However, for Cycle P0810-5, we found that mesopelagic mesozooplankton predation on small vertical migrators was 233–423 mg C m^{-2} d^{-1} (95% CI), indicating a higher degree of confidence that this flow was substantial at this location. Investigation of the confidence intervals can thus inform which conclusions can be considered robust. Developing even better-resolved ecosystem models likely requires incorporation of more diverse measurement types, such as ^{15}N isotopic data (Stukel et al., 2018a).

The Biological Carbon Pump and Mesopelagic Flux Attenuation

Reports of active transport by vertically migrating biota have long suggested that these organisms can transport a globally significant amount of carbon to depth. However, most early studies suggested that active transport was substantially less important than passive flux of sinking particles (Morales, 1999; Davison et al., 2013; Steinberg and Landry, 2017). At the oligotrophic BATS station off Bermuda, Dam et al. (1995) found that respiration by mesozooplankton augmented the passive carbon flux at 150 m by 18–70%. Also at BATS, Steinberg et al. (2000) reported a significant vertical transfer of nitrogen by zooplankton, including dissolved organic nitrogen (DON). In fact, vertical migrators were found to perform 15–66% of the total nitrogen transport. Hansen and Visser (2016) estimated that across the North Atlantic active transport by mesozooplankton may constitute 27% of total export out of the surface mixed layer. In addition to zooplankton, vertical migrations by micronekton can also lead to significant export fluxes (Angel and Pugh, 2010; Davison et al., 2013; Hernandez-Leon et al., in review). Using biomass estimates and metabolic relationships, Davison et al. (2013) found micronekton contributions of 22–24 mg C m^{-2} d^{-1} (or 15–17% of estimated passive export) in the northeast Pacific at 150 m water depth. In the North Pacific Subtropical Gyre, Al-Mutairi and Landry (2001) estimated that active transport due to zooplankton respiration was responsible for carbon flux equal to 18% of passive flux at 150 m. Using a conservative approach (Longhurst et al., 1990), estimated that active export by zooplankton DVM was 13–58% that of passive flux at 150 m when accounting for respiration alone in subtropical waters, which is similar to our results where the LIEM suggests that mesozooplankton respiration at depth is 9–113% (median: 34%) that of passive export at 100 m. Global modeling estimates have indicated that active transport may be responsible for 14% (Archibald et al., 2019) or 15 to 40% (Bianchi et al., 2013) increases in carbon export out of the euphotic zone relative to sinking particles alone. More recent results have suggested increased importance for active transport, potentially rivaling that of passive flux. In the Costa Rica Dome, a region with high mesozooplankton biomass like the CCE, Stukel et al. (2018b) identified active transport by zooplankton DVM as responsible for 21–45% of total euphotic zone export. Hernández-León et al. (in review) found that active transport was equal to one quarter of passive flux in oligotrophic regions, but was 2-fold higher than passive flux in eutrophic areas of the tropical and subtropical Atlantic. Our results that total active transport (zooplankton and nekton) may be responsible for 18–84% (median: 42%) of total carbon export at 100 m in the CCE are thus somewhat higher than found in most studies, but consistent with recently published values for high zooplankton biomass regions. Furthermore, our results are in line with other biogeochemical and ecological expectations (e.g., mesopelagic carbon demand, euphotic zone new production, mesozooplankton energy partitions). We thus suggest that active transport in high biomass regions may be more important, in fact, than some previous studies suggest, and we recommend focused research to investigate the potentially conservative assumptions made in previous studies that rely on standard (rather than active) estimates of zooplankton metabolic rates.

Within the mesopelagic, zooplankton also play an important biogeochemical role in the attenuation of particle flux (Steinberg et al., 2008; Buesseler and Boyd, 2009; Stukel et al., 2019) and in effecting elemental cycling (Kiko et al., in review; Robinson et al., 2010). Our results suggest that mesozooplankton detritivory accounted for the consumption of 57–71% of sinking particles from the epipelagic, with bacterially mediated remineralization of the majority of the remainder (i.e., mesopelagic export efficiency is $< 10\%$). Notably, 3 of the 4 cycles with the lowest proportion of detritivory and the largest proportion of carnivory in the resident mesopelagic zooplankton were during upwelling cycles. This is opposite to the findings of Wilson et al. (2010), who observed increases in fatty-acid biomarkers associated with carnivory at station Aloha relative to K2 and attributed the increase to the lower primary productivity at station Aloha. Our result that zooplankton rely more heavily on carnivory in the mesopelagic agrees with fecal pellet characteristic analyses and fatty acid biomarkers measured by Wilson et al. (2008) and Wilson et al. (2010), respectively. However, given the advective nature of an eastern boundary current and frequency of non-steady state conditions, it is difficult to generalize from our results to the rest of the Pacific. Clearly additional studies are necessary.

CONCLUSIONS

The LIEM used here incorporated numerous *in situ* measurements made during quasi-Lagrangian experiments in the CCE in order to constrain carbon flows through the ecosystem. These observations were made in water parcels spanning a wide range of conditions from highly productive upwelling regions to an oligotrophic offshore domain and consistently found that active transport of carbon by mesozooplankton was important to supplying the mesopelagic carbon demand. The model suggests that, relative to total export, gravitational settling contributes 12–55% (median: 37%) and subduction contributes 2–32% (median: 14%) of carbon flux. This finding has implications for the interpretation of sediment trap and ^{234}Th disequilibrium measurements and for helping to reconcile the long-studied imbalance in the mesopelagic carbon budget. The LIEM also highlights the central importance of zooplankton in marine food webs and

biogeochemistry. Excretion by vertical migrants is important for meeting bacterial carbon demand, while predation on vertical migrants supports mesopelagic resident fish communities. Our analysis comprises a unique, fully resolved phytoplankton-to-fish coupled food web of the epipelagic and mesopelagic ocean. Nevertheless, substantial uncertainties remain, and targeted studies are necessary to validate the suggested relationships *in situ* and to test their applicability across the global ocean.

DATA AVAILABILITY

All datasets generated for this study are included in the manuscript and/or the **Supplementary Files**.

AUTHOR CONTRIBUTIONS

ML was responsible for cruise design and protistan zooplankton data. MO was responsible for mesozooplankton data. RG was responsible for phytoplankton data. PD was responsible for myctophid data. MS was responsible for particle export data. TK and MS designed the model. TK wrote the manuscript. All authors contributed to editing the manuscript.

ACKNOWLEDGMENTS

The authors would like to thank the crews and captains of the *R/V Thompson* and *Melville* for their superlative assistance in collecting the wide variety of observations used in this study. We thank our colleagues in the CCE for their continued support, energy and commitment to long-term ecological research of the pelagic. We would like to thank the editor and two reviewers on their constructive comments and expertise. Additionally, the open source R community provided valuable technical support, and both directly and indirectly assisted in the development of the code used for the calculations presented here. This work was supported by NSF Biological Oceanography grants to the CCE LTER Program: OCE-0417616, OCE-1026607, OCE-1637632, and OCE-1614359. The source code and data used for the LIEM can be freely obtained under the MIT open-source license at https://github.com/tbrycekelly/Inverse_DVM or by contacting TK.

SUPPLEMENTARY MATERIAL

The Supplementary Material for this article can be found online at: https://www.frontiersin.org/articles/10.3389/fmars.2019.00508/full#supplementary-material

REFERENCES

Al-Mutairi, H., and Landry, M. R. (2001). Active export of carbon and nitrogen at station ALOHA by diel migrant zooplankton. *Deep Sea Res. Part II Top. Stud. Oceanogr.* 48, 2083–2103. doi: 10.1016/S0967-0645(00)00174-0

Anderson, T. R., Martin, A. P., Lampitt, R. S., Trueman, C. N., Henson, S. A., and Mayor, D. J. (2018). Quantifying carbon fluxes from primary production to mesopelagic fish using a simple food web model. *ICES J. Mar. Sci.* 76, 690–701. doi: 10.1093/icesjms/fsx234

Angel, M. V., and Pugh, P. R. (2010). Quantification of diel vertical migration by micronektonic taxa in the northeast Atlantic. *Hydrobiologia* 440, 161–179. doi: 10.1023/A:1004115010030

Archibald, K. M., Siegel, D. A., and Doney, S. C. (2019). Modeling the impact of zooplankton diel vertical migration on the carbon export flux of the biological pump. *Glob. Biogeochem. Cycles.* 33, 181–199. doi: 10.1029/2018GB005983

Aumont, O., Maury, O., Lefort, S., and Bopp, L. (2018). Evaluating the potential impacts of the diurnal vertical migration by marine organisms on marine biogeochemistry. *Glob. Biogeochem. Cycles* 32, 1622–1643. doi: 10.1029/2018GB005886

Bandara, K., Varpe, Ø., Ji, R., and Eiane, K. (2018). A high-resolution modeling study on diel and seasonal vertical migrations of high-latitude copepods. *Ecol. Model.* 368, 357–376. doi: 10.1016/j.ecolmodel.2017.12.010

Benitez-Nelson, C. R., Buesseler, K. O., Van Der Loeff, M. R., Andrews, J., Ball, L., Crossin, G., et al. (2001). Testing a new small-volume technique for determining 234Th in seawater. *J. Radioanalyt. Nucl. Chem.* 248, 795–799. doi: 10.1023/A:1010621618652

Bettencourt, J. H., López, C., García, E. H., Montes, I., Sudre, J., Dewitte, B., et al. (2015). Boundaries of the peruvian oxygen minimum zone shaped by coherent mesoscale dynamics. *Nat. Geosci.* 8, 937–940. doi: 10.1038/ngeo2570

Bianchi, D., Stock, C., Galbraith, E. D., and Sarmiento, J. L. (2013). Diel vertical migration: ecological controls and impacts on the biological pump in a one-dimensional ocean model. *Glob. Biogeochem. Cycles* 27, 478–491. doi: 10.1002/gbc.20031

Boyd, P. W., and Trull, T. W. (2007). Understanding the export of biogenic particles in oceanic waters: is there consensus? *Prog. Oceanogr.* 72, 276–312. doi: 10.1016/j.pocean.2006.10.007

Buesseler, K. O., and Boyd, P. W. (2009). Shedding light on processes that control particle export and flux attenuation in the twilight zone of the open ocean. *Limnol. Oceanogr.* 54, 1210–1232. doi: 10.4319/lo.2009.54.4.1210

Burd, A. B., Hansell, D. A., Steinberg, D. K., Anderson, T. R., Arístegui, J., Baltar, F., et al. (2010). Assessing the apparent imbalance between geochemical and biochemical indicators of meso- and bathypelagic biological activity: What the @$#! is wrong with present calculations of carbon budgets? *Deep Sea Res. Part II Top. Stud. Oceanogr.* 57, 1557–1571. doi: 10.1016/j.dsr2.2010.02.022

Chavez, F. P., and Messié, M. (2009). A comparison of Eastern boundary upwelling ecosystems. *Prog. Oceanogr.* 83, 80–96. doi: 10.1016/j.pocean.2009.07.032

Choy, C. A., Popp, B. N., Hannides, C. C. S., and Drazen, J. C. (2015). Trophic structure and food resources of epipelagic and mesopelagic fishes in the north pacific subtropical gyre ecosystem inferred from nitrogen isotopic compositions. *Limnol. Oceanogr.* 60, 1156–1171. doi: 10.1002/lno.10085

Cohen, J. H., and Forward, R. B. (2009). Zooplankton diel vertical migration — a review of proximate control. *Ocean. Mar. Biol. Annu. Rev.* 47, 77–109. doi: 10.1201/9781420094220.ch2

Conover, R. J. (1966). Assimilation of organic by zooplankton. *Limnol. Oceanogr.* 11, 338–345. doi: 10.4319/lo.1966.11.3.0338

Dam, H. G., and Peterson, W. T. (1988). The effect of temperature on the gut clearance rate constant of planktonic copepods. *J. Exp. Mar. Biol. Ecol.* 123, 1–14. doi: 10.1016/0022-0981(88)90105-0

Dam, H. G., Roman, M. R., and Youngbluth, M. J. (1995). Downward export of respiratory carbon and dissolved inorganic nitrogen by diel-migrant mesozooplankton at the JGOFS Bermuda time-series station. *Deep-Sea Res. Part I* 42, 1187–1197. doi: 10.1016/0967-0637(95)00048-B

Davison, P., Lara-Lopez, A., and Anthony Koslow, J. (2015). Mesopelagic fish biomass in the southern California current ecosystem. *Deep-Sea Res. Part II Top. Stud. Oceanogr.* 112, 129–142. doi: 10.1016/j.dsr2.2014.10.007

Davison, P. C., Checkley, D. M., Koslow, J. A., and Barlow, J. (2013). Carbon export mediated by mesopelagic fishes in the northeast Pacific Ocean. *Prog. Oceanogr.* 116, 14–30. doi: 10.1016/j.pocean.2013.05.013

del Giorgio, P. A., and Cole, J. J. (1998). Bacterial growth efficiency in natural aquatic systems. *Annu. Rev. Ecol. Syst.* 29, 503–541. doi: 10.1146/annurev.ecolsys.29.1.503

del Giorgio, P. A., and Duarte, C. M. (2002). Respiration in the open ocean. *Nature* 420, 379–384. doi: 10.1038/nature01165

Dickson, M.-L., Orchardo, J., Barber, R. T., Marra, J., McCarthy, J. J., and Sambrotto, R. N. (2001). Production and respiration rates in the Arabian Sea during the 1995 northeast and southwest monsoons. *Deep Sea Res. Part II Top. Stud. Oceanogr.* 48, 1199–1230. doi: 10.1016/S0967-0645(00)00136-3

Dubois, S., Del Amo, Y., Grami, B., Jude, F., Marquis, E., David, V., et al. (2012). Network analysis of the planktonic food web during the spring bloom in a semi enclosed lagoon (Arcachon, SW France). *Acta Oecologica.* 40, 40–50. doi: 10.1016/j.actao.2012.02.002

Ducklow, H. W., and Harris, R. P. (1993). Introduction to the JGOFS North Atlantic bloom experiment. *Deep-Sea Res. Part II* 40, 1–8. doi: 10.1016/0967-0645(93)90003-6

Ekau, W., Auel, H., Pörtner, H.-O., and Gilbert, D. (2010). Impacts of hypoxia on the structure and processes in pelagic communities (zooplankton, macro-invertebrates and fish). *Biogeosciences* 7, 1669–1699. doi: 10.5194/bg-7-1669-2010

Franks, P. J. S. (2002). NPZ models of plankton dynamics: their construction, coupling to physics, and application. *J. Oceanogr.* 58, 379–387. doi: 10.1023/A:1015874028196

Gasol, J. M., Alonso-Sáez, L., Vaqué, D., Baltar, F., Calleja, M. L., Duarte, C. M., et al. (2009). Mesopelagic prokaryotic bulk and single-cell heterotrophic activity and community composition in the NW Africa-Canary Islands coastal-transition zone. *Prog. Oceanogr.* 83, 189–196. doi: 10.1016/j.pocean.2009.07.014

Gilly, W. F., Beman, J. M., Litvin, S. Y., and Robison, B. H. (2013). Oceanographic and biological effects of shoaling of the oxygen minimum zone. *Annu. Rev. Mar. Sci.* 5, 393–420. doi: 10.1146/annurev-marine-120710-100849

Gontikaki, E., van Oevelen, D., Soetaert, K., and Witte, U. (2011). Food web flows through a sub-arctic deep-sea benthic community. *Prog. Oceanogr.* 91, 245–259. doi: 10.1016/j.pocean.2010.12.014

Gorsky, G., Ohman, M. D., Picheral, M., Gasparini, S., Stemmann, L., Romagnan, J.-B., et al. (2010). Digital zooplankton image analysis using the ZooScan integrated system. *J. Plankton Res.* 32, 285–303. doi: 10.1093/plankt/fbp124

Hannides, C. C. S., Drazen, J. C., and Popp, B. N. (2015). Mesopelagic zooplankton metabolic demand in the North Pacific Subtropical Gyre. *Limnol. Oceanogr.* 60, 419–428. doi: 10.1002/lno.10032

Hansen, A. N., and Visser, A. W. (2016). Carbon export by vertically migrating zooplankton: an optimal behavior model. *Limnol. Oceanogr.* 61, 701–710. doi: 10.1002/lno.10249

Helly, J. J., and Levin, L. A. (2004). Global distribution of naturally occurring marine hypoxia on continental margins. *Deep Sea Res. Part Oceanogr. Res. Pap.* 51, 1159–1168. doi: 10.1016/j.dsr.2004.03.009

Henson, S. A., Sanders, R., Madsen, E., Morris, P. J., Le Moigne, F., and Quartly, G. D. (2011). A reduced estimate of the strength of the ocean's biological carbon pump. *Geophys. Res. Lett.* 38, 10–14. doi: 10.1029/2011GL046735

Henson, S. A., Yool, A., and Sanders, R. (2015). Variability in efficiency of particulate organic carbon export: a model study. *Glob. Biogeochem. Cycles* 29, 33–45. doi: 10.1002/2014GB004965

Ikeda, T. (1985). Metabolic rates of epipeagic marine zooplankton as a function of body mass and temperature. *Mar. Biol.* 85, 1–11. doi: 10.1007/BF00396409

Ikeda, T., Kanno, Y., Ozaki, K., and Shinada, A. (2001). Metabolic rates of epipelagic marine copepods as a function of body mass and temperature. *Mar. Biol.* 139, 587–596. doi: 10.1007/s002270100608

Jackson, G. A., and Eldridge, P. M. (1992). Food web analysis of a planktonic system off Southern California. *Prog. Oceanogr.* 30, 223–251. doi: 10.1016/0079-6611(92)90014-Q

Kiko, R., Hauss, H., Buchholz, F., and Melzner, F. (2016). Ammonium excretion and oxygen respiration of tropical copepods and euphausiids exposed to oxygen minimum zone conditions. *Biogeosciences* 13, 2241–2255. doi: 10.5194/bg-13-2241-2016

Knauer, G. A., Martin, J. H., and Bruland, K. W. (1979). Fluxes of particulate carbon, nitrogen, and phosphorus in the upper water column of the northeast Pacific. *Deep Sea Res. Part Oceanogr. Res. Pap.* 26, 97–108. doi: 10.1016/0198-0149(79)90089-X

Kones, J. K., Soetaert, K., van Oevelen, D., and Owino, J. O. (2009). Are network indices robust indicators of food web functioning? a monte carlo approach. *Ecol. Model.* 220, 370–382. doi: 10.1016/j.ecolmodel.2008.10.012

Krause, J. W., Brzezinski, M. A., Goericke, R., Landry, M. R., Ohman, M. D., Stukel, M. R., et al. (2015). Variability in diatom contributions to biomass, organic matter production and export across a frontal gradient in the California Current Ecosystem. *J. Geophys. Res. Oceans* 120, 1032–1047. doi: 10.1002/2014JC010472

Kroes, H. W. (1977). The niche structure of ecosystems. *J. Theor. Biol.* 65, 317–326. doi: 10.1016/0022-5193(77)90327-7

Landry, M. R., Brown, S. L., Rii, Y. M., Selph, K. E., Bidigare, R. R., Yang, E. J., et al. (2008). Depth-stratified phytoplankton dynamics in cyclone opal, a subtropical mesoscale eddy. *Deep Sea Res. Part II Top. Stud. Oceanogr.* 55, 1348–1359. doi: 10.1016/j.dsr2.2008.02.001

Landry, M. R., Ohman, M. D., Goericke, R., Stukel, M. R., Barbeau, K. A., Bundy, R., et al. (2012). Pelagic community responses to a deep-water front in the California Current Ecosystem: overview of the a-front study. *J. Plankton Res.* 34, 739–748. doi: 10.1093/plankt/fbs025

Landry, M. R., Ohman, M. D., Goericke, R., Stukel, M. R., and Tsyrklevich, K. (2009). Lagrangian studies of phytoplankton growth and grazing relationships in a coastal upwelling ecosystem off Southern California. *Prog. Oceanogr.* 83, 208–216. doi: 10.1016/j.pocean.2009.07.026

Landry, M. R., Selph, K. E., Taylor, A. G., Décima, M., Balch, W. M., and Bidigare, R. R. (2011). Phytoplankton growth, grazing and production balances in the HNLC equatorial Pacific. *Deep Sea Res. Part II Top. Stud. Oceanogr.* 58, 524–535. doi: 10.1016/j.dsr2.2010.08.011

Laws, E. A., D'Sa, E., and Naik, P. (2011). Simple equations to estimate ratios of new or export production to total production from satellite-derived estimates of sea surface temperature and primary production. *Limnol. Oceanogr. Methods* 9, 593–601. doi: 10.4319/lom.2011.9.593

Laws, E. A., Landry, M. R., Barber, R. T., Campbell, L., Dickson, M.-L., and Marra, J. (2000). Carbon cycling in primary production bottle incubations: inferences from grazing experiments and photosynthetic studies using 14C and 18O in the Arabian Sea. *Deep Sea Res. Part II Top. Stud. Oceanogr.* 47, 1339–1352. doi: 10.1016/S0967-0645(99)00146-0

Lefevre, D., Minas, H. J., Minas, M., Robinson, C., Le, B., Williams, P. J., et al. (1997). Review of gross community production, primary production, net community production and dark community respiration in the Gulf of Lions. *Deep Sea Res. Part II Top. Stud. Oceanogr.* 44, 801–832. doi: 10.1016/S0967-0645(96)00091-4

Longhurst, A. R., Bedo, A. W., Harrison, W. G., Head, E. J. H., and Sameoto, D. D. (1990). Vertical flux of respiratory carbon by oceanic diel migrant biota. *Deep Sea Res. Part Oceanogr. Res. Pap.* 37, 685–694. doi: 10.1016/0198-0149(90)90098-G

Marra, J. (2009). Net and gross productivity: weighing in with 14C. *Aquat. Microb. Ecol.* 56, 123–131. doi: 10.3354/ame01306

Milligan, A. J., Halsey, K. H., and Behrenfeld, M. J. (2015). Horizons: advancing interpretations of 14C-uptake measurements in the context of phytoplankton physiology and ecology. *J. Plankton Res.* 37, 692–698. doi: 10.1093/plankt/fbv051

Morales, C. E. (1999). Carbon and nitrogen fluxes in the oceans: the contribution by zooplankton migrants to active transport in the North Atlantic during the joint global ocean flux study. *J. Plankton Res.* 21, 1799–1808. doi: 10.1093/plankt/21.9.1799

Morozov, A. Y., and Kuzenkov, O. A. (2016). Towards developing a general framework for modelling vertical migration in zooplankton. *J. Theor. Biol.* 405, 17–28. doi: 10.1016/j.jtbi.2016.01.011

Morrow, R. M., Ohman, M. D., Goericke, R., Kelly, T. B., Stephens, B. M., and Stukel, M. R. (2018). CCE V: primary production, mesozooplankton grazing, and the biological pump in the California Current Ecosystem: variability and response to El Niño. *Deep Sea Res. Part Oceanogr. Res. Pap.* 140, 52–62. doi: 10.1016/j.dsr.2018.07.012

Ohman, M. D., Powell, J. R., Picheral, M., and Jensen, D. W. (2012). Mesozooplankton and particulate matter responses to a deep-water frontal system in the southern California Current System. *J. Plankton Res.* 34, 815–827. doi: 10.1093/plankt/fbs028

Ohman, M. D., and Romagnan, J. B. (2016). Nonlinear effects of body size and optical attenuation on diel vertical migration by zooplankton. *Limnol. Oceanogr.* 61, 765–770. doi: 10.1002/lno.10251

Peterson, B. J. (1980). Productivity and the 14C-CO2 method : a history of the productivity problem. *Ecology* 11, 359–385. doi: 10.1146/annurev.es.11.110180.002043

Pike, S. M., Buesseler, K. O., Andrews, J., and Savoye, N. (2005). Quantification of234Th recovery in small volume sea water samples by inductively

coupled plasma-mass spectrometry. *J. Radioanal. Nucl. Chem.* 263, 355–360. doi: 10.1007/s10967-005-0062-9

Powell, J. R., and Ohman, M. D. (2012). Use of glider-class acoustic doppler profilers for estimating zooplankton biomass. *J. Plankton Res.* 34, 563–568. doi: 10.1093/plankt/fbs023

Powell, J. R., and Ohman, M. D. (2015). Changes in zooplankton habitat, behavior, and acoustic scattering characteristics across glider-resolved fronts in the Southern California Current System. *Prog. Oceanogr.* 134, 77–92. doi: 10.1016/j.pocean.2014.12.011

Robinson, C., Steinberg, D. K., Anderson, T. R., Arístegui, J., Carlson, C. A., Frost, J. R., et al. (2010). Mesopelagic zone ecology and biogeochemistry – a synthesis. *Deep Sea Res. Part II Top. Stud. Oceanogr.* 57, 1504–1518. doi: 10.1016/j.dsr2.2010.02.018

Sailley, S. F., Ducklow, H. W., Moeller, H. V, Fraser, W. R., Schofield, O. M., Steinberg, D. K., et al. (2013). Carbon fluxes and pelagic ecosystem dynamics near two western Antarctic Peninsula adélie penguin colonies: an inverse model approach. *Mar. Ecol. Prog. Ser.* 492, 253–272. doi: 10.3354/meps10534

Saint-béat, B., Vézina, A. F., Asmus, R., Asmus, H., and Niquil, N. (2013). The mean function provides robustness to linear inverse modelling flow estimation in food webs : a comparison of functions derived from statistics and ecological theories. *Ecol. Model.* 258, 53–64. doi: 10.1016/j.ecolmodel.2013.01.023

Samo, T. J., Pedler, B. E., Ball, G. I., Pasulka, A. L., Taylor, A. G., Aluwihare, L. I., et al. (2012). Microbial distribution and activity across a water mass frontal zone in the California Current Ecosystem. *J. Plankton Res.* 34, 802–814. doi: 10.1093/plankt/fbs048

Savoye, N., Benitez-Nelson, C., Burd, A. B., Cochran, J. K., Charette, M., Buesseler, K. O., et al. (2006). 234Th sorption and export models in the water column: a review. *Mar. Chem.* 100, 234–249. doi: 10.1016/j.marchem.2005.10.014

Seibel, B. A. (2011). Critical oxygen levels and metabolic suppression in oceanic oxygen minimum zones. *J. Exp. Biol.* 214, 326–336. doi: 10.1242/jeb.049171

Siegel, D. A., Buesseler, K. O., Doney, S. C., Sailley, S. F., Behrenfeld, M. J., and Boyd, P. W. (2014). Global assessment of ocean carbon export by combining satellite observations and food-web models. *Glob. Biogeochem. Cycles* 28, 181–196. doi: 10.1002/2013GB004743

Steinberg, D. K., Carlson, C. A., Bates, N. R., Goldthwait, S. A., Madin, L. P., and Michaels, A. F. (2000). Zooplankton vertical migration and the active transport of dissolved organic and inorganic carbon in the Sargasso Sea. *Deep Sea Res. Part Oceanogr. Res. Pap.* 47, 137–158. doi: 10.1016/S0967-0637(99)00052-7

Steinberg, D. K., and Landry, M. R. (2017). Zooplankton and the ocean carbon cycle. *Annu. Rev. Mar. Sci.* 9, 413–444. doi: 10.1146/annurev-marine-010814-015924

Steinberg, D. K., Van Mooy, B. A. S., Buesseler, K. O., Boyd, P. W., Kobari, T., and Karl, D. M. (2008). Bacterial vs. zooplankton control of sinking particle flux in the ocean's twilight zone. *Limnol. Oceanogr.* 53, 1327–1338. doi: 10.4319/lo.2008.53.4.1327

Straile, D. (1997). Gross growth efficiencies of protozoan and metazoan zooplankton and their dependence on food concentration, predator-prey weight ratio, and taxonomic group. *Limnol. Oceanogr.* 42, 1375–1385. doi: 10.4319/lo.1997.42.6.1375

Stukel, M. R., Décima, M., and Kelly, T. B. (2018a). A new approach for incorporating 15N isotopic data into linear inverse ecosystem models with markov chain monte carlo sampling. *PLoS ONE* 13:e0199123. doi: 10.1371/journal.pone.0199123

Stukel, M. R., Décima, M., Landry, M. R., and Selph, K. E. (2018b). Nitrogen and isotope flows through the costa rica dome upwelling ecosystem: the crucial mesozooplankton role in export flux. *Glob. Biogeochem. Cycles* 32, 1815–1832. doi: 10.1029/2018GB005968

Stukel, M. R., Kahru, M., Benitez-Nelson, C. R., Décima, M., Goericke, R., Landry, M. R., et al. (2015). Using lagrangian-based process studies to test satellite algorithms of vertical carbon flux in the eastern North Pacific Ocean. *J. Geophys. Res. Oceans* 120, 7208–7222. doi: 10.1002/2015JC011264

Stukel, M. R., Kelly, T. B., Aluwihare, L. I., Barbeau, K. A., Goericke, R., Krause, J. W., et al. (2019). The Carbon:^{234} Thorium ratios of sinking particles in the California current ecosystem 1: relationships with plankton ecosystem dynamics. *Mar. Chem.* 212, 1–15. doi: 10.1016/j.marchem.2019.01.003

Stukel, M. R., Landry, M. R., Ohman, M. D., Goericke, R., Samo, T., and Benitez-nelson, C. R. (2012). Do inverse ecosystem models accurately reconstruct plankton trophic flows? comparing two solution methods using fi eld data from the California current. *J. Mar. Syst.* 91, 20–33. doi: 10.1016/j.jmarsys.2011.09.004

Stukel, M. R., Ohman, M. D., Kelly, T. B., and Biard, T. (2019). The roles of filter-feeding and flux-feeding zooplankton as gatekeepers of particle flux into the mesopelagic ocean. *Front. Mar. Sci.* 6:397. doi: 10.3389/fmars.2019.00397

Stukel, M. R., Ohman, M. M. D., Benitez-Nelson, C. R. C., and Landry, M. M. R. (2013). Contributions of mesozooplankton to vertical carbon export in a coastal upwelling system. *Mar. Ecol. Prog. Ser.* 491, 47–65. doi: 10.3354/meps10453

Stukel, M. R., Song, H., Goericke, R., and Miller, A. J. (2018c). The role of subduction and gravitational sinking in particle export, carbon sequestration, and the remineralization length scale in the California Current Ecosystem. *Limnol. Oceanogr.* 63, 363–383. doi: 10.1002/lno.10636

Tanaka, T., and Rassoulzadegan, F. (2004). Vertical and seasonal variations of bacterial abundance and production in the mesopelagic layer of the NW Mediterranean Sea: bottom-up and top-down controls. *Deep Sea Res. Part Oceanogr. Res. Pap.* 51, 531–544. doi: 10.1016/j.dsr.2003.12.001

Taylor, A. G., Goericke, R., Landry, M. R., Selph, K. E., Wick, D. A., and Roadman, M. J. (2012). Sharp gradients in phytoplankton community structure across a frontal zone in the California Current ecosystem. *J. Plankton Res.* 34, 778–789. doi: 10.1093/plankt/fbs036

Teuber, L., Kiko, R., Séguin, F., and Auel, H. (2013). Respiration rates of tropical Atlantic copepods in relation to the oxygen minimum zone. *J. Exp. Mar. Biol. Ecol.* 448, 28–36. doi: 10.1016/j.jembe.2013.06.012

van den Meersche, K., Soetaert, K., van Oevelen, D., Meersche, K., Van den, Soetaert, K., and Van Oevelen, D. (2009). xsample(): an R function for sampling linear inverse problems. *J. Stat. Softw. Code Snippets* 30, 1–15. doi: 10.18637/jss.v030.c01

van Oevelen, D., Soetaert, K., and Heip, C. (2012). Carbon flows in the benthic food web of the porcupine abyssal plain: the (un)importance of labile detritus in supporting microbial and faunal carbon demands. *Limnol. Oceanogr.* 57, 645–664. doi: 10.4319/lo.2012.57.2.0645

van Oevelen, D., van den Meersche, K., Meysman, F. J. R., Soetaert, K., Middelburg, J. J., and Vézina, A. F. (2010). Quantifying food web flows using linear inverse models. *Ecosystems* 13, 32–45. doi: 10.1007/s10021-009-9297-6

Vézina, A., Platt, T., Vezina, A. F., and Platt, T. (1988). Food web dynamics in the ocean. I. Best-estimates of flow networks using inverse methods. *Mar. Ecol. Prog. Ser.* 42, 269–287. doi: 10.3354/meps042269

Wilson, S. E., Steinberg, D. K., and Buesseler, K. O. (2008). Changes in fecal pellet characteristics with depth as indicators of zooplankton repackaging of particles in the mesopelagic zone of the subtropical and subarctic North Pacific Ocean. *Deep Sea Res. Part II Top. Stud. Oceanogr.* 55, 1636–1647. doi: 10.1016/j.dsr2.2008.04.019

Wilson, S. E., Steinberg, D. K., Chu, F.-L. E., and Bishop, J. K. B. (2010). Feeding ecology of mesopelagic zooplankton of the subtropical and subarctic North Pacific Ocean determined with fatty acid biomarkers. *Deep Sea Res. Part Oceanogr. Res. Pap.* 57, 1278–1294. doi: 10.1016/j.dsr.2010.07.005

Yebra, L., Almeida, C., and Hernández-León, S. (2005). Vertical distribution of zooplankton and active flux across an anticyclonic eddy in the Canary Island waters. *Deep Sea Res. Part Oceanogr. Res. Pap.* 52, 69–83. doi: 10.1016/j.dsr.2004.08.010

Yokokawa, T., Yang, Y., Motegi, C., and Nagata, T. (2013). Large-scale geographical variation in prokaryotic abundance and production in meso- and bathypelagic zones of the central Pacific and Southern ocean. *Limnol. Oceanogr.* 58, 61–73. doi: 10.4319/lo.2013.58.1.0061

Conflict of Interest Statement: The authors declare that the research was conducted in the absence of any commercial or financial relationships that could be construed as a potential conflict of interest.

APPENDIX A

TABLE A1 | Measurement constraints used in the LIEM.

	Quantity	P07.1		P0704-2		P0704-4		P0810-1		P0810-2		P0810-3		P0810-4		P0810-5		P0810-6	
		μ	σ	μ	σ	μ	σ	μ	σ	μ	σ	μ	σ	μ	σ	μ	σ	μ	σ
1	C-14PP	1233	74	587	35	2314	139	554	33	484	29	893	54	674	40	1672	100	325	19
2	Delta PHY	−322	209	18	253	−80	602	538	1680	−1	50	−76	166	−399	4771	−325	173	−5	62
3	Microzooplankton Grazing	659	238	717	135	1282	225	472	301	243	51	357	74	277	41	498	48	138	43
4	SMZ Grazing	2249	1132	123	37	856	652	21	9	90	26	199	53	48*	21*	836*	688*	85*	37*
5	LMZ Grazing	93	87	42	18	123	55	18	12	14	9	66	26	21*	15*	51*	55*	19*	14*
6	vmSMZ Grazing	2092	907	137	44	669	499	50	30	110	34	249	113	72*	50*	753*	538*	101*	47*
7	vmLMZ Grazing	232	171	42	18	132	42	19	11	20	10	51	25	19*	14*	95*	101*	22*	16*
8	SMZ + LMZ Grazing	2342	1077	166	57	979	763	35	31	104	44	265	65	67*	38*	887*	668*	104*	61*
9	vmLMZ + vmSMZ Grazing	2306	1137	203	82	622	238	86	42	165	11	336	163	107*	70*	809*	650*	150*	41*
10	Sed Trap @ 100m	144	13	32	6	170	41	74	11	69	13	78	7	149	36	127	22	107	5
11	Thorium @ 100m	77	11	32	10	121	45	32	60	51	29	18	22	46	38	53	13	54	8
12	Fecal Pellet Flux @ 100m	135		4		54		4		8		5		35		14		4	
13	Minimum Subduction	39		47		25		11		33		13		26		10		31	
14	Maximum Subduction	79		55		45		33		47		15		51		19		59	
15	Epi Bacterial Prod (0–100 m)	66	27	22	12	53	30	240	137	80	17	148	21	351	60	400	37	101	8
16	Min dBAC BP	16		5		8		16		13		14		27		102		21	
17	Max dBAC BP	52		16		27		52		41		45		89		336		69	
18	Deep NM Resp (dMYC)	2.8	5.5	3.4	1.0	2.2	0.7	4.6	2.2	3.6	1.7	3.8	0.8	3.8	4.4	6.7	0.9	7.3	1.8
19	Deep NM Poop (dMYC)	1.2	2.4	1.5	0.5	1.0	0.3	2.1	1.0	1.6	0.7	1.7	0.4	1.7	1.9	3.0	0.4	3.3	0.8
20	Deep NM Mort (dMYC)	2.8	5.5	3.4	1.1	2.2	0.7	4.7	2.3	3.7	1.7	3.9	0.8	3.9	4.4	6.8	1.0	7.4	1.8
21	Epi VM Resp (vmMYC)	7.5	14.7	2.8	2.2	12.2	4.8	12.0	2.8	2.8	0.6	14.5	4.1	8.0	4.8	8.9	1.0	5.5	2.0
22	Deep VM Resp (vmMYC)	9.5	18.6	3.5	2.8	15.5	6.0	14.9	3.4	3.0	0.7	16.9	5.0	9.7	6.0	10.6	0.8	6.2	2.1
23	Deep VM Poop (vmMYC)	5.1	10.0	1.9	1.5	8.3	3.2	8.1	1.9	1.8	0.4	9.5	2.8	5.3	3.3	5.9	0.5	3.5	1.3
24	Deep VM Mort (vmMYC)	6.0	11.7	2.2	1.8	9.8	3.8	9.5	2.2	2.1	0.5	11.1	3.2	6.3	3.8	6.9	0.6	4.1	1.5

Values given show the mean (μ) and 1 SD (σ) for each cycle except for min/max constraints which are blank. Marked values (*) were assumed values calculated from cycles of the same classification (see section Mesozooplankton and Nekton Constraints). All values are given in mg C m^{-2} d^{-1}.

TABLE A2 | Mesozooplankton biomass and minimum respiration estimates used in the LIEM.

Quantity	P0704-1	P0704-2	P0704-4	P0810-1	P0810-2	P0810-3	P0810-4	P0810-5	P0810-6
Epipeleagic Min Resp (SAR)	8.0	8.6	8.0	0.0	0.0	0.0	0.0	8.9	0.0
SMZ Min Resp	24.4	5.1	20.6	4.8	26.3	18.0	36.3	31.6	27.3
vmSMZ Min Resp	5.3	0.4	5.5	16.4	3.3	8.6	0.0	21.5	0.0
dSMZ Min Resp	2.6	2.6	5.7	9.4	2.5	7.1	1.1	14.5	3.3
LMZ Min Resp	7.0	3.3	11.9	5.5	10.4	5.7	7.8	3.0	5.8
vmLMZ Min Resp	19.9	1.5	63.2	24.7	14.9	50.9	11.1	64.2	11.8
dLMZ Min Resp	3.2	5.4	6.7	20.4	7.6	13.3	4.9	31.3	13.5
GEL Min Resp	0.2	0.1	0.1	0.3	0.7	0.2	0.0	0.0	0.7
dGEL Min Respiration	0.4	0.1	0.5	0.4	1.1	0.3	0.1	0.4	0.8
SMZ Biomass	654	106	511	106	833	509	1249	1891	1346
vmSMZ Biomass	104	33	115	722	127	282	0	1120	0
dSMZ Biomass	499	280	715	968	307	834	111	1430	381
LMZ Biomass	424	173	478	971	586	1126	867	938	1763
vmLMZ Biomass	557	347	5175	993	1557	9859	1681	6122	1671
dLMZ Biomass	5928	2839	5702	7180	1818	3579	1395	7134	3942

Respiration is given in mg C m^{-2} d^{-1} and biomass in mg C m^{-2}.

frontiers in Marine Science

ORIGINAL RESEARCH
published: 05 December 2019
doi: 10.3389/fmars.2019.00751

Copepod Grazing Influences Diatom Aggregation and Particle Dynamics

*Jordan Toullec[1], Dorothée Vincent[2,3], Laura Frohn[1], Philippe Miner[4], Manon Le Goff[1], Jérémy Devesa[1] and Brivaëla Moriceau[1]**

[1] Univ Brest, CNRS, IRD, Ifremer, LEMAR, Plouzané, France, [2] UMR 8187 Laboratoire d'Océanologie et de Géosciences, CNRS, Université du Littoral-Côte d'Opale, Wimereux, France, [3] Agence Française pour la Biodiversité, Direction de l'Appui aux Politiques et aux Acteurs, Service Connaissance, Evaluation et Surveillance du Milieu Marin, Espace Giraudeau, Brest, France, [4] Ifremer, Univ Brest, CNRS, IRD, LEMAR, Plouzané, France

In marine ecosystems, carbon export is driven by particle flux which is modulated by aggregation, remineralization, and grazing processes. Zooplankton contribute to the sinking flux through the egestion of fast sinking fecal pellets but may also attenuate the flux by tearing apart phytoplankton aggregates into small pieces through swimming activity or direct ingestion. Freely suspended cells, artificial monospecific aggregates from two different diatom species (*Chaetoceros neogracile* and *Skeletonema marinoi*) and natural aggregates of *Melosira* sp. were independently incubated with five different copepod species (*Acartia clausi*, *Temora longicornis*, *Calanus helgolandicus*, *Euterpina acutifrons*, and *Calanus hyperboreus*). During the grazing experiments initiated with free diatoms, *E. acutifrons* feeding activity evidenced by ingestion rates of 157 ± 155 ng Chl a ind^{-1} d^{-1}, induced a significant increase of *S. marinoi* aggregation. Transparent exopolymeric particles (TEP) production was only slightly boosted by the presence of grazers and turbulences created by swimming may be the main trigger of the aggregation processes. All copepods studied were able to graze on aggregates and quantitative estimates led to chlorophyll a ingestion rates (expressed in Chla a equivalent, i.e., the sum of chlorophyll *a* and pheopigments in their guts) ranging from 4 to 23 ng Chl a_{eq} ind^{-1} d^{-1}. The relation between equivalent spherical diameters (ESDs) and sinking velocities of the aggregates did not significantly change after grazing, suggesting that copepod grazing did not affect aggregate density as also shown by Si:C and C:N ratios. Three main trends in particle dynamics could be identified and further linked to the copepod feeding behavior and the size ratio between prey and predators: (1) Fragmentation of *S. marinoi* aggregates by the cruise feeder *T. longicornis* and of *Melosira* sp. aggregates by *C. hyperboreus* at prey to predator size ratios larger than 15; (2) no change of particle dynamics in the presence of the detritic cruise feeder *E. acutifrons*; and finally (3) re-aggregation of *C. neogracile* and *S. marinoi* aggregates when the two filter feeders *A. clausi* and *C. helgolandicus* were grazing on aggregate at prey to predator size ratios lower than 10. Aggregation of freely suspended cells or small aggregates was facilitated by turbulence resulting from active swimming of small copepods. However, stronger turbulence created by larger cruise feeders copepods prevent aggregate formation and even made them vulnerable to breakage.

Keywords: diatom aggregate, grazing experiment, copepod, sinking velocity, particle dynamics

OPEN ACCESS

Edited by:
Morten Hvitfeldt Iversen, Alfred Wegener Institute, Helmholtz Centre for Polar and Marine Research (AWI), Germany

Reviewed by:
Jun Sun, Tianjin University of Science and Technology, China
Xiaodong Wang, Jinan University, China

***Correspondence:**
Brivaëla Moriceau
Brivaela.Moriceau@univ-brest.fr

Specialty section:
This article was submitted to Marine Biogeochemistry, a section of the journal Frontiers in Marine Science

Received: *06 May 2019*
Accepted: *19 November 2019*
Published: *05 December 2019*

Citation:
Toullec J, Vincent D, Frohn L, Miner P, Le Goff M, Devesa J and Moriceau B (2019) Copepod Grazing Influences Diatom Aggregation and Particle Dynamics. Front. Mar. Sci. 6:751. doi: 10.3389/fmars.2019.00751

INTRODUCTION

In marine ecosystems, diatoms play a key role in the biological carbon pump (Jin et al., 2006; Tréguer et al., 2017). Diatom contribution to the export is mainly driven by particle dynamics such as aggregate formation, by coagulation of freely suspended phytoplankton cells or small detritus into a sticky matrix made of transparent exopolymeric particles (TEPs). Considering the balance between sinking and remineralization, only large and fast sinking particles formed in the mixed layer can reach the sequestration depth (Moriceau et al., 2007), i.e., 1000 m depth considering that an efficient carbon entrapment is longer than a thousand year (Passow and Carlson, 2012). This mechanistic view is confirmed by *in situ* profiles of particle fluxes (Guidi et al., 2007). Yet, viable freely suspended cells were collected at depth down to 4000 m (Agustí et al., 2015). Due to their slow sinking rates (1–5 m d^{-1}, Bienfang, 1981) isolated living cells cannot reach water layer as deep. Living cells may require transportation to depth *via* aggregates and then dispersed after disaggregation of the fast sinking particle by unknown processes. Strong decrease of the particle size with depth confirm the attenuation of particle fluxes under the mixed layer depth (Guidi et al., 2007). From *in situ* observations in the NW Mediterranean Sea, Stemmann et al. (2004) proposed different processes possibly explaining fragmentation of sinking particles, namely microbial activity and zooplankton feeding. Zooplankton grazers can strongly modulate the particle fluxes in the water column. Organisms such as salps, appendicularians, and copepods are acknowledged to be important contributors to carbon export *via* the production of fast sinking fecal pellets resulting from grazing (Stemmann et al., 2002; Turner, 2002, 2015; Boyd and Trull, 2007; Stamieszkin et al., 2015; Lalande et al., 2016). Overall, the contribution of fecal pellets to the total particle carbon flux varies from 1 to 100%, most values being <40% (Turner, 2015). In addition, during vertical migrations, zooplankton egest fecal pellets deeper than the mixed layer (Wilson et al., 2008; Brierley, 2014) resulting in an active transport of fresh organic matter at depth (Gorgues et al., 2019) as observed in the Scotia Sea and the Southern Ocean (Cavan et al., 2015, 2017; Bode et al., 2018). As a consequence, a significant proportion of the particle flux may escape remineralization processes in the upper pelagic zone (Cavan et al., 2015). Additional metabolic processes such as respiration and excretion occurring deeper during zooplankton migration also contribute to transport dissolved carbon to the deep sea (Turner, 2015; Steinberg and Landry, 2017; Hernández-León et al., 2019). Direct relation between increasing carbon export and copepod abundance was evidenced *in situ* in Kongsfjorden (Norway, Lalande et al., 2016) when diatoms dominate the community as well as during a mesocosm study conducted in the Bay of Hopavagen (Norway, Moriceau et al., 2018). However, in the latter case, this increase in carbon export was only visible when cyanobacteria (and not diatoms) dominated the phytoplankton community. Other zooplankton organisms, such as appendicularians, are major contributors to vertical particle carbon flux (Alldredge et al., 2005), *via* the production of cellulosic houses embedded with detritus or other plankton organisms (Gorsky et al., 1999; Vargas et al., 2002; Lombard and Kiørboe, 2010; Lombard et al., 2013a).

Moreover, zooplankton may also attenuate vertical particle fluxes through different activities. Swimming of large Euphausiids was demonstrated to fragment marine aggregates into small particles that sink more slowly, become accessible to small grazers and microbial organisms, thus enhancing remineralization and carbon cycling (Dilling and Alldredge, 2000; Goldthwait et al., 2004, 2005). Sinking organic materials such as marine snow aggregates and fecal pellets could also constitute alternative food sources for mesozooplankton (Dagg, 1993; Lampitt et al., 1993; Steinberg, 1995; Dilling et al., 1998; Kiørboe, 2000; Dilling and Brzezinski, 2004; Koski et al., 2017). Ostracods, cladocerans, ascidian larvae, and copepods are aggregate colonizers, and can feed either on prokaryotic community located inside or at the surface of the aggregates, or directly on the aggregate matrix (Green and Dagg, 1997; Shanks and Walters, 1997). From 20 to 70% of the aggregate carbon biomass may be degraded by these colonizers during their sinking under the euphotic zone (Kiørboe, 2000). In a recent study investigating copepod grazing behavior on aggregated particles, Koski et al. (2017) demonstrated that both harpacticoida and poecilostomatoida copepods were able to feed on aggregates and could thus attenuate the particle carbon flux. Aggregation processes and dynamics are increasingly understood *via* the combination of laboratory experiments and models (Beauvais et al., 2006; Passow and De La Rocha, 2006; Gärdes et al., 2011; Jackson, 2015; Prairie et al., 2019), mesocosm experiments (Alldredge et al., 1995; Passow and Alldredge, 1995b; Svensen et al., 2001, 2002; Moriceau et al., 2018; Cisternas-Novoa et al., 2019), and *in situ* observations (Lampitt et al., 2010; Laurenceau-Cornec et al., 2015; Nowald et al., 2015; Giering et al., 2017; Cavan et al., 2018; Bach et al., 2019). In the meantime, studies focusing on disaggregation processes due to remineralization or zooplankton activity (Goldthwait et al., 2004; Taucher et al., 2018) remain limited despite their importance in providing new insights to better understand particle export in the mesopelagic zone. As dominant components of zooplankton communities, copepods may be considered as "gatekeepers of the biological carbon pump" if they limit carbon export by breaking aggregates as previously suggested in laboratory (Goldthwait et al., 2004), mesocosm experiments (Moriceau et al., 2018; Taucher et al., 2018), and *in situ* studies (Dilling and Alldredge, 2000). They may also enhance carbon export by (1) egesting large sinking fecal pellets (Turner, 2015; Lalande et al., 2016; Steinberg and Landry, 2017), (2) boosting the aggregation, as seen for cyanobacteria, appendicularians, and doliolids (Moriceau et al., 2018; Taucher et al., 2018), and (3) increasing the particle sinking rates when increasing the silicon content of diatoms (Pondaven et al., 2007). Swimming activity being intrinsically linked to feeding, copepod flexible diet may also modulate particle fluxes through differential grazing between free diatoms and aggregated diatoms (Bochdansky and Herndl, 1992; Bochdansky et al., 1995) or by changing the composition of the phytoplankton community (Bach et al., 2019). Their distinct functional feeding traits as filter feeders or ambush feeders

(Kiørboe, 2011; Lombard et al., 2013b; Koski et al., 2017) make them organisms of particular interest to study particle dynamics. Recognizing that only very few studies have dealt with the interactions between large particles and grazers under laboratory conditions, we propose here to study the effects of both copepod grazing and swimming activities on diatom aggregate dynamics (i.e., changes in size, sinking velocity, and elemental composition) using rolling tank experiments (Shanks and Edmondson, 1989).

MATERIALS AND METHODS

Experimental Set-Up

Two types of incubation experiments were carried out to estimate the effect of copepod grazing on particle dynamics. The first set of experiments tested whether copepod activities influence coagulation rate of free diatoms and/or the size, sinking velocity, and composition of the resulting aggregates (Experiments 1–3). The second set of experiments monitored the changes in diatom aggregate abundance, size, sinking velocity, and composition under grazing pressure (Experiments 4–8; **Figure 1**). Aggregates studied here were visible to the naked eyes starting in length from 1 mm.

Phytoplankton Cultures

For laboratory experiments (Experiments 1–7), *Skeletonema marinoi* (strain CCAP 1077/5) and *Chaetoceros neogracile* (strain CCAP 1010/3) were obtained from Ifremer collection (Laboratory of Functional Physiology of Marine Organism, Ifremer Brittany's Centre, France). They were continuously grown in Conway medium (Conway et al., 1976) prepared with autoclaved 1 μm filtered seawater from the Bay of Brest (Brittany, France). Cells were maintained in exponential growth phase in 2 L glass round bottom balloons at 20°C under continuous irradiance (100 μmoles photons m^{-2} s^{-1}). Balloons were kept in constant aeration and CO_2 was supplied to keep the pH between 7.5 and 7.9. These cultures were directly used for experiments using free diatom cells as prey type (Experiments 1–3, **Table 1**). Subsamples of the cultures were used for chemical analyses at T_{init} (see below).

Aggregate Preparation From Diatom Cultures and *in situ* Aggregate Collection

In order to perform Experiments 4–8, monospecific aggregates were produced in the laboratory. Once diatom cultures reached the stationary phase, i.e., stable cell concentrations of 10^6–10^7 for *S. marinoi* and 10^8 cell mL^{-1} for *C. neogracile*, 2 L were diluted into 10 L cylindrical rolling tanks containing 1 μm filtered UV sterilized seawater (FSW hereafter, **Figure 1**). Cultures were then maintained at 18°C under a 12:12 h photoperiod cycle, for 2–10 days, and rotated at 3 rpm on a rolling table to promote cell collision and aggregation (Shanks and Edmondson, 1989). As soon as aggregates were formed inside the 10 L rolling tank, 10–20 aggregates were carefully transferred inside a set of 1 L rolling tanks containing FSW using a large aperture plastic pipette (10 mL). Similar sampling was done to measure the initial chemical conditions (T_{init}) of the aggregates (see below).

For the *in situ* experiment (Experiment 8), large floating mono-specific aggregates of *Melosira* sp. were sampled from the surface from a zodiac boat on the 3rd of July 2016 during the GreenEdge expedition on-board the NGCC Amundsen. The aggregates were sampled at station 600 (70°30.653 N, 63°59.258 W) using a 0.1 mm mesh sieve (**Figure 1**). *Melosira* sp. aggregates were diluted into 200 mL of 0.7 μm FSW sampled with a Niskin bottle at 50 m depth (salinity 32.7, T^0 −1.5°C). The mixture was homogenized and divided into four aliquots. The first aliquot was kept for biogeochemical analyses [particulate organic carbon (POC)/nitrogen (PON) and $bSiO_2$ content] and for taxonomic analysis of phytoplankton. The three other aliquots were distributed into three rolling tanks (4 L) containing *in situ* 0.7 μm FSW. Rolling tanks were stored in the dark in a cold room (4°C) and rotated on a rolling table at 3.3 rpm. This incubation ended up in the formation of a large aggregate (26.8–34 mm, **Figure 1**).

Copepod Sampling and Rearing Phase

Four copepod species (*Euterpina acutifrons*, *Temora longicornis*, *Acartia clausi*, and *Calanus helgolandicus*) were selected for the laboratory experiments on diatom free cells and aggregates (**Tables 1**, **2**). They were chosen for their easiness of cultivation, as their presence generally matches phytoplankton spring blooms in the area (Schultes et al., 2013), and because they display different functional traits (Benedetti et al., 2015) regarding feeding strategies and sizes. *A. clausi* (0.9 mm total length) and *C. helgolandicus* (2.7 mm total length) are both omnivorous filter feeders with a clear tendency to herbivory, the latter being able to migrate vertically (Andersen et al., 2001, 2004). *T. longicornis* (0.8 mm total length) and *E. acutifrons* (0.5 mm total length) are described as cruise feeders (Lombard et al., 2013b), *E. acutifrons* having the tendency to feed on detrital matter (Benedetti et al., 2015). Copepods used in the experiments were collected at the Lanveoc sampling site (48°18.00 N, 4°27.360 W) during cruises on-board the oceanographic ship "Albert Lucas" (INSU-CNRS-UBO) from January to April in years 2017 and 2018. Zooplankton were collected with a WP2 plankton net (200 μm mesh size) fitted with a 2 L filtering cod-end during horizontal net tows (speed < 1 m s^{-1} for <10 min) at 3 m depth. After each plankton haul, zooplankton samples were immediately diluted in 30 L of surface seawater, stored in the dark in a cool box, and brought back within few hours to the laboratory. To initiate the rearing phase, a ratio of 1 male per 5 females was assured with at least 100 (for *E. acutifrons*) to 250 (for calanoid copepods) adult females of each species individually sorted under a dissecting microscope. The copepods were placed in polycarbonate beakers of varying volume (from 7 to 20 L according to species size) containing 1 μm FSW. During at least 1 week of acclimation inside the culture room, copepods were kept at 18°C, at 33 salinity, and under 12:12 h day:night photoperiod for about up to 1 month. They were daily fed in excess with a mixture of algae continuously cultured (*Rhodomonas salina*, *Thalassiosira weissflogii*, *Tisochrysis lutea*, and *Tetraselmis suecica*, grown under the same condition as for *S. marinoi* and *C. neogracile*) at concentration exceeding

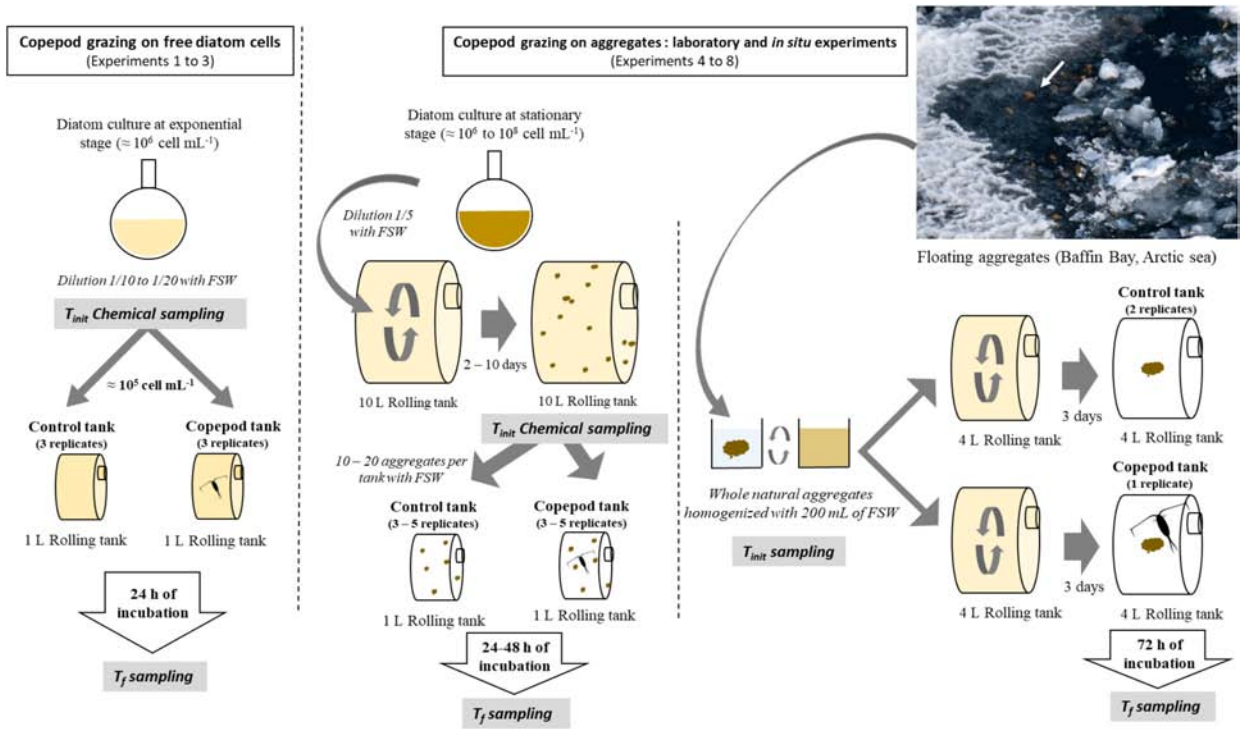

FIGURE 1 | Experimental design. **(Left)** Copepod grazing experiments on free diatom cells (Experiments 1–3). **(Right)** Copepod grazing experiments on diatom aggregates (Experiments 4–8). Photo on the **right** corresponds to *in situ* floating *Melosira* sp. aggregates between the ice packs, taken from the deck of the NGCC Amundsen at about 15 m distance.

10^3–10^4 cell mL^{-1} (Berggreen et al., 1988; Vincent et al., 2007), thus avoiding predation of calanoid copepods on younger stages (Bonnet et al., 2004; Boersma et al., 2014). Seawater was renewed every other day by adding 10–20% volume of 1 μm FSW and air was supplied *via* small bubbles in each rearing tank. Twenty-four hours prior to the beginning of the experiment, 30 (*C. helgolandicus*) to 100 (*E. acutifrons*) cultured copepods were isolated in 1 L beakers containing 0.2 μm FSW without food. This starving phase allowed gut evacuation and maximized feeding during incubation.

Wild *Calanus hyperboreus* (6.3 mm total length) were collected during the GreenEdge expedition on-board the NGCC Amundsen in July 2016. *C. hyperboreus* displays an omnivorous suspensive feeding behavior (Conover, 1966; Huntley, 1981; Greene, 1988; Darnis et al., 2008, 2012). Collection of zooplankton organisms *via* plankton nets resulted in retrieving high amounts of dead or injured individuals. The exact cause of this mortality could not be inferred and to undertake the grazing experiment, copepods were collected from 24 Niskin bottles (10 L) deployed over the 0–300 m depth at station 615 (70°29.926 N, 59°31.504 W). 240 L of seawater from the Niskin bottles was sieved over a 200 μm mesh sieve partially immersed in seawater to avoid individual stress. Only copepods of the *C. hyperboreus* species were collected. Immediately after sieving, copepods were isolated *via* pipetting in 1 L of 0.7 μm FSW and left for 24 h in the dark to limit stress and allow gut evacuation. On the day of the experiment, only the most active specimens ($N = 18$) were collected using a sieve and added to the 4 L rolling tank containing the large *Melosira* sp. aggregate (Experiment 8).

Grazing Experiments

A set of eight laboratory experiments were carried out and allowed to integrate variable predator to prey size ratios, the latter ranging in size and type from small isolated diatom cell [6–10 μm equivalent spherical diameter (ESD)] up to few centimeters aggregates (**Tables 1**, **2**). For three out of the eight experiments carried out at laboratory (**Table 1**, Experiments 1–3), isolated diatom cells at exponential growth state were provided as food source at concentration higher than bloom density in the area (2.3–5.3 × 10^5 cell mL^{-1}), i.e., maximum cell concentrations of 10^4 cell mL^{-1} are generally recorded during bloom for *Chaetoceros* sp. and *Skeletonema* sp. (Soudant and Belin, 2018). This high diatom cell concentration was set on purpose to induce diatom collision and provided high likelihood to form aggregates during the course of the incubation. Aggregation of *S. marinoi* was indeed shown to take >40 h at cell density <10^5 cell mL^{-1} (Grossart et al., 2006). This high cell concentration was also chosen considering that even though copepod grazing could induce a large decrease in cell density (e.g., up to 50% of the initial stocks over the incubation at food density matching bloom), cell concentration would still remain close enough in controls compare to copepod tanks. The only differences in parameters promoting aggregation between the two tanks being related to copepod presence (i.e., swimming and grazing and possible

TABLE 1 | Initial conditions in incubations using freely suspended diatoms as prey (Experiments 1–3).

Experiment	Diatom species	Copepod species	Number of replicates	Copepod abundance (ind L^{-1})	Cell concentration (10^5 cell mL^{-1})	POC (µmol C L^{-1})	PON (µmol N L^{-1})	$bSiO_2$ (µmol Si L^{-1})	TEP (mg X_{eq} L^{-1})	C:N (mol:mol)	Si:C (mol:mol)
1	*S. marinoi*	*E. acutifrons*	3	28.2 ± 0.0	5.3 ± 0.8	710 ± 124	45 ± 1	81 ± 2	5.2 ± 0.6	16 ± 3	0.11 ± 0.02
		C.helgolandicus	3	10.9 ± 0.6							
2	*S. marinoi*	*E. acutifrons*	3	33.9 ± 1.8	2.4 ± 0.2	414 ± 87	35 ± 0	74 ± 0	4.4 ± 1.7	12 ± 2	0.18 ± 0.04
3	*C. neogracile*	*E. acutifrons*	3	35.3 ± 0.0	2.3 ± 0.2	253 ± 11	30 ± 1	70 ± 1	3.5 ± 0.1	9 ± 0	0.28 ± 0.02
		A. clausi	3	14.9 ± 2.3							

Results are means ± SE.

change in mucus production, Malej and Harris, 1993). In the remaining four experiments (**Table 2**, Experiments 4–7), diatom aggregates were used as exclusive prey type. The incubation was initiated using 10–20 aggregates per roller tank (Guidi et al., 2008). Since the initial aggregate abundance varied during the first hours of the experiment as aggregation/disaggregation processes occurred before reaching an "equilibrium," the latter was chosen as the time set for estimating copepod effects (T_0). "Copepod tanks" received a known number of reared copepods as detailed in **Tables 1**, **2**. In order to obtain a significant grazing signal, copepod abundance in rolling tanks was set high, i.e., being 2–4 times higher for calanoids and 10 times higher for *E. acutifrons* than those commonly measured *in situ* during the decline of phytoplankton blooms in the North Atlantic Ocean (typically 4 ind L^{-1} for calanoid copepods such as *T. longicornis*, *A. clausi*, and *C. helgolandicus* and 0.2 ind L^{-1} for harpacticoida (Schultes et al., 2013). However such high copepod abundances are totally congruent with those recorded over a 3-year survey in the eutrophic system of Long Island (Capriulo et al., 2002) with 30–50 ind L^{-1} for *T. longicornis* and >35 ind L^{-1} for *Acartia hudsonica*. These chosen abundance remained also highly comparable to values used in most experimental studies ranging from 8 to >15 ind L^{-1} (Sautour and Castel, 1993; Vincent and Hartmann, 2001; Sarthou et al., 2008). For all experiments, dead and injured individuals were discarded and living ones were individually pipetted to 1 L rolling tanks containing prey assemblages. Rolling tanks were then filled to the rim with FSW, avoiding air bubbles introduction and placed on the rolling table at 3 rpm. Tank rotation allowed prey homogenization and mimicked continuous settling of aggregates in the water column. Incubation was carried out at 18°C under natural photoperiod regime. Preliminary experiments permitted to set optimal incubation duration between 24 and 48 h (T_f end of incubation) so as to measure adequate growth and grazing rates and limit bottle effects (Roman and Rublee, 1980).

During Experiment 8, the large *Melosira* sp. aggregate (26–34 mm) was incubated with wild copepods (*C. hyperboreus*) by adding 18 living individuals to a 4-L roller tank. The grazing experiment was undertaken at 4°C. *Melosira* sp. aggregates were shown to have strong negative buoyancy under light regime due to bubble formation induced by photosynthesis (Fernández-Méndez et al., 2014). Therefore, to keep aggregates suspended in the rolling tank during the experiment, the incubation with *C. hyperboreus* was undertaken in the dark and during 72 h to follow the temporal dynamic of the fragmentation and potential changes in copepod behavior.

Aggregates Enumeration, Size, and Sinking Velocity

Aggregate morphological characteristics were measured at T_0 and T_f in rolling tanks before aggregate sampling. Image analyses were based on pictures and videos taken using a digital camera (Canon EOS 600D). Video recordings allowed to avoid aggregate manipulation and bias due to sampling. Aggregates were enumerated in each tank using image of the whole tank. Diameter (d, mm) and height (h, mm) of each aggregate (with $d > h$) were

TABLE 2 | Initial conditions in incubations using aggregates as prey (Experiments 4–8).

Experiment	Diatom species	Copepod species	Number of replicates	Copepod abundance (ind L^{-1})	POC (µmol C L^{-1})	PON (µmol N L^{-1})	$bSiO_2$ (µmol Si L^{-1})	C:N (mol:mol)	Si:C (mol:mol)
4	*C. neogracile*	Control	4	–	64 ± 2	8.5 ± 0.2	2.6 ± 0.1	7.6 ± 0.2	0.04 ± 0.00
		E. acutifrons	4	34.3 ± 1.5					
5	*C. neogracile*	Control	4	–	na	na	na	na	na
		A. Clausi	4	16.6 ± 1.0					
6	*S. marinoi*	Control	4	–	128 ± 7	18 ± 1	13 ± 1	7 ± 0	0.10 ± 0.01
		T. longicornis	5	12.4 ± 2.0					
7	*S. marinoi*	Control	3	–	32 ± 2	2.8 ± 0.1	1.7 ± 0.1	11.5 ± 0.4	0.05 ± 0.01
		E. acutifrons	3	33.9 ± 1.8					
		C. helgolandicus	3	11.3 ± 0.6					
8	*Melosira* sp.	Control	2	–	33 ± 0	2.0 ± 0.1	2.8 ± 0.4	16.5 ± 0.6	0.08 ± 0.01
		C. hyperboreus	1	4.5					

Results are means ± SE; na stands for data not available.

derived from the pictures and estimated using an image system analysis software (Inkscape®) calibrated with the rolling tank characteristics (e.g., front diameter, back diameter, and width), measurement precision was 0.3 mm. A minimum of six images was used for each tank, all aggregates were individually measured on each picture unless aggregate concentration was >20 agg L^{-1}. In this case a minimum of 20 aggregates were analyzed in each picture (aggregate volume and ESD computations are presented in **Table 3**).

Aggregate sinking velocities (U_{agg}, m d^{-1}) were measured directly in the tank, using the method of Ploug et al. (2010). Sinking velocities of all aggregates were directly measured in the rolling tanks having aggregate concentrations <20 agg L^{-1}. In the tank where aggregate concentrations were higher, a minimum of 20 sinking velocities were independently measured. At steady state, aggregates follow a circular trajectory. For each aggregate, the rotation center of the aggregate was located using small video recordings and the software Inkscape®. Sinking velocities were deduced from the rotation of the tank and from the distance between the rotation center of the aggregate and the center of the tank, using Eq. 1.

$$U_{agg} = \frac{X_a}{T} \times 2\pi \quad (1)$$

where T is the tank rotation period (in d), and X_a the distance between the rotation center of the aggregate and the center of the tank (in m). As such, the error linked to sinking velocity computations is directly related to the minimum X_a measurable (0.3 mm) using image analysis, and the associated uncertainty is 0.7 m d^{-1}. Diatom aggregates are fractal particles, their sinking velocities increase with size according to a power law curve defined in Eq. 2 (Alldredge and Gotschalk, 1988; Iversen et al., 2010). The relation between sinking velocity (U_{agg}) and aggregate size (ESD) was computed for *S. marinoi* and *C. neogracile* aggregates, using a non-linear relation function nls() function; R software® (R Core Team, 2017).

$$U_{agg} = A(\mathrm{ESD})^B \quad (2)$$

where A and B are the unidimensional parameters of the regression.

Final Sampling (T_f)

Aggregates were carefully removed from the rolling tank using a large aperture plastic pipette (10 mL) and isolated inside 50 mL falcon tubes containing FSW (one to four tubes were used depending on the amount of material). After being homogenized by vigorous shaking, subsamples were taken for chemical analyses. Once aggregates were removed, copepods were carefully retrieved from each rolling tank by sieving seawater through an immersed 200 µm mesh sieve. For Experiments 1–3 and 8, copepods were sorted and preserved in formalin solution (4% final concentration) for stage analyses and size estimations (length and width of the prosome and urosome). For Experiments 4–7, copepods were placed in 2 mL cryotubes (one per tank), flash frozen in liquid nitrogen in order to estimate aggregate ingestion *via* the gut content fluorescence method of Mackas and Bohrer (1976). Size measurements were made concurrently from 75 *A. clausi*, 79 *C. helgolandicus*, 100 *T. longicornis*, and 173 *E. acutifrons*, randomly sieved from the copepod culture over a 200 µm mesh sieve and preserved in formalin. Copepod size measurements were performed under a dissecting microscope and measurement precision was 10 µm.

Calanus helgolandicus fecal pellets from Experiments 1 (free cells) and 7 (aggregate) were recovered after the 24 h incubation by filtering the remaining seawater of each rolling tank onto a 40 µm mesh sieve. Fecal pellets retained on the mesh sieve were resuspended in FSW in a plankton counting chamber (Dolfuss cuvette, 6 mL volume), pipetted, and pooled into a 50 mL falcon tubes for size measurements and counting (see below).

Chemical Analyses

Biogenic Silica ($bSiO_2$)

Ten milliliters of the free cells or aggregate suspension were filtered through 0.4 µm polycarbonate filters (Millipore). For fecal pellet measurements, 100–200 fecal pellets of

TABLE 3 | Equations used to calculate volume (μm^3 and mm^3) and equivalent spherical diameter (ESD; μm and mm) for aggregates, fecal pellets, and copepods.

Description	Shape	Equation	Parameters	References
Aggregate volume (V_{agg}, μm^3)	Prolate spheroid shape	$V_{agg} = \frac{\pi}{6} \times d^2 \times h$	d = Aggregate diameter (μm) h = Aggregate height (μm)	Hillebrand et al., 1999
Fecal pellet volume (V_{PF}, μm^3)	Cylinder with two half spheres	$V_{PF} = \pi \times d^2 \times \left(\frac{L}{4} + \frac{d}{6}\right)$	L = Fecal pellet length (μm) d = Fecal pellet diameter (μm)	Hillebrand et al., 1999
Aggregate and fecal pellet equivalent spherical diameter (ESD, μm)		$ESD = \sqrt[3]{\frac{6 \times V}{\pi}}$		Hillebrand et al., 1999
T. longicornis volume (V_{cop}, μm^3)	Prolate spheroid shape (total volume)	$V_{cop} = \frac{4}{3} \times \pi\eta^2 \times \left(\frac{a}{2}^3\right)$	a = Prosome length (μm) η = Aspect ratio derived	Conway, 2006; Jiang and Kiørboe, 2011b
A. clausi, *C. helgolandicus*, and *C. hyperboreus* volume (V_{cop}, μm^3)	Ellipsoid shape (Prosome)	$V_p = \frac{\pi}{6} \times a \times b \times c$	a = Prosome length (μm) b = Prosome width (μm) c = Prosome height (μm)	Hillebrand et al., 1999
	Cylindrical shape (Urosome)	$V_u = r^2 \times \pi \times l$	l = Urosome length (μm) r = Urosome diameter (μm)	Hillebrand et al., 1999
		$V_{cop} = V_p + V_u$		
E. acutifrons volume (V_{cop}, μm^3)	Body shape-dependent conversion factors C	$V_{cop} = L \times W^2 \times C$	L = Total body length (μm) W = Total body width (μm) C = 485 for fusiform harpacticoid copepods	Warwick and Gee, 1984; Veit-Köhler, 2005
Copepod equivalent spherical diameter (ESD, μm)		$ESD_{cop} = \left(\frac{V_{cop}}{0.523}\right)^{1/3}$		Hansen et al., 1994

C. helgolandicus were directly placed on the filter. All filters were individually placed in petri dishes and dried at 55°C for 24 h. They were then kept at room temperature until $bSiO_2$ analysis following Moriceau et al. (2007). Briefly, filters were digested in 8 mL of sodium hydroxide (NaOH 0.2 M) during 4 h at 90°C under constant agitation. Digestion was stopped by cooling the solution to 4°C and neutralized with 2 mL of chloride acid (HCl 1 M). Digestates containing the dissolved silica (dSi) were analyzed using an AutoAnalyzer (Bran and Luebbe Technicon Autoanalyzer 0.1% precision).

Particulate Organic Carbon and Nitrogen

Ten milliliters of the free cell or aggregate suspensions were filtered through pre-combusted (4 h 450°C) glass fiber filters (Whatman GF/F). For fecal pellets measurements, 100–200 fecal pellets of *C. helgolandicus* were directly placed on the filter. All filters were then rinsed with 10 mL of FSW. The filters were placed inside aluminum foil, dried at 55°C for 24 h, and analyzed for elemental C and N using a Carlo Erba NA-1500 elemental analyzer (Aminot and Kérouel, 2004).

Transparent Exopolymeric Particles

Transparent exopolymeric particles were measured following the method of Passow and Alldredge (1995a) for Experiments 1–3. Sub-samples of 10 mL were pipetted from the cell suspension, and filtered onto 0.4 μm polycarbonate filters (Whatman) under low vacuum pressure (<60 mm Hg) in order to prevent TEP forcing through the filter pores. Filters were stained with 0.5 mL of Alcian blue solution for 2 s (0.02% in aqueous solution, 0.06% acetic acid, pH 2.5, filtered through 0.2 μm before use) and kept frozen (−20°C) until analysis. Filters were then soaked for 2 h in 6 mL of 80% H_2SO_4 solution under constant agitation. The absorption of the obtained solution was measured at 787 nm (spectrophotometer prim'Light SECOMAM) in a 1 cm cuvette and was converted into mg of Gum Xanthan equivalent per liter (mg X_{eq} L^{-1}) using a calibration curve valid for our working solution of Alcian blue and made onto 0.2 μm polycarbonate filters. TEP concentrations were expressed in g X_{eq} L^{-1} and ng X_{eq} $cell^{-1}$, the latter taking into account the growth of the cells during the incubation. TEP production (ng X_{eq} $cell^{-1}$ d^{-1}) was calculated from the difference between TEP concentrations over the course of the incubation normalized by cell concentration at T_{init} and T_f.

Copepod ESD Computation

Copepod ESD was computed for each species from copepod volumes using shapes and equations from the literature (**Table 3**).

Specific Growth Rate and Grazing Parameters

Phytoplankton growth rates (k, d^{-1}), copepod grazing rates (g, d^{-1}), clearance rates (F, mL ind^{-1} d^{-1}), and ingestion rates were calculated from cell counts in Experiments 1–3 according to Frost (1972). At the beginning (T_{init}) and the end of incubation (T_f), 5 mL sub-samples of seawater from each tank were pipetted and preserved in acid Lugol solution (2% final concentration). Phytoplankton cell concentration was estimated using a Malassez cell counting chamber. Depending on cell density in the roller tanks, 3–12 sub-samples were counted corresponding to the enumeration of 120–300 cells per sample. When cell concentrations at T_f

were not significantly different between controls and copepod tanks, grazing was considered under the detection limit (i.e., <dl in **Table 4**). Ingestion rates were converted to ng Chl a ind^{-1} d^{-1} using a literature-based mean value of 0.10 pg Chl a $cell^{-1}$ for *S. marinoi* (Norici et al., 2011; Chandrasekaran et al., 2014; Orefice et al., 2016; Smerilli et al., 2019) and 0.35 pg Chl a $cell^{-1}$ for *C. neogracile* (unpublished data from González-Fernández et al., 2019).

Copepod Gut Content

For gut content analyses (Experiments 4–7), copepods were individually sorted from freshly thawed samples under a cool light stereomicroscope. Individuals were rinsed with 0.2 µm FSW to eliminate phytoplankton cells and aggregates stuck to feeding appendages, and were then transferred into 4 mL acetone (90%). Individuals (N = 6–27 copepods per replicate) were grinded and chlorophyllian pigments (Chlorophyll a and pheopigments) were extracted in the dark at 4°C overnight. Fluorescence of the extract was measured before and after acidification with 10% HCl (Parsons et al., 1984) using a Fluorometer (Turner design). Copepod gut content (G_{cop}, ng Chl a_{eq} ind^{-1}) was obtained by addition of Chlorophyll *a* and pheopigments concentrations and values were not corrected for pigment degradation on the recommendation of Durbin and Campbell (2007). Ingestion rates (ng Chl a_{eq} ind^{-1} h^{-1}) were derived from gut content (G_{cop}) using Eq. 3:

$$I = 60 \times G_{cop} \times k \quad (3)$$

where k is the gut evacuation rate (min^{-1}), computed following the model of Dam and Peterson (1988) which accounts for the temperature of incubation.

Fecal Pellet Production, Size, and Sinking Velocities

Fecal pellets production (FP ind^{-1} d^{-1}) was estimated in experiments with *C. helgolandicus* (Experiments 1–7). Up to six sub-samples of the total fecal pellet suspension were counted. Each fecal pellet was measured (length and width in µm) with 10 µm precision (see **Table 3** for shape and volume computations).

Fecal pellet sinking velocities (U_{FP}, m d^{-1}) follow Stokes' law and were computed following Eq. 4 (Komar et al., 1981).

$$U_{\mathrm{FP}} = 0.0790 \times \frac{1}{\mu} \times (\rho_{\mathrm{SW}} - \rho_{\mathrm{PF}}) \times g \times L^2 \left(\frac{L}{d}\right)^{-1.604} \quad (4)$$

where µ is the kinetic viscosity of seawater (0.0123 g cm^{-1} s^{-1}), ρ_{SW} and ρ_{PF} are the density of seawater (1.071 g cm^{-3} at 18°C) and of *C. helgolandicus* fecal pellets (1.26 g cm^{-3}; Cole et al., 2016), respectively, L and d the fecal pellet length (cm) and width (cm), respectively, and g is the acceleration due to gravity (981 cm s^{-2}).

Statistical Analyses

Results are expressed in mean ± standard error (SE), or ±cumulative error when manipulations or analysis involved error propagation (e.g., aggregates abundances, TEP production, Si:C ratios, and C:N ratios). Statistics were performed using Sigmaplot® 14.0 software. As data distribution matched the parametric assumption of normality (using Shapiro–Wilk test, $p < 0.05$), the effects of copepod grazing on the mean size, aggregate abundance, and stoichiometric ratios during the incubation were tested by one-way ANOVA. Tukey's *post hoc* tests were used to determine specific copepod influence on measured parameters. Covariance between ESD and sinking velocity was analyzed on logarithmic transformed data using an ANCOVA. Linear correlation between two variables was analyzed using Pearson correlation test under assumption of normality, and using Spearman rank correlation test when otherwise.

RESULTS

First Set of Experiments: Effects of Copepod Grazing/Swimming on Diatom Aggregation

Copepod Ingestion Rates

During the incubations, copepods actively grazed on *S. marinoi* (Experiments 1 and 2) but no grazing was measurable on *C. neogracile* (Experiment 3), i.e., phytoplankton growth exceeded grazing rates as evidenced by similar cell abundance

TABLE 4 | Final cell concentration (10^5 cell mL^{-1}) and copepod clearance (mL ind^{-1} d^{-1}) and ingestion rates (ng Chl a ind^{-1} d^{-1}) for Experiments 1–3.

Experiment	Diatom species	Copepod species	Final cell concentration (10^5 cell mL^{-1})	Clearance rate (mL ind^{-1} d^{-1})	Ingestion rate (ng Chl a ind^{-1} d^{-1})
1	*S. marinoi*	Control	5.8 ± 0.8	–	–
		E. acutifrons	5.9 ± 1.0	3 ± 3	157 ± 155
		C. helgolandicus	4.4 ± 0.3	24 ± 6	1159 ± 248
2	*S. marinoi*	Control	3.6 ± 0.1	–	–
		E. acutifrons	2.63 ± 0.03	9.6 ± 0.3	225 ± 6
3	*C. neogracile*	Control	2.8 ± 0.2	–	–
		E. acutifrons	3.0 ± 0.1	<dl	<dl
		A. clausi	3.07 ± 0.04	<dl	<dl

Results are means ± SE; <dl, under the detection limit.

in controls and copepod tanks at T_f (**Table 4**). *E. acutifrons* ingestion rates ranged from 157 ± 155 to 225 ± 6 ng Chl a ind^{-1} d^{-1} (**Table 4**). *C. helgolandicus* ingestion rates were five to eight times higher, reaching 1159 ± 248 ng Chl a ind^{-1} d^{-1} (**Table 4**). During the incubation with *S. marinoi*, *C. helgolandicus* egestion averaged 64 ± 55 fecal pellets ind^{-1} d^{-1} (Experiment 1). Their average ESD was 173 ± 24 μm, with a carbon content of 30 ± 7 nmol C PF^{-1} and a sinking velocity of 122 ± 32 m d^{-1}. The majority of fecal pellets recovered at the end of the incubation were intact.

Aggregation of Free Diatom Cells

Sizes and sinking velocities of the *S. marinoi* aggregates formed in the presence of *E. acutifrons* and *C. helgolandicus* were not significantly different from the controls with respective mean values of 1.6 ± 0.0 mm ESD and 230 ± 1 m d^{-1} (**Table 5** and **Figure 2A**). At lower cell density, *S. marinoi* formed less but bigger aggregates than during Experiment 1, with a mean ESD of 3.1 ± 0.6 mm (**Table 5** and **Figure 2C**) and an average sinking velocity of 320 ± 10 m d^{-1} (**Table 5**). However, mean aggregate abundance was significantly higher (p-value < 0.05) in Experiment 1 in the presence of *E. acutifrons* (288 ± 80 agg L^{-1}) compared to controls (145 ± 25 agg L^{-1}) and *C. helgolandicus* (113 ± 35 agg L^{-1}) (**Table 5** and **Figure 2B**). At lower initial cell concentration (Experiment 2), aggregate abundance was also slightly higher (but not significantly) in *E. acutifrons* tanks, with a mean of 60 ± 9 agg L^{-1} compared to 46 ± 9 agg L^{-1} in controls (**Table 5** and **Figure 2D**). A non-significant but systematic increase in the TEP concentration or production by *S. marinoi* was measured in the presence of *E. acutifrons* and *C. helgolandicus* (**Table 5**). Concerning Experiment 3 with *C. neogracile*, aggregates were formed in two out of the six copepod tanks (**Table 5**). In the rolling tanks containing *A. clausi* (Experiment 3), TEP production was significantly higher than in controls (4 ± 2 versus 10 ± 3 pg X_{eq} $cell^{-1}$ d^{-1}, p = 0.045). *C. neogracile* formed larger aggregates than *S. marinoi* with average ESD of 4.5 ± 0.5 and 4.3 ± 1.5 mm in the presence of *E. acutifrons* and *A. clausi,* respectively. In this experiment, *C. neogracile* aggregates were too numerous and had too low contrast in pictures and videos to measure their sinking velocity, probably due to their low cell content. Indeed, the percentage of aggregated cells was only 0.3 ± 0.3% (**Table 5**).

Elemental Cell Composition

Si:C ratios of *S. marinoi* significantly increased from 0.14 ± 0.04 to 0.21 ± 0.04 (p = 0.018) in the presence of *E. acutifrons* (Experiment 1), whereas *C. helgolandicus* grazing did not influence Si:C nor C:N ratios (Experiment 1). In general *S. marinoi* C:N ratios decreased similarly in all rolling tanks ($p < 0.05$), except for Experiment 1 where *E. acutifrons* grazing led to a stronger decrease of *S. marinoi* C:N ratio. *C. neogracile* elementary ratios were not modified during incubation in the presence or absence of copepods (controls), as shown by the marked stability in mean values of Si:C and C:N ratios (**Table 5**).

TABLE 5 | Final conditions in incubations (Experiments 1–3) using free diatom cells as prey.

Experiment	Diatom species	Copepod species	Aggregate abundance (agg L^{-1})	ESD (mm)	Sinking velocity (m d^{-1})	Aggregated cells (% of total cells)	Final TEP concentration (mg X_{eq} L^{-1})	TEP production (pg X_{eq} $cell^{-1}$ d^{-1})	Final C:N (mol:mol)	Final Si:C (mol:mol)
1	*S. marinoi*	Control	145 ± 25	1.6 ± 0.1	230 ± 65	29 ± 12	5.9 ± 0.8	1 ± 2	10.2 ± 2.4	0.14 ± 0.04
		E. acutifrons	288 ± 80*	1.6 ± 0.0	228 ± 54	39 ± 6	6.7 ± 0.6	3 ± 1	6.4 ± 0.6	0.21 ± 0.04*
		C. helgolandicus	113 ± 35	1.6 ± 0.1	232 ± 64	29	6.4 ± 0.9	2 ± 2	8.0 ± 2.5	0.16 ± 0.06
2	*S. marinoi*	Control	46 ± 9	3.0 ± 0.3	310 ± 16	32 ± 10	5.1 ± 0.5	2 ± 2	8.6 ± 0.3	0.21 ± 0.01
		E. acutifrons	60 ± 9	3.1 ± 0.2	330 ± 12	13 ± 2	6.0 ± 0.5	7 ± 2	7.7 ± 0.4	0.19 ± 0.02
3	*C. neogracile*	Control	No agg.	No agg.	No agg.	0	4.4 ± 0.7	4 ± 2	7.8 ± 0.7	0.26 ± 0.05
		E. acutifrons	47 ± 47	4.5 ± 0.5	<dl	23 ± 23	5.7 ± 1.3	9 ± 5	10.1 ± 1.2	0.21 ± 0.03
		A. clausi	2 ± 2	4.3 ± 1.5	<dl	0.3 ± 0.3	6.2 ± 0.9*	10 ± 3*	7.5 ± 0.8	0.26 ± 0.03

*Results are means ± SE, except for aggregate abundance, TEP production, and C:N and Si:C ratios where means ± cumulative error are indicated. *p-value < 0.05; <dl, under the detection limit; No agg., no aggregation.*

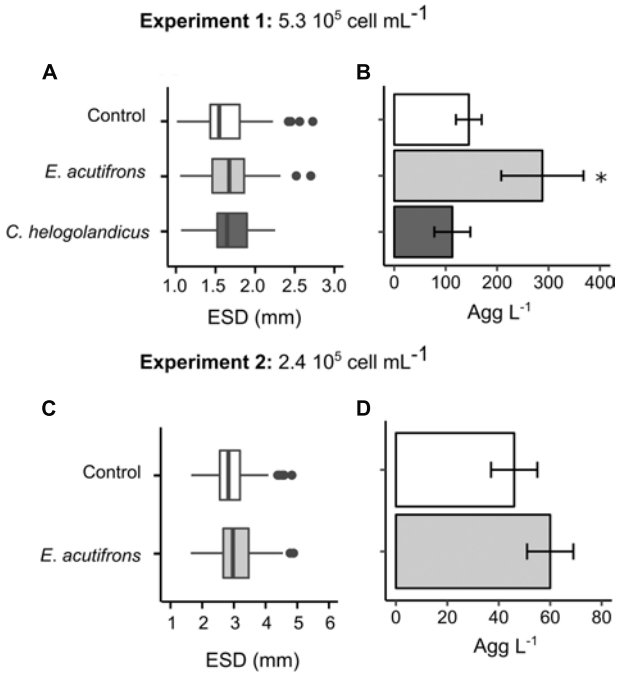

FIGURE 2 | Influence of copepod grazing on aggregation of free *S. marinoi* cells at high **(top)** and low **(bottom)** initial concentrations. Graphs **(A)** and **(C)** display boxplot of *S. marinoi* aggregate ESD (mm) at the end of the incubations (n = 60). Graphs **(B)** and **(D)** display *S. marinoi* aggregate abundance (agg L^{-1}; mean ± cumulative error) at the end of the incubations. *p-value < 0.05.

Second Set of Experiments: Effects of Copepod Grazing/Swimming on Aggregate Dynamics

Copepod Grazing on *C. neogracile* Aggregates

Chaetoceros neogracile aggregates were grazed by both *E. acutifrons* and *A. clausi* as proven by copepod mean gut contents values reaching 0.08 ± 0.03 and 0.12 ± 0.04 ng Chl a_{eq} ind^{-1} for *E. acutifrons* and *A. clausi*, respectively (**Table 6**). Derived ingestion rates ranged from 4 ± 1 to 6 ± 2 ng Chl a_{eq} ind^{-1} d^{-1} for *E. acutifrons* and *A. clausi*, respectively (**Table 6**).

C. neogracile Aggregate Distribution and Sinking Velocity

In Experiment 4, no significant changes in *C. neogracile* aggregate abundance, ESD, and sinking velocity were observed in the presence of *E. acutifrons* (**Table 7** and **Figures 3A,B**). During Experiment 5, re-aggregation was observed in all rolling tanks causing a shift in aggregate abundance (from 18 ± 6 to 3 ± 1 agg L^{-1} in controls and from 15 ± 3 to 1.7 ± 0.6 agg L^{-1} with *A. clausi*), size (from 1.8 ± 0.1 to 5 ± 1 mm in controls and from 1.9 ± 0.1 to 5 ± 1 mm with *A. clausi*), and sinking velocity (from 141 ± 27 to 439 ± 153 m d^{-1} in controls and from 145 ± 26 to 501 ± 106 m d^{-1} with *A. clausi*), between T_0 and T_f (**Table 7** and **Figures 3C,D**). This pattern was similar in copepod and control tanks suggesting that grazing by *A. clausi* had no influence on aggregation dynamics (**Table 7** and **Figures 3C,D**).

TABLE 6 | Copepod gut contents (ng Chl a_{eq} ind^{-1}) and ingestion rates (ng Chl a_{eq} ind^{-1} d^{-1}) while grazing on aggregates (Experiments 4–7).

Experiment	Diatom species	Copepod species	Gut content (ng Chl a_{eq} ind^{-1})	Ingestion rate (ng Chl a_{eq} ind^{-1} d^{-1})
4	C. *neogracile*	*E. acutifrons*	0.08 ± 0.03	4 ± 1
5	C. *neogracile*	*A. clausi*	0.12 ± 0.04	6 ± 2
6	S. *marinoi*	*T. longicornis*	0.5 ± 0.3	23 ± 14
7	S. *marinoi*	*E. acutifrons*	0.05 ± 0.02	2.6 ± 0.9
		C. helgolandicus	0.3 ± 0.2	14 ± 9

Results are means ± SE.

Elemental Composition of the *C. neogracile* Aggregates

Euterpina acutifrons grazing on *C. neogracile* aggregates did not influence the particulate organic matter elemental composition and mean values remained stable, with final C:N ratios of 7.9 ± 0.3, and final Si:C ratios of 0.04 ± 0.02 (**Table 7**). Due to technical problems, no data were available for Experiment 5.

Copepod Grazing on *S. marinoi* Aggregates

All copepods studied fed on *S. marinoi* aggregates (Experiments 6 and 7). This resulted in mean gut content values of 0.5 ± 0.3 ng Chl a_{eq} ind^{-1} for *T. longicornis* and 0.3 ± 0.2 ng Chl a_{eq} ind^{-1} for *C. helgolandicus*. The smallest copepod *E. acutifrons* exhibited the lowest values with an average of 0.05 ± 0.02 ng Chl a_{eq} ind^{-1} (**Table 6**). Derived ingestion rates reached 23 ± 14 ng Chl a_{eq} ind^{-1} d^{-1} for *T. longicornis*, 14 ± 9 ng Chl a_{eq} ind^{-1} d^{-1} for *C. helgolandicus*, and 2.6 ± 0.9 ng Chl a_{eq} ind^{-1} d^{-1} for *E. acutifrons* (**Table 6**).

Calanus helgolandicus fecal pellets collected were intact, and fecal pellet mean production rate was 25 ± 3 FP ind^{-1} d^{-1}, which is a twofold lower value than what was observed when grazing on free *S. marinoi* (Experiment 1). Fecal pellets produced were smaller when aggregates were the only prey, averaging 145 ± 25 μm in ESD. Corresponding carbon content (33 ± 7 nmol C PF^{-1}) and sinking velocity (97 ± 31 m d^{-1}) were also lower.

S. marinoi Aggregates Distribution and Sinking Velocity

The presence of *T. longicornis* induced a fragmentation of aggregates evidenced by a significant increase in aggregate abundance (from 3 ± 1 to 14 ± 8 agg L^{-1}; p = 0.039) and a significant decrease in their mean ESD (from 9 ± 3 to 4.1 ± 0.7 mm; p = 0.013). As a consequence, corresponding sinking velocities were twofold higher in controls at T_f compared to copepod tanks (**Table 7** and **Figures 4A,B**). During Experiment 7, re-aggregation processes were observed in all incubations suggesting no influence of copepod presence (**Table 7** and **Figures 4C–E**).

TABLE 7 | Initial and final aggregate abundances (agg L^{-1}), ESD (mm), and associated sinking velocities (m d^{-1}) in incubations using aggregates as copepod prey (Experiments 4–8).

Experiment	Diatom species	Copepod species	Initial aggregate abundance (agg L^{-1})	Final aggregate abundance (agg L^{-1})	Initial ESD (mm)	Final ESD (mm)	Initial sinking velocity (m d^{-1})	Final sinking velocity (m d^{-1})	Final C:N (mol:mol)	Final Si:C (mol:mol)
4	*C. neogracile*	Control	3 ± 1	1.8 ± 0.9	7 ± 2	9 ± 2	265 ± 105	384 ± 78	7.9 ± 0.2	0.04 ± 0.02
		E. acutifrons	6 ± 1	4 ± 2	4.5 ± 0.4	10 ± 5	191 ± 28	423 ± 199	8 ± 0.2	0.04 ± 0.02
5	*C. neogracile*	Control	18 ± 6	3 ± 1	1.8 ± 0.1	5 ± 1	141 ± 27	439 ± 153	NA	NA
		A. clausi	15 ± 3	1.7 ± 0.6	1.9 ± 0.1	5 ± 1	145 ± 26	501 ± 106	NA	NA
6	*S. marinoi*	Control	3 ± 2	4 ± 3	13 ± 7	10 ± 4	967 ± 755	809 ± 378	6.8 ± 0.1	0.12 ± 0.05
		T. longicornis	3 ± 1	14 ± 8*	9 ± 3	4.1 ± 0.7*	840 ± 505	367 ± 70	6.8 ± 0.2	0.14 ± 0.08
7	*S. marinoi*	Control	7 ± 1	1.9 ± 0.6	2.00 ± 0.02	4 ± 1	401 ± 30	457 ± 179	7 ± 2	0.10 ± 0.06
		E. acutifrons	6 ± 2	2.4 ± 0.8	2.3 ± 0.1	4.2 ± 0.7	474 ± 7	482 ± 131	4 ± 2	0.2 ± 0.1
		C. helgolandicus	11 ± 4	1.4 ± 0.4	1.9 ± 0.1	4.5 ± 0.7	382 ± 15	498 ± 143	6 ± 1	0.18 ± 0.06
8	*Melosira* sp.	Control	0.25	0.3 ± 0	26.75 ± 0.05	30 ± 4	1540 ± 70	1633 ± 422	11 ± 2	0.18 ± 0.03
		C. hyperboreus	0.25	13 ± 1 (at T 72 h)	34	10 ± 4 (at T 48 h)	1779	740 ± 351 (at T 48 h)	10 ± 1 (at T 72 h)	0.14 ± 0.03 (at T 72 h)

*Results are means ± SE, except for C:N and Si:C ratios where means ± cumulative error are indicated. *p-value < 0.05.*

Elemental Composition of *S. marinoi* Aggregates

We did not observed any significant variation of Si:C and C:N ratios over time and between tanks. Ratios remained stable reaching respective mean ratios of 0.13 ± 0.07 and 6.8 ± 0.2 for Si:C and C:N, respectively, in Experiment 6 and mean ratios of 0.14 ± 0.11 and 6 ± 3 for Si:C and C:N, respectively, in Experiment 7 (**Table 7**).

In situ Experiment: Effects of *C. hyperboreus* Grazing/Swimming on *Melosira* sp. Aggregate Characteristics and Elemental Composition

The *Melosira* sp. aggregates formed at T_{init} were stable in size and sinking rates over the 72 h incubation in controls (**Table 7**). By contrast, after 24 h incubation with *C. hyperboreus* the fragmentation of this large aggregate into seven smaller ones (1.75 agg L^{-1}) of 14.3 ± 7.0 mm ESD and associated mean sinking velocity of 1017 ± 257 m d^{-1} was evidenced. Fragmentation processes were ongoing over time and after 48 h resulted in an aggregate abundance of 4.8 agg L^{-1} (with respective ESD of 9.8 ± 2.7 mm and average sinking velocity of 740 ± 351 m d^{-1}, **Table 7** and **Figure 5**). After 72 h, incubation with copepods resulted in 50 ± 12 aggregates (12.5 ± 1.2 agg L^{-1}). Due to the huge amount of small particles and the low quality of the video recordings, size and sinking velocities measurements could not be done at 72 h.

While it was not possible to measure ingestion, analyses of videos showed active interactions between copepods and aggregates. Copepods were ripping aggregates or swimming through aggregates. We observed a switch in *C. hyperboreus* swimming behavior between T_0 and T_f. In fact, during the first hours of incubation while only one large aggregate was present, copepods were passively swept within the rolling tank rotation and only exhibited few jumps. After 48 h of incubation, copepods were more active and we observed several jumps, and changes in swimming trajectories to avoid collision with aggregates (**Figure 6** and **Supplementary Videos S2, S3**).

When *C. hyperboreus* were incubated during 72 h with *Melosira* sp. aggregates, we did not observe any changes in Si:C and C:N ratios, compared to the controls and mean values were 0.16 ± 0.02 and 11 ± 1, respectively (**Table 7**).

DISCUSSION

Methodological Considerations

The main purpose of this study was to investigate the influence of copepod grazing/swimming on aggregate formation and dynamics. Aggregate formation depends on coagulation processes regulated by particle stickiness and collision rate inside the tank, the latter being directly linked to particle concentration (Jackson, 1990, 2015; Riebesell, 1991). Our experimental set up allowed to study if copepod activity favored or prevented aggregate formation, independently from particle concentration variations due to grazing and swimming. Despite the high cell concentrations needed to promote aggregation in 24 h, grazing

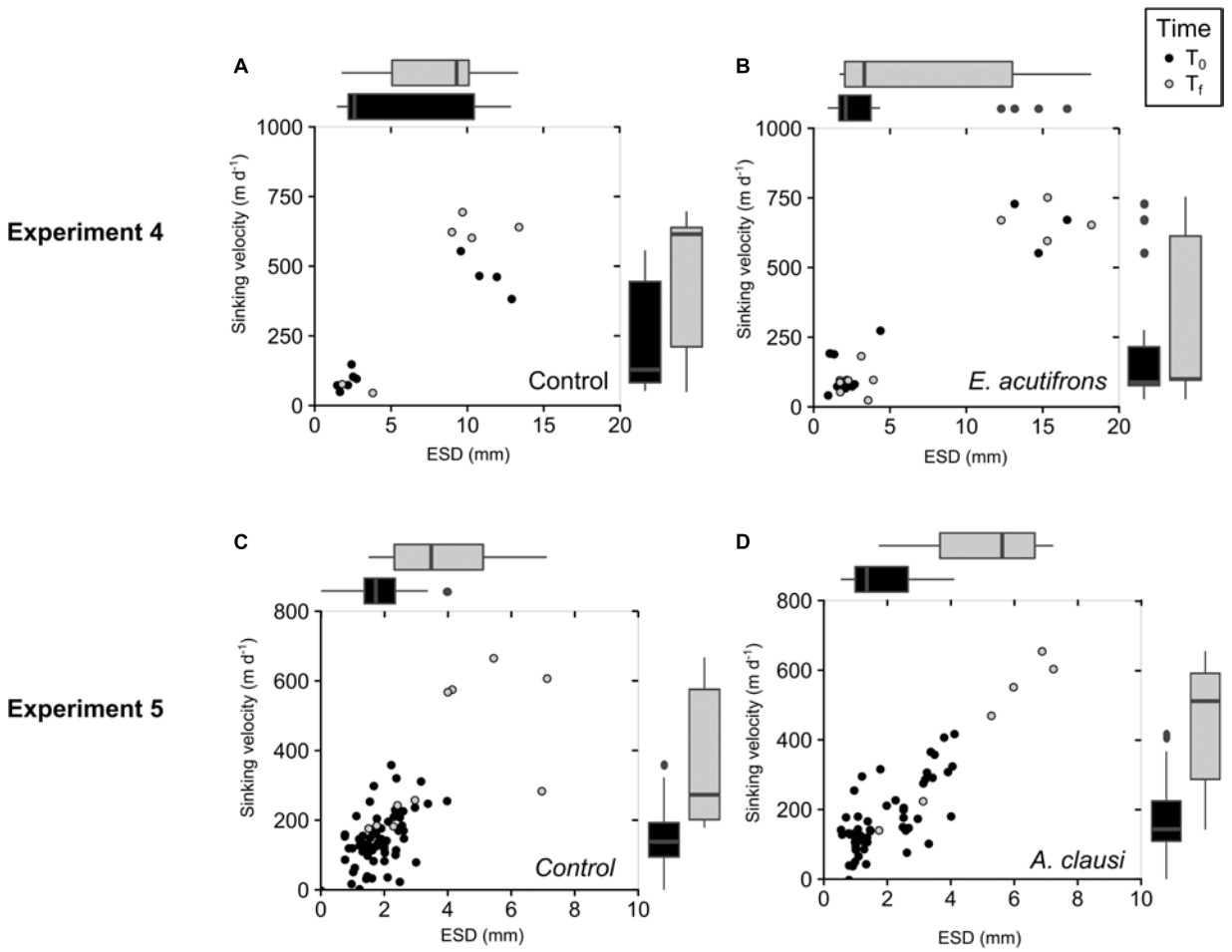

FIGURE 3 | Change in *C. neogracile* aggregate characteristics over the course of the incubation (Experiments 4 and 5): on the left for controls **(A,C)** and on the right in copepod tanks containing *E. acutifrons* **(B)** and *A. clausi* **(D)**. Depicted are the sinking velocities of aggregates (m d^{-1}) over ESD (mm) at the beginning (T_0, black dots) and at the end (T_f, gray dots); boxplots of aggregate size distribution (ESD, mm; on top of the graph), and sinking velocities (m d^{-1}; on the right part of the graph) at the beginning (T_0, black boxes) and end (T_f, gray boxes) of the incubations.

activity was still measurable in all experiments except Experiment 3. Clearance rates of 3–9.6 mL ind^{-1} d^{-1} for *E. acutifrons* and of 24 ± 6 mL ind^{-1} d^{-1} for *C. helgolandicus* were congruent with literature values for the same species, e.g., from 2.8 to 31 mL ind^{-1} d^{-1} for *E. acutifrons* (Sautour and Castel, 1993; de Melo Júnior et al., 2013), and from 36 to 126 mL ind^{-1} d^{-1} for *C. helgolandicus* (Fileman et al., 2007). The same holds for ingestion rates, our values for *E. acutifrons* are highly comparable with values recorded during laboratory experiments (157–225 ng Chl a ind^{-1} d^{-1}, this study vs. 360–408 ng Chl a ind^{-1} d^{-1} in Sautour and Castel, 1993). By contrast, *C. helgolandicus* exhibited ingestion rates twofold higher (1159 ± 248 ng Chl a ind^{-1} d^{-1}) than the value found in Irigoien et al. (2000) (600 ng Chl a ind^{-1} d^{-1}) and rates commonly range between 30 and 300 ng Chl a ind^{-1} d^{-1}, depending on food concentration (Mauchline, 1998; Fileman et al., 2007). In our study, this discrepancy could be explained by the combined effects of high prey concentration, the absence of stress due to predation, and the 24 h starvation phase prior to the beginning of the experiment, all these factors being acknowledged to maximize ingestion (Bollens and Frost, 1989a,b, 1991; Bollens and Stearns, 1992; Mauchline, 1998).

In the second set of experiments (Experiments 4–7), it was impossible to use the Frost (1972) method to compute grazing rates. Firstly because aggregates are complex cell assemblages preventing the measurement of the exponential phytoplankton growth. Secondly, the high heterogeneity of aggregates does not allow to rely precisely on the same initial Chl a concentration in each tank, and may thus introduce biases in rate computations. As an alternative, ingestion rates were estimated from the gut fluorescent content method (Mackas and Bohrer, 1976) which is often performed at laboratory or *in situ* to estimate zooplankton herbivory. It constitutes a fast and easy method to set up that could be carried out on a variety of planktonic (copepods, salps, and krill; Pakhomov et al., 1996; Perissinotto and Pakhomov, 1998; Lópes et al., 2007), pelagic (herring larvae, Denis et al., 2018), and benthic organisms (Díaz et al., 2012; Gaonkar and Anil, 2012). Although potential issues exist regarding gut pigments destruction (Conover et al., 1986;

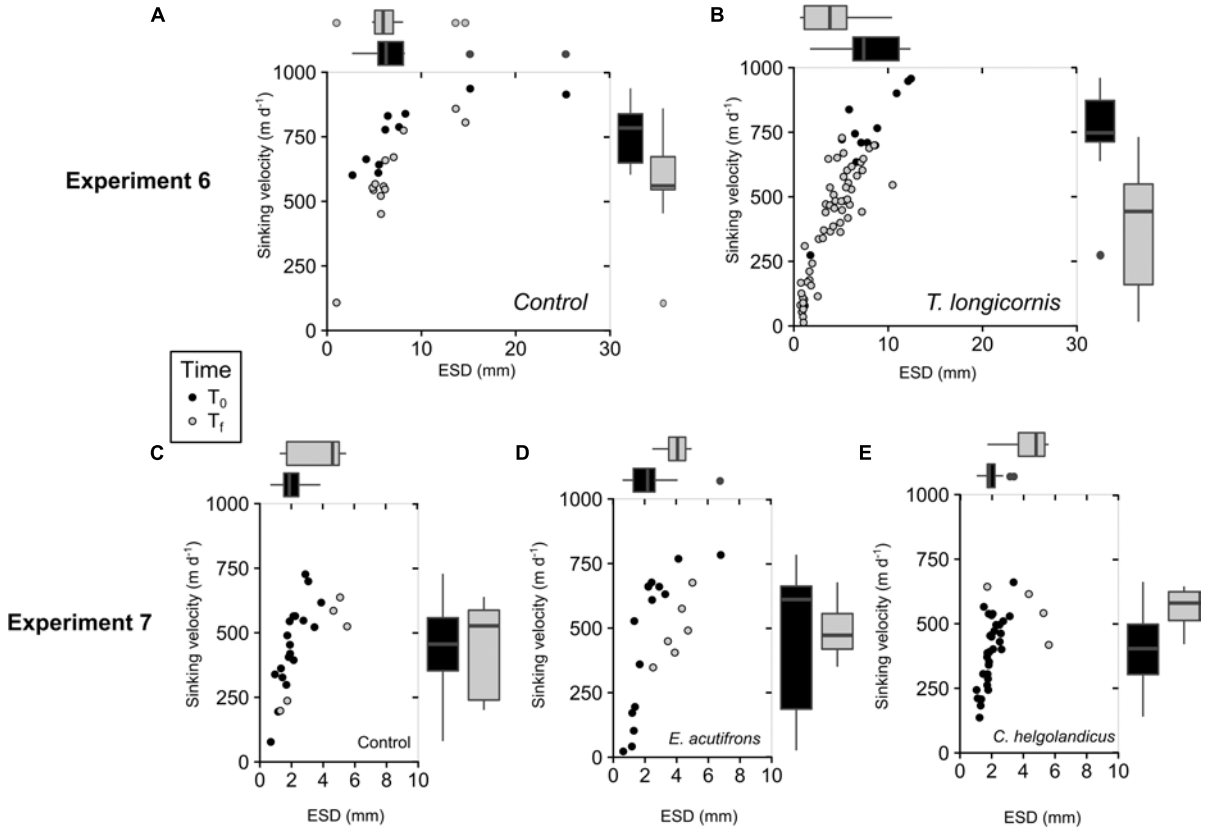

FIGURE 4 | Change in *S. marinoi* aggregate characteristics over the course of the incubation (Experiments 6 and 7) for controls **(A,C)** and for copepod tanks containing *T. longicornis* **(B)**, *E. acutifrons* **(D)**, and *C. helgolandicus* **(E)**. Depicted are the sinking velocities of aggregates (m d^{-1}) over ESD (mm) at the beginning (T_0, black dots) and end (T_f, gray dots); boxplots of aggregate size distribution (ESD, mm; on top of the graph), and sinking velocities (m d^{-1}; on the right part of the graph) at the beginning (T_0, black boxes) and end (T_f, gray boxes) of the incubations.

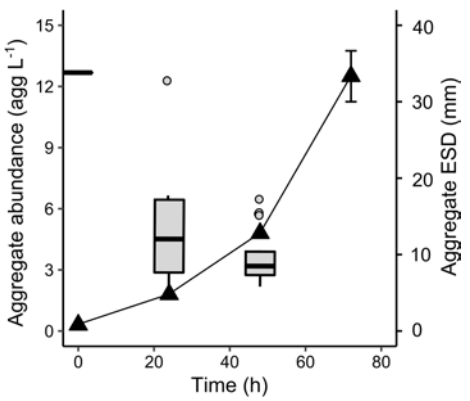

FIGURE 5 | Aggregate dynamics for natural *Melosira* sp. aggregate incubated with *C. hyperboreus*. Black triangles represent the aggregate abundances (agg L^{-1}) and boxes the aggregate ESD (mm) distribution, both plotted over the course of the experiment (h).

Durbin and Campbell, 2007) and gut evacuation rate estimates (Perissinotto and Pakhomov, 1996), the method appeared well suited to quantify aggregate ingestion by copepods, using total chlorophyllian pigments as a proxy of prey biomass. The ingestion rates obtained *via* gut content are, however, not directly comparable to those estimated from cell decrease (e.g., Frost, 1972) and rather correspond to a snapshot of the amount of aggregates ingested at the time of sampling. In any case, our results highlighting significant ingestion of most copepod species while offered aggregate as prey, revealed copepod ability to deal with larger and more complex preys (i.e., containing a mix of cell and mucus assemblage) such as whole or fragmented aggregates as shown by Iversen and Poulsen (2007), when copepods were offered fecal pellets as food. If copepod preferences for fragmented aggregates could not be inferred from our study, direct feeding on large aggregates was observed for *E. acutifrons* and *C. hyperboreus*, and individuals seemed to hang on aggregates while feeding (**Supplementary Video S1** for *E. acutifrons*).

First Set of Experiments: Copepod Grazing/Swimming Effects on Diatom Aggregation

Different processes could explain how copepod presence have modified cell aggregation dynamic in our study.

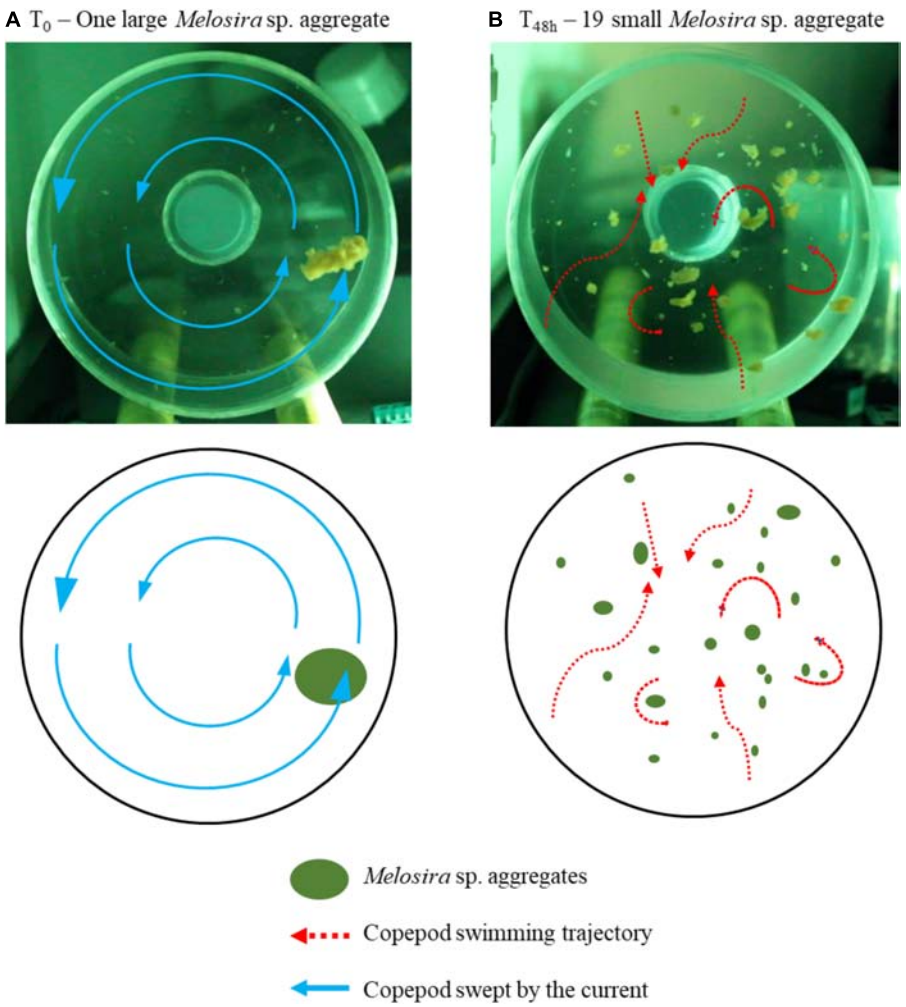

FIGURE 6 | *Calanus hyperboreus* swimming trajectories drawn from video recordings (Experiment 8). Comparison of the feeding strategy of *C. hyperboreus* at the beginning of the incubation with one large *Melosira* sp. aggregate **(A)**, and after 48 h with 19 fragmented aggregates **(B)**.

Cell stickiness may be enhanced when TEP production is boosted. Exudation of organic compounds and polymers by zooplankton is well known (Alldredge and Silver, 1988; Schuster and Herndl, 1995). In general, copepod cues may also induce physiological responses in marine phytoplankton. For instance, copepodamides are compounds that may induce defensive traits such as increase in toxin production by dinoflagellates (Selander et al., 2011, 2015), change in *S. marinoi* chain size (Bergkvist et al., 2012, 2018; Amato et al., 2018; Grebner et al., 2018) and increase the silica content of *T. weissflogii* (Pondaven et al., 2007). In line with the study of Malej and Harris (1993) who measured an inhibition of copepod feeding rate due to high molecular weight polysaccharides produced by phytoplankton, we hypothesized in our experiments that copepod activities may promote mucus production as observed for nutrient limitation stress (Engel, 2000; Passow, 2002). Indeed TEP production in Experiment 3 was higher when *A. clausi* grazed on *C. neogracile* and slightly higher (though not significantly) in the presence of *E. acutifrons* (Experiment 1) than in controls. However, while more aggregates were produced with *E. acutifrons*, we did not observe an increase in aggregate formation with *A. clausi*. Conversely to the general postulate stating that aggregation is positively correlated to TEP concentrations, in our study, higher TEP production did not always result in higher aggregation rate, at least during the 24 h of incubation. Moreover, no significant correlation was found between TEP production or concentration and aggregate abundance or size. While TEP are important to trigger aggregation, TEP concentrations and production alone are not sufficient to explain our aggregation patterns.

The collision rates may be modified by two parameters: micro-turbulences created when copepods swim around and particle abundances associated to differential sinking due to egestion of fast sinking fecal pellets and manipulation of TEP by copepods. To aggregate, the particles must collide and then stick together. However, if the collision is too violent (high energy dissipation rates see Alldredge et al., 1990), no coagulation follows and disaggregation processes may even occur (Alldredge et al., 1990). In rolling tanks without copepods, collision is promoted through

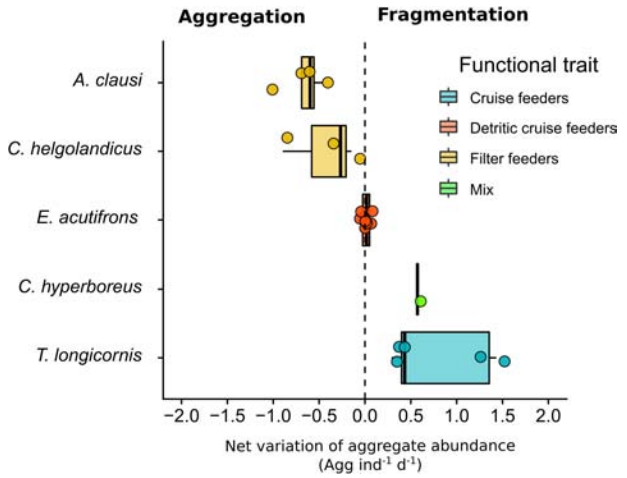

FIGURE 7 | Influence of different functional traits on aggregate dynamics for each copepod species. Each dot represents the variation in aggregate abundance between T_0 and T_f divided by the variation between T_0 and T_f in controls. For a given experiment, the net variation is then divided by the copepod abundance (ind L^{-1}) and the duration of the incubation (in d). The figure depicts the functional traits associated to copepod species *sensu* Benedetti et al. (2015).

differential sinking only whereas *in situ* collision is due to both differential sinking and turbulence (Alldredge et al., 1990; Riebesell, 1991; Jiang and Osborn, 2004; Jackson, 2015). Different feeding behavior of copepods may create at least two types of turbulence. When filtering, copepods generate double shear field (Strickler, 1982) and thus induce micro circulation on the order of 1 to 18 mm s^{-1} (Kiørboe, 1997; Jiang and Kiørboe, 2011b). Moreover, copepod swimming behavior when foraging such as jump and swimming phases of ambush feeders create wake vortex with velocity of 240 mm s^{-1} (Kiørboe, 1997; Jiang and Kiørboe, 2011a,b). In our study the two suspension feeders (*A. clausi* and *C. helgolandicus*) we used did not promote aggregation. By comparison, in Experiments 1 and 2, activity of the small cruise feeder *E. acutifrons* induced aggregation. This suggests that turbulences created by filtering activity only were not enough to promote collisions whereas turbulence induced by small cruise feeder behavior (Strickler, 1982; Kiørboe, 1997; Jiang and Kiørboe, 2011b) seemed to favor cell collisions without disrupting coagulation. Possibly, turbulences created by larger cruise feeder such as *C. helgolandicus* may be too strong and prevent the coagulation of the cells by providing too much energy. Future studies focusing on microfluidic disturbance generated by copepod feeding and foraging are required to highlight the effects on coagulation process, and therefore confirm this statement. Collision rates are additionally related to the amount of particles in the tank (Jackson, 2015). In comparison to *E. acutifrons*, the lower aggregate abundance formed in the presence of *C. helgolandicus* could be related to its higher ingestion rates (**Table 4**). By increasing particle abundance and the differential sinking velocity, we expected that the fecal pellets produced would have increased collision rates (Burd and Jackson, 2009). This was much anticipated as fecal pellets sink much faster than free cells (100–200 vs. 1–5 m d^{-1} for fecal

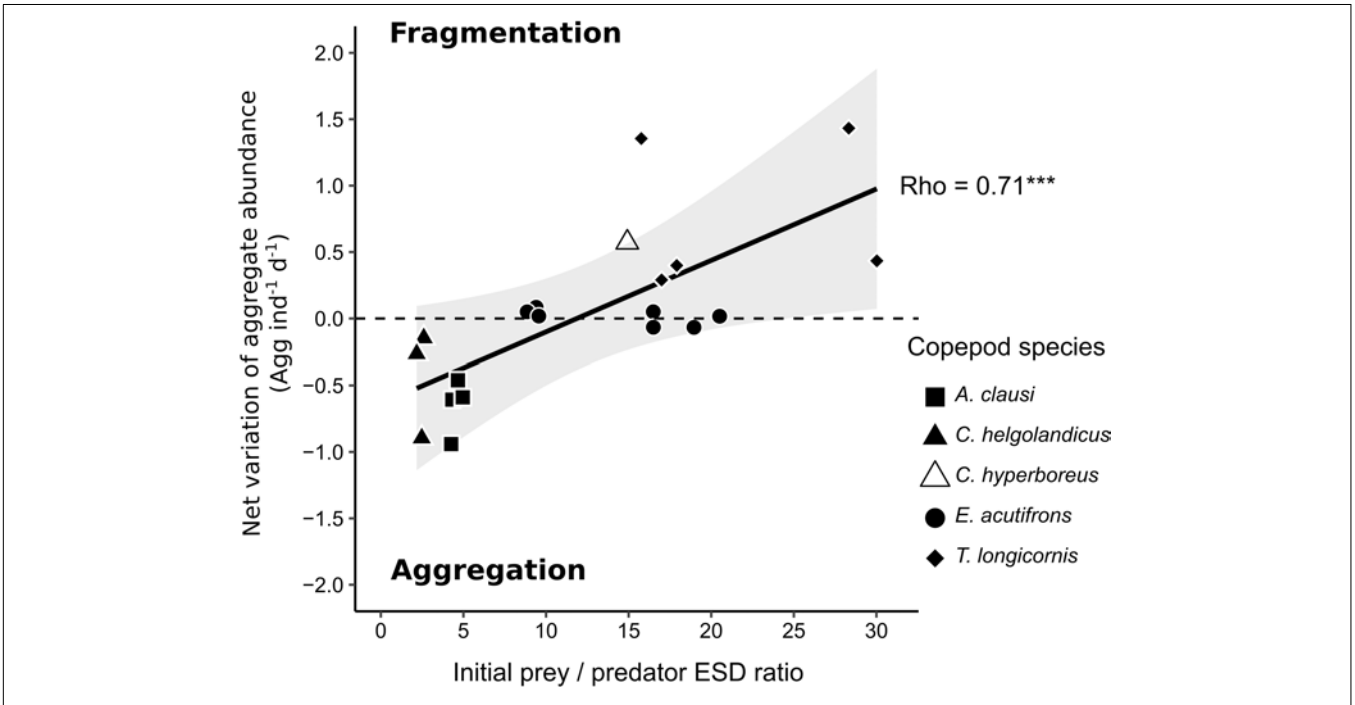

FIGURE 8 | Influence of prey to predator size ratios (expressed as ESD) on aggregate dynamics: the net variation of aggregate abundance (agg ind^{-1} d^{-1}) is correlated to prey to predator size ratios (average aggregate ESD/copepod ESD). Each point represents one rolling tank. Gray shading corresponds to 99% confidence interval of the linear regression. ***p-value < 0.001 of Spearman's rho rank correlation test.

pellets and free cells, respectively; Yoon et al., 2001; Bienfang, 1981; Turner, 2015). Our set up did not allow to directly observe if fecal pellets got trapped into the aggregates formed but despite *C. helgolandicus* producing large (145 ± 25 μm) and abundant fecal pellets (190–1528 per tank) no significant change in aggregate formation was evidenced. Therefore, the increase in particle abundance related to fecal pellet production did not compensate aggregate fragmentation linked to copepod grazing (i.e., increase in turbulence and decrease in cell concentration). Another process possibly affecting the collision rate is a modification of the size of the TEP. In fact, copepods do not actively feed on TEP, but could passively influence TEP size spectra by increasing the coagulation of small TEP into larger ones (Prieto et al., 2001). Turbulences due to swimming might induce TEP formation (Schuster and Herndl, 1995). Additionally, TEP size might be increased when TEP are caught into the feeding current, compacted by feeding appendages and rejected after capture (Young et al., 1997). In our study, we can hypothesize that by manipulating TEP with their feeding appendages, copepods may have contributed to increase the likelihood of collision between TEP, diatoms, and fecal pellets. However, to verify such a hypothesis required to use the microscopic TEP assay method to quantify TEP (Passow and Alldredge, 1995a; Mari et al., 2005).

Overall, our results are consistent with what was observed in a mesocosm study conducted in Norway (Moriceau et al., 2018). During this study, phytoplankton aggregation increased with copepod abundance when cyanobacteria were the dominant species. However, when diatoms constituted the bulk of the phytoplankton community, the net impact of copepods on carbon export was negative, suggesting that in this particular case, the balance between aggregation and fragmentation was in favor of particle fragmentation.

Second Set of Experiments: Implications of Grazing and Swimming of Copepods on Aggregate Characteristics

The influence of copepod grazing on aggregate size and abundance after 24 h incubation could be the result of either their direct grazing on aggregates or of their swimming activity while foraging. Similar studies were carried out with zooplankton and marine snow inside rolling tanks (Bochdansky and Herndl, 1992; Bochdansky et al., 1995). For instance, Bochdansky and Herndl (1992) showed that *A. clausi* does not significantly feed on marine snow, and concluded that the major fraction of free-living filter feeders are unable to use phytoplankton when embedded in a mucoid matrix. On the contrary, quantitative ingestion rates measured here on the four copepod species (including *A. clausi*) clearly evidenced an active grazing on diatoms even when embedded in aggregates. Direct feeding on aggregates was observed for *E. acutifrons* (see **Supplementary Video S1**) increase in gut content could not exclude feeding on both aggregate fragments and disaggregated diatoms. However, we assume the latter negligible since free diatoms were not visible when checking the incubation media *via* microscopy. Trophic interactions between zooplankton and phytoplankton aggregates were also demonstrated for protists (Artolozaga et al., 2002), euphausiids (Dilling and Brzezinski, 2004), copepods, appendicularians, and doliolids (Taucher et al., 2018), but the process involved remain unknown.

Changes in aggregate structure were explored as a possible pathway for copepods to influence the particle flux. We hypothesized that zooplankton may change the aggregate density by repackaging or increasing Si:C ratios of the cells constituting the aggregates. First of all, in our experiments, Si:C ratios were not affected by the 24 h of grazing. Another test was through the parameters obtained from the fit of the ESD and sinking velocities data for *C. neogracile* and *S. marinoi* aggregates. Power law regressions between aggregates ESD and sinking velocity are characterized by *A* and *B* constant parameters that are comparable to those described in literature for *in situ* marine snow (Shanks, 2002; Iversen et al., 2010), with *B* values ranging from 0.4 to 1.3, corresponding to fractal dimensions between 1.4 and 2.3 (calculated using equation 6 from Xiao et al., 2012). In every situation where copepods fragmented the large aggregates or re-aggregated the small aggregates, the regression linking aggregate ESD and sinking velocities remained the same with unchanged *A* and *B* and so the fractal dimension *D* that may be derived from *B* (Long et al., 2015). These results suggested that copepod activities did not altered the aggregate porosity and excess density.

Particle dynamics was affected by our distinct experimental conditions regarding prey and predator types. We distinguished three different patterns: (1) fragmentation, (2) no change in the particle dynamic, and (3) re-aggregation in larger aggregates. **Figures 7**, **8** summarize re-aggregation and fragmentation patterns induced by copepods, using the variation in aggregate abundance between T_0 and T_f divided by the variation between T_0 and T_f in controls. For a given experiment, the net variation was then divided by the copepods abundance (ind L^{-1}) and the duration of the incubation (in d). **Figure 7** relates copepod functional traits to fragmentation/aggregation predominance. In **Figure 8**, we tested the impact of prey to predator size ratios onto aggregation/fragmentation balance.

Aggregate fragmentation was evidenced when a significant increase in particle abundance was associated to a decrease in their size spectra and sinking velocity. This pattern was observed for prey to predator size ratios higher than 15 (**Figure 8**) in the experiment with *T. longicornis* and *C. hyperboreus* feeding on *S. marinoi* and *Melosira* aggregates, respectively (**Table 7** and **Figures 4**, **5**, **7**, **8**). The cruise feeder *T. longicornis* was actively feeding on aggregates as also evidenced in previous experiments demonstrating the ability of *T. longicornis* to eat on sinking organic materials (Kiørboe, 2011; Lombard et al., 2013b). To our knowledge, no studies have quantified copepod ingestion while grazing on aggregates. However, our gut content values are comparable to experimental studies using phytoplankton cells as prey. We measured similar but smaller ingestion rates for *T. longicornis* in our rolling tank incubations (0.5 ± 0.3 ng Chl a_{eq} ind^{-1} d^{-1}) compared to measurements done during batch laboratory experiments (117–217 ng Chl a_{eq} ind^{-1} d^{-1}, Wang and Conover, 1986). In the experiment with *C. hyperboreus* and the natural *Melosira* sp. aggregate, videos showed that different types of interactions were at play and may explain the observed

decrease in the aggregate size. In fact, the videos evidenced that large pieces of aggregate were broken up by copepod jumping through the aggregate. Copepod swimming velocities range between 0.1 and 100 mm s^{-1} (Yamazaki and Squires, 1996) and they jump at velocities reaching up to 400 mm s^{-1} creating wake vortex with velocity of 240 mm s^{-1} (Jiang and Kiørboe, 2011a,b), which in the vicinity of fragile aggregates could be sufficient to break them. We even observed copepods hanging on aggregate before jumping, thus triggering the fragmentation of the aggregate into pieces. Interestingly when the particles were smaller and more abundant (as a result of the fragmentation), copepods swam more actively around aggregates (**Figure 6** and **Supplementary Videos S2, S3**). *C. hyperboreus* is generally considered as a passive filter feeder (Conover, 1966; Huntley, 1981; Greene, 1988). However, we observed a switch of swimming behavior from passive swept into the current when copepods were incubated with one large aggregate to active cruising when the aggregates became smaller and more numerous (as described in Strickler, 1982; Kiørboe et al., 2018). This change in their feeding foraging strategy may explain why fragmentation accelerated after 48 h (**Figure 5**). Overall, the more aggregates are fragmented, the more small aggregate abundance increases and the more copepods increase fragmentation, as can be seen from the exponential increase in aggregate abundance over time (**Figure 5**). *C. hyperboreus* seemed to be more active when aggregates ESD decreased during this experiment, suggesting that they may feed more on fragments than on whole aggregates.

Active feeding evidenced by ingestion rates in the range of 2.6 ± 0.9 to 4 ± 1 ng Chl a_{eq} ind^{-1} d^{-1} is congruent with the direct feeding on whole aggregates evidenced *via* video recording (**Supplementary Video S1**). However, no changes in the *S. marinoi* and *C. neogracile* aggregate size or abundance have been observed with *E. acutifrons* (**Table 7** and **Figures 3**, **4**, **7**, **8**). Cruise feeders detritivores (such as *E. acutifrons*) feeding on marine snow has already been demonstrated (Koski et al., 2005, 2007, 2017) and is often associated to particle flux attenuation. However in our study, *E. acutifrons* with prey to predator size ratios ranging from 7 to 20 did not significantly change the particle spectra neither in size nor in abundance or sinking rates (**Figure 8**). These results suggest that measuring grazing on aggregates is not sufficient on its own to conclude on flux attenuation.

Re-aggregation implies a decrease of aggregate abundance and an increase of the aggregate size compared to controls. This was observed for the experiments with *A. clausi* and *C. helgolandicus* feeding on *C. neogracile* and *S. marinoi* aggregates (**Figures 7**, **8**). **Figures 7**, **8** tend to suggest that aggregation processes prevailed over disaggregation for prey to predator size ratios lower than 6 and/or when filter feeders are predators. We believe that this pattern may be explained by the small sizes of the aggregates tested (Initial ESD = 1.9 mm in incubation with *A. clausi* and *C. helgolandicus* vs. 9 mm for the incubations with *T. longicornis* and 34 mm for *C. hyperboreus*). Small aggregates are more resistant to shear than large aggregates (Jackson, 1990), at a given shear (as induced by copepod swimming) aggregation may be facilitated between small aggregates. Reversely bigger and more fragile aggregates may be broken by the same shear (Jackson, 1990). Unfortunately due to the impossibility to stabilize aggregate at a given size we couldn't test this hypothesis by incubating large aggregates with filter feeders and small aggregates with cruise feeders.

CONCLUSION

Our work suggested that the ability to predict the consequences of copepod activity on particle dynamic could necessitate better understanding of copepod functional traits. The general trend emerging from our study was that in the surface layer aggregation of freely suspended cells or small aggregates may be facilitated by the turbulence resulting from active swimming of small copepods. However, aggregates are fragile and their formation may be prevented by stronger turbulences as those created by larger cruise feeder copepods. As they grow in size, aggregates become more vulnerable to breakage and the same shear that was favoring aggregation of freely suspended cells (swimming of cruise feeders) or even of small aggregates preferentially fragment bigger aggregates. The main difficulty in testing this hypothesis is to stabilize aggregate at a given size in rolling tanks. While we also observed a slight increase in the diatom TEP production, our experimental set up, both in duration and in chemical analysis did not permitted to conclude on this matter. Indeed, we only measured the total pool of >0.4 μm TEP, and not the chemical composition, such as the proportion of sulfate half ester groups that may be responsible for most chemical bridges leading to aggregation (Mopper et al., 1995; Passow, 2002). We could not link either zooplankton activity to TEP size spectra which would only have been possible *via* microscopical measurements of the Alcian blue-stained TEP.

Our work may help to better understand the mechanisms driving the biological pump of carbon. Considering that carbon is efficiently isolated from the atmosphere at a depth approaching 1000 m, many recent studies start differentiating between the export efficiency and the transfer efficiency (Henson et al., 2012; Maiti et al., 2013; Cavan et al., 2017). The first is the amount of carbon produced in surface reaching the export depth (100–200 m) while the second is the proportion of the exported carbon reaching the sequestration depth. Large-scale observations suggested that ecosystems with high export efficiency such as high latitude ecosystems dominated by diatoms have a low transfer efficiency (Maiti et al., 2013). Reversely ecosystems with low export efficiency have high transfer efficiency (Henson et al., 2012; Guidi et al., 2015). Considering that aggregation of freely suspended cells and small aggregates are favored by copepod feeding activity while big aggregates are preferentially fragmented, this mechanisms may partly explained the discrepancy observed between diatoms dominated ecosystems and low productive ecosystem. Diatoms ecosystems tend to form bigger aggregates that may be exported very fast (Alldredge and Gotschalk, 1989; Cisternas-Novoa et al., 2015) but are more vulnerable to breakage by the turbulences created when copepods are feeding. Reversely, ecosystems dominated by cyanobacteria tend to form smaller aggregates (Cisternas-Novoa et al., 2015) that sink more slowly and may thus lead to smaller

export (Henson et al., 2012) but believing our results may be more resistant to copepods swimming activities.

DATA AVAILABILITY STATEMENT

The raw data supporting the conclusions of this article will be made available by the authors, without undue reservation, to any qualified researcher.

AUTHOR CONTRIBUTIONS

JT: writing the manuscript, performing laboratory experiments, sample analyses, and data treatment. DV: copepod collection and rearing, support during laboratory experiments, writing the manuscript, and supervision. LF: support in lab experiments. PM: diatom cultures and support in lab experiments. ML: nutrients and $bSiO_2$ analysis. JD: POC and PON measurements. BM: support in laboratory experiments and *in situ* experiment, writing the manuscript, supervision, and PI of the BIOPSIS project.

FUNDING

This work was supported by the ANR BIOPSIS project, grant ANR-16-CE-0002-01 of the French Agence Nationale de la Recherche, and the CHIBIDO team of the LEMAR. JT was funded by a French doctoral research grant from LabexMer axe 2 (50%) and the ANR BIOPSIS project (50%). The Green Edge project is funded by the following Canadian and French programs and agencies: the Network of Centres of Excellence ArcticNet, the Canada Foundation for Innovation (Amundsen Science), Canada's Excellence in Research Chair (CERC) program, ANR (Contract #111112), CNES (Project #131425), French Arctic Initiative, Fondation Total, CSA, LEFE, and IPEV (Project #1164).

ACKNOWLEDGMENTS

We would like to thank Ifremer for providing the diatom strains and the Albert-Lucas crew for their help at sea, during zooplankton collection. We thank everyone in LEMAR and particularly the technical staff from PFOM-ARN-Ifremer for assistance during the experiments and copepod feeding and maintenance every week-end. We also thank the two reviewers, especially one of them who gave precious comments and constructive suggestions on a previous version of this manuscript. We are very thankful to the crew of the NGCC Amundsen, for their enthusiastic help and technical support, to Marcel Babin, PI of the project, and to Joannie Ferland, Marie-Hélène Forget, and Flavienne Bruyant who organized the expeditions with so much efficiency.

SUPPLEMENTARY MATERIAL

The Supplementary Material for this article can be found online at: https://www.frontiersin.org/articles/10.3389/fmars.2019.00751/full#supplementary-material

VIDEO S1 | Copepod (*E. acutifrons*) eating on diatom aggregate (*C. neogracile*).

VIDEO S2 | *Melosira* sp. aggregate fragmentation due to copepod jump (*C. hyperboreus*).

VIDEO S3 | *Melosira* sp. aggregate fragmentation during the 72 h of incubation.

REFERENCES

Agustí, S., González-Gordillo, J. I., Vaqué, D., Estrada, M., Cerezo, M. I., Salazar, G., et al. (2015). Ubiquitous healthy diatoms in the deep sea confirm deep carbon injection by the biological pump. *Nat. Commun.* 6:7608. doi: 10.1038/ncomms8608

Alldredge, A. L., Gorsky, G., Youngbluth, M., and Deibel, D. (2005). "The contribution of discarded appendicularian houses to the flux of particulate organic carbon from oceanic surface waters," in: *Response of Marine Ecosystems to Global Change: Ecological Impact of Appendicularians*, eds G. Gorsky, M. Youngbluth, and D. Deibel (Paris: GB Science Publishers-Editions Scientifiques), 309–326.

Alldredge, A. L., and Gotschalk, C. (1988). In situ settling behavior of marine snow. *Limnol. Oceanogr.* 33, 339–351. doi: 10.1016/j.scitotenv.2016.09.115

Alldredge, A. L., and Gotschalk, C. (1989). Direct observations of the mass flocculation of diatom blooms: characteristics, settling velocities and formation of diatom aggregates. *Deep Sea Res. Part A. Oceanogr. Res. Pap.* 36, 159–171. doi: 10.1016/0198-0149(89)90131-90133

Alldredge, A. L., Gotschalk, C., Passow, U., and Riebesell, U. (1995). Mass aggregation of diatom blooms: insights from a mesocosm study. *Deep Sea Res. Part II Top. Stud. Oceanogr.* 42, 9–27. doi: 10.1016/0967-0645(95)00002-8

Alldredge, A. L., Granata, T. C., Gotschalk, C., and Dickey, T. D. (1990). The physical strength of marine snow and its implications for particle disaggregation in the ocean. *Limnol. Oceanogr.* 35, 1415–1428. doi: 10.4319/lo.1990.35.7.1415

Alldredge, A. L., and Silver, M. W. (1988). Characteristics, dynamics and significance of marine snow. *Prog. Oceanogr.* 20, 41–82. doi: 10.1016/0079-6611(88)90053-90055

Amato, A., Sabatino, V., Nylund, G. M., Bergkvist, J., Basu, S., Andersson, M. X., et al. (2018). Grazer-induced transcriptomic and metabolomic response of the chain-forming diatom *Skeletonema marinoi*. *ISME J.* 12, 1594–1604. doi: 10.1038/s41396-018-0094-0

Aminot, A., and Kérouel, R. (2004). *Hydrologie Des Écosystèmes Marins: Paramètres Et Analyses*. Versailles: Editions Quae.

Andersen, V., Devey, C., Gubanova, A., Picheral, M., Melnikov, V., Tsarin, S., et al. (2004). Vertical distributions of zooplankton across the Almeria–Oran frontal zone (Mediterranean Sea). *J. Plankton Res.* 26, 275–293. doi: 10.1093/plankt/fbh036

Andersen, V., Gubanova, A., Nival, P., and Ruellet, T. (2001). Zooplankton community during the transition from spring bloom to oligotrophy in the open NW mediterranean and effects of wind events. 2. vertical distributions and migrations. *J. Plankton Res.* 23, 243–261. doi: 10.1093/plankt/23.3.243

Artolozaga, I., Valcárcel, M., Ayo, B., Latatu, A., and Iriberri, J. (2002). Grazing rates of bacterivorous protists inhabiting diverse marine planktonic microenvironments. *Limnol. Oceanogr.* 47, 142–150. doi: 10.4319/lo.2002.47.1.0142

Bach, L. T., Stange, P., Taucher, J., Achterberg, E. P., Algueró-Muñiz, M., Horn, H., et al. (2019). The influence of plankton community structure on sinking velocity and remineralization rate of marine aggregates. *Glob. Biogeochem. Cycles* 33, 971–994. doi: 10.1029/2019GB006256

Beauvais, S., Pedrotti, M. L., Egge, J., Iversen, K., and Marrasé, C. (2006). Effects of turbulence on TEP dynamics under contrasting nutrient conditions: implications for aggregation and sedimentation processes. *Mar. Ecol. Prog. Ser.* 323, 47–57. doi: 10.3354/meps323047

Benedetti, F., Gasparini, S., and Ayata, S. D. (2015). Identifying copepod functional groups from species functional traits. *J. Plankton Res.* 38, 159–166. doi: 10.1093/plankt/fbv096

Berggreen, U., Hansen, B., and Kiørboe, T. (1988). Food size spectra, ingestion and growth of the copepodAcartia tonsa during development: implications for determination of copepod production. *Mar. Biol.* 99, 341–352. doi: 10.1007/BF02112126

Bergkvist, J., Klawonn, I., Whitehouse, M. J., Lavik, G., Brüchert, V., and Ploug, H. (2018). Turbulence simultaneously stimulates small- and large-scale CO 2 sequestration by chain-forming diatoms in the sea. *Nat. Commun.* 9:3046. doi: 10.1038/s41467-018-05149-w

Bergkvist, J., Thor, P., Jakobsen, H. H., Wängberg, S.-A., and Selander, E. (2012). Grazer-induced chain length plasticity reduces grazing risk in a marine diatom. *Limnol. Oceanogr.* 57, 318–324. doi: 10.4319/lo.2012.57.1.0318

Bienfang, P. K. (1981). Sinking rates of heterogeneous, temperate phytoplankton populations. *J. Plankton Res.* 3, 235–253. doi: 10.1093/plankt/3.2.235

Bochdansky, A. B., and Herndl, G. J. (1992). Ecology of amorphous aggregations (marine snow) in the Northern Adriatic Sea. 111. Zooplankton interactions with marine snow. *Mar. Ecol. Prog. Ser.* 87, 135–146. doi: 10.3354/meps087135

Bochdansky, A. B., Puskaric, S., and Herndl, G. J. (1995). Influence of zooplankton grazing on free dissolved enzymes in the sea. *Mar. Ecol. Prog. Ser.* 121, 53–63. doi: 10.3354/meps121053

Bode, M., Koppelmann, R., Teuber, L., Hagen, W., and Auel, H. (2018). Carbon budgets of mesozooplankton copepod communities in the Eastern Atlantic Ocean-regional and vertical patterns between 24°N and 21°S. *Glob. Biogeochem. Cycles* 32, 840–857. doi: 10.1029/2017GB005807

Boersma, M., Wesche, A., and Hirche, H.-J. (2014). Predation of calanoid copepods on their own and other copepods' offspring. *Mar. Biol.* 161, 733–743. doi: 10.1007/s00227-013-2373-2377

Bollens, S. M., and Frost, B. W. (1989a). Predator-induced diet vertical migration in a planktonic copepod. *J. Plankton Res.* 11, 1047–1065. doi: 10.1093/plankt/11.5.1047

Bollens, S. M., and Frost, B. W. (1989b). Zooplanktivorous fish and variable diel vertical migration in the marine planktonic copepod *Calanus pacificus*. *Limnol. Oceanogr.* 34, 1072–1083. doi: 10.4319/lo.1989.34.6.1072

Bollens, S. M., and Frost, B. W. (1991). Diel vertical migration in zooplankton: rapid individual response to predators. *J. Plankton Res.* 13, 1359–1365. doi: 10.1093/plankt/13.6.1359

Bollens, S. M., and Stearns, D. E. (1992). Predator-induced changes in the diel feeding cycle of a planktonic copepod. *J. Exp. Mar. Biol. Ecol.* 156, 179–186. doi: 10.1016/0022-0981(92)90244-90245

Bonnet, D., Titelman, J., and Harris, R. (2004). Calanus the cannibal. *J. Plankton Res.* 26, 937–948. doi: 10.1093/plankt/fbh087

Boyd, P. W., and Trull, T. W. (2007). Understanding the export of biogenic particles in oceanic waters: is there consensus? *Prog. Oceanogr.* 72, 276–312. doi: 10.1016/j.pocean.2006.10.007

Brierley, A. S. (2014). Diel vertical migration. *Curr. Biol.* 24, R1074–R1076. doi: 10.1016/j.cub.2014.08.054

Burd, A. B., and Jackson, G. A. (2009). Particle aggregation. *Ann. Rev. Mar. Sci.* 1, 65–90.

Capriulo, G. M., Smith, G., Troy, R., Wikfors, G. H., Pellet, J., and Yarish, C. (2002). The planktonic food web structure of a temperate zone estuary, and its alteration due to eutrophication. *Nutr. Eutrophicat. Estuar. Coast. Waters* 445, 263–333. doi: 10.1007/978-94-017-2464-7_23

Cavan, E. L., Giering, S. L. C., Wolff, G. A., Trimmer, M., and Sanders, R. (2018). Alternative particle formation pathways in the eastern tropical north pacific's biological carbon pump. *J. Geophys. Res.* 123, 2198–2211. doi: 10.1029/2018JG004392

Cavan, E. L., Henson, S. A., Belcher, A., and Sanders, R. (2017). Role of zooplankton in determining the efficiency of the biological carbon pump. *Biogeosciences* 14, 177–186. doi: 10.5194/bg-14-177-2017

Cavan, E. L., Moigne, F. A. C. L., Poulton, A. J., Tarling, G. A., Ward, P., Daniels, C. J., et al. (2015). Attenuation of particulate organic carbon flux in the Scotia Sea, Southern Ocean, is controlled by zooplankton fecal pellets. *Geophys. Res. Lett.* 42, 821–830. doi: 10.1002/2014GL062744

Chandrasekaran, R., Barra, L., Carillo, S., Caruso, T., Corsaro, M. M., Dal Piaz, F., et al. (2014). Light modulation of biomass and macromolecular composition of the diatom *Skeletonema marinoi*. *J. Biotechnol.* 192, 114–122. doi: 10.1016/j.jbiotec.2014.10.016

Cisternas-Novoa, C., Lee, C., and Engel, A. (2015). Transparent exopolymer particles (TEP) and Coomassie stainable particles (CSP): differences between their origin and vertical distributions in the ocean. *Mar. Chem.* 175, 56–71. doi: 10.1016/j.marchem.2015.03.009

Cisternas-Novoa, C., Lee, C., Tang, T., de Jesus, R., and Engel, A. (2019). Effects of higher CO2 and temperature on exopolymer particle content and physical properties of marine aggregates. *Front. Mar. Sci.* 5:500. doi: 10.3389/fmars.2018.00500

Cole, M., Lindeque, P. K., Fileman, E., Clark, J., Lewis, C., Halsband, C., et al. (2016). Microplastics alter the properties and sinking rates of zooplankton faecal pellets. *Environ. Sci. Technol.* 50, 3239–3246. doi: 10.1021/acs.est.5b05905

Conover, R. J. (1966). Assimilation of organic matter by zooplankton. *Limnol. Oceanogr.* 11, 338–345. doi: 10.4319/lo.1966.11.3.0338

Conover, R. J., Durvasula, R., Roy, S., and Wang, R. (1986). Probable loss of chlorophyll-derived pigments during passage through the gut of zooplankton, and some of the consequences. *Limnol. Oceanogr.* 31, 878–886. doi: 10.4319/lo.1986.31.4.0878

Conway, D. V. P. (2006). *Identification of the Copepodite Developmental Stages of Twenty-Six North Atlantic Copepods*. Plymouth: Marine Biological Association of the United Kingdom.

Conway, H. L., Harrison, P. J., and Davis, C. O. (1976). Marine diatoms grown in chemostats under silicate or ammonium limitation. II. Transient response of Skeletonema costatum to a single addition of the limiting nutrient. *Mar. Biol.* 35, 187–199. doi: 10.1007/bf00390940

Dagg, M. J. (1993). Sinking particles as a possible source of nutrition for the large calanoid copepod *Neocalanus cristatus* in the subarctic Pacific Ocean. *Deep Sea Res. Part I Oceanogr. Res. Pap.* 40, 1431–1445. doi: 10.1016/0967-0637(93)90121-I

Dam, H. G., and Peterson, W. T. (1988). The effect of temperature on the gut clearance rate constant of planktonic copepods. *J. Exp. Mar. Biol. Ecol.* 123, 1–14. doi: 10.1016/0022-0981(88)90105-90100

Darnis, G., Barber, D. G., and Fortier, L. (2008). Sea ice and the onshore–offshore gradient in pre-winter zooplankton assemblages in southeastern Beaufort Sea. *J. Mar. Syst.* 74, 994–1011. doi: 10.1016/j.jmarsys.2007.09.003

Darnis, G., Robert, D., Pomerleau, C., Link, H., Archambault, P., Nelson, R. J., et al. (2012). Current state and trends in canadian Arctic marine ecosystems: II. heterotrophic food web, pelagic-benthic coupling, and biodiversity. *Clim. Chang.* 115, 179–205. doi: 10.1007/s10584-012-0483-488

de Melo Júnior, M., Miyashita, L. K., Silva, N. J., Gaeta, S. A., and Lopes, R. M. (2013). Reproductive traits of *Euterpina acutifrons* in a coastal area of Southeastern Brazil. *Mar. Ecol.* 34, 363–372. doi: 10.1111/maec.12041

Denis, J., Vincent, D., Antajan, E., Vallet, C., Mestre, J., Lefebvre, V., et al. (2018). Gut fluorescence technique to quantify pigment feeding in downs herring larvae. *Mar. Ecol. Prog. Ser.* 607, 129–142. doi: 10.3354/meps12775

Díaz, E. R., Kraufvelin, P., and Erlandsson, J. (2012). Combining gut fluorescence technique and spatial analysis to determine *Littorina littorea* grazing dynamics in nutrient-enriched and nutrient-unenriched littoral mesocosms. *Mar. Biol.* 159, 837–852. doi: 10.1007/s00227-011-1860-y

Dilling, L., and Alldredge, A. L. (2000). Fragmentation of marine snow by swimming macrozooplankton: a new process impacting carbon cycling in the sea. *Deep Sea Res. Part I Oceanogr. Res. Pap.* 47, 1227–1245. doi: 10.1016/s0967-0637(99)00105-3

Dilling, L., and Brzezinski, M. A. (2004). Quantifying marine snow as a food choice for zooplankton using stable silicon isotope tracers. *J. Plankton Res.* 26, 1105–1114. doi: 10.1093/plankt/fbh103

Dilling, L., Wilson, J., Steinberg, D., and Alldredge, A. (1998). Feeding by the euphausiid *Euphausia pacifica* and the copepod *Calanus pacificus* on marine snow. *Mar. Ecol. Prog. Ser.* 170, 189–201. doi: 10.3354/meps170189

Durbin, E. G., and Campbell, R. G. (2007). Reassessment of the gut pigment method for estimating in situ zooplankton ingestion. *Mar. Ecol. Prog. Ser.* 331, 305–307.

Engel, A. (2000). The role of transparent exopolymer particles (TEP) in the increase in apparent particle stickiness (α) during the decline of a diatom bloom. *J. Plankton Res.* 22, 485–497. doi: 10.1093/plankt/22.3.485

Fernández-Méndez, M., Wenzhöfer, F., Peeken, I., Sørensen, H. L., Glud, R. N., and Boetius, A. (2014). Composition, buoyancy regulation and fate of ice algal aggregates in the central Arctic Ocean. *PLoS One* 9:e107452. doi: 10.1371/journal.pone.0107452

Fileman, E., Smith, T., and Harris, R. (2007). Grazing by *Calanus helgolandicus* and Para-*Pseudocalanus* spp. on phytoplankton and protozooplankton during the spring bloom in the Celtic Sea. *J. Exp. Mar. Biol. Ecol.* 348, 70–84. doi: 10.1016/j.jembe.2007.04.003

Frost, B. W. (1972). Effects of size and concentration of food of the particles on the feeding behavior marine planktonic copepod *Calanus Pacificus*. *Limnol. Oceanogr.* 17, 805–815. doi: 10.4319/lo.1972.17.6.0805

Gaonkar, C. A., and Anil, A. C. (2012). Gut fluorescence analysis of barnacle larvae: an approach to quantify the ingested food. *Estuar. Coast. Shelf Sci.* 111, 147–150. doi: 10.1016/j.ecss.2012.07.005

Gärdes, A., Iversen, M. H., Grossart, H.-P., Passow, U., and Ullrich, M. S. (2011). Diatom-associated bacteria are required for aggregation of *Thalassiosira weissflogii*. *ISME J.* 5, 436–445. doi: 10.1038/ismej.2010.145

Giering, S. L. C., Sanders, R., Martin, A. P., Henson, S. A., Riley, J. S., Marsay, C. M., et al. (2017). Particle flux in the oceans: challenging the steady state assumption: challenging the steady state assumption. *Glob. Biogeochem. Cycles* 31, 159–171. doi: 10.1002/2016GB005424

Goldthwait, S., Yen, J., Brown, J., and Alldredge, A. (2004). Quantification of marine snow fragmentation by swimming euphausiids. *Limnol. Oceanogr.* 49, 940–952. doi: 10.4319/lo.2004.49.4.0940

Goldthwait, S. A., Carlson, C. A., Henderson, G. K., and Alldredge, A. L. (2005). Effects of physical fragmentation on remineralization of marine snow. *Mar. Ecol. Prog. Ser.* 305, 59–65. doi: 10.3354/meps305059

González-Fernández, C., Toullec, J., Lambert, C., Le Goïc, N., Seoane, M., Moriceau, B., et al. (2019). Do transparent exopolymeric particles (TEP) affect the toxicity of nanoplastics on *Chaetoceros neogracile*? *Environ. Pollut.* 250, 873–882. doi: 10.1016/j.envpol.2019.04.093

Gorgues, T., Aumont, O., and Memery, L. (2019). Simulated changes in the particulate carbon export efficiency due to diel vertical migration of zooplankton in the North Atlantic. *Geophys. Res. Lett.* 46, 5387–5395. doi: 10.1029/2018gl081748

Gorsky, G., Chrétiennot-Dinet, M. J., Blanchot, J., and Palazzoli, I. (1999). Picoplankton and nanoplankton aggregation by appendicularians: Fecal pellet contents of *Megalocercus huxleyi* in the equatorial Pacific. *J. Geophys. Res.* 104, 3381–3390. doi: 10.1029/98JC01850

Grebner, W., Berglund, E. C., Berggren, F., Eklund, J., Harðadóttir, S., Andersson, M. X., et al. (2018). Induction of defensive traits in marine plankton-new copepodamide structures: New copepodamide structures. *Limnol. Oceanogr.* 64, 820–831. doi: 10.1002/lno.11077

Green, E. P., and Dagg, M. J. (1997). Mesozooplankton associations with medium to large marine snow aggregates in the northern Gulf of Mexico. *J. Plankton Res.* 19, 435–447. doi: 10.1093/plankt/19.4.435

Greene, C. H. (1988). Foraging tactics and prey-selection patterns of omnivorous and carnivorous calanoid copepods. *Hydrobiologia* 167, 295–302. doi: 10.1007/978-94-009-3103-9_29

Grossart, H.-P., Czub, G., and Simon, M. (2006). Algae–bacteria interactions and their effects on aggregation and organic matter flux in the sea. *Environ. Microbiol.* 8, 1074–1084. doi: 10.1111/j.1462-2920.2006.00999.x

Guidi, L., Gorsky, G., Claustre, H., Miquel, J. C., Picheral, M., and Stemmann, L. (2008). Distribution and fluxes of aggregates> 100 μm in the upper kilometer of the South-Eastern Pacific. *Biogeosciences* 5, 1361–1372. doi: 10.5194/bg-5-1361-2008

Guidi, L., Legendre, L., Reygondeau, G., Uitz, J., Stemmann, L., and Henson, S. A. (2015). A new look at ocean carbon remineralization for estimating deepwater sequestration: Ocean remineralization and sequestration. *Glob. Biogeochem. Cycles* 29, 1044–1059. doi: 10.1002/2014GB005063

Guidi, L., Stemmann, L., Legendre, L., Picheral, M., Prieur, L., and Gorsky, G. (2007). Vertical distribution of aggregates (> 110 μm) and mesoscale activity in the northeastern Atlantic: effects on the deep vertical export of surface carbon. *Limnol. Oceanogr.* 52, 7–18. doi: 10.4319/lo.2007.52.1.0007

Hansen, B., Bjornsen, P. K., and Hansen, P. J. (1994). The size ratio between planktonic predators and their prey. *Limnol. Oceanogr.* 39, 395–403. doi: 10.4319/lo.1994.39.2.0395

Henson, S. A., Sanders, R., and Madsen, E. (2012). Global patterns in efficiency of particulate organic carbon export and transfer to the deep ocean. *Glob. Biogeochem. Cycles* 26:GB1028. doi: 10.1029/2011GB004099

Hernández-León, S., Putzeys, S., Almeida, C., Bécognée, P., Marrero-Díaz, A., Arístegui, J., et al. (2019). Carbon export through zooplankton active flux in the Canary Current. *J. Mar. Syst.* 189, 12–21. doi: 10.1016/j.jmarsys.2018.09.002

Hillebrand, H., Dürselen, C.-D., Kirschtel, D., Pollingher, U., and Zohary, T. (1999). Biovolume calculation for pelagic and benthic microalgae. *J. Phycol.* 35, 403–424. doi: 10.1046/j.1529-8817.1999.3520403.x

Huntley, M. (1981). Nonselective, nonsaturated feeding by three calanoid copepod species in the Labrador Sea1. *Limnol. Oceanogr.* 26, 831–842. doi: 10.4319/lo.1981.26.5.0831

Irigoien, X., Head, R. N., Harris, R. P., Cummings, D., Harbour, D., and Meyer-Harms, B. (2000). Feeding selectivity and egg production of *Calanus helgolandicus* in the english channel. *Limnol. Oceanogr.* 45, 44–54. doi: 10.4319/lo.2000.45.1.0044

Iversen, M. H., Nowald, N., Ploug, H., Jackson, G. A., and Fischer, G. (2010). High resolution profiles of vertical particulate organic matter export off cape blanc, mauritania: degradation processes and ballasting effects. *Deep Sea Res. Part I Oceanogr. Res. Pap.* 57, 771–784. doi: 10.1016/j.dsr.2010.03.007

Iversen, M. H., and Poulsen, L. K. (2007). Coprorhexy, coprophagy, and coprochaly in the copepods *Calanus helgolandicus*, *Pseudocalanus elongatus*, and *Oithona similis*. *Mar. Ecol. Prog. Ser.* 350, 79–89. doi: 10.1021/acs.est.5b05905

Jackson, G. A. (1990). A model of the formation of marine algal flocs by physical coagulation processes. *Deep Sea Res. Part A Oceanogr. Res. Pap.* 37, 1197–1211. doi: 10.1016/0198-0149(90)90038-w

Jackson, G. A. (2015). Coagulation in a rotating cylinder: coagulation in a rotating tank. *Limnol. Oceanogr. Methods* 13:e10018. doi: 10.1002/lom3.10018

Jiang, H., and Kiørboe, T. (2011a). Propulsion efficiency and imposed flow fields of a copepod jump. *J. Exp. Biol.* 214, 476–486. doi: 10.1242/jeb.049288

Jiang, H., and Kiørboe, T. (2011b). The fluid dynamics of swimming by jumping in copepods. *J. R. Soc. Inter.* 8, 1090–1103. doi: 10.1098/rsif.2010.0481

Jiang, H., and Osborn, T. R. (2004). Hydrodynamics of copepods: a review. *Surv. Geophys.* 25, 339–370. doi: 10.1093/icb/icv051

Jin, X., Gruber, N., Dunne, J. P., Sarmiento, J. L., and Armstrong, R. A. (2006). Diagnosing the contribution of phytoplankton functional groups to the production and export of particulate organic carbon, CaCO2, and opal from global nutrient and alkalinity distributions: diagnosing phytoplankton functional groups. *Glob. Biogeochem. Cycles* 20:GB2015.

Kiørboe, T. (1997). Small-scale turbulence, marine snow formation, and planktivorous feeding. *Sci. Mar.* 61, 141–158.

Kiørboe, T. (2000). Colonization of marine snow aggregates by invertebrate zooplankton: abundance, scaling, and possible role. *Limnol. Oceanogr.* 45, 479–484. doi: 10.4319/lo.2000.45.2.0479

Kiørboe, T. (2011). How zooplankton feed: mechanisms, traits and trade-offs. *Biol. Rev.* 86, 311–339. doi: 10.1111/j.1469-185X.2010.00148.x

Kiørboe, T., Saiz, E., Tiselius, P., and Andersen, K. H. (2018). Adaptive feeding behavior and functional responses in zooplankton. *Limnol. Oceanogr.* 63, 308–321. doi: 10.1002/lno.10632

Komar, P. D., Morse, A. P., Small, L. F., and Fowler, S. W. (1981). An analysis of sinking rates of natural copepod and euphausiid fecal pellets 1. *Limnol. Oceanogr.* 26, 172–180. doi: 10.4319/lo.1981.26.1.0172

Koski, M., Boutorh, J., and de la Rocha, C. (2017). Feeding on dispersed vs. aggregated particles: the effect of zooplankton feeding behavior on vertical flux. *PLoS One* 12:e0177958. doi: 10.1371/journal.pone.0177958

Koski, M., Kiørboe, T., and Takahashi, K. (2005). Benthic life in the pelagic: aggregate encounter and degradation rates by pelagic harpacticoid copepods. *Limnol. Oceanogr.* 50, 1254–1263. doi: 10.4319/lo.2005.50.4.1254

Koski, M., Møller, E. F., Maar, M., and Visser, A. W. (2007). The fate of discarded appendicularian houses: degradation by the copepod, *Microsetella norvegica*, and other agents. *J. Plankton Res.* 29, 641–654. doi: 10.1093/plankt/fbm046

Lalande, C., Moriceau, B., Leynaert, A., and Morata, N. (2016). Spatial and temporal variability in export fluxes of biogenic matter in *Kongsfjorden*. *Polar Biol.* 39, 1725–1738. doi: 10.1007/s00300-016-1903-4

Lampitt, R. S., Salter, I., de Cuevas, B. A., Hartman, S., Larkin, K. E., and Pebody, C. A. (2010). Long-term variability of downward particle flux in the deep northeast Atlantic: causes and trends. *Deep Sea Res. Part II Top. Stud. Oceanogr.* 57, 1346–1361. doi: 10.1016/j.dsr2.2010.01.011

Lampitt, R. S., Wishner, K. F., Turley, C. M., and Angel, M. V. (1993). Marine snow studies in the Northeast Atlantic Ocean: distribution, composition and role as a food source for migrating plankton. *Mar. Biol.* 116, 689–702. doi: 10.1007/bf00355486

Laurenceau-Cornec, E., Trull, T. W., Davies, D. M., Bray, S. G., Doran, J., Planchon, F., et al. (2015). The relative importance of phytoplankton aggregates and zooplankton fecal pellets to carbon export: insights from free-drifting sediment trap deployments in naturally iron-fertilised waters near the Kerguelen Plateau. *Biogeosciences* 12, 1007–1027. doi: 10.5194/bg-12-1007-2015

Lombard, F., Guidi, L., and Kiørboe, T. (2013a). Effect of type and concentration of ballasting particles on sinking rate of marine snow produced by the Appendicularian *Oikopleura dioica*. *PLoS One* 8:e75676. doi: 10.1371/journal.pone.0075676

Lombard, F., Koski, M., and Kiørboe, T. (2013b). Copepods use chemical trails to find sinking marine snow aggregates. *Limnol. Oceanogr.* 58, 185–192. doi: 10.4319/lo.2013.58.1.0185

Lombard, F., and Kiørboe, T. (2010). Marine snow originating from appendicularian houses: age-dependent settling characteristics. *Deep Sea Res. Part I Oceanogr. Res. Pap.* 57, 1304–1313. doi: 10.1016/j.dsr.2010.06.008

Long, M., Moriceau, B., Gallinari, M., Lambert, C., Huvet, A., Raffray, J., and Soudant, P. (2015). Interactions between microplastics and phytoplankton aggregates: impact on their respective fates. *Mar. Chem.* 175, 39–46. doi: 10.1016/j.marchem.2015.04.003

Lópes, R. M., Dam, H. G., Aquino, N. A., Monteiro-Ribas, W., and Rull, L. (2007). Massive egg production by a salp symbiont, the poecilostomatoid copepod Sapphirina angusta Dana, 1849. *J. Exp. Mar. Biol. Ecol.* 348, 145–153. doi: 10.1016/j.jembe.2007.04.005

Mackas, D., and Bohrer, R. (1976). Fluorescence analysis of zooplankton gut contents and an investigation of diel feeding patterns. *J. Exp. Mar. Biol. Ecol.* 25, 77–85. doi: 10.1016/0022-0981(76)90077-0

Maiti, K., Charette, M. A., Buesseler, K. O., and Kahru, M. (2013). An inverse relationship between production and export efficiency in the Southern Ocean. *Geophys. Res. Lett.* 40, 1557–1561. doi: 10.1002/grl.50219

Malej, A., and Harris, R. P. (1993). Inhibition of copepod grazing by diatom exudates: a factor in the development of mucus aggregates? *Mar. Ecol. Prog. Ser.* 96, 33–42. doi: 10.3354/meps096033

Mari, X., Rassoulzadegan, F., Brussaard, C. P., and Wassmann, P. (2005). Dynamics of transparent exopolymeric particles (TEP) production by Phaeocystis globosa under N- or P-limitation: a controlling factor of the retention/export balance. *Harmful algae* 4, 895–914. doi: 10.1016/j.hal.2004.12.014

Mauchline, J. (1998). "Biology of calanoid copepods," in *The Advances in Marine Biology*, eds J. Blaxter, B. Douglas, and P. Tyler, (Cambridge, MA: Academic Press).

Mopper, K., Zhou, J., Sri Ramana, K., Passow, U., Dam, H. G., and Drapeau, D. (1995). The role of surface-active carbohydrates in the flocculation of a diatom bloom in a mesocosm. *Deep Sea Res. Part II Top. Stud. Oceanogr.* 42, 47–73. doi: 10.1016/0967-0645(95)00004-A

Moriceau, B., Garvey, M., Passow, U., and Ragueneau, O. (2007). Evidence for reduced biogenic silica dissolution rates in diatom aggregates. *Mar. Ecol. Prog. Ser.* 333, 129–142. doi: 10.3354/meps333129

Moriceau, B., Iversen, M. H., Gallinari, M., Evertsen, A.-J. O., Le Goff, M., Beker, B., et al. (2018). Copepods boost the production but reduce the carbon export efficiency by diatoms. *Front. Mar. Sci.* 5:82. doi: 10.3389/fmars.2018.00082

Norici, A., Bazzoni, A. M., Pugnetti, A., Raven, J. A., and Giordano, M. (2011). Impact of irradiance on the C allocation in the coastal marine diatom *Skeletonema marinoi* sarno and zingone. *Plant Cell Environ.* 34, 1666–1677. doi: 10.1111/j.1365-3040.2011.02362.x

Nowald, N., Iversen, M. H., Fischer, G., Ratmeyer, V., and Wefer, G. (2015). Time series of in-situ particle properties and sediment trap fluxes in the coastal upwelling filament off Cape Blanc Mauritania. *Prog. Oceanogr.* 137, 1–11. doi: 10.1016/j.pocean.2014.12.015

Orefice, I., Chandrasekaran, R., Smerilli, A., Corato, F., Caruso, T., Casillo, A., et al. (2016). Light-induced changes in the photosynthetic physiology and biochemistry in the diatom *Skeletonema marinoi*. *Algal Res.* 17, 1–13. doi: 10.1016/j.algal.2016.04.013

Pakhomov, E. A., Perissinotto, R., and McQuaid, C. D. (1996). Prey composition and daily rations of myctophid fishes in the Southern Ocean. *Mar. Ecol. Prog. Ser.* 134, 1–14. doi: 10.3354/meps134001

Parsons, T. R., Maita, Y., and Lalli, C. M. (1984). "Determination of chlorophylls and total carotenoids: spectrophotometric method," in *A Manual of Chemical and Biological Methods For Seawater Analysis*, eds T. R. Parsons, Y. Maita, and C. M. Lalli, (Oxford: Pergamon Press), 101–112.

Passow, U. (2002). Transparent exopolymer particles (TEP) in aquatic environments. *Prog. Oceanogr.* 55, 287–333. doi: 10.1016/S0079-6611(02)00138-136

Passow, U., and Alldredge, A. L. (1995a). A dye-binding assay for the spectrophotometric measurement of transparent exopolymer particles (TEP). *Limnol. Oceanogr.* 40, 1326–1335. doi: 10.4319/lo.1995.40.7.1326

Passow, U., and Alldredge, A. L. (1995b). Aggregation of a diatom bloom in a mesocosm: the role of transparent exopolymer particles (TEP). *Deep Sea Res. Part II Top. Stud. Oceanogr.* 42, 99–109. doi: 10.1016/0967-0645(95)00006-C

Passow, U., and Carlson, C. (2012). The biological pump in a high CO2 world. *Mar. Ecol. Prog. Ser.* 470, 249–271. doi: 10.3354/meps09985

Passow, U., and De La Rocha, C. L. (2006). Accumulation of mineral ballast on organic aggregates. *Glob. Biogeochem. Cycles* 20:GB1013. doi: 10.1029/2005GB002579

Perissinotto, R., and Pakhomov, E. A. (1996). Gut evacuation rates and pigment destruction in the Antarctic krill *Euphausia superba*. *Mar. Biol.* 125, 47–54. doi: 10.1007/BF00350759

Perissinotto, R., and Pakhomov, E. A. (1998). The trophic role of the tunicate Salpa thompsoni in the Antarctic marine ecosystem. *J. Mar. Syst.* 17, 361–374. doi: 10.1016/S0924-7963(98)00049-49

Ploug, H., Terbrüggen, A., Kaufmann, A., Wolf-Gladrow, D., and Passow, U. (2010). A novel method to measure particle sinking velocity in vitro, and its comparison to three other in vitro methods. *Limnol. Oceanogr. Methods* 8, 386–393. doi: 10.4319/lom.2010.8.386

Pondaven, P., Gallinari, M., Chollet, S., Bucciarelli, E., Sarthou, G., Schultes, S., et al. (2007). Grazing-induced changes in cell wall silicification in a marine diatom. *Protist* 158, 21–28. doi: 10.1016/j.protis.2006.09.002

Prairie, J. C., Montgomery, Q. W., Proctor, K. W., and Ghiorso, K. S. (2019). Effects of phytoplankton growth phase on settling properties of marine aggregates. *J. Mar. Sci. Eng.* 7:265. doi: 10.3390/jmse7080265

Prieto, L., Sommer, F., Stibor, H., and Koeve, W. (2001). Effects of planktonic copepods on transparent exopolymeric particles (tep) abundance and size spectra. *J. Plankton Res.* 23, 515–525. doi: 10.1093/plankt/23.5.515

R Core Team (2017). *R: A Language and Environment for Statistical Computing*. Vienna: R Foundation for Statistical Computing. Available at: https://www.R-project.org/

Riebesell, U. (1991). Particle aggregation during a diatom bloom. II. Biological aspects. *Mar. Ecol. Prog. Ser.* 69, 281–291. doi: 10.3354/meps069281

Roman, M. R., and Rublee, P. A. (1980). Containment effects in copepod grazing experiments: a plea to end the black box approach1. *Limnol. Oceanogr.* 25, 982–990. doi: 10.4319/lo.1980.25.6.0982

Sarthou, G., Vincent, D., Christaki, U., Obernosterer, I., Timmermans, K. R., and Brussaard, C. P. (2008). The fate of biogenic iron during a phytoplankton bloom induced by natural fertilisation: impact of copepod grazing. *Deep Sea Res. Part II Top. Stud. Oceanogr.* 55, 734–751. doi: 10.1016/j.dsr2.2007.12.033

Sautour, B., and Castel, J. (1993). Feeding behaviour of the coastal copepod Euterpina acutifrons on small particles. *Cah. Biol. Mar.* 34, 239–251.

Schultes, S., Sourisseau, M., Le Masson, E., Lunven, M., and Marié, L. (2013). Influence of physical forcing on mesozooplankton communities at the Ushant tidal front. *J. Mar. Syst.* 109–110, S191–S202. doi: 10.1016/j.jmarsys.2011.11.025

Schuster, S., and Herndl, G. J. (1995). Formation and significance of transparent exopolymeric particles in the northern Adriatic Sea. *Mar. Ecol. Prog. Ser.* 124, 227–236. doi: 10.3354/meps124227

Selander, E., Jakobsen, H. H., Lombard, F., and Kiørboe, T. (2011). Grazer cues induce stealth behavior in marine dinoflagellates. *PNAS* 108, 4030–4034. doi: 10.1073/pnas.1011870108

Selander, E., Kubanek, J., Hamberg, M., Andersson, M. X., Cervin, G., and Pavia, H. (2015). Predator lipids induce paralytic shellfish toxins in bloom-forming algae. *PNAS* 112, 6395–6400. doi: 10.1073/pnas.1420154112

Shanks, A. L. (2002). The abundance, vertical flux, and still-water and apparent sinking rates of marine snow in a shallow coastal water column. *Cont. Shelf Res.* 22, 2045–2064. doi: 10.1016/s0278-4343(02)00015-8

Shanks, A. L., and Edmondson, E. W. (1989). Laboratory-made artificial marine snow: a biological model of the real thing. *Mar. Biol.* 101, 463–470. doi: 10.1007/bf00541648

Shanks, A. L., and Walters, K. (1997). Holoplankton, meroplankton, and meiofauna associated with marine snow. *Mar. Ecol. Prog. Ser.* 156, 75–86. doi: 10.3354/meps156075

Smerilli, A., Balzano, S., Maselli, M., Blasio, M., Orefice, I., Galasso, C., et al. (2019). Antioxidant and photoprotection networking in the coastal diatom *Skeletonema marinoi*. *Antioxidants* 8:154. doi: 10.3390/antiox8060154

Soudant, D., and Belin, C. (2018). *Trente Années D'observation Des Micro-Algues Et Des Toxines D'algues Sur Le Littoral*. Versailles: Editions Quae.

Stamieszkin, K., Pershing, A. J., Record, N. R., Pilskaln, C. H., Dam, H. G., and Feinberg, L. R. (2015). Size as the master trait in modeled copepod fecal pellet carbon flux. *Limnol. Oceanogr.* 60, 2090–2107. doi: 10.1002/lno.10156

Steinberg, D. K. (1995). Diet of copepods (*Scopalatum vorax*) associated with mesopelagic detritus (giant larvacean houses) in monterey bay, California. *Mar. Biol.* 122, 571–584. doi: 10.1007/bf00350679

Steinberg, D. K., and Landry, M. R. (2017). Zooplankton and the Ocean carbon cycle. *Ann. Rev. Mar. Sci.* 9, 413–444. doi: 10.1146/annurev-marine-010814-015924

Stemmann, L., Gorsky, G., Marty, J.-C., Picheral, M., and Miquel, J.-C. (2002). Four-year study of large-particle vertical distribution (0–1000m) in the NW Mediterranean in relation to hydrology, phytoplankton, and vertical flux. *Deep Sea Res. Part II Top. Stud. Oceanogr.* 49, 2143–2162. doi: 10.1016/S0967-0645(02)00032-32

Stemmann, L., Jackson, G. A., and Ianson, D. (2004). A vertical model of particle size distributions and fluxes in the midwater column that includes biological and physical processes—Part I: model formulation. *Deep Sea Res. Part I Oceanogr. Res. Pap.* 51, 865–884. doi: 10.1016/j.dsr.2004.03.001

Strickler, J. R. (1982). Calanoid copepods, feeding currents, and the role of gravity. *Science* 218, 158–160. doi: 10.1126/science.218.4568.158

Svensen, C., Egge, J. K., and Stiansen, J. E. (2001). Can silicate and turbulence regulate the vertical flux of biogenic matter? A mesocosm study. *Mar. Ecol. Prog. Ser.* 217, 67–80. doi: 10.3354/meps217067

Svensen, C., Nejstgaard, J. C., Egge, J. K., and Wassmann, P. (2002). Pulsing versus constant supply of nutrients (N, P and Si): effect on phytoplankton, mesozooplankton and vertical flux of biogenic matter. *Sci. Mar.* 66, 189–203. doi: 10.3989/scimar.2002.66n3189

Taucher, J., Stange, P., Algueró-Muñiz, M., Bach, L. T., Nauendorf, A., Kolzenburg, R., et al. (2018). In situ camera observations reveal major role of zooplankton in modulating marine snow formation during an upwelling-induced plankton bloom. *Prog. Oceanogr.* 164, 75–88. doi: 10.1016/j.pocean.2018.01.004

Tréguer, P., Bowler, C., Moriceau, B., Dutkiewicz, S., Gehlen, M., Aumont, O., et al. (2017). Influence of diatom diversity on the ocean biological carbon pump. *Nat. Geosci.* 11, 27–37. doi: 10.1038/s41561-017-0028-x

Turner, J. T. (2002). Zooplankton fecal pellets, marine snow and sinking phytoplankton blooms. *Aquat. Microb. Ecol.* 27, 57–102. doi: 10.3354/ame027057

Turner, J. T. (2015). Zooplankton fecal pellets, marine snow, phytodetritus and the ocean's biological pump. *Prog. Oceanogr.* 130, 205–248. doi: 10.1016/j.pocean.2014.08.005

Vargas, C. A., Tnnesson, K., Sell, A., Maar, M., Mller, E. F., Zervoudaki, T., et al. (2002). Importance of copepods versus appendicularians in vertical carbon fluxes in a Swedish fjord. *Mar. Ecol. Prog. Ser.* 241, 125–138. doi: 10.3354/meps241125

Veit-Köhler, G. (2005). Influence of biotic and abiotic sediment factors on abundance and biomass of harpacticoid copepods in a shallow Antarctic bay. *Sci. Mar.* 69, 135–145. doi: 10.3989/scimar.2005.69s2135

Vincent, D., and Hartmann, H. J. (2001). Contribution of ciliated microprotozoans and dinoflagellates to the diet of three copepod species in the Bay of Biscay. *Hydrobiologia* 443, 193–204.

Vincent, D., Slawyk, G., L'Helguen, S., Sarthou, G., Gallinari, M., Seuront, L., et al. (2007). Net and gross incorporation of nitrogen by marine copepods fed on 15N-labelled diatoms: methodology and trophic studies. *J. Exp. Mar. Biol. Ecol.* 352, 295–305. doi: 10.1016/j.jembe.2007.08.006

Wang, R., and Conover, R. J. (1986). Dynamics of gut pigment in the copepod *Temora longicornis* and the determination of in situ grazing rates. *Limnol. Oceanogr.* 31, 867–877. doi: 10.4319/lo.1986.31.4.0867

Warwick, R. M., and Gee, J. M. (1984). Community structure of estuarine meiobenthos. *Mar. Ecol. Prog. Ser.* 18, 97–111. doi: 10.1016/j.marpolbul.2016.06.041

Wilson, S. E., Steinberg, D. K., and Buesseler, K. O. (2008). Changes in fecal pellet characteristics with depth as indicators of zooplankton repackaging of particles in the mesopelagic zone of the subtropical and subarctic North Pacific Ocean. *Deep Sea Res. Part II Top. Stud. Oceanogr.* 55, 1636–1647. doi: 10.1016/j.dsr2.2008.04.019

Xiao, F., Li, X., Lam, K., and Wang, D. (2012). Investigation of the hydrodynamic behavior of diatom aggregates using particle image velocimetry. *J. Environ. Sci.* 24, 1157–1164. doi: 10.1016/S1001-0742(11)60960-60961

Yamazaki, H., and Squires, K. D. (1996). Comparison of oceanic turbulence and copepod swimming. *Mar. Ecol. Prog. Ser.* 144, 299–301. doi: 10.3354/meps144299

Yoon, W. D., Kim, S. K., and Han, K. N. (2001). Morphology and sinking velocities of fecal pellets of copepod, molluscan, euphausiid, and salp taxa in the northeastern tropical Atlantic. *Mar. Biol.* 139, 923–928. doi: 10.1007/s002270100630

Young, S., Palm, M., Grover, J. P., and McKee, D. (1997). How Daphnia cope with algae selected for inedibility in long- running microcosms. *J. Plankton Res.* 19, 391–397. doi: 10.1093/plankt/19.3.391

Conflict of Interest: The authors declare that the research was conducted in the absence of any commercial or financial relationships that could be construed as a potential conflict of interest.

The handling Editor declared a past co-authorship with one of the authors, BM.

frontiers in Marine Science

ORIGINAL RESEARCH
published: 06 December 2019
doi: 10.3389/fmars.2019.00741

On the Estimation of Zooplankton-Mediated Active Fluxes in Oxygen Minimum Zone Regions

Rainer Kiko[1,2]* *and Helena Hauss*[1]

[1] Marine Ecology, GEOMAR Helmholtz Institute for Ocean Research Kiel, Kiel, Germany, [2] Laboratoire d'Océanographie de Villefranche, Sorbonne Université, Villefranche-sur-Mer, France

In the Peruvian upwelling system, the mesopelagic oxygen minimum zone (OMZ) is the main vertically structuring feature of the pelagic habitat. Several zooplankton and nekton species undertake diel vertical migrations (DVMs) into anoxic depths. It has been argued that these migrations contribute substantially to the oxygen consumption and release of dissolved compounds (in particular ammonium) in subsurface waters. However, metabolic suppression as a response to low ambient oxygen partial pressure (pO_2) has not been accounted for in these estimates. Here, we present estimates of zooplankton- and nekton-mediated oxygen consumption and ammonium release based on vertically stratified net hauls (day/night, upper 1,000 m). Samples were scanned, followed by image analysis and size-/taxon-specific estimation of metabolic rates of all identified organisms as a function of their biomass as well as ambient temperature and pO_2. The main crustacean migrants were euphausiids (mainly *E. mucronata*) on offshore stations and the commercially exploited squat lobster *Pleuroncodes monodon* on the upper shelf, where it often undertakes migration to the seafloor during the day. Correction for metabolic suppression results in a substantial reduction of both respiration and ammonium excretion within the OMZ core. Ignoring this mechanism leads to a 10-fold higher estimate of DVM-mediated active export of carbon by respiration to below 100 m depth at deep-water stations. The DVM-mediated release of ammonium by euphausiids into the 200–400 m depth layer ranges between 0 and 36.81 $\mu mol\ NH_4\ m^{-2}\ d^{-1}$, which is insufficient to balance published estimates of ammonium uptake rates due to anammox. It seems critical to account for the modulation of zooplankton metabolic activity at low oxygen in order to correctly represent the contribution of migrating species to the biological pump.

Keywords: zooplankton, Humboldt current, export flux, krill, biological carbon pump

Edited by:
Sanjeev Kumar, Physical Research Laboratory, India

Reviewed by:
John Patrick Dunne, Geophysical Fluid Dynamics Laboratory (GFDL), United States
Jyothibabu Retnamma, Council of Scientific and Industrial Research, India

***Correspondence:**
Rainer Kiko
rainer.kiko@obs-vlfr.fr

Specialty section:
This article was submitted to Marine Biogeochemistry, a section of the journal Frontiers in Marine Science

Received: *20 May 2019*
Accepted: *14 November 2019*
Published: *06 December 2019*

Citation:
Kiko R and Hauss H (2019) On the Estimation of Zooplankton-Mediated Active Fluxes in Oxygen Minimum Zone Regions. Front. Mar. Sci. 6:741. doi: 10.3389/fmars.2019.00741

1. INTRODUCTION

Zooplankton organisms occupy an important role in pelagic ecosystems as they provide the link between primary and tertiary trophic levels and to a large extent shapes elemental cycles. Depth-integrated mesozooplankton carbon ingestion and respiration of primary production in the global open ocean is estimated at 34–63 and 17–32%, respectively (Hernández-León and Ikeda, 2005). Zooplankton organisms feed on all kinds of small particulate matter (e.g., phytoplankton,

detritus, other zooplankton) and egested fecal pellets contribute substantially to the passive sinking flux out of the surface layer.

The diel vertical migration (DVM) of zooplankton and micronekton is the largest concerted movement of animal biomass on earth. In the most common form, zooplankton organisms actively feed in the productive euphotic zone during the night and migrate down to a few hundred meters depth during the day to mainly hide from visual predation (Lampert, 1989). These DVMs result in the active export of organic and inorganic matter from the surface layer as zooplankton organisms excrete, defecate, respire and are preyed upon at depth (e.g., Longhurst et al., 1990). The daytime depth is strongly dependent on water transparency and is deepest in the oligotrophic blue ocean. In the Peruvian upwelling system, one of the most productive regions on the planet, microbial degradation of sinking organic matter (Kalvelage et al., 2015) and respiration by metazoans, in concert with sluggish ventilation (Czeschel et al., 2011) have led to the formation of a permanent oxygen minimum zone (OMZ) with often virtually anoxic oxygen concentrations in its core (e.g., Revsbech et al., 2009). The core of this midwater OMZ coincides with the daytime depth of many DVM species as indicated by large scale analysis of acoustic backscatter data (Bianchi et al., 2013, 2014). The upper oxycline, which is located directly below the mixed layer, is considered the single most important vertically structuring feature of the pelagic habitat in the Humboldt Current Ecosystem (Chavez and Messié, 2009; Bertrand et al., 2010). At the same time, oxygen levels play an essential role in nutrient cycling. Under anoxic conditions, N loss processes (denitrification and anammox, Lam et al., 2009) result in a nitrogen deficit in the upwelling regions. Bianchi and Mislan (2016) suggested that zooplankton DVM is a major contributor to providing dissolved ammonium to the OMZ by excretion at the daytime depth. However, they did not account for changes in zooplankton metabolism at low oxygen levels.

Zooplankton organisms ultimately rely on aerobic respiration. They developed different, species-specific hypoxia tolerance thresholds (Childress and Seibel, 1998) and some tolerate anoxia for prolonged periods of time. OMZs therefore shape the distribution of zooplankton within the pelagic ecosystem (e.g., Saltzman and Wishner, 1997; Wishner et al., 1998; Auel and Verheye, 2007). Off Peru, only few metazoan species are able to tolerate anoxic conditions in the OMZ core. These include the endemic krill species *Euphausia mucronata* (Kiko et al., 2016) and the squat lobster *Pleuroncodes monodon* (Kiko et al., 2015). They achieve this by downregulation of their aerobic metabolism. As they "hold their breath," oxygen consumption is not measurable, but also ammonium excretion is substantially reduced (Kiko et al., 2015, 2016). Up to now, this metabolic suppression has not been accounted for in estimations of DVM-mediated fluxes.

Here, we examine the vertical distribution and migration of zooplankton in the upper 1,000 m off Peru. We develop a new method to include the impact of low oxygen levels on metabolic function to better constrain zooplankton impacts on the carbon, nitrogen and oxygen budget of the area.

2. MATERIALS AND METHODS

2.1. Field Sampling

Data and samples were collected during RV Meteor cruise 93 to the Peruvian upwelling region in February and March 2013 (2013/02/06 to 2013/03/10, Callao/Peru to Cristobal/Panama), At the time of the cruise, southeasterly winds prevailed ($1 - 9\ m\ s^{-1}$, Thomsen et al., 2016), resulting in nutrient upwelling typical of austral summer conditions. At five stations, we took depth-specific mesozooplankton samples conducting 10 vertical hauls ($1\ m\ s^{-1}$) with a Hydrobios MultiNet Maxi (0.50 m^2 mouth opening, 333 μm mesh size, 9 nets). During each station occupation, a day haul and a night haul were obtained within 24 h and in very close proximity (average distance 0.15 km, range 0–0.7 km) to each other, representing a pair of day-night hauls for the assessment of diel vertical migration patterns. Sampling was avoided during local dusk or dawn ±1 h. The day hauls were brought on deck ±5 h of local solar noon, whereas the night hauls were brought on deck ±4 h of local midnight (see **Figure 1** for sampling locations and **Table 1** for further location and time information for each haul used). Sampling depths were 1,000–600, 600–400, 400–200, 200–100, 100–50, 50–30, 30–20, 20–10, and 10–0 m depth when water depth was >1,000 m. Otherwise, a finer depth resolution within these general depth steps was established. Temperature, salinity and oxygen concentration from RV Meteor cruise 93 were measured by the Physical Oceanography department at the GEOMAR Helmholtz Centre for Ocean Research Kiel and are published by Krahmann (2015). In short, a Seabird SBE 9-plus CTD on a 24-niskin rosette was deployed directly before or after the net haul. The CTD carried duplicate temperature, salinity and oxygen (optode) probes. Oxygen from the optodes was calibrated by a combination of Winkler titration (Grasshoff et al., 2009) and STOX sensor measurements (Revsbech et al., 2009). Zooplankton samples were formaldehyde-fixed on board and brought to the GEOMAR laboratory.

2.2. Zooplankton Imaging and Biomass Calculation

In the laboratory, each sample was size-fractionated (small: 333–500 μm, medium: 500–1000 μm and large: $> 1,000\ \mu m$). For the small and medium fraction, subsamples with about 1,000 zooplankton items per subsample were generated using a Motoda-Splitter, whereas the entire large fraction was used for further analysis. The plankton items contained in each fraction were distributed and separated on a 20*30 cm glass tray and the glass tray scanned using an Epson perfection V750 pro flatbed scanner. Scans were 8bit grayscale, 2,400 dpi images (tagged image file format; *.tif). Object segmentation was conducted using Zooprocess (Gorsky et al., 2010) and taxonomic units were assigned automatically using Plankton Identifier or the prediction options in EcoTaxa (Picheral et al., 2019). Assignments were thereafter corrected manually on the EcoTaxa platform. Analysis of the biomass-size spectrum showed that organisms with an equivalent spherical diameter of 12.41 mm were not quantitatively sampled. Therefore, this value was chosen as a digital cut-off in our analysis, meaning that all objects larger then

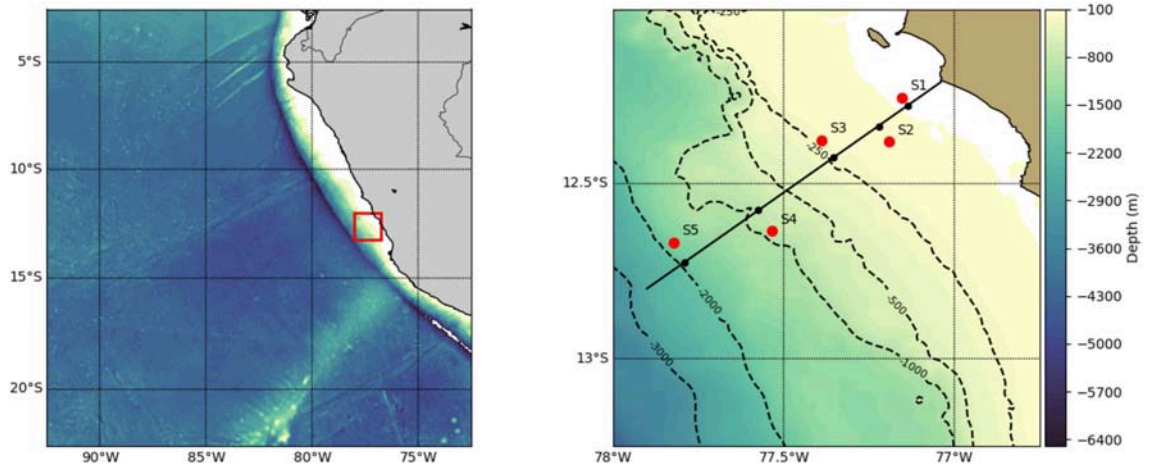

FIGURE 1 | Map of the Eastern Tropical South Pacific **(left)** with a red rectangle indicating study area **(right)** and red dots indicating sites (S1–S5). At each of the five sampling sites, a pair of day and night hauls were obtained.

TABLE 1 | Metadata for each pair of hauls used in this publication.

Pair ID (–)	Haul ID (–)	Date (–)	Time (UTC)	Lat. (°)	Lon. (°)	Noon (UTC)	Delta to noon (h)	Category (–)	In pair dist. (km)	Dist. to coast (km)	Max. depth sampled (m)
s1	mn25	2013-03-02	22:22	−12.254	−77.152	17:20	05:01	Day	0.11	12.8	70
s1	mn26	2013-03-03	02:29	−12.254	−77.153	17:20	09:08	Night	0.11	12.8	70
s2	mn02	2013-02-10	21:10	−12.38	−77.191	17:22	03:47	Day	0.0	24.2	125
s2	mn03	2013-02-11	02:58	−12.38	−77.191	17:22	09:35	Night	0.0	24.2	125
s3	mn20	2013-02-24	21:35	−12.377	−77.388	17:22	04:12	Day	0.0	41.6	210
s3	mn19	2013-02-24	07:58	−12.377	−77.388	17:22	14:35	Night	0.0	41.6	210
s4	mn05	2013-02-11	20:58	−12.639	−77.531	17:24	03:33	Day	0.69	71.0	1000
s4	mn04	2013-02-11	09:30	−12.633	−77.537	17:24	16:05	Night	0.69	71.0	1000
s5	mn14	2013-02-20	18:47	−12.668	−77.821	17:24	01:22	Day	0.0	98.5	1000
s5	mn13	2013-02-20	08:05	−12.668	−77.821	17:25	14:39	Night	0.0	98.5	1000

this size were not further considered when calculating biomass or metabolic rates. Likewise, the small fraction (333–500 μm) was not included, as preliminary analysis showed almost no DVM-activity into the OMZ in this size fraction. Taxon-specific area-to-drymass conversion factors for subtropical zooplankton (Lehette and Hernández-León, 2009) were used to calculate the dryweight of each specimen according to $dw = a * area^b$. Likewise, taxon-specific drymass to C conversion factors (Kiørboe, 2013) were used to calculate the C content of each zooplankton organism scanned. Taxonomic units and biomass conversion factors used are listed in **Table 2**. Abundance and biomass estimates are lower bounds, as some organisms sticked together, produced an undiscernable mass with detritus or in case of gelatinous organisms did not produce a clearly identifiable image due to the low contrast of the tissue. Such individuals were not included in the respective calculations.

The following categories cannot be discerned in the preserved net samples, as many of their members are either damaged by the net or the fixation and therefore do not yield quantifiable images: thaliacea, cnidaria other then calycophoran siphonophores, ctenophores, all rhizaria.

We consider the following categories to be well-conserved and constrain our analyses on these: crustacea, chaetognatha, calycophoran siphonophores, annelida, and mollusca. Fish are also well-conserved, but not included in the literature on zooplankton individual biomass estimates or metabolic rates (Lehette and Hernández-León, 2009; Kiørboe, 2013; Ikeda, 2014) we use.

2.3. Estimation of Physiological Rates—Respiration

Taxon-specific equations for biomass and temperature dependence of respiration (Ikeda, 2014) were applied to calculate the depth-specific respiration rate of each scanned crustacean specimen. A detailed description on the experimental procedure to estimate these rates is given in Ikeda (1985). The average temperature for the sampled depth layer was obtained from the concomitant CTD deployments. We applied a correction for the oxygen-dependence of respiration if the mean oxygen level for a given net was below the critical oxygen partial pressure p_{crit} of *Euphausia mucronata* and *Pleuroncodes monodon* (Kiko et al., 2015, 2016). The p_{crit} is a threshold value below which the

TABLE 2 | Conversion factors and functions used in this publication.

Group	BM exponent	BM multiplicator	Respi. factor	Excr. factor	DW to C
Copepoda	1.59	45.25	n.a.	n.a.	0.48
Amphipoda	1.51	43.9	0.416	0.262	0.34
Crustacea	1.51	43.9	0.416	0.262	0.34
Cladocera	1.51	43.9	−0.393	−1.356	0.435
Decapoda	1.51	43.9	0.631	n.a.	0.435
Euphausiacea	1.51	43.9	0.697	n.a.	0.419
Ostracoda	1.51	43.9	−0.393	−1.356	0.435
Chaetognatha	1.19	23.45	−0.448	n.a.	0.367
Ctenophora[a]	1.02	43.17	−1.257	−1.397	0.051
Siphonophorae	1.02	43.17	−0.480	−0.558	0.132
Mollusca[b]	1.54	43.38	n.a.	−0.550	0.289
Annelida	1.54	43.38	0.382	n.a.	0.37

[a] *Formula for siphonophores was used as no specific formula is given in Lehette and Hernández-León (2009).*

[b] *Formula for general mesozooplankton was used as no specific formula is given in Lehette and Hernández-León (2009). Biomass was calculated as biomass = BMmultiplicator ∗ area^{BMexponent}. Respi. factor and Excr. factor from Ikeda (2014). DW to C conversion factors from Kiørboe (2013). n.a., not applicable.*

regulation of oxygen uptake fails, resulting in a drastic metabolic reduction (Childress and Seibel, 1998). As we only have data on the p_{crit} of these two species from the Peruvian upwelling, we use the mean of these values (0.6 kPa) as a general p_{crit} for crustaceans in the region. These p_{crit} values were obtained at 13°C and in order to calculate corrected respiration rates we need to extrapolate the p_{crit} to the environmental temperatures observed. For this, we use Equation (1) by Deutsch et al. (2015):

$$\Phi = A_0 B^n \frac{pO_2}{exp(-E_0/k_B T)} \quad (1)$$

where Φ is the metabolic index as defined by Deutsch et al. (2015), A_0 is the ratio of rate coefficients for oxygen supply and metabolic rate, B is body mass, n is the difference between the allometric scalings of respiratory efficacy and resting metabolic demand, E_0 is the temperature dependence of resting metabolic demand and k_B is the Boltzmann constant. For further details regarding this calculation please consult Deutsch et al. (2015).

If $pO_2 = p_{crit}$, Φ becomes 1. It follows that the $p_{crit}x$ measured at temperature x (Tx) and the $p_{crit}z$ measured at temperature z (Tz) relate to each other in the following way:

$$\frac{p_{crit}x}{exp(-E_0/k_B Tx)} = \frac{p_{crit}z}{exp(-E_0/k_B Tz)} \quad (2)$$

If we know $p_{crit}z$ and Tz, we can solve this equation to yield $p_{crit}x$ at the required target temperature Tx:

$$p_{crit}x = p_{crit}z * exp((-E_0/k_B Tx) - (-E_0/k_B Tz)) \quad (3)$$

We use an E_0 of 0.55, which is the mean of values published for crustaceans in Deutsch et al. (2015). The E_0 values provided by Deutsch et al. (2015) range from 0.36 (*Sergestes tenuiremis*) to 0.74 (Atlantic rock crab). We assume a linear decrease of the respiration rate from the p_{crit} to zero, as we have observed that both crustaceans investigated can tolerate zero oxygen levels and do respire all oxygen if maintained in a closed bottle. Hence, we assume a constant respiration rate for oxygen levels above the extrapolated p_{crit} (calculated according to Ikeda, 2014) and a linear decrease from p_{crit} to zero pO_2. **Figure 2** delineates the general strategy of this approach. To convert oxygen respiration to carbon release, we use a respiratory quotient of 0.97 (Steinberg and Landry, 2017).

2.4. Estimation of Physiological Rates—Ammonium Excretion

Ammonium excretion at different oxygen levels was calculated using a reevaluation of the data by Kiko et al. (2016) of rates measured at 13°C and different oxygen levels for *E. mucronata*.

$$Excr_{std} = a * {pO_2}^b + c \quad (4)$$

with a = 1.275, b = 0.363, and c = 1.0e-10. This yields the excretion rate for 1 $g\ DW$ of a 0.1 $g\ DW$ standard individual in $\mu mol\ h^{-1} g^{-1}$. Division by 10 yields the rate for 0.1 $g\ DW$ of the 0.1 $g\ DW$ standard individual in $\mu mol\ h^{-1}$, so essentially the individual excretion rate.

An allometric weight adjustment according to Moloney and Field (1989) was applied using:

$$Excr = Excr_{std} * ((0.1/x)^{0.25}) \quad (5)$$

with x being the biomass of the individual in $g\ DW$. This yields the excretion rate of 0.1 $g\ DW$ of an organism with biomass x in $\mu mol\ h^{-1}$. Multiplication of this rate with the biomass x (in $g\ DW$) divided by 0.1 $g\ DW$ (biomass factor, indicates how much heavier or lighter then 0.1 the individual is) yields the excretion rate of the individual with biomass x in $\mu mol\ h^{-1}$. To scale the rates to the measured *in situ* temperature, another adjustment was applied using a Q_{10} of 2. For comparison, ammonium excretion rates were also calculated according to Ikeda (2014), which includes an adjustment for temperature, but not for oxygen. At a pO_2 of 24 kPa, both calculation methods yield almost identical results (e.g., see Kiko et al., 2016).

2.5. Calculation of Day-Night Biomass Differences and Active Fluxes

Migratory fluxes from the surface layer to below 100 m depth were calculated as the day-night difference of the integrated biomass at 100–1,000 m depth (or the bottom) to avoid artifacts due to sampling net avoidance in the surface layer at daytime (Ianson et al., 2004). A residence time at depth of 12 h was assumed to calculate metabolic rate related fluxes.

3. RESULTS

3.1. Environmental Conditions

Sea surface temperature (SST) increased from the shelf stations to the offshore stations, with 17.6°C at the innermost and 20.5°C at the outermost station, respectively (**Figure 3**). Likewise, the

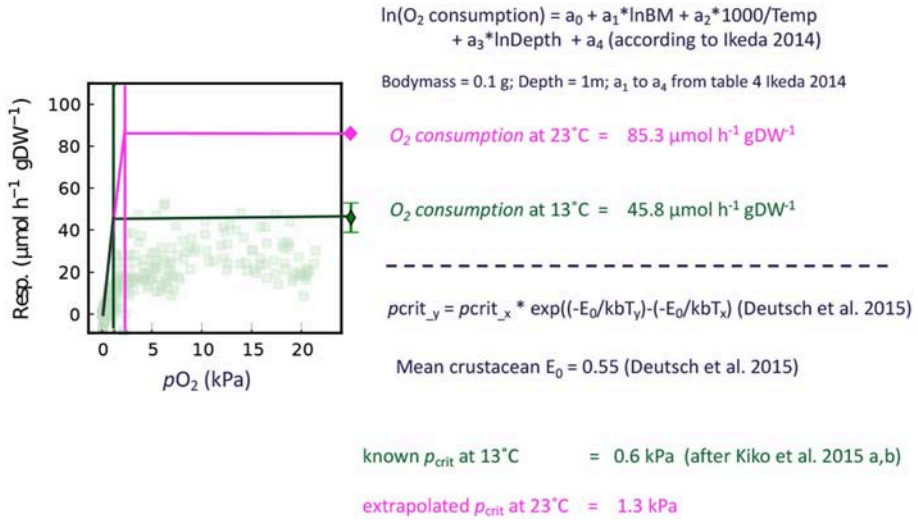

FIGURE 2 | Schematic of the respiration rate correction for environmental partial pressures below the p_{crit}. The example calculations are conducted for *Euphausiacea* and the transparent dots in the figure indicate individual respiration rate measurements of *E. mucronata* from Kiko et al. (2016).

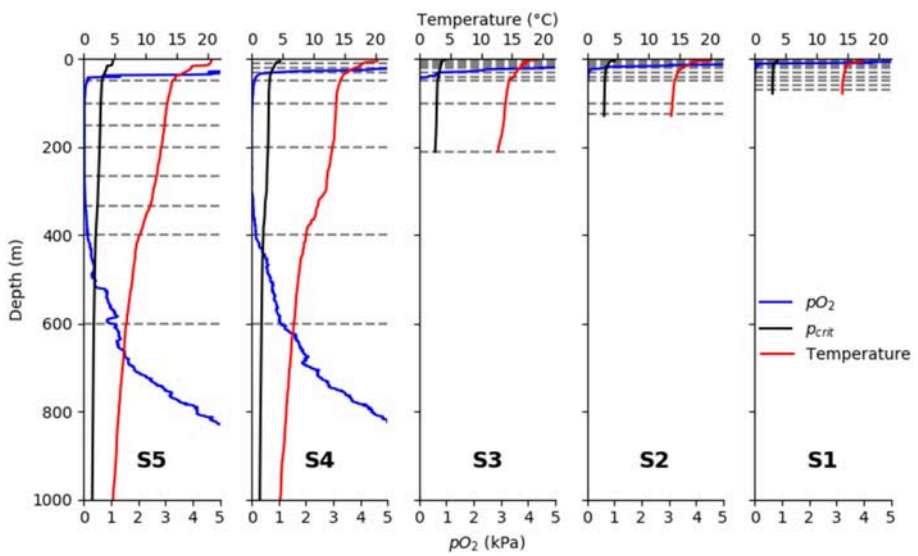

FIGURE 3 | Vertical profiles of observed pO_2 (blue), temperature (red), and p_{crit} (black) calculated after Equation (3). From left to right: S5, S4, S3, S2, S1 horizontal gray lines denote sampling intervals of the multinet.

thermo- and oxycline depths decreased from shelf to offshore. The oxygen concentration dropped to $< 5\ \mu mol\ O_2\ kg^{-1}$ at 11, 22, 39, 33, and 42 m depth, respectively, at the five stations (from shelf to offshore). In the OMZ core (between ~100 and 400 m depth), oxygen content was frequently $< 0.5\ \mu mol\ O_2\ kg^{-1}$ and often reached the detection limit of the optode. At the two deep stations, an increase in oxygen levels at the base of the OMZ was observed from around 450 m depth, with values higher than $5\ \mu mol\ O_2\ kg^{-1}$ at 520 and 527 m, respectively. The depth where the observed pO_2 fell below the temperature-dependent p_{crit} value calculated according to Equation (3) for crustaceans decreased continuously from nearshore to offshore (11 m at s1 and 42 m at s2; **Figure 3**).

3.2. Night- and Daytime Biomass Distribution Along the Sampled Transect

Night- and daytime biomass distribution along the sampled transect is shown for the entire well-preserved zooplankton in **Figure 4**, top row, for minor groups of well-preserved zooplankton (amphipoda, ostracoda, siphonophora, mollusca, chaetognatha, annelida; abbreviated as MG) in **Figure 4**, middle row, for decapoda, which were strongly dominated by *Pleuroncodes monodon* in **Figure 4**, bottom row and separately

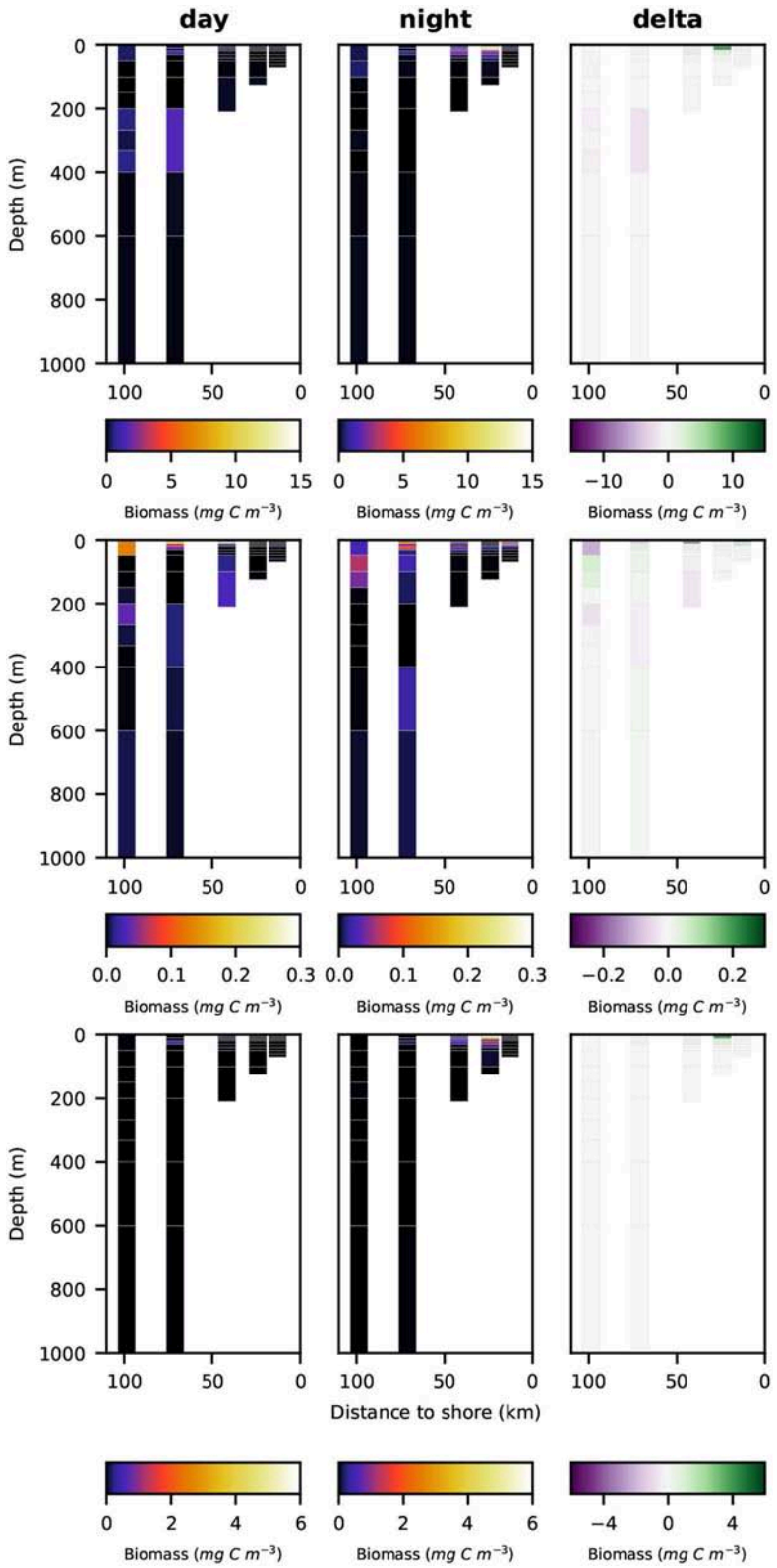

FIGURE 4 | Vertical distribution of zooplankton biomass (*mg C* m^{-3}) along the transect at day (left panels), night (middle panels), and the difference of the two (right panels). Top row: total well-preserved zooplankton, middle row: minor-groups, bottom row: Decapoda.

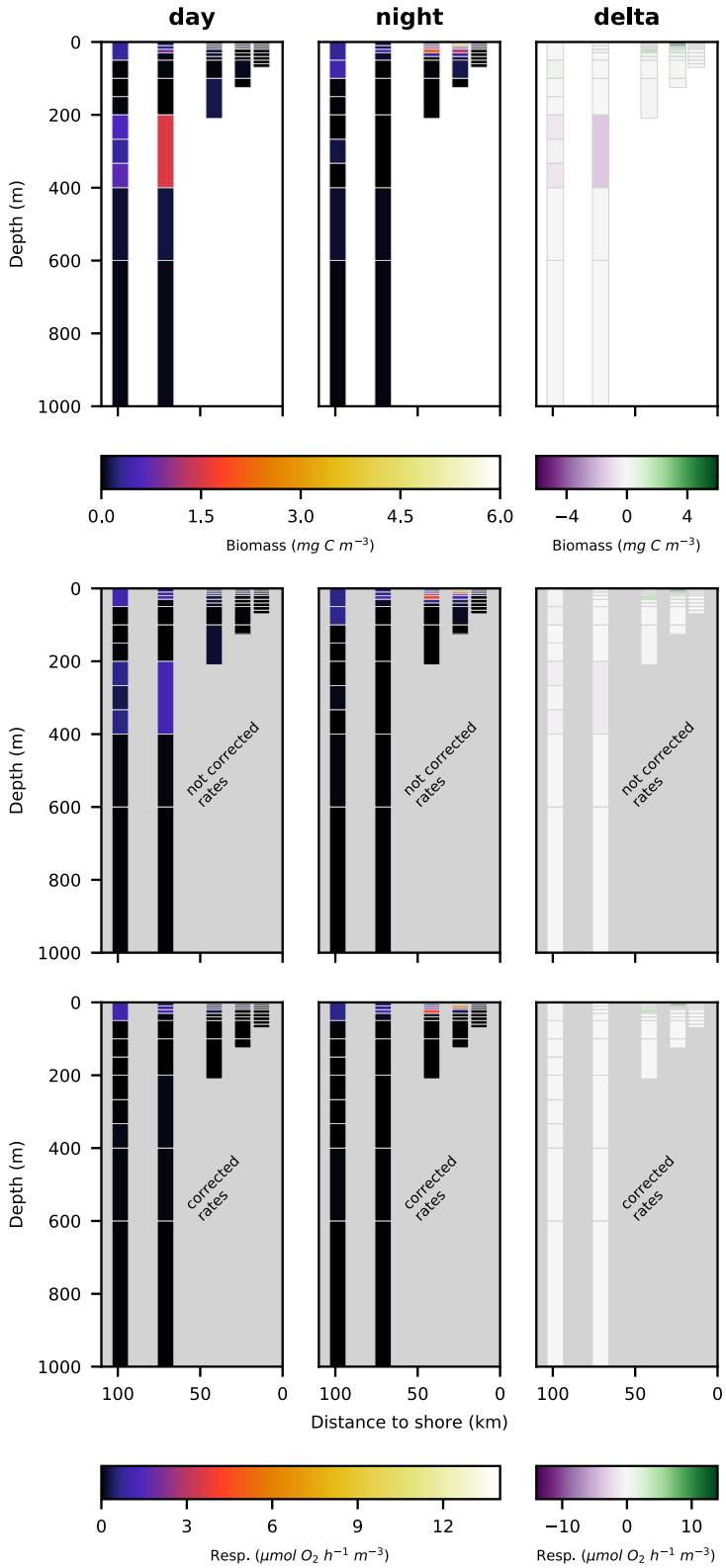

FIGURE 5 | Vertical distribution of total crustacean biomass (top row; *mg C* m^{-3}), not corrected respiration rates (middle row; $\mu mol\ O_2\ h^{-1}\ m^{-3}$) and corrected respiration rates (bottom row; $\mu mol\ O_2\ h^{-1}\ m^{-3}$) along the transect at day (left panels), night (middle panels), and the difference of the two (right panels).

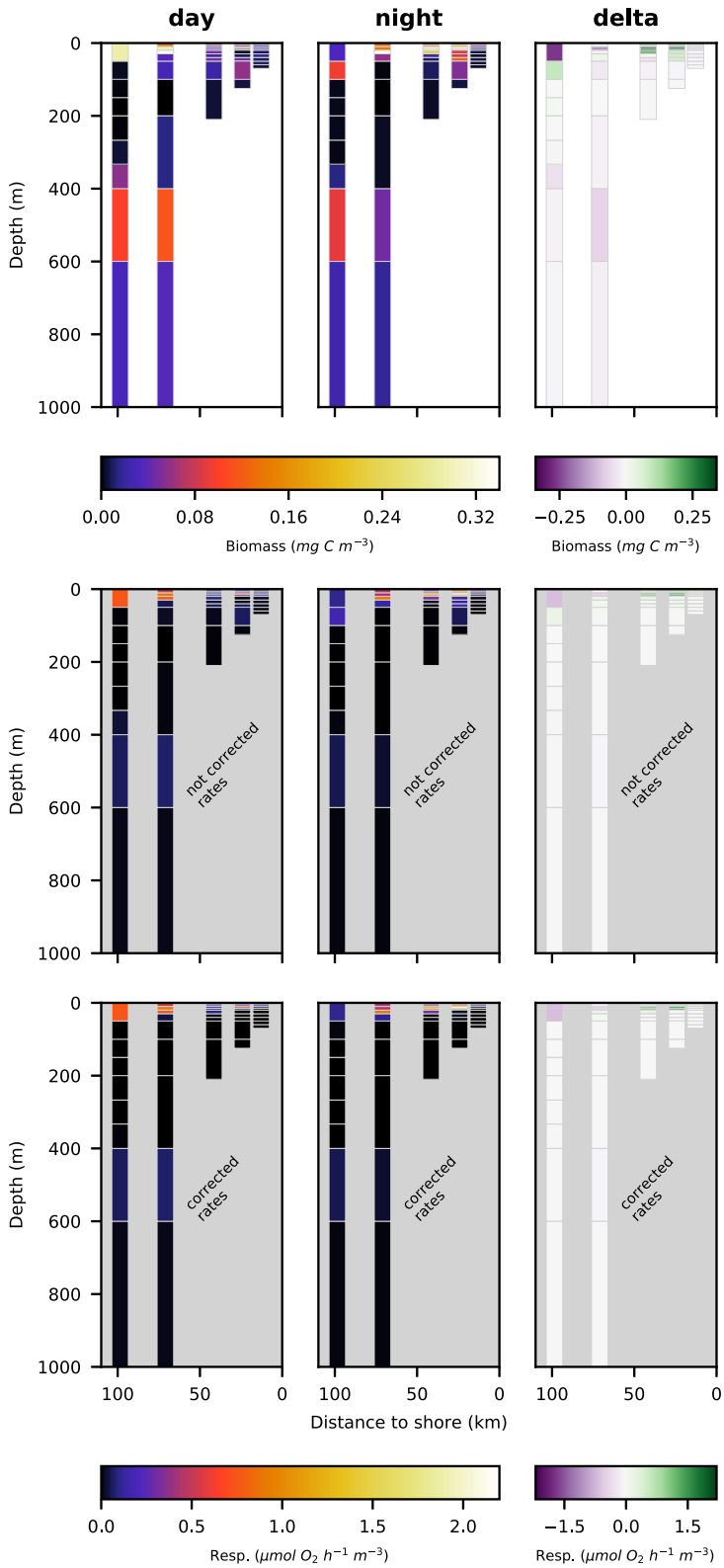

FIGURE 6 | Vertical distribution of copepoda biomass (top row; *mg C* m^{-3}), not corrected respiration rates (middle row; $\mu mol\ O_2\ h^{-1}\ m^{-3}$) and corrected respiration rates (bottom row; $\mu mol\ O_2\ h^{-1}\ m^{-3}$) along the transect at day (left panels), night (middle panels), and the difference of the two (right panels).

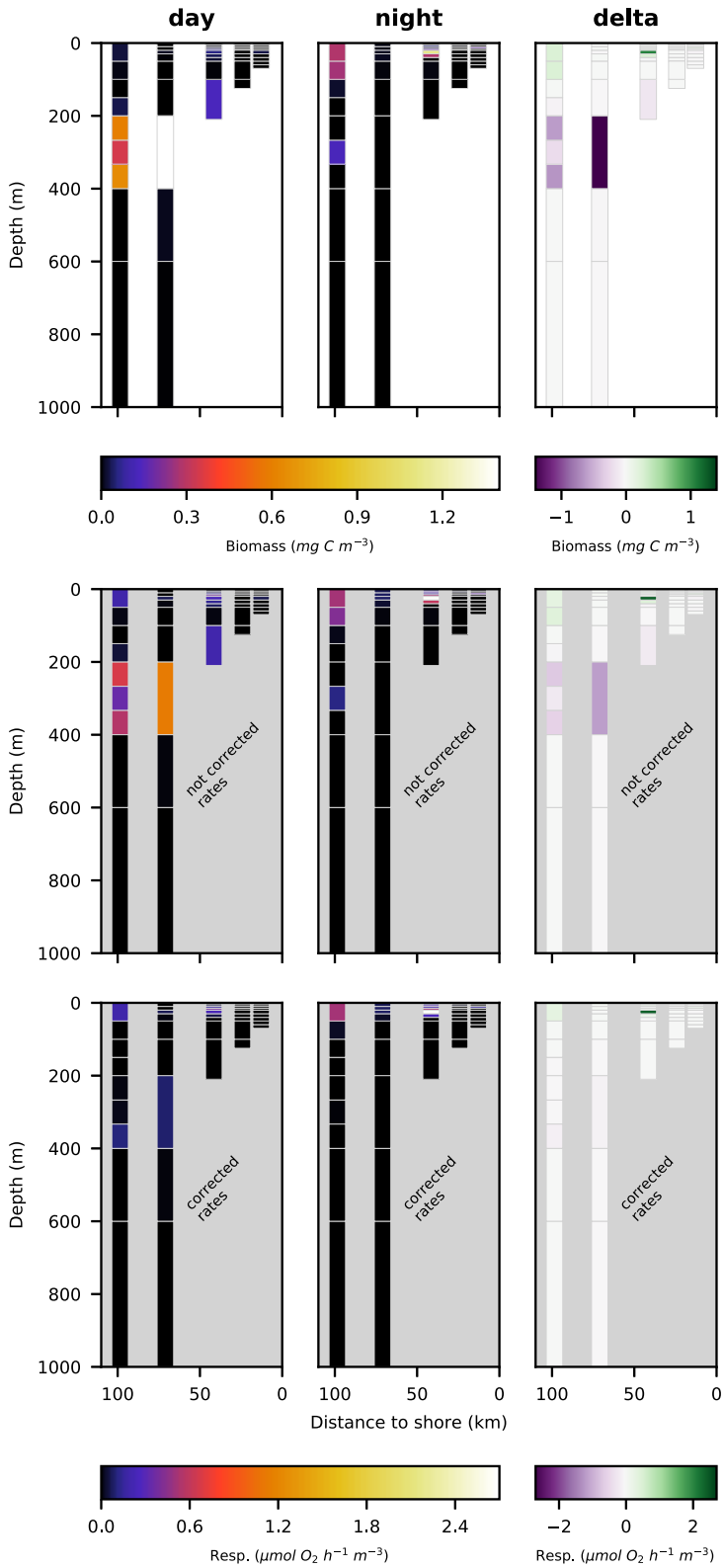

FIGURE 7 | Vertical distribution of euphausiacea biomass (top row; *mg C* m^{-3}), not corrected respiration rates (middle row; $\mu mol\ O_2\ h^{-1}\ m^{-3}$) and corrected respiration rates (bottom row; $\mu mol\ O_2\ h^{-1}\ m^{-3}$) along the transect at day (left panels), night (middle panels), and the difference of the two (right panels).

TABLE 3 | Integrated biomass and respiration rates.

Category	Parameter	Unit	s5	s4	s3	s2	s1
Copepod	Biomass C night	$mg\ C\ m^{-2}$	438.1	310.4	148.6	153.9	13.1
Copepoda	Biomass C day	$mg\ C\ m^{-2}$	621.8	616.3	44.8	64.2	12.3
Euphausiacea	Biomass C night	$mg\ C\ m^{-2}$	452.0	15.8	192.1	0.5	11.0
Euphausiacea	Biomass C day	$mg\ C\ m^{-2}$	1,322.1	3,657.6	201.4	0.1	4.2
Decapoda	Biomass C night	$mg\ C\ m^{-2}$	33.8	104.0	132.0	1,041.2	9.6
Decapoda	Biomass C day	$mg\ C\ m^{-2}$	14.1	111.8	19.8	0.2	0.2
Crustacea total	Biomass C night	$mg\ C\ m^{-2}$	1,617.9	856.1	572.4	2,776.7	36.1
Crustacea total	Biomass C day	$mg\ C\ m^{-2}$	2,378.1	4,943.0	318.5	123.0	35.8
Minor groups	Biomass C night	$mg\ C\ m^{-2}$	107.4	143.3	18.6	3.2	27.3
Minor groups	Biomass C day	$mg\ C\ m^{-2}$	157.5	102.9	67.3	0.6	1.6
Well-preserved total	Biomass C night	$mg\ C\ m^{-2}$	1,725.4	999.4	591.1	2,779.9	63.3
Well-preserved total	Biomass C day	$mg\ C\ m^{-2}$	2,535.6	5,045.9	385.8	123.5	37.4
Copepoda	Resp. not corrected night	$mg\ C\ m^{-2}\ d^{-1}$	33.2	32.8	19.0	33.9	4.2
Copepoda	Resp. not corrected day	$mg\ C\ m^{-2}\ d^{-1}$	62.3	49.6	5.8	11.3	3.2
Euphausiacea	Resp. not corrected night	$mg\ C\ m^{-2}\ d^{-1}$	56.9	4.3	39.0	0.2	1.8
Euphausiacea	Resp. not corrected day	$mg\ C\ m^{-2}\ d^{-1}$	119.1	232.2	31.5	0.0	0.8
Decapoda	Resp. not corrected night	$mg\ C\ m^{-2}\ d^{-1}$	2.7	9.1	23.5	122.5	3.2
Decapoda	Resp. not corrected day	$mg\ C\ m^{-2}\ d^{-1}$	3.6	8.5	3.4	0.1	0.1
Crustacea total	Resp. not corrected night	$mg\ C\ m^{-2}\ d^{-1}$	143.1	88.0	108.6	425.5	10.0
Crustacea total	Resp. not corrected day	$mg\ C\ m^{-2}\ d^{-1}$	219.6	350.2	51.6	19.4	8.8
Minor groups	Resp. not corrected night	$mg\ C\ m^{-2}\ d^{-1}$	16.4	17.7	8.4	1.0	10.4
Minor groups	Resp. not corrected day	$mg\ C\ m^{-2}\ d^{-1}$	35.0	20.5	21.1	0.2	0.7
Well-preserved total	Resp. not corrected night	$mg\ C\ m^{-2}\ d^{-1}$	159.5	105.7	117.0	426.5	20.4
Well-preserved total	Resp. not corrected day	$mg\ C\ m^{-2}\ d^{-1}$	254.5	370.7	72.6	19.6	9.5
Copepoda	Resp. corrected night	$mg\ C\ m^{-2}\ d^{-1}$	23.7	31.4	17.8	27.3	3.4
Copepoda	Resp. corrected day	$mg\ C\ m^{-2}\ d^{-1}$	59.2	46.0	3.1	6.6	1.4
Euphausiacea	Resp. corrected night	$mg\ C\ m^{-2}\ d^{-1}$	28.5	3.6	34.9	0.2	0.8
Euphausiacea	Resp. corrected day	$mg\ C\ m^{-2}\ d^{-1}$	19.8	23.2	6.3	0.0	0.0
Decapoda	Resp. corrected night	$mg\ C\ m^{-2}\ d^{-1}$	1.0	9.1	23.2	107.0	3.0
Decapoda	Resp. corrected day	$mg\ C\ m^{-2}\ d^{-1}$	3.6	8.5	1.9	0.1	0.1
Crustacea total	Resp. corrected night	$mg\ C\ m^{-2}\ d^{-1}$	94.3	75.4	95.8	378.5	7.5
Crustacea total	Resp. corrected day	$mg\ C\ m^{-2}\ d^{-1}$	112.1	109.1	12.9	10.5	4.4
Minor groups	Resp. corrected night	$mg\ C\ m^{-2}\ d^{-1}$	0.0	0.0	0.0	0.0	0.0
Minor groups	Resp. corrected day	$mg\ C\ m^{-2}\ d^{-1}$	0.0	0.0	0.0	0.0	0.0
Well-preserved total	Resp. corrected night	$mg\ C\ m^{-2}\ d^{-1}$	94.3	75.4	95.8	378.5	7.5
Well-preserved total	Resp. corrected day	$mg\ C\ m^{-2}\ d^{-1}$	112.1	109.1	12.9	10.5	4.4

for crustacea, copepoda and euphausiacea in **Figures 5–7**, respectively. Values integrated over the entire water column are shown in **Table 3**, whereas migratory biomass to below 100 m depth is shown in **Table 4**.

Total well-preserved zooplankton biomass (**Figure 4**, top row) was dominated by *Pleuroncodes monodon* on the shelf and euphausiacea at the offshore stations. In depth layers where these two groups were absent or low in abundance, total well-preserved zooplankton biomass was below 0.1 mg m^{-3}.

Only very little MG zooplankton were found at stations s1 and s2—the two stations closest to the coast (**Figure 4**, middle row)—and MG zooplankton was dominated by annelida in the surface layers. Highest biomass of the MG group was found at the middle station s3 at daytime, but also stations s4 and s5 featured high MG biomass in the surface layer, dominated by siphonophora. Siphonophora also generally contributed most to the MG zooplankton biomass. Day-night differences in biomass distribution of the MG zooplankton group showed no clear patterns.

Pleuroncodes monodon was found in high abundance and generated the highest biomass value of 165 $mg\ DW\ m^{-3}$ (62.6 $mg\ C\ m^{-3}$) along the entire transect in surface waters at station S2 at nighttime. Few further specimens were observed at station s3 in surface waters at nighttime and at station s4 in surface waters at daytime. Virtually no specimens were found in surface waters at daytime at stations s2 and s3.

The biomass of copepoda at station s1 (closest to the shore) was very low, both at day- and at nighttime. The highest biomass of copepoda was found at station s3 in the surface layer at nighttime. Nighttime biomass was also high at stations s2 and

TABLE 4 | Integrated day-night differences below the 100 m depth level.

Category	Parameter	Unit	s5	s4	s3	s2	s1
Copepod	Biomass C	$mg\ C\ m^{-2}$	84.3	277.1	1.9	0.0	n.a.
Euphausiacea	Biomass C	$mg\ C\ m^{-2}$	1,181.4	3,651.0	175.9	0.0	n.a.
Decapoda	Biomass C	$mg\ C\ m^{-2}$	−32.4	−24.9	8.4	0.0	n.a.
Crustacea total	Biomass C	$mg\ C\ m^{-2}$	1,005.6	4,097.3	200.3	45.7	n.a.
Minor groups	Biomass C	$mg\ C\ m^{-2}$	24.4	−29.8	36.7	0.4	n.a.
Well-preserved total	Biomass C	$mg\ C\ m^{-2}$	1,030.0	4,067.5	237.0	46.1	n.a.
Copepoda	Resp. not corrected	$mg\ C\ m^{-2}\ d^{-1}$	0.7	1.9	0.0	0.0	n.a.
Euphausiacea	Resp. not corrected	$mg\ C\ m^{-2}\ d^{-1}$	13.8	32.2	3.2	0.0	n.a.
Decapoda	Resp. not corrected	$mg\ C\ m^{-2}\ d^{-1}$	−0.3	−0.0	0.1	0.0	n.a.
Crustacea total	Resp. not corrected	$mg\ C\ m^{-2}\ d^{-1}$	12.4	37.7	3.8	0.6	n.a.
Minor groups	Resp. not corrected	$mg\ C\ m^{-2}\ d^{-1}$	0.8	0.5	1.3	0.0	n.a.
Well-preserved total	Resp. not corrected	$mg\ C\ m^{-2}\ d^{-1}$	13.3	38.1	5.1	0.6	n.a.
Copepoda	Resp. corrected	$mg\ C\ m^{-2}\ d^{-1}$	0.5	1.6	0.0	0.0	n.a.
Euphausiacea	Resp. corrected	$mg\ C\ m^{-2}\ d^{-1}$	1.3	3.1	0.0	0.0	n.a.
Decapoda	Resp. corrected	$mg\ C\ m^{-2}\ d^{-1}$	−0.1	−0.0	0.0	0.0	n.a.
Crustacea total	Resp. corrected	$mg\ C\ m^{-2}\ d^{-1}$	−0.3	4.8	0.0	0.0	n.a.
Minor groups	Resp. corrected	$mg\ C\ m^{-2}\ d^{-1}$	0.0	0.0	0.0	0.0	n.a.
Well-preserved total	Resp. corrected	$mg\ C\ m^{-2}\ d^{-1}$	−0.3	4.8	0.0	0.0	n.a.

n.a., not applicable.

s4 in the surface layer. Daytime abundance in the surface layer was low at stations s2 and s3, but comparatively high at stations s4 and s5. A secondary maximum of copepod biomass could be observed at the lower boundary of the OMZ in the two offshore stations s4 and s5 in the 400–600 m depth layer. Day-night differences in biomass distribution of copepoda revealed no clear patterns.

Euphausiacea were almost absent at day and nighttime from the two innermost stations s1 and s2 where water depth was shallower then 200 m. At daytime, euphausiacea biomass was very low in the upper 200 m also at stations s4 and s5, whereas few specimens were found in the 100–200 m depth layer at station s3. Nighttime biomass was high at stations s3 and s5 in the oxygenated surface layer. At stations s4 and s5, high euphausiacea biomass was found in the 200–400 m depth layer at daytime, but not further below. Day-night differences in euphausiacea biomass distribution indicate that specimens in this group mainly spent the day in the oxygen minimum zone at daytime and migrated to the surface at nighttime.

3.3. Respiration Rates of Copepoda and Euphausiacea

Respiration rate estimates for copepoda and euphausiacea are shown in **Figures 6**, **7**. The middle panels show the uncorrected rate estimates, whereas the bottom panels show the corrected rate estimates. It is important to note that the uncorrected rates are only shown for comparative purposes, only the corrected rates are valid estimates of copepoda and euphausiacea respiration rates. Uncorrected respiration rates more or less mirrored the biomass distribution of copepoda and euphausiacea in the surface layer. Lower temperatures below 100 m depth resulted in a decrease of the respiration rate estimate in comparison to the biomass. Copepoda biomass below 100 m was very low, therefore uncorrected and corrected respiration rate estimates can not be visualized in **Figure 6**. Uncorrected copepoda respiration rate estimates for station s4 and s5 at 100–400 m depth ranged between 0.23 and 40.54 μmol O_2 h^{-1} m^{-3}. Uncorrected copepoda respiration rate estimates for station s4 and s5 at 400–600 m depth ranged between 34 and 76 μmol O_2 h^{-1} m^{-3}. Corrected copepoda respiration rate estimates at 0–50 m depth were similar to the uncorrected rates, as the oxygen levels above 50 m depth were mostly above the p_{crit} estimates we use in the correction formula. Corrected respiration rate estimates of 0.013 $\mu mol\ O_2\ h^{-1}\ m^{-3}$ at station s5 for the 50–100 m depth layer were about 12-fold lower than not corrected rates. Corrected copepoda respiration rate estimates for station s4 and s5 at 100–400 m depth ranged between 0.004 and 7.9 $nmol\ O_2\ h^{-1}\ m^{-3}$. For station s4 and s5 at 400–600 m depth, corrected estimates were identical to the uncorrected rates as the oxygen levels in this layer are comparatively high again. Uncorrected euphausiacea respiration rate estimates ranged between 0.34 and 1.14 $\mu mol\ O_2\ h^{-1}\ m^{-3}$at daytime in the 200–400 m depth layer at stations s4 and s5, whereas corrected values ranged between 0.0 and 0.11 $\mu mol\ O_2\ h^{-1}\ m^{-3}$. Likewise, substantial daytime respiration would be assumed for the 100–200 m depth layer at station s3 if no correction for metabolic suppression is conducted. Uncorrected rates yield considerable day-night differences in respiratory activity for the 100–400 m depth range at stations s3–s5. Applying the proposed correction yielded much lower (factor of 0.18–0.87) corrected respiration rate estimates. Likewise, day-night differences in respiration and hence active flux of carbon to these depths were rather small. We find that the active flux due to respiration to 100–1,000 m water depth off Peru should be estimated at 0.0, 4.8, and −0.3

TABLE 5 | Integrated ammonium excretion rates of Euphausiacea for the 200–400 m depth level. A 12 h residence time in this layer at daytime was assumed.

Category	Parameter	Unit	s5	s4	s3	s2	s1
Day	Not corrected	$\mu mol\ NH_4\ m^{-2}\ d^{-1}$	82.3	179.7	16.6	0.0	n.a.
Night	Not corrected	$\mu mol\ NH_4\ m^{-2}\ d^{-1}$	7.1	0.0	0.0	0.0	n.a.
Delta	Not corrected	$\mu mol\ NH_4\ m^{-2}\ d^{-1}$	75.2	179.7	16.6	0.0	n.a.
Day	Corrected	$\mu mol\ NH_4\ m^{-2}\ d^{-1}$	16.4	36.8	0.0	0.0	n.a.
Night	Corrected	$\mu mol\ NH_4\ m^{-2}\ d^{-1}$	1.3	0.0	0.0	0.0	n.a.
Delta	Corrected	$\mu mol\ NH_4\ m^{-2}\ d^{-1}$	15.1	36.8	0.0	0.0	n.a.

n.a., not applicalbe.

$mg\ C\ m^{-2}\ d^{-1}$ for stations s3–s5 (**Table 4**), values that are at least 8-fold lower then those obtained omitting the necessary correction for metabolic suppression.

3.4. Ammonium Excretion of Euphausiids

Integrated ammonium excretion rates of Euphausiids for the 200–400 m depth layer are listed in **Table 5**. We only calculated rates for this depth interval, as the only published function to calculate oxygen-dependent ammonium excretion rates was obtained for measurements conducted at 13°C (Kiko et al., 2016). Mean temperatures in the 200–400 m depth layer were found to range between 10 and 16°C. Euphausiids were observed in this depth range at stations s3–s5. Ammonium excretion rates at daytime ranged between 0 and 36.81 $\mu mol\ NH_4\ m^{-2}\ d^{-1}$ ($n = 3$), at nighttime between 0 and 1.33 $\mu mol\ NH_4\ m^{-2}\ d^{-1}$ ($n = 3$). The resulting diel vertical migration flux of Ammonium into the 200–400 m depth layer ranged between 0 and 36.81 $\mu mol\ NH_4\ m^{-2}\ d^{-1}$. Ammonium excretion rates not corrected for the metabolic suppression due to hypoxia were about 4-fold higher at stations s4 and s5 than the corrected rates. At station s3, corrected rates were 0 $\mu mol\ NH_4\ m^{-2}\ d^{-1}$, whereas the non-corrected daytime rate and DVM-related flux was 16.57 $\mu mol\ NH_4\ m^{-2}\ d^{-1}$.

4. DISCUSSION

4.1. General Remarks

In the Tropical Pacific, zooplankton biomass is inversely related to depth of the thermocline and is positively related to chlorophyll, primary production and concentration of nutrients (Fernández-Álamo and Färber-Lorda, 2006). In the productive Humboldt upwelling system (HUS) off Peru, zooplankton biomass is extremely high. It is therefore very interesting to consider the role of zooplankton in the biogeochemical cycles of the HUS, both due to their local impacts on elemental cycles of e.g., carbon, nitrogen and oxygen, but also due to the possibly basin-wide implications of these impacts. Here, we focus on the impact of the OMZ on the metabolic activity of DVM organisms. Earlier estimates of zooplankton mediated fluxes to the OMZ are likewise too high, as active flux due to respiration was estimated as 0.12 times the migratory biomass (Escribano et al., 2009). The factor 0.12 stems from a global analysis of zooplankton and biomass respiration rate data that specifically excluded upwelling areas (Hernández-León and Ikeda, 2005). It therefore seems inappropriate to apply it in upwelling systems. High active export fluxes in OMZ regions were also assumed in earlier modeling work, which also proposed that diel vertical migrants are one of the major sources of dissolved ammonium to anoxic waters as well as major consumers of oxygen at depth (Bianchi et al., 2013, 2014). For the first time, we have now incorporated metabolic suppression of migrating crustaceans (Kiko et al., 2015, 2016) into an estimate of active transport according to experimental results. Our results indicate that for OMZ regions, oxygen is a key environmental variable that does not only drive species distribution, but also scales metabolic activity, and therefore needs to be included in modeling efforts of zooplankton-mediated elemental fluxes.

4.2. Biomass Distribution Along the Transect Sampled

According to Ayón et al. (2008) and references therein, zooplankton are numerically dominated by crustaceans off Peru. The main zooplankton groups off central Peru are copepods (which are by far the most abundant group) and euphausiids. Among those taxa that are also abundant are e.g., chaetognaths, siphonophores, polychaetes, and salps. Because some of these organisms are large, they do contribute substantially to total biomass despite their high water content. Still, we have to keep in mind that our values are likely underestimates, as also the gear in use leads to a truncated size spectrum. We did not include organisms passing through a 500 μm mesh in this analysis, and active swimming macrozooplankton/micronekton as well as rare species are not sampled quantitatively by the multinet. Despite the high upwelling and productivity at the shelf stations, total integrated biomass was lower at the two nearshore stations. This was mainly due to the dominance of small copepods, the extremely shallow oxycline and the water depth being too shallow for organisms conducting DVM, except for *P. monodon*, which partly resides at the seafloor during the day (Kiko et al., 2015). According to Antezana (2009), the mean daytime depth of *E. mucronata* is ∼250 m. At the 210 m deep station s3, integrated euphausiid biomass (and, thus, also migrant biomass) was already markedly reduced to ∼ 460 $mg\ DW\ m^{-2}$, compared to the outer stations with >1, 000 $mg\ DW\ m^{-2}$ (except in the nighttime haul at s4 where only few euphausiids where caught in the surface layer). Except for that haul, the contribution of euphausiids to total well-preserved biomass at water depths >200 m ranged between 25 and 71%, which is lower than that reported by Antezana (2010) at 10°S and 14°S off Peru. An increasing shelf-slope-offshore trend in epipelagic integrated biomass estimated acoustically by night was also reported for macrozooplankton off Peru (6–18°S) by Ballón et al. (2011), albeit with substantially higher values (around 100 $g\ DW\ m^{-2}$), since their approach included species that are capable of net avoidance (which is to some extent the case for euphausiids). In the same study, epipelagic zooplankton biomass was also determined by vertical 300 μm net hauls, and these estimates are

well within the range of our values, with $\sim$ 1–20 $g\ DW\ m^{-2}$). Also, volume-specific euphausiid biomass in the different depth layers was $\sim$10 times lower compared to Escribano et al. (2009), who used a 1 m^2 Tucker trawl towed at 5 kn. Thus, our calculated total biomass is well comparable to mesozooplankton estimates using other methods, but underestimates the biomass of macrozooplankton/micronekton, which is mostly due to a gear effect (avoidance of the relatively small/slow Hydrobios Multinet Maxi).

4.3. Metabolic Activity of Zooplankton Off Peru

Depth-resolved estimates of zooplankton metabolic activity that account for the metabolic suppression due to anoxic conditions do not yet exist for the HUS. Hernández-León and Ikeda (2005) excluded the upwelling areas from their analysis of global zooplankton respiration, likely due to the lack of appropriate data. They found maximum integrated oceanic zooplankton respiration rates in the 10°N to 20°N latitudinal range of about 240 $mg\ C\ m^{-2}\ d^{-1}$. Our corrected integrated respiration rate estimates (only for well-preserved zooplankton, size fraction $300 - 500\ \mu m$ excluded) range from 4.4 to 378.5 $mg\ C\ m^{-2}\ d^{-1}$. Values at the two offshore stations s4 and s5 range between 75.4 and 112.1 $mg\ C\ m^{-2}\ d^{-1}$ and are therefore within the lower range of the estimates by Hernández-León and Ikeda (2005). Low integrated rates despite extremely high biomass are due to the suppression of metabolic activity. Not corrected rates are with 105.73 to 370.68 $mg\ C\ m^{-2}\ d^{-1}$ within the range reported by Hernández-León and Ikeda (2005).

Also Ekau et al. (2018) calculated integrated zooplankton respiration rates using a constant factor of 54.6 $mL\ O_2\ g^{-1}\ DM\ d^{-1}$ (which is $\sim$ 2.44 $\mu mol\ O_2\ mg^{-1}\ DM\ d^{-1}$) for the Benguela upwelling system, although this system features an intense OMZ. Their values generally range between 45 and 135 $\mu mol\ O_2\ m^{-2}\ d^{-1}$, with maxima of 900 $\mu mol\ O_2\ m^{-2}\ d^{-1}$ (10.71 $mg\ C\ m^{-2}\ d^{-1}$). These values likely also require a downward correction, although in this system zooplankton rather tend to avoid extremely low oxygen values, which means that metabolic suppression might not occur.

It is even more important to consider the metabolic suppression when studying DVM-mediated active export of respiratory carbon. Not considering this mechanism leads to 10-fold overestimation of DVM-mediated carbon export to below 100 m depth at stations s4 and s5. At station s3 we would assume a considerable export of 5.08 $mg\ C\ m^{-2}\ d^{-1}$, where there is none. Likewise, Escribano et al. (2009) calculated a DVM-mediated active export of 4417.4 $mg\ C\ m^{-2}\ d^{-1}$ via respiration to the 60–600 m depth layer, which should likely be reduced to zero due to the fact that the oxygen concentrations at their sampling location were extremely low between 60 and at least 500 m depth.

Another dataset of zooplankton mediated active export from an upwelling region was collected in the California Current system (Stukel et al., 2013). Here, oxygen values of about 40 $\mu mol\ O_2\ kg^{-1}$ are found at 400 m depth (Ren et al., 2018). These oxygen concentrations are likely high enough to allow normal respiratory activity. Stukel et al. (2013) report a DVM-mediated respiratory flux of 2.4 *to* 47.1 $mg\ C\ m^{-2}\ d^{-1}$, which is rather high in comparison to the corrected fluxes we observe, but would be consistent with non-corrected rates. In general, our work suggests that DVM-mediated respiratory carbon export into the OMZ is rather low in the Peruvian upwelling.

It was previously suggested that ammonium excretions by diel vertical migrant species might support anammox—a nitrogen loss process occurring in severely hypoxic to anoxic waters—to a large extent (Bianchi et al., 2014). Our first estimates of ammonium excretion by euphausiids in the Peruvian OMZ show that this is likely not the case. We do calculate integrated transport rates of 15.05 and 36.81 $\mu mol\ NH_4\ m^{-2}\ d^{-1}$ into the 200–400 m depth layer. This yields maximum rates of 0.008 $nmol\ NH_4\ L^{-1}\ h^{-1}$. *E. mucronata* migrations are rather confined to about 200–250 m depth. Assuming that all ammonium is released at this depth, would therefore result in ammonium release rates of 0.032 $nmol\ NH_4\ L^{-1}\ h^{-1}$. Kalvelage et al. (2011) list ammonium uptake rates due to anammox of 0.41 and 0.79 $nmol\ NH_4\ L^{-1}\ h^{-1}$ at 180 and 250 m depth, respectively (measured at 16°S, 75°W). Lam et al. (2009) provide rates of 2.5 and 3.3 $nmol\ NH_4\ L^{-1}\ h^{-1}$ for the 200 and 400 m depth level, respectively (measured at 12°S, 78°W). Our maximum ammonium supply estimates therefore can not sustain these anammox rates, suggesting that anammox is fueled by other ammonium sources.

4.4. Implications for Zooplankton Ecophysiology

This work relies on the summary of respiration rate estimates for different zooplankton functional groups described by Ikeda (2014). Further efforts are needed to integrate novel data, to refine and to test these functions. E.g., Ikeda (2014) mostly used closed bottle approaches with several individuals for his measurements. However, work on single individuals using Clarke-type sensors (e.g., Maas et al., 2012; Seibel et al., 2018) or optodes (e.g., Kiko et al., 2016) enables more detailed studies of e.g., the p_{crit} and avoids crowding effects. Especially the temperature dependence of the p_{crit}, but also large scale geographical differences in p_{crit} require further study. Likewise, further measurements of ammonium excretion at different oxygen and temperature levels are needed.

One important aspect of DVM into severely hypoxic or even anoxic depth layers is the build-up of an oxygen debt through the accumulation of metabolic waste products during the stay at depth. The ability of *E. mucronata* to survive anoxia is likely a result of an efficient anoxic metabolism, as high lactate dehydrogenase levels are reported for this species (Gonzalez and Quiñones, 2002). Migrating organisms need to get rid of the metabolic waste products (e.g., lactate) upon return to well-oxygenated surface water, which might lead to an increase in metabolic activity following OMZ exposure. Chaston (1969) reports a doubling of the respiration rate within the first hour after return from anoxia to normoxia in *Cyclops varicans*. How

metabolic activity changes in diel vertical migrators upon return to the oxic region therefore requires further study, as such an activity increase will result in a retention of metabolic activity in the oxygenated region.

4.5. Implications for Zooplankton Sampling

Currently, published datasets are often either taxonomically well-resolved abundance data, lacking information on size and biomass of the identified groups (e.g., Criales-Hernández et al., 2008 in the same region as the present study), or only contain bulk zooplankton biomass (or biovolume) data, which do not allow for the consideration of the impact of size distribution or taxonomic and functional composition on metabolic rates and fluxes as well as food web interactions (Ayón et al., 2011). Physiological rates generally do not scale linearly with body size (Moloney and Field, 1989) and therefore changes in the size distribution can go in hand with changes in zooplankton mediated biogeochemical fluxes despite unchanged bulk biomass. Detailed taxonomic analyses are very valuable for diversity studies, but it would be interesting to also integrate size measurements (e.g., via imaging) into the laboratory routine to enable individual-based studies on biogeochemical fluxes. The necessity for bulk measurements should be carefully assessed and best be accompanied by measurements of the size distribution, e.g., with imaging approaches.

One restriction of our analysis is the use of vertically hoisted, integrating nets for our sampling. Apart from missing the fragile part of the zooplankton community which is destroyed by nets (Hoving et al., 2018), net catches integrate over a range of environmental conditions, e.g., a temperature and oxygen gradient at the oxycline. The exact location of an organism and the environmental conditions where it was active can not be retrieved with integrating nets and our metabolic rate estimates are rather uncertain when the net integrated over a strong vertical gradient of temperature and/or oxygen. Optical *in situ* observations, e.g., using a VPR or a UVP5, Pelagios, ROVs, etc. will be helpful to ameliorate both problems, but do have the problem of instrument avoidance by optically orienting organisms (e.g., Benoit-Bird et al., 2010). In general, both approaches should be combined, optimally in an integrated camera-net instrument package to obtain a more complete understanding of zooplankton distribution.

We base our calculations on area-biomass functions obtained in the subtropical Atlantic, and the work by Lehette and Hernández-León (2009) is to our knowledge the only comprehensive work assessing this issue. Further work on area-biomass relationships is needed and the underlying individual raw data (images, weights and any further information, such as C-, N-, P-content) should be stored in an international database [e.g., in EcoTaxa (Picheral et al., 2019)], similar to the NCBI database of genomic sequences. Such data will enable us to better unlock the secrets that are hidden in the image data from the zooscan approach and other optical methods that are currently being collected. Also for these data, EcoTaxa seems to be the currently best developed solution for image hosting, collaborative online sorting and data sharing. Some of these ideas have already been discussed in Lombard et al. (2019), an outlook paper that details the needs for a globally consistent strategy in plankton ocean observation, but the need for a database that contains individual high-quality images and data should not be overlooked.

4.6. Implications for Other Regions, Global Biogeochemistry, and Modeling

Our sampling is restricted to a very small area and our estimates are only valid for the HUS region where oxygen levels go down to almost anoxic levels. Metabolic suppression effects are obviously strongest in this region, leading to an almost complete shutdown of metabolic activity. Similar effects are to be expected for the northern part of the Indian Ocean, the Black sea, the Baltic sea and other severe OMZs. Regions further offshore, as well as north and south of our sampling region feature less severe OMZ conditions. This might enable stronger DVM activity, also by taxonomic groups other than euphausiids, which might also feature different p_{crit} values (Seibel et al., 2016). It seems necessary to specifically map the zooplankton community composition and the metabolic capacities of DVM-organisms in transitional areas between extreme OMZs and well-oxygenated waters in order to better estimate zooplankton-mediated impacts on OMZ biogeochemistry.

Currently, the global ocean is losing oxygen and midwater OMZs are intensifying and expanding under global warming conditions (Stramma et al., 2008; Schmidtko et al., 2017) due to changes in ocean mixing and reduced oxygen solubility (Matear and Hirst, 2003; Bopp et al., 2013; Cocco et al., 2013). Large scale feedbacks between changing oxygen levels and the role of zooplankton in the elemental cycling of oxygen, carbon and nitrogen are to be expected. Oxygen levels in less extreme oceanic OMZ regions may in the near future fall below the p_{crit} of vertically migrating species. Oxygen loss will likely result in a dampening of zooplankton metabolic activity in OMZ regions, first via avoidance of the OMZ by non-tolerant species and second through metabolic suppression in tolerant species. Respiration activity of zooplankton should therefore decline with declining OMZ oxygen levels. The zooplankton community composition could be a relevant factor in determining the deoxygenation rate and might influence if an OMZ stabilizes at a region-specific oxygen level. Feedbacks on nutrient cycling might include the retention of nitrogen in the surface layer, as ammonium excretion at depth is reduced.

It seems critical that metabolic suppression in DVM organisms is also considered in efforts to model the role of zooplankton organisms in biogeochemical cycles. Bianchi et al. (2013) and Bianchi et al. (2014) did not take this into account and used a model formulation that resulted in a linear relationship between passive particle export and oxygen utilization or ammonium release. Their zooplankton-mediated fluxes are likely too high in extreme OMZ regions. Aumont et al. (2018) and Archibald et al. (2019) on the other hand impose minimum oxygen thresholds of 5 $\mu mol\ O_2\ kg^{-1}$ and 15 $\mu mol\ O_2\ kg^{-1}$, respectively below which migratory organisms cannot reside. Aumont et al. (2018) need this constraint as their

model formulation would otherwise predict negative oxygen concentrations due to ongoing respiration. The parameterization with a fixed oxygen threshold might result in an appropriate estimation of metabolic rates (but for the wrong reasons), as migrating organisms are artificially displaced to shallower depth levels, where e.g., temperatures are generally higher and therefore metabolic rate estimates elevated. The inappropriate displacement of the DVM organisms might also result in other errors in the model, e.g., the gut flux and mortality occur at shallower depth. Using our approach to account for downregulated metabolic activity below the p_{crit} might yield a more realistic model formulation. In general, we hope that our first oxygen utilization and ammonium release rates for the DVM community of the HUS might help to better constrain future biogeochemical models.

DATA AVAILABILITY STATEMENT

CTD data used in this publication is available at https://doi.pangaea.de/10.1594/PANGAEA.848017. Data from scanned zooplankton images is available at https://ecotaxa.obs-vlfr.fr/ (password protected, access provided upon reasonable request).

AUTHOR CONTRIBUTIONS

RK and HH developed the sampling plan, conducted the sampling, and performed all the sample analysis. RK developed and realized the calculation of individual-based biomass and metabolic rate estimates, including the correction for metabolic suppression. RK and HH outlined and wrote the article together.

FUNDING

This work was a contribution of the SFB 754 Climate-Biogeochemistry Interactions in the Tropical Ocean (www.sfb754.de) which was supported by the German Science Foundation (DFG).

ACKNOWLEDGMENTS

We thank the crew, chief scientists, and CTD teams of RV Meteor expedition M93. We are grateful to Svenja Christiansen and Jannik Faustmann for their help in the Zooscan lab. This work would not have been possible without the generous support by PD Dr. Frank Melzner and Prof. Dr. Ulrich Sommer.

REFERENCES

Antezana, T. (2009). Species-specific patterns of diel migration into the oxygen minimum zone by euphausiids in the humboldt current ecosystem. *Prog. Oceanogr.* 83, 228–236. doi: 10.1016/j.pocean.2009.07.039

Antezana, T. (2010). Euphausia mucronata: a keystone herbivore and prey of the humboldt current system. *Deep Sea Res. Part II Top. Stud. Oceanogr.* 57, 652–662. doi: 10.1016/j.dsr2.2009.10.014

Archibald, K. M., Siegel, D. A., and Doney, S. C. (2019). Modeling the impact of zooplankton diel vertical migration on the carbon export flux of the biological pump. *Glob. Biogeochem. Cycles* 33, 181–199. doi: 10.1029/2018GB005983

Auel, H., and Verheye, H. M. (2007). Hypoxia tolerance in the copepod calanoides carinatus and the effect of an intermediate oxygen minimum layer on copepod vertical distribution in the northern Benguela current upwelling system and the Angola–Benguela front. *J. Exp. Mar. Biol. Ecol.* 352, 234–243. doi: 10.1016/j.jembe.2007.07.020

Aumont, O., Maury, O., Lefort, S., and Bopp, L. (2018). Evaluating the potential impacts of the diurnal vertical migration by marine organisms on marine biogeochemistry. *Glob. Biogeochem. Cycles* 32, 1622–1643. doi: 10.1029/2018GB005886

Ayón, P., Criales-Hernandez, M. I., Schwamborn, R., and Hirche, H.-J. (2008). Zooplankton research off Peru: a review. *Prog. Oceanogr.* 79, 238–255. doi: 10.1016/j.pocean.2008.10.020

Ayón, P., Swartzman, G., Espinoza, P., and Bertrand, A. (2011). Long-term changes in zooplankton size distribution in the Peruvian Humboldt current system: conditions favouring sardine or anchovy. *Mar. Ecol. Prog. Ser.* 422, 211–222. doi: 10.3354/meps08918

Ballón, M., Bertrand, A., Lebourges-Dhaussy, A., Gutiérrez, M., Ayón, P., Grados, D., et al. (2011). Is there enough zooplankton to feed forage fish populations off Peru? An acoustic (positive) answer. *Prog. Oceanogr.* 91, 360–381. doi: 10.1016/j.pocean.2011.03.001

Benoit-Bird, K. J., Moline, M. A., Schofield, O. M., Robbins, I. C., and Waluk, C. M. (2010). Zooplankton avoidance of a profiled open-path fluorometer. *J. Plankton Res.* 32, 1413–1419. doi: 10.1093/plankt/fbq053

Bertrand, A., Ballón, M., and Chaigneau, A. (2010). Acoustic observation of living organisms reveals the upper limit of the oxygen minimum zone. *PLoS ONE* 5:e10330. doi: 10.1371/journal.pone.0010330

Bianchi, D., Babbin, A. R., and Galbraith, E. D. (2014). Enhancement of anammox by the excretion of diel vertical migrators. *Proc. Natl. Acad. Sci. U.S.A.* 111, 15653–15658. doi: 10.1073/pnas.1410790111

Bianchi, D., Galbraith, E. D., Carozza, D. A., Mislan, K., and Stock, C. A. (2013). Intensification of open-ocean oxygen depletion by vertically migrating animals. *Nat. Geosci.* 6, 545–548. doi: 10.1038/ngeo1837

Bianchi, D., and Mislan, K. A. S. (2016). Global patterns of diel vertical migration times and velocities from acoustic data. *Limnol. Oceanogr.* 61, 353–364. doi: 10.1002/lno.10219

Bopp, L., Resplandy, L., Orr, J. C., Doney, S. C., Dunne, J. P., Gehlen, M., et al. (2013). Multiple stressors of ocean ecosystems in the 21st century: projections with cmip5 models. *Biogeosciences* 10, 6225–6245. doi: 10.5194/bg-10-6225-2013

Chaston, I. (1969). Anaerobiosis in cyclops varicans1. *Limnol. Oceanogr.* 14, 298–301.

Chavez, F. P., and Messié, M. (2009). A comparison of eastern boundary upwelling ecosystems. *Prog. Oceanogr.* 83, 80–96. doi: 10.1016/j.pocean.2009.07.032

Childress, J. J., and Seibel, B. A. (1998). Life at stable low oxygen levels: adaptations of animals to oceanic oxygen minimum layers. *J. Exp. Biol.* 201, 1223–1232.

Cocco, V., Joos, F., Steinacker, M., Frölicher, T., Bopp, L., Dunne, J., et al. (2013). Oxygen and indicators of stress for marine life in multi-model global warming projections. *Biogeosciences* 10, 1849–1868. doi: 10.5194/bg-10-1849-2013

Criales-Hernández, M., Schwamborn, R., Graco, M., Ayón, P., Hirche, H.-J., and Wolff, M. (2008). Zooplankton vertical distribution and migration off central Peru in relation to the oxygen minimum layer. *Helgoland Mar. Res.* 62:85. doi: 10.1007/s10152-007-0094-3

Czeschel, R., Stramma, L., Schwarzkopf, F. U., Giese, B. S., Funk, A., and Karstensen, J. (2011). Middepth circulation of the eastern tropical South Pacific and its link to the oxygen minimum zone. *J. Geophys. Res. Oceans* 116:C01015. doi: 10.1029/2010JC006565

Deutsch, C., Ferrel, A., Seibel, B., Pörtner, H. O., and Huey, R. B. (2015). Climate change tightens a metabolic constraint on marine habitats. *Science* 348, 1132–1135. doi: 10.1126/science.aaa1605

Ekau, W., Auel, H., Hagen, W., Koppelmann, R., Wasmund, N., Bohata, K., et al. (2018). Pelagic key species and mechanisms driving energy flows in the northern Benguela upwelling ecosystem and

their feedback into biogeochemical cycles. *J. Mar. Syst.* 188, 49–62. doi: 10.1016/j.jmarsys.2018.03.001

Escribano, R., Hidalgo, P., and Krautz, C. (2009). Zooplankton associated with the oxygen minimum zone system in the northern upwelling region of chile during march 2000. *Deep Sea Res. II Top. Stud. Oceanogr.* 56, 1083–1094. doi: 10.1016/j.dsr2.2008.09.009

Fernández-Álamo, M. A., and Färber-Lorda, J. (2006). Zooplankton and the oceanography of the eastern tropical Pacific: a review. *Prog. Oceanogr.* 69, 318–359. doi: 10.1016/j.pocean.2006.03.003

Gonzalez, R. R., and Quiñones, R. A. (2002). Ldh activity in *Euphausia mucronata* and *Calanus chilensis*: implications for vertical migration behaviour. *J. Plankton Res.* 24, 1349–1356. doi: 10.1093/plankt/24.12.1349

Gorsky, G., Ohman, M. D., Picheral, M., Gasparini, S., Stemmann, L., Romagnan, J.-B., et al. (2010). Digital zooplankton image analysis using the zooscan integrated system. *J. Plankton Res.* 32, 285–303. doi: 10.1093/plankt/fbp124

Grasshoff, K., Kremling, K., and Ehrhardt, M. (2009). *Methods of Seawater Analysis*. Weinheim: John Wiley & Sons.

Hernández-León, S., and Ikeda, T. (2005). A global assessment of mesozooplankton respiration in the ocean. *J. Plankton Res.* 27, 153–158. doi: 10.1093/plankt/fbh166

Hoving, H.-J. T., Christiansen, S., Fabrizius, E., Hauss, H., Kiko, R., Linke, P., et al. (2018). The pelagic *in situ* observation system (pelagios) to reveal biodiversity, behavior and ecology of elusive oceanic fauna. *Ocean Sci.* 15, 1327–1340. doi: 10.5194/os-15-1327-2019

Ianson, D., George A. Jackson, G. A., Angel, M. V., Lampitt, R. S., and Burd, A. B. (2004). Effect of net avoidance on estimates of diel vertical migration. *Limnol. Oceanogr.* 49, 2297–2303. doi: 10.4319/lo.2004.49.6.2297

Ikeda, T. (1985). Metabolic rates of epipelagic marine zooplankton as a function of body mass and temperature. *Mar. Biol.* 85, 1–11.

Ikeda, T. (2014). Respiration and ammonia excretion by marine metazooplankton taxa: synthesis toward a global-bathymetric model. *Mar. Biol.* 161, 2753–2766. doi: 10.1007/s00227-014-2540-5

Kalvelage, T., Jensen, M. M., Contreras, S., Revsbech, N. P., Lam, P., Günter, M., et al. (2011). Oxygen sensitivity of anammox and coupled n-cycle processes in oxygen minimum zones. *PLoS ONE* 6:e29299. doi: 10.1371/journal.pone.0029299

Kalvelage, T., Lavik, G., Jensen, M. M., Revsbech, N. P., Löscher, C., Schunck, H., et al. (2015). Aerobic microbial respiration in oceanic oxygen minimum zones. *PLoS ONE* 10:e0133526. doi: 10.1371/journal.pone.0133526

Kiko, R., Hauss, H., Buchholz, F., and Melzner, F. (2016). Ammonium excretion and oxygen respiration of tropical copepods and euphausiids exposed to oxygen minimum zone conditions. *Biogeosciences* 13, 2241–2255. doi: 10.5194/bg-13-2241-2016

Kiko, R., Hauss, H., Dengler, M., Sommer, S., and Melzner, F. (2015). The squat lobster pleuroncodes monodon tolerates anoxic "dead zone" conditions off Peru. *Mar. Biol.* 162, 1913–1921. doi: 10.1007/s00227-015-2709-6

Kiørboe, T. (2013). Zooplankton body composition. *Limnol. Oceanogr.* 58, 1843–1850. doi: 10.4319/lo.2013.58.5.1843

Krahmann, G. (2015). Physical oceanography during METEOR cruise M93. *PANGAEA*. doi: 10.1594/PANGAEA.848017

Lam, P., Lavik, G., Jensen, M. M., van de Vossenberg, J., Schmid, M., Woebken, D., et al. (2009). Revising the nitrogen cycle in the peruvian oxygen minimum zone. *Proc. Natl. Acad. Sci. U.S.A.* 106:4752. doi: 10.1073/pnas.0812444106

Lampert, W. (1989). The adaptive significance of diel vertical migration of zooplankton. *Funct. Ecol.* 3, 21–27.

Lehette, P., and Hernández-León, S. (2009). Zooplankton biomass estimation from digitized images: a comparison between subtropical and antarctic organisms. *Limnol. Oceanogr. Methods* 7, 304–308. doi: 10.4319/lom.2009.7.304

Lombard, F., Boss, E., Waite, A. M., Uitz, J., Stemmann, L., Sosik, H. M., et al. (2019). Globally consistent quantitative observations of planktonic ecosystems. *Front. Mar. Sci.* 6:196. doi: 10.3389/fmars.2019.00196

Longhurst, A., Bedo, A., Harrison, W., Head, E., and Sameoto, D. (1990). Vertical flux of respiratory carbon by oceanic diel migrant biota. *Deep Sea Res. A Oceanogr. Res. Papers* 37, 685–694.

Maas, A. E., Wishner, K. F., and Seibel, B. A. (2012). Metabolic suppression in thecosomatous pteropods as an effect of low temperature and hypoxia in the eastern tropical North Pacific. *Mar. Biol.* 159, 1955–1967. doi: 10.1007/s00227-012-1982-x

Matear, R. J., and Hirst, A. C. (2003). Long-term changes in dissolved oxygen concentrations in the ocean caused by protracted global warming. *Glob. Biogeochem. Cycles* 17:1125. doi: 10.1029/2002GB001997

Moloney, C. L., and Field, J. G. (1989). General allometric equations for rates of nutrient uptake, ingestion, and respiration in plankton organisms. *Limnol. Oceanogr.* 34, 1290–1299.

Picheral, M., Colin, S., and Irisson, J. (2019). *Ecotaxa, A Tool for the Taxonomic Classification of Images*. Available online at: https://ecotaxa.obs-vlfr.fr

Ren, A. S., Chai, F., Xue, H., Anderson, D. M., and Chavez, F. P. (2018). A sixteen-year decline in dissolved oxygen in the Central California current. *Sci. Rep.* 8:7290. doi: 10.1038/s41598-018-25341-8

Revsbech, N. P., Larsen, L. H., Gundersen, J., Dalsgaard, T., Ulloa, O., and Thamdrup, B. (2009). Determination of ultra-low oxygen concentrations in oxygen minimum zones by the stox sensor. *Limnol. Oceanogr. Methods* 7, 371–381. doi: 10.4319/lom.2009.7.371

Saltzman, J., and Wishner, K. F. (1997). Zooplankton ecology in the eastern tropical Pacific oxygen minimum zone above a seamount: 1. General trends. *Deep Sea Res. I Oceanogr. Res. Papers* 44, 907–930.

Schmidtko, S., Stramma, L., and Visbeck, M. (2017). Decline in global oceanic oxygen content during the past five decades. *Nature* 542:335. doi: 10.1038/nature21399

Seibel, B. A., Luu, B. E., Tessier, S. N., Towanda, T., and Storey, K. B. (2018). Metabolic suppression in the pelagic crab, pleuroncodes planipes, in oxygen minimum zones. *Compar. Biochem. Physiol. B Biochem. Mol. Biol.* 224, 88–97. doi: 10.1016/j.cbpb.2017.12.017

Seibel, B. A., Schneider, J. L., Kaartvedt, S., Wishner, K. F., and Daly, K. L. (2016). Hypoxia tolerance and metabolic suppression in oxygen minimum zone euphausiids: implications for ocean deoxygenation and biogeochemical cycles. *Integr. Compar. Biol.* 56, 510–523. doi: 10.1093/icb/icw091

Steinberg, D. K., and Landry, M. R. (2017). Zooplankton and the ocean carbon cycle. *Annu. Rev. Mar. Sci.* 9, 413–444. doi: 10.1146/annurev-marine-010814-015924

Stramma, L., Johnson, G. C., Sprintall, J., and Mohrholz, V. (2008). Expanding oxygen-minimum zones in the tropical oceans. *Science* 320, 655–658. doi: 10.1126/science.1153847

Stukel, M. R., Ohman, M. D., Benitez-Nelson, C. R., and Landry, M. R. (2013). Contributions of mesozooplankton to vertical carbon export in a coastal upwelling system. *Mar. Ecol. Prog. Ser.* 491, 47–65. doi: 10.3354/meps10453

Thomsen, S., Kanzow, T., Colas, F., Echevin, V., Krahmann, G., and Engel, A. (2016). Do submesoscale frontal processes ventilate the oxygen minimum zone off Peru? *Geophys. Res. Lett.* 43, 8133–8142. doi: 10.1002/2016GL070548

Wishner, K. F., Gowing, M. M., and Gelfman, C. (1998). Mesozooplankton biomass in the upper 1000 m in the arabian sea: overall seasonal and geographic patterns, and relationship to oxygen gradients. *Deep Sea Res. II Top. Stud. Oceanogr.* 45, 2405–2432.

Conflict of Interest: The authors declare that the research was conducted in the absence of any commercial or financial relationships that could be construed as a potential conflict of interest.

frontiers in Marine Science

ORIGINAL RESEARCH
published: 21 January 2020
doi: 10.3389/fmars.2019.00825

Mesozooplankton and Micronekton Active Carbon Transport in Contrasting Eddies

Lian E. Kwong[1], Natasha Henschke[1], Evgeny A. Pakhomov[1,2,3], Jason D. Everett[4,5] and Iain M. Suthers[5,6]*

[1] Department of Earth, Ocean and Atmospheric Sciences, University of British Columbia, Vancouver, BC, Canada, [2] Institute for the Oceans and Fisheries, University of British Columbia, Vancouver, BC, Canada, [3] Hakai Institute, Heriot Bay, BC, Canada, [4] Centre for Applications in Natural Resource Mathematics, The University of Queensland, St. Lucia, QLD, Australia, [5] Evolution and Ecology Research Centre, University of New South Wales Sydney, Sydney, NSW, Australia, [6] Sydney Institute of Marine Science, Mosman, NSW, Australia

Mesozooplankton (June 2015 and September 2017) and micronekton (September 2017) were sampled along the eastern coast of Australia. Depth stratified mesozooplankton and micronekton were collected using a Multiple Opening/Closing Net and Environmental Sensing System (MOCNESS) and an International Young Gadoid Pelagic Trawl (IYGPT) equipped with an opening/closing codend. Sampling was undertaken at the center and edge of a frontal cold-core eddy (F-CCE Center and Edge) in 2015, and at the center of a cold-core eddy (B-CCE) and two warm-core eddies (R-WCE and WCE) in 2017. We assess the diel vertical structure, biomass, and downward active carbon transport by mesozooplankton and micronekton in eddies. Total water column mesozooplankton and micronekton biomass did not vary substantially across water masses, while the extent and depth of diel vertical migration did. Using *in situ* measurements of temperature and measurements of mesozooplankton and micronekton abundance and biomass, we estimated the contribution of respiration, dissolved organic carbon (DOC) excretion, gut flux, and mortality to total downward active carbon transport in each water mass. Overall, active carbon transport by mesozooplankton and micronekton below the mixed layer varied substantially across water masses. We corrected estimates of micronekton migratory biomass and active carbon transport assuming 50% net efficiency. In the R-WCE mesozooplankton remained within the mixed layer during the day and night; only 50% of the total micronekton population migrated below the mixed layer contributing to carbon transport, equating to 2.89 mg C m^{-2} d^{-1}. Mesozooplankton actively transported 16.1 and 8.0 mg C m^{-2} d^{-1} at the F-CCE Center and Edge, respectively. Mesozooplankton and micronekton active carbon transport in the B-CCE were 5.4 and 0.74 mg C m^{-2} d^{-1}, and in the WCE 88 and 13.4 mg C m^{-2} d^{-1}. Differences in carbon export were dependent on food availability, temperature, time spent migrating, and mixed layer depth. These findings suggest that under certain conditions mesoscale eddies can act as important carbon sinks.

Keywords: mesozooplankton, micronekton, southwest Pacific, diel vertical migration, active carbon transport

OPEN ACCESS

Edited by:
Morten Hvitfeldt Iversen, Alfred Wegener Institute, Helmholtz Centre for Polar and Marine Research (AWI), Germany

Reviewed by:
Suzanne Jane Painting, Centre for Environment, Fisheries and Aquaculture Science (CEFAS), United Kingdom
Santiago Hernández-León, University of Las Palmas de Gran Canaria, Spain

****Correspondence:***
Lian E. Kwong
lkwong@eoas.ubc.ca

Specialty section:
This article was submitted to Marine Ecosystem Ecology, a section of the journal Frontiers in Marine Science

Received: *04 June 2019*
Accepted: *20 December 2019*
Published: *21 January 2020*

Citation:
Kwong LE, Henschke N, Pakhomov EA, Everett JD and Suthers IM (2020) Mesozooplankton and Micronekton Active Carbon Transport in Contrasting Eddies. Front. Mar. Sci. 6:825. doi: 10.3389/fmars.2019.00825

INTRODUCTION

The planktivorous mesopelagic fishes arguably have the Earth's largest fish biomass, which is likely underestimated by an order of magnitude due in part to the unknown energy transfer through the zooplankton component of pelagic food webs (Irigoien et al., 2014). Energy fluxes between the epipelagic (<200 m) and the mesopelagic (200–1000 m) layers vary globally and play a key role in determining marine productivity and fisheries (Young et al., 2011, 2015; Kiko et al., 2017; Reygondeau et al., 2017). The permanent mesopelagic inhabitants (non-vertical migrators) rely on both the passive sinking of epipelagic particles and migratory organisms as a food source, although the proportional importance is still debated (Hannides et al., 2013; Choy et al., 2015). Due to surface waters warming, epipelagic productivity and vertical energy flux dynamics are expected to change as animals retreat to cooler waters resulting in vertical and/or latitudinal shifts (Poloczanska et al., 2016). Therefore, resolving the factors that influence vertical energy flux is central to understanding the implications of environmental change on commercially valuable fisheries and vertical carbon flux.

Mesozooplankton (0.2–20 mm) and micronekton (20–200 mm) undergo extensive diel vertical migrations (DVMs), feeding in the highly productive surface waters at night and migrating back down to depth during the day where they reside to avoid predation (Iwasa, 1982; Hays et al., 1997) and improve metabolism (McLaren, 1974; Enright, 1977; Iwasa, 1982; Hernández-León et al., 2010). Depending on the assemblages and their body size, they can migrate to depths of 500–1000 m (Baird et al., 1975; Irigoien et al., 2014). Once at depth, these organisms metabolize surface-derived nutrients releasing carbon by way of respiration, dissolved organic carbon (DOC) excretion, gut flux, and mortality (Steinberg et al., 2000; Ducklow et al., 2001; Davison et al., 2013; Steinberg and Landry, 2017). As these processes are largely size, temperature, and pressure dependent they can therefore be calculated for whole communities by applying a size-based approach (Zhang and Dam, 1997; Steinberg et al., 2000; Ikeda, 2013a, 2014, 2016). Larger organisms likely transport more carbon due to their deeper migrations (Sameoto et al., 1987; Moteki et al., 2009), body size/mass (Hansen and Visser, 2016), large fecal pellets (Turner, 2002), and long gut passage times (GPTs) (Baird et al., 1975; Dagg and Wyman, 1983; Reinfelder and Fisher, 1994; Pakhomov et al., 1996).

The importance of vertically migrating zooplankton and micronekton to biogeochemical cycling is becoming increasingly apparent, although it remains largely unquantified (Tsubota et al., 1999; Hansen and Visser, 2016; Gorgues et al., 2019). Most studies focus on specific aspects of active carbon transport such as the respiration, DOC excretion, gut flux, and/or mortality of individual species (Kobari et al., 2008), groups (i.e., orders or classes of zooplankton and micronekton; Hidaka et al., 2001; Davison et al., 2013) or specific size ranges (e.g., 0.1–1 mm total length; Hernández-León et al., 2001; Davison et al., 2013; Ariza et al., 2015). It is rare that all fluxes (i.e., respiration, DOC excretion, gut flux, and mortality) are considered when estimating active carbon transport via mesozooplankton and micronekton (Steinberg and Landry, 2017). By neglecting certain species/taxa, sizes, or fluxes, we are underestimating carbon export to the deep ocean, leading to inconsistencies between models (Falkowski et al., 2003; Usbeck et al., 2003; Martz et al., 2008; Davison et al., 2013). There remains a high uncertainty in active carbon transport estimates stemming largely from methodological approaches and spatial variability (Steinberg and Landry, 2017).

Distinct biological communities develop in mesoscale eddies, which are particularly effective at retaining and transporting organisms that undergo DVM (Mackas and Galbraith, 2002). Within eddies, differences in phytoplankton composition and zooplankton biomass, respiration, and fecal pellet production have been observed between the center and periphery of eddies (Mackas and Coyle, 2005; Yebra et al., 2005; Goldthwait and Steinberg, 2008; Landry et al., 2008). To our knowledge only four studies have looked at the effects of mesoscale eddies on active carbon transport (Yebra et al., 2005, 2018; Landry et al., 2008; Shatova et al., 2012). These studies looked at specific fluxes (i.e., gut flux and respiratory flux) by mesozooplankton. No studies have looked at the contribution of micronekton to carbon transport, though some suggest that micronekton aggregate in and around eddy centers (Sabarros et al., 2009; Drazen et al., 2011).

In the southwestern Pacific Ocean, there are no studies that look at active carbon transport of both mesozooplankton and micronekton within or across eddies, but one study assessed the contribution of pelagic tunicates (Henschke et al., 2019). Some mesozooplankton and micronekton studies have focused on the subtropical convergence off eastern Tasmania (Young and Blaber, 1986; Young et al., 1987, 1988), while the mesozooplankton and micronekton communities in the temperate Tasman Sea are comparatively understudied. Changes in zooplankton communities have been observed off southeastern Australia as a result of a southerly extension of the East Australian Current (EAC) and its eddy field, with continued changes likely to have impacts on pelagic fish and fisheries in the area (Hobday et al., 2011; Kelly et al., 2016).

In the southwest Pacific, the EAC transports warm, tropical water southwards along the coast until it diverges eastward at ∼32°S (Suthers et al., 2011; Cetina-Heredia et al., 2014). Associated with the EAC is a dynamic mesoscale eddy field, where frequent cyclonic (cold-core) and anti-cyclonic (warm-core) eddies are formed (Everett et al., 2012). Generally, cold-core eddies in this region have been found to create more productive pelagic habitats compared to warm-core eddies (Greenwood et al., 2007; Everett et al., 2012). The pelagic environments of cold- and warm-core eddies are often different to each other, and to the surrounding water due to a range of eddy-driven processes such as entrainment (Greenwood et al., 2007; Everett et al., 2015), eddy induced Ekman pumping (McGillicuddy and Robinson, 1997; Martin and Richards, 2001), or eddy trapping (Chenillat et al., 2018).

In this study, our overall goal was to compare the biomass, diel-vertical migration, and vertical fluxes of mesozooplankton and micronekton communities across a range of eddy environments along the eastern coast of Australia during

the winter of 2015 and the spring of 2017. Specifically, our aims were to (a) assess the diel vertical structure of mesozooplankton and micronekton biomass between eddies, and to (b) quantify downward active carbon transport mediated by mesozooplankton and micronekton.

MATERIALS AND METHODS

Study Area

Sampling was undertaken from the *RV Investigator* in the western Tasman Sea during winter (2–18 June 2015) and spring (6–15 September 2017) voyages. The sampling area extended from Brisbane (27.5°S) south to Batemans Bay (35.7°S; **Figure 1**). The hydrographic features in the region were identified using a combination of satellite-derived chlorophyll *a* [Moderate Resolution Imaging Spectroradiometer; MODIS-Aqua via Integrated Marine Observing System (IMOS)], sea-surface temperature (MODIS-Aqua via IMOS[1]), and altimetry (IMOS and bathymetry data; General Bathymetric Chart of the Oceans; GEBCO).

Five water types were sampled during this study. In June 2015, the center and the edge of an ∼35 km frontal cold-core eddy ("F-CCE") was sampled off Forster (∼33°S; **Figures 1B,C**). This productive eddy formed adjacent to the continental shelf a week prior to sampling, entraining shelf water, before moving off the shelf into the warmer EAC (Roughan et al., 2017). In September 2017, three eddies were sampled (**Figures 1D,E**): an ∼150 km cold-core eddy off Brisbane (∼27.5°S; "B-CCE"), a large (∼200 km) warm-core eddy (WCE) that formed from the retroflection of the EAC (∼33°S; R-WCE), and an ∼150 km WCE sampled south of the Tasman Front (∼35°S) that was also formed from EAC water (Henschke et al., 2019).

Eddies were identified using a combination of satellite SST and altimetry, and an onboard Acoustic Doppler Current Profiler (ADCP). The 2015 F-CCE was too small to be visible using altimetry, but was clearly visible in SST, and verified using the ADCP (**Figure 1B**). The 2017 eddies were all large enough to be observed using satellite altimetry (**Figure 1D**).

Oceanographic Sampling

At each eddy a Seabird SBE911-plus Conductivity–Temperature–Depth (CTD) probe equipped with a calibrated Chelsea Aqua-Tracker Mk3 fluorometer and fitted with 12 L bottles on a rosette sampler was used to profile temperature, salinity, and fluorescence. Mixed later depth (MLD) for each eddy was calculated following Levitus (1982) as the depth at which $\sigma_T >$ surface $\sigma_T + 0.125$, where σ_T is the density. Water samples taken from the rosette at various depths were used to measure nutrients and calibrate oxygen and chlorophyll *a* from the CTD. Dissolved inorganic nutrient measurements were made using automated continuous flow with colorimetric detection following CSIRO standard operating procedures (Rees et al., 2018). Fluorescence was converted to chlorophyll *a* concentrations through regression analyses as described in Roughan et al. (2017) for 2015 samples ($r^2 = 0.81$, $n = 66$) and Henschke et al. (2019) for 2017 samples ($r^2 = 0.84$, $n = 20$) to provide full water column chlorophyll *a* estimates. Dissolved oxygen concentrations were determined using the Winkler-titration method (Strickland and Parsons, 1972).

Mesozooplankton (June 2015 and September 2017) and micronekton (September 2017) sampling was concentrated in the eddy centers. Additional mesozooplankton sampling was undertaken outside the eddy in 2015 (**Supplementary Table S1**).

Mesozooplankton

Depth-stratified sampling for mesozooplankton was undertaken during the day and night using a Multiple Open-Closing Net and Environmental Sensing System (MOCNESS). The MOCNESS had a mouth-opening of 1 m^2 and consisted of five nets that can be triggered remotely, all fitted with 500 μm mesh. The MOCNESS was lowered to 500 m and five oblique tows were performed while the vessel was traveling at 1.5 m s^{-1}: 500–400, 400–300, 300–200, 200–100, and 100 m to the surface. Immediately after collection, approximate mesozooplankton size classes were determined by gently rinsing the contents of each cod-end through a sieve column to four size classes: 500–1000, 1000–2000, 2000–4000, and >4000 μm. All organisms that were >4000 μm were individually measured, counted, and grouped into two additional logarithmic size classes: 4000–8000 and 8000–16,000 μm. The groups were placed onto pre-weighed petri dishes, oven dried at 50°C, and weighed to the nearest 0.01 g. Dry weight was converted to carbon weight (mg C m^{-3}) assuming carbon weight = 0.4 * dry weight (Parsons et al., 1984; Steinberg et al., 2000). Total biomass (mg C m^{-3}) for each tow was total carbon weight captured in each tow divided by volume filtered. Abundance of each size fraction was calculated as follows. A representative biovolume for an animal equal to the mid-size of the size-fraction was calculated by assuming ellipsoid shape and near-neutral density following Suthers et al. (2004). Wet weights were then converted to dry weight assuming dry weight = 0.1 * wet weight (Weibe et al., 1975). Finally, we calculated total mesozooplankton abundance in each size-fraction (i.e., counts per tow) by dividing total dry weight of the size fraction by the mean animal dry mass.

Volume of water filtered was calculated using the G.O. mechanical flow meter (General Oceanics Inc., Miami, United States) mounted on the MOCNESS.

Micronekton

In 2017, additional sampling was undertaken to quantify micronekton (20–200 mm) biomass in each eddy using a 157.5-m^2 International Young Gadoid Pelagic Trawl (IYGPT). Mesh size of the trawl reduced from 200 mm stretched mesh width at the mouth to 10 mm in the codend. The trawl was equipped with a MID water Open and Closing net system (MIDOC; Marouchos et al., 2017), with a 1-m^2 mouth area and six cod-ends graduating from 10 mm mesh to 500 μm mesh. The MIDOC was lowered to two target depths (500 and 1000 m) during both the day and night while the vessel maintained a speed of 1 m s^{-1}. We employed two different depth stratified sampling strategies: (1) 1000–900, 900–800, 800–700, 700–600, 600–500, and 500–0 m, and (2) 0–500,

[1]http://imos.aodn.org.au/imos/

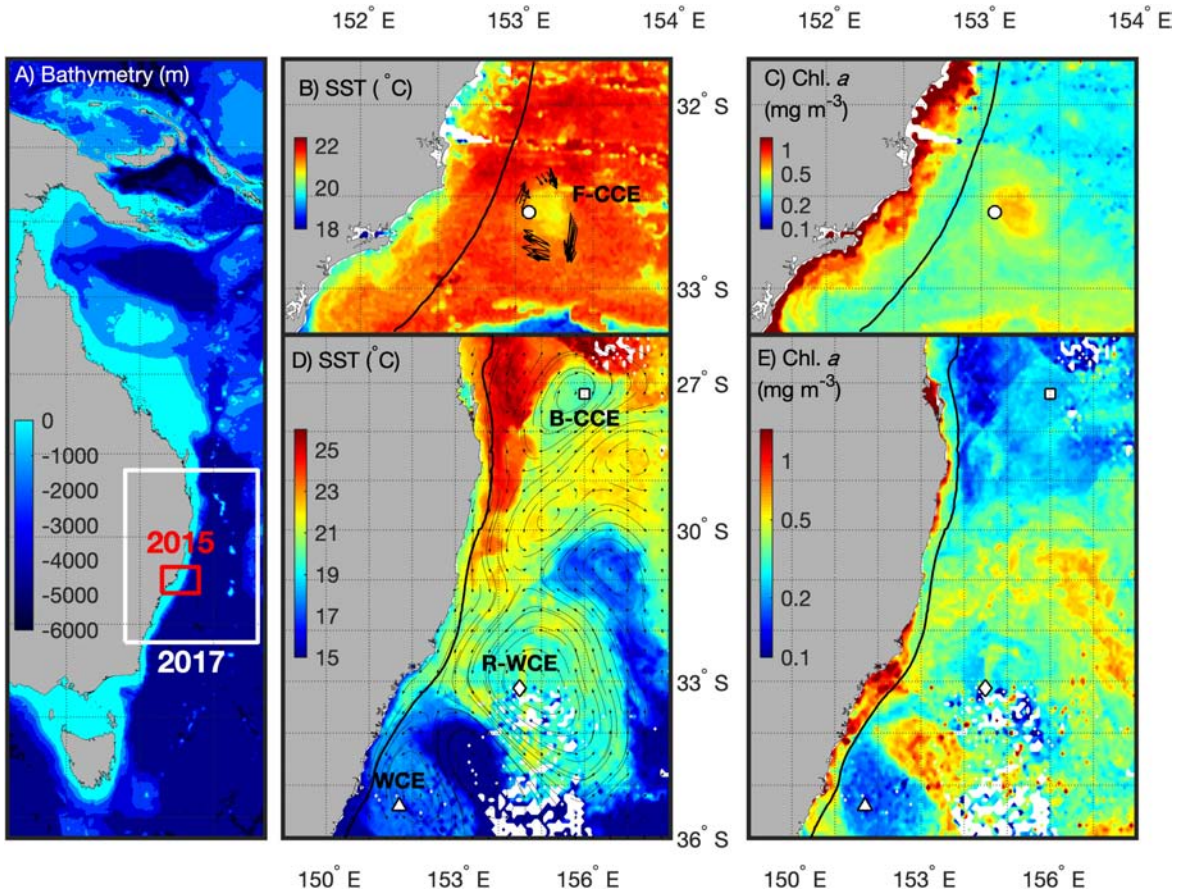

FIGURE 1 | Southeast coast of Australia **(A)** highlighting the 2015 (red) and 2017 (white) sampling locations with bathymetry overlaid. For 2015 (top) the F-CCE location **(○)** is shown with **(B)** Sea Surface Temperature (SST) and ADCP data (Roughan et al., 2017), and **(C)** chlorophyll *a* (Chl. *a*) data from the 8–9 June 2015. For 2017 (bottom) the locations of the B-CCE **(□)**, R-WCE **(◇)**, and WCE **(△)** are shown with **(D)** SST and altimetry data from IMOS, and **(B)** Chl. *a* data from the 3–5 September 2017. The black line represents the 200 m shelf **(B–E)**.

500–400, 400–300, 300–200, 200–100, and 100–0 m. Each depth stratum was sampled for ∼20–40 min (**Supplementary Table S1**). The volume of water filtered was calculated based on the spread and height of the MIDOC doors and the distance traveled through the water column.

Immediately after collection, micronekton were separated into major taxonomic groups, identified to the lowest possible taxonomic level, counted, individually weighed, and photographed for body length (mm). The major taxonomic groups included myctophids, decapods, and cephalopods (for a complete species list, see **Supplementary Table S2**). We did not include gelatinous organisms (i.e., siphophores, jellyfish, and salps) in our analysis, as they were often damaged in net tows. Carbon weights were calculated using individual lengths and length to weight relationships (LWRs) from the literature or FishBase Bayesian LWR (Froese et al., 2014), by directly weighing the individuals, or by using the average LWR of the genus or family (**Supplementary Table S3**). Where no direct carbon weight to wet weight relationship was available, we assumed carbon weight = 20% of wet weight (Crabtree, 1995; Andersen et al., 2016). Abundance for each size class (mesozooplankton) and taxon (micronekton) was determined by dividing the number of individuals captured in each tow by the volume of water filtered.

For our analysis, we include organisms from the MOCNESS ranging from 0.5 to 16 mm in size and from the MIDOC 20 to 200 mm total length. All values are reported as mean ± standard error (S.E.).

Data Analysis

To test the day and night differences in mesozooplankton and micronekton biomass at each eddy we applied ANOVA, but first tested the assumptions using Bartlett's test (homogeneity of variance) and Shapiro–Wilk test (normality) using R Statistical Software (R Core Team). All statistical values are reported in **Supplementary Tables S4**, **S5**.

Active Carbon Transport

The migratory community refers to the portion of mesozooplankton and micronekton that actively migrate into the mixed layer during the night to feed and reside below the mixed layer during the day. This portion of the

community was calculated based on day and night differences in biomass within the mixed layer. Thus, only the biomass migrating below the MLD were included in our calculation of downward active carbon flux at each location. Organisms that do not migrate below the MLD instead contribute to carbon "recycling" within the MLD, whereby, they consume organic matter and respire, excrete, die, and produce fecal pellets that remain within the MLD.

To determine depth of vertical migration, we calculated the weighted mean depth (WMD, m) for each taxonomic group as follows:

$$\mathrm{WMD}_{ji} = \frac{\sum (b_{ji} * d_{ji})}{\sum b_{ji}}$$

where b_{ji} is the biomass (mg CW m^{-3}) and d_{ji} is the midpoint of the depth stratum (m) for taxon j in each sampling location (i).

For mesozooplankton we infer total abundance (N) in each size bin using geomean carbon weight (GM; mg ind.$^{-1}$), which represents mean carbon weight of an individual (ind.) in size bin x, and total carbon weight (CW; mg) within size bin x as follows:

$$N = \frac{\mathrm{CW}_x}{\mathrm{GM}_x}.$$

To calculate the contribution of mesozooplankton and micronekton to active carbon transport, we must first calculate individual respiration, DOC excretion, gut flux (defecation), and mortality. To do so, we calculate individual rate processes using size-dependent rate equations. Individual rates are then scaled up using migratory densities, and the depth of export is assumed using WMD. Finally, we also calculate the carbon flux to migratory biomass ratio for each group to assess the downward contribution per day.

Respiration

Respiratory oxygen uptake (RO; μL O_2 ind.$^{-1}$ h^{-1}) was calculated using size, temperature, and taxon-specific rate equations (**Supplementary Table S6**). Respiratory oxygen uptake was converted into respiratory carbon equivalent (RC; μg C ind.$^{-1}$ d^{-1}) as follows:

$$\mathrm{RC} = \mathrm{RO} * \mathrm{RQ} \frac{12}{22.4} * \mathrm{TD}$$

where RQ is the respiratory quotient (**Supplementary Table S6**), 12 is the molar weight of carbon (g mol^{-1}), 22.4 is the molar volume (mol L^{-1}) of an ideal gas at standard pressure and temperature, and TD is the time spent at depth. Community respiration was then calculated by adding together individual respiration rates for each depth stratum.

Excretion

Dissolved organic carbon excretion was assumed to be 31% of CO_2 respiration based on Steinberg et al. (2000). The study reported that DOC excretion was on average 31% of CO_2 respiration (μg C respired) or 24% of the total metabolized carbon (i.e., excreted + respired), and found similar variation, depending on environmental temperature and organism weight, across crustacean species. We apply the same relationship for DOC excretion to myctophids, as estimates for fishes are lacking in the literature (Hudson et al., 2014).

Mortality

We apply two different approaches to calculate zooplankton and micronekton mortality to ease comparison with other studies, and to demonstrate the vast variability in estimates.

For our model, downward carbon flux arising from zooplankton and micronekton mortality was calculated based on the Zhang and Dam (1997) adaptation of Peterson and Wroblewski (1984). This approach assumes that predation scales in an isometric fashion.

$$M_{\mathrm{h}} = \frac{(5.26 * 10^{-3}) * \mathrm{DW}^{-0.25}}{24}$$

where M_h is the hourly weight-specific mortality rate based on individual dry weight (DW; g). M_h can be multiplied by the number of hours spent at depth to obtain individual contribution to downward flux attributed to natural mortality.

For comparison, we also calculate mortality from growth as in Hernández-León et al. (2019). Assuming our systems are in steady-state, growth should be approximately equivalent to mortality. We calculate zooplankton growth according to Ikeda and Motoda (1978), where Growth = 0.75 * Respiration. For micronekton, we use the growth/metabolism ratio (0.66) from Brett and Groves (1979).

Gut Flux

We assume that organisms migrating into the surface waters during the night are feeding to complete satiation, and use the average index of stomach fullness (ISF; dry weight of stomach contents/dry weight of organism) and organism size (DW; mg) to calculate food ball dry weight (FB; mg):

$$\mathrm{FB} = \mathrm{DW} * \mathrm{ISF}.$$

Taxon-specific estimates of mean ISF were compiled from the literature and are provided in **Supplementary Table S7**. Food ball dry weight is converted to carbon units assuming carbon weight = 0.4 * dry weight (Parsons et al., 1984; Steinberg et al., 2000). We apply an assimilation efficiency of 88% to calculate the average carbon weight of the daily egested material (E; mg C d^{-1}) (Hopkins and Baird, 1977). Assuming egestion is constant throughout the day, we divide daily egestion (E) by 24 h to obtain hourly egestion. To contribute to downward gut flux, GPT (**Supplementary Table S7**) must exceed the amount of time spent on downward migration (DM; h) (**Table 1**); where this is not the case (i.e., GPT ≤ DM) gut flux was automatically set to zero. Time spent on downward migration, at depth, and at the surface were estimated based on the acoustic backscatter from the onboard EK60 (Suthers, 2017). Therefore, total downward gut flux is:

$$\mathrm{GF} = \left(\frac{E}{24\,\mathrm{h}}\right) * (\mathrm{GPT} - \mathrm{DM}).$$

Gut passage times (h) for the various taxa captured were compiled from the literature (**Supplementary Table S7**). Gut flux of polychaetes and mollusks was calculated assuming that they

TABLE 1 | Hours micronekton spent migrating upward, staying at the surface (night), migrating downward and staying at depth (day), and during diel vertical migrations derived from EK60.

	Upward migration (h)	Surface (h)	Downward migration (h)	Depth (h)
B-CCE	2	11.5	0.75	9.75
R-WCE	1	11.5	1.5	10
WCE	2.5	11	1	9.5

had the same ISF and GPT as copepods, as no specific estimates were available from the literature. Previous studies argue that pelagic mollusks exhibit similar feeding strategies as copepods, with short GPTs (Dagg and Wyman, 1983; Reinfelder and Fisher, 1994). For the MOCNESS data, copepods and mollusks made up the majority of the biomass. Therefore, we assume short GPTs (1.04 h; Dagg and Wyman, 1983; Reinfelder and Fisher, 1994). As no echogram is available for the 2015 voyage, we assume the downward migration at the F-CCE (center and edge) will be similar to that of the B-CCE (i.e., 0.75 h).

RESULTS

Oceanographic Setting

The F-CCE Center (58 m) and F-CCE Edge (102 m) had shallow mixed layers (**Figure 2A**) and temperature and salinity profiles were characteristic of shelf water and EAC water, respectively (Roughan et al., 2017). The F-CCE Center was less saline and had significantly higher chlorophyll *a* concentrations (0.96 ± 0.12; $F_{4,29} = 82.66$, $p < 0.001$) in the surface layer (0–50 m) compared to other water masses. Nutrient levels were low in surface waters, but increased rapidly from 50 m. In comparison, the F-CCE Edge was more saline, warmer, and had lower chlorophyll *a* and nutrient concentrations than the F-CCE Center. Dissolved oxygen declined sharply below the mixed layer to minimums near 100 (Center) and 150 m (Edge) (**Figure 2E**).

The B-CCE was starting to decay, as evidenced from the rising sea-level anomaly (not shown; Ocean Current via IMOS[2]). It had a shallow mixed layer depth (MLD) (91 m; **Figure 2A**), low surface nutrients (**Figure 2D**), and low chlorophyll *a*, with a chlorophyll *a* max (0.51 mg m^{-3}) occurring near the MLD (**Figure 2C**). Below the mixed layer, dissolved oxygen declined rapidly until ∼100 m, but did not reach hypoxic conditions (**Figure 2E**).

The R-WCE and WCE were both approximately 1–2 months old and formed from the EAC. Both the R-WCE (MLD, 236 m) and WCE (MLD, 322 m) were deeply mixed and characterized by saline, oligotrophic water (**Figures 2A–C**). Across all water masses, nutrient levels were the highest in surface waters (0–50 m) of the WCE (2.17 ± 0.02; $F_{4,17} = 2073.45$, $p < 0.001$), and both nutrients and chlorophyll *a* remained well mixed in the top 200 m of the WCE. Nutrient levels were low and well mixed in the R-WCE to 300 m. Prior to and during sampling, the complex R-WCE was entraining oligotrophic EAC water, resulting in a lower nutrient concentration, as was observed in the CTD profiles. Hence, it is difficult to observe the R-WCE from satellite SST and chlorophyll *a* (**Figure 1**). Dissolved oxygen remained high in the mixed layers of both the R-WCE and WCE, reaching minimums at 460 and 380 m, respectively (**Figure 2E**).

Mesozooplankton and Micronekton

Total Water Column Biomass

In 2015, mesozooplankton biomass in the F-CCE ranged from 1.2 to 2.3 mg C m^{-3}. Our data met the assumptions of homogeneity of variance and normality (**Supplementary Table S4**). We detected no statistically significant difference in total water-column mesozooplankton biomass between the F-CCE Center and Edge ($p = 0.41$). Day and night mesozooplankton biomass was significantly different at the F-CCE Center ($p = 0.007$), while no difference was detected at the F-CCE Edge ($p = 0.649$) (**Supplementary Table S5**). Generally, biomass at both the F-CCE Center and Edge was higher at night (2.31 ± 0.09 and 1.68 ± 0.33 mg C m^{-3}, respectively) than during the day (1.24 ± 0.007 and 1.41 ± 0.54 mg C m^{-3}, respectively) (**Figure 3**).

In 2017, the total water-column mesozooplankton biomass ranged from 0.55 to 2.2 mg C m^{-3}. The mesozooplankton biomass in the B-CCE did not vary significantly between day and night ($p = 0.77$; **Supplementary Table S7**). Daytime biomass in the R-WCE was higher than nighttime, while the WCE showed the opposite trend with substantially higher biomass at night (**Figure 3**). We were unable to test these differences statistically due to lack of replication.

Mean micronekton biomass was consistently higher at night than during the day and ranged from 0.07 to 0.21 mg C m^{-3}. However, day and night differences were not statistically significant in all three eddies ($p > 0.32$; **Figure 3**; **Supplementary Table S5**). This suggests that our sampling captured similar overall micronekton biomass during the day and night across all three eddies (see the section "Vertical Migration and Active Carbon Transport" for discussion of net avoidance). The majority of micronekton biomass (68–83%) was made up of myctophids (38–62%) and decapods (22–31%). Cephalopods (4–14%) and other fish (7–15%) were the next most dominant in terms of carbon biomass. All other groups contributed <5% to the total biomass (**Table 2**). Thus, we calculate migratory biomass and active carbon transport for all micronekton, and present only the results for myctophids and decapods in detail.

Vertically Resolved Biomass

In 2015, mesozooplankton biomass (mean ± SE) in the top 100 m increased by >200% at night in the F-CCE Center (night = 15 ± 0.6 and day = 6 ± 0.05 mg C m^{-3}) and increased by 50% in the F-CCE Edge (night = 9 ± 0.7 and day = 6 mg C m^{-3}) (**Figure 4**). All other depth strata showed minimal changes between the day and night at the F-CCE Center and Edge (**Figure 4**), suggesting that mesozooplankton from below our maximum sampling depth (500 m) were migrating into the top 100 m of the water column at night.

In 2017, mesozooplankton biomass was highest at night in the top 100 m except for the R-WCE, which had higher biomass during the day in the 100 m depth stratum (**Figure 5**). Overall,

[2]http://oceancurrent.imos.org.au/

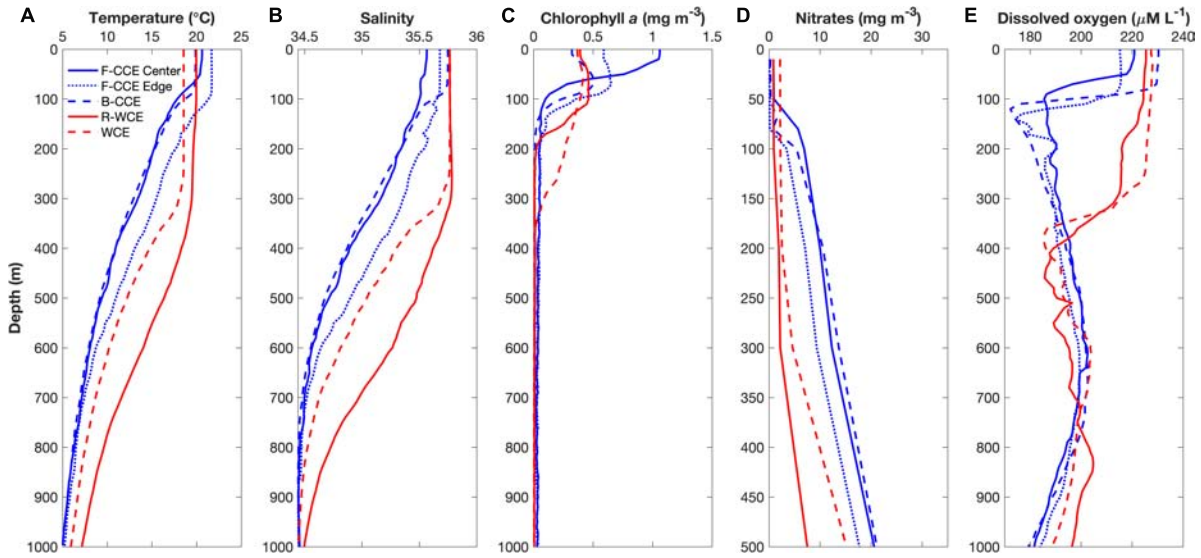

FIGURE 2 | Depth profiles of **(A)** temperature (°C), **(B)** salinity, **(C)** chlorophyll *a* (mg m^{-3}), **(D)** nitrates (mg m^{-3}), and **(E)** dissolved oxygen (μM L^{-1}) in the F-CCE Center (blue solid), F-CCE Edge (blue dotted), B-CCE (blue dashed), R-WCE (red solid), and WCE (red dashed).

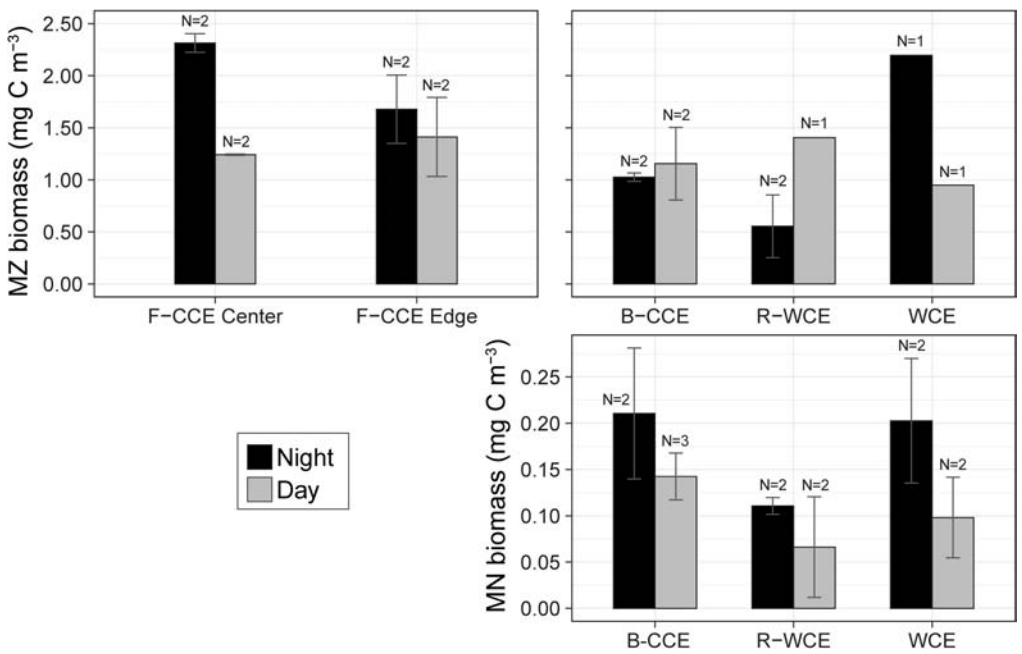

FIGURE 3 | Total water column mean mesozooplankton (MZ; **top**) and micronekton (MN; **bottom**) biomass (mg C m^{-3}) in the top 500 (MZ) and 1000 m (MN) during the night (black) and day (gray) at the F-CCE Center, F-CCE Edge, B-CCE, R-WCE, and WCE. Bars indicate ± standard error of the mean.

mesozooplankton biomass in the top 100 m at night was at least three times greater in the WCE (134 mg C m^{-3}) than in the B-CCE (44 ± 3 mg C m^{-3}) and the R-WCE (38 mg C m^{-3}) (**Figure 5**). During the day, biomass in the top 100 m decreased in the B-CCE (35 ± 6 mg C m^{-3}) and the WCE (27 mg C m^{-3}), while biomass in the R-WCE increased (62 mg C m^{-3}). Biomass was generally higher in all other depth strata during the night except for the WCE 400–300 m depth stratum (**Figure 5**). Thus, mesozooplankton were performing DVM into the top 100 m at night in the B-CCE and the WCE, and reverse DVM into the top 100 m during the day in the R-WCE (**Figure 5**).

Total micronekton biomass increased at night in the top 100 m in the R-WCE and the WCE, while remaining relatively constant in the B-CCE (**Figure 5**). Notable changes in the contribution of myctophids and decapods to total biomass in each depth stratum were observed during the day and night. In the B-CCE,

TABLE 2 | Proportion of micronekton carbon biomass by major taxonomic group captured in the MIDOC.

	Proportion of micronekton biomass (%)		
Group	**B-CCE**	**R-WCE**	**WCE**
Amphipoda	1	1	<1
Cephalopoda	**9**	**4**	**14**
Chaetognatha	<1	<1	<1
Decapoda	**23**	**22**	**31**
Sternoptychidae	3	3	2
Mollusca	1	2	<1
Myctophidae	**58**	**62**	**38**
Pyrosoma	1	<1	1
Other fish	4	5	13
Other crustaceans	<1	<1	<1

Dominant taxonomic groups are bolded.

myctophids and decapods were more prevalent >300m at night and <300 m during the day (**Figure 5D**), with decapods making up the majority of the migratory biomass (**Table 3**). The R-WCE showed a similar trend, although myctophid and decapods were more prevalent >200 m at night and <100 m during the day (**Figure 5E**), with myctophids made up the majority of the migratory biomass (**Table 3**). In the WCE, myctophids were prevalent in the top 100 m during both the day and night, yet biomass increased below 600 m during the day (**Figure 5F**), with decapods making up the majority of the migratory biomass (**Table 3**). A notable increase in decapod biomass in the top 100 m was observed at night in the WCE (**Figure 5F**).

Overall, the WMD of myctophids and decapods became shallower at night in the B-CCE and the WCE (**Figures 5D,F**), indicating that the populations were undergoing DVM. Myctophids migrated from daytime WMDs of 497 and 652 m to nighttime WMDs of 296 and 202 m in the B-CCE and the WCE, respectively. Similarly, decapods migrated from daytime WMDs of 634 and 577 m to nighttime WMDs of 262 and 286 m in the B-CCE and the WCE. Total migratory biomass into the MLD was substantially higher in the WCE (262 μg C m^{-3} d^{-1}) than in the B-CCE (50 μg C m^{-3} d^{-1}). In the R-WCE, WMDs for myctophids and decapods were shallower during the day than at night (**Figure 4**). For myctophids, WMD was 205 m during the day and 292 m at night and for decapods 237 m during the day and 469 m at night. Further, 44 and 42% of the myctophid and decapod population were remaining within the MLD during the day (**Figure 4**), while the rest were migrating below the MLD.

Active Carbon Transport

Total downward carbon flux by mesozooplankton and micronekton varied across water masses. In 2015, mesozooplankton downward carbon export at the F-CCE Center (16.1 mg C m^{-2} d^{-1}) was double that at the F-CCE Edge (8.0 mg C m^{-2} d^{-1}) (**Table 3**).

In 2017, total migratory mesozooplankton and micronekton biomass was highest in the WCE (**Table 3**). Similarly, total mesozooplankton and micronekton downward carbon flux below the MLD was substantially higher in the WCE (88 and 6.7 mg C m^{-2} d^{-1}, respectively) than in the B-CCE (5.4 and 0.4 mg C m^{-2} d^{-1}, respectively) (**Table 3**). Mesozooplankton migrated within the MLD in the R-WCE, recycling carbon in the top 200 m of the water column (2.2 mg C m^{-2} d^{-1}) (**Table 3**). Additionally, only 56 and 58% of the myctophid and decapod biomass were migrating below the MLD, while all other micronekton remained within the MLD during the day and night (**Figure 5**). Therefore, 50% of the total biomass and 51% of the active carbon flux in R-WCE were being exported below the MLD during DVM, equating to 1.5 mg C m^{-2} d^{-1} (**Table 3**).

Overall, respiratory and mortality flux contributed the most to downward carbon transport in all three water masses (**Table 4**). We found that mortality flux varied substantially depending on the model approach (**Table 5**). When estimated from growth, mortality was greater for mesozooplankton in the F-CCE Center and Edge, and lower for mesozooplankton in the B-CCE and WCE (**Table 5**). In contrast, both approaches yielded similar results for micronekton, though estimates derived from growth were generally more conservative.

Although mesozooplankton contributed more to overall downward carbon transport in each water mass, when scaled based on migratory biomass (i.e., carbon flux/migratory biomass for each group) micronekton ultimately contributed more to downward carbon transport (**Table 4**). Of all micronekton groups, myctophids and decapods contributed the most to carbon flux in all three water masses (**Table 3**). Specifically, myctophids contributed more in the B-CCE and WCE, while decapods contributed more in the R-WCE when scaled based on migratory biomass (**Table 4**).

DISCUSSION

This study quantifies mesozooplankton and micronekton active carbon flux in contrasting eddies. Although differences in mesozooplankton and micronekton composition in warm- and cold-core eddies have previously been assessed (e.g., The Ring Group, 1981; Goldthwait and Steinberg, 2008; Eden et al., 2009), their contribution to active carbon flux within and across eddies remains poorly understood (e.g., Goldthwait and Steinberg, 2008; Landry et al., 2008). Despite similarities in total water column biomass, we observed notable differences in mesozooplankton and micronekton migratory biomass and their contribution to carbon export across eddies. Mesozooplankton and micronekton were contributing to downward carbon export below the MLD in the F-CCE Center and Edge, B-CCE, and WCE, and recycling carbon in the R-WCE.

Mesozooplankton and Micronekton Total Water Column Biomass

Eddies form partially isolated and distinct biological communities which can be transported large distances (Mackas and Galbraith, 2002; Batten and Crawford, 2005; Eden et al., 2009; Suthers et al., 2011; Condie and Condie, 2016). They can aggregate micronekton populations due to bottom-up effects intensifying food-web interactions. This aggregation

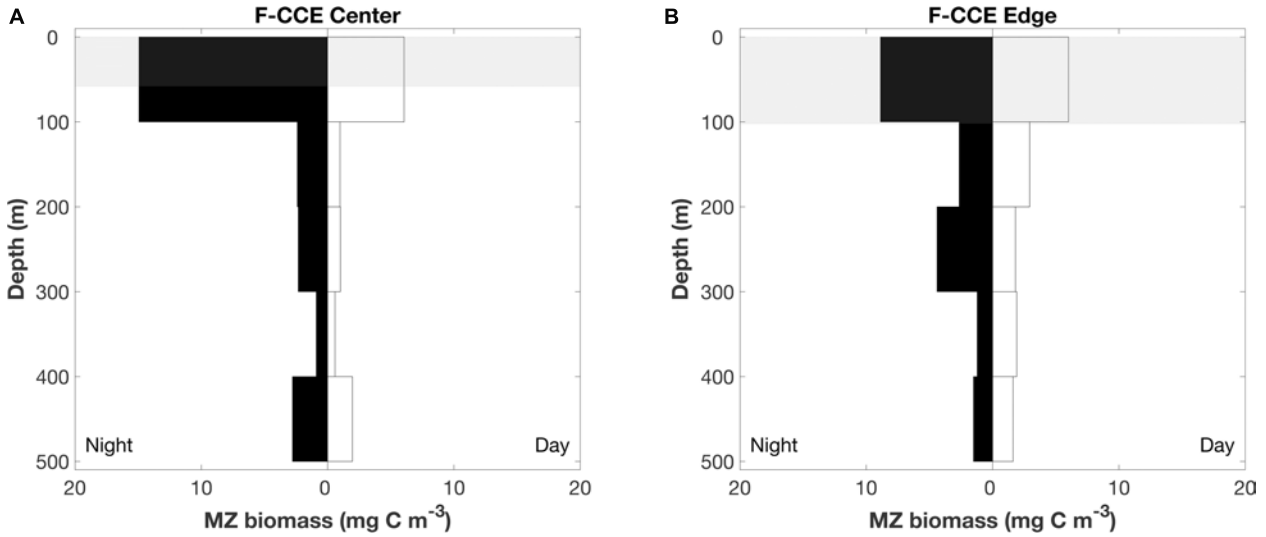

FIGURE 4 | Depth profile of mesozooplankton at the **(A)** F-CCE Center and **(B)** F-CCE Edge. Nighttime profiles are left-hand panes, and daytime profiles are right-hand panes. Shaded gray areas represent mean (±SD) mixed layer depth.

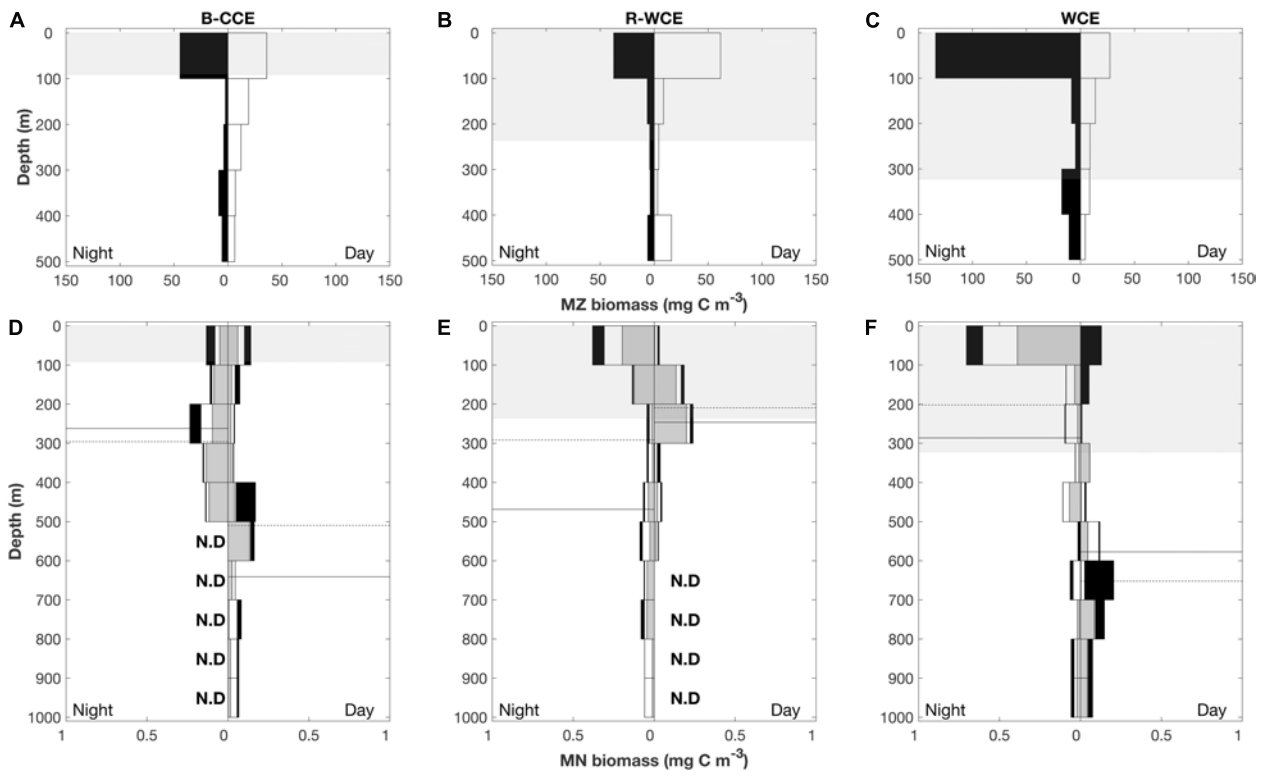

FIGURE 5 | Depth profile of mesozooplankton (MZ; **A–C**) and micronekton (MN; **D–F**) in the B-CCE, R-WCE, and WCE. Micronekton biomass is split into myctophids (gray), decapods (white), and all other micronekton (black). Nighttime profiles are left-hand panes, and daytime profiles are right-hand panes. Dashed lines represent weighted mean depths for myctophids solid lines represent weighted mean depths for decapods. Shaded gray areas represent mean (±SD) mixed layer depth. N.D indicates no data.

occurs primarily at the eddy periphery rather than center where production is highest (Sabarros et al., 2009; Drazen et al., 2011). We observed minimal differences in mesozooplankton total water column biomass between the F-CCE Center and Edge. This is contrary to most studies which report elevated mesozooplankton abundance and biomass at eddy centers

(e.g., Mackas et al., 2005; Landry et al., 2008; Everett et al., 2011). However, differences between day and night total water-column biomass were more pronounced at the F-CCE Center than the F-CCE Edge, suggesting intensified DVM in eddy centers (Eden et al., 2009). As our study only sampled mesozooplankton down to 500 m in 2015, it is possible that a portion of the nighttime biomass was originating from below our sampling depth (see the section "Vertical Migration and Active Carbon Transport").

Factors influencing the biological community within eddies include eddy age, size, phase (Eden et al., 2009), retention time (Condie and Condie, 2016), and the characteristics of the source waters (Olson, 1991; Strzelecki et al., 2007; Mullaney and Suthers, 2013). In this study, mesozooplankton and micronekton total water column biomass was similar in cold- and warm-core eddies. This is consistent with past studies reporting similar zooplankton biomass in contrasting eddies, despite vast differences in eddy type and chlorophyll *a* concentration (Goldthwait and Steinberg, 2008; Eden et al., 2009). These studies suggest that the two eddy types may be equally productive depending on conditions of their formation (Goldthwait and Steinberg, 2008; Eden et al., 2009; Dufois et al., 2016). In our sampling region, cold-core eddies are generally more productive due to upwelling of nutrient rich waters fueling primary production (Govoni et al., 2010; Everett et al., 2012); hence, we expected to see higher biomass of mesozooplankton and micronekton in the B-CCE. During sampling, however, the B-CCE was in the decay phase, as the sea level anomaly was subsiding, and surface nutrient and chlorophyll *a* were low. Therefore, differences in biota that may have existed at the eddy formation could have been undetectable at the time of sampling (The Ring Group, 1981; Eden et al., 2009). Indeed, all three eddies sampled in 2017 had similar chlorophyll *a* in the top 100 m layer. Considering the decaying productivity in the B-CCE, the similarities in total water column biomass across eddy types in 2017 could be attributed to their similar source waters (i.e., Coral Sea and EAC; Jyothibabu et al., 2015).

TABLE 3 | Total migratory biomass (mg C m^{-2}) and active carbon flux (mg C m^{-2}) by mesozooplankton and micronekton for each water mass.

Water mass	Taxa	Migratory biomass (mg C m^{-2})	Carbon flux (mg C m^{-2} d^{-1})
F-CCE Center	Mesozooplankton	214.1	16.1
F-CCE Edge	Mesozooplankton	90.6	8.0
B-CCE	Mesozooplankton	63.6	5.4
	Micronekton		
	Myctophid	0.5	0.16
	Decapod	1.0	0.1
	Pyrosoma	0.2	0.02
	Other[a]	2.3	0.1
	Total	4.0	0.4
R-WCE	Mesozooplankton	(332.3)[b]	(2.2)
	Micronekton[c]		
	Myctophid	4.1(3.9)	1.0(0.8)
	Decapod	0.7(0.5)	0.5(0.7)
	Pyrosoma[d]	0.6	0.002
	Other	(1.5)	(0.3)
	Total	5.4(5.9)	1.5(1.8)
WCE	Mesozooplankton	1,421	88
	Micronekton		
	Myctophid	10.6	3.05
	Decapod	15.7	3.6
	Pyrosoma	0.9	0.004
	Other	0.6	0.05
	Total	26.9	6.7

*[a]Primarily non-cephalopod mollusks. [b]Mesozooplankton increased during the day in the top 100 m (N = 1). [c]Fifty percent of the total micronekton population remained within the MLD (recycling carbon), whereas the remainder migrated below (exporting carbon). [d]Pyrosomes (Pyrosoma atlanticum) migrated below the MLD in the R-WCE (Henschke et al., 2019). Estimates of pyrosome carbon flux for the R-WCE and the WCE were calculated in Henschke et al. (2019) (**Figure 6**). Values in brackets indicate biomass remaining within the MLD, thus recycling carbon.*

Vertical Migration and Active Carbon Transport

Past studies have reported intensification of DVM within mesoscale eddies (Yebra et al., 2005; Goldthwait and Steinberg, 2008; Landry et al., 2008; Eden et al., 2009). However, only a few studies have attempted to quantify carbon export in eddies (e.g., Yebra et al., 2005; Landry et al., 2008). To our knowledge, this study represents the first assessment of active carbon flux incorporating both mesozooplankton and micronekton across contrasting eddies in the southwest Pacific Ocean.

The magnitude of day and night differences in total water column biomass (see the section "Mesozooplankton and Micronekton Total Water Column Biomass") as well as total nighttime biomass in the top 100 m were both substantially higher at the F-CCE Center than Edge, suggesting intensified mesozooplankton DVM at eddy centers (Goldthwait and Steinberg, 2008; Landry et al., 2008; Eden et al., 2009). Chlorophyll *a* at the F-CCE Center was more than double that of the F-CCE Edge. Thus, we attribute these differences in DVM behavior and carbon export at the F-CCE Center versus Edge to higher food availability, as zooplankton may decrease the extent of their vertical migrations when food availability is low (Huntley and Brooks, 1982; Lampert, 1989). Mesozooplankton biomass in the top 100 m increased at night in the B-CCE and the WCE, and during the day in the R-WCE. The latter points to reverse DVM in the R-WCE, although only one daytime replicate was available for the R-WCE. As chlorophyll *a* was similar in all three eddies these differences in DVMs were not solely driven by the food availability. In the B-CCE and the R-WCE mesozooplankton, biomass in the top 100 m were substantially lower than in the WCE indicating lower food availability prior to sampling, assuming all three eddies had similar source waters. Mesozooplankton exhibit DVM behavior as a means to improve metabolism (McLaren, 1963; McLaren, 1974; Enright, 1977; Iwasa, 1982; Hernández-León et al., 2010) and reduce exposure to visual predation (Iwasa, 1982; Hays et al., 1997). Temperature decreased more rapidly below the MLD in the B-CCE than in the R-WCE, indicating that the benefits of DVM related to improved metabolism were likely higher in the former. Further, the MLD was much shallower in

TABLE 4 | Migratory micronekton biomass (mg C m^{-2}) and active carbon fluxes (expressed in mg C m^{-2} d^{-1} and d^{-1}) out of the MLD in the F-CCE Center, Edge, B-CCE, and WCE, and carbon recycling in the R-WCE.

Water mass	Taxa	Migratory biomass (mg C m^{-2})	Active carbon flux (mg C m^{-2} d^{-1})				Active carbon flux (d^{-1}) (carbon flux/ migratory biomass)			
			MF	RF	EF	GF	MF	RF	EF	GF
(A) Raw										
F-CCE Center	MZ	214.1	0.03	9.4	2.9	3.8	0.0001	0.04	0.01	0.02
F-CCE Edge	MZ	90.6	0.005	4.0	1.2	2.8	0.0001	0.04	0.01	0.03
B-CCE	MZ	63.6	1.3	3.1	1.0	0.001	0.02	0.05	0.02	0.00
	MN	4.0	0.16	0.17	0.05	0.001	0.04	0.04	0.01	0.00
R-WCE*	MZ	(332.3)	(0.6)	(1.2)	(0.4)	(0.01)	(0.0001)	(0.004)	(0.001)	(0.00)
	MN	5.4 (5.9)	0.5 (0.57)	0.56 (0.63)	0.17 (0.19)	0.30 (0.41)	0.09 (0.97)	0.10 (0.11)	0.03 (0.03)	0.06 (0.07)
WCE	MZ	1,421	23.6	48.6	15.1	0.001	0.02	0.03	0.01	0.00
	MN	26.9	2.22	2.75	0.85	0.89	0.08	0.10	0.03	0.03
(B) Corrected with 50% net efficiency										
B-CCE	MN	8.0	0.32	0.32	0.1	0.001	0.04	0.04	0.01	0.00
R-WCE	MN	10.8 (11.8)	0.96 (1.06)	1.08 (1.2)	0.34 (0.38)	0.51 (0.7)	0.09 (0.09)	0.01 (0.10)	0.03 (0.03)	0.05 (0.06)
WCE	MN	53.8	4.4	5.5	1.7	1.8	0.08	0.10	0.03	0.03
(C) Corrected with 14% net efficiency										
B-CCE	MN	26.4	1.1	1.2	0.4	0.01	0.04	0.05	0.02	0.00
R-WCE	MN	37.9 (42.1)	3.43 (3.79)	3.86 (4.29)	1.21 (1.36)	1.79 (2.50)	0.09 (0.09)	0.10 (0.10)	0.03 (0.03)	0.05 (0.06)
WCE	MN	191.1	15.86	19.6	6.07	6.29	0.08	0.10	0.03	0.03

**R-WCE mesozooplankton were recycling carbon in the top 100 m of the water, while P. atlanticum (100%) and a portion of the myctophid (56%) and decapod (58%) populations were exporting carbon below the MLD in the R-WCE. We provide (A) Raw values for migratory biomass and active carbon transport for mesozooplankton (MZ) and micronekton (MN), and (B,C) corrected values of micronekton migratory biomass and active carbon transport out of the MLD, which are first corrected for diel differences in net avoidance (see the section "Vertical Migration and Active Carbon Transport"), and then for (B) 50% capture efficiency, and (C) 14% capture efficiency. MF, mortality flux; RF, respiratory flux; EF, excretory flux; and GF, gut flux. Values in brackets indicate carbon recycled within the MLD.*

the B-CCE (91 m) than in the R-WCE (236 m), suggesting that mesozooplankton may have had lower metabolic costs in getting to a metabolically advantageous depth in the B-CCE. It is thus possible that mesozooplankton in the R-WCE were undergoing reverse DVM primarily to reduce exposure to visual predation by micronekton, which were exhibiting concurrent normal DVM within the MLD (Ohman, 1986). However, it should be noted that no mesozooplankton replicates were available during the day in the R-WCE. Only 50% of the micronekton population migrated below the MLD during the day in the R-WCE. The reduced DVM by micronekton in the R-WCE is likely explained by relatively low food availability (i.e., chlorophyll *a* and mesozooplankton biomass) and reduced metabolic benefits, as temperature remained relatively high down to 400 m, after which it slowly decreased.

Differences in DVM and MLD between eddies led to considerable differences in the magnitude and depth of carbon export across water types. The shallower MLD in cold-core eddies than in warm-core eddies (Waite et al., 2019) suggests that organisms must migrate deeper to effectively contribute to carbon export in warm-core eddies. In this study, mesozooplankton and micronekton were vertically migrating below the MLD, thus contributing to downward active carbon flux in the F-CCE Center and Edge, B-CCE and WCE. Our results support past studies reporting higher active carbon fluxes by mesozooplankton at eddy centers (Yebra et al., 2005; Landry et al., 2008), as export at the F-CCE Center (16.1 mg C m^{-2} d^{-1}) was more double that of the F-CCE Edge (8.0 mg C m^{-2} d^{-1}). In the Canary Islands, Yebra et al. (2005) assessed respiratory and gut flux of mesozooplankton in a WCE, reporting similarly

TABLE 5 | Comparison of two different approaches to estimate mortality of mesozooplankton and micronekton: (1) Zhang and Dam (1997) isometric approach based on Peterson and Wroblewski (1984), and (2) assuming the system is under steady-state and mortality is approximately equivalent to growth, various growth rate equations have been applied.

Water mass	Category	Mortality (mg C m^{-2} d^{-1})	
		Zhang and Dam (1997)	Growth ≈ mortality
F-CCE Center	MZ	0.03	7.1
F-CCE Edge	MZ	0.005	2.9[1]
B-CCE	MZ	1.3	0.159[1]
	MN	0.16	0.11[2]
R-WCE*	MZ	(0.6)	(0.85)[1]
	MN	0.5 (0.57)	0.37 (0.33)[2]
WCE	MZ	23.6	4.3[1]
	MN	2.22	1.82[2]

*[1]Ikeda and Motodo (1978) where growth = 0.75 × respiration. [2]Brett and Groves (1979) where growth:metabolism = 0.66. *R-WCE mesozooplankton were recycling carbon in the top 100 m of the water, while P. atlanticum (100%) and a portion of the myctophid (56%) and decapod (58%) populations were exporting carbon below the MLD in the R-WCE. Values in brackets indicate the portion of mortality that is contributing to recycling above the MLD. MZ, mesozooplankton; MN, micronekton.*

elevated respiratory carbon fluxes at the eddy center compared to the eddy edge and minimal differences in gut flux relative to total biomass. We did not sample the eddy edges in 2017. In the B-CCE and the WCE, mesozooplankton contributed 5.4 and 88 mg C m^{-2} d^{-1} to downward active carbon transport, respectively. In the R-WCE mesozooplankton biomass remained unchanged during the day and night, suggesting that they were recycling carbon (2.2 mg C m^{-2} d^{-1}) within the MLD. Our estimates of mesozooplankton respiratory and mortality flux (9.97–23.53 mg C m^{-2} d^{-1}) were similar to Hidaka et al. (2001) in the western equatorial Pacific at the B-CCE, F-CCE Center and Edge, while the WCE was an order of magnitude higher. The higher carbon export in the WCE was supported by substantially higher mesozooplankton migratory biomass.

In the B-CCE, R-WCE, and WCE micronekton contributed 0.4, 1.5, and 6.7 mg C m^{-2} d^{-1} to downward carbon export. Only 50% of the micronekton population was contributing to downward carbon transport in the R-WCE, while the remainder was recycling carbon within the MLD. It is well documented that nets may under sample micronekton by an order of magnitude due to avoidance (Koslow et al., 1997; Kaardvedt et al., 2012). This avoidance reportedly exhibits diel variation, with greater net avoidance during the day than at night (e.g., Wiebe et al., 1982), which may lead to overestimated migratory and active carbon fluxes (Angel and Pugh, 2000). Therefore, we first re-scaled the biomass of our highly migratory groups (i.e., myctophids and decapods), such that total water column biomass during the day and night were equivalent, and then re-ran our model. This only corrects for the discrepancy between day and night net avoidance (**Supplementary Table S1**). Our micronekton biomass was an order of magnitude lower than mesozooplankton biomass; based on ecological theory, we would expect to see equal biomass within equally logarithmic size bins (Sheldon et al., 1972; Blanchard et al., 2017). This discrepancy could be due to net efficiency, which typically ranges from 4 to 14% for micronekton net sampling (Gjøsaeter, 1984; May and Blaber, 1989; Koslow et al., 1997; Davison, 2011; Kaardvedt et al., 2012). To correct for this, we applied an additional correction of 14% from Koslow et al. (1997) that was calculated for a similar micronekton community in southeastern Australia. While this is the best available correction for our data, it should be noted that our sampling approach differs slightly from that of Koslow et al. (1997) in terms of tow speed (1 vs. 1.5 m/s), net dimension (157.5 vs. 105 m^2), and mesh size (200 mm tapering to 10 mm at the codend vs. 100 mm tapering to 10 mm at the codend), which may influence the overall net efficiency. Thus, we also apply a more conservative correction for net efficiency of 50% for comparison with other studies in the literature (i.e., Hernández-León et al., 2019). All conversions are shown in **Supplementary Table S8**. Similar to Hernández-León et al. (2019), we found that different net efficiencies led to vast differences in overall downward carbon export (**Table 4**). We provide values for both efficiencies (**Table 4**), but estimate and discuss active carbon transport going forward using the more conservative net efficiency of 50% (**Figure 6**).

Myctophids and decapods contributed the most to micronekton downward carbon flux in all three eddies. Except for Henschke et al. (2019), no other study had focused on active carbon transport of micronekton within eddies making it difficult to compare our results with previous studies. Estimates of active carbon transport by decapods and myctophids vary substantially spatially and temporally (Hidaka et al., 2001; Davison et al., 2013; Schukat et al., 2013; Ariza et al., 2015; Pakhomov et al., 2018; Gorgues et al., 2019), thus caution must be taken when comparing estimates. When corrected with a net efficiency of 50%, and expressed as d^{-1} (downward carbon export/migratory biomass; see **Table 4**) our estimates were comparable to past studies of Hidaka et al. (2001) in western equatorial Pacific (14% net efficiency correction for micronekton respiratory and gut flux: 15.2–29.9 mg C m^{-2} d^{-1}), Ariza et al. (2015) near the Canary Islands (micronekton respiratory flux: 2.9 mg C m^{-2} d^{-1}) and Angel and Pugh (2000) in the northeast Atlantic (12.5–58 mg C m^{-2} d^{-1}). Davison et al. (2013) assessed fish-mediated export in the highly productive California Current, reporting values substantially higher than those of the WCE. However, a direct comparison is difficult without knowing the precise size range of fishes used in Davison et al. (2013). *Pyrosoma atlanticum* contributed minimally to active carbon flux (<1–7% of total flux in the B-CCE, WCE, and R-WCE; **Figure 6**). Although when biomass is high pyrosomes may export up to 11 mg C m^{-2} d^{-1} (Henschke et al., 2019). Our study demonstrates that myctophids and decapods are equally important as micronekton in their contribution to downward carbon transport. In some cases, the contribution of decapods to downward carbon transport may even exceed that of myctophids in mesoscale eddies. Hernández-León et al. (2019) reported that decapods coincided with sharp oxygen minimum zones (OMZs) in the subtropical Atlantic Ocean. In our study, the B-CCE exhibited a sharp decline in oxygen at the base of the MLD (∼100 m), in this case the migratory biomass of decapods exceeded that of myctophids. This finding supports Hernández-León et al. (2019), as decapods are known to be more tolerant of low oxygen concentrations (Childress, 1975). Thus, it is important to consider all groups, including highly variable and/or patchy species when making active flux estimates.

Contrary to Hidaka et al. (2001), we found that mesozooplankton contributed more to downward carbon export than micronekton in the B-CCE and WCE, while only micronekton were contributing to export in the R-WCE. This difference was primarily driven by the higher metabolic rates, and thus respiratory flux, of mesozooplankton when compared to micronekton (Ikeda, 1985, 2016). However, our sampling was concentrated in eddy centers, so it is possible that we missed the portion of micronekton that is thought to aggregate at eddy peripheries (Sabarros et al., 2009; Drazen et al., 2011). Our mesozooplankton and micronekton showed similar trends, with the highest export occurring in the WCE, followed by the B-CCE and R-WCE.

Although we only collected mesozooplankton at the F-CCE Center and Edge in 2015, we would expect this trend to hold true as Hernández-León et al. (2019) reported a significant positive relationship between zooplankton and micronekton total active flux. Our findings suggest that mesoscale eddies can act as important carbon sinks.

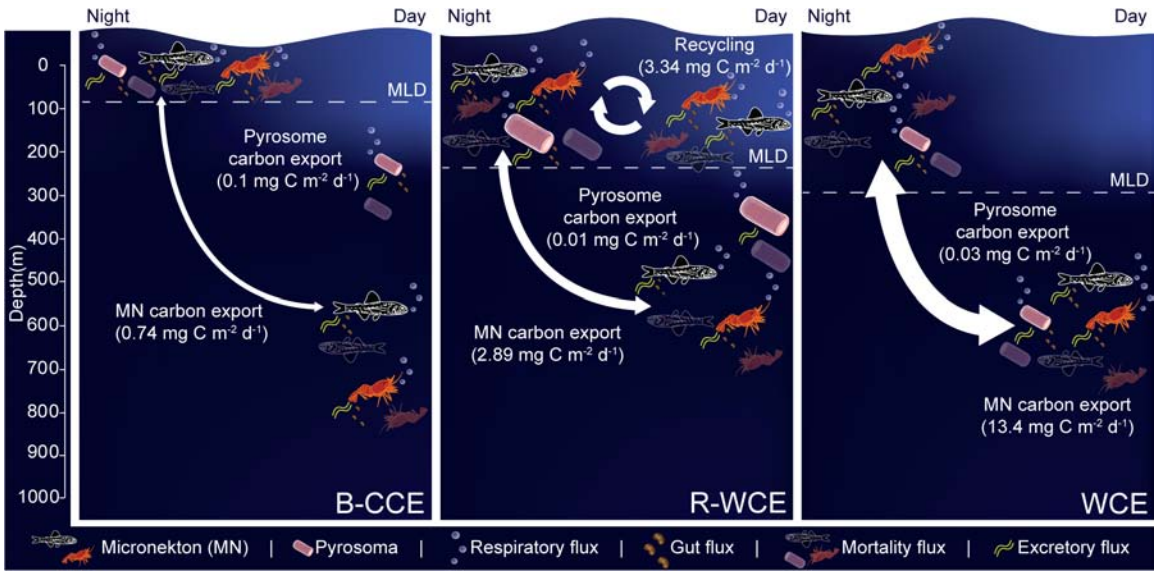

FIGURE 6 | Micronekton active carbon flux and depth of vertical migration in the B-CCE, R-WCE, and WCE. Dashed line represents the mixed layer depth (MLD). Estimates of pyrosome (*Pyrosoma atlanticum*) active carbon for the R-WCE and WCE were calculated in Henschke et al. (2019). Values reported assume 50% net efficiency (**Table 4**). MF, mortality flux; GF, gut flux; RF, respiratory flux; and EF, excretory flux.

Uncertainty and Limitations

A number of empirical equations from the literature were applied to estimate respiration, DOC excretion, mortality, and gut flux. The uncertainty associated with the models may indeed plague such estimates. Respiration was estimated using empirical allometric relationships dependent on carbon weight and *in situ* temperature from the literature (Ikeda, 2013b, 2014, 2016; Henschke et al., 2019). For all relationships used, temperature and weight explained >86% of the variation in oxygen uptake, suggesting minimal uncertainty with the models. DOC excretion was estimated based on excretory rates of several different taxonomic groups, including shrimp, euphausiids, copepods, amphipods, and polychaetes compiled in Steinberg et al. (2000). The study found that excretory flux was consistently ∼31% of respiratory flux across all taxonomic groups. Similar to respiration, DOC excretion rates were dependent on temperature and organism dry weight (Steinberg et al., 2000). The error margin associated with excretory flux is considered minor. In addition, this flux contributed minimally to the total carbon export budget. For estimates of gut flux, we compiled values of ISF and GPT from the literature for various taxa (**Supplementary Table S7**). To be conservative, where multiple values were available, we used the shortest values in our model. All values were corrected for differences in temperature and applied on an individual basis. Uncertainty may arise with gut flux estimates as none of these values take into consideration organism size, feeding history, overall stomach fullness, which may lead to variable GPTs. We assumed that organisms were continuously feeding at night in the mixed layer. This may lead to some overestimation as they may conduct intermittent feeding that can be difficult to quantify. However, while the contribution of gut flux to active carbon transport can be great, in this study it was minimal in all water masses. Most active carbon flux studies choose not to include mortality flux as it is highly variable and dependent on food availability, environmental, and predator abundance.

Mortality was calculated using the Zhang and Dam (1997) adaptation of Peterson and Wroblewski (1984) size-dependent mortality rate model for fishes ranging from 0.1 mg (eggs) to 1000 g (adults) dry weight. This model spans a wide variety of species and sizes of organisms and may lead to overestimation, particularly at the extremes of the mass range. This study simply represents a starting point, as stomiid predation on mesopelagic fish alone is estimated to range from 58 to 230% (Clarke, 1982; Hopkins et al., 1996; Davison et al., 2013). Thus, we provide a direct comparison with our values and the approach taken in Hernández-León et al. (2019), which assumes that the system is in steady-state and thus mortality is approximately equivalent to growth (**Table 5**). Our results demonstrate that vastly different estimates of mortality flux can be obtained by the two different approaches, and that one is not consistently more conservative than the other. Therefore, we recommend that future studies focus on refining the uncertainty associated with estimating gut and mortality flux.

Mesozooplankton were sampled using a MOCNESS with a 500-μm mesh. Therefore, smaller mesozooplankton (200–500 μm) were not captured leading to underestimates in total mesozooplankton abundance and biomass, particularly in the spring (i.e., 2017) when nauplii and copepodites numbers are high (Kimmerer and McKinnon, 1987).

The largest uncertainty pertains to micronekton sampling. We were unable to account for escapement and herding. Nets with tapering mesh often lead to underestimates in micronekton biomass, as small weak swimming micronekton often escape

through the coarse mesh at the mouth of the net, while large strong swimming micronekton are "herded" toward the back of the net where the mesh size is small enough for retention (Lee et al., 1996; Koslow et al., 1997; Voronina and Pakhomov, 1998). A degree of error pertaining to the calculation of volume filtered for the MIDOC also exists. This value is calculated based on the spread and height of the midwater trawl doors, which can vary throughout a tow. We used the average spread and height of the trawl to calculate volume filtered, but at present have no way of correcting for deviations that can arise due to currents and winds inflicted on the net as well as animal herding by the net (Voronina and Pakhomov, 1998; Heino et al., 2011). Thus, we assume our uncorrected estimates of micronekton biomass to be conservative and likely on the lower end.

Finally, past studies have reported seasonal variation in the migratory behavior of mesopelagic fishes (e.g., Staby and Aksnes, 2011; Urmy et al., 2012), suggesting that the intensity (i.e., depth) of DVM is suppressed during the spring for some mesopelagic fishes. As our sampling was conducted during the winter of 2017 and the spring of 2015, micronekton were likely exhibiting less intense DVM, and thus contributing less to downward carbon export.

CONCLUSION

We assessed the vertical distribution and carbon export by mesozooplankton and micronekton in contrasting eddies. The magnitude and depth of DVM varied across water masses. Mesozooplankton exhibited intensified DVM and carbon export at the F-CCE Center in comparison to the edge. We observed similar total water column mesozooplankton and micronekton biomass in the B-CCE, R-WCE, and WCE, likely attributable to their similar source waters. However, notable differences in carbon export across eddies were observed. Generally, cold-core eddies had shallower MLD than warm-core eddies, suggesting that in order to contribute to carbon export (i.e., transport below the MLD) organisms had to migrate deeper in warm-core eddies. In the R-WCE, the MLD was deeper and temperatures were higher, suggesting that mesozooplankton were undergoing reverse DVM primarily to reduce exposure to visual predation as the metabolic advantages of DVM were reduced. Mesozooplankton contributed more to downward carbon export than micronekton in the B-CCE and WCE, and only micronekton were contributing to export in the R-WCE. Differences in carbon export appear to depend on food availability, temperature, time spent migrating, and MLD. Our findings suggest that under certain conditions mesoscale eddies can act as important carbon sinks.

DATA AVAILABILITY STATEMENT

The raw datasets generated for this study are included in the article/**Supplementary Material**. Additional data will be provided on request.

ETHICS STATEMENT

The animal study was reviewed and approved by the Animal Care and Ethics Committee (ACEC) of the University of New South Wales.

AUTHOR CONTRIBUTIONS

LK and NH conducted the data analysis and wrote the first draft of the manuscript. LK, NH, EP, and IS participated in the data collection and sample processing. IS, JE, and EP contributed to design and interpretation of results. All authors contributed to writing, revising, and approving the submitted version of the manuscript.

FUNDING

This work was partially funded by the Australian Research Council Discovery Projects scheme (DP140101340 and DP150102656), and a Natural Sciences and Engineering Research Council of Canada (NSERC) Discovery Grant (funding reference number RGPN-2014-05107). LK and NH were funded by the University of British Columbia funding to EP. The voyages (IN2015v03 and IN2017v04) were supported by ship-time grants to IS and JE from the CSIRO Marine National Facility.

ACKNOWLEDGMENTS

We would like to thank the CSIRO Marine National Facility (MNF) for its support in the form of sea time on the R/V *Investigator*, support personnel, scientific equipment, and data management. Finally, we would like to thank our fellow researchers who assisted in collecting samples in June 2015 and September 2017. Satellite data were sourced from the Integrated Marine Observing System (IMOS).

SUPPLEMENTARY MATERIAL

The Supplementary Material for this article can be found online at: https://www.frontiersin.org/articles/10.3389/fmars.2019.00825/full#supplementary-material

TABLE S1 | Number of samples performed at each location.

TABLE S2 | Presence/absence species list for MIDOC catches, where 1 = present and 0 = absent in the B-CCE, R-WCE, and WCE in September 2017.

TABLE S3 | Length to weight relationships used to calculate carbon weight (CW; in mg) for micronekton captured in the MIDOC. Lengths are reported as either total length (TL) or standard length (SL) in millimeters.

TABLE S4 | Testing the assumptions of ANOVA. The results for Bartlett's test of homogeneity of variance and Shapiro-Wilk's test for normality for total water column mesozooplankton and micronekton.

TABLE S5 | Results of ANOVA comparing day and night total water column mesozooplankton (EZ net) and micronekton (MIDOC) biomass captured in the F-CCE Center, F-CCE Edge, B-CCE, R-WCE, and WCE.

TABLE S6 | Regression equations used to calculate respiratory oxygen uptake (RO; $\mu L\ O_2 \cdot ind \cdot^{-1}\ h^{-1}$), where DW is individual dry weight (mg), WW is individual wet weight (mg), T is temperature (°C), and D is depth (m).

TABLE S7 | Values of ISF (% of total body weight) and gut passage time (GPT; h) used to calculate active carbon transport. Where values were not available for specific species of fish the average ISF and GPT for mesopelagic fish were applied. Only organisms that were undergoing DVM are included. Where DW = dry weight (mg), CW = carbon weight (mg), T = temperature (°C), and FP = daily fecal pellet production.

TABLE S8 | Day/night avoidance variability correction and overall net avoidance calculation for migratory micronekton carbon fluxes (mg C m^{-2} d^{-1}) out of the MLD in the B-CCE and WCE, and carbon recycling (values in brackets) in the R-WCE. Micronekton biomass is first corrected for diel differences in net avoidance (see the section "Vertical Migration and Active Carbon Transport"), and then for overall micronekton net avoidance assuming a net efficiency of 14% (Koslow et al., 1997). MF = mortality flux, RF = respiratory flux, EF = excretory flux, and GF = gut flux.

DATA SHEET S1 | Raw data.

REFERENCES

Andersen, K. H., Berge, T., Gonçalves, R. J., Hartvig, M., Heuschele, J., Hylander, S., et al. (2016). Characteristic sizes of life in the oceans, from bacteria to whales. *Ann. Rev. Mar. Sci.* 8, 217–241. doi: 10.1146/annurev-marine-122414-034144

Angel, M. V., and Pugh, P. R. (2000). Quantification of diel vertical migration by micronektonic taxa in the northeast Atlantic. *Hydrobiologia* 440, 161–179. doi: 10.1023/A:1004115010030

Ariza, A., Garijo, J. C., Landeira, J. M., Bordes, F., and Hernández-León, S. (2015). Migrant biomass and respiratory carbon flux by zooplankton and micronekton in the subtropical northeast Atlantic Ocean (Canary Islands). *Prog. Oceanogr.* 134, 330–342. doi: 10.1016/j.pocean.2015.03.003

Baird, R. C., Hopkins, T. L., Wilson, D. F., and Bay, Y. (1975). Diet and feeding chronology of *Diaphus taaningi* (Myctophidae) in the Cariaco Trench. *Am. Soc. Ichthyol. Herpetol.* 1975, 356–365.

Batten, S. D., and Crawford, W. R. (2005). The influence of coastal origin eddies on oceanic plankton distributions in the eastern Gulf of Alaska. *Deep. Res. Part II Top. Stud. Oceanogr.* 52, 991–1009. doi: 10.1016/j.dsr2.2005.02.009

Blanchard, J. L., Heneghan, R. F., Everett, J. D., Trebilco, R., and Richardson, A. J. (2017). From bacteria to whales: using functional size spectra to model marine ecosystems. *Trends Ecol. Evol.* 32, 174–186. doi: 10.1016/j.tree.2016.12.003

Brett, J. R., and Groves, T. D. D. (1979). Physiological energetics. *Fish Physiol.* 8, 280–352.

Cetina-Heredia, P., Roughan, M., van Sebille, E., and Coleman, M. A. (2014). Long-term trends in the East Australian current separation latitude and eddy driven transport. *J. Geophys. Res. Ocean.* 119, 4351–4366. doi: 10.1002/2014JC010192. Received

Chenillat, F., Franks, P. J. S., Capet, X., Rivière, P., Grima, N., Blanke, B., et al. (2018). Eddy properties in the Southern California current system. *Ocean Dyn.* 68, 761–777. doi: 10.1007/s10236-018-1158-4

Childress, J. J. (1975). The respiratory rates of midwater crustaceans as a function of depth of occurrence and relation to the oxygen minimum layer off Southern California. *Comp. Biochem. Physiol. A. Comp. Physiol.* 50, 787–799. doi: 10.1016/0300-9629(75)90146-2

Choy, C. A., Popp, B. N., Hannides, C. C. S., and Drazen, J. C. (2015). Trophic structure and food resources of epipelagic and mesopelagic fishes in the north pacific subtropical Gyre ecosystem inferred from nitrogen isotopic compositions. *Limnol. Oceanogr.* 60, 1156–1171. doi: 10.1002/lno.10085

Clarke, T. A. (1982). Feeding habits of stomiatoid fishes from Hawaiian waters. *Fish. Bull.* 80, 287–304.

Condie, S., and Condie, R. (2016). Retention of plankton within ocean eddies. *Glob. Ecol. Biogeogr.* 25, 1264–1277. doi: 10.1111/geb.12485

Crabtree, R. E. (1995). Chemical composition and energy content of deep-sea demersal fishes from tropical and temperate regions of the western North Atlantic. *Bull. Mar. Sci.* 56, 434–449.

Dagg, M. J., and Wyman, K. D. (1983). Natural ingestion of the copepods Neocalanus plumchrus and N. cristatus calculeted from gut contents. *Mar. Ecol. Prog. Ser.* 13, 37–46.

Davison, P. C. (2011). *The Export of Carbon Mediated by Mesopelagic Fishes in the Northeast Pacific Ocean*. PhD Thesis, University of California, San Diego, CA.

Davison, P. C., Checkley, D. M., Koslow, J. A., and Barlow, J. (2013). Carbon export mediated by mesopelagic fishes in the northeast Pacific Ocean. *Prog. Oceanogr.* 116, 14–30. doi: 10.1016/j.pocean.2013.05.013

Drazen, J. C., De Forest, L. G., and Domokos, R. (2011). Micronekton abundance and biomass in Hawaiian waters as influenced by seamounts, eddies, and the moon. *Deep. Res. Part I Oceanogr. Res. Pap.* 58, 557–566. doi: 10.1016/j.dsr.2011.03.002

Ducklow, H., Steinberg, D., and Buesseler, K. (2001). Upper ocean carbon export and the biological pump. *Oceanography* 14, 50–58. doi: 10.5670/oceanog.2001.06

Dufois, F., Hardman-Mountford, N. J., Greenwood, J., Richardson, A. J., Feng, M., and Matear, R. J. (2016). Anticyclonic eddies are more productive than cyclonic eddies in subtropical gyres because of winter mixing. *Sci. Adv.* 2:e1600282. doi: 10.1126/sciadv.1600282

Eden, B. R., Steinberg, D. K., Goldthwait, S. A., and McGillicuddy, D. J. (2009). Zooplankton community structure in a cyclonic and mode-water eddy in the Sargasso Sea. *Deep. Res. Part I Oceanogr. Res. Pap.* 56, 1757–1776. doi: 10.1016/j.dsr.2009.05.005

Enright, J. T. (1977). Diurnal vertical migration: adaptive significance and timing. Part 1. Selective advantage: a metabolic model. *Limnol. Oceanogr.* 22, 856–886.

Everett, J. D., Baird, M. E., Oke, P. R., and Suthers, I. M. (2012). An avenue of eddies: quantifying the biophysical properties of mesoscale eddies in the Tasman Sea. *Geophys. Res. Lett.* 39, 1–5. doi: 10.1029/2012GL053091

Everett, J. D., Baird, M. E., and Suthers, I. M. (2011). Three-dimensional structure of a swarm of the salp Thalia democratica within a cold-core eddy off southeast Australia. *J. Geophys. Res. Ocean.* 116, 1–14. doi: 10.1029/2011JC007310

Everett, J. D., Macdonald, H., Baird, M. E., Humphries, J., Roughan, M., and Suthers, I. M. (2015). Cyclonic entrainment of preconditioned shelf waters into a frontal eddy. *J. Geophys. Res. Ocean.* 120, 677–691. doi: 10.1002/2014JC010472

Falkowski, P. G., Laws, E. A., Barber, R. T., and Murray, J. W. (2003). "Phytoplankton and their role in primary, new, and export production," in *Ocean Biogeochemistry*, ed. M. J. R. Fasham, (Berlin: Springer-Verlag), 99–121.

Froese, R., Thorson, J. T., and Reyes, R. B. (2014). A Bayesian approach for estimating length-weight relationships in fishes. *J. Appl. Ichthyol.* 30, 78–85. doi: 10.1111/jai.12299

Gjøsaeter, J. (1984). Mesopelagic fish, a large potential resource in the Arabian Sea. *Deep Sea. Res.* 31, 1019–1035.

Goldthwait, S. A., and Steinberg, D. K. (2008). Elevated biomass of mesozooplankton and enhanced fecal pellet flux in cyclonic and mode-water eddies in the Sargasso Sea. *Deep. Res. Part II Top. Stud. Oceanogr.* 55, 1360–1377. doi: 10.1016/j.dsr2.2008.01.003

Gorgues, T., Aumont, O., and Memery, L. (2019). Simulated changes in the particulate carbon export efficiency due to diel vertical migration of zooplankton in the North Atlantic. *Geophy. Res. Lett.* 46, 5387–5395.

Govoni, J. J., Hare, J. A., Davenport, E. D., Chen, M. H., and Marancik, K. E. (2010). Mesoscale, cyclonic eddies as larval fish habitat along the southeast United States shelf: a Lagrangian description of the zooplankton community. *ICES J. Mar. Sci.* 67, 403–411. doi: 10.1093/icesjms/fsp269

Greenwood, J. E., Feng, M., and Waite, A. M. (2007). A one-dimensional simulation of biological production in two contrasting mesoscale eddies in the south eastern Indian Ocean. *Deep. Res. Part II Top. Stud. Oceanogr.* 54, 1029–1044. doi: 10.1016/j.dsr2.2006.10.004

Hannides, C. C. S., Popp, B. N., Choy, A. C., and Drazen, J. C. (2013). Midwater zooplankton and suspended particle dynamics in the North Pacific Subtropical Gyre: a stable isotope perspective. *Limnol. Oceanogr.* 58, 1931–1936. doi: 10.4319/lo.2013.58.6.1931

Hansen, A. N., and Visser, A. W. (2016). Carbon export by vertically migrating zooplankton: an optimal behavior model. *Limnol. Oceanogr.* 61, 701–710. doi: 10.1002/lno.10249

Hays, G. C., Harris, R. P., and Head, R. N. (1997). The vertical nitrogen flux caused by zooplankton diel vertical migration. *Mar. Ecol. Prog. Ser.* 160, 57–62. doi: 10.3354/meps160057

Heino, M., Porteiro, F. M., Sutton, T. T., Falkenhaug, T., Godø, O. R., and Piatkowski, U. (2011). Catchability of pelagic trawls for sampling deep-living

nekton in the mid-North Atlantic. *ICES J. Mar. Sci.* 68, 377–389. doi: 10.1093/icesjms/fsq089

Henschke, N., Pakhomov, E. A., Kwong, L. E., Everett, J. D., Laiolo, L., Coghlan, A. R., et al. (2019). Large vertical migrations of *Pyrosoma atlanticum* play an important role in active carbon transport. *J. Geophys. Res. Biogeosciences* 124:2018JG004918. doi: 10.1029/2018JG004918

Hernández-León, S., Almeida, C., Gómez, M., Torres, S., Montero, I., and Portillo-Hahnefeld, A. (2001). Zooplankton biomass and indices of feeding and metabolism in island-generated eddies around Gran Canaria. *J. Mar. Syst.* 30, 51–66. doi: 10.1016/S0924-7963(01)00037-9

Hernández-León, S., Franchy, G., Moyano, M., Menéndez, I., Schmoker, C., and Putzeys, S. (2010). Carbon sequestration and zooplankton lunar cycles: could we be missing a major component of the biological pump? *Limnol. Oceanogr.* 55, 2503–2512. doi: 10.4319/lo.2010.55.6.2503

Hernández-León, S., Olivar, M. P., Fernández de Puelles, M. L., Bode, A., Castellón, A., López-Pérez, C., et al. (2019). Zooplankton and micronekton active flux across the tropical and subtropical Atlantic Ocean. *Front. Mar. Sci.* 6:535. doi: 10.3389/fmars.2019.00535

Hidaka, K., Kawaguchi, K., Murakami, M., and Takahashi, M. (2001). Downward transport of organic carbon by diel migratory micronekton in the western equatorial Pacific. *Deep Sea Res. Part I Oceanogr. Res. Pap.* 48, 1923–1939. doi: 10.1016/s0967-0637(01)00003-6

Hobday, A. J., Young, J. W., Moeseneder, C., and Dambacher, J. M. (2011). Defining dynamic pelagic habitats in oceanic waters off eastern Australia. *Deep. Res. Part II Top. Stud. Oceanogr.* 58, 734–745. doi: 10.1016/j.dsr2.2010.10.006

Hopkins, T. L., and Baird, R. C. (1977). "Aspects of the feeding ecology of oceanic midwater fishes," in *Oceanic Sound Scattering Prediction*, eds N. R. Andersen, and B. J. Zahuranec, (New York, NY: Plenum Press).

Hopkins, T. L., Sutton, T. T., and Lancraft, T. M. (1996). The trophic structure and predation impact of a low latitude midwater fish assemblage. *Prog. Oceanogr.* 38, 205–239.

Hudson, J. M., Steinberg, D. K., Sutton, T. T., Graves, J. E., and Latour, R. J. (2014). Myctophid feeding ecology and carbon transport along the northern Mid-Atlantic Ridge. *Deep. Res. Part I Oceanogr. Res. Pap.* 93, 104–116. doi: 10.1016/j.dsr.2014.07.002

Huntley, M., and Brooks, E. R. (1982). Effects of age and food availability on diel vertical migration of Calanus pacificus. *Mar. Biol.* 71, 23–31. doi: 10.1007/BF00396989

Ikeda, T. (1985). Metabolic rates of epipelagic marine zooplantkon as a function of body mass and temperature. *Mar. Biol.* 85, 1–11.

Ikeda, T. (2013a). Metabolism and chemical composition of pelagic decapod shrimps: synthesis toward a global bathymetric model. *J. Oceanogr.* 69, 671–686. doi: 10.1007/s10872-013-0200-x

Ikeda, T. (2013b). Respiration and ammonia excretion of euphausiid crustaceans: synthesis toward a global-bathymetric model. *Mar. Biol.* 160, 251–262. doi: 10.1007/s00227-012-2150-z

Ikeda, T. (2014). Synthesis toward a global model of metabolism and chemical composition of medusae and ctenophores. *J. Exp. Mar. Bio. Ecol.* 456, 50–64. doi: 10.1016/j.jembe.2014.03.006

Ikeda, T. (2016). Routine metabolic rates of pelagic marine fishes and cephalopods as a function of body mass, habitat temperature and habitat depth. *J. Exp. Mar. Bio. Ecol.* 480, 74–86. doi: 10.1016/j.jembe.2016.03.012

Ikeda, T., and Motoda, S. (1978). Estimated zooplankton prodction and their ammonia excretion in the Kuroshio and adjacent seas. *Fish. Bull.* 76, 357–367.

Irigoien, X., Klevjer, T. A., Røstad, A., Martinez, U., Boyra, G., Acuña, J. L., et al. (2014). Large mesopelagic fishes biomass and trophic efficiency in the open ocean. *Nat. Commun.* 5:3271. doi: 10.1038/ncomms4271

Iwasa, Y. (1982). Vertical migration of zooplankton: a game between predator and prey. *Am. Nat.* 120, 171–180.

Jyothibabu, R., Vinayachandran, P. N., Madhu, N. V., Robin, R. S., Karnan, C., Jagadeesan, L., et al. (2015). Phytoplankton size structure in the southern Bay of Bengal modified by the Summer Monsoon current and associated eddies: implications on the vertical biogenic flux. *J. Mar. Syst.* 143, 98–119. doi: 10.1016/j.jmarsys.2014.10.018

Kaardvedt, S., Staby, A., and Aksnes, D. L. (2012). Efficient trawl avoidance by mesopelagic fishes causes large underestimation of their biomass. *Mar. Ecol. Prog. Ser.* 456, 1–6.

Kelly, P., Clementson, L., Davies, C., Corney, S., and Swadling, K. (2016). Zooplankton responses to increasing sea surface temperatures in the southeastern Australia global marine hotspot. *Estuar. Coast. Shelf Sci.* 180, 242–257. doi: 10.1016/j.ecss.2016.07.019

Kiko, R., Biastoch, A., Brandt, P., Cravatte, S., Hauss, H., Hummels, R., et al. (2017). Biological and physical influences on marine snowfall at the equator. *Nat. Geosci.* 10, 852–858. doi: 10.1038/NGEO3042

Kimmerer, W. J., and McKinnon, A. D. (1987). Growth, mortality, and secondary production of the copepod Acartia tranteri in Westernport Bay. *Australia. Limnol. Oceanogr.* 32, 14–28.

Kobari, T., Steinberg, D. K., Ueda, A., Tsuda, A., Silver, M. W., and Kitamura, M. (2008). Impacts of ontogenetically migrating copepods on downward carbon flux in the western subarctic Pacific Ocean. *Deep. Res. Part II Top. Stud. Oceanogr.* 55, 1648–1660. doi: 10.1016/j.dsr2.2008.04.016

Koslow, A. J., Kloser, R. J., and Williams, A. (1997). Pelagic biomass and community structure over the mid-continental slope off southeastern Australia based upon acoustic and midwater trawl sampling. *Mar. Ecol. Prog. Ser.* 146, 21–35.

Lampert, W. (1989). The adaptive significance of diel vertical migration of zooplankton. *Funct. Ecol.* 3, 21–27. doi: 10.2307/2389671

Landry, M. R., Decima, M., Simmons, M. P., Hannides, C. C. S., and Daniels, E. (2008). Mesozooplankton biomass and grazing responses to Cyclone Opal, a subtropical mesoscale eddy. *Deep. Res. Part II Top. Stud. Oceanogr.* 55, 1378–1388. doi: 10.1016/j.dsr2.2008.01.005

Lee, K., Lee, M., and Wang, J. (1996). Behavioural responses of larval anchovy schools herded within large-mesh wings of trawl net. *Fish. Res.* 28, 57–69.

Levitus, S. (1982). *Climatological atlas of the World Ocean. NOAA Professional Paper 13*. Washington, DC: US Government Printing Office.

Mackas, D., and Galbraith, M. (2002). Zooplankton distribution and dynamics in a North Pacific Eddy of coastal origin. I. Transport and loss of contrinental margin species. *Deep. Res. Part II* 58, 725–738.

Mackas, D. L., and Coyle, K. O. (2005). Shelf-offshore exchange processes, and their effects on mesozooplankton biomass and community composition patterns in the northeast Pacific. *Deep. Res. Part II Top. Stud. Oceanogr.* 52, 707–725. doi: 10.1016/j.dsr2.2004.12.020

Mackas, D. L., Tsurumi, M., Galbraith, M. D., and Yelland, D. R. (2005). Zooplankton distribution and dynamics in a North Pacific Eddy of coastal origin: II. Mechanisms of eddy colonization by and retention of offshore species. *Deep. Res. Part II Top. Stud. Oceanogr.* 52, 1011–1035. doi: 10.1016/j.dsr2.2005.02.008

Marouchos, A., Underwood, M., Malan, J., Sherlock, M., and Kloser, R. (2017). *MIDOC: An Improved Open and Closing Net System for Stratified Sampling of Mid-Water Biota*. Aberdeen: IEEE, 1–5. doi: 10.1109/OCEANSE.2017.8084931

Martin, A. P., and Richards, K. J. (2001). Mechanisms for vertical nutrient transport within a North Atlantic mesoscale eddy. *Deep. Res. Part II Top. Stud. Oceanogr.* 48, 757–773. doi: 10.1016/S0967-0645(00)00096-5

Martz, T. R., Johnson, K. S., and Riser, S. C. (2008). Ocean metabolism observed with oxygen sensors on profiling floats in the South Pacific. *Limnol. Oceanogr.* 53, 2094–2111. doi: 10.4319/lo.2008.53.5_part_2.2094

May, J. L., and Blaber, S. J. M. (1989). Benthic and pelagic fish biomass of the upper continental slope off eastern Tasmania. *Mar. Biol.* 101, 11–25.

McGillicuddy, D. J., and Robinson, A. R. (1997). Eddy-induced nutrient supply and new production in the Sargasso Sea. *Deep. Res. Part I Oceanogr. Res. Pap.* 44, 1427–1450. doi: 10.1016/S0967-0637(97)00024-1

McLaren, I. A. (1963). Effects of temperature on growth of zooplankton, and the adaptive value of vertical migration. *J. Fish. Res. Board Canada* 20, 685–727. doi: 10.1139/f63-046

McLaren I. A. (1974). Demographic strategy of vertical migration by a Marine copepod. *Am. Nat.* 108, 91–102.

Moteki, M., Horimoto, N., Nagaiwa, R., Amakasu, K., Ishimaru, T., and Yamaguchi, Y. (2009). Pelagic fish distribution and ontogenetic vertical migration in common mesopelagic species off Lützow-Holm Bay (Indian Ocean sector, Southern Ocean) during austral summer. *Polar Biol.* 32, 1461–1472. doi: 10.1007/s00300-009-0643-0

Mullaney, T. J., and Suthers, I. M. (2013). Entrainment and retention of the coastal larval fish assemblage by a short-lived, submesoscale, frontal eddy of the East Australian current. *Limnol. Oceanogr.* 58, 1546–1556. doi: 10.4319/lo.2013.58.5.1546

Ohman, M. D. (1986). Predator-limited population-growth of the copepod *Pseudocalanus* Sp. *J. Plankton Res.* 8, 673–713. doi: 10.1093/plankt/8.4.673

Olson, D. (1991). Rings in the ocean. *Annu. Rev. Earth Planet. Sci.* 19, 283–311. doi: 10.1146/annurev.earth.19.1.283

Pakhomov, E. A., Perissinotto, R., and Mcquaid, C. D. (1996). Prey composition and daily rations of myctophid fishes in the Southern Ocean. *Mar. Ecol. Prog. Ser.* 134, 1–14.

Pakhomov, E. A., Podeswa, Y., Hunt, B. P. V., and Kwong, L. E. (2018). Vertical distribution and active carbon transport by pelagic decapods in the North Pacific Subtropical Gyre. *ICES J. Mar. Sci.* 76, 702–717. doi: 10.1093/icesjms/fsy134

Parsons, T. R., Takahashi, M., and Hargrave, B. (1984). *Biological Oceanographic Processes*. New York, NY: Pergamon Press.

Peterson, I., and Wroblewski, J. S. (1984). Mortality rate of fishes in the pelagic ecosystem. *Can. J. Fish. Aquat. Sci.* 41, 1117–1120.

Poloczanska, E. S., Burrows, M. T., Brown, C. J., García Molinos, J., Halpern, B. S., Hoegh-Guldberg, O., et al. (2016). Responses of marine organisms to climate change across oceans. *Front. Mar. Sci.* 3:62. doi: 10.3389/fmars.2016.00062

Rees, C., Pender, L., Sherrin, K., Schwanger, C., Hughes, P., Tibben, S., et al. (2018). Methods for reproducible shipboard SFA nutrient measurement using RMNS and automated data processing. *Limnol. Oceanog. Methods* 17, 25–41.

Reinfelder, J. R., and Fisher, N. S. (1994). By marine planktonic the assimilation of elements ingested bivalve larvae. *Limnology* 39, 12–20.

Reygondeau, G., Guidi, L., Beaugrand, G., Henson, S. A., Koubbi, P., MacKenzie, B. R., et al. (2017). Global biogeochemical provinces of the mesopelagic zone. *J. Biogeogr.* 00, 1–15. doi: 10.1111/jbi.13149

Roughan, M., Keating, S. R., Schaeffer, A., Cetina Heredia, P., Rocha, C., Griffin, D., et al. (2017). A tale of two eddies: the biophysical characteristics of two contrasting cyclonic eddies in the East Australian Current System. *J. Geophyiscal Res. Ocean.* 122, 2494–2518.

Sabarros, P. S., Ménard, F., Lévénez, J. J., Tew-Kai, E., and Ternon, J. F. (2009). Mesoscale eddies influence distribution and aggregation patterns of micronekton in the Mozambique Channel. *Mar. Ecol. Prog. Ser.* 395, 101–107. doi: 10.3354/meps08087

Sameoto, D., Guglielmo, L., and Lewis, M. K. (1987). Day/night vertical distribution of euphausiids in the eastern tropical Pacific. *Mar. Biol.* 96, 235–245. doi: 10.1007/BF00427023

Schukat, A., Bode, M., Auel, H., Carballo, R., Martin, B., Koppelmann, R., et al. (2013). Pelagic decapods in the northern Benguela upwelling system: distribution, ecophysiology and contribution to active carbon flux. *Deep. Res. Part I Oceanogr. Res. Pap.* 75, 146–156. doi: 10.1016/j.dsr.2013.02.003

Shatova, O., Koweek, D., Conte, M. H., and Weber, J. C. (2012). Contribution of zooplankton fecal pellets to deep ocean particle flux in the Sargasso Sea assessed using quantitative image analysis. *J. Plankton Res.* 34, 905–921. doi: 10.1093/plankt/fbs053

Sheldon, R. W., Prakash, A., and Sutcliffe, H. (1972). The size distribution of particles in the ocean. *Limnol. Oceanogr.* 17, 327–340.

Staby, A., and Aksnes, D. L. (2011). Follow the light—diurnal and seasonal variations in vertical distribution of the mesopelagic fish *Maurolicus muelleri*. *Mar. Ecol. Prog. Ser.* 422, 265–273.

Steinberg, D. K., Carlson, C. A., Bates, N. R., Goldthwait, S. A., Madin, L. P., and Michaels, A. F. (2000). Zooplankton vertical migration and the active transport of dissolved organic and inorganic carbon in the Sargasso Sea. *Deep Sea Res. Part I Oceanogr. Res. Pap.* 47, 137–158. doi: 10.1016/S0967-0637(99)00052-7

Steinberg, D. K., and Landry, M. R. (2017). Zooplankton and the Ocean carbon cycle. *Ann. Rev. Mar. Sci.* 9, 413–444. doi: 10.1146/annurev-marine-010814-015924

Strickland, J. D. H., and Parsons, T. R. (1972). *A Practical Handbook of Seawater Analysis*. Ottawa: Fisheries Research Board of Canada.

Strzelecki, J., Koslow, J. A., and Waite, A. (2007). Comparison of mesozooplankton communities from a pair of warm- and cold-core eddies off the coast of Western Australia. *Deep. Res. Part II Top. Stud. Oceanogr.* 54, 1103–1112. doi: 10.1016/j.dsr2.2007.02.004

Suthers, I. M. (2017). *RV Investigator voyage summary: IN2017_V04*. Hobart, TAS: Australian Ocean Data Network

Suthers, I. M., Taggart, C. T., Kelley, D., Rissik, D., and Middleton, J. H. (2004). Entrainment and advection in an island's tidal wake, as revealed by light attenuance, zooplankton, and ichthyoplankton. *Limnol. Oceanogr.* 49, 283–296. doi: 10.4319/lo.2004.49.1.0283

Suthers, I. M., Young, J. W., Baird, M. E., Roughan, M., Everett, J. D., Brassington, G. B., et al. (2011). The strengthening East Australian Current, its eddies and biological effects - an introduction and overview. *Deep. Res. Part II Top. Stud. Oceanogr.* 58, 538–546. doi: 10.1016/j.dsr2.2010.09.029

The Ring Group (1981). Gulf stream cold-core righs: their physics. Chemistry, and Biolgoy. *Science* 212, 1091–1100.

Tsubota, H., Ishizaka, J., Nishimura, A., and Watanabe, Y. W. (1999). Overview of NOPACCS (Northwest Pacific Carbon Cycle Study). *J. Oceanogr.* 55, 645–653.

Turner, J. T. (2002). Zooplankton fecal pellets, marine snow and sinking phytoplankton blooms. *Aquat. Microb. Ecol.* 27, 57–102.

Urmy, S. S., Horne, J. K., and Barbee, D. H. (2012). Measuring the vertical distributional variability of pelagic fauna in Monterey Bay. *ICES J. Mar. Sci. J. Cons.* 69, 184–196.

Usbeck, R., Schlitzer, R., Fischer, G., and Wefer, G. (2003). Particle fluxes in the ocean: comparison of sediment trap data with results from inverse modeling. *J. Mar. Syst.* 39, 167–183. doi: 10.1016/S0924-7963(03)00029-0

Voronina, N., and Pakhomov, E. (1998). How accurate are trawl krill biomass estimates? *Oceanology* 38, 211–212.

Waite, A. M., Raes, E., Beckley, L. E., Thompson, P. A., Griffin, D., Saunders, M., et al. (2019). Production and ecosystem structure in cold-core vs. warm-core eddies: implications for the zooplankton isoscape and rock lobster larvae. *Limnol. Oceanogr.* 9999, 1–19. doi: 10.1002/lno.11192

Weibe, P. H., Boyd, S., and Cox, J. L. (1975). Relationships between zooplankton displacement volume, wet weight, dry weight, and carbon. *Fish. Bull.* 73, 777–786.

Wiebe, P. H., Boyd, S. H., Davis, B. M., and Cox, J. L. (1982). Avoidance of towed nets by the euphausiid *Nematoscelis megalops*. *Fish. Bull.* 80, 75–91.

Yebra, L., Almeida, C., and Hernández-León, S. (2005). Vertical distribution of zooplankton and active flux across an anticyclonic eddy in the Canary Island waters. *Deep. Res. Part I Oceanogr. Res. Pap.* 52, 69–83. doi: 10.1016/j.dsr.2004.08.010

Yebra, L., Herrera, I., Mercado, J. M., Cortés, D., Gómez-Jakobsen, F., Alonso, A., et al. (2018). Zooplankton production and carbon export flux in the western Alboran Sea gyre (SW Mediterranean). *Prog. Oceanogr.* 167, 64–77. doi: 10.1016/j.pocean.2018.07.009

Young, J. W., and Blaber, S. J. M. (1986). Feeding ecology of three species of midwater fishes associated with the continental slope of eastern Tasmania. *Australia. Mar. Biol.* 93, 147–156. doi: 10.1007/BF00428663

Young, J. W., Blaber, S. J. M., and Rose, R. (1987). Reproductive biology of three species of midwater fishes associated with the continental slope of eastern Tasmania. *Australia. Mar. Biol.* 332, 323–332.

Young, J. W., Bulman, C. M., Blaber, S. J. M., and Wayte, S. E. (1988). Age and growth of the lanternfish *Lampanyctodes hectoris* (Myctophidae) from eastern Tasmania. *Australia. Mar. Biol.* 99, 569–576. doi: 10.1007/BF00392564

Young, J. W., Hobday, A. J., Campbell, R. A., Kloser, R. J., Bonham, P. I., Clementson, L. A., et al. (2011). The biological oceanography of the East Australian Current and surrounding waters in relation to tuna and billfish catches off eastern Australia. *Deep. Res. Part II Top. Stud. Oceanogr.* 58, 720–733. doi: 10.1016/j.dsr2.2010.10.005

Young, J. W., Hunt, B. P. V., Cook, T. R., Llopiz, J. K., Hazen, E. L., Pethybridge, H. R., et al. (2015). The trophodynamics of marine top predators: current knowledge, recent advances and challenges. *Deep. Res. Part II Top. Stud. Oceanogr.* 113, 170–187. doi: 10.1016/j.dsr2.2014.05.015

Zhang, X., and Dam, H. G. (1997). Downward export of carbon by die1 migrant mesozooplankton in the central equatorial Pacific. *Deep. Res. Part II* 44, 2191–2202.

Conflict of Interest: The authors declare that the research was conducted in the absence of any commercial or financial relationships that could be construed as a potential conflict of interest.

frontiers in Marine Science

CORRECTION
published: 04 September 2020
doi: 10.3389/fmars.2020.00708

Corrigendum: Mesozooplankton and Micronekton Active Carbon Transport in Contrasting Eddies

Lian E. Kwong[1]*, *Natasha Henschke*[1], *Evgeny A. Pakhomov*[1,2,3], *Jason D. Everett*[4,5] *and Iain M. Suthers*[5,6]

[1] Department of Earth, Ocean and Atmospheric Sciences, University of British Columbia, Vancouver, BC, Canada, [2] Institute for the Oceans and Fisheries, University of British Columbia, Vancouver, BC, Canada, [3] Hakai Institute, Heriot Bay, BC, Canada, [4] Centre for Applications in Natural Resource Mathematics, The University of Queensland, St. Lucia, QLD, Australia, [5] Evolution and Ecology Research Centre, University of New South Wales Sydney, Sydney, NSW, Australia, [6] Sydney Institute of Marine Science, Mosman, NSW, Australia

OPEN ACCESS

Edited and reviewed by:
Morten Hvitfeldt Iversen, Alfred Wegener Institute Helmholtz Centre for Polar and Marine Research (AWI), Germany

***Correspondence:**
Lian E. Kwong
lkwong@eoas.ubc.ca

Specialty section:
This article was submitted to Marine Ecosystem Ecology, a section of the journal Frontiers in Marine Science

Received: *01 July 2020*
Accepted: *04 August 2020*
Published: *04 September 2020*

Citation:
Kwong LE, Henschke N, Pakhomov EA, Everett JD and Suthers IM (2020) Corrigendum: Mesozooplankton and Micronekton Active Carbon Transport in Contrasting Eddies. Front. Mar. Sci. 7:708. doi: 10.3389/fmars.2020.00708

Keywords: mesozooplankton, micronekton, southwest Pacific, diel vertical migration, active carbon transport

A Corrigendum on

Mesozooplankton and Micronekton Active Carbon Transport in Contrasting Eddies
by Kwong, L. E., Henschke, N., Pakhomov, E. A., Everett, J. D., and Suthers, I. M. (2020). Front. Mar. Sci. 6:825. doi: 10.3389/fmars.2019.00825

In the original article, there was a mistake in the legend for **Table S-3** as published. Units were not included in the original table legend. The correct legend appears below.

Table S-3. Length to weight relationships used to calculate carbon weight (CW; in mg) for micronekton captured in the MIDOC. Lengths are reported as either total length (TL) or standard length (SL) in millimeters.

Additionally, there was a mistake in **Table S-3** as published. We have re-configured some of the equations within the table to add clarity for those that wish to apply these equations with their own data. In the original table the wet weight to carbon conversions on some of the equations were improperly placed. The corrected **Table S-3** appears below.

The authors apologize for these errors and state that they do not change the scientific conclusions of the article in any way. The original article has been updated.

TABLE S-3 | Length to weight relationships used to calculate carbon weight (CW; in mg) for micronekton captured in the MIDOC.

Group	Species	Regression
Chaetognath	Chaetognath[1,2]	$CW = 0.0001352*TL^{3.1545}*0.367$
Crustacean	Amphipod[1,3]	$CW = 10^{(2.717*\log_{10}(TL) - 1.911)}*0.345$
Crustacean	Decapod[1,4]	$CW = 10^{(3.787*\log_{10}(TL) - 3.972)}*0.435$
Crustacean	Euphausiid[1,3]	$CW = 10^{(3.23*\log_{10}(TL) - 3.261)}*0.419$
Crustacean	Isopod[1,5,6]	$CW = 10^{(2.751*\log_{10}(TL) - 1.69)}*0.435$
Fish	Alepisauridae[7]	$CW = 0.2*(0.00389*(\frac{TL}{10})^{3.12})$
Fish	Alepocephalidae[8]	$CW = 0.2*WW$
Fish	Anoplogastridae[7]	$CW = 0.2*(0.00829*(SL)^{2.38})$
Fish	Bathylagidae[7]	$CW = 0.2*(0.00537*(\frac{TL}{10})^{2.98})$
Fish	Bramidae[8]	$CW = 0.2*WW$
Fish	Bregmacerotidae[7,9,10]	$CW = e^{(3.143*ln(1.312*\frac{SL}{10}) - 4.2475)}*84.7$
Fish	Carangidae[7]	$CW = 10^{(2.8047*\log_{10}(TL) - 4.6581)}*0.2$
Fish	Carapidae[7]	$CW = 10^{(2.8047*\log_{10}(TL) - 4.6581)}*0.2$
Fish	Caristiidae[7]	$CW = 0.2*WW$
Fish	Centrolophidae[7]	$CW = 10^{(2.8047*\log_{10}(TL) - 4.6581)}*0.2$
Fish	Ceratiidae[7]	$CW = 0.2*(0.01995*(\frac{TL}{10})^{3.01})$
Fish	Cetomimidae[7]	$CW = 10^{(2.8047*\log_{10}(TL) - 4.6581)}*0.2$
Fish	Chaunacidae[7]	$CW = 10^{(2.8047*\log_{10}(TL) - 4.6581)}*0.2$
Fish	Chiasmodontidae[7]	$CW = 10^{(2.8047*\log_{10}(TL) - 4.6581)}*0.2$
Fish	Dalatiidae[7,9]	$CW = \left(0.00363*(SL*0.1164)^{3.12}\right)*84.7$
Fish	Derichthyidae[7]	$CW = 0.2*(0.00102*(\frac{TL}{10})^{3.06})$
Fish	Diretmidae[7]	$CW = 0.2*(0.01698*(\frac{TL}{10})^{3})$
Fish	Emmelichthyidae[7]	$CW = 10^{(2.8047*\log_{10}(TL) - 4.6581)}*0.2$
Fish	Epigonidae[7]	$CW = 0.2*(0.0174*(\frac{TL}{10})^{2.95})$
Fish	Evermannellidae[7]	$CW = 0.2*(0.00427*(\frac{TL}{10})^{3.12})$
Fish	Gempylidae[7,9]	$CW = \left(0.00363*(SL*0.1164)^{3.12}\right)*84.7$
Fish	Gigantactinidae[7]	$CW = 0.2*(0.01995*(\frac{TL}{10})^{3.01})$
Fish	Gonostomatidae[9,11]	$CW = 10^{(2.945*\log_{10}(SL) - 5.282)}*0.053$
Fish	Grammicolepididae[7]	$CW = 0.2*(0.02451*(\frac{TL}{10})^{2.891})$
Fish	Howellidae[9]	$CW = 0.0847*(0.01122*(\frac{TL}{10})^{3.04})$
Fish	Leptocephalus[9]	$CW = 10^{(1.857*\log_{10}(SL) - 1.877)}*0.0847$
Fish	Linophrynidae[7]	$CW = 10^{(2.52*\log_{10}(SL) - 1.593)}*0.046$
Fish	Macroramphosidae[7]	$CW = 0.2*(0.0312*(\frac{TL}{10})^{2.268})$
Fish	Melamphaidae[9,11]	$CW = 10^{(3.259*\log_{10}(SL) - 2.164)}*0.039$
Fish	Melanocetidae[7]	$CW = 10^{(2.52*\log_{10}(SL) - 1.593)}*0.046$
Fish	Microstomatidae[7]	$CW = 0.2*(0.00537*(\frac{TL}{10})^{2.98})$
Fish	Myctophidae[9,11]	$CW = 10^{(2.902*\log_{10}(SL) - 1.797)}*0.092$
Fish	Nemichthyidae[7]	$CW = 10^{(1.857*\log_{10}(SL) - 1.877)}*0.0847$
Fish	Nomeidae[7,9]	$CW = 84.7*(0.0122*(1.186*\frac{SL}{10})^{2.949})$
Fish	Notosudidae[7]	$CW = 0.2*(0.00295*(\frac{TL}{10})^{3.18})$
Fish	Opisthoproctidae[8,9]	$CW = 10^{(2.16*\log_{10}(SL) - 0.025)}*0.0525$
Fish	Photostylus argenteus[13]	$CW = (0.0009*SL^{3.2857})*0.0847$
Fish	Paralepididae[7,9,10]	$CW = e^{(ln(0.000002) + 2.824*ln(SL*1.0482))}*84.7$
Fish	Phosichthyidae[9,11]	$CW = 10^{(4.036*\log_{10}(SL) - 3.418)}*0.0847$
Fish	Pleuronectiformes[7]	$CW = 0.2*(0.01047*(\frac{TL}{10})^{3})$
Fish	Regalecidae[7]	$CW = 0.2*(0.00102*(\frac{TL}{10})^{3.06})$
Fish	Serrivomeridae[13,14,15]	$CW = 450.9*(0.000001*(\frac{SL}{10})^{4.45})$
Fish	Setarchidae[7]	$CW = 0.2*(0.01*(\frac{TL}{10})^{3.04})$

(Continued)

TABLE S-3 | Continued

Group	Species	Regression
Fish	Sternoptychidae[9,11]	$CW = 10^{(2.95*\log_{10}(SL) - 1.52)*0.06}$
Fish	*Sternoptyx* spp. [9,11]	$CW = 10^{(2.877*\log_{10}(SL) - 1.08)*0.056}$
Fish	Stomiidae[9,11]	$CW = 10^{(2.52*\log_{10}(SL) - 1.593)*0.046}$
Fish	Tetraodontidae[7]	$CW = 0.2*(0.01*(\frac{TL}{10})^{3.04})$
Fish	Trachipteridae[7]	$CW = 0.2*(0.00112*(\frac{TL}{10})^{3.06})$
Fish	Trichiuridae[8,9]	$CW = 10^{(3.23*\log_{10}(\frac{SL}{10}) - 2.189)*84.7}$
Fish	Unidentified Fish[7]	$CW = 10^{(2.8047*\log_{10}(TL) - 4.6581)*0.2}$
Fish	Zeniontidae[7]	$CW = 0.2*(0.0396*(\frac{TL}{10})^{2.609})$
Jellyfish	Jellyfish[3,16,17]	$CW = 10^{(2.767*\log_{10}(TL) - 3.643)}$
Mollusk	Cephalopod[12,14]	$CW = 10^{(2.611*\log_{10}(TL) - 3.5)*55.44}$
Mollusk	Heterpod[18]	$CW = (0.0888*TL^{2.161})*0.028$
Mollusk	Mollusk[1,3]	$CW = 10^{(1.646*\log_{10}(TL) - 0.915)*0.289}$
Tunicate	Pyrosome[19]	$CW = (0.0013*TL^2 + 0.0151*TL)*39.2$
Polychaete	Polychaete[1,3,20]	$CW = 10^{(1.798*\log_{10}(TL) - 2.17)*0.37}$

References

[1]Kiørboe (2013)
[2]Feigenbaum (1979)
[3]Mizdalski (1988)
[4]Podeswa (2012)
[5]Strong and Dabron (1979)
[6]Defeo and Martinez (2003)
[7]Froese et al., (2014)
[8]Individual measurements in lab
[9]Childress et al., (1990)
[10]Bernardes and Rossi-Wongtschowski (2000)
[11]Davison (2011)
[12]Lindsay (2003)
[13]Pakhomov (Unpublished data)
[14]Villanueva and Guerra, (1991)
[15]Alpoim et al., (2002)
[16]Haddad and Nogueira (2006)
[17]Uye and Shimauchi (2005)
[18]Davis and Wiebe (1985)
[19]Henschke et al. (2019)
[20]Uye (1982)

Lengths are reported as either total length (TL) or standard length (SL) in millimeters.

frontiers in Marine Science

ORIGINAL RESEARCH
published: 14 February 2020
doi: 10.3389/fmars.2020.00064

Running the Gauntlet: Assessing the Threats to Vertical Migrators

Bruce H. Robison, Rob E. Sherlock, Kim R. Reisenbichler and Paul R. McGill*

Monterey Bay Aquarium Research Institute, Moss Landing, CA, United States

Diel vertical migrations (DVM) by zooplankton and nekton are driven by the selective advantage of avoiding visually cued predators near the surface during the hours of daylight. And just as there is a second set of predators that occupy the migrators' dark daytime depths, there is also a diverse suite of predators that comprise a gauntlet of threats during the migrations. Here we examine these migrations from the perspective of the migrators, to enumerate the kinds of predatory threats they face and to assess the threat potential of various predator types. The study is based on thousands of hours of *in situ* observations and measurements of the mesopelagic community in Monterey Bay, California, conducted chiefly by remotely operated vehicles (ROVs). We provide accounts of some predator/prey interactions, and we introduce a means to calculate the threat potential of specific predators, based on MBARI's long-term time-series of quantitative video surveys.

Keywords: vertical migration, mesopelagic, predators, prey, ROV

OPEN ACCESS

Edited by:
Amy Elizabeth Maas, Bermuda Institute of Ocean Sciences, Bermuda

Reviewed by:
Michael R. Stukel, Florida State University, United States
Rudi Schuech, University of Lincoln, United Kingdom

****Correspondence:***
Bruce H. Robison
robr@mbari.org

Specialty section:
This article was submitted to Marine Biogeochemistry, a section of the journal Frontiers in Marine Science

Received: *29 March 2019*
Accepted: *28 January 2020*
Published: *14 February 2020*

Citation:
Robison BH, Sherlock RE, Reisenbichler KR and McGill PR (2020) Running the Gauntlet: Assessing the Threats to Vertical Migrators. Front. Mar. Sci. 7:64. doi: 10.3389/fmars.2020.00064

INTRODUCTION

The dusk and dawn migrations of epi-mesopelagic animals comprise a tidal cycle of shifting biomass in a tide driven not by gravity, but by light. Twice a day a diverse aggregation of species traverses the water column, with most individuals covering hundreds of meters each way (Marshall, 1979). Distributed along the migratory path are passive predators, lying in wait to ensnare, entangle, or engulf the vertical commuters. Also attendant are layers of active predators, who lure, track, or chase their migrating prey. In the 17th century, some Native American tribes imposed ritualistic punishment on prisoners by forcing them to run between two lines of warriors who would reach out to strike the captive as he raced past. Similar practices are known from military history as far back as the ancient Greeks. In modern parlance, "running the gauntlet" has come to mean passing through a series of challenges or attacks, and it can be applied to fraternity hazing, military boot camp, or to the diel vertical migrations (DVM) of midwater animals.

Vertically migrating animals comprise an active component of the biological pump, and when compared with passively sinking detritus, the migrators contribute significantly to the overall flux of particulate organic carbon (Robinson et al., 2010; Davison et al., 2013; Steinberg and Landry, 2017; Archibald et al., 2019). The migration strategy balances the risk of predation with feeding opportunity – factors that vary based on latitude, time of year, turbidity, the size of the animal, and more (Hansen and Visser, 2016; Ohman and Romagnan, 2016). Our historical perspective on vertical migrations has been shaped by the means through which we study them, and for the most part our spatial resolution has been indirect and relatively coarse. The trawl nets with which scientists have traditionally gathered data on DVM are blunt tools for examining complex behaviors

like predation and predator avoidance. Even the most precise midwater trawling systems cannot resolve animal distribution patterns in the vertical plane at scales of less than tens of meters. And in the horizontal plane, net tows integrate distribution patterns over hundreds or thousands of meters. The best way to determine the fine-scale aspects of vertical migration is directly, *in situ*. The first scientist to take this approach was Eric Barham of the U.S. Navy Electronics Laboratory. Barham (1963, 1966) used human-occupied vehicles (HOVs) coupled with shipboard acoustic systems to delineate the composition and structure of sonic scattering layers (SSL). He observed, for the first time, migrating fishes, siphonophores, and crustaceans at their daytime and nighttime depths as well as during their ascents and descents.

This paper examines diel vertical migration from the standpoint of the migrators, to assess the threats they face during their movements. It is based on thousands of hours of *in situ* observations and measurements made with HOVs, remotely operated vehicles (ROVs), and autonomous underwater vehicles (AUVs) in Monterey Bay, California. The value of *in situ* midwater research has increased dramatically with the development of new vehicles and advanced technologies that enable investigative practices which were previously possible only in terrestrial and shallow-water research. These include manipulative experimental work, detailed behavioral observations, high-precision small-scale resolution of distribution and abundance, and direct measurements of physiological processes *in situ* (Robison et al., 2017). A consequence of technological advances is that we can now more thoroughly investigate DVM, as Barham did, from within SSL. Here we provide examples of the predatory threats faced by some migratory species, and a means to quantify the threat potential of different types of predators.

Here, threat potential is a measure of the latent risk of encountering a potential predator or obstacle during diel vertical migration. It does not equate to mortality nor is it a proxy for predation rate or predatory impact.

MATERIALS AND METHODS

Data Acquisition

The quantitative data and observations reported here were generated in Monterey Bay, California, principally during a long-term series of ROV dives initiated in 1988. Dive sites were situated most commonly over the axis of the Monterey Submarine Canyon, at locations where the bottom depths ranged from 1600 to 3500 m. Three different ROVs were used to conduct the research, each carrying what, at the time, was a state-of-the-art high-resolution video camera that recorded continuously throughout each dive. The video footage, coupled with coincident hydrographic measurements, was annotated and incorporated into MBARI's Video Annotation and Reference System (VARS) database (Schlining and Stout, 2006). The video data can be arranged into two categories: transect data and transit data.

The quantitative data presented here come from MBARI's midwater time series, 1997–2015; which constituted 1893 mesopelagic video transects conducted during daylight hours. Transect data were generated during horizontal excursions of the vehicle at a single reference station in a vertically stacked series of specific depth intervals from 50 to 1000 m. Transects were run at a constant speed and depth with the camera's lens at its widest field of view. Lighting was uniform. The area viewed was calculated based upon test tank calibrations. The volume of water surveyed was calculated by multiplying the viewed area by the distance traveled, which was measured precisely by an acoustic current meter (Robison et al., 2005; Katija et al., 2017). Animals in each transect were counted and summed to give abundance and that value was divided by the volume to give the number of individuals per cubic meter. Transect data were collected on approximately a monthly basis after 1994 as the core of MBARI's midwater time-series database.

Transit data were derived from video footage recorded during all non-transecting, midwater dive time. That is, when the vehicle was ascending, descending, searching, observing, making measurements, conducting manipulative work, and all other activities in the water column. Transit data provide behavioral observations, information on predator/prey interactions and context for the quantitative transect data. Because our ROVs have variable ballast systems, behavioral observations can be made stealthily, with minimal use of thrusters to keep the vehicle in position (Robison et al., 2017). As was the case with transecting, all transit video footage was annotated by highly skilled technicians to identify and count the animals encountered, then logged into VARS. Concurrent hydrographic data were likewise logged into the database, linked by time code to each annotation.

In addition to the data generated during ROV and AUV dives, observations of Monterey Bay's mesopelagic community and its vertical migrations were made from several HOVs: *Deep Rover, Alvin, Mir, Deep Worker,* and *Nadir*. These HOVs along with MBARI's ROV *Tiburon* and the *i2MAP* AUV are all electrically powered and thus are relatively quiet. MBARI's two hydraulically powered ROVs *Ventana* and *Doc Ricketts* are noisy, which limits their ability to make observations of fishes.

Seasonality of Monterey Bay

Monterey Bay is bisected by the Monterey Submarine Canyon that brings the deep ocean close to shore. Coastal upwelling delivers nutrient-rich water during spring and into the summer months (Skogsberg, 1936; Bolin and Abbott, 1963; Pennington and Chavez, 2000). Skogsberg and Phelps (1946) initially described three oceanic seasons in Monterey Bay – a pattern subsequently accepted by many scientists like Barham (1957), Bolin and Abbott (1963), and thoroughly discussed by Pennington and Chavez (2000). However, the parameters of temperature, oxygen and nutrient concentrations depend largely upon whether upwelling is, or is not, occurring (Bolin and Hopkins Marine Station, 1964).

When upwelling is underway, the mixed layer is shallow, with increased nutrient levels and primary production (Olivieri and Chavez, 2000). Data for Monterey Bay indicate that the majority of primary production occurs within this shallow mixed layer (SML) (Pennington and Chavez, 2000). In a broad sense

then, the seasonality of Monterey Bay may be categorized by mixed layer depth, shallow versus deep, and estimated by whether upwelling (m d^{-1}) is positive or negative. Mean daily upwelling velocities calculated from a 12-year data set indicate that, on average, upwelling velocity is positive from ∼ calendar days 92 (April) through 305 (November) in Monterey Bay (Olivieri and Chavez, 2000; Silguero and Robison, 2000). These dates were used to define our transect data as having occurred during the upwelling/SML or deep mixed layer (DML) season.

Calculating Threat Potential

In order to calculate the likelihood that an individual migrator would encounter a specific type of predator or threat during ascent or descent, we first calculated mean predator density per cubic meter using daytime transect data from 1997 to 2015. Logistical constraints limited our opportunities for nighttime transecting. Because transects occur at set depths in the water column (50 m, and then 100–1000 m by 100 m increments), we integrated predator abundance across the vertical depth range that the migratory prey traverse using trapezoidal integration (Dull, 1941), the Bolstad2 package (Curran, 2013) within the software R (R Core Team, 2013) and/or Mathematica (Wolfram Research Inc, 2019). After calculating areal density, the cross-sectional area (CSA) for a given predator was approximated based on its shape and size as did Jackson et al. (1993) who calculated the CSA of pteropod feeding webs. Since prey travel vertically, the likelihood of an encounter with a predator will depend on the CSA of that predator (e.g., the spread of its tentacles in the case of the siphonophore, *Nanomia bijuga*) and it is the predators' horizontal spacing which matters most to the prey, not their vertical distribution. For example, two predators might overlie one another completely, but occur at different depths. For a vertically migrating prey in our model, this amounts to a single predator, not two. Building on the model of Jackson et al. (1993) we account for one predator shadowing another by randomly distributing points, based on predator density, and representing the CSA of the predators across a space of 1 m^2, then calculating the percentage of predator-occupied space in that 1 m^2 using Mathematica (**Figure 1**). Predator density was calculated from time-series data (**Figure 2**). The probability of encountering a predator while migrating vertically is equal to the fraction of the square meter occupied by predators. For each predator, this simulation was repeated 1000 times (a normal Poisson distribution was usually reached after 500 permutations and in all cases by 1000) to generate a mean threat potential – the chance of a prey item encountering, but not necessarily being captured by, a predator while migrating vertically.

There are several important assumptions made using this initial approach: predators are randomly spaced with respect to prey and to each other, prey travel in a straight, vertical path through the water column, there is no predator avoidance by prey, and predators are always ready to capture prey (i.e., negligible time is spent handling prey or relocating). Because at least some of the predators (e.g., *N. bijuga* and *Chiroteuthis calyx*) migrate with their prey, the prey stands a chance of encountering the same individual predator more than once – a factor not included in our estimates.

Estimates of a predator's CSA were based on one or all of the following: (1) lab measurements (squids), (2) ROV video (*Bathochordaeus* spp., siphonophores and ctenophores) and laser measurements (Katija et al., 2017, *Bathochordaeus* spp., see **Figure 3**), and (3) published data. Because siphonophores are contractile, even an individual colony's size will vary with behavior, thus making size a difficult parameter to quantify precisely. However, as an adult colony, *Nanomia bijuga* ranges from approximately 10 to 30 cm long. When these siphonophores deploy their tentacles to "fish" for prey, they typically form a J-shaped posture with their tentilla stretching into the water column around them, approximating a circle from the perspective of vertically migrating prey like a euphausiid (**Figure 1**). Based on the variability of adult size, a conservative estimate for the radius, *r*, of this circle of tentacular influence is approximately 5 cm (0.05 m), and the CSA = $\pi * r^2$.

With its lobes outstretched, the ctenophore *Thalassocalyce inconstans* (**Figure 3A**) forms a roughly circular threat that can span in excess of 30 cm in diameter. However, to estimate their threat potential a diameter of 15 cm was chosen because *Thalassocalyce* are observed in a range of sizes over depth and season. The cross section of water occupied by the tentacles of longer siphonophores, like *Praya dubia*, which typically stretch out in the horizontal plane, can be approximated using an elliptical shape: $\pi * a * b$, with a and b equal to the major and minor radii of the ellipse. Although *P. dubia* commonly reach lengths in excess of 30 m (Robison, 2004), we adopted 15 m as a conservative measure for the length of the colony and 1.0 m for the horizontal extent of the tentacles. The houses of giant larvaceans like *Bathochordaeus* spp. are similarly elliptical in cross section and can exceed a meter in longest dimension (**Figure 3B**). The threat potential of *Bathochordaeus* spp. was calculated based on a house 1 m in length by 0.3 m width.

The depth range of the vertically migrating prey must also be considered. In the midwater time series, the majority of euphausiids in Monterey Bay are found in the top 300 m of the water column while the daytime distribution of *N. bijuga* commonly extends down to 500 m (**Figures 2A,B**). Predators occurring below the prey's depth range pose no threat.

The squids, *C. calyx* and *Gonatus* spp. feed on fishes, and by day most mesopelagic fish occur in the 400–600 m transects. When calculating the threat potential to the fishes by these squid, transect data from 50 to 600 m were used (**Figures 2C,D**). *Gonatus* spp. are fast-swimming predators of fishes and of each other (Hoving and Robison, 2016), with an estimated sphere of influence approximately 1.0 m in diameter. *Chiroteuthis* fishes for its prey with long, dangling feeding tentacles that have bioluminescent photophores to attract prey from a distance. The threat potential of *Chiroteuthis* was estimated to be double that of *Gonatus*, or 2.0 m.

RESULTS

What follows is a series of accounts depicting interactions between some vertically migrating prey and some of their

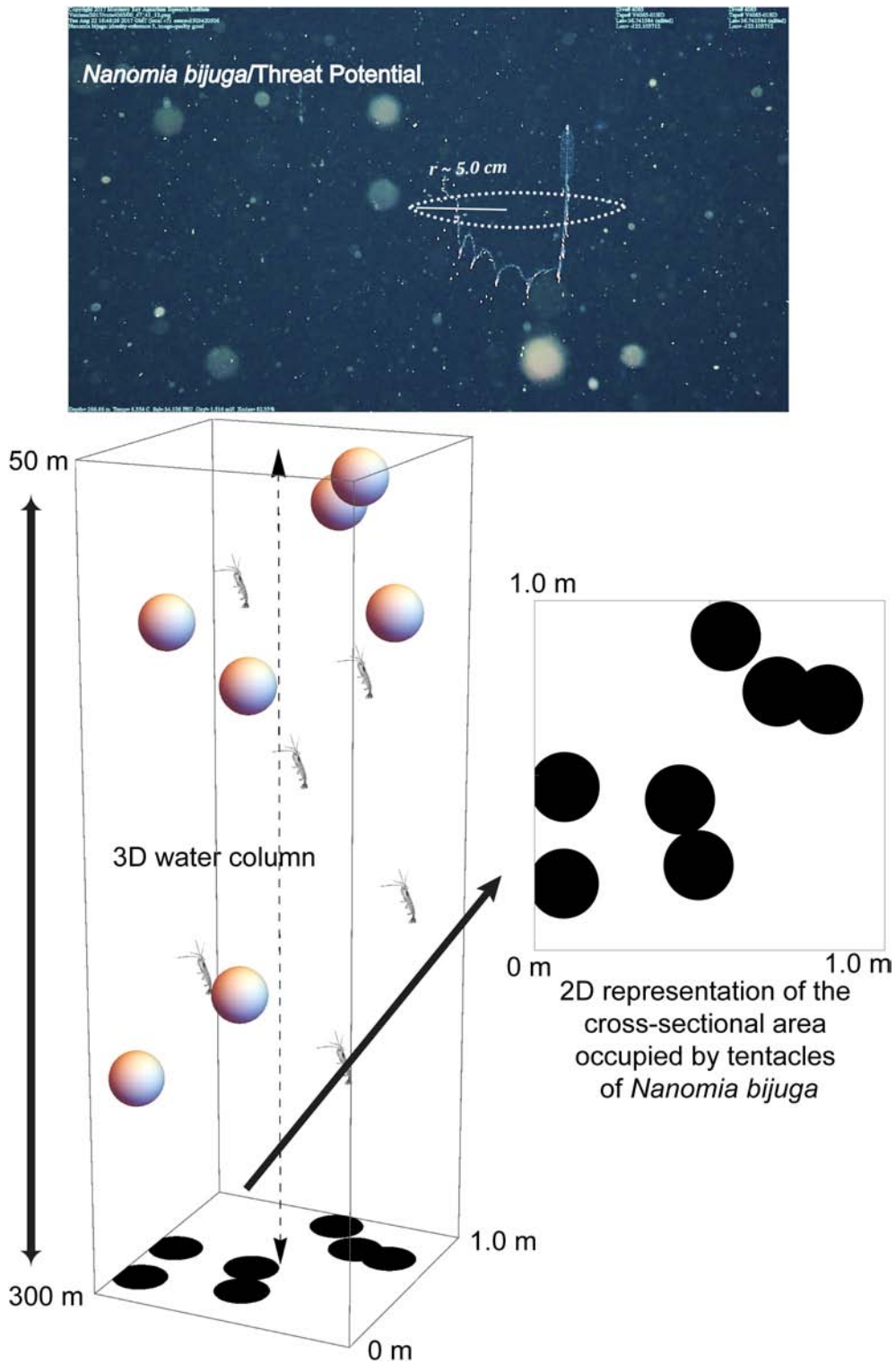

FIGURE 1 | ROV video frame grab of the physonect siphonophore, *Nanomia bijuga*, fishing with its siphosome forming a "J" shape and tentilla with nematocysts (stinging cells) emanating outward and around the animal. A radius of 5 cm constitutes an average threat potential of ~ 4–8% for the siphonophore, depending on seasonal abundance. The 3D diagram illustrates *N. bijuga* (spheres) in the 1 m^2 × 250 m water column through which the vertically migrating prey (euphausiids) traverse. The threat potential was calculated based on the space occupied by the predator's tentacles (dark circles) versus unoccupied space in the 2D illustration. Not to scale.

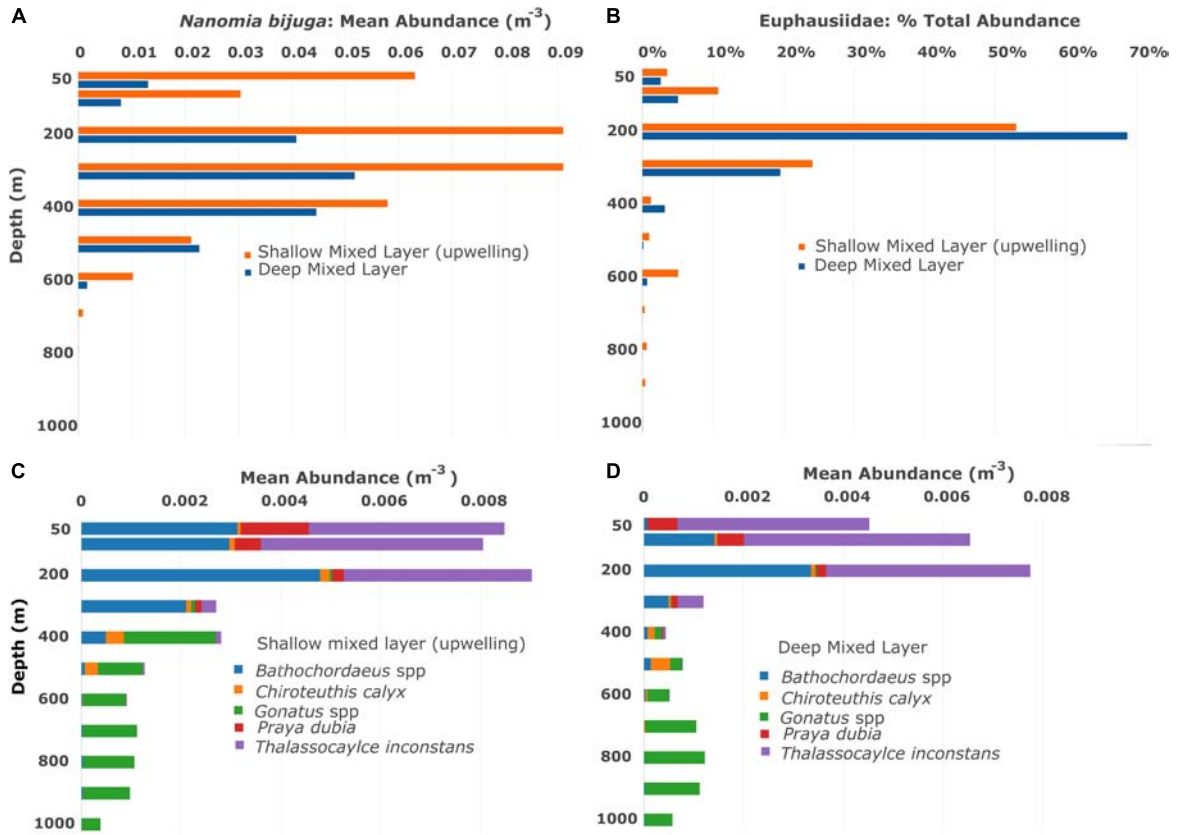

FIGURE 2 | Vertical and seasonal distributions based on the Midwater Time Series, from 1997–2015 for **(A)** the siphonophore *Nanomia bijuga*, **(B)** euphausiid krill, **(C,D)** giant larvaceans *Bathochordaeus* spp., the squids *Chiroteuthis calyx* and *Gonatus* spp., the siphonophore *Praya dubia* and the lobate ctenophore *Thalassocalyce inconstans*. The mixed layer of nutrients is shallow when upwelling is occurring and deeper when it is not, thus seasonality in Monterey Bay is broadly defined here by mixed layer depth. Mean abundances indicate that many mesopelagic animals are more abundant when the mixed layer is shallow and upwelling is occurring. Note that krill are expressed in percent abundance because quantifying each euphausiid on video is not always possible.

predators. Each synopsis is based on direct observations made from undersea vehicles, *in situ*, primarily in Monterey Bay.

Prey and Predator Profiles

Krill and *Nanomia*

Krill in Monterey Bay consist chiefly of two euphausiid species: *Euphausia pacifica* and *Thysanoessa spinifera*. They occur at depths principally between 100 and 300 m during the day (**Figures 2A,B**) and they migrate to shallower depths at night. Euphausiids are keystone forage for a broad range of predators from whales and birds to fish, squid, and jellies. Krill abundance and the composition of the euphausiid community can vary seasonally and episodically but they are a consistent presence year-round (Marinovic et al., 2002) with about 90% occurring within the top 300 m irrespective of mixed-layer depth (**Figures 2A,B**). While krill occasionally form dense swarms, we most often see them separated from each other by centimeter- to meter-scale distances. Their appearance during transects run within their depth range is usually patchy.

Nanomia bijuga is a small (10–30 cm) physonect siphonophore and a principal predator of krill in Monterey Bay. These siphonophores capture krill with nematocyst batteries at the ends of retractile tentacles based near the openings of a dozen or so gastrozooids (stomachs) arranged in a linear chain. Typically *N. bijuga* has 6–12 swimming bells (the nectosome), a gas-filled pneumatophore, and 20–30 siphosome elements, the portion of the colony behind the propulsive units. Most *Nanomia* migrate in concert with their krill prey and form a prominent constituent of the local sonic scattering layer (Barham, 1963). *Nanomia* itself is preyed upon by the abundant, non-migratory narcomedusae *Solmissus incisa* and *S. marshalli* (Raskoff, 2002), which broadly overlap *Nanomia*'s entire depth range.

Nanomia shows stereotypical behavior during prey capture and handling. It typically positions itself in a J-shaped fishing posture with its tentacles splayed outward and its nectosome angled up (**Figure 1**). When krill contact and struggle against a tentacle, *Nanomia* begins swimming rapidly, which aligns the body with the trailing tentacle and its captured prey. While swimming, *Nanomia* contracts the tentacle and the prey is drawn in until it can be grasped by other tentacles and then maneuvered into a nearby gastrozooid. This behavior explains why the posterior gastrozooids are more likely to contain food than those near the nectosome, although we commonly observe *Nanomia* continuing to "fish" after one or more gastrozooids are

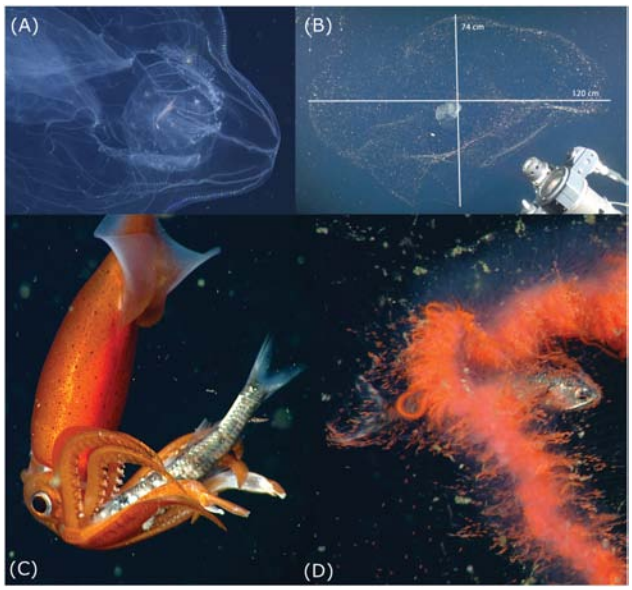

FIGURE 3 | Potential threats to vertical migrators. Note that the images are not at the same scale. **(A)** The ctenophore *Thalassocalyce* has trapped a euphausiid krill within its lobes and is slowly transporting the prey using ciliary action, toward its mouth. This predator uses its transparent lobes to intercept vertically migrating prey. **(B)** The mucus "house" of the giant larvacean *Bathochordaeus stygius,* which can present an obstacle for vertically migrating zooplankton and micronekton, often spans >1 m in greatest dimension. The outer structure is a coarse-mesh filter and the inner portion is a fine-mesh filter within which the animal sits. When the filters become clogged, the larvacean discards them and extrudes another house. Precise measurements of structures too large and fragile to collect can be made with Deep-PIV (Katija et al., 2017) seen in the lower right corner. **(C)** The squid *Gonatus onyx* is holding a myctophid fish, *Stenobrachius leucopsarus,* with its arms, after catching it with long feeding tentacles. The squid disables the fish, using its beak to sever the spinal cord. **(D)** This undescribed, orange, physonect siphonophore has captured a myctophid fish, *S. leucopsarus,* with its tentacles and is maneuvering the prey into a gastrozooid (stomach). Access to additional data on these and other predators and prey is available through the MBARI Deep-Sea Guide: http://dsg.mbari.org/dsg/home.

already full. After ingestion *Nanomia* settles again into its feeding posture and relocates every few minutes. These tactics are well-suited for feeding on prey that aggregate in patches (Robison and Connor, 1999; Robison, 2004). However, such movements are not accounted for in our model.

When predators like *Nanomia* migrate vertically along with their prey, encounter rates will vary based on their respective swimming speeds (Gerritsen and Strickler, 1977; Harvey et al., 2013). If fast-moving prey can outswim their predators, then survival depends on the length of the gauntlet through which they move and not the speed at which they swim. However, since krill swim more slowly than *Nanomia*, the speed of migration is important and their survival will vary proportionally to it (Anderson et al., 2005). Swimming speeds for these animals may be calculated based on various traits, such as size and life history stage (Torres and Childress, 1983; Dorman et al., 2015), some of which we have documented. However, we do not know how the presence of one affects the swimming behavior of the other. In the laboratory, the gastrozooids of *Nanomia* elongate and show increased movement in the presence of krill and can readily attach to a stationary krill without assistance from any tentacles. So, *Nanomia* can clearly sense the presence of nearby krill. While we know how *Nanomia* fishes, we do not know how often they cast their nets to fish while migrating, nor how that changes in the presence of prey.

Seasonal cycles of local primary production are clearly reflected in the abundance of *Nanomia*. Upwelling-driven phytoplankton blooms occur during the summer, followed about a month later by large increases in grazer populations. These, in turn, lead to rapid expansion of the *Nanomia* population, which reaches its maximum abundance approximately 3 months after the onset of seasonal upwelling and 1–2 months after krill numbers are at their peak (Robison et al., 1998).

Threat potential for *Nanomia bijuga* = 8.1% (SML), 4.4% (DML).

Some Additional Threats to Krill

Thalassocalyce inconstans is a diaphanous and delicate lobate ctenophore that feeds on krill, copepods, and other small zooplankton. It occurs throughout the deep water column of Monterey Bay but is concentrated above 300 m during the day (**Figures 2C,D**; MBARI Deep-Sea Guide[1]). Individual *T. inconstans* are not particularly abundant nor are they known to undertake vertical migrations. In its fishing posture, *Thalassocalyce* spreads its two lobes broadly into a thin, flattened plane. Small prey, such as copepods, are trapped by a sticky mucus coating on the inner surface of a lobe and are transported to the mouth by cilia (Harbison et al., 1978). Larger prey, like krill, become trapped within a globe-like enclosure formed by rapid contraction of the lobes when they are touched (Swift et al., 2009). Subsequent contractions reduce the size of the enclosed volume and direct the krill toward the ctenophore's mouth (**Figure 3A**). Within the enclosed volume krill gently probe the walls of the interior with their antennae, seeking a gap between the lobes that will allow escape (Swift et al., 2009). Additional ctenophores that prey upon krill are the periodically abundant cydippids *Hormiphora californiensis* and *Pleurobrachia bachei*, both are sit-and-wait predators that deploy multiple tentilla from each of their two tentacles; each tentillum is tipped with a sticky colloblast for capturing prey. Typically, *Hormiphora* sits with its tentacles held above the body, while *Pleurobrachia* holds them below.

Threat potential for *Thalassocalyce inconstans* = 0.5% (SML), 0.4% (DML).

The calycophoran siphonophore *P. dubia* can attain lengths of as much as 30–40 m (Robison and Connor, 1999; Robison, 2004), with a thousand or more zooids in its siphosome. Large siphonophores can deploy their tentacles in a curtain that hangs below the chain of zooids along the stem, or they can be spread out radially from the stem like the bristles of a bottle brush. Because they are passive predators, *Praya* colonies capture whatever encounters their tentacles and cannot swim away, and thus they consume a broad spectrum of zooplankton and

[1]http://dsg.mbari.org/dsg/home

micronekton, including krill. *Praya* typically occupies depths between 50 and 400 m. Two additional elongate siphonophores, the physonects *Apolemia uvaria* and *A. rubriversa,* overlap the lower portion of *Praya*'s depth range (MBARI Deep-Sea Guide) and extend a similar predatory threat down to 950 m.

Threat potential for *Praya dubia* = 53.9% (SML), 39.2% (DML).

Giant larvaceans of the genus *Bathochordaeus* do not feed on krill, however, their large mucus houses pose a potential threat to many vertically migrating species by presenting an obstacle that can entangle smaller zooplankters (**Figure 3B**). Functioning to prevent large detritus particles from clogging the finer mesh of the larvacean's inner filters, the outer structure can reach dimensions as large as a meter across (Hamner and Robison, 1992). The three species of *Bathochordaeus* in Monterey Bay (Sherlock et al., 2017) produce new filter houses on a daily basis (Robison et al., 2005). A factor in this timing is likely to be that many of these delicate structures are shredded by the passage of animals like fishes and larger crustaceans during DVM.

Threat potential for *Bathochordaeus* spp. = 27.6% (SML), 17.1% (DML).

Krill are also consumed by many species, which, like *Nanomia*, also undertake DVM. These include myctophid fishes, the bathylagid fish *Leuroglossus stilbius,* and sergestid shrimp.

Myctophids and Squid

Myctophid lanternfish comprise a significant biomass component of the SSL in Monterey Bay and they are regarded as quintessential vertical migrators (Marshall, 1979). Their predators include several species of squid whose prey-capture tactics involve either direct attack (e.g., *Gonatus onyx* and *Dosidicus gigas*) or aggressive mimicry using lures (e.g., *C. calyx* and *Grimalditeuthis bonplandi*). *G. onyx* and its congener *G. berryi* have a wide depth range within the mesopelagic of the study area but they show little evidence of an intrinsic diel vertical migration behavior. Instead, it appears that they remain below the mixed layer and seize myctophids, principally *Stenobrachius leucopsarus* and *Tarletonbeania crenularis,* during the myctophids' vertical migratory runs and at depth during the day (Hoving and Robison, 2016). As is typical of piscivorous squid, once captured, the spinal cord of the myctophid is severed by the squid's beak and the fish is then manipulated into a head-first position for ingestion (**Figure 3C**). The two species of *Gonatus* also exhibit a significant level of cannibalism, feeding on their own species as well as their congeners (Hoving and Robison, 2016). We have observed the large Humboldt squid, *D. gigas,* on several occasions feeding within aggregations of S. *leucopsarus*. These squid grab the fish individually with one or both feeding tentacles and transfer the prey to their mouth, while the dexterous arm tips are used for smaller prey.

Threat potential for *Gonatus onyx* = 19.4% (SML), 3.9% (DML).

Chiroteuthis calyx exhibits a complex behavioral repertoire, especially for an animal that lives perpetually in a habitat of little or no ambient illumination (Burford et al., 2015). The fourth arm on each side of *C. calyx* is thicker and longer than the other three, and has a groove through which the slender feeding tentacle is deployed. The tentacle slides through the groove then out of the supporting arm to hang suspended below. Serial light organs along the tentacle flash while the tentacle is moved up and down, presumably to attract prey (Robison, 2004). We have observed *C. calyx* grasping captured myctophids on several occasions. Another squid that lures its prey is *Grimalditeuthis bonplandi,* which is unique in that the club at the terminus of its feeding tentacle is capable of self-propulsion (Hoving et al., 2013). The actions of the club, which are deployed at the terminus of a very long filamentous tentacle, resemble the movements of a small swimming animal and are believed to be employed in attracting the squid's prey.

Threat potential for *Chiroteuthis calyx* = 18.0% (SML), 3.9% (DML).

We have not calculated threat potentials for *D. gigas* or *G. bonplandi* because in the former case, their presence in Monterey Bay is episodic (Field et al., 2007; Zeidberg and Robison, 2007) and for the latter species our observations are much too rare.

Some Additional Threats to Myctophids and Other Micronekton, Not Quantified

Threats to vertically migrating myctophids include both sit-and-wait predators as well as wide-ranging, highly mobile forms. Medusae and siphonophores comprise the bulk of the passive gelatinous piscivores and both utilize toxin-injecting nematocyst batteries to catch and immobilize their prey. We typically see smaller myctophids caught by medusae like *Periphylla periphylla,* while larger fishes seem more likely to be seized by siphonophore colonies. Many of these cnidarians have red or orange pigmentation (**Figure 3D**) which selectively absorbs blue light – the principal wavelengths available at these depths. This renders the predators essentially invisible. With siphonophores, the diel danger to a myctophid is a dense, unseen cloud of fine tentacles deployed in the path of its migration.

For many highly mobile predators of vertically migratory micronektonic fishes, depth changes made during periods of DVM do not appear to be an intrinsic pattern. Fast-moving fishes like Pacific hake, *Merluccius productus,* actively pursue myctophids, often in schools, and we see them near the surface during daytime as well as at night. Stomiid dragonfish, like *Tactostoma macropus, Idiacanthus antrostomus*, and *Chauliodus macouni,* are solitary hunters with broad vertical ranges. As is the case with the squid *C. calyx,* dragonfish appear to use bioluminescent lures to bait their prey.

DISCUSSION

It is becoming clear that the DVM of most deep-sea zooplankton and nekton are driven by the selective advantage of avoiding visually cued predation in near-surface waters during the hours of daylight (Bollens et al., 1992; Childress, 1995; Robison, 2003). It is equally apparent that there is a diverse aggregation of predators who lie in wait for the migrators during their daily travels through the water column. Analyzing and assessing these predator/prey

interactions is one of the goals of MBARI's ROV-based Midwater Ecology Program (Choy et al., 2017; Robison et al., 2017).

In the present case, threat potential is an assessment of the inherent risk of confronting a potential predator or obstacle during diel vertical migration. The calculations of threat potential derived here are based on average numbers of predators measured during hundreds of transecting dives between 1997 and 2015. During that time span we also recorded many variations of environmental conditions, differences in relative abundance within predator and prey populations, as well as changes in the composition of the midwater community overall. Dynamic variables are rife in the deep pelagic habitat and they occur on day-to-day time scales, seasonally, episodically, and in patterns we cannot yet resolve or link to any particular explanation. Despite the vagaries imposed by such variability, one great value of a multi-decadal time series is that consistent and repeating patterns emerge during analysis which can reveal some of the fundamental ecological characteristics of the animals that comprise these vast communities (Robison et al., 2005; Zeidberg and Robison, 2007; Burford et al., 2015).

The threats we have enumerated here are only a fraction of the full range of predatory challenges that confront diel vertical migrators, who regularly face a wide array of predatory strategies, tactics, and mechanisms. Collectively, these risks would make the odds of successful migration seem very small. However, high threat potentials are unlikely to result in equally high rates of mortality for vertically migrating prey. Indeed, vertical migration occurs in large part to avoid predation (Bollens et al., 1992). Vertical migrators have many ways to mitigate the threats, including mimicry (Robison, 1999; Burford et al., 2015), bioluminescence (Case et al., 1977; Widder, 2010), schooling or swarming (Hamner et al., 1983), and finely tuned sensory systems (Frank, 2017); overall, displaying a variety of behavioral responses to environmental conditions as well as to encounters with other species (Bollens and Frost, 1991; Visser and Thygesen, 2003).

Given the multitude of predators that lie in wait for individual vertical migrators, the threat potentials we have calculated would seem to be overwhelming but clearly, the prey populations persist. Other factors that reduce the likelihood of predation impact reaching calculated threat potential include: handling time (e.g., squid cannot gulp down a meal directly as most fishes can, instead with typical prey, they must secure, immobilize, and then chop their food into bite-size chunks with their beaks); partial tentacle deployment (e.g., *Nanomia* seldom appear with all of their tentacles fully extended, thus effectively reducing their CSA); satiation (e.g., many predators with obviously full guts are quiescent, apparently not in active feeding mode); prey manipulation (*Thalassocalyce* cannot use its lobes to capture additional prey when they are being used to enclose and direct prey toward the mouth); relocation (many ambush predators, like small siphonophores, change their location when feeding in one spot is not productive).

The threat potentials calculated here provide a metric for comparison of risk for migrators beyond other measures such as predator abundance or biomass. For example, *Nanomia bijuga* is typically more abundant than *P. dubia* by several orders of magnitude (**Figures 2A,C,D**), yet the threat to migrators posed by *P. dubia* on average (53.9%) is comparable to that of *N. bijuga* at the highest daytime densities we have observed (up to 1.4/m^3 which equates to threat potential of 46.1%).

One key difference between the direct, *in situ* approach used here for studying DVM ecology, and the traditional, indirect approach is that nets and acoustics grossly underestimate the great abundance and diversity of gelatinous predators (Haddock, 2004; Robison, 2004; Choy et al., 2017). The advent of undersea vehicles as research platforms in midwater has revealed not only the predatory roles of medusae, ctenophores, and siphonophores in DVM dynamics, but also their very broad depth distribution through the deep oceanic water column (Robison et al., 2010).

A second advantage conferred by HOVs and ROVs is the ability to document behavior. *In situ* observations have revealed the behavior patterns of many predators, both hard-bodied and gelatinous. Understanding a predator's behavior provides a new dimension for quantifying and predicting their impact on prey populations. Likewise, learning the avoidance tactics of prey species will help us to anticipate the effects of shifting predator populations in the face of unbridled exploitation. Looking forward, the advent of autonomous vehicles is providing extended dive time for day/night comparisons of DVM (Reisenbichler et al., 2016) and promises to expand the scope of *in situ* investigations to mesoscale levels. These perspectives will become increasingly important as we strive to understand and measure (and consider exploiting) DVM, an enormous energy-exchange process in the changing global ocean.

DATA AVAILABILITY STATEMENT

The datasets generated for this study are available on request to the corresponding author.

AUTHOR CONTRIBUTIONS

BR formulated the study. RS and PM managed the data extraction and manipulation. PM is responsible for modeling threat potential in Mathematica. BR, KR, and RS contributed to data collection and *in situ* observations. All authors contributed to writing the manuscript.

FUNDING

This work was supported by the David and Lucile Packard Foundation.

ACKNOWLEDGMENTS

We are grateful to Daniel Davis for his insights and guidance in developing the mathematics presented here. Joost Daniels and Kakani Katija provided images and measurements from DeepPIV. We thank the crews of MBARI's R/Vs *Point Lobos, Rachel Carson,* and *Western Flyer,* and the pilots of our ROVs *Ventana, Tiburon,* and *Doc Ricketts.* The three reviewers added to the clarity of the manuscript.

REFERENCES

Anderson, J. J., Gurarie, E., and Zabel, R. W. (2005). Mean free-path length theory of predator-prey interactions: application to juvenile salmon migration. *Ecol. Modell.* 186, 196–211. doi: 10.1016/j.ecolmodel.2005.01.014

Archibald, K. M., Siegel, D. A., and Doney, S. C. (2019). Modeling the impact of zooplankton diel vertical migration on the carbon export flux of the biological pump. *Global Biogeochem. Cycles* 33, 181–199. doi: 10.1029/2018gb005983

Barham, E. G. (1957). *The Ecology of Sonic Scattering Layers in Monterey Bay*. Ph.D. thesis, Stanford University, Palo Alto, CA.

Barham, E. G. (1963). Siphonophores and the deep scattering layer. *Science* 140, 826–828. doi: 10.1126/science.140.3568.826

Barham, E. G. (1966). Deep scattering layer migration and composition: observations from a diving saucer. *Science* 151, 1399–1403. doi: 10.1126/science.151.3716.1399

Bolin, R. L., and Abbott, D. P. (1963). Studies on the marine climate and phytoplankton of the central coast area of California, 1954–1960. *Calif. Coop. Fish. Invest. Rep.* 9, 23–45.

Bolin, R. L., and Hopkins Marine Station, (1964). *Hydrographic Data From the Area of the Monterey Submarine Canyon, 1951-1955: Final Report, July 30, 1964. Pacific Grove*. California: Stanford University.

Bollens, S. M., and Frost, B. W. (1991). Diel vertical migration in zooplankton: rapid individual response to predators. *J. Plankton Res.* 13, 1359–1365. doi: 10.1093/plankt/13.6.1359

Bollens, S. M., Frost, B. W., Thoreson, D. S., and Watts, S. J. (1992). Diel vertical migration in zooplankton: a field test of the predator avoidance hypothesis. *Hydrobiologia* 234, 33–39. doi: 10.1007/bf00010777

Burford, B. P., Robison, B. H., and Sherlock, R. E. (2015). Behaviour and mimicry in the juvenile and subadult life stages of the mesopelagic squid Chiroteuthis calyx. *J. Mar. Biol. Assoc. U.K.*95, 1221–1235. doi: 10.1017/S0025315414001763

Case, J. F., Warner, J., Barnes, A. T., and Lowenstine, M. (1977). Bioluminescence of lantern fish (Myctophidae) in response to changes in light intensity [34]. *Nature* 265, 179–181. doi: 10.1038/265179

Childress, J. J. (1995). Are there physiological and biochemical adaptations of metabolism in deep-sea animals? *Trends Ecol. Evol.* 10, 30–36. doi: 10.1016/S0169-5347(00)88957-0

Choy, C. A., Haddock, S. H. D., and Robison, B. H. (2017). Deep pelagic food web structure as revealed by in situ feeding observations. *Proc. Biol. Sci.* 284:20172116. doi: 10.1098/rspb.2017.2116

Curran, J. (2013). *Bolstad2*: Bolstad Functions. R Package Version 1.0-28. Available at: https://Cran.R-project.org/package=Bolstad2 (accessed February, 2019).

Davison, P. C., Checkley, D. M., Koslow, J. A., and Barlow, J. (2013). Carbon export mediated by mesopelagic fishes in the northeast Pacific Ocean. *Prog. Oceanogr.* 116, 14–30. doi: 10.1016/j.pocean.2013.05.013

Dorman, J. G., Sydeman, W. J., Bograd, S. J., and Powell, T. M. (2015). An individual-based model of the krill Euphausia pacifica in the California Current. *Prog. Oceanogr.* 138, 504–520. doi: 10.1016/j.pocean.2015.02.006

Dull, R. W. (1941). *Mathematics for Engineers*, 2nd Edn. New York, NY: McGraw–Hill Book Co.

Field, J. C., Baltz, K. E. N., and Walker, W. A. (2007). Range expansion and trophic interactions of the jumbo squid, Dosidicus gigas, in the California Current. *CalCOFI Rep.* 48, 131–146.

Frank, T. M. (2017). Ontogenetic adaptations in the visual systems of deep-sea crustaceans. *Philos. Trans. R. Soc. B Biol. Sci.* 372:20160071. doi: 10.1098/rstb.2016.0071

Gerritsen, J., and Strickler, J. R. (1977). Encounter probabilities and community structure in zooplankton: a mathematical model. *J. Fish. Res. Bd. Can.*34, 73–82. doi: 10.1139/f77-008

Haddock, S. H. D. (2004). A golden age of gelata: past and future research on planktonic ctenophores and cnidarians. *Hydrobiologia* 530, 549–556. doi: 10.1007/978-1-4020-2762-8_62

Hamner, W. M., Hamner, P. P., Strand, S. W., and Gilmer, R. W. (1983). Behavior of Antarctic krill, Euphausia superba: chemoreception, feeding, schooling, and molting. *Science* 220, 433–435. doi: 10.1126/science.220.4595.433

Hamner, W. M., and Robison, B. H. (1992). In situ observations of giant appendicularians in monterey bay. *Deep-Sea Res. A* 39, 1299–1313. doi: 10.1016/0198-0149(92)90070-A

Hansen, A. N., and Visser, A. W. (2016). Carbon export by vertically migrating zooplankton: an optimal behavior model. *Limnol. Oceanogr.* 61, 701–710. doi: 10.1002/lno.10249

Harbison, G. R., Madin, L. P., and Swanberg, N. R. (1978). On the natural history and distribution of oceanic ctenophores. *Deep Sea Res.* 25, 233–256. doi: 10.1016/0146-6291(78)90590-8

Harvey El, L., Jeong, H. J., and Menden-Duer, S. (2013). Avoidance and attraction: chemical cues influence predator-prey interactions of planktonic protists. *Limnol.Oceanogr.*58, 1176–1184. doi: 10.4319/lo.2013.58.4.1176

Hoving, H. J. T., and Robison, B. H. (2016). Deep-sea in situ observations of gonatid squid and their prey reveal high occurrence of cannibalism. *Deep-Sea Res. I* 116, 94–98. doi: 10.1016/j.dsr.2016.08.001

Hoving, H. J. T., Zeidberg, L. D., Benfield, M. C., Bush, S. L., Robison, B. H., and Vecchione, M. (2013). First in situ observations of the deep-sea squid Grimalditeuthis bonplandi reveal unique use of tentacles. *Proc. R. Soc. B Biol. Sci.* 280:20131463. doi: 10.1098/rspb.2013.1463

Jackson, G. A., Najjar, R. G., and Toggweiler, J. R. (1993). Flux feeding as a mechanism for zooplankton grazing and its implications for vertical particulate flux. *Limnol. Oceanogr.* 38, 1328–1331. doi: 10.4319/lo.1993.38.6.1328

Katija, K., Sherlock, R. E., Sherman, A. D., and Robison, B. H. (2017). New technology reveals the role of giant larvaceans in oceanic carbon cycling. *Sci. Adv.* 3, e1602374. doi: 10.1126/sciadv.1602374

Marinovic, B. B., Croll, D. A., Gong, N., Benson, S. R., and Chavez, F. P. (2002). Effects of the 1997-1999 El Niño and La Niña events on zooplankton abundance and euphausiid community composition within the Monterey Bay coastal upwelling system. *Prog. Oceanogr.* 54, 265–277. doi: 10.1016/S0079-6611(02)00053-8

Marshall, N. B. (1979). *Developments in Deep-Sea Biology*. Poole Dorset: Blandford Press.

Ohman, M. D., and Romagnan, J.-B. (2016). Nonlinear effects of body size and optical attenuation on diel vertical migration by zooplankton. *Limnol. Oceanogr.* 61, 765–770. doi: 10.1002/lno.10251

Olivieri, R. A., and Chavez, F. P. (2000). A model of plankton dynamics for the coastal upwelling system of Monterey Bay. *California. Deep-Sea Res. II* 47, 1077–1106. doi: 10.1016/S0967064599)00137-X

Pennington, T. J., and Chavez, F. P. (2000). Seasonal fluctuations of temperature, salinity, nitrate, chlorophyll and primary production at station H3/M1 over 1989–1996 in Monterey Bay. California. *Deep-Sea Res. II Top. Stud. Oceanogr.* 47, 947–973. doi: 10.1016/S0967-0645(99)00132-0

R Core Team, (2013). *R: A Language and Environment for Statistical Computing*. Vienna: R Foundation for Statistical Computing. doi: 10.1016/s0967-0645(99)00132-0

Raskoff, K. A. (2002). Foraging, prey capture, and gut contents of the mesopelagic narcomedusa *Solmissus* spp. (*Cnidaria*: *Hydrozoa*). *Mar. Biol.* 141, 1099–1107. doi: 10.1007/s00227-002-0912-8

Reisenbichler, K. R., Chaffey, M. R., Cazenave, F. C., McEwen, R. S., Henthorn, R. H., Sherlock, R. E., et al. (2016). "Automating MBARI's midwater time-series video surveys: the transition from ROV to AUV," in *OCEANS 2016 MTS/IEEE Monterey* (Monterey, CA: IEEE).

Robinson, C., Steinberg, D. K., Anderson, T. R., Arístegui, J., Carlson, C. A., Frost, J. R., et al. (2010). Mesopelagic zone ecology and biogeochemistry - a synthesis. *Deep-Sea Res. II* 57, 1504–1518. doi: 10.1016/j.dsr2.2010.02.018

Robison, B. H. (1999). Shape change behavior by mesopelagic animals. *Mar. Freshw. Behav. Physiol.* 32, 17–25. doi: 10.1080/10236249909379034

Robison, B. H. (2003). What drives the diel vertical migrations of Antarctic midwater fish? *J. Mar. Biol. Assoc. U.K.*83, 639–642. doi: 10.1017/S0025315403007586h

Robison, B. H. (2004). Deep pelagic biology. *J. Exp. Mar. Bio. Ecol.* 300, 253–272. doi: 10.1016/j.jembe.2004.01.012

Robison, B. H., and Connor, J. (1999). *The Deep Sea. Monterey B*. Monterey, CA: Monterey Bay Aquarium Press.

Robison, B. H., Reisenbichler, K. R., and Sherlock, R. E. (2017). The coevolution of midwater research and ROV technology at MBARI. *Oceanography* 30, 26–37. doi: 10.5670/oceanog.2017.421

Robison, B. H., Reisenbichler, K. R., Sherlock, R. E., Silguero, J. M. B., and Chavez, F. P. (1998). Seasonal abundance of the siphonophore. Nanomia bijuga, in Monterey Bay. *Deep-Sea Res. II* 45, 1741–1751. doi: 10.1016/S0967-0645(98)80015-5

Robison, B. H., Sherlock, R. E., and Reisenbichler, K. R. (2010). The bathypelagic community of Monterey Canyon. *Deep-Sea Res. II* 57, 1551–1556. doi: 10.1016/j.dsr2.2010.02.021

Robison, B. H. H., Reisenbichler, K. R., and Sherlock, R. E. (2005). Giant larvacean houses: rapid carbon transport to the deep sea floor. *Science* 308, 1609–1611. doi: 10.1126/science.1109104

Schlining, B. M., and Stout, N. J. (2006). *MBARI's Video Annotation and Reference System. in OCEANS 2006*. IEEE Computer Society, doi: 10.1109/OCEANS.2006.306879

Sherlock, R. E., Walz, K. R., Schlining, K. L., and Robison, B. H. (2017). Morphology, ecology, and molecular biology of a new species of giant larvacean in the eastern North Pacific: *Bathochordaeus mcnutti* sp. nov. *Mar. Biol.* 164:20. doi: 10.1007/s00227-016-3046-0

Silguero, J. M. B., and Robison, B. H. (2000). Seasonal abundance and vertical distribution of mesopelagic calycophoran siphonophores in Monterey Bay, CA. *J. Plankt. Res.* 22, 1139–1153. doi: 10.1093/plankt/22.6.1139

Skogsberg, T. (1936). Hydrography of Monterey Bay, California. Thermal conditions, 1929-1933. *Trans. Am. Philos. Soc.* 29, i–152.

Skogsberg, T., and Phelps, A. (1946). Hydrography of Monterey Bay, California. Thermal Conditions, Part II (1934-1937). *Proc. Am. Philos. Soc.* 90, 350–386.

Steinberg, D. K., and Landry, M. R. (2017). Zooplankton and the ocean carbon cycle. *Ann Rev Mar Sci* 9, 413–444. doi: 10.1146/annurev-marine-010814-015924

Swift, H. F., Hamner, W. M., Robison, B. H., and Madin, L. P. (2009). Feeding behavior of the ctenophore Thalassocalyce inconstans: Revision of anatomy of the order Thalassocalycida. *Mar. Biol.* 156, 1049–1056. doi: 10.1007/s00227-009-1149-6

Torres, J. J., and Childress, J. J. (1983). Relationship of oxygen consumption to swimming speed in Euphausia pacifica. *Mar. Biol.* 74, 79–86. doi: 10.1007/bf00394278

Visser, A. W., and Thygesen, U. H. (2003). Random motility of plankton: diffusive and aggregative contributions. *J. Plankton Res.* 25, 1157–1168. doi: 10.1093/plankt/25.9.1157

Widder, E. A. (2010). Bioluminescence in the ocean. *Science* 328, 704–708. doi: 10.1126/science.1174269

Wolfram Research Inc, (2019). *Mathematica, Version 12.0*.

Zeidberg, L. D., and Robison, B. H. (2007). Invasive range expansion by the Humboldt squid, Dosidicus gigas, in the eastern North Pacific. *Proc. Natl. Acad. Sci. U. S. A.* 104, 12948–12950. doi: 10.1073/pnas.0702043104

Conflict of Interest: The authors declare that the research was conducted in the absence of any commercial or financial relationships that could be construed as a potential conflict of interest.

frontiers in Marine Science

ORIGINAL RESEARCH
published: 29 May 2020
doi: 10.3389/fmars.2020.00358

Zooplankton-Mediated Fluxes in the Eastern Tropical North Atlantic

Rainer Kiko[1,2]*, *Peter Brandt*[2,3], *Svenja Christiansen*[2,4], *Jannik Faustmann*[2,3], *Iris Kriest*[2], *Elizandro Rodrigues*[5], *Florian Schütte*[2] and *Helena Hauss*[2,3]

[1] Laboratoire d'Océanographie de Villefranche-sur-mer, Sorbonne Université, Villefranche-sur-mer, France, [2] GEOMAR Helmholtz Center for Ocean Research Kiel, Kiel, Germany, [3] Faculty of Mathematics and Natural Sciences, Kiel University, Kiel, Germany, [4] Department of Biosciences, University of Oslo, Oslo, Norway, [5] Instituto do Mar, I.P., Mindelo, Cabo Verde

Zooplankton organisms are a central part of pelagic ecosystems. They feed on all kinds of particulate matter and their egested fecal pellets contribute substantially to the passive sinking flux to depth. Some zooplankton species also conduct diel vertical migrations (DVMs) between the surface layer (where they feed at nighttime) and midwater depth (where they hide at daytime from predation). These DVMs cause the active export of organic and inorganic matter from the surface layer as zooplankton organisms excrete, defecate, respire, die, and are preyed upon at depth. In the Eastern Tropical North Atlantic (ETNA), the daytime distribution depth of many migrators (300–600 m) coincides with an expanding and intensifying oxygen minimum zone (OMZ). We here assess the day and night-time biomass distribution of mesozooplankton with an equivalent spherical diameter of 0.39–20 mm in three regions of the ETNA, calculate the DVM-mediated fluxes and compare these to particulate matter fluxes and other biogeochemical processes. Integrated mesozooplankton biomass in the ETNA region is about twice as high at a central OMZ location (cOMZ; 11° N, 21° W) compared to the Cape Verde Ocean Observatory (CVOO; 17.6° N, 24.3° W) and an oligotrophic location at 5° N, 23° W (5N). An Intermediate Particle Maximum (IPM) is particularly strong at cOMZ compared to the other regions. This IPM seems to be related to DVM activity. Zooplankton DVM was found to be responsible for about 31–41% of nitrogen loss from the upper 200m of the water column. Gut flux and mortality make up about 31% of particulate matter supply to the 300–600 m depth layer at cOMZ, whereas it makes up about 32% and 41% at CVOO and 5N, respectively. Resident and migrant zooplankton are responsible for about 7–27% of the total oxygen demand at 300–600 m depth. Changes in zooplankton abundance and migration behavior due to decreasing oxygen levels at midwater depth could therefore alter the elemental cycling of oxygen and carbon in the ETNA OMZ and impact the removal of nitrogen from the surface layer.

Keywords: zooplankton, tropical Atlantic, oxygen minimum zone, diel vertical migration, biogeochemical fluxes, martin curve, Cape Verde ocean observatory

OPEN ACCESS

Edited by:
Carol Robinson,
University of East Anglia,
United Kingdom

Reviewed by:
Geraint A. Tarling,
British Antarctic Survey (BAS),
United Kingdom
Michael R. Stukel,
Florida State University, United States

***Correspondence:**
Rainer Kiko
rainer.kiko@obs-vlfr.fr

Specialty section:
This article was submitted to Marine Biogeochemistry, a section of the journal Frontiers in Marine Science

Received: *28 June 2019*
Accepted: *27 April 2020*
Published: *29 May 2020*

Citation:
Kiko R, Brandt P, Christiansen S, Faustmann J, Kriest I, Rodrigues E, Schütte F and Hauss H (2020) Zooplankton-Mediated Fluxes in the Eastern Tropical North Atlantic. Front. Mar. Sci. 7:358. doi: 10.3389/fmars.2020.00358

1. INTRODUCTION

1.1. The Oxygen Minimum Zone of the Eastern Tropical North Atlantic

The Eastern Tropical North Atlantic (ETNA) harbors a mesopelagic Oxygen Minimum Zone (OMZ) at about 300–600 m water depth (Karstensen et al., 2008) that vertically expanded and intensified in the last 50 years (Stramma et al., 2008). Its core coincides with the daytime depth of many vertically migrating zooplankton and nekton species (Bianchi et al., 2013). Oceanic OMZs mainly result from sluggish ventilation associated with weak thermocline circulation and enhanced consumption in proximity to the eastern boundary upwelling systems. Zooplankton and nekton respiration and the remineralization of organic matter by aerobic microbes contribute to the oxygen demand, whereas horizontal and vertical mixing contribute to the oxygen supply (Karstensen et al., 2008; Fischer et al., 2013; Hahn et al., 2014). Weak mean advection by zonal current bands that are ubiquitous in the tropical Pacific and Atlantic contribute to the ventilation of the eastern basins from the well-ventilated western boundaries (Brandt et al., 2015). Minimum oxygen levels in the ETNA in the OMZ core are observed to be slightly below 40 $\mu mol\ O_2\ kg^{-1}$, compared to about 200 $\mu mol\ O_2\ kg^{-1}$ in the upper mixed layer. Oceanic OMZs are expected to further expand under global warming conditions. Reduced oxygen solubility and increased stratification associated with shallowing ventilation and reduced mixing are thought to be the main drivers of future oceanic oxygen loss (Matear and Hirst, 2003; Bopp et al., 2013; Cocco et al., 2013; Oschlies et al., 2018).

1.2. The Role of Zooplankton in Biogeochemical Cycling

Zooplankton occupies an important role in pelagic ecosystems as it provides the link between primary and tertiary trophic levels and to a large extent shapes elemental cycles. Global, depth-integrated mesozooplankton carbon ingestion and respiration is estimated at 34–63 and 17–32%, respectively, of primary production in the global open ocean (Hernández-León and Ikeda, 2005). Zooplankton feeds on all kinds of small particulate matter (e.g., phytoplankton, detritus, smaller zooplankton organisms) and egested fecal pellets contribute substantially to the passive sinking flux out of the surface layer (e.g., Turner, 2015; Steinberg and Landry, 2017) as they sink much faster than the individual food particles ingested (e.g., Liszka et al., 2019). On the other hand, zooplankton respiration and excretion impacts the oxygen and nutrient distribution. Mesozooplankton excretion for example provides a substantial fraction of the estimated N and P requirements of phytoplankton (>50% in the oligotrophic tropical and subtropical Atlantic (Isla and Anadón, 2004). Zooplankton organisms developed different, species-specific tolerance thresholds for low oxygen availability (Childress and Seibel, 1998). OMZs therefore shape the distribution of zooplankton within the pelagic ecosystem of the subtropical and tropical oceans (e.g., Saltzman and Wishner, 1997; Wishner et al., 1998; Auel and Verheye, 2007). Some zooplankton organisms also conduct diel vertical migrations (DVMs) between the surface layer, where they feed at nighttime and midwater depth below the sunlit euphotic zone, where they hide from predation at daytime (Lampert, 1989). These DVMs create related migratory fluxes (Steinberg et al., 2000, 2002) and result in the active export of organic and inorganic matter from the surface layer as zooplankton organisms excrete, defecate, respire, die, and get eaten at depth (e.g., Longhurst et al., 1990). Global biogeochemical model studies that include some first zooplankton DVM parameterizations also suggest that the active flux can locally contribute up to 50% of the sinking flux to the mesopelagic (Bianchi et al., 2013; Aumont et al., 2018; Archibald et al., 2019), and lower oxygen concentrations in these depths by 15 $\mu mol\ kg^{-1}$ (Aumont et al., 2018) up to almost 50 $\mu mol\ kg^{-1}$ (Bianchi et al., 2013). However, these models do not represent the behavior of zooplankton in extreme OMZs well (Kiko and Hauss, 2019) as hypoxia threshold levels are used that are unrealistic in some regions. Feedbacks between changing oxygen levels and the role of zooplankton in the elemental cycling of oxygen and carbon are to be expected and might also impact the elemental cycling of nitrogen. Many important processes such as excretion, defecation and mortality are very difficult and time consuming to observe directly, but can be deduced from zooplankton data (abundance, size and taxonomic identity) obtained during oceanographic surveys using allometric relationships and results from process studies. As physiological rates (Ikeda, 2014), but also e.g., the size of fecal pellets (Stamieszkin et al., 2015; Turner, 2015) scale with body size and vary with organism type, changes in the zooplankton size distribution and composition can go in hand with changes in zooplankton mediated biogeochemical fluxes despite unchanged bulk biomass. It is hence critical to observe the zooplankton size distribution, e.g., with optical methods (Gorsky et al., 2010) if we want to come to a more complete understanding of biogeochemical cycling in a given region (Lombard et al., 2019).

Determining the zooplankton size distribution using optical methods also has the advantage that aggregates, fibers and other non-zooplankton components, as well as organisms that are not-quantitatively caught due to an unfavorable abundance to volume ratio (Lombard et al., 2019) can be digitally removed from the analysis. On the other hand, the analysis of zooplankton net catches with the given method delivers lower-bound biomass estimates, as some organisms get entangled with each other and detritus on the scanner surface and can therefore not be analyzed optically. Net catches and subsequent fixation are also not favorable for fragile, gelatinous organisms such as rhizaria and various gelatinous meso- and macrozooplankton (Remsen et al., 2005). These methods are therefore only suitable for "well-preserved" zooplankton in a sampling specific size range.

1.3. Zooplankton Research in the Eastern Tropical North Atlantic

The ETNA features dust input from the Sahara (e.g., Baker et al., 2007) and an extended OMZ associated with the coastal upwelling and the Guinea Dome. Oxygen levels within the OMZ are not severely low, but long term observations indicate that they are declining and that the OMZ is expanding (Stramma et al., 2008; Schmidtko et al., 2017). The ETNA is hence

particularly interesting regarding biogeochemical processes in the North Atlantic. Very limited zooplankton data are available for the ETNA. A study by Chahsavar-Archard and Razouls (1982) provided a faunistic evaluation for several stations, with two net catches conducted down to 600 m depth, but no quantitative data on zooplankton abundance or biomass. Quantitative sampling efforts such as those undertaken routinely during the Atlantic Meridional Transect (AMT) cruises and the extensive collections of researchers from the former Soviet Union were mostly restricted to the upper 200 m of the water column (Piontkovski and Castellani, 2009). This hampers the estimation of zooplankton-mediated fluxes out of the surface layer and into the OMZ as net avoidance during daytime might occur at the surface (Ianson et al., 2004) and the organisms that take refuge at depth during daytime might do so at different depth levels. In a recent study, Hauss et al. (2016) observed the impact of an individual mesoscale eddy near Cape Verde on the distribution and vertical migration of zooplankton and Christiansen et al. (2018) investigated the distribution of a holopelagic polychaete in relation to particle abundance and mesoscale eddy dynamics across the tropical Atlantic, demonstrating that hypoxia tolerance is variable between species. For a migrating euphausiid (*Euphausia gibboides*) and a migrating copepod (*Pleuromamma abdominalis*), we have experimentally determined the critical oxygen partial pressure p_{crit} at which aerobic metabolism can no longer be maintained independently of the environmental pO_2 (Kiko et al., 2016). A companion paper in this research topic (Hernández-León et al., 2019) conducted five day-night stations between 2 and 20° N.

1.4. Target Regions of Our Work

We here constrain zooplankton impacts on the particle size distribution and the carbon, nitrogen and oxygen budget of the ETNA. We focus our analysis on three regions of interest: the Cape Verde Ocean Observatory (CVOO; at 17.6°N, 24.3°W), the center of the OMZ in the ETNA (cOMZ; at 11°N, 21°W) and an oligotrophic area (5N; at 5°N, 23°W). According to previous studies, the region is largely N-limited (Hauss et al., 2013) and in addition to diapycnal flux of dissolved N substantially fuelled by diazotrophy in the upper mixed layer, with the colonial cyanobacterium *Trichodesmium* sp. being a key species (Sandel et al., 2015). Among the three regions, the cOMZ region features the shallowest pycnocline and highest productivity (Sandel et al., 2015). CVOO is located north of the Cape Verde archipelago close to the Cape Verde frontal zone. The upper layers in this region are mostly affected by North Atlantic central water (NACW) that is more saline and warmer than South Atlantic central water (SACW) (Schütte et al., 2016a). cOMZ stations are located in the spatial center of the mesopelagic OMZ. Here, the lowest average oxygen concentrations in the tropical North Atlantic are found at the boundary between central water masses above and intermediate water masses, mostly Antarctic intermediate water (AAIW), below. In addition to the mesopelagic OMZ in the cOMZ region, a well-developed shallow OMZ related to the proximity of the eastern boundary upwelling region with high surface productivity has been identified (Brandt et al., 2015). The water masses in the cOMZ region are a mixture of NACW and SACW. The 5N region is mostly dominated by fresher and colder SACW (Hahn et al., 2017). In addition the water masses are more oxygenated due to better ventilation by the eastward flow within the North Equatorial Counter Current and the North Equatorial Undercurrent, which supply oxygenated waters from the western boundary of the Atlantic Ocean toward the oxygen minimum near the eastern boundary (Brandt et al., 2015). Mesoscale eddies in the observation area are known to feature rather different biogeochemical properties (Schütte et al., 2016a,b). Anticyclonic modewater eddies are known to be exceptionally productive and often feature severely hypoxic subsurface oxygen levels (Karstensen et al., 2015; Hauss et al., 2016). We here excluded all mesoscale eddies identified in Christiansen et al. (2018) from the data analysis in order to provide information on the background conditions.

Specifically, we (1) provide estimates of integrated and depth-resolved mesozooplankton biomass for the different regions and relate these to the general environmental conditions, (2) discuss the importance of DVMs for nitrogen fluxes out of the upper 200 m of the water column and for the carbon and oxygen budget of the 300–600 m depth layer, (3) analyze the impact of zooplankton DVMs on POC content and flux observed using an Underwater Vision Profiler 5 and (4) conduct a first comparison of our data to biogeochemical model results.

2. MATERIALS AND METHODS

2.1. Onboard Sampling

During RV Maria S. Merian cruise MSM22 and RV Meteor cruises M97, M105, M106, M119, and M130 to the ETNA region in November 2012, June 2013, March/April 2014, September 2015, and September 2016, respectively, we collected depth-specific mesozooplankton samples from 34 vertical hauls with a Hydrobios MultiNet Midi (0.25 m^2 mouth opening, 200 μm mesh size, five nets). On each station, a day and a night haul were obtained in very close proximity (average distance 2.4 km, range 0–7.0 km) to each other, representing a pair of day-night hauls for the assessment of diel vertical migration patterns. Sampling was avoided during local dusk or dawn ± 1 h and the day hauls were brought on deck ± 5 h of local solar noon, whereas the night hauls were brought on deck between ± 4 h of local midnight (see **Figure 1** for sampling locations and **Table 1** for further location and time information for each haul used). Sampling depths were 1,000–600, 600–300, 300–200, 200–100, and 100–0 m depth during all cruises. Temperature, salinity, chlorophyll-a and oxygen concentration were measured during concomitant profiles of a Seabird SBE 11plus CTD (conductivity, temperature, depth) equipped with dual oxygen sensors (calibrated during the cruises with discrete samples) and a fluorescence probe. Additionally, an Underwater Vision Profiler 5 (UVP5; Picheral et al., 2010) was mounted on the CTD to measure the particle abundance and size distribution as well as the *Trichodesmium* sp. abundance. Nitrate was analyzed either on board or after storage at −20°C after Grasshoff et al. (2009). Furthermore, we analyze backscatter data from the vessel mounted 38 kHz Acoustic Doppler Current Profiler (ADCP). The regions targeted in this work are the area of the Cape Verde Ocean Observatory

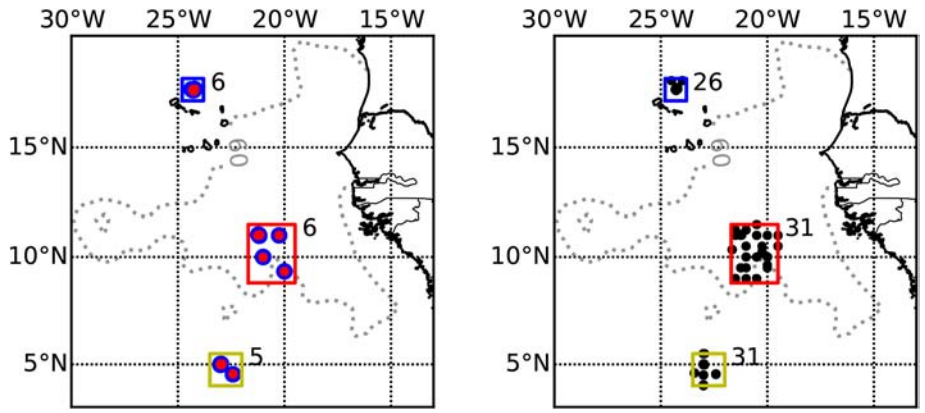

FIGURE 1 | Map showing the sampling area in the ETNA and the three sampling regions. Boxes indicate the area boundaries from which CTD or ADCP data were included in the analysis (blue: CVOO, red: cOMZ, yellow: 5N). **(Left)** Multinet deployments. **(Right)** CTD deployments. Numbers next to the boxes indicate the number of day-night multinet pairs or CTDs obtained in the respective region. Within the cOMZ, a random subsampling was conducted to reduce the number of CTD profiles used to 31. Gray dotted contour line indicates 60 $\mu mol\ O_2\ kg^{-1}$ oxygen (World Ocean Atlas 2018) at 400 m depth. Lower values are found at cOMZ.

(CVOO), the central region of the ETNA OMZ (cOMZ) and stations located in the North Equatorial Counter Current at about 5°N, 23°W (5N). We make use of CTD, UVP5 and ADCP data obtained within ±0.5° distance to the Multinet deployments from the respective cruises. The boxes from which these data are obtained are: 5N (4.0°N to 5.5°N, 24°W to 22°W), cOMZ (8.8°N to 11.5°N, 21.7°W to 19.5°W), and CVOO (17.1°N to 18.1°N, 24.8°W to 23.8°W) (**Figure 1**). Data obtained within mesoscale eddies identified in Christiansen et al. (2018) was excluded from the analysis. A list of CTD-sampling locations, dates and times can be found in **Tables S1A–C**.

2.2. Laboratory Analysis of Multinet Catches

Samples were fixed in borax-buffered formaldehyde in seawater solution and brought to the home laboratory. Here, each sample was size-fractionated (small: 200–500 μm, medium: 500–1,000 μm and large: > 1,000 μm). The small fraction was not further used in this analysis. For the medium fraction, subsamples with about 1,000 zooplankton items per subsample were generated using a Motoda Splitter, whereas the entire large fraction was used for further analysis. The plankton items contained in each fraction were distributed and separated on a 20*30 cm glass tray and the glass tray scanned using an Epson perfection V750 pro flatbed scanner. Object segmentation was conducted using Zooprocess (Gorsky et al., 2010) and taxonomic units were assigned automatically using Plankton Identifier or the prediction options in EcoTaxa (Picheral et al., 2017). Assignments were thereafter corrected manually on the EcoTaxa platform. Analysis of the biovolume-size spectrum (**Figure S1**) showed that organisms with an equivalent spherical volume smaller than 0.032 mm^{-3} (equivalent to a equivalent spherical diameter of 0.39 mm) and larger than 4,188 mm^{-3} (equivalent to an equivalent spherical diameter of 20.0 mm) were not quantitatively sampled. We therefore excluded these from further analysis. See **Figure S1** for further details. Taxon-specific area-to-drymass conversion factors for subtropical zooplankton (Lehette and Hernández-León, 2009) and drymass to carbon (C) and nitrogen (N) conversion factors (Kiørboe, 2013) were used to calculate the biomass, C and N content of each zooplankton organism scanned. Taxonomic units and biomass conversion factors used are listed in **Table 2**. Abundance and biomass estimates are lower bounds, as some organisms touched each other (multiple) or were entangled in an indiscernable mass with detritus. We consider the following categories to be well conserved and constrain our analyses on these: crustacea, chaetognatha, calycophoran siphonophores, annelida, and mollusca. Fish are also well-conserved, but not included in the literature on zooplankton individual biomass estimates or metabolic rates (Lehette and Hernández-León, 2009; Kiørboe, 2013; Ikeda, 2014) we use. The following categories can not be quantitatively evaluated, as many of their members are either damaged by the net or the fixation: all rhizaria, thaliacea, ctenophores, cnidaria other than calycophoran siphonophores. Our estimates of total biomass as well as zooplankton-mediated fluxes should therefore be considered lower bound estimates.

2.3. Calculation of Mesozooplankton Biomass, Metabolic Activity, and Mortality

Taxon-specific equations for biomass and temperature dependence of respiration and ammonium excretion (Ikeda, 2014) were applied to calculate the depth-specific respiration and ammonium excretion rate of each scanned specimen (see **Table 2** for equations and taxon specific factors used). The average temperature for the sampled depth layer was obtained from the concomitant CTD deployments. The environmental pO_2 was generally much higher than the estimated p_{crit} for migrating euphausiids and copepods (Kiko et al., 2016, see also **Figure 2**). Therefore, unlike to our companion paper (Kiko and Hauss, 2019), we did not apply a correction of oxygen-dependent depression of metabolic activity. Daily mortality of copepods was calculated according to Hirst and Kiørboe (2002)

TABLE 1 | Metadata for each pair of hauls used in this publication.

Pair	Cruise	Haul	Date	Time	Latitude	Longitude	Noon	Delta to noon	Category	Distance
1	MSM022-1	mn02	2012-10-25	13:01	17.535	-24.251	13:21	00:20	day	4.47
1	MSM022-1	mn01	2012-10-25	00:04	17.579	-24.25	13:21	10:42	night	4.47
2	MSM022-1	mn07	2012-10-30	11:50	5.013	-22.998	13:15	01:25	day	1.77
2	MSM022-1	mn08	2012-10-31	00:55	4.997	-22.992	13:15	11:39	night	1.77
3	MSM022-1	mn11	2012-11-01	15:49	4.551	-22.416	13:13	02:35	day	1.86
3	MSM022-1	mn10	2012-11-01	03:39	4.533	-22.417	13:13	14:25	night	1.86
4	MSM022-1	mn34	2012-11-20	15:45	17.626	-24.212	13:22	02:22	day	1.05
4	MSM022-1	mn35	2012-11-20	22:16	17.634	-24.218	13:22	08:53	night	1.05
5	M097-1	mn02	2013-05-26	16:02	17.566	-24.283	13:34	02:27	day	0.24
5	M097-1	mn01	2013-05-26	05:02	17.567	-24.285	13:34	15:27	night	0.24
6	M097-1	mn06	2013-06-03	11:15	10.999	-20.25	13:19	02:04	day	0.1
6	M097-1	mn05	2013-06-02	22:01	11.0	-20.25	13:18	08:42	night	0.1
7	M097-1	mn15	2013-06-18	09:00	9.33	-20.0	13:21	04:21	day	0.53
7	M097-1	mn14	2013-06-18	05:05	9.335	-19.999	13:20	15:44	night	0.53
8	M105-1	mn10	2014-03-24	11:41	9.9893	-21.0024	13:30	01:49	day	1.15
8	M105-1	mn09	2014-03-24	05:23	10.0001	-20.9999	13:30	15:52	night	1.15
9	M106-1	mn02	2014-04-20	13:38	17.6	-24.25	13:35	00:02	day	0.0
9	M106-1	mn01	2014-04-20	05:11	17.6	-24.25	13:36	15:34	night	0.0
10	M106-1	mn08	2014-04-25	17:50	11.01	-21.208	13:22	04:27	day	3.17
10	M106-1	mn07	2014-04-24	23:39	11.036	-21.223	13:23	10:15	night	3.17
11	M106-1	mn11	2014-04-29	14:41	5.017	-22.933	13:29	01:11	day	5.6
11	M106-1	mn12	2014-04-30	02:44	5.025	-22.983	13:29	13:14	night	5.6
12	M119-1	mn03	2015-09-09	16:55	17.6035	-24.2977	13:34	03:20	day	6.96
12	M119-1	mn01	2015-09-09	02:40	17.6179	-24.3592	13:35	13:04	night	6.96
13	M119-1	mn06	2015-09-14	13:49	11.0041	-21.2468	13:20	00:28	day	4.85
13	M119-1	mn07	2015-09-14	23:52	11.0293	-21.21	13:20	10:31	night	4.85
14	M119-1	mn09	2015-09-18	13:52	4.9728	-22.9658	13:26	00:25	day	3.48
14	M119-1	mn10	2015-09-19	01:44	4.977	-22.9971	13:26	12:17	night	3.48
15	M130-1	mn02	2016-08-30	14:26	17.5828	-24.2842	13:37	00:48	day	0.06
15	M130-1	mn01	2016-08-30	03:50	17.5825	-24.2837	13:37	14:12	night	0.06
16	M130-1	mn06	2016-09-08	16:15	11.0178	-21.157	13:22	02:52	day	4.74
16	M130-1	mn07	2016-09-09	00:59	10.9802	-21.1812	13:22	11:36	night	4.74
17	M130-1	mn09	2016-09-11	14:21	5.0002	-22.9998	13:28	00:52	day	0.02
17	M130-1	mn10	2016-09-11	23:32	5.0003	-22.9998	13:28	10:03	night	0.02

Time and local noon are UTC in HH:MM, Delta to noon in HH:MM, distance in km.

as $\ln(mortality) = 0.047 * Temperature - 0.154 * ln(DW) - 2.532$, thereby treating all copepods as broadcast spawners (DW = Dryweight in μg, Temperature in Celsius). Mortality of all other groups was calculated according to Hirst and Kiørboe (2002) as $log10(mortality) = (-0.325 * log10(DW) - 0.154) / 2^{(15-temperature)/10}$, thereby applying a Q10 of 2 (DW = Dryweight in g, Temperature in Celsius). Individual daily mortality was multiplied with the individual biomass and summed up to yield mortality per day in mg Carbon. Day-night differences of total respiration, ammonium excretion and mortality were calculated for each depth level in order to include effects of temperature and size-distribution. For depth below 100 m, these day-night differences coincide with the migratory fluxes. Migratory losses from the 0 to 200 m depth layer were calculated as the sum of the integrated day-night difference of fluxes at 200 to 1,000 m depth to avoid artifacts due to sampling net avoidance in the surface layer at daytime (Ianson et al., 2004) and reduction of metabolic activity at depth due to lower temperatures. A residence time at depth of 12 h was assumed. To test for statistical significance of day-night differences, a one-sided students t-Test against zero was conducted ($p < 0.05$).

2.4. Calculation of POC Content and POC Flux From UVP5 Data

High-resolution full depth particle size spectra (0.14–44 mm equivalent spherical diameter, ESD) were obtained with an Underwater Vision Profiler 5 (UVP5 Picheral et al., 2010), mounted on the CTD-Rosette used during the respective cruise. Calculating POC flux from UVP5 data relies on assumptions about the relationship between particle size and POC content and particle size and sinking speed (Kriest, 2002; Giering et al.,

TABLE 2 | Conversion factors and functions used in this publication.

Group	BM exponent	BM multiplicator	Respiration factor	Excretion factor	DWtoC	CtoN
copepoda	1.59	45.25	0	0	0.48	5.1
amphipoda	1.51	43.9	0.416	0.262	0.34	5.1
crustacea	1.51	43.9	0.416	0.262	0.34	5.1
cladocera	1.51	43.9	-0.393	-1.356	0.435	4.9
decapoda	1.51	43.9	0.631	0	0.435	4.9
euphausiacea	1.51	43.9	0.697	0	0.419	4.1
ostracoda	1.51	43.9	-0.393	-1.356	0.435	4.9
chaetognatha	1.19	23.45	-0.448	0	0.367	4.0
ctenophora[1]	1.02	43.17	-1.257	-1.397	0.051	4.4
siphonophorae	1.02	43.17	-0.480	-0.558	0.132	4.0
mollusca[2]	1.54	43.38	0	-0.550	0.289	5.9
annelida	1.54	43.38	0.382	0	0.37	4.2

[1]*formula for siphonophores was used as no specific formula is given in Lehette and Hernández-León (2009);* [2]*formula for general mesozooplankton was used as no specific formula is given in Lehette and Hernández-León (2009). Biomass was calculated as biomass = BM multiplicator ∗ area*$^{BM\ exponent}$*. Respiration and Excretion factors from Ikeda (2014). Respiration was calculated according to Ikeda (2014) as* $\ln(respiration) = 18.775 + 0.766 * \ln(DW) - 5.256 * 1000/Temperature - 0.113 * \ln(Depth) + Respiration\ factor$*. Excretion was calculated according to Ikeda (2014) as* $\ln(excretion) = 15.567 + 0.796 * \ln(DW) - 5.010 * 1000/Temperature - 0.115 * \ln(Depth) + Excretion\ factor$*; DW = Dryweight in mg, Temperature in K, Depth in meter) DW to C and C to N conversion factors from Kiørboe (2013).*

2020). These vary widely with particle type and regional estimates of particle flux from sediment traps should be used to validate the UVP5 derived POC flux estimates (Guidi et al., 2008). We therefore calculated POC flux using parameterizations proposed by Kriest (2002), Guidi et al. (2008), and Iversen et al. (2010) (see **Figure S2**) and compared these to published POC flux measurements from the region (Engel et al., 2017; Hernández-León et al., 2019) obtained with surface-tethered sediment traps. The parameterization by Iversen et al. (2010) leads to a strong overestimation of POC flux, whereas the parameterization of Guidi et al. (2008) leads to an underestimation. Only the parameterization by Kriest (2002) fits the data reasonably well and matches the data from Hernández-León et al. (2019) almost perfectly. Data obtained by Engel et al. (2017) coincide well at depth, but are generally higher in the surface area. In both cases surface tethered sediment traps were used, but Hernández-León et al. (2019) deployed only one trap, whereas Engel et al. (2017) deployed a chain of traps. It is likely that surface tethered trap chains are not moving freely with the surface current, as their deeper traps act as a drogue, and therefore the upper traps are experiencing drag through the water column. Thus, (a) the individual traps might hang shallower than determined with the given rope length, and (b) traps at different depths might show differing trapping efficiencies, as they might experience different current speeds and be tilted differently. Buesseler et al. (2000) observed that a chain of traps indicated a strong flux attenuation with depth, which was not observed in parallel deployments of neutrally buoyant traps. They suggest that surface tethered trap chains might overestimate sedimenting flux by up to 30%. Given these uncertainties, we decided to use the parameterization by Kriest (2002) to calculate POC content and flux from UVP5 data. This parameterization assumes that particle mass and sinking speed can be calculated using empirically derived relationships for marine aggregates (see Kriest, 2002, reference 2a of Table 1 and reference 9 of Table 2 for mass and sinking speed of a particle, respectively). Assuming a C:N ratio of 106:16, this yields an expression for the sinking flux (in $mg\ C\ m\ d^{-1}$) of a single particle characterized by its diameter ESD (in cm) of $2.8649 * ESD^{2.24}$. Multiplying with the particle number in a particle size class (in particles m^{-3}), and integrating over all size classes between 0.13 and 1 mm, we obtain the total POC flux ($mg\ C\ m^{-2}\ d^{-1}$) for this size range. This parameterization was derived from *in situ* measurements of particulate matter sinking speeds and carbon content and has been shown to best reproduce profiles of marine snow and particulate organic matter at the same time (Kriest, 2002). To calculate the POC flux, we here use the total abundance of all objects of 0.13–1 mm size as it is not possible to discern different objects in this size range. Images of all objects larger than 1 mm were sorted into feces, aggregates and other classes (e.g., copepods, rhizarians etc.) using EcoTaxa (https://ecotaxa.obs-vlfr.fr). POC content and flux were calculated for each single feces or aggregate item using above described formula and added to the POC-flux calculated for the 0.13–1 mm fraction to yield the total flux. The largest detritus item observed had an equivalent spherical diameter of 44 mm.

2.5. ADCP Data Analysis

During the cruises M105, M106, M119, and M130 a 38 kHz RDI Ocean Surveyor (OS38) was mounted in the ship's sea chest and worked continuously. Depending on the region and sea state, the range covered by the instruments is around 1,000 m. The minimum size of particles that influences the sound scattering of the OS38 are 10–20 mm therefore, large copepods, euphausiids and small pelagic fishes contribute most to the backscatter amplitude recorded by the OS38. To investigate the vertical migration of the zooplankton the echo amplitude of the OS38 was transformed into volumetric backscatter Sv (dB) (Mullison, 2017) to correct the depth dependency of the data. Furthermore, Sv between 10:00 to 14:00 and 22:00 to 2:00 o'clock local time were selected for every 24 h and averaged in daytime and nighttime profiles. To obtain the difference in volumetric backscatter the daytime values were subtracted from the nighttime values. In addition a two-sample t-Test was applied (p-value < 0.05) to identify in which depths the day and night-time values were significantly different.

2.6. Model Setup

To investigate the potential necessity to include zooplankton gut flux and respiration in global models we here investigate a global biogeochemical model (Kriest and Oschlies, 2015, setup RemHigh) that was designed to represent the oxidant cycles in OMZs, but excludes vertical migration of zooplankton. The biogeochemical model was coupled to a global offline circulation model based on the Transport Matrix Method (Khatiwala, 2007), using 12 monthly mean transport matrices derived from the

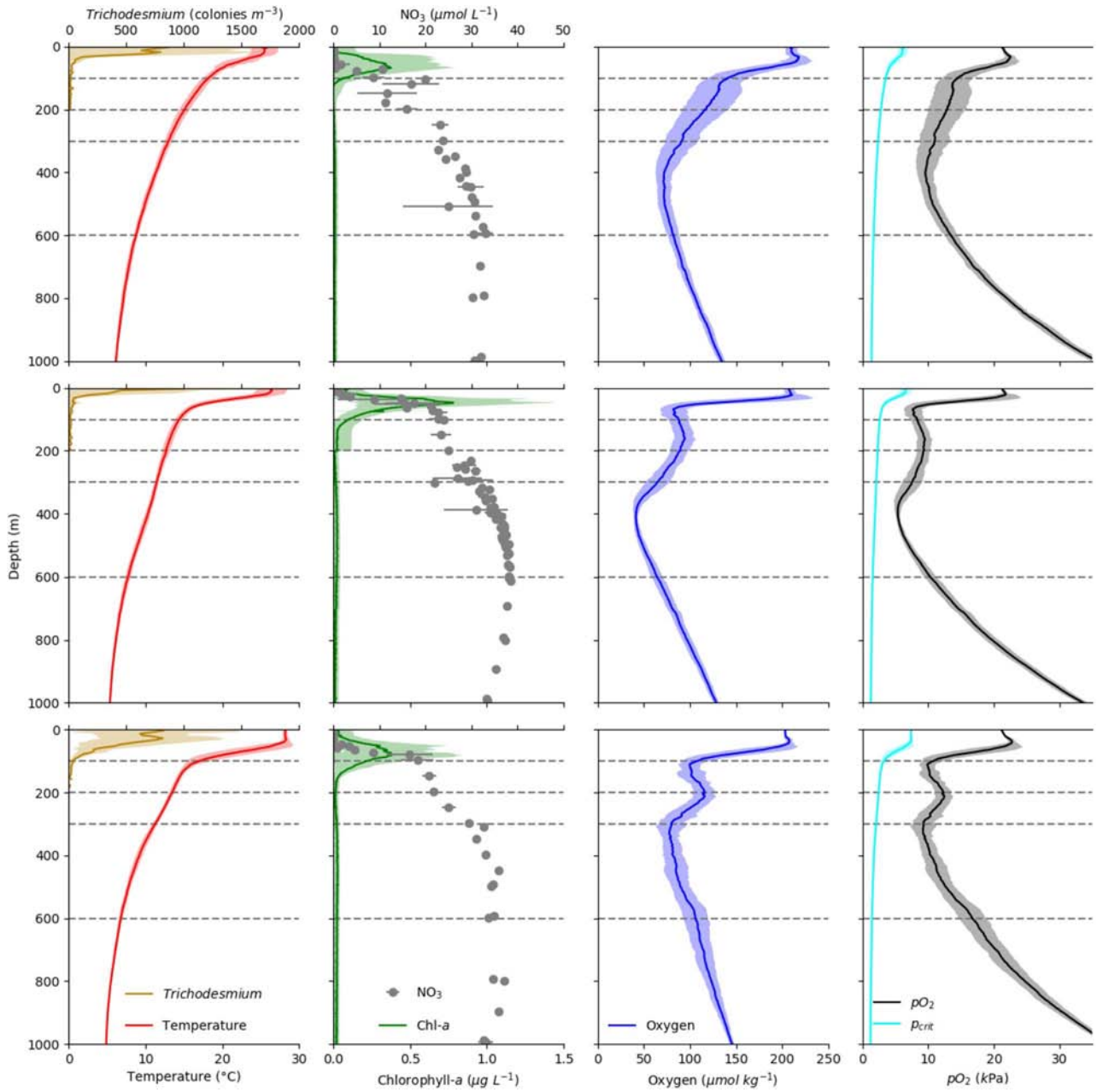

FIGURE 2 | Vertical profiles of Temperature (°C, red line), *Trichodesmium* sp. abundance (*individuals* m^{-3}, yellow line), Chlorophyll-a (*mg* m^{-3}, green line), Nitrate concentration ($\mu mol\ O_2\ kg^{-1}$, gray dots), oxygen concentration ($\mu mol\ O_2\ kg^{-1}$, blue line), and pO_2 (*kPa*, black line) as well as estimated p_{crit} (*kPa*, cyan line) of the migrating euphausiid species *Euphausia gibboides* in the three regions CVOO **(top)**, cOMZ **(middle)**, and 5N **(bottom)**. Dashed lines indicate the depth strata of our multinet deployments.

Estimating the Circulation and Climate of the Ocean (ECCO) project, which provides circulation fields that yield a best fit to hydrographic and remote sensing observations over a 10-year period (). The global model has a horizontal resolution of 1° × 1° with 23 vertical levels in the vertical. Three model configurations with different power-law exponents (analogous to Martin et al., 1987) describing the particle flux to the ocean interior b (0.6435, 0.858, and 1.0725) were simulated over 9000 years, i.e., until near steady state. In addition we test a biogeochemical model configuration in the same circulation, in which we optimized six biogeochemical parameters of the coupled global model against observed nutrients and oxygen. Optimization was carried out as described by Kriest et al. (2017). Optimized b was estimated at 1.46. The other optimal parameters

and further details of model performance can be found in Kriest et al. (2020).

3. RESULTS

3.1. Environmental Conditions at the Three Sampling Regions

Temperature profiles in the surface layers at 5N, cOMZ, and CVOO are markedly different (**Figure 2**). The mixed layer was deepest and sea surface temperature highest at 5N. Beneath, a uniform temperature of approximately 27–28°C was found in the upper 40 m at 5N, which then declined to a mean (± *SD*) of 17.0 (± 1.6)°C at 100 m depth, whereas mixed layer temperatures at cOMZ and CVOO were slightly lower (approximately 25–26°C at cOMZ and 23–25°C at CVOO) and declined gradually to 14.4 (± 0.5) and 18.2 (± 0.7)°C at 100 m depth at cOMZ and CVOO, respectively. The colder temperatures at cOMZ at 100 m are due to a shallowing of the isopycnals associated with the presence of the Guinea Dome. Temperature profiles between 100 and 1,000 m depth were rather similar, with temperatures in the 300–600 m depth layer ranging between 8.8 and 13.0 (CVOO; median: 10.6), 7.7 and 11.5 (cOMZ; median 9.6), and 6.8 and 11.2 (5N; median 8.4) °C, respectively. The chlorophyll a maximum was shallowest at cOMZ and deepest at 5N. Integrated chlorophyll a concentrations were lowest at 5N with a mean of 26.7 $mg\ m^{-2}$ (Standard Error = 3.2, n = 30), and similar at CVOO (27.6 $mg\ m^{-2}$, SE = 4.6, $n = 17$) and highest at cOMZ (35.4 $mg\ m^{-2}$, SE = 3.7, $n = 31$). This observation was in line with the nitracline depth. Mean nitrate concentrations exceeded 15 $\mu mol\ L^{-1}$ at 45, 75, and 100 m depth at cOMZ, 5N, and CVOO, respectively. *Trichodesmium* sp. abundance was by far highest at 5N, with a mean integrated abundance of 43.7 $*10^3$ colonies m^{-2}, while 24.4 and $15.5*10^3$ colonies m^{-2} were observed at CVOO and cOMZ, respectively. Primary productivity estimates from satellite data (https://www.science.oregonstate.edu/ocean.productivity/) obtained within the same week (8-day time window) as the CTD profiles were found to be 490.1 ± 82.6 *sd* (5N), 679.4 ± 322.2 *sd* (cOMZ), and 510.1 ± 108.4 *sd* (CVOO) $mg\ C\ m^{-2}\ d^{-1}$. In addition also the oxygen profiles in the three regions differ, with a pronounced subsurface OMZ and a fully developed midwater OMZ at 5N and cOMZ, with the latter reaching lower oxygen concentrations. Oxygen partial pressure is first of all a function of oxygen concentration, but also impacted by temperature and salinity, with lower partial pressures at higher temperatures and salinities. The decline of temperature with depth therefore leads to a tilted pO_2 profile in comparison to the oxygen concentration profile. Both 5N and cOMZ feature two pO_2 minima, the first at 100 m depth and the second at 300 and 400 m depth at 5N and cOMZ, respectively. At 5N, pO_2 dropped to about 9.2 *kPa* in the two minima, whereas they lie at about 5.4 *kPa* at cOMZ. At CVOO, only one pO_2 minimum with a value of about 9.6 *kPa* was observed at about 400 m depth. Mean pO_2 values were below or very close to 10 *kPa* between 50 and 600 m depth at cOMZ throughout, between 100 and 150 and about 270–400 m depth at 5N, and between about 325–470 m depth at CVOO. At none of the stations, the pO_2 fell below the extrapolated p_{crit} of *E. gibboides* (**Figure 2**).

3.2. Mesozooplankton Biomass Distribution

Integrated biomass of well-preserved zooplankton (size range 0.39–20.00 mm) calculated from day and night hauls was highest at cOMZ (1589.7 $mg\ C\ m^{-2}$) and comparatively low at both CVOO and 5N (987.8 $mg\ C\ m^{-2}$ and 685.7 $mg\ C\ m^{-2}$, respectively, **Table 3**). Daytime biomass was high at the surface, declined in the 100–200 and 200–300 m depth layers and then increased again slightly in the 300–600 m depth layer at 5N and CVOO, whereas it increased markedly in this depth layer at cOMZ (**Figure 3**, **Table S2**). Low biomass values were again found in the 600–1,000 m depth layer at daytime, but they were also low at nighttime. Biomass in the 300–600 m depth layer was lower at nighttime at all three stations, but a significant deviation from zero in the daytime minus nighttime biomass was only found at cOMZ (One-sided Students *t*-Test, $p < 0.05$). Here, median nighttime biomass was 2.0-fold higher than daytime biomass. Increases in nighttime biomass were observed in the 100–200 and 0–100 m depth layer. Highest median biomass (9.5 $mg\ C\ m^{-3}$; quartiles: 8.7 $mg\ C\ m^{-3}$, 10.1 $mg\ C\ m^{-3}$) was observed in the 0–100 m depth layer at cOMZ. Crustaceans contributed most to biomass at all depths and increased from a median contribution of 54 (CVOO), 80 (cOMZ) and 83 % (5N) in the 0–100 m depth layer to a median contribution of 95 (cOMZ), 95 (CVOO), and 83 % (5N) in the 300–600 m depth layer (**Table S3**). Within crustaceans, copepods and euphausiids were the major contributors to biomass (data not shown). The day-nighttime biomass difference at 300–600 m depth was almost exclusively related to the difference in crustacean biomass. Mortality expressed as biomass in mg C lost per day and cubic meter follows very similar patterns as the biomass distribution itself. Detailed values can be found in **Table S4**. **Figure S3** shows the respective plots.

3.3. Mesozooplankton Ammonium Excretion and Respiration

Ammonium excretion and respiration rates followed similar patterns as the biomass distribution patterns. Median

TABLE 3 | Biomass, respiration, and excretion estimates integrated for the upper 1,000 m at the three sampling locations.

Region	Parameter	Unit	Median	1q	3q	n
5N	biomass	$mg\ C\ m^{-2}$	685.7	574.92	936.48	10.0
5N	respiration	$\mu mol\ O_2\ m^{-2}\ d^{-1}$	133.76	102.98	155.89	10.0
5N	NH_4 excretion	$\mu mol\ NH_4\ m^{-2}\ d^{-1}$	13.39	10.01	15.05	10.0
cOMZ	biomass	$mg\ C\ m^{-2}$	1589.73	1469.18	1773.19	12.0
cOMZ	respiration	$\mu mol\ O_2\ m^{-2}\ d^{-1}$	239.42	209.99	258.51	12.0
cOMZ	NH_4 excretion	$\mu mol\ NH_4\ m^{-2}\ d^{-1}$	24.75	21.64	26.98	12.0
CVOO	biomass	$mg\ C\ m^{-2}$	987.8	869.93	1086.92	12.0
CVOO	respiration	$\mu mol\ O_2\ m^{-2}\ d^{-1}$	138.69	105.89	165.36	12.0
CVOO	NH_4 excretion	$\mu mol\ NH_4\ m^{-2}\ d^{-1}$	14.31	11.55	16.35	12.0

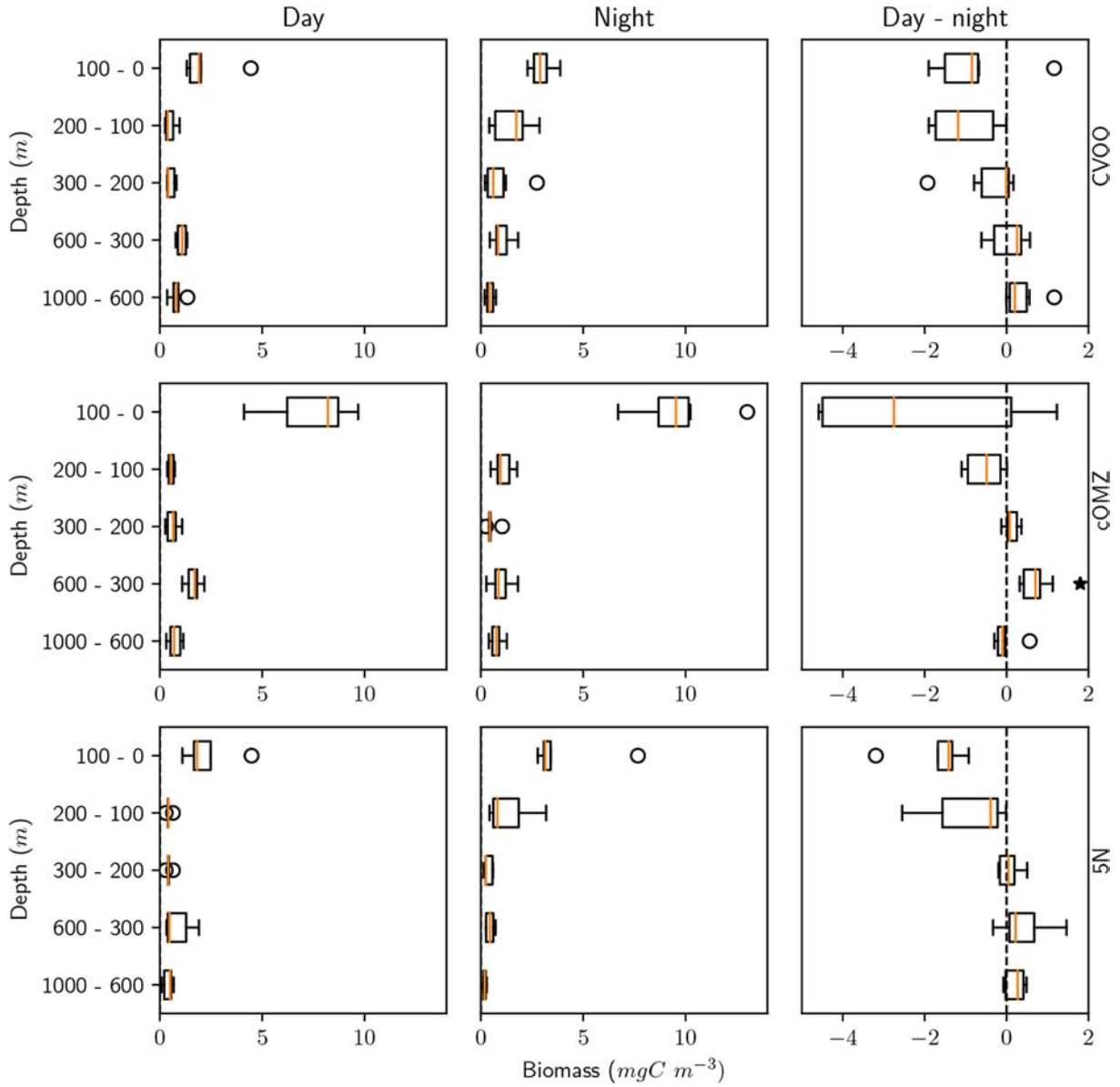

FIGURE 3 | Mesozooplankton biomass for day, night, and the day-night difference in each layer and for the three different sampling regions. An asterisk (*) denotes a significant difference (one-sided Students *t*-test, $p < 0.05$) of the day-night difference from zero.

ammonium excretion rates integrated for the 1,000–0 m depth layer sampled were comparatively low at 5N and CVOO (13.4 $\mu mol\ NH_4\ m^{-2}\ d^{-1}$ and 14.3 $\mu mol\ NH_4\ m^{-2}\ d^{-1}$, respectively), whereas median rates were almost twice as high at cOMZ (24.8 $\mu mol\ NH_4\ m^{-2}\ d^{-1}$, **Table 3**). Likewise, integrated respiration rates of 133.8 $\mu mol\ O_2\ m^{-2}\ d^{-1}$ and 138.7 $\mu mol\ O_2\ m^{-2}\ d^{-1}$ were found at 5N and CVOO, respectively, and almost twice as high values at cOMZ (239.4 $\mu mol\ O_2\ m^{-2}\ d^{-1}$, **Table 3**). Daytime ammonium excretion rates in the upper 100 m were 1.53 $\mu mol\ NH_4\ m^{-3}\ d^{-1}$ at 5N and 1.49 $\mu mol\ NH_4\ m^{-3}\ d^{-1}$ at CVOO (**Figure 4**, **Table S5**), respiration rates were 15.6 $\mu mol\ O_2\ m^{-3}\ d^{-1}$ (5N) and 12.6 $\mu mol\ O_2\ m^{-3}\ d^{-1}$ (CVOO; **Figure 5**, **Table S6**). Approximately three times higher rates were observed at cOMZ (ammonium excretion rate 4.44 $\mu mol\ NH_4\ m^{-3}\ d^{-1}$, respiration rate 39.9 $\mu mol\ O_2\ m^{-3}\ d^{-1}$). Nighttime surface excretion rates increased to 2.74 $\mu mol\ NH_4\ m^{-3}\ d^{-1}$ (5N), 2.25 $\mu mol\ NH_4\ m^{-3}\ d^{-1}$ (CVOO), and 4.79 $\mu mol\ NH_4\ m^{-3}\ d^{-1}$ (cOMZ), whereas respiration rates increased to 29.4 $\mu mol\ O_2\ m^{-3}\ d^{-1}$ (5N), 21.8 $\mu mol\ O_2\ m^{-3}\ d^{-1}$ (CVOO), and 48.3 $\mu mol\ O_2\ m^{-3}\ d^{-1}$ (cOMZ). Excretion and respiration rates at 300 to 600 m depth were substantially reduced and values are very similar, with median values ranging between 0.1 $\mu mol\ NH_4\ m^{-3}\ d^{-1}$ and 0.2 $\mu mol\ NH_4\ m^{-3}\ d^{-1}$ for ammonium excretion and between 0.9

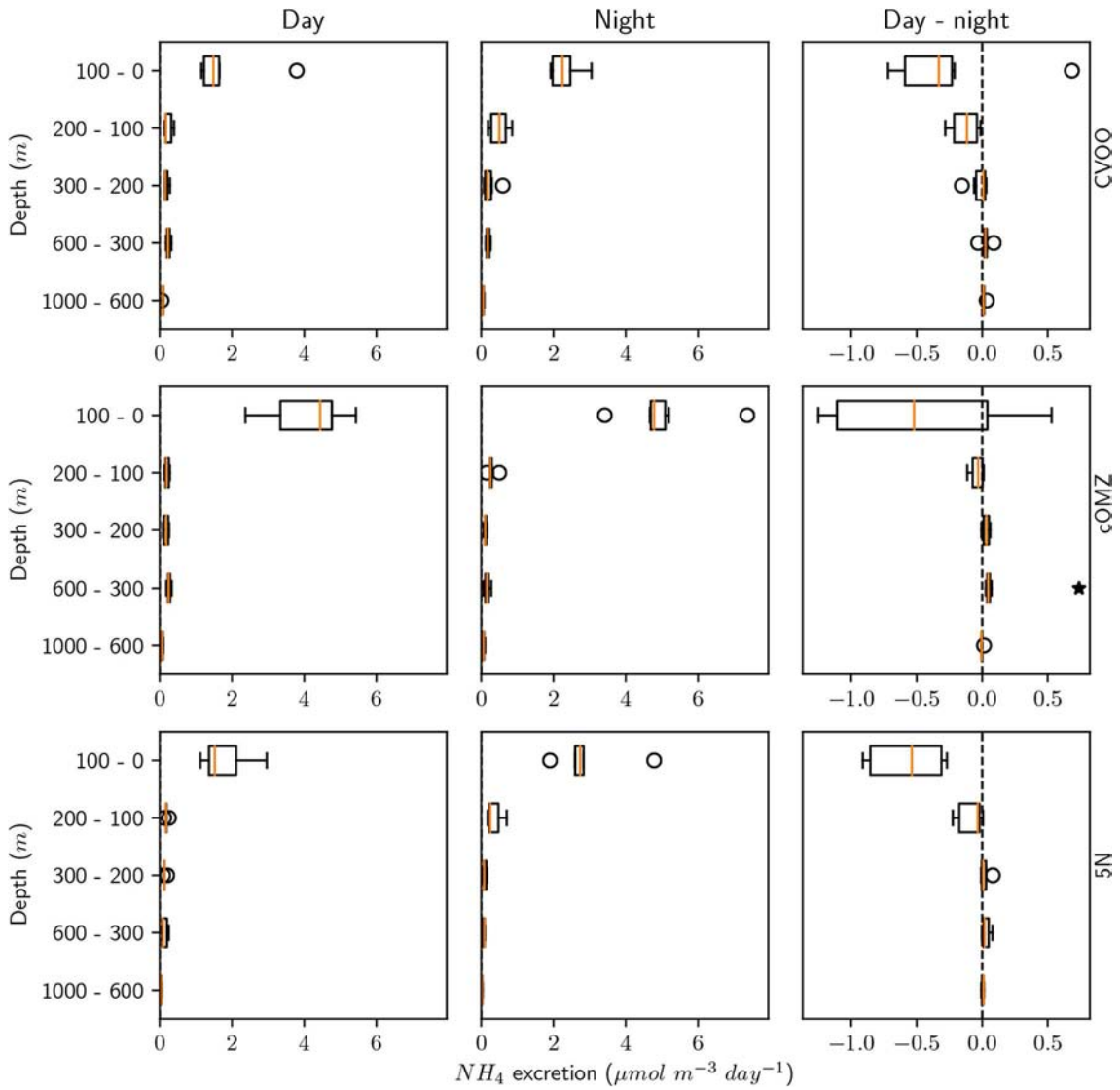

FIGURE 4 | Mesozooplankton ammonium excretion for day, night and the day-night difference in each layer and for the three different sampling regions. An asterisk (*) denotes a significant difference (one-sided Students *t*-test, $p < 0.05$) of the day-night difference from zero.

$\mu mol\ O_2\ m^{-3}\ d^{-1}$ and 2.8 $\mu mol\ O_2\ m^{-3}\ d^{-1}$ for respiration in all regions. The day-night excretion and respiration rate difference at depth was only significantly different from zero in the cOMZ region, where the day excretion and respiration rates were higher than the night rates (with a difference of 0.05 $\mu mol\ NH_4\ m^{-3}\ d^{-1}$ and 0.6 $\mu mol\ O_2\ m^{-3}\ d^{-1}$, respectively).

3.4. POC Content and Flux From *in situ* Particle Imaging

POC content and flux calculated from UVP5 data (**Figure 6**, **Table 4**) varies markedly between the three investigation areas. Average POC content in the surface area (0–100 m depth) was highest at cOMZ (average 2.9 ± 1.2 $mg\ C\ m^{-3}$, $n = 30$), followed by 5N (average 2.6 ± 0.9 $mg\ C\ m^{-3}$, $n = 31$) and then CVOO (average 2.2 ± 0.7 $mg\ C\ m^{-3}$, $n = 26$). In all regions the POC content is substantially lower in the 100–200 and 200–300 m depth layer. Whereas the average POC content declines further in the 300–600 m depth layer at CVOO to average values of 0.8 ± 0.1 $mg\ C\ m^{-3}$, $n = 22$, it increases again slightly at 5N (average 0.5 ± 0.1 $mg\ C\ m^{-3}$, $n = 24$) and markedly at cOMZ (0.9 ± 0.1 $mg\ C\ m^{-3}$, $n = 27$), thus resembling an intermediate particle maximum (IPM) in the OMZ core. POC content declines again rather gradually below about 500 m depth in all three regions. Mean POC content in the 600–1,000 m depth layer is highest at cOMZ (average 0.7 ± 0.1 $mg\ C\ m^{-3}$, $n = 27$), followed by CVOO (average 0.6 ± 0.1 $mg\ C\ m^{-3}$, $n = 22$), and 5N (average 0.5 ± 0.1 $mg\ C\ m^{-3}$, $n = 24$). POC flux follows similar patterns, but the flux increase at midwater depth is less pronounced (cOMZ) or barely visible (5N and CVOO). Detailed POC flux values for the described depth layers can be found in **Table 4**. POC flux at 200

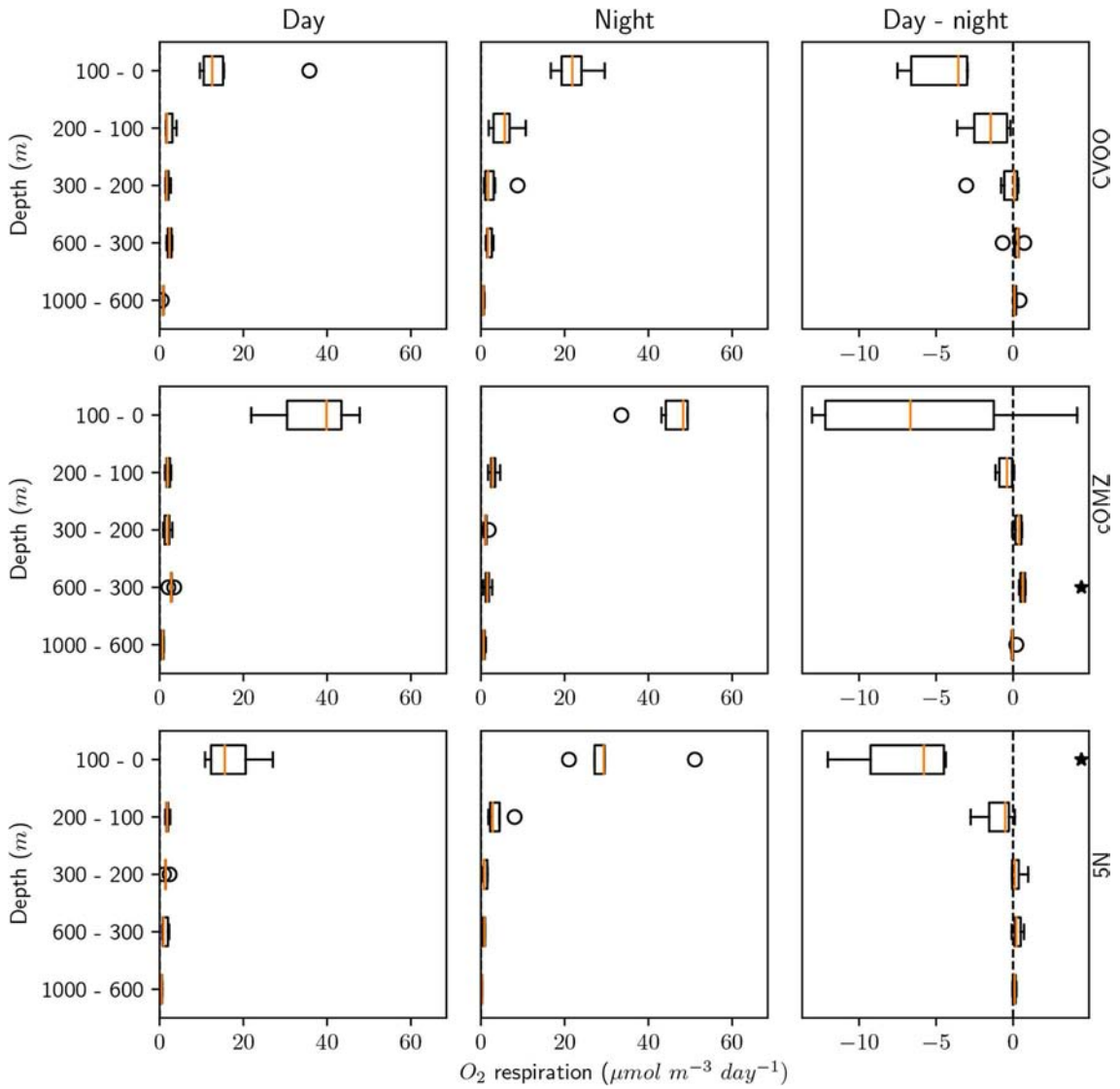

FIGURE 5 | Mesozooplankton respiration for day, night, and the day-night difference in each layer and for the three different sampling regions. An asterisk (*) denotes a significant difference (one-sided Students *t*-test, $p < 0.05$) of the day-night difference from zero.

m depth (average of the values observed between 190 and 210 m depth) amounts to 9.3 $mg\ C\ m^{-2}\ d^{-1}$, 18.1 $mg\ C\ m^{-2}\ d^{-1}$, and 16.4 $mg\ C\ m^{-2}\ d^{-1}$ at 5N, cOMZ and CVOO, respectively. POC flux at 300 m depth (average of the values observed between 290 and 310 m depth) is highest at cOMZ (16.2 $mg\ C\ m^{-2}\ d^{-1}$), where it declines to 14.1 $mg\ C\ m^{-2}\ d^{-1}$ at 600 m (average of the values observed between 590 and 610 m depth). POC flux at 300 m depth at CVOO is slightly lower (14.8 $mg\ C\ m^{-2}\ d^{-1}$) and declines to 11.1 $mg\ C\ m^{-2}\ d^{-1}$ at 600 m depth. Lowest POC flux at 300 m depth is observed at 5N with 9.1 $mg\ C\ m^{-2}\ d^{-1}$ and slightly lower values at 600 m depth (7.4 $mg\ C\ m^{-2}\ d^{-1}$).

3.5. Nitrogen Fluxes Out of the Top 200 m

The median active export of dissolved ammonium via DVM from the 0 to 200 m depth layer can be estimated at 10.9 $\mu mol\ N\ m^{-2}\ d^{-1}$ (5N), 15.1 $\mu mol\ N\ m^{-2}\ d^{-1}$ (cOMZ), and 12.8 $\mu mol\ N\ m^{-2}\ d^{-1}$ (CVOO; **Figure 7**). These values are calculated as the sum of integrated differences for the 200–1,000 m depth layer. The DON export calculated assuming a DON excretion to ammonium excretion ratio of 0.32 Steinberg et al. (2002) is estimated at 3.5 $\mu mol\ N\ m^{-2}\ d^{-1}$ (5N), 4.8 $\mu mol\ N\ m^{-2}\ d^{-1}$ (cOMZ), and 4.1 $\mu mol\ N\ m^{-2}\ d^{-1}$ (CVOO) $\mu mol\ DON\ m^{-2}\ day^{-1}$. Estimating the active N gut flux as a result of defecation at 1% of the migrating biomass [calculated from Schnetzer and Steinberg (2002)] and the N loss at depth due to mortality with the allometric equations provided by Hirst and Kiørboe (2002) results in a flux of 56.6 $\mu mol\ N\ m^{-2}\ d^{-1}$ (5N), 67.9 $\mu mol\ N\ m^{-2}\ d^{-1}$ (cOMZ), and 69.1 $\mu mol\ N\ m^{-2}\ d^{-1}$ (CVOO) $\mu mol\ N\ m^{-2}\ day^{-1}$ out of the 0–200 m depth layer (for detailed mortality estimates see **Table S4**), values are converted from C to N using a Redfield ratio of 106 C : 16 N). Combined

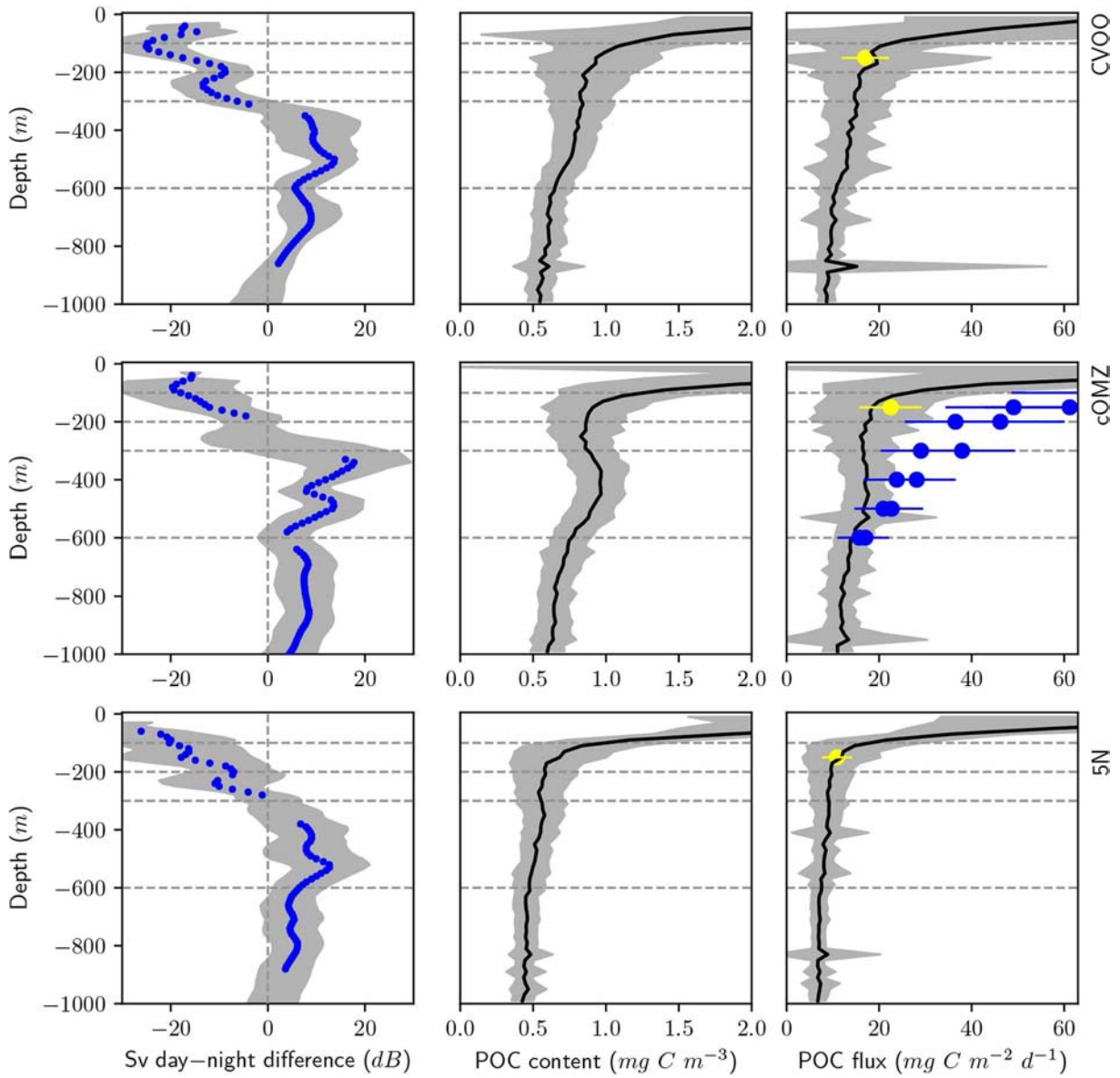

FIGURE 6 | Day-night backscatter difference from the vessel mounted 38 kHz ADCP **(left)**, average POC content **(middle)**, and POC flux **(right)** from UVP5 data obtained during CTD deployments in the respective regions. Top panels: CVOO, Middle panels: cOMZ, Bottom panels: 5N. Gray shading indicates the standard deviation of the respective parameter. Blue dots in the left panels indicate the mean ADCP backscatter if the day and night values are significantly different from each other. Blue dots in the right panels indicate sediment trap data from Engel et al. (2017), yellow dots indicate sediment trap data from Hernández-León et al. (2019). An approximate 30% uncertainty of sediment trap estimates is indicated with error bars. Dashed lines indicate the depth levels of our multinet deployments.

with the fluxes due to excretion these values add up to a loss of 70.9 $\mu mol\ N\ m^{-2}\ d^{-1}$ (5N), 87.9 $\mu mol\ N\ m^{-2}\ d^{-1}$ (cOMZ), and 86.0 $\mu mol\ N\ m^{-2}\ d^{-1}$ (CVOO) $\mu mol\ N\ m^{-2}\ day^{-1}$ due to DVM-related processes. Converting passive POC sinking fluxes at 200 m depth to PON fluxes using a Redfield ratio of 106 C: 16 N results in 100.4 $\mu mol\ N\ m^{-2}\ day^{-1}$, 195.1 $\mu mol\ N\ m^{-2}\ day^{-1}$, and 176.3 $\mu mol\ N\ m^{-2}\ day^{-1}$ at 5N, cOMZ, and CVOO, respectively. DVM-mediated losses make up 32 (CVOO), 31 (cOMZ), and 41 (5N) % of total N-loss at 200 m depth.

3.6. Carbon and Oxygen Fluxes at Midwater Depth

Active carbon supply to the 300–600 m depth layer via DVM gut flux, mortality and DOC excretion [calculated as 31% of respiration, Steinberg et al. (2000)] amounts to 243.6 $\mu mol\ O_2\ m^{-2}\ day^{-1}$ (CVOO), 444.3 $\mu mol\ O_2\ m^{-2}\ day^{-1}$ (cOMZ), 169.6 $\mu mol\ O_2\ m^{-2}\ day^{-1}$ (5N) (**Figure 8**; all values shown are converted to $\mu mol\ O_2$ using a respiratory quotient of 0.86 to allow for comparison with the oxygen demand). Passive flux amounts to 1057.1 $\mu mol\ O_2\ m^{-2}\ d^{-1}$ (CVOO), 1158.8

TABLE 4 | Average values and standard deviation of POC content and POC flux calculated from UVP5 data for the five depth layers of interest.

Region	Parameter	Depth start (m)	Depth end (m)	Avg	Stddev	n
5N	POC content	0	100	2.63	0.87	31
5N	POC content	100	200	0.68	0.3	31
5N	POC content	200	300	0.53	0.15	30
5N	POC content	300	600	0.54	0.1	24
5N	POC content	600	1000	0.45	0.07	24
cOMZ	POC content	0	100	2.93	1.18	30
cOMZ	POC content	100	200	0.98	0.34	30
cOMZ	POC content	200	300	0.89	0.22	30
cOMZ	POC content	300	600	0.93	0.14	27
cOMZ	POC content	600	1000	0.69	0.09	27
CVOO	POC content	0	100	2.17	0.73	26
CVOO	POC content	100	200	0.96	0.37	26
CVOO	POC content	200	300	0.84	0.28	24
CVOO	POC content	300	600	0.77	0.14	22
CVOO	POC content	600	1000	0.59	0.08	22
5N	POC flux	0	100	60.84	25.73	31
5N	POC flux	100	200	12.49	8.22	31
5N	POC flux	200	300	9.12	3.91	30
5N	POC flux	300	600	9.85	2.76	24
5N	POC flux	600	1000	8.22	2.4	24
cOMZ	POC flux	0	100	77.18	39.27	30
cOMZ	POC flux	100	200	24.14	21.55	30
cOMZ	POC flux	200	300	19.1	8.65	30
cOMZ	POC flux	300	600	19.12	4.19	27
cOMZ	POC flux	600	1000	13.58	2.45	27
CVOO	POC flux	0	100	53.18	29.77	26
CVOO	POC flux	100	200	20.22	14.16	26
CVOO	POC flux	200	300	16.47	9.04	24
CVOO	POC flux	300	600	14.5	5.58	22
CVOO	POC flux	600	1000	10.56	3.01	22

POC content in mgC m^{-3}, POC flux in mgC m^{-2} d^{-1}. n, number of available profiles in the respective depth bin.

$\mu mol\ O_2\ m^{-2}\ d^{-1}$ (cOMZ), and 652.4 $\mu mol\ O_2\ m^{-2}\ d^{-1}$ (5N) at 300 m depth, whereas it amounts to 795.3 $\mu mol\ O_2\ m^{-2}\ d^{-1}$ (CVOO), 1012.1 $\mu mol\ O_2\ m^{-2}\ d^{-1}$ (cOMZ), and 527.7 $\mu mol\ O_2\ m^{-2}\ d^{-1}$ (5N) at 600 m depth. 32 (CVOO), 31 (cOMZ), and 41% (5N) of the total flux into the 300–600 m depth layer are DVM-mediated. For the 300–600 m depth stratum, we estimate median integrated respiration rates of 510.0 $\mu mol\ O_2\ m^{-2}\ day^{-1}$, 480.0 $\mu mol\ O_2\ m^{-2}\ day^{-1}$, and 270.0 $\mu mol\ O_2\ m^{-2}\ day^{-1}$ of resident zooplankton (calculated from nighttime hauls only) at CVOO, cOMZ, and 5N, respectively. Integrated migratory oxygen demand can be estimated at 90.0 $\mu mol\ O_2\ m^{-2}\ day^{-1}$ (CVOO), 180.0 $\mu mol\ O_2\ m^{-2}\ day^{-1}$ (cOMZ), and 60.0 $\mu mol\ O_2\ m^{-2}\ day^{-1}$ (5N).

3.7. Comparison to Model Results

We here compare observed oxygen concentration and organic matter flux via sinking particles to our model results with

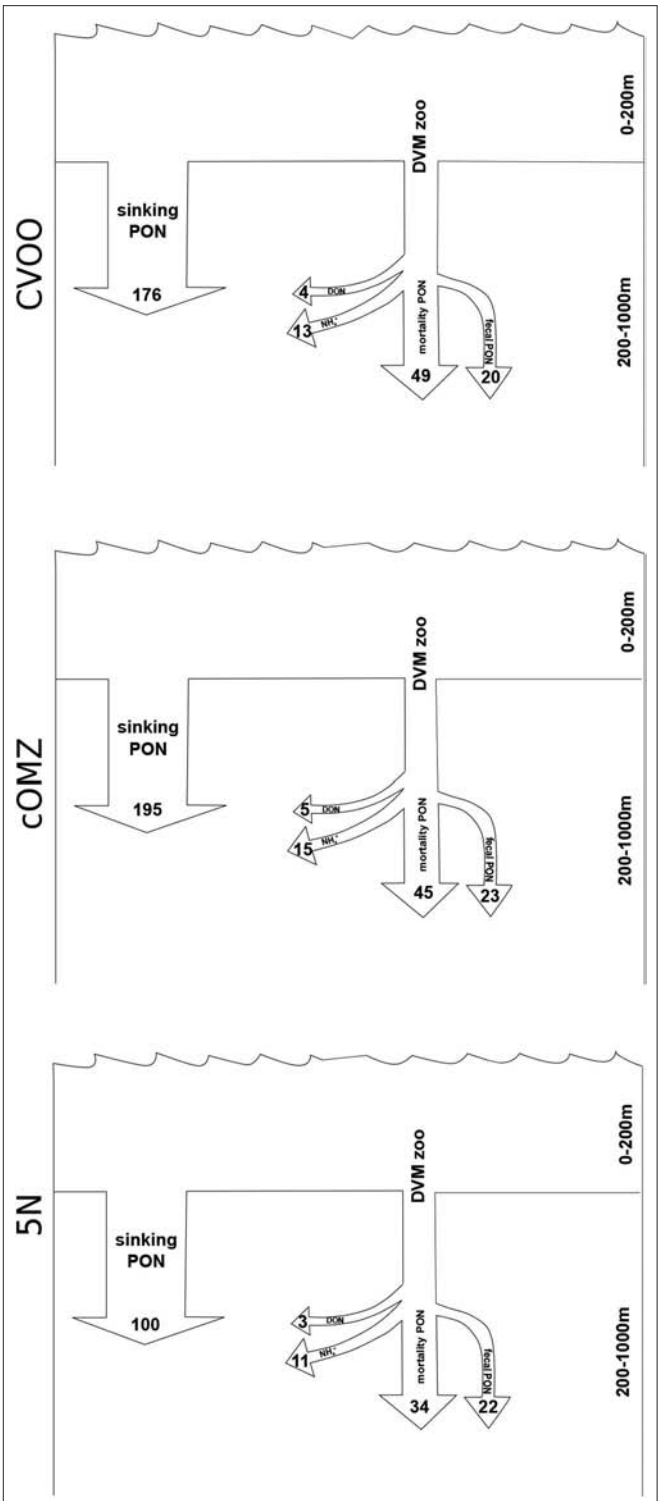

FIGURE 7 | Nitrogen fluxes out of the upper 200 m for the three regions. All values in $\mu mol\ N\ m^{-3}\ day^{-1}$. Estimate of the sinking PON flux is the average from our UVP5 data calculated for 190–210 m depth. Zooplankton related DVM fluxes (DVM zoo) are the median fluxes calculated from the sum of integrated day-night differences observed in the 200–300, 300–600, and 600–1,000 m depth layers.

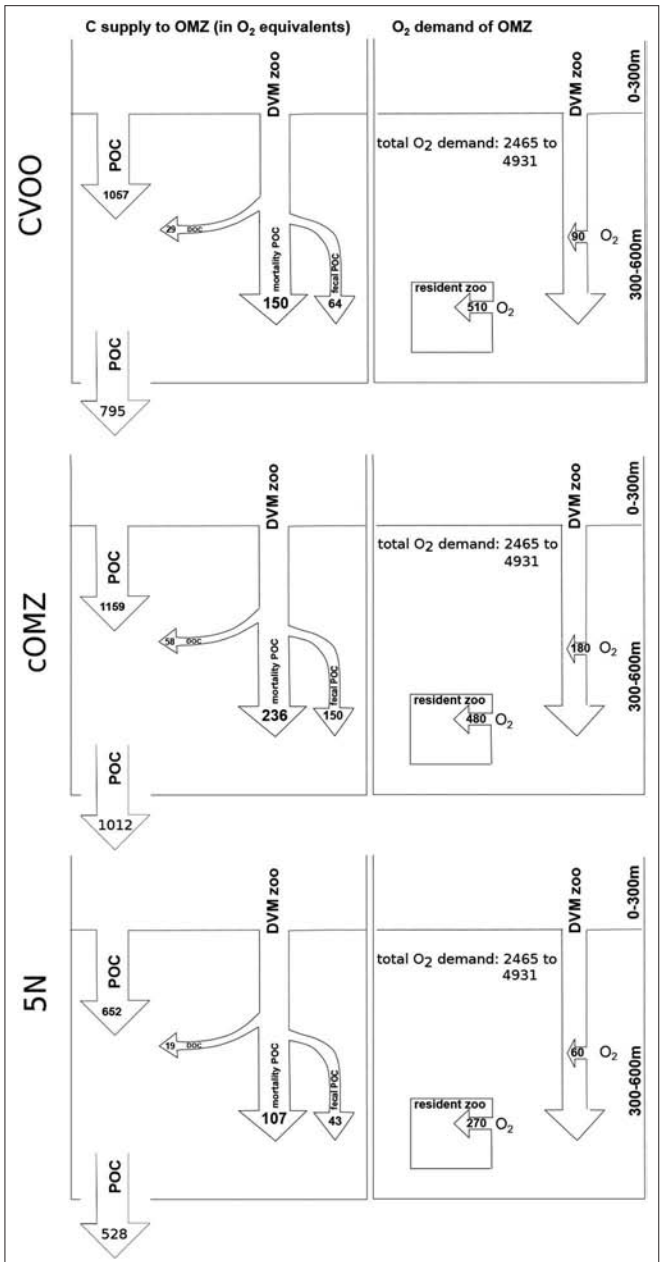

FIGURE 8 | Carbon supply and oxygen demand budget of the 300–600 m depth layer for the three regions. Carbon supply is converted to oxygen equivalents using a respiratory quotient of 0.86. All values in $\mu mol\ O_2\ m^{-2}\ day^{-1}$. POC flux is the average from our UVP5 data calculated for 290–310 m and 590–610 m depth. All zooplankton related rates are median values. Total oxygen demand from Karstensen et al. (2008) (3–6 $\mu mol\ O_2\ kg^{-1}\ year^{-1}$ converted $\mu mol\ O_2\ m^{-2}\ day^{-1}$).

the coupled global biogeochemical model MOPS (Kriest and Oschlies, 2015) in **Figure 9**. In sensitivity experiments carried out by Kriest and Oschlies (2015) the power-law exponent describing the particle flux to the ocean interior b was increased from b=0.6435 over $b = 0.858$ to $b = 1.0725$, i.e., from deep to shallower remineralization of particulate organic matter. In agreement with observations, all model experiments exhibit a steep subsurface decline of oxygen, down to values of about 30 $mmol\ m^{-3}$ in the optimized model. However, no model setup reflects the double OMZ observed at cOMZ and 5N. Even objective parameter optimization against global data sets of nutrients and oxygen (as carried out by Kriest et al., 2020) does not yield any significant improvement at the three locations analyzed here. At CVOO and cOMZ the optimized model and the experiment with relatively shallow remineralization (as represented by $b = 1.0725$) show a good match to the observed oxygen below 400 m. On the other hand, at 5N the best fit to observed oxygen is obtained with $b = 0.858$ or less. Thus, CVOO and cOMZ, the two regions with stronger zooplankton migration and respiration (**Figure 8**), require model setups with rather shallow remineralization in order to match oxygen between ≈ 400-600 m, while the region at 5N is simulated best with the "classical" exponent of $b = 0.858$ (Martin et al., 1987).

Deep particle flux at CVOO is represented best by a particle flux with a b value between 0.6345 and 1.0725, even though the lower values would result in an overestimate of deep oxygen by about 20 to 40 $mmolO_2\ m^{-3}$ (see above). At cOMZ particle flux between 400 and 600 m (about the target depth of DVM) derived from UVP5 data is simulated best by $b = 0.858$; again, this value leads to an overestimate of oxygen between 400 and 600 m of about 20 mmol m^{-3}. Only the model with a very steep particle flux profile ($b = 0.6435$) matches the trap fluxes observed by Engel et al. In this case, the model overestimates deep oxygen by ≈ 50 mmol m^{-3} at 400 m. Finally, at 5N observed particle flux is matched best by b defined by a range between 0.858 and 1.0725. The lowest value of b (comparable to faster settling particles) results in an overestimate of particle flux. Yet, as shown above this experiment could still produce a reasonable oxygen profile.

4. DISCUSSION

Our work aims to provide a quantitative assessment of zooplankton biomass, diel vertical migration, and related biogeochemical fluxes in the ETNA. We here combine data from several cruises since 2012 to the region. In the following, we will first consider the constraints of optical plankton and particle assessments and the application of allometric relationships to such ocean optics data and will then discuss the derived estimates. First comparisons to model data show that independently developed models and data coincide reasonably well, but differ in important details. Our observations could be used to further constrain the models and improve parameterizations.

4.1. Estimating Biomass, Physiological Rates, and Fluxes From Ocean Optics Data—Problems and Uncertainties

Our biomass estimates of zooplankton and particles rely on empirical relationships between size and carbon or nitrogen content (Kriest, 2002; Lehette and Hernández-León, 2009), include only zooplankton that is not destroyed during net sampling and preservation in formalin and can be imaged well on a scanner. Likewise, we used allometric relationships

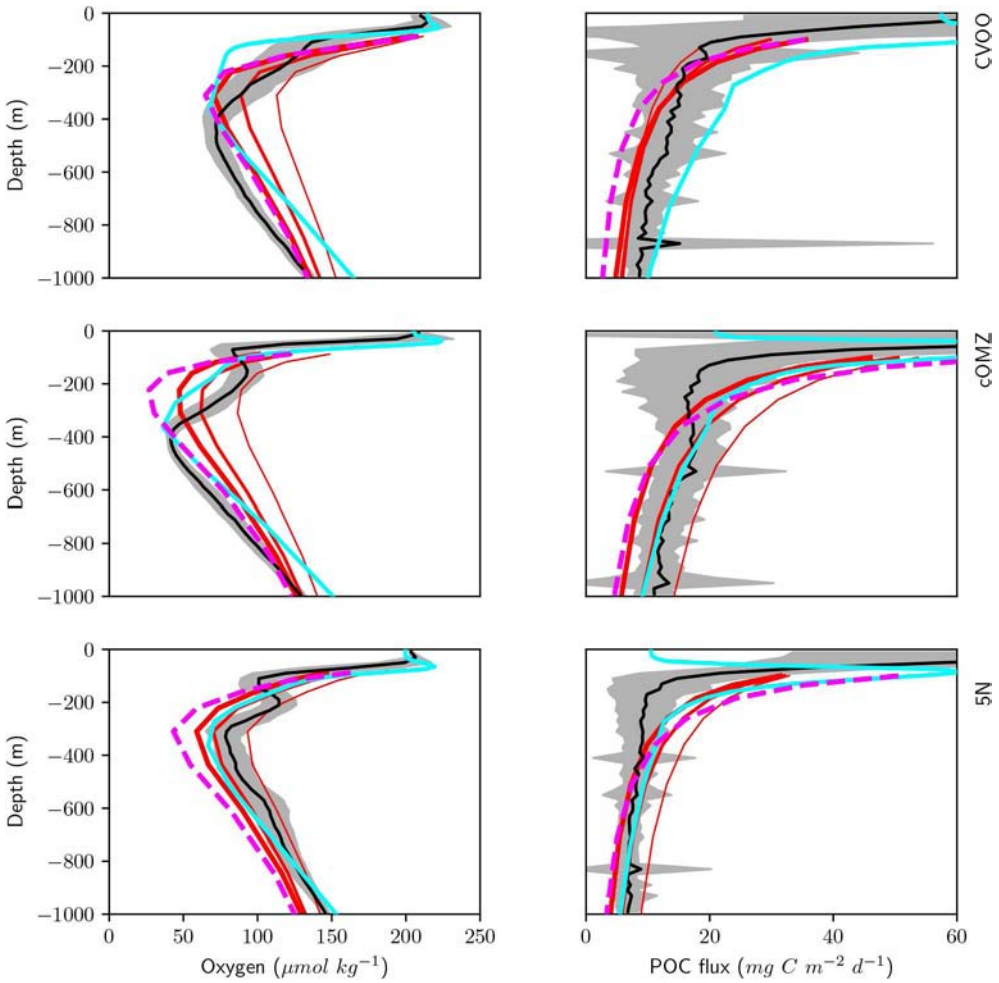

FIGURE 9 | Simulated (red, magenta, and cyan) and observed (black and gray) oxygen **(left)** and POC flux **(right)** below 100 m depth averaged over the three different regions CVOO (top), cOMZ (middle), and 5N (bottom). Model results are annual means of year 9000 of simulation RemHigh (Kriest and Oschlies, 2015) with three different exponents b for the particle flux curve. Thick red lines: $b = 1.0725$; medium red lines: $b = 0.858$; thin red lines: $b = 0.6345$. Magenta dashed lines show results of the same model optimized against observed nutrients and oxygen (Kriest et al., 2020). Cyan lines show results from Aumont et al. (2018).

that link size and particle sinking speed to obtain particle flux (Kriest, 2002), as well as relationships to calculate respiration, excretion and mortality rates based on size, temperature and taxonomic grouping (Hirst and Kiørboe, 2002; Ikeda, 2014). Whereas, the location and size of organisms and particles are well-defined, uncertainties of the derived estimates stem from uncertainties of the respective parameterizations. Applying such calculations is nevertheless necessary to convert the abundance and size estimates to biomass, fluxes and rates in SI units, which allows for comparison with other studies. The only parameter for which we could not find an allometric relationship is the gut flux. Here, we used data from Schnetzer and Steinberg (2002) to estimate gut flux at 1% of the migrating biomass. A general factor of 1% is not very satisfactory, as gut flux might vary according to composition and size distribution of the migrating community. The cited study was conducted at the Bermuda Atlantic Time Series Station, where the community composition may be different from the one we observed. We estimate the particulate matter supply via mortality of migrating organisms at depth by combining biomass and mortality estimates. Uncertainty with respect to this parameter is related to the fate of the dead body and the estimated mortality. Whereas natural mortality will directly contribute to the particle inventory, consumptive mortality will contribute to it via sloppy feeding and as defecation of the respective predator. Hence, the dead biomass that contributes to the POC flux might be lower than the total mortality flux. The mortality estimates we use are community estimates of consumptive and natural mortality of epipelagic communities (Hirst and Kiørboe, 2002). To our knowledge, no mortality estimates for mesopelagic zooplankton communities exist. It therefore needs to be stressed that mortality rates at depth might be different to those estimated here. However, Robison et al. (2020) note that many different, sometimes specialized mid-water predators pose

a considerable threat to the migrating community. Furthermore, the migration activity itself, the changes in abiotic conditions (e.g., temperature, oxygen) and the lack of food might have so far unknown effects on the mortality of the migratory community. Natural and/or consumptive mortality might also vary regionally, depending e.g., on the oxygen level at the migration depth or the predator community composition (Robison et al., 2020). Further work, especially to parameterize zooplankton gut flux to and mortality at mid-water depth is needed and will help to reduce the uncertainties associated with the estimation of DVM-mediated fluxes. With the mentioned constraints in mind, we will in the following discuss the biomass distribution of well-preserved zooplankton and the impacts of DVM-mediated fluxes on biogeochemical cycles of nitrogen, carbon and oxygen in the ETNA.

4.2. Zooplankton Biomass Distribution

Integrated zooplankton biomass was found to be almost twice as high at cOMZ compared to 5N and CVOO. Likewise, migrator biomass was highest at cOMZ. Several indicators mark the cOMZ region as the most productive of the three regions investigated, however, none of them is changed by a factor of two. The cOMZ region is characterized by a higher integrated chlorophyll-a, as well as ocean color-derived net primary productivity, a shallower nutricline/pycnocline depth and a lower integrated *Trichodesmium* sp. abundance. Sandel et al. (2015) observed a lower diapycnal nutrient flux between 7 and 15°N at 23°W [a region largely coinciding with our cOMZ region; referenced to as "Guinea Dome" (GD) by Sandel et al. (2015)], compared to the Oligotrophic North Atlantic ("ONA"), which largely coincides with our 5N region and the greater CVOO region. However, these fluxes were determined across the nitracline depth, which was particularly shallow at GD, and high chlorophyll-a concentrations were still observed below this depth by Sandel et al. (2015). The elevation of the pycno- and nitracline in the GD/cOMZ region creates beneficial conditions for primary productivity, which likely is the main reason for the elevated integrated and migrating biomass in this region. *Trichodesmium* sp. was found to synthesize several defense molecules and therefore likely has a rather poor nutritional value for most zooplankton (Codd, 1995), which also could partly explain why zooplankton biomass is lower at 5N and CVOO, where *Trichodesmium* sp. is more abundant. DVM species might also benefit from the OMZ refuge at depth at cOMZ (see also Bianchi et al., 2014). Only for two endemic pelagic species in the study area p_{crit} values are available, *E. gibboides* and *P. abdominalis* (Kiko et al., 2016). Oxygen partial pressures at depth were found to be well above the p_{crit} of these species in all three regions, but only at cOMZ they are with 5.2 kPa at about 350 m depth low enough to possibly exclude fast-swimming predators with a high respiratory demand such as billfishes (Prince et al., 2010; Stramma et al., 2012) or cephalopods. In support of this hypothesis, we note that the absolute peak in day-night 38 kHz backscatter difference (an indicator for the migratory fraction of larger zooplankton like krill and nekton) actually coincides with the minimum pO_2. pO_2 minima and day-night difference peaks do not coincide at CVOO and 5N, where oxygen values are also considerably higher and a refuge due to particularly low oxygen partial pressures is therefore not created. Another reason for the observed differences might be that biomass is elevated in parts of the zooplankton size spectrum which we did not observe or in the gelatinous/fragile component of the zooplankton community.

We here specifically excluded observations obtained within mesoscale eddies that featured particularly large anomalies in any of the observed parameters. Comparison of our results to earlier work especially on low-oxygen anticyclonic modewater eddies (Karstensen et al., 2008; Fiedler et al., 2016; Hauss et al., 2016; Christiansen et al., 2018) can indicate zooplankton distribution changes we could possibly expect in the "non-eddy" situation if mean oxygen levels further decline in the ETNA. Christiansen et al. (2018) observed that the flux-feeding polychaete *Poeobius* sp. was particularly abundant in several anticyclonic modewater eddies with low oxygen levels in their core. The average oxygen concentration in the shallow oxygen minimum at 85 to 120 m depth of the eddy studied by Karstensen et al. (2008), Hauss et al. (2016), and Fiedler et al. (2016) was 6.6 $\mu mol\ kg^{-1}$ (0.56 kPa O_2). Acoustic observations (shipboard ADCP, 75kHz) revealed that larger zooplankton and nekton were avoiding this zone and were compressed at the surface (Hauss et al., 2016). In general, we therefore expect diel vertical migration activity in the ETNA to weaken if oxygen levels in the migration range fall below about 30 $\mu mol\ O_2\ kg^{-1}$. This weakening would reduce the related oxygen demand and carbon supply to the OMZ and would therefore stabilize oxygen levels, at least for some time at this level. Increases in the abundance of flux feeders such as *Poeobius* sp. might also occur, with strong repercussions on particle distribution and flux (Christiansen et al., 2018).

4.3. Nitrogen Flux Out of the Surface Layer

DVM mediated nitrogen loss from the surface layer (here defined as the upper 200 m, which contains the target layers of the nighttime ascent) contributes substantially to total nitrogen loss (**Figure 7**). Approximately 41 (5N), 31 (cOMZ), and 32% (CVOO) of the total N loss from the surface layer (PON and DVM-mediated losses combined) is lost via DVM-mediated fluxes. Such estimates are consistent with other observations (e.g., Steinberg et al., 2000, 2002; Putzeys, 2013) and highlight the importance of DVM-mediated fluxes for the nutrient budget of the surface layer. Diapycnal nitrogen supply at the 200 m depth level ranges between approximately 500 and 1,000 $\mu mol\ N\ m^{-2}\ day^{-1}$ (Sandel et al., 2015). The given range, however, has a large uncertainty due to the sporadic occurrence of elevated mixing events in the upper thermocline associated, e.g., with shear instability of rarely occurring near-inertial waves (Bourlès et al., 2019). Nevertheless, the given range suggests that total nitrogen losses (passive flux and dvm-mediated fluxes combined) of 262.0 (CVOO), 283.0 (cOMZ), and 171.0 $\mu mol\ N\ m^{-2}\ day^{-1}$ (5N) observed at 200 m depth are already compensated by the diapycnal supply. Sandel et al. (2015) estimate atmospheric input at about 1,000 $\mu mol\ N\ m^{-2}\ day^{-1}$ at ONA and NCV, which largely coincide with 5N and CVOO, respectively. For the Guinea Dome region they estimate an atmospheric input of about 400 $\mu mol\ N\ m^{-2}\ day^{-1}$. Given the large uncertainties in all these estimates, and given the fact

that further loss processes, e.g. through the migration of larger organisms (Hernández-León et al., 2019) likely occur, it seems that our loss estimates are consistent with the supply estimates.

4.4. Oxygen and Carbon Budget of the DVM Target Depth

Comparing the possible active carbon supply routes via DVM gut flux, mortality, and DOC excretion with the POC supply via sedimenting particles for the three different areas investigated, we find that the carbon supply via DVM contributes 32 (CVOO), 41 (5N), and 31 % (cOMZ) to the combined supply. These results are consistent with other observations (Putzeys, 2013; Steinberg and Landry, 2017; Hernández-León et al., 2019) and highlight the importance of zooplankton mediated fluxes.

Much of the carbon supplied via passive sinking at 300 m depth is also lost this way at 600 m depth. If we calculate the relative carbon demand of the resident zooplankton considering only the POC that "disappears" at midwater depth, then we find that resident zooplankton consumes about 100 (CVOO), 81 (cOMZ), and 91 % (5N) of the supply. We do not consider the carbon demand of the migrating zooplankton in this calculation, as this should cover its carbon demand in the surface layer (Giering et al., 2014). It follows that, at least based on our assessment, only very little carbon should be available for other respiratory processes such as bacterial and microzooplankton respiration. Carbon supply at CVOO via the mechanisms investigated (POC flux and DVM-mediated processes) seems to be rather low in comparison to the likely demand. Further supply is expected to originate from larger migrators (Hernández-León et al., 2019). Lateral and vertical (via diapycnal mixing) supply of suspended and dissolved carbon might also contribute (Kelly et al., 2019). This supply pathway would mainly support the bacterial carbon demand.

Estimates of oxygen consumption at 300 to 600 m depth range between 3 and 6 $mmol\ O_2\ m^{-3}\ year^{-1}$ (Karstensen et al., 2008; Hahn et al., 2014). Our respiration rate estimates suggest that about 7.0 to 13.0% (5N), 12.0 to 24.0 % (CVOO), and 13.0 to 27.0 % (cOMZ) of the oxygen demand is caused by resident and migrating mesozooplankton. These estimates are somehow at odds with above described estimates of carbon supply and demand, but as mentioned, further carbon supply mechanisms need to be investigated. The estimates by Karstensen et al. (2008) include all oxygen loss and supply processes along the subduction pathway and might not represent those realized at 5N, cOMZ, or CVOO. Especially at cOMZ we would expect higher total respiration rates due to a larger POC supply compared to other regions along the subduction pathway.

4.5. Diel Vertical Migration Seems to Feed an Intermediate Particle Maximum

Particulate matter supply via gut flux, natural and consumptive mortality should contribute to the particle inventory at DVM depth. We previously reported that an equatorial Intermediate Particle Maximum (IPM) in the Atlantic and Pacific occurs at the depth of DVM activity and is strongest where day-night difference of the ADCP backscatter signal is largest. We therefore suggested that the IPM and resultant POC flux increase at midwater depth are DVM-related (Kiko et al., 2017). IPMs have been revealed by optical backscatter and turbidity, as well as UVP5 measurements in different oceanic environments (e.g., McCave, 2009; Roullier et al., 2014). They might not only be the result of zooplankton-mediated particle supply, but they could also (exclusively or additionally) be related to nepheloid layers shedding from the benthic boundary layer of coastal shelfs (Inthorn et al., 2006; Karakaş et al., 2006) and to enhanced microbial abundance in OMZs. In our current study, we also detected an IPM at 300–600 m depth at cOMZ (and to a lesser degree also at CVOO and 5N), coinciding with both the core of the OMZ and the daytime depth of DVM zooplankton. We here provide further data that suggest a link between the IPM and DVM-mediated particle supply. At cOMZ, both the IPM (as indicated by the estimated POC content) and the ADCP backscatter difference are largest and we see a significant difference to zero in the migratory zooplankton biomass obtained from our net catches. No clear IPM signal is observed at 5N and CVOO, where the ADCP backscatter signal is more stretched and smaller, and the migratory biomass difference not significant. The POC flux calculated from the particle size distribution also is clearly enhanced at 300–600 m depth at cOMZ, but not at 5N or CVOO. As we know the carbon flux into and out of the 300–600 m depth layer and the POC content (derived from the UVP5 data i.e., for the particle size range 0.14–26.8 mm) of this layer, we can derive the needed active supply of particulate matter to maintain the IPM and counter the particle remineralization. The active flux needed can be calculated as remineralisation rate * POC content + Flux out - Flux in [see also Extended data Figure 9 from Kiko et al. (2017)]. The active flux we observe at cOMZ would fully support the IPM if the remineralization rate would be 2.6% per day. Iversen and Ploug (2013) find individual particle remineralization rates of about 0.5–6% per day at 4°C. Temperatures at 300–600 m depth in the ETNA are approximately twice as high, which should increase the remineralization rate by about a factor of 1.5. As Iversen and Ploug (2013) use fresh surface material, whereas the nutritional value of material arriving at midwater depth might be more reduced, it seems reasonable that remineralization rates of 2.6% per day are possible. Considering also the uncertainties of our gut flux and mortality estimates and taking into account that we here did not consider macrozooplankton and nekton gut flux and mortality, we can not falsify the hypothesis that the IPM is a result of DVM-mediated active supply of particulate matter to depth.

4.6. Comparison to Model Results

Considering DVM-mediated fluxes at midwater depth might also improve the representation of OMZs in global biogeochemical models. We here compare model simulations by Kriest and Oschlies (2015) and Kriest et al. (2020) described above (both without DVM-mediated processes; hereafter referred to as "MOPS"), as well as results of the NEMO/PISCES/APECOSM model by Aumont et al. (2018) which does include DVM-mediated processes. Modifications of the particle settling velocity in model MOPS show that the model run with more slowly settling particles (equivalent to shallow remineralization and a

large attenuation coefficient b) matches observed deep oxygen at CVOO and cOMZ, but underestimates deep particle flux, while those model runs that match observed particle flux overestimate deep oxygen by ≈ 20–50 mmol m^{-3}.

It cannot be ruled out that the models' circulation, resolution, and possibly erroneous physical oxygen supply associated with mean advection, diapycnal mixing, and lateral eddy fluxes, causes some of the mismatches between simulated and observed oxygen. Furthermore, resident zooplankton and nekton might be underestimated in the models, which could also explain some of the mismatch. On the other hand, Bianchi et al. (2013) and Aumont et al. (2018) suggest that the impact of zooplankton on deep oxygen concentrations in highly productive upwelling areas is within the "required" range. Apparently, a considerable amount of mesopelagic remineralization is needed at CVOO and cOMZ in order to represent oxygen profiles. However, when this is achieved with a b corresponding to shallow remineralization, simulated particle flux is too low. Importantly, even after optimization of model parameters, among them the particle flux parameter b, the MOPS model is not able to simultaneously fit observed particle flux and oxygen profiles in the three regions.

In the NEMO/PISCES/APECOSM model, which parameterizes DVM, the OMZ is situated slightly deeper than in the other model experiments, but slightly shallower than in reality. Again, it remains to be investigated if and how much this feature is associated with the model physics and the distribution of resident zooplankton and nekton. The POC-flux profile actually shows a small change at the DVM-depth, which may be related to the DVM-mediated POC supply, and is supported by our observations. Therefore, in agreement with other modeling studies (Bianchi et al., 2013; Aumont et al., 2018; Archibald et al., 2019) our analysis suggests that parameterization of zooplankton and nekton diel vertical migration, its organic matter supply to the deep ocean and deep oxygen consumption can affect global and regional model performance. Comparison to our observations suggests that the NEMO/PISCES/APECOSM model still underestimates the effects, whereas the inclusion of DVM could help to improve the performance of MOPS in this region, and possibly elsewhere. Our comprehensive data set that includes zooplankton as well as particle concentrations and derived fluxes should help to further constrain such modeling efforts in terms of model parameterization, optimization, and evaluation.

4.6.1. Major Findings and Conclusions of Our Study

(1) Integrated biomass is highest at cOMZ and rather similar at 5N and CVOO. Only at cOMZ we do observe a significant day-night mesozooplankton biomass difference at 300 to 600 m depth. The oxygen levels in the three regions are not (yet) below the p_{crit} of two common migrators (*E. gibboides* and *P. abdominalis*). It is hence unlikely that their migration patterns are directly impacted by oxygen availability, but mesozooplankton predators might be excluded at cOMZ, creating a refuge.

(2) DVM activity removes between 31 to 41% of nitrogen from the upper 200 m of the water column. Total nitrogen loss (DVM-mediated and via passively sinking particles) from the upper 200 m of the water column is well-covered in all regions via diapycnal diffusion, nitrogen fixation, dry, and wet deposition (Sandel et al., 2015).

(3) Resident zooplankton utilizes 81 (cOMZ), 91 (5N), and 100% (CVOO) of carbon supplied to the 300–600 m depth layer via DVM and passively sinking particles (supply at 300 m minus loss at 600 m depth), indicating slightly different carbon balances in the three regions. Water column oxygen respiration at 300–600 m depth is estimated at 3–6 $mmol\ O_2\ m^{-3}\ year^{-1}$ (Karstensen et al., 2008) and our results indicate that zooplankton is responsible for 7–27% of it.

(4) The intermediate particle maximum is strongest at cOMZ and can probably be explained by gut flux and mortality of migrating zooplankton. Weaker impacts of diel vertical migration on the particle size spectrum can also be observed in the other regions.

(5) A first comparison of our POC-flux data to global biogeochemical model simulations indicates that the overall POC-flux estimates coincide but the contribution of DVM-mediated fluxes seems to be lacking or to be underestimated. More appropriate parameterizations might improve the representation of the biological carbon pump and the global oxygen distribution.

DATA AVAILABILITY STATEMENT

Datasets analyzed in this study are available in the Pangaea collection: https://doi.pangaea.de/10.1594/PANGAEA.903023. Data not listed in this collection is available from the authors upon reasonable request. Data from scanned zooplankton images and the UVP5 is also available on https://ecotaxa.obs-vlfr.fr/.

AUTHOR CONTRIBUTIONS

RK and HH designed the study. RK developed all routines for the biomass and metabolic rate estimation of scanned zooplankton as well as UVP5 data. RK, HH, SC, JF, and ER collected, scanned, and analyzed the zooplankton samples. PB and FS obtained and processed the CTD and ADCP data. IK designed and analyzed the biogeochemical model. RK drafted the manuscript. All authors contributed to the writing of the manuscript and agree to the submitted version.

FUNDING

This work is a contribution of the SFB 754 Climate—Biogeochemistry Interactions in the Tropical Ocean (www.sfb754.de, grant/award no. 27542298) which is supported by the German Science Foundation (DFG). This paper was furthermore supported by the projects TRIATLAS and iAtlantic, which have received funding from the European Union's Horizon 2020 research and innovation programme under grant agreement No 817578 and 818123, respectively. RK furthermore received a Make Our Planet Great Again grant of the French National Research Agency within the Programme d'Investissements d'Avenir; reference ANR-19-MPGA-0012.

ACKNOWLEDGMENTS

We are grateful to the crew and chief scientists of the research vessels Maria S. Merian and Meteor as well as the colleagues collecting nutrient data on the various cruises. Pieter Vandromme obtained Multinet samples and UVP5 data during FS Meteor cruise M119. Furthermore, we would like to thank all our colleagues of the SFB754 who supported us, provided interesting feedback regarding our work and generated a motivating work environment. Lars Stemman and Marc Picheral (Laboratoire d'Océanographie de Villefranche-sur-Mer) provided a UVP5 for cruises MSM22 and M97 and supported the optical analysis. Technical support by Hydroptic for UVP5 deployments is greatly appreciated. A special thank you also goes to the GEOMAR data management team (Hela Mehrtens, Carsten Schirnick and colleagues) and Christiane Schelten, the coordinator of the SFB754.

SUPPLEMENTARY MATERIAL

The Supplementary Material for this article can be found online at: https://www.frontiersin.org/articles/10.3389/fmars.2020.00358/full#supplementary-material

REFERENCES

Archibald, K. M., Siegel, D. A., and Doney, S. C. (2019). Modeling the impact of zooplankton diel vertical migration on the carbon export flux of the biological pump. *Glob. Biogeochem. Cycles* 33, 181–199. doi: 10.1029/2018GB005983

Auel, H., and Verheye, H. M. (2007). Hypoxia tolerance in the copepod calanoides carinatus and the effect of an intermediate oxygen minimum layer on copepod vertical distribution in the northern benguela current upwelling system and the angola-benguela front. *J. Exp. Mar. Biol. Ecol.* 352, 234–243. doi: 10.1016/j.jembe.2007.07.020

Aumont, O., Maury, O., Lefort, S., and Bopp, L. (2018). Evaluating the potential impacts of the diurnal vertical migration by marine organisms on marine biogeochemistry. *Glob. Biogeochem. Cycles* 32, 1622–1643. doi: 10.1029/2018GB005886

Baker, A. R., Weston, K., Kelly, S. D., Voss, M., Streu, P., and Cape, J. N. (2007). Dry and wet deposition of nutrients from the tropical atlantic atmosphere: links to primary productivity and nitrogen fixation. *Deep Sea Res. Part I* 54, 1704–1720. doi: 10.1016/j.dsr.2007.07.001

Bianchi, D., Babbin, A. R., and Galbraith, E. D. (2014). Enhancement of anammox by the excretion of diel vertical migrators. *Proc. Natl. Acad. Sci. U.S.A.* 111, 15653–15658. doi: 10.1073/pnas.1410790111

Bianchi, D., Galbraith, E. D., Carozza, D. A., Mislan, K., and Stock, C. A. (2013). Intensification of open-ocean oxygen depletion by vertically migrating animals. *Nat. Geosci.* 6, 545–548. doi: 10.1038/ngeo1837

Bopp, L., Resplandy, L., Orr, J. C., Doney, S. C., Dunne, J. P., Gehlen, M., et al. (2013). Multiple stressors of ocean ecosystems in the 21st century: projections with CMIP5 models. *Biogeosciences* 10, 6225–6245. doi: 10.5194/bg-10-6225-2013

Bourlés, B., Araujo, M., McPhaden, M. J., Brandt, P., Foltz, G. R., Lumpkin, R., et al. (2019). Pirata: A sustained observing system for tropical atlantic climate research and forecasting. *Earth Space Sci.* 6, 577–616. doi: 10.1029/2018EA000428

Brandt, P., Bange, H. W., Banyte, D., Dengler, M., Didwischus, S.-H., Fischer, T., et al. (2015). On the role of circulation and mixing in the ventilation of oxygen minimum zones with a focus on the eastern tropical North Atlantic. *Biogeosciences* 12, 489–512. doi: 10.5194/bg-12-489-2015

Buesseler, K. O., Steinberg, D. K., Michaels, A. F., Johnson, R. J., Andrews, J. E., Valdes, J. R., et al. (2000). A comparison of the quantity and composition of material caught in a neutrally buoyant versus surface-tethered sediment trap. *Deep Sea Res. Part I* 47, 277–294. doi: 10.1016/S0967-0637(99)00056-4

Chahsavar-Archard, V., and Razouls, C. (1982). Les copépodes pélagiques au sud-est des iles du cap vert, i. aspects qualitatifs (mission guidôme du no "j. charcot", septembre-octobre 1976). *Vie Milieu* 32, 25–45.

Childress, J. J., and Seibel, B. A. (1998). Life at stable low oxygen levels: adaptations of animals to oceanic oxygen minimum layers. *J. Exp. Biol.* 201, 1223–1232.

Christiansen, S., Hoving, H.-J., Schütte, F., Hauss, H., Karstensen, J., Körtzinger, A., et al. (2018). Particulate matter flux interception in oceanic mesoscale eddies by the *Polychaete poeobius* sp. *Limnol. Oceanogr.* 63, 2093–2109. doi: 10.1002/lno.10926

Cocco, V., Joos, F., Steinacker, M., Frölicher, T., Bopp, L., Dunne, J., et al. (2013). Oxygen and indicators of stress for marine life in multi-model global warming projections. *Biogeosciences* 10, 1849–1868. doi: 10.5194/bg-10-1849-2013

Codd, G. (1995). Cyanobacterial toxins: occurrence, properties and biological significance. *Water Sci. Technol.* 32, 149–156. doi: 10.2166/wst.1995.0177

Engel, A., Wagner, H., Le Moigne, F. A., and Wilson, S. T. (2017). Particle export fluxes to the oxygen minimum zone of the eastern tropical North Atlantic. *Biogeosciences* 14, 1825–1838. doi: 10.5194/bg-14-1825-2017

Fiedler, B., Grundle, D. S., Schütte, F., Karstensen, J., Löscher, C. R., Hauss, H., et al. (2016). Oxygen utilization and downward carbon flux in an oxygen-depleted eddy in the eastern tropical North Atlantic. *Biogeosciences* 13, 5633–5647. doi: 10.5194/bg-13-5633-2016

Fischer, T., Banyte, D., Brandt, P., Dengler, M., Krahmann, G., Tanhua, T., et al. (2013). Diapycnal oxygen supply to the tropical North Atlantic oxygen minimum zone. *Biogeosciences* 10, 5079–5093. doi: 10.5194/bg-10-5079-2013

Giering, S. L., Sanders, R., Lampitt, R. S., Anderson, T. R., Tamburini, C., Boutrif, M., et al. (2014). Reconciliation of the carbon budget in the ocean's twilight zone. *Nature* 507, 480–483. doi: 10.1038/nature13123

Giering, S. L. C., Cavan, E. L., Basedow, S. L., Briggs, N., Burd, A. B., Darroch, L. J., et al. (2020). Sinking organic particles in the ocean-flux estimates from in situ optical devices. *Front. Mar. Sci.* 6:834. doi: 10.3389/fmars.2019.00834

Gorsky, G., Ohman, M. D., Picheral, M., Gasparini, S., Stemmann, L., Romagnan, J.-B., et al. (2010). Digital zooplankton image analysis using the ZooScan integrated system. *J. Plankton Res.* 32, 285–303. doi: 10.1093/plankt/fbp124

Grasshoff, K., Kremling, K., and Ehrhardt, M. (2009). *Methods of Seawater Analysis*. Weinheim: John Wiley & Sons.

Guidi, L., Jackson, G. A., Stemmann, L., Miquel, J. C., Picheral, M., and Gorsky, G. (2008). Relationship between particle size distribution and flux in the mesopelagic zone. *Deep Sea Res. Part I* 55, 1364–1374. doi: 10.1016/j.dsr.2008.05.014

Hahn, J., Brandt, P., Greatbatch, R. J., Krahmann, G., and Körtzinger, A. (2014). Oxygen variance and meridional oxygen supply in the tropical North East Atlantic oxygen minimum zone. *Clim. Dyn.* 43, 2999–3024. doi: 10.1007/s00382-014-2065-0

Hahn, J., Brandt, P., Schmidtko, S., and Krahmann, G. (2017). Decadal oxygen change in the eastern tropical North Atlantic. *Ocean Sci.* 13, 551–576. doi: 10.5194/os-13-551-2017

Hauss, H., Christiansen, S., Schütte, F., Kiko, R., Lima, M. E., Rodrigues, E., et al. (2016). Dead zone or oasis in the open ocean? Zooplankton distribution and migration in low-oxygen modewater eddies. *Biogeosciences* 13, 1977–1989. doi: 10.5194/bg-13-1977-2016

Hauss, H., Franz, J. M., Hansen, T., Struck, U., and Sommer, U. (2013). Relative inputs of upwelled and atmospheric nitrogen to the eastern tropical North Atlantic food web: spatial distribution of δ15n in mesozooplankton and relation to dissolved nutrient dynamics. *Deep Sea Res. Part I* 75, 135–145. doi: 10.1016/j.dsr.2013.01.010

Hernández-León, S., and Ikeda, T. (2005). A global assessment of mesozooplankton respiration in the ocean. *J. Plankton Res.* 27, 153–158. doi: 10.1093/plankt/fbh166

Hernández-León, S., Olivar, M. P., Fernández de Puelles, M. L., Bode, A., Castellón, A., López-Pérez, C., et al. (2019). Zooplankton and micronekton active flux

across the tropical and subtropical Atlantic Ocean. *Front. Mar. Sci.* 6:535. doi: 10.3389/fmars.2019.00535

Hirst, A., and Kiørboe, T. (2002). Mortality of marine planktonic copepods: global rates and patterns. *Mar. Ecol. Prog. Ser.* 230, 195–209. doi: 10.3354/meps230195

Ianson, D., George A. Jackson, G. A., Angel, M. V., Lampitt, R. S., and Burd, A. B. (2004). Effect of net avoidance on estimates of diel vertical migration. *Limnol. Oceanogr.* 49, 2297–2303. doi: 10.4319/lo.2004.49.6.2297

Ikeda, T. (2014). Respiration and ammonia excretion by marine metazooplankton taxa: synthesis toward a global-bathymetric model. *Mar. Biol.* 161, 2753–2766. doi: 10.1007/s00227-014-2540-5

Inthorn, M., Mohrholz, V., and Zabel, M. (2006). Nepheloid layer distribution in the benguela upwelling area offshore namibia. *Deep Sea Res. Part I* 53, 1423–1438. doi: 10.1016/j.dsr.2006.06.004

Isla, J. A., and Anadón, R. (2004). Mesozooplankton size-fractionated metabolism and feeding off NW Spain during autumn: effects of a poleward current. *ICES J. Mar. Sci.* 61, 526–534. doi: 10.1016/j.icesjms.2004.03.014

Iversen, M. H., Nowald, N., Ploug, H., Jackson, G. A., and Fischer, G. (2010). High resolution profiles of vertical particulate organic matter export off cape blanc, mauritania: degradation processes and ballasting effects. *Deep Sea Res. Part I* 57, 771–784. doi: 10.1016/j.dsr.2010.03.007

Iversen, M. H., and Ploug, H. (2013). Temperature effects on carbon-specific respiration rate and sinking velocity of diatom aggregates-potential implications for deep ocean export processes. *Biogeosciences* 10:4073. doi: 10.5194/bg-10-4073-2013

Karakaş, G., Nowald, N., Blaas, M., Marchesiello, P., Frickenhaus, S., and Schlitzer, R. (2006). High-resolution modeling of sediment erosion and particle transport across the Northwest African shelf. *J. Geophys. Res.* 111. doi: 10.1029/2005JC003296

Karstensen, J., Fiedler, B., Schütte, F., Brandt, P., Körtzinger, A., Fischer, G., et al. (2015). Open ocean dead zones in the tropical North Atlantic Ocean. *Biogeosciences* 12, 2597–2605. doi: 10.5194/bg-12-2597-2015

Karstensen, J., Stramma, L., and Visbeck, M. (2008). Oxygen minimum zones in the eastern tropical Atlantic and Pacific oceans. *Prog. Oceanogr.* 77, 331–350. doi: 10.1016/j.pocean.2007.05.009

Kelly, T. B., Davison, P. C., Goericke, R., Landry, M. R., Ohman, M. D., and Stukel, M. R. (2019). The importance of mesozooplankton diel vertical migration for sustaining a mesopelagic food web. *Front. Mar. Sci.* 6:508. doi: 10.3389/fmars.2019.00508

Khatiwala, S. (2007). A computational framework for simulation of biogeochemical tracers in the ocean. *Global Biogeochem. Cy.* 21:GB3001. doi: 10.1029/2007GB002923

Kiko, R., Biastoch, A., Brandt, P., Cravatte, S., Hauss, H., Hummels, R., et al. (2017). Biological and physical influences on marine snowfall at the equator. *Nat. Geosci.* 10:852. doi: 10.1038/ngeo3042

Kiko, R., and Hauss, H. (2019). On the estimation of zooplankton-mediated active fluxes in oxygen minimum zone regions. *Front. Mar. Sci.* 6:741. doi: 10.3389/fmars.2019.00741

Kiko, R., Hauss, H., Buchholz, F., and Melzner, F. (2016). Ammonium excretion and oxygen respiration of tropical copepods and euphausiids exposed to oxygen minimum zone conditions. *Biogeosciences* 13, 2241–2255. doi: 10.5194/bg-13-2241-2016

Kiørboe, T. (2013). Zooplankton body composition. *Limnol. Oceanogr.* 58, 1843–1850. doi: 10.4319/lo.2013.58.5.1843

Kriest, I. (2002). Different parameterizations of marine snow in a 1D-model and their influence on representation of marine snow, nitrogen budget and sedimentation. *Deep Sea Res. Part I* 49, 2133–2162. doi: 10.1016/S0967-0637(02)00127-9

Kriest, I., Kähler, P., Koeve, W., Kvale, K., Sauerland, V., and Oschlies, A. (2020). One size fits all?-calibrating an ocean biogeochemistry model for different circulations. *Biogeosci. Discuss.* 2020, 1–40. doi: 10.5194/bg-2020-9

Kriest, I., and Oschlies, A. (2015). MOPS-1.0: towards a model for the regulation of the global oceanic nitrogen budget by marine biogeochemical processes. *Geosci. Model Dev.* 8, 2929–2957. doi: 10.5194/gmd-8-2929-2015

Kriest, I., Sauerland, V., Khatiwala, S., Srivastav, A., and Oschlies, A. (2017). Calibrating a global three-dimensional biogeochemical ocean model (MOPS-1.0). *Geosci. Model Dev.* 10, 127–154. doi: 10.5194/gmd-10-127-2017

Lampert, W. (1989). The adaptive significance of diel vertical migration of zooplankton. *Funct. Ecol.* 3, 21–27. doi: 10.2307/2389671

Lehette, P., and Hernández-León, S. (2009). Zooplankton biomass estimation from digitized images: a comparison between subtropical and Antarctic organisms. *Limnol. Oceanogr.* 7, 304–308. doi: 10.4319/lom.2009.7.304

Liszka, C. M., Manno, C., Stowasser, G., Robinson, C., and Tarling, G. A. (2019). Mesozooplankton community composition controls faecal pellet flux and remineralisation depth in the Southern Ocean. *Front. Mar. Sci.* 6:230. doi: 10.3389/fmars.2019.00230

Lombard, F., Boss, E., Waite, A. M., Vogt, M., Uitz, J., Stemmann, L., et al. (2019). Globally consistent quantitative observations of planktonic ecosystems. *Front. Mar. Sci.* 6:196. doi: 10.3389/fmars.2019.00196

Longhurst, A., Bedo, A., Harrison, W., Head, E., and Sameoto, D. (1990). Vertical flux of respiratory carbon by oceanic diel migrant biota. *Deep Sea Res. Part A* 37, 685–694. doi: 10.1016/0198-0149(90)90098-G

Martin, J. H., Knauer, G. A., Karl, D. M., and Broenkow, W. W. (1987). VERTEX: carbon cycling in the northeast pacific. *Deep Sea Res. Part A* 34, 267–285. doi: 10.1016/0198-0149(87)90086-0

Matear, R. J., and Hirst, A. C. (2003). Long-term changes in dissolved oxygen concentrations in the ocean caused by protracted global warming. *Glob. Biogeochem. Cycles* 17. doi: 10.1029/2002GB001997

McCave, I. N. (2009). "Nepheloid layers," in *Elements of Physical Oceanography: A Derivative of the Encyclopedia of Ocean Sciences*, eds S. A. Thorpe, K. K. Turekian (Elsevier), 282. doi: 10.1016/B978-012374473-9.00671-8

Mullison, J. (2017). *Backscatter Estimation Using Broadband Acoustic Doppler Current Profilers - Updated*. Available online at: http://www.teledynemarine.com/Documents/Brand%20Support/RD%20INSTRUMENTS/Technical%20Resources/Technical%20Notes/WorkHorse%20-%20ADCP%20Special%20Applications%20and%20Modes/FSA031.pdf

Oschlies, A., Brandt, P., Stramma, L., and Schmidtko, S. (2018). Drivers and mechanisms of ocean deoxygenation. *Nat. Geosci.* 11:467. doi: 10.1038/s41561-018-0152-2

Picheral, M., Colin, S., Irisson, J-O. (2017). EcoTaxa, a tool for the taxonomic classification of images. Available online at: http://ecotaxa.obs-vlfr.fr

Picheral, M., Guidi, L., Stemmann, L., Karl, D. M., Iddaoud, G., and Gorsky, G. (2010). The underwater vision profiler 5: an advanced instrument for high spatial resolution studies of particle size spectra and zooplankton. *Limnol. Oceanogr.* 8, 462–473. doi: 10.4319/lom.2010.8.462

Piontkovski, S., and Castellani, C. (2009). Long-term declining trend of zooplankton biomass in the Tropical Atlantic. *Hydrobiologia* 632, 365–370. doi: 10.1007/s10750-009-9854-1

Prince, E. D., Luo, J., Phillip Goodyear, C., Hoolihan, J. P., Snodgrass, D., Orbesen, E. S.,et al. (2010). Ocean scale hypoxia-based habitat compression of Atlantic istiophorid billfishes. *Fish. Oceanogr.* 19, 448–462. doi: 10.1111/j.1365-2419.2010.00556.x

Putzeys, S. (2013). *Carbon active fluxes in the Northeast Atlantic Subtropical Gyre* (Doctoral thesis). Universidad de Las Palmas de Gran Canaria, Las Palmas de Gran Canaria, Spain.

Remsen, A., Hopkins, T. L., and Samson, S. (2005). What you see is not what you catch: a comparison of concurrently collected net, optical plankton counter, and shadowed image particle profiling evaluation recorder data from the Northeast Gulf of Mexico. *Deep Sea Res. Part I* 51, 129–151. doi: 10.1016/j.dsr.2003.09.008

Robison, B. H., Sherlock, R. E., Reisenbichler, K. R., and McGill, P. R. (2020). Running the gauntlet: assessing the threats to vertical migrators. *Front. Mar. Sci.* 7:64. doi: 10.3389/fmars.2020.00064

Roullier, F., Berline, L., Guidi, L., Durrieu De Madron, X., Picheral, M., Sciandra, A., et al. (2014). Particle size distribution and estimated carbon flux across the Arabian Sea oxygen minimum zone. *Biogeosciences* 11, 4541–4557. doi: 10.5194/bg-11-4541-2014

Saltzman, J., and Wishner, K. F. (1997). Zooplankton ecology in the eastern tropical Pacific oxygen minimum zone above a seamount: 1. General trends. *Deep Sea Res. Part I* 44, 907–930. doi: 10.1016/S0967-0637(97)00007-1

Sandel, V., Kiko, R., Brandt, P., Dengler, M., Stemmann, L., Vandromme, P., et al. (2015). Nitrogen fuelling of the pelagic food web of the Tropical Atlantic. *PLoS ONE* 10:e0131258. doi: 10.1371/journal.pone.0131258

Schmidtko, S., Stramma, L., and Visbeck, M. (2017). Decline in global oceanic oxygen content during the past five decades. *Nature* 542:335. doi: 10.1038/nature21399

Schnetzer, A., and Steinberg, D. (2002). Natural diets of vertically migrating zooplankton in the Sargasso Sea. *Mar. Biol.* 141, 89–99. doi: 10.1007/s00227-002-0815-8

Schütte, F., Brandt, P., and Karstensen, J. (2016a). Occurrence and characteristics of mesoscale eddies in the tropical northeastern Atlantic Ocean. *Ocean Sci.* 12, 663–685. doi: 10.5194/os-12-663-2016

Schütte, F., Karstensen, J., Krahmann, G., Hauss, H., Fiedler, B., Brandt, P., et al. (2016b). Characterization of "dead-zone" eddies in the eastern tropical North Atlantic. *Biogeosciences* 13, 5865–5881. doi: 10.5194/bg-13-5865-2016

Stamieszkin, K., Pershing, A. J., Record, N. R., Pilskaln, C. H., Dam, H. G., and Feinberg, L. R. (2015). Size as the master trait in modeled copepod fecal pellet carbon flux. *Limnol. Oceanogr.* 60, 2090–2107. doi: 10.1002/lno.10156

Stammer, D., Ueyoshi, K., Köhl, A., Large, W. G., Josey, S. A., and Wunsch, C. (2004) Estimating air-sea fluxes of heat, freshwater, and momentum through global ocean data assimilation. *J. Geophys. Res.* 109. doi: 10.1029/2003JC002082

Steinberg, D. K., Carlson, C. A., Bates, N. R., Goldthwait, S. A., Madin, L. P., and Michaels, A. F. (2000). Zooplankton vertical migration and the active transport of dissolved organic and inorganic carbon in the Sargasso Sea. *Deep Sea Res. Part I* 47, 137–158. doi: 10.1016/S0967-0637(99)00052-7

Steinberg, D. K., Goldthwait, S. A., and Hansell, D. A. (2002). Zooplankton vertical migration and the active transport of dissolved organic and inorganic nitrogen in the Sargasso Sea. *Deep Sea Res. Part I* 49, 1445–1461. doi: 10.1016/S0967-0637(02)00037-7

Steinberg, D. K., and Landry, M. R. (2017). Zooplankton and the ocean carbon cycle. *Annu. Rev. Mar. Sci.* 9, 413–444. doi: 10.1146/annurev-marine-010814-015924

Stramma, L., Johnson, G. C., Sprintall, J., and Mohrholz, V. (2008). Expanding oxygen-minimum zones in the tropical oceans. *Science* 320, 655–658. doi: 10.1126/science.1153847

Stramma, L., Prince, E. D., Schmidtko, S., Luo, J., Hoolihan, J. P., Visbeck, M., et al. (2012). Expansion of oxygen minimum zones may reduce available habitat for tropical pelagic fishes. *Nat. Clim. Change* 2:33. doi: 10.1038/nclimate1304

Turner, J. T. (2015). Zooplankton fecal pellets, marine snow, phytodetritus and the ocean's biological pump. *Progr. Oceanogr.* 130, 205–248. doi: 10.1016/j.pocean.2014.08.005

Wishner, K. F., Gowing, M. M., and Gelfman, C. (1998). Mesozooplankton biomass in the upper 1000 m in the Arabian Sea: overall seasonal and geographic patterns, and relationship to oxygen gradients. *Deep Sea Res. Part II* 45, 2405–2432. doi: 10.1016/S0967-0645(98)00078-2

Conflict of Interest: The authors declare that the research was conducted in the absence of any commercial or financial relationships that could be construed as a potential conflict of interest.

Advantages of publishing in Frontiers

OPEN ACCESS
Articles are free to read for greatest visibility and readership

FAST PUBLICATION
Around 90 days from submission to decision

HIGH QUALITY PEER-REVIEW
Rigorous, collaborative, and constructive peer-review

TRANSPARENT PEER-REVIEW
Editors and reviewers acknowledged by name on published articles

Frontiers
Avenue du Tribunal-Fédéral 34
1005 Lausanne | Switzerland

Visit us: www.frontiersin.org
Contact us: info@frontiersin.org | +41 21 510 17 00

REPRODUCIBILITY OF RESEARCH
Support open data and methods to enhance research reproducibility

DIGITAL PUBLISHING
Articles designed for optimal readership across devices

FOLLOW US
@frontiersin

IMPACT METRICS
Advanced article metrics track visibility across digital media

EXTENSIVE PROMOTION
Marketing and promotion of impactful research

LOOP RESEARCH NETWORK
Our network increases your article's readership